SCOUR OF CAPTURED SEDIMENT FROM A STORMWATER HYDRODYNAMIC DEVICE

by

HUMBERTO F. AVILA RANGEL

A DISSERTATION

Submitted in partial fulfillment of the requirements for the degree of
Doctor of Philosophy in the Department of Civil,
Construction, and Environmental Engineering
in the Graduate School of
The University of Alabama

TUSCALOOSA, ALABAMA

2008

Submitted by Humberto F. Avila Rangel in partial fulfillment of the requirements for the degree of Doctor of Philosophy specializing in Civil Engineering.

Accepted on behalf of the Faculty of the Graduate School by the dissertation committee:

____
S. Rocky Durrans, Ph.D.

____
Michael Triche, Ph.D.

____
Lisa Davis, Ph.D.

____
Shirley E. Clark, Ph.D.

____
Jason T. Kirby, Ph.D.

____
Kenneth J. Fridley, Ph.D.

____
Robert E. Pitt, Ph.D.
Chairperson

____
Kenneth J. Fridley, Ph.D.
Department Chairperson

____
Date

____
David A. Francko, Ph.D.
Dean of the Graduate School

____
Date

DEDICATION

To my wife, Edith, for her unconditional love, and to my daughter, Isabella, for bringing joy to my life.

LIST OF ABREVIATIONS AND SYMBOLS

$b_{Q,D}$	Constants for regression model based on linear functions
C_d	Coefficient of drag (theoretical equations)
D	Sediment particle size
D	Depth or diameter of a pipe
DRG	Drag coefficient (CFD model)
f_L	Liquid fraction
f_S	Solid volume fraction
$f_{S,CO}$	Cohesive solid fraction
$f_{S,CR}$	Critical solid fraction
f_{SED}	Fraction of sediment in cell
g	Gravitational acceleration
H	Overlaying water depth, or, Depth below the outlet
K	Coefficient of reduction of shear stress
$m_{Q,D}$	Constants for regression model based on linear functions
n_s	Vector normal to the packed bed surface
Q	Flow rate
R_*	Reynolds number of the particle
SSC	Suspended Sediment Concentration
TSDRG	Constant for drag coefficient

u	Velocity
u_*	Shear velocity
V	Velocity
w	Settling velocity of particles
α	Dimensionless parameter that represents the probability of sediment suspension
Φ	Dimensionless shear stress
φ	Local slope of the packed bed
ν	Kinematics viscosity of the water
ρ	Density of water
ρ_s	Density of particles
τ_*	Dimensionless shear stress
τ_o	Critical shear stress
ζ	Angle of repose of the particle
τ	Acting shear stress

ACKNOWLEDGEMENTS

I would like to thank my advisor, Dr. Robert Pitt, for his continuous guidance, trust, and support in conducting this research. I would also like to thank the University of Alabama, the Universidad del Norte, COLCIENCIAS, and LASPAU for their financial support. I would like to thank Dr. S. Rocky Durrans, who is part of my committee, for his trust and advice during this research. I would like to thank the remaining members of my committee, Drs. Shirley Clark, Lisa Davis, Michael Triche, Jason Kirby, and Kenneth Fridley, for their assistance during this research. I would also like to thank the Department of Civil, Construction, and Environmental Engineering of the University of Alabama for giving me the great opportunity to teach.

I would like to thank Tim Ryan for helping me to build the physical model and offering me his friendship. To Dr. James Richardson, thank you for helping me in one of tests. I would like to thank the faculty, staff, and students in the Civil, Construction, and Environmental Engineering Department.

Finally, I would like to thank my beloved wife Edith, who helped me to perform all the physical tests. To my parents, Humberto and Mery, my brothers, Boris and Leandro, and my mother-in-law, Yenedith, thank you for your love, advice, and trust.

CONTENTS

LIST OF TABLES

LIST OF FIGURES

ABSTRACT

Hydrodynamic devices have long been proposed as sediment traps in storm drainage systems. A number of research studies have investigated the performance of catchbasins as stormwater quality control devices by evaluating the sediment and pollutant removal capacity of those structures. However, little information is available on the potential scour of previously captured sediment in hydrodynamic devices, and regulators, vendors, and stormwater managers are trying to understand its significance.

The purpose of this research was to evaluate the sediment scour in catchbasin sumps, analyzing the effect of flow rate, overlaying water depth, inlet geometry, and sediment particle sizes. Full-scale physical experimentation and Computational Fluid Dynamic (CFD) modeling were performed to determine the Suspended Sediment Concentration (SSC) associated with the scour rate under different conditions. The conditions of the tests were the following: flow rates between 0.3 and 20 L/s, overlaying water depths above the sediment surface between 10 and 106 cm, circular and rectangular inlet geometries, a sediment mixture, and sediment with homogeneous particle sizes.

The overlaying water depth, sediment particle sizes, and the armoring sediment layer were shown to be highly significant in minimizing scour potential by reducing the SSC exponentially. In contrast, SSC increased as a fractional power function of flow rate. Differences in the scour patterns were found for a sediment mixture and for sediment with a homogeneous sediment particle size. The absence of an armoring layer on the

sediment surface caused the SSC to stay constant within the 30 min of analysis while showing no indication of reduction. A new scour model code was written and implemented in Flow-3D v.9.2 to simulate the scour scenarios for homogeneous sediment material from a catchbasin sump with a rectangular inlet. A total of 40 scenarios, including the calibration and validation, were simulated. Regression models were generated to estimate the scour rate for a sediment mixture and for homogeneous particle sizes. The models calculated SSC as a function of flow rate, overlaying water depth, and sediment particle size.

Recommendations and future research subjects are proposed, including enhancements of the basic geometry of a catchbasin sump, a methodology for scour test protocols, evaluation of the armoring properties of different particles sizes, and the creation of a scour model implemented in a CFD model to evaluate sediment mixtures.

ABSTRACT OF DISSERTATION

The University of Alabama Graduate School

Degree: Doctor of Philosophy **Major Subject**: Civil Engineering

Name of Candidate: Humberto F. Avila Rangel

Title of Dissertation: Scour of Captured Sediment from a Stormwater Hydrodynamic Device

Hydrodynamic devices have long been proposed as sediment traps in storm drainage systems. A number of research studies have investigated the performance of catchbasins as stormwater quality control devices by evaluating the sediment and pollutant removal capacity of those structures. However, little information is available on the potential scour of previously captured sediment in hydrodynamic devices, and regulators, vendors, and stormwater managers are trying to understand its significance.

The purpose of this research was to evaluate the sediment scour in catchbasin sumps, analyzing the effect of flow rate, overlaying water depth, inlet geometry, and sediment particle sizes. Full-scale physical experimentation and Computational Fluid Dynamic (CFD) modeling were performed to determine the Suspended Sediment Concentration (SSC) associated with the scour rate under different conditions. The conditions of the tests were the following: flow rates between 0.3 and 20 L/s, overlaying water depths above the sediment surface between 10 and 106 cm, a 30-cm diameter (12 inch) circular and a 50-cm wide rectangular inlet geometries, a sediment mixture, and sediment with homogeneous particle sizes.

The overlaying water depth, sediment particle sizes, and the armoring sediment layer were shown to be highly significant in minimizing the scour potential by reducing SSC exponentially. In contrast, SSC increased as a fractional power function of flow rate. Differences in the scour patterns were found for a sediment mixture and for sediment with a homogeneous sediment particle size. The absence of an armoring layer on the sediment surface caused the SSC to stay constant within the 30 min of analysis while showing no indication of reduction. A new scour model code was written and implemented in Flow-3D v.9.2 to simulate the scour scenarios for homogeneous sediment material from a catchbasin sump with a rectangular inlet. A total of 40 scenarios, including the calibration and validation, were simulated. Regression models were generated to estimate the scour rate for a sediment mixture and for homogeneous particle sizes. The models calculated SSC as a function of flow rate, overlaying water depth, and sediment particle size.

Recommendations and future research subjects were proposed, including enhancements of the basic geometry of a catchbasin sump, a methodology for scour test protocols, evaluation of the armoring properties of different particles sizes, and the creation of a scour model implemented in a CFD model to evaluate sediment mixtures.

Abstract Approved: Chairman of
Dissertation Committee ______________________________
Robert E. Pitt, Ph.D.

Head of Department
or College ______________________________
Kenneth J. Fridley, Ph.D.

Date___________ Dean of the
Graduate School______________________________
David A. Francko, Ph.D.

CHAPTER 1

INTRODUCTION

1.1 Overview

Hydrodynamic devices have long been proposed as sediment traps in storm drainage systems. The earliest and simplest hydrodynamic device was an inlet with a catchbasin sump (Lager et al. 1977). Early uses of these devices had been to act as a trap to capture large debris, minimizing their deposition in the storm drainage system. However, a number of research studies have investigated the performance of catchbasins as stormwater quality control devices by evaluating the sediment and pollutant removal capacity of these structures (Aronson, Watson, and Pisano 1983; Butler and Karunaratne 1995; Lager et al. 1977; Pitt et al. 1979, 1985, 1994, 1998, 1999). Hydrodynamic devices have been also developed recently to specially provide stormwater quality control benefits (de Brujin and Clark, 2003; New Jersey Corporation for Advanced Technology (NJCAT), 2002, 2004a, 2004b, 2004c, 2005a, 2005b).

Accumulation of sediment and potential subsequent scour is one of the sediment transport processes in a stormwater drainage system (Pitt 2004). Sediment can be captured in inlets and catchbasins during rainfall events. The accumulation rate, or sediment-retaining performance, depends on the size and geometry of the device, flow rate, sediment size, and specific gravity of the sediment. The sediment removal performance in catchbasin sumps has been reported to be between 14 and 99% (Lager et al. 1977). Typically, up to about 30% of the total stormwater particulates are captured during actual rainfall tests (Pitt 1985). WinSLAMM, the Source Loading and Management Model, for example, uses the surface overflow rate (SOR), or upflow velocity concept, to model sediment capture in hydrodynamic devices. However, once the sediment is captured, there is risk of washing out that sediment due to scour, increasing the pollution load in the stormwater system.

Previous studies performed by the American Public Work Association (APWA 1969) concluded that catchbasins may be an important source of pollution from stormwater flows, as the overburden water was felt to be more contaminated than stormwater and is displaced during rains. However, during extensive testing of overburden water, Pitt and Bissonette (1984) did not find any significant difference between the two waters for the same events. Stormwater pollution has been associated with runoff sediment load; toxicity in stormwater, for example, was associated with suspended sediment in stormwater runoff (Burton and Pitt 2002). The Department of Natural Resources (DNR) of the state of Wisconsin and the New Jersey Corporation for Advanced Technology (NJCAT) have developed and/or are improving protocols to consider sediment scour as one of the performance criteria for removal efficiency (Brzozowski 2006).

1.2 Significance of the Study

The significance and need of this research is based on the following:

Understanding the scour phenomenon in catchbasin devices is an actual need when implementing protocols and rules for preventing and managing polluted stormwater runoff. Currently, sediment scour is a major subject of concern when evaluating the performance of catchbasins and related hydrodynamic separators in stormwater systems and when developing protocols for scour evaluation (Brzozowski 2006).

A number of recent research studies have investigated the performance of catchbasins as stormwater quality control devices by evaluating the sediment removal capacity (Aronson et al. 1983; Butler et al. 1995; Lager et al. 1977; Pitt et al. 1979, 1985, 1994, 1998, 1999). Also, hydrodynamic separators have been developed to provide some stormwater quality control benefits (NJCAT 2002, 2004, 2005). However, the evaluation of several technologies has been mostly concentrated in the sediment removal capacity, and little information is available on the scour potential of previously captured sediment. Removal capacity does not necessarily imply the ability to prevent the sediment from being scoured, especially when the remaining sediment capacity volume of the device is small and the flow rates are high. Studies on a screened hydrodynamic separator performed by Sansalone et al. (2007) showed that particles smaller than 50 μm are sensitive to scour in this type of device.

Maintenance of catchbasin devices is fundamental to ensure the operating efficiency of sediment removal. Field observations have shown that the scour depth in catchbasins is generally about 300 mm below the outlet (Pitt 1985), which is also mentioned by U.S. EPA (1999) as a signal to perform catchbasin cleaning. However, no information has been found relating to specific overlaying water depths at which scour may be minimized as a function of the flow rate and mean particle size.

1.3 Hypotheses

This research addresses the following hypotheses:

1. Scour of pre-deposited sediment from a stormwater catchbasin sump can be estimated through knowledge of the major factors involved in the process, such as flow rate, characteristics of the sediment, and overlying water depth above the sediment.
2. In addition to the data collected from physical experimentation to determine the relationship of the scour rate with those major factors, the sediment scour rate can also be determined by using the initial motion and initial suspension threshold criteria implemented in a Computational Fluid Dynamics (CFD) model. Differences between actual field observations and the CFD model are likely caused by bed armoring, highly variable flows, and a mixture of sediment particle sizes. The CFD modeling is highly valuable in understanding the basic processes inherent in scour from these devices.

1.3.1 *Methods and Analyses to Test the Hypotheses*

In order to test the hypotheses, the following methods and analyses were performed:

- Full-scale physical experimentation:
    - A full-scale physical model was built based on the optimal geometry of a catchbasin sump proposed by Lager et al. (1977). The model had a maximum flow capacity of 10 L/s and the flexibility of modifying the inlet geometry.

  - Hydrodynamic tests were conducted to evaluate the velocity field generated in the water domain of a catchbasin sump. Two inlet geometries were evaluated: a 50-cm wide rectangular inlet and a 30-cm circular pipe inlet. Each inlet was tested with three flow rates: 2.5, 5, and 10 L/s. Velocity vectors were measured on different locations in the water domain of the catchbasin sump.
  - Sediment scour tests were conducted with two different pre-deposited sediment materials: a sediment mixture and sediment with a homogeneous particle size distribution. Composite samples were collected from both experiments to determine the Suspended Sediment Concentration (SSC). The scour tests were performed at different overlaying water depths and flow rates.
- Computational Fluid Dynamic (CFD) modeling:
  - Hydrodynamic simulations were conducted with two CFD software packages: *Fluent v.6.2* (ANSYS © 2008), and *Flow-3D* v.*9.2* (Flow Science © 2008). 3-dimensional (3D) and 2-dimensional (2D) analyses were performed. Velocity vectors were evaluated and compared to experimental data. Calibration and validation of the hydrodynamic model were conducted prior to the sediment scour analysis with CFD modeling.
  - Sediment scour simulations were performed with CFD software package *Flow-3D* v.*9.2*. A 2D-customized scour model code was created, calibrated, and validated to evaluate the sediment scour. Four particle sizes were evaluated: 50, 180, 500, and 1000 μm, at different elevations: 15, 24, 35, 40, and 45 cm below the outlet, and three different flow rates: 5, 10, and 20 L/s.
- Statistical analysis:

- Experimental data:
    - One-way ANOVA (Analysis of Variance) tests with Bonferroni t-test for paired comparisons were applied to the experimental data obtained from the hydrodynamic and sediment scour tests to determine the significant factors on the sediment scour potential.
    - Multiple linear regression and customized regression models were determined to estimate SSC as a function of flow rate and overlaying water for a sediment mixture. Response surfaces were created to compare experimental data to the values estimated by the model. Residual analysis was conducted to evaluate the level of error of the estimates.
- CFD results:
    - Simple linear regression and multiple linear regression models were determined to estimate SSC as a function of flow rate and overlaying water depth for sediment with a homogeneous particle size. Response surfaces were created to compare experimental data to the values estimated by the model. Residual analysis was performed to evaluate the level of error of the estimated values.

1.4 Objectives

The objectives of this research are as follows:

- Determine the significant factors involved in the sediment scour phenomenon in a catchbasin sump.

- Evaluate the hydrodynamic characteristics of the flow in a catchbasin sump associated with the sediment scour potential.
- Determine the Suspended Sediment Concentration (SSC) for different conditions of flow rate, sediment characteristics, and overlaying water depth above the sediment.
- Implement a Computational Fluid Dynamics (CFD) model supported by physical experimentation to determine the sediment scour rate under different conditions.
- Evaluate the relationship between individual significant factors involved in the scour phenomenon and the scour rate.
- Develop a verified theoretical model to predict the scour rate given the significant factors and their interactions.

1.5 Contribution

The significant contributions of this research are as follow:

- Identifying mathematical relationships between individual significant factors involved in the scour phenomenon and the sediment scour rate in a catchbasin sump.
- Creating and implementing a computational model for sediment scour in catchbasin sumps.
- Contributing to the understanding and improvement of existing, and the development of new stormwater control devices, protocols, and rules for preventing and managing polluted stormwater runoff.

CHAPTER 2

LITERATURE REVIEW

This chapter includes a description of different geometries and functions of catchbasin sumps, the typical operating conditions in terms of quantity and quality of water, the hydrodynamics involved in catchbasin sumps, and sediment scour theory.

2.1 Definitions

A catchbasin is an underground chamber that receives surface runoff from streets and has the capability of retaining coarse and fine material (sediment, leaves, etc.) from the storm runoff water (Lager et al. 1977) before delivering the water to a manhole, a main sewer pipe, or a receiving water body. Manholes are located along the storm drainage system and connect two or more segments of sewer pipes to convey the water to a single and greater-size pipe. Manholes are installed for cleaning and maintenance purposes or when pipe segments change direction. An inlet is an entrance structure located on the curbline and is used to capture the surface runoff to deliver it to a manhole or directly to a main sewer pipe. Simple inlets do not have sumps to trap the sediment in the runoff. Catchbasins with sumps are installed on the curbline instead of simple inlets. Sometimes, manholes may also have sumps.

Pitt and Field (1998) presented the characteristics of an efficient storm drain inlet. The goal is a storm drainage inlet device that:

- Does not cause flooding when it clogs with debris,
- Does not force stormwater through the captured material,
- Does not have adverse hydraulic head loss properties,
- Maximizes pollutant reductions, and
- Requires inexpensive and infrequent maintenance.

2.2 Classifications and Geometries of Catchbasins

Catchbasin sumps can be classified by their location as surface-inlet catchbasins, in-line catchbasins, and off-line catchbasins. Also, they can be classified by their performance as catchbasins, which function to prevent sewer clogging by trapping coarse debris and to prevent odor emanations from the sewer by providing a water seal, and enhanced catchbasins, known as hydrodynamic separators, which function to treat the combined sewage or stormwater by reducing the Suspended Sediment Concentration (SSC) and floatable material from the water.

Surface-inlet catchbasins receive the stormwater directly from the surface (streets, parking lots, etc.) through inlets, and then they convey the water to a manhole or a main sewer pipe. Most catchbasins fall within this classification. In Europe, catchbasins (termed gully pots) are generally smaller in size, serving smaller drainage areas (Lager et al. 1977). Hooded sumps can be used to prevent sewer gases from escaping from the sewerage in combined sewer systems and to prevent floatables from entering the drainage system.

The optimal catchbasin geometry was recommended by Lager et al. (1977) and tested by Pitt (1979, 1985, 1994). In this catchbasin, if the outlet diameter is *d*, the total height of the manhole is *6.5d* and the inside diameter is *4d*; the outlet has to be located *4d* above the bottom and *2.5d* below the top of the manhole (Figure 1).

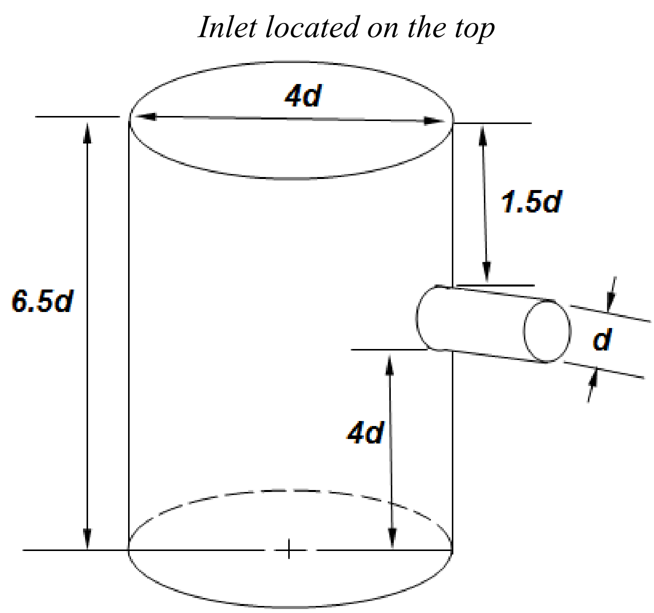

Figure 1. Optimal catchbasin geometry recommended by Lager et al. (1977).

Different types of inlet structures can be found in catchbasins. The most typical are the grate inlet, the curb opening inlet with or without depression, the combination inlet, and the slotted drain inlet (Chin 2006).

In-line hydrodynamic devices are located along the sewer system, receiving the combined or stormwater directly from a sewer pipe and delivering it back downstream to another sewer pipe segment. Hydrodynamic separators are designed to remove sediment, floatables, and oil from the water and can also be placed in-line.

Off-line hydrodynamic devices receive the combined sewage or separate stormwater through a derivation from a main sewer system or manhole. These devices can have storage and sediment removal functions in either separated or combined sewer systems. Off-line devices can deliver the treated water back to the storm sewer system or directly to a water body if they are working as a combined sewer overflow (CSO) structure.

2.3 Sediment Characteristics and Removal Capacity in Catchbasins

Particle size distributions in catchbasin sumps differ from the sediment distribution in the inflowing water being treated. Large particle sizes are more easily captured by catchbasins than fine particles. High flow rates also reduce the sediment removal capacity of catchbasins (Lager et al. 1977). Valiron and Tabuchi (1992) summarized the results of the particle size distribution of sediment collected in five gully pots in northern France, which are shown in Table 1. Most of the solids trapped were sand-sized, with a mean diameter close to 300 µm.

Table 1. Mean Particle Size Distributions of Dried Solids Collected in Five Gully Pots (Valiron and Tabuchi 1992)

Particle size (µm)	**< 50**	**50 – 100**	**100 - 200**	**200 - 500**	**500 - 1000**	**1000 - 2000**	**> 2000**
gully # 1	24	3	6	11	6	8	42
gully # 2	24	6	8	18	14	17	13
gully # 3	5	2	5	16	13	15	44
gully # 4	15	4	14	29	11	10	17
gully # 5	56	6	8	12	7	8	4
Mean distribution	24.8	4.2	8.2	17.2	10.2	11.6	24

Pitt and Khambhammettu (2006) evaluated the particle size distribution of a catchbasin sump at a monitoring location in Tuscaloosa, AL, at the end of 10-month monitoring period; the results are shown in Table 2. The median particle size was about 450 µm. The specific gravity values varied from about 1.5 to 3.0, with a mass-weighted specific gravity value of 2.5; the lower values of specific gravity were for the smallest and largest particles. Table 2 also shows chemical characteristics of the sediment, which were considered similar to previous studies.

Table 2. Observed Quantity and Quality of Sediment Collected from Catchbasin Sump (Pitt and Khambhammettu 2006)

Sediment Size Range (µm)	% of total amount in sump in size range	Specific density (g/cm^3)	COD, (mg/kg)	P, (mg/kg)	Fe (mg/kg)	Cu (mg/kg)	Cr (mg/kg)	Zn (mg/kg)
<75	2.0	1.47	233,000	3,580	6,050	190	21.2	1,340
75-150	2.9	2.09	129,000	1,620	4,960	99.8	17.4	958
150-250	6.6	2.64	35,500	511	3,010	48.2	8.0	501
250-425	21.5	2.17	60,100	315	2,790	33.6	6.7	539
425-850	31.9	2.99	45,000	496	2,290	22.1	3.7	270
850-2,000	19.6	2.69	29,200	854	4,050	27.8	6.9	414
2,000-4,750	8.9	1.85	143,000	1,400	4,430	54.9	10.5	450
>4,750	6.5	1.85	251,000	1,700	7,000	48.7	9.3	564
Total	100.0	2.50						

In contrast to these particle sizes trapped in catchbasin and gully pot sumps, particle size distributions of suspended solids in the inflowing water were evaluated by

Pitt et al. (1999) at 121 stormwater inlets that were not affected by stormwater controls in New Jersey, Alabama, and Wisconsin. The median particle sizes at these locations ranged from 0.6 to 38 µm, with an average of 14 µm. The ninetieth percentile size ranged from 0.5 to 11 µm (average was 3 µm). Stormwater particle size distributions, including the bed load component, were determined from samples collected at the inlet to the Monroe St. wet detention pond in Madison, WI. The median particle size ranged from 2 to 25 µm and averaged 8 µm. The bed load represented particles larger than about 300 µm, and comprised about 10 percent of the annual total solids loading, but ranged from 2 to 25 percent for individual sampling periods (Pitt et al. 1999).

Figure 2 shows the average particle size distribution for inflowing stormwater collected at inlets by Pitt et al. (1999) in comparison with the particle size distribution in catchbasin sediments observed by Valiron and Tabuchi (1992) and Pitt and Khambhammettu (2006). This figure shows that while the median particle size in the stormwater at the inlet was about 8 µm, the median particle size in the catchbasin sediment was about 400 µm. This shows that fine particles either are not trapped by catchbasins or are trapped during low flow rate events and then washed out during high flow rate events. In all cases, it is evident that scour potential represents a main issue concerning the sediment removal performance of a catchbasin.

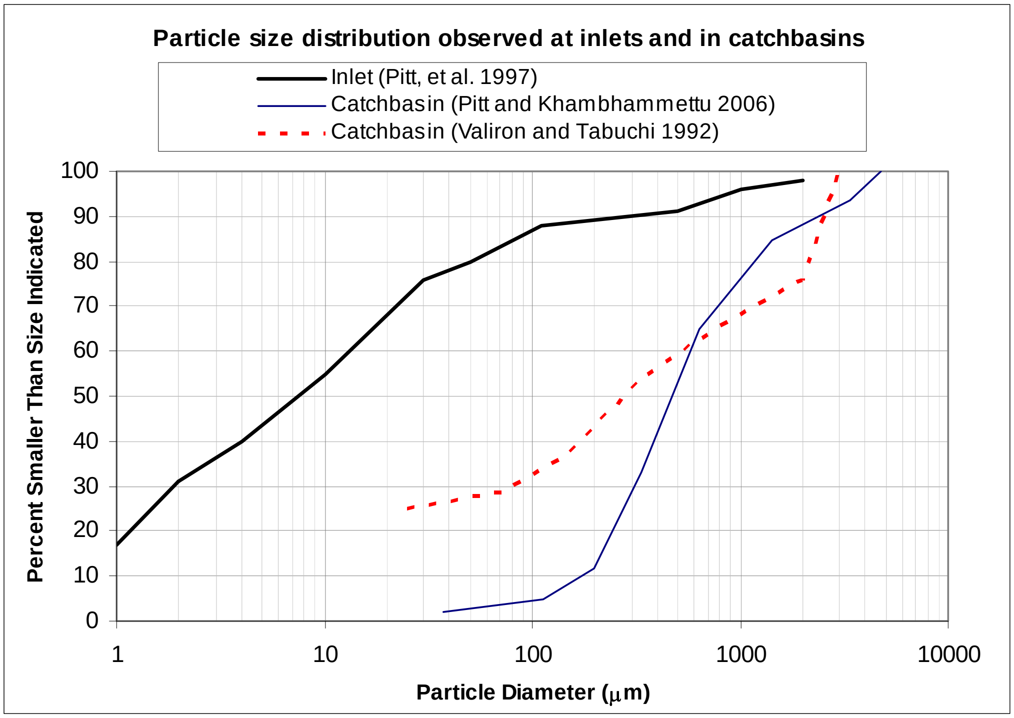

Figure 2. Particle size distributions observed for inflowing water at inlets and for trapped sediment in gully pots and catchbasins.

Butler and Karunaratne (1995) also evaluated the particle size distribution of sediment deposited in catchbasin sumps. It was found that only large particles are trapped by the catchbasins; the median particle size was between about 300 and 3,000 μm, and less than 10% of the particles were smaller than 100 μm.

Early investigations concluded that catchbasins are hydraulically inefficient, with insufficient sedimentation capacity and a high level of resuspension of solids at moderate flow rates (APWA 1969; Sartor and Boyd 1972). In general, it is important to consider that sediment settling and scour are dependent primarily on the size and the density of the particles and the flow rate. Lager et al. (1977) conducted experiments to evaluate the sediment capture capacity in catchbasins. They evaluated different geometries and determined efficiency curves of the percentage of sediment retained as a function of the flow rate for the optimal catchbasin geometry in this series of experiments. These results showed that catchbasins can have high removal capabilities for large particles and low flows, but the removal capabilities decreased for small sediment particles and high flow rates. However, the flow rates tested by Lager et al. (from 1 to 7 cfs) were relatively high compared to typical flow rates, as shown in Table 3.

Lager et al. (1977) also concluded that the primary control for removal performance of catchbasins is the storage basin depth, and the efficiency improves with increasing depth. Butler and Karunaratne (1995), in contrast, concluded that the depth of sediment has a smaller effect on sediment capture than the flow rate and particle size in gully pots, which are smaller in size than the catchbasins used in U.S. and Canada.

Figure 3 shows the critical particle size captured for different sumps areas and flow rates calculated by Pitt and Khambhammettu (2006). Particles larger than the sizes shown on the diagonal lines would be captured for the concurrent flow and sump size conditions. These calculations are based on the up-flow velocity related to the terminal settling velocity of different sediment particle sizes, assuming a 2.5 specific gravity.

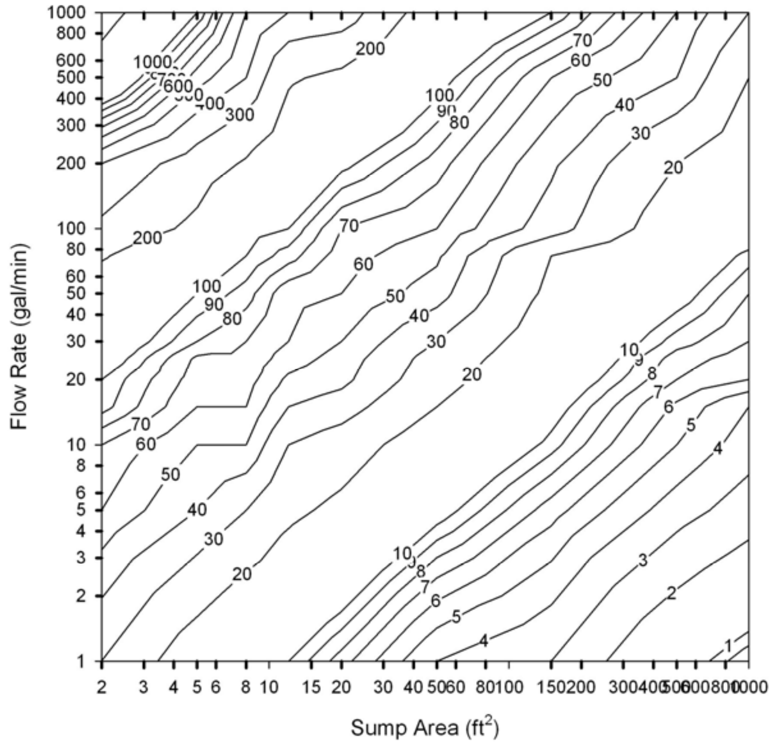

Figure 3. Critical particle sizes (μm) captured for different sump areas and flow rates (Pitt and Khambhammettu 2006).

2.4 Treatment Flow Rates and Hydraulic Capacity

WinSLAMM, the Source Loading and Management Model, is typically used for continuous simulations using several decades of rain data to predict stormwater quality conditions. Table 3 shows typical flow rate values (in gallons per minute) for an acre of pavement (a typical drainage area for a single inlet) for five different US cities during a single typical rain year. These values show the treatment flow rates that would be needed to treat different percentages of the annual flows for an acre of pavement in these cities. The treatment flow rates assume that these flows would treat all runoff events up to these flows and these amounts for larger rains.

Table 3. Annual Flow Rate Distributions (GPM/Acre Pavement), (1 L/s ≈ 16 GPM) (Pitt and Khambhammettu 2006)

Location	50th Percentile	70th Percentile	90th Percentile	Maximum flow rate expected during typical rain year
Seattle, WA	16	28	44	60
Portland, ME	31	52	80	130
Milwaukee, WI	35	60	83	210
Phoenix, AZ	38	60	150	190
Atlanta, GA	45	65	160	440

The hydraulics of a catchbasin system are determined by the flow capacity of the top inlet entrance and the outflow capacity through the outlet pipe. When the outlet is submerged due to backwater conditions, the outflow rate depends on the hydraulic gradient between the head in the barrel and the head at the end of the outlet pipe (Lager et al. 1977). In most cases, the hydraulic capacity of a storm drain inlet is determined by the inlet located at the street.

2.5 Hydrodynamics in Catchbasins

The hydrodynamics in catchbasins are mainly defined by two conditions: the plunging effect of the incoming cascading water and the outlet characteristics. The free-falling cascading water, either rectangular or circular, increases its falling vertical velocity due to gravity until it impacts the surface of the water volume contained in the catchbasin sump, which causes a plunge pool velocity decay phenomenon. McKeigh (1978) found that an undeveloped free-falling circular jet, characterized with a solid and non-aerated water core, spreads out as it penetrates the plunge pool. McKeigh defined the zone of flow establishment as the zone where the solid jet core completely decays. Ervine and Falvey (1987) provided approximations for estimating the velocity of a circular undeveloped jet in a plunge pool based on McKeigh's results. They suggested using the impact velocity until the depth at which the inner core completely decays. Below this zone of flow establishment, the velocity may be estimated by Equation 1. Ervine and Falvey assumed that the core decays at $4d_i$ deep.

$$V_{\max} \approx \frac{4V_i d_i}{H}, \qquad \text{Equation 1}$$

where V_{max} is the maximum velocity of the jet at depth L, H is the depth beneath the water surface, V_i is the jet velocity at impact with the water surface, and d_i is the diameter of the circular jet core at impact.

Bohrer et al. (1998) developed an empirical equation to predict the plunge pool velocity decay of a free-falling rectangular jet. Equation 2 includes the changes of density of the rectangular jet due to air entrainment caused by the turbulent conditions at the impacting zone.

$$\frac{V}{V_i} = 0.0675\left[\frac{\rho_i}{\rho}\cdot\frac{V_i^2}{gL}\right] + 0.1903 \qquad \text{Equation 2}$$

This equation is limited to a range of:

$$0.51 < \left[\frac{\rho_i}{\rho}\cdot\frac{V_i^2}{gL}\right] < 5.76, \qquad \text{Equation 3}$$

where V is the average velocity of a jet at depth L, ρ_i is the average density of the air entrained jet at impact with the water surface, ρ is the density of water, and g equals the gravitational acceleration.

The impacting cascading water will disturb the volume of control up to a certain depth, transferring momentum and creating variation in velocity. However, the velocity field pattern in the volume of control will be mainly controlled by the characteristics of the outlet. Given the geometry of the sump (generally cylindrical), the geometry, dimension, and location of the outlet will control the flow pattern. Detailed information about typical magnitudes and directions of velocity vectors in the volume of control of a catchbasin sump were not found in the existing literature. This research will contribute this information.

2.6 Sediment Settling Process

Sedimentation is a solid-liquid separation by gravitational settling (Lee and Lin 1999). The type of sedimentation that predominates in catchbasins is Type 1, which is discrete particle settling. The terminal settling velocity at which a particle will no longer accelerate during the settling process is determined by balancing the forces acting on a submerged particle; these forces are particle weight, the buoyancy force, and the drag force. The particle weight and the buoyancy force can be expressed as the submerged weight of the particle (F_w), as given by Equation 4.

$$F_w = \frac{\pi D^3}{6}(\rho_s - \rho)g \,, \qquad \text{Equation 4}$$

where F_w is the submerged or buoyed particle weight, D is the diameter of the particle, ρ is the mass density of the fluid, ρ_s equals the mass density of the fluid, and g is the acceleration of gravity.

A general expression described by Newton's Law is presented Equation 5 (ASCE 1975).

$$w = \left[\frac{4g(\rho_s - \rho)D}{3C_d \rho} \right]^{1/2}, \qquad \text{Equation 5}$$

where w is the settling velocity of particles, g equals gravitational acceleration, ρ_s is the density of particles, ρ equals the density of water, D is the diameter of particles, and C_d is the coefficient of drag.

The drag coefficient depends on the ratio of inertial forces related to the particle and viscous forces related to the fluid, which is defined as the Particle Reynolds Number (R') in Equation 6. The drag coefficient decreases as the Particle Reynolds Number increases.

$$R' = \frac{wD\rho}{\mu}, \qquad \text{Equation 6}$$

where μ is the dynamic viscosity.

Given the Particle Reynolds Number, the drag coefficient can be calculated by using the following expressions:

If $R' < 1$,

$$C_d = \frac{24}{R'}. \qquad \text{Equation 7}$$

At this range, the terminal settling velocity results in the Stokes equation, given as:

$$w = \frac{g(\rho_s - \rho)D^2}{18\mu} \qquad \text{Equation 8}$$

If *1 < R' < 1000,*

$$C_d = \frac{24}{R'} + \frac{3}{\sqrt{R'}} + 0.34 \,. \qquad \text{Equation 9}$$

This previous expression was presented by Fair, Geyer, and Okun (1968).

If *R' > 1000*

$$C_d = 0.34 \;\; to \;\; 0.40 \qquad \text{Equation 10}$$

However, the ASCE (1990) presented a $C_d \approx 0.44$ when $1000 < R' < 200{,}000$, with which the terminal settling velocity results in Newton's equation, given as:

$$w = 1.74 \left[\frac{g(\rho_s - \rho)D}{\rho} \right]^{1/2} . \qquad \text{Equation 11}$$

If R' is greater than 200,000, C_d is less than 0.1 for spherical particles, and no sedimentation occurs at this level of turbulence (Lee and Lin 1999).

2.7 Sediment Resuspension - Scour Process

Sediment resuspension and transport have been widely studied by many researchers, especially relating to sediment transport in open channel flow (including rivers and artificial channels). However, the study of scour caused by local hydraulic effects has not been as extensively studied as open channels. In open channels, there is a dominant velocity direction tangential to the bed, which creates a tractive force on the bottom surface which is responsible for the incipient motion of the sediment particles. The sediment is re-suspended and transported in the predominant direction of the flow with a spatial distribution caused by the turbulence of the flow. However, scour created by local effects in hydraulic structures, such as piers and sumps, results in the velocity vectors possibly acting vertically on the sediment bed or having similar magnitudes in all three directions (x, y, and z). Therefore, the resuspension may be caused by several factors not considered in open channels, such as vertical components of velocity, shear stress at any direction, high momentum transfer in any direction, and the effect of the interface slope between the sediment and water layers. However, the fundamental theory of sediment transport applies to cases of scour where flowing water or sediment are involved.

2.7.1 *Initial Motion*

Sediment resuspension is first related to the condition for incipient motion of deposited sediment particles. Three different approaches have been used to evaluate the condition of incipient motion (Garde and Ranga 1977):

Competent velocity. In this concept, the size of the bed material is related to the mean velocity of the flow, which causes the particle to move. It was first studied by DuBuant, and then by others researchers such as Tu, Rubey, and Brahms and Airy.

Goncharov (1967) defined a nondisplacement velocity U_p (Equation 12), which is the highest average flow velocity at which bed particles do not move and the maximum magnitude of fluctuating lift force that does not exceed the submerged weight of the particle. He also defined the detachment velocity U_n (Equation 13). The detachment velocity is the lowest average flow velocity at which individual bed particles become detached and at which the average magnitude of fluctuating lift force is approximately equal to the submerged weight of the particle.

$$U_p = \log \frac{8.8d}{D} \sqrt{\frac{2g(\gamma_s - \gamma)D}{1.75\gamma}}$$ Equation 12

$$U_n = \log \frac{8.8d}{D} \sqrt{\frac{2g(\gamma_s - \gamma)D}{3.5\gamma}} ,$$ Equation 13

where *d* is the depth of the flow, *D* is the diameter of the particle, γ_s is the specific weight of the sediment, and γ is the specific weight of the fluid.

Neil (1968) determined an equation for the mean critical velocity U_{cr} (Equation 14).

$$\frac{U_{cr}}{\sqrt{(\gamma_s - \gamma)d / \rho}} = 1.414 \left(\frac{D}{d} \right)^{1/6}$$ Equation 14

In general, the detachment velocity defined by Goncharov (1967) has been found to be close to the critical velocity used by most investigators (Garde and Ranga 1977).

Lift concept. The upward force due to the flow (lift) is greater than the submerged weight of the particle, which causes incipient motion. This concept was studied by several investigators such as Jeffreys.

Einstein and El-Samni (1949) found Equation 15 to be only valid for flows along rough beds.

$$L = C_L \rho \cdot u^2 / 2 ,$$ Equation 15

where C_L equals 0.178, u is the velocity of flow at a distance 0.35 D_{35} from the theoretical bed, and D_{35} is the sieve size for which 35 percent of the material, by weight, is finer.

Critical shear stress. The incipient motion of the sediment particles is caused by the shear stress exerted by the flow water on the channel bed in the direction of flow. Empirical, semi-theoretical, and theoretical analyses have been performed by several researchers, and critical shear stress criterion is currently the most often-used method in the evaluation of scour and stream stability.

In general, empirical equations try to relate the critical shear stress to the relative density of the sediment particles, the particle diameter, and empirical coefficients obtained from experimental observations. Some of the investigators are Kramer, the United States Waterways Experimental Station – USWES, Chang, Krey, Indri, Schoklistsch, Aki and Sato, and Sakai (Garde and Ranga 1977).

Theoretical and semi-theoretical analysis, based on the study of the equilibrium and the beginning sediment particle movement, considering the forces acting on the particle, have been performed by several researchers such as Shields (1936), White (1940), Iwagaki (1956), and Cheng and Chiew (1999).The critical shear stress defines the limiting conditions at which the sediment will move or not move from the sediment bed. Typically, the critical shear stress analysis is based upon the Shield's diagram to determine the initial motion at which bed load will occur.

Shields (1936), whose results have been widely accepted and used, derived his equation by applying dimensional analysis to the forces acting on the particle at the beginning of motion. His equation (Equation 16) relates the dimensionless shear stress to the shear Reynolds's number (R_*).

$$\tau_* = \frac{\tau_o}{(\gamma_s - \gamma)d} = f(R_*). \qquad \text{Equation 16}$$

where τ_* is the dimensionless shear stress, τ_o is the critical shear stress for initial motion, $R_* = \frac{u_* d}{\upsilon}$, ν is the kinematics viscosity of the water, u_* is the shear velocity at incipient motion, which can be calculated as $\sqrt{\frac{\tau}{\rho}}$, g is the acceleration of gravity, R equals the hydraulic radius, and S equals slope.

Figure 4 shows the Shields' diagram, which was first proposed by Rouse (ASCE 1975). The curve was developed for fully-developed turbulent flow and artificial flattened beds with no cohesive sediments (ASCE 1975). The graph also includes data obtained by several other workers such as White, USWES, Kramer, Gilbert, and Casey. Shields' results have been widely accepted as incipient motion criteria, although some other investigators have reported different results for the parameters.

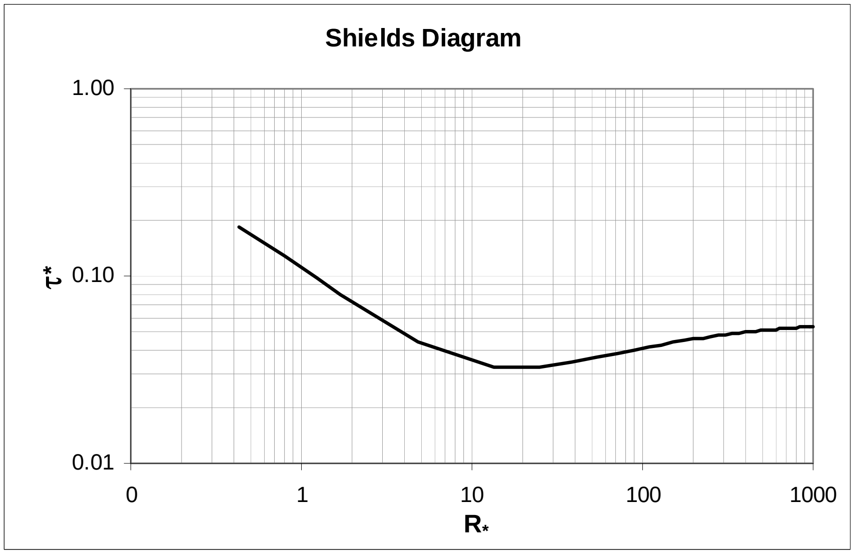

Figure 4. Shields diagram (ASCE 1975).

Shields' curve can be calculated with Equation 17 and 18 (COE 1995). These equations are useful for computational purposes.

$$\tau_* = 0.22\beta + 0.06 \cdot 10^{-7.7\beta},$$ Equation 17

where

$$\beta = \left(\frac{1}{\upsilon} \sqrt{\left(\frac{\gamma_s - \gamma}{\gamma} \right) g d^3} \right)^{-0.6}.$$ Equation 18

It is important to consider that the Shields' (1936) critical shear stress parameter may not be useful for predicting the erodibility of a sediment bed in some cases,for two main reasons. First, Shields' experiment was performed using a flat bottom channel with total roughness determined by the size of the granular bottom. Actually, the sediment bed is a loose boundary layer that creates bed forms and channel irregularities by the action of the flow, and therefore, the roughness coefficient is expected to be larger than that estimated from a flat bed. Secondly, Shields used uniform bed material, so the shear stress for a given size particle in a sediment mixture may be different from the shear stress of the same size particle in a uniform bed (COE 1995).

Considering the previous reasons and the absence of critical shear stress values for channels with granular and cohesive materials, the U.S. Bureau of Reclamation and the Corp of Engineering estimated permissible shear stress values for granular and cohesive materials (Chow 1959). However, these permissible shear stress values are specifically for open channels and likely are not applicable to sumps.

2.7.2 *Initial Suspension*

In the case of scour in catchbasin sumps, it is necessary to consider not only the initial motion criterion, but also the initial suspension criterion. Scour in catchbasins is associated with the migration of sediment out of the sump. This obviously involves the initial motion of the sediment, which will cause a sediment bed to shift. However, because the surface of the sediment layer deposited in the sump is located below the outlet elevation, sediment bed shifting will not necessarily represent migration out of the device, because the sediment does not necessarily reach the outlet. Therefore, only suspended sediment will be expected to leave the catchbasin sump.

Different shear stress criteria were reviewed in order to formulate a better approach for the initial motion and initial suspension thresholds as a function of sediment characteristics and critical shear stress. Shields (1936), White(1940), and Iwagaki (1956) studied the critical shear stress for initial motion. These analyses were consistent with experimental values obtained by other researchers, such as Kramer, Indri, and Chang, among others (summarized in Garden and Raju 1977). These criteria give a better approach to the critical shear stress for initial motion, considering they are based on theoretical and semi-theoretical analysis and have also been widely used, especially the Shields approach.

In addition to the criteria mentioned above, the Cheng-Chiew (1999) criterion, which involves both initial motion and initial suspension, was also evaluated (Equation 19). This criterion relates the critical shear stress to the probability that sediment with a particular specific gravity, diameter, and settling velocity becomes bed load or gets suspended.

$$\tau_* = \frac{\left(\sqrt{25 + 1.2D_*^2} - 5\right)^3}{\left(w/u_*\right)^2 D_*^3}, \qquad \text{Equation 19}$$

where D_* is the dimensionless diameter of particles, $D_* = \left(\frac{g}{\nu^2}\left(\frac{\rho_s - \rho}{\rho}\right)\right)^{1/3} D$, w is the settling velocity of the particles, u_* equals shear velocity at incipient motion, and ν equals kinematic viscosity.

The relationship w/u_* is related to the probability of incipient motion of the particle or initiation of suspension from the bed load occurring. The initial suspension of the sediment particle occurs when the vertical velocity fluctuation v', created by turbulent flow, is greater than the settling velocity, w, of the particle ($v' > w$). Also, it is evident that when $v' < w$, there is a termination of suspension of the sediment particles at any elevation. Then, Cheng and Chiew (1999) defined the probability that the sediment particle is suspended as $P = P(v' > w)$, a Gaussian distribution based on previous research work on vertical turbulence fluctuation near the bed surface. Additionally, previous experimental studies found that the vertical velocity fluctuation, *v'*, near a rough bed is almost equal to the shear velocity, u_*. The probability function for initial suspension is given by Equation 20.

$$P = 0.5 - 0.5\sqrt{1 - \exp\left(-\frac{2}{\pi}\frac{w^2}{u_*^2}\right)} \qquad \text{Equation 20}$$

According to Cheng and Chiew (1999), the initial motion threshold is determined when the probability of suspension is close to zero ($1\text{x}10^{-7}$), and the initial suspension threshold is determined when the probability is about 1%. Obviously, there is not a specific line that determines when the sediment will be suspended, but usually a range is used, and according to Cheng and Chiew, this value may be adopted for determining the initial suspension. Figure 5 shows the dimensionless shear stress (τ_*) as a function of the Reynolds number of the grain (R_*), calculated with the Cheng-Chiew criterion. Shields, Van Rijn and Xie criteria (Cheng and Chiew 1999) were also included in this analysis.

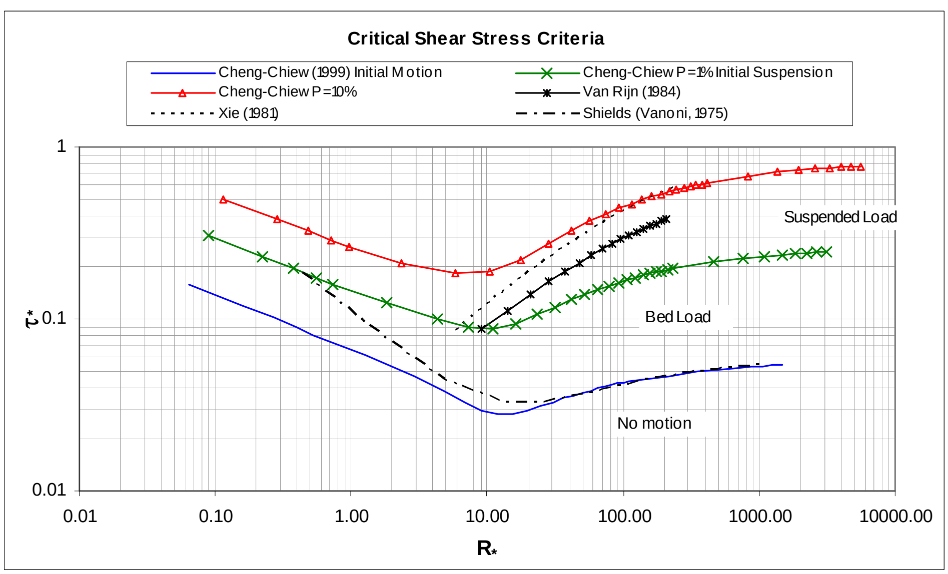

Figure 5. Critical shear stress criteria for initial motion and initial suspension.

Other values of the relationship u_* / w as experimental limits for the initiation of suspension have been proposed by Van Rijn (1984) (Equation 21) and Niño, López, and García (2003) (Equation 22).

$$u_* / w = \begin{cases} 4.0 R_p^{-2/3} & 1 \le R_P \le 32 \\ 0.4 & R_P \le 32 \end{cases} \qquad \text{Equation 21}$$

$$u_* / w = \begin{cases} 21.2 R_p^{-1.2} & 1 \le R_P \le 27.3 \\ 0.4 & R_P \le 27.3 \end{cases} \qquad \text{Equation 22}$$

Figure 5 clearly shows that the dimensionless critical shear stress calculated by Cheng and Chiew (1999) is less than the value calculated by Shields (1936) for Reynolds numbers of the grain less than 30. Therefore, the selection of the Cheng-Chiew criterion gives a conservative value for initial motion shear stress. Moreover, the Cheng-Chiew criterion involves the criteria of Xie and Van Rijn for the initial suspension threshold. Therefore, the Cheng-Chiew criterion was selected to determine the critical shear stress for initial motion and initial suspension thresholds. Figure 6 shows the critical shear stress obtained from the Cheng-Chiew criterion as a function of sediment size (diameter). This graph shows the critical shear stress for particles between 10 and 10,000 μm, with a specific gravity of 2.5. However, this graph can also be determined for any particle size range and specific gravity.

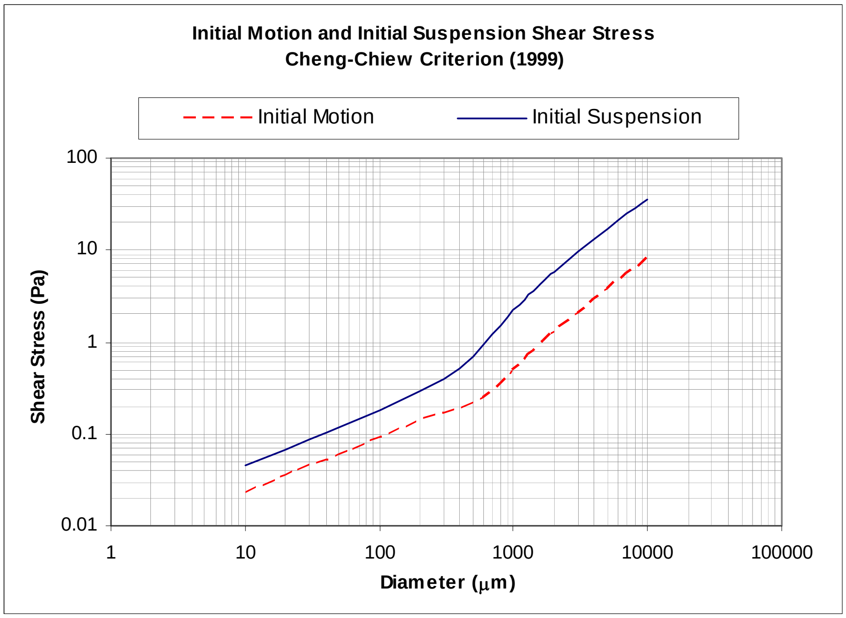

Figure 6. Initial motion and initial suspension shear stress as a function of particle size with specific gravity 2.5 – Cheng-Chiew Criterion.

2.8 Sediment Scour Model for Local Effects

A main component of this research focused on Computational Fluid Dynamics (CFD) modeling. Flow-3D v.9.2 (Flow Science, Inc.) will be extensively used to evaluate the hydrodynamics and sediment scour under different scenarios. Fluent v.6.2 (Fluent, Inc.), another CFD model that has been commonly used by others doing hydrodynamic stormwater modeling (Adamsson, Stovin, and Bergdahl 2003; Faram, Harwood, and Deahl 2003; Phipps et al. 2004; Sansalone et al. 2007), was used to obtain results during the initial sensitivity analyses. However, only Flow-3D has the capability of evaluating sediment scour from a dense sediment bed while considering consolidation of the sediment as packed sediment, suspended solids concentration, movement of the sediment surface, and tracking of the sediment surface interface.

Sediment scour and transport equations have mostly been developed for open channel flow, and empirical methods based on depth-average values are not capable of determining local scour in a confined volume, such as a catchbasin sump or a hydrodynamic device (Brethour 2001). Empirical and semi-empirical methods have been developed to predict local scour at bridge piers and abutments and scour by vertical drops and by horizontal jets (Aderibigbe and Rajaratnam 1998; Dey and Raikar 2007; Hoffmans and Pilarczyk 1995; Meilan, Fujisak, and Tanaka 2001; Melville 1997). Most of those methods are not applicable to any type of structure, and some cannot be applied to 3D systems; however, their results have been used to develop and validate computational scour models. Other investigators have focused on mathematical models based on the fundamental laws of mass continuity, momentum, and energy implemented in computational models (Brethour 2001; Dey and Bose 1994; Dou and Jones 2000; Jia, Kitamura, and Wang 2001; Li and Cheng 1999). Brethour (2001, 2003) presented a sediment scour and deposition model which was validated with experimental data and is built in Flow-3D v.9.2 to evaluate sediment scour in any possible 3D geometry.

According to Brethour (2001, 2003), there are two concentration fields: the suspended sediment and the packed sediment. The suspended sediment originates from inflow boundaries or from erosion or packed sediment. The packed sediment is not transported but eroded into suspended sediment at the packed sediment-fluid interface.

The sediment concentration is stored in units of mass/volume, and the mean fluid viscosity is enhanced by the suspended sediment, as given in Equation 23.

$$\mu^* = \mu_f \left[1 - \frac{\min(f_S, f_{S,CO})}{f_{S,CR}} \right], \qquad \text{Equation 23}$$

where f_S is the solid volume fraction, f_L is the liquid fraction, which is equal to $1 - f_S$, $f_{S,CO}$ is the cohesive solid fraction, and $f_{S,CR}$ is the critical solid fraction, which is the solid fraction at which the sediment particles are completely bound together in a solid-like mass.

The drag coefficient, DRG, is given as:

$$DRG = \begin{cases} 0 & \text{if } f_S < f_{S,CO} \\ \left[\dfrac{f_{S,CR} - f_{S,CO}}{f_{S,CR} - f_S}\right]\left[\dfrac{f_{S,CR} - f_{S,CO}}{f_{S,CR} - f_S} - 1\right] & \text{if } f_{S,CO} < f_S < f_{S,CR} \\ \infty & \text{if } f_S > f_{S,CR} \end{cases} \qquad \text{Equation 24}$$

or

$$DRG = TSDRG \frac{f_{SED}^2}{(1 - f_{SED})^3}, \qquad \text{Equation 25}$$

where *TSDRG* is the constant for drag coefficient, f_{SED} is the fraction of sediment in the cell, which is incorporated into the momentum equations.

The macroscopic density of the mix fluid-sediment is given as:

$$\bar{\rho} = \rho_L + f_S(\rho_S - \rho_L), \qquad \text{Equation 26}$$

where ρ_L and ρ_S are the macroscopic density of the fluid and sediment, respectively.

The drift velocity, u_{drift}, which is the velocity of the fluid particle relative to the fluid, is given by:

$$u_{drift} = \frac{f_L D^2}{18\mu} \frac{\nabla P}{\bar{\rho}} (\rho_S - \rho_L). \qquad \text{Equation 27}$$

The sediment scour from the packed sediment bed is a function of the critical Shields' parameter, as shown in Equation 28. If the shear stress acting on the bed is greater than the critical shear stress, τ_o, the sediment particles will lift and become suspended sediment when the advection-dispersion model is applied. In order to have an estimate of the rate at which sediment is lifted away from the packed bed interface, a critical lift velocity as a function of the excess shear velocity can be used, given by:

$$u_{lift} = \alpha \mathbf{n}_S \sqrt{\frac{\tau - \tau_o}{\bar{\rho}}}, \qquad \text{Equation 28}$$

where n_s is the vector normal to the packed bed surface and α is the dimensionless parameter that represents the probability that a particle is lifted away from the packed bed.

Another component of the scour model is the effect of the interface slope. The critical shear stress values that apply for flat surfaces are reduced by the following factor when the particles are located on a slope:

$$\tau_{o,Slope} = \tau_o \sqrt{1 - \frac{\sin^2 \varphi}{\sin^2 \zeta}}, \qquad \text{Equation 29}$$

where φ is the local slope of the packed bed and ζ is the angle of repose of the particle.

The implementation of a computational model for sediment scour in catchbasin sumps requires calibration and validation based on experimental results obtained from physical experimentation. A detailed description of the methodology and experiments conducted with a full-scale physical model, as well as the description of the computational model used in this research, are explained in the next chapter.

CHAPTER 3

METHODOLOGY AND DESCRIPTION OF THE EXPERIMENT

3.1 Introduction

The methodology of this research consisted of the following major components:

Full-scale physical model. A full-scale physical model of the optimal catchbasin sump proposed by Lager et al. (1977) was built to perform a series of tests to evaluate the hydrodynamics of the flow in the sump under the effect of a plunging water jet and also to evaluate the scour of pre-deposited sediment.

Hydrodynamic tests – physical experimentation. Velocities were measured in the catchbasin sump to determine the effect of a plunging water jet (coming from an inlet) on the hydrodynamics of the flow in the sump. A series of experiments were conducted for different flow rates and inlet geometries.

Sediment scour tests – physical experimentation. Suspended Solid Concentration (SSC), Particle Size Distribution (PSD), and turbidity were measured to determine the mass and pattern of sediment scoured under different conditions of flow rates and overlaying water depth (water depth between the invert elevation of the outlet and the sediment surface).

Implementation of a CFD model. The calibration and validation of a CFD model was conducted to be able to simulate a series of scenarios of sediment scour for different sediment particle sizes, flow rates, and overlaying water depth. The creation of a scour model code was needed given the limitation of the CFD software package.

3.2 Full-Scale Physical Modeling

3.2.1 *Description of the Full-scale Physical Model*

The geometry of the catchbasin sump used for the experiments was based on the optimal geometry recommended by Lager et al. (1977) and tested by Pitt et al. (1979, 1985, 1998). For this geometry, if the outlet diameter is *d*, the total height of the catchbasin sump is 6.5*d*, and the inside diameter is 4*d*; the outlet has to be located 4*d* above the bottom and 1.5*d* below the top of the catchbasin. The outlet diameter (*d*) was selected as 300 mm (approximately 12 inches) (see Figure 7).

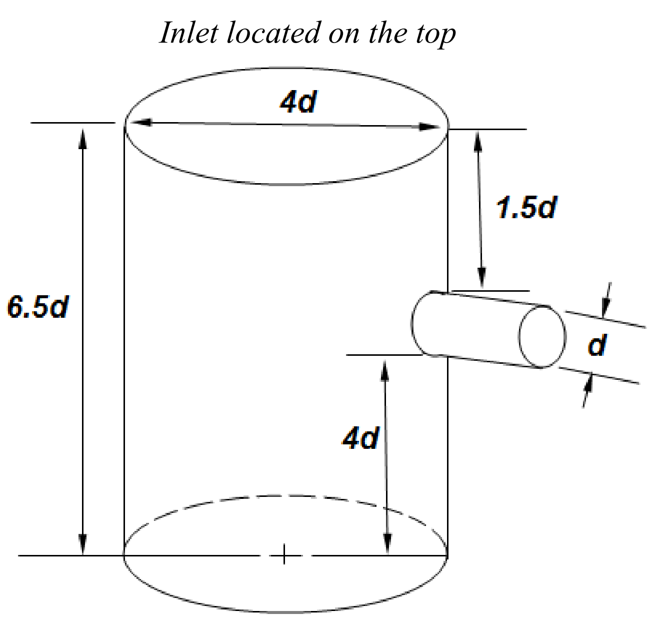

Figure 7. Optimal catchbasin geometry (Larger et al. 1977) used to build the full-scale physical model.

The physical model consisted of the following components, which are indicated in Figure 8 and 9:

1. A cylindrical plastic tank of 116 cm in internal diameter. The invert elevation of the outlet, which was 29 cm in diameter, was located at 116 cm above the bottom of the tank.
2. A structure placed on a trailer with dimensions 1.8 m x 3.0 m.
3. A 50-cm wide channel placed on the wooden structure. This channel was modified to a pipe of 30 cm (12 inches) in diameter during the hydrodynamic tests with a circular inlet.
4. A turbulent dissipation tank located on the top of the wooden structure upstream from the channel.
5. A pump with a maximum capacity of 10 L/s and a maximum head of 6.0 m.
6. Pipes of 76 mm (3 inches) and 38 mm (1.5 inches) for large and small flow rates, respectively.
7. A set of valves to control the flow rate.
8. Two flow meters (Midwest Instruments & Control Corp.); one for the 76-mm (3 inches) pipe and another for the 38-mm (1.5 inches) pipe. The reading ranges for the flow meters were between 2.5 and 30.0 L/s for the 76-mm (3 inches) pipe and between 0.65 and 8.0 L/s for the 38-mm (1.5 inches) pipe.
9. A pool located downstream from the catchbasin used for water recirculation during the hydrodynamic tests and also used as sediment trap during the scour tests.

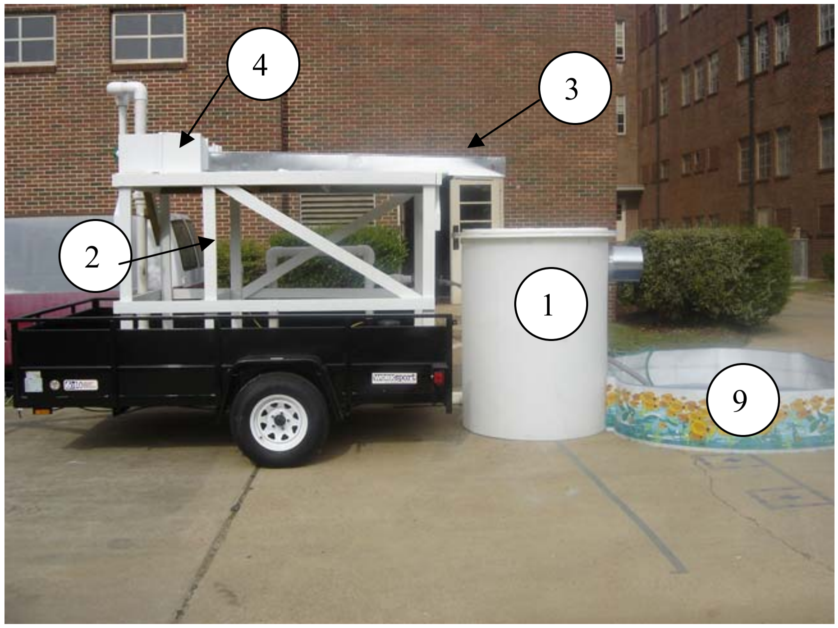

Figure 8. Full-scale physical model, lateral view.

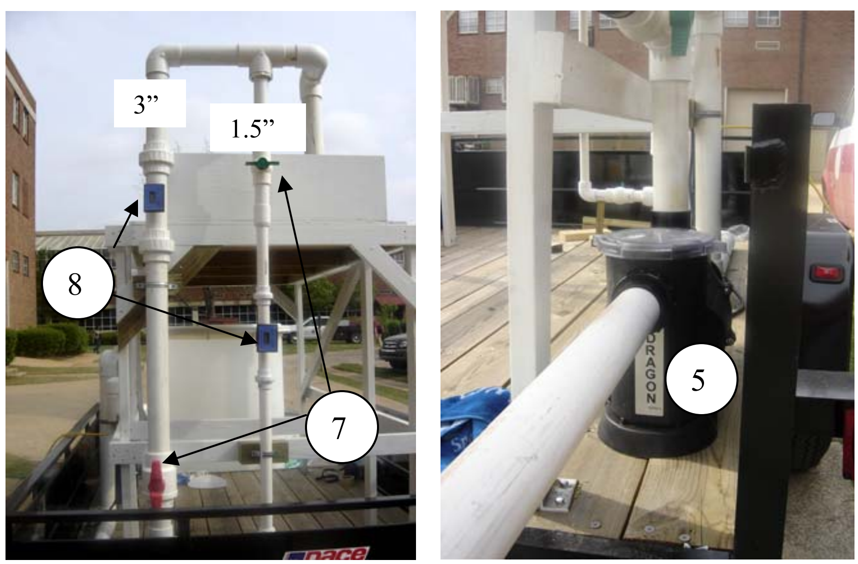

Figure 9. Full-scale physical model, pipeline system and flow meters (left) and pump (right).

Two types of tests were performed with this model: hydrodynamic tests to measure velocities at different elevations in the control volume and scour tests to evaluate the scoured mass of pre-deposited sediment placed at different depths in the catchbasin sump. The hydrodynamic tests were conducted at the facilities of the University of Alabama using clear water.

3.2.2 *Description of Hydrodynamic Tests and Experimental Design*

The hydrodynamic tests consisted of the measurement of velocities in x, y, and z directions in the control volume to determine the effect of the plunging water jet on the hydrodynamic conditions in the catchbasin sump. An Acoustic Doppler Velocity Meter (FlowTracker Handheld ADV, Sontek) was used for this purpose. The velocities were measured at 155 different locations within the control volume of the sump, distributed on 5 layers with 31 points each. An instantaneous velocity was measured every 1 second during a 30-sec period, which resulted in 930 velocity measurements for each layer and 4,650 velocity measurements for each test. Figure 10 shows the location of each layer at 16, 36, 56, 76, and 96 cm below the outlet. Figure 11 shows the location of the 31 points on each layer.

Figure 10. Full-scale physical model with the elevations for velocity measurements.

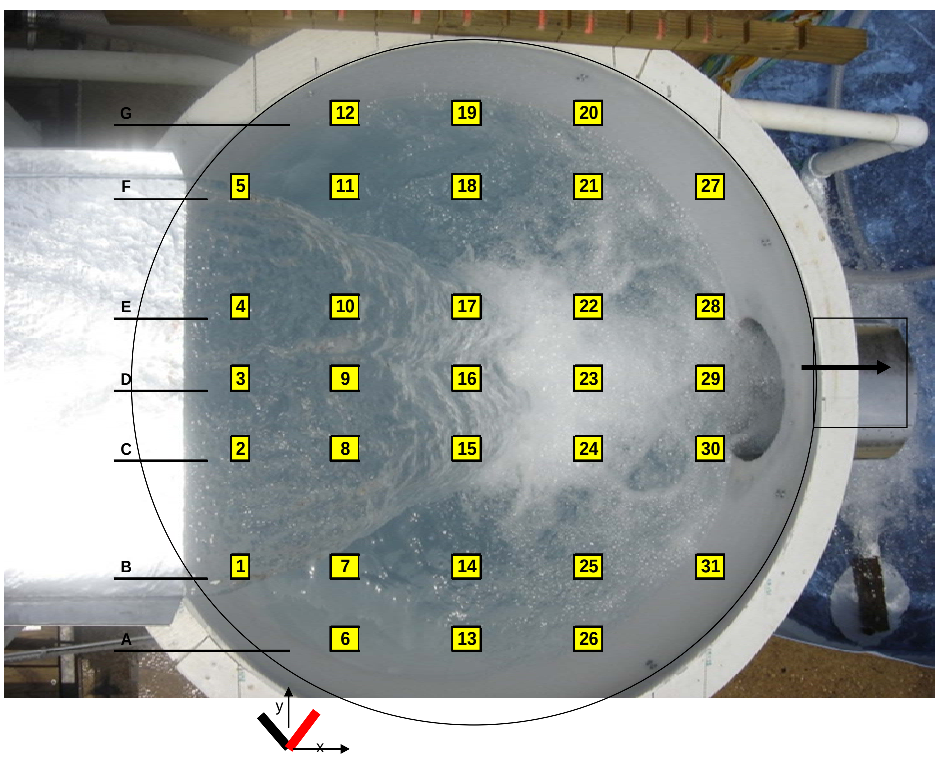

Figure 11. Plan view of a layer with 31 points for measuring velocities; velocity was measured at 5 different elevations.

Three flow rates, 2.5, 5.0, and 10 L/s, and two types of inlet geometries, a 50 cm-wide rectangular inlet and a 30 cm circular pipe inlet, were evaluated. A total of six tests were performed. The water temperature was between 25 and 30^{o}C.

3.2.3 *Description of Scour Tests and Experimental Design*

The scour tests consisted of the measurement of the Suspended Solid Concentration (SSC) at the effluent of the catchbasin sump to determine the sediment mass loss. Turbidity and Particle Size Distribution (PSD) were also measured. Two types of scour tests were performed. The first series of scour tests were performed with a sediment mixture at Lake Lureen State Park, Northport, AL, as once-through tests using the lake water. The second scour tests were performed with sediment with a homogeneous particle size at the facilities of the University of Alabama.

The scour tests were conducted with a 50-cm wide rectangular inlet. Two different PSD mixtures were used as pre-deposited sediment in the catchbasin sump. The first PSD mixture was a prepared sediment mixture having a PSD similar to the measured values from deposited sediment sampled from catchbasin sumps observed by Valiron and Tabuchi (1992) and Pitt and Khambhammettu (2006). The characteristic diameters of this sediment mixture are D_{10} = 90 μm, D_{50} = 500 μm, and D_{90} = 2000 μm. Figure 12 shows the PSD of the sediment mixtures and also the particle size distributions for the separate components used to make the mixture.

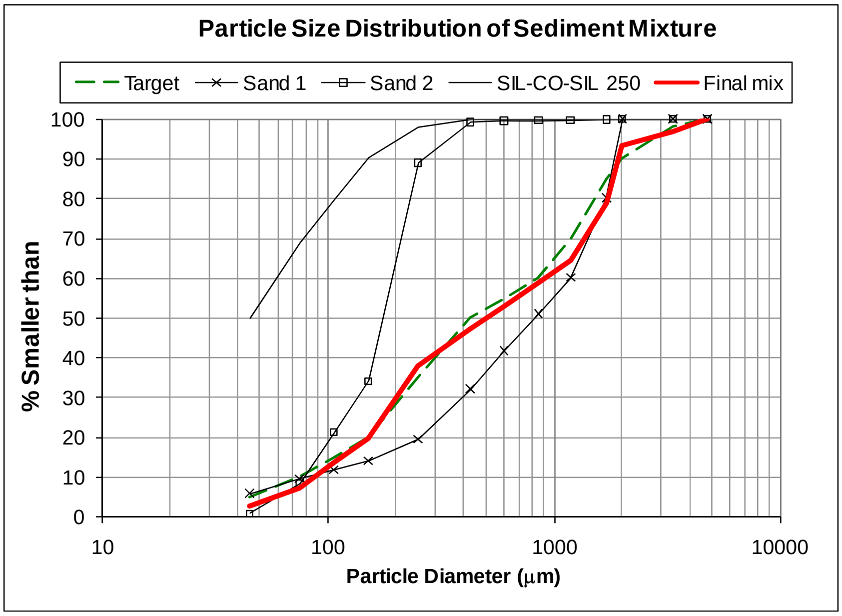

Figure 12. Particle Size Distribution (PSD) of sediment mixture prepared for scour test.

The wide range of this PSD in the sump contributes to the formation of bed armoring, which is the development of an erosion-resistant layer of relatively large particles created by the preferential washing of fine particles from the surface layers due to the velocity field acting on the sediment surface.

The second PSD mixture corresponded to a sediment material with a fairly homogeneous PSD, with D_{10} = 80 μm, D_{50} = 180 μm, and D_{90} = 250 μm (See Figure 13). The sediment scour results obtained with this homogeneous PSD were used for calibration and validation of the CFD model.

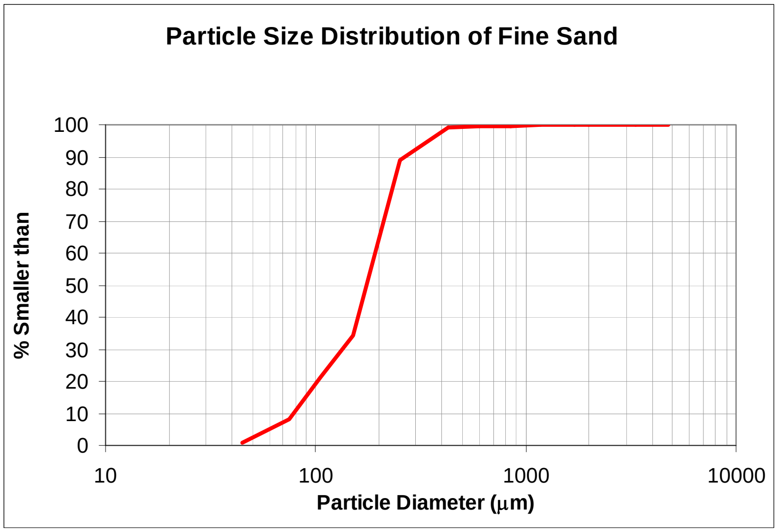

Figure 13. Particle Size Distribution (PSD) of an approximately homogeneous sediment material.

Table 4 describes the series of scour experiments performed.

Table 4. Description of the Series of Scour Experiments

Type of Sediment	Flow rate (L/s)	Depth below the outlet (cm)	Duration (min)	Sampling (Composite samples)	Total composite samples
Mixture	0.3, 1.3, 3.0, 6.3, and 10	10	25 min for each flow rate	First 5-min, and last 20-min for each flow rate. Inlet samples for each elevation.	36
		25			
		46			
		106			
	10	10	4 impacts with prolonged flow of 3 min each	One composite sample for each impact	16
		25			
		46			
		106			
Homogeneous	10	24	30 min for each elevation	3-min composite samples at influent and effluent.	40
		35			

The sediment was placed and leveled at different elevations inside the catchbasin sump (Figure 14). The sediment scour was evaluated under different flow rates. Additionally, a series of tests with fluctuating flow rates were conducted with the sediment mixture.

Figure 14. Placement of sediment at 25 cm below the outlet (left); performing scour test (right).

The SSC and PSD for the tests performed with the sediment mixture were determined by wet sieving through successive sieves: 2000, 1200, 425, 250, 150, 106, 45, 32, 20 μm, and finally a membrane filter of 0.45 μm to capture particulates. Figure 16 shows an image of the equipment used to determine SSC. The wet sieve analysis was performed with 10 subsamples of 100 mL, each obtained from splitting a 1.0 L composite effluent sample with a USGS/Decaport cone water sample splitter (Figure 15). The particle size information of the lake water was subtracted from the effluent sample observations to remove the background effects. Only a member filter of 0.45 μm was used to determine the SSC from the composite samples collected during the scour tests with sediment with homogeneous PSD.

Figure 15. USGS/Decaport cone water sample splitter and 1-Liter sampling bottles.

Figure 16. Procedure to determine SSC from the composite samples collected during the scour tests; sieving setup (left); a 0.45 μm micro-pore with sediment (right).

The composite samples collected from the tests with fine sand were only analyzed for SSC, considering that the original PSD was fairly uniform. The USGS/Decaport cone water sample splitter was used to split a 1.0 L composite sample into 10 subsamples of 100 mL. The SSC was determined by filtering 100-mL subsamples through a membrane filter of 0.45 μm and weighting the mass retained by the membrane. A turbidity time series was obtained for each test using a Water Quality Sensor (HORIBA Probe) located next to the outlet (see Figure 17).

Figure 17. Location of HORIBA probe to measure turbidity next to the outlet.

3.3 Computational Fluid Dynamic (CFD) Modeling

The specifications of the CFD software packages and the computers used are as follow:

- *Fluent v.6.2* (ANSYS © 2008). The model was run with a multi-user system UNIX SERVER having 8 Hyper Threaded processors Intel Xeon 64 bit of 3.33 Ghz, 28 Gigs of RAM and an 29 Gig Swap Partition.
- *Flow-3D* v.*9.2* (Flow Science © 2008). The model was run with a Personal Computer Dell 690 (750W-32bits) having 2 Dual Core Intel Xeon processors of 3.0 GHz-4MB L2 working in parallel and 4GB of RAM Memory.

The models were run with the following specifications:

- Units in cgs (cm, grams, and seconds).
- One fluid with air entrainment: The main fluid was water with a density of 1.0 g/cm^3. The density of the air was 0.001225 g/cm^3. The air entrainment coefficient was set at 0.5, the average coefficient for undeveloped free falling jet (Bohrer 1998).
- Specific gravity of 2.5 for the sediment particle sizes.
- Viscosity and Turbulence model: turbulent flow with Newtonian fluid.
- Mesh size: A range between 100,000 and 200,000 cells for the 3-dimentional (3D) model and 9,000 cells for the 2-dimensional (2D) model. The CFD model automatically checks the quality of the mesh by evaluating the adjacent cell size and the aspect ratio of the cells.
- Boundary conditions: velocity at the inlet, pressure at the outlet (specifying atmospheric pressure), symmetry at the top and walls on the sides.
- Initial conditions: The catchbasin sump is initialized with water up to the minimum outlet elevation. If sediment is included, different elevations and particle sizes were specified.

Figure 18 shows the solid and the multi-block mesh of the 3D-CFD model evaluated. Also, the figure shows a screenshot of the boundary conditions used for the preliminary evaluations that have been carried out during this research.

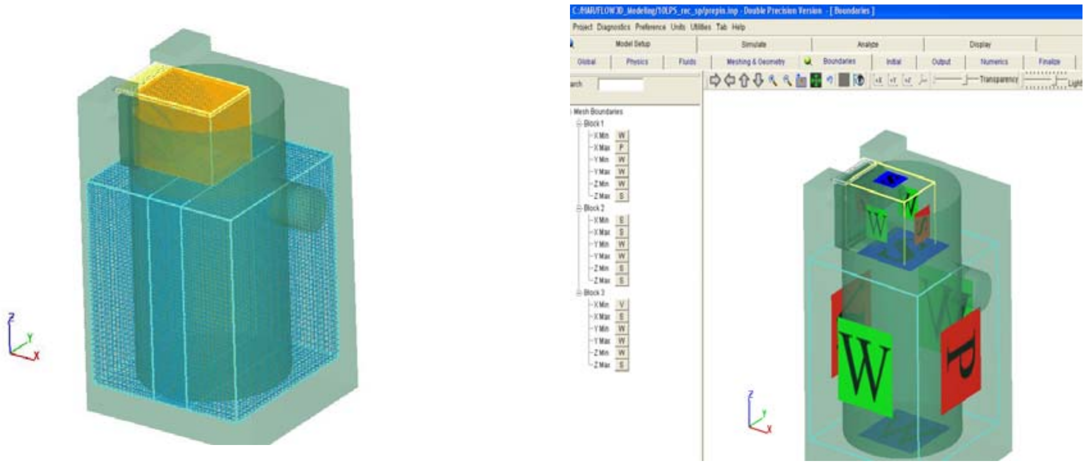

Figure 18. Geometry and multi-block mesh of 3D-CFD model (left) and boundary conditions display of Flow-3D (right).

The computational models were based on three fundamental physical equations of Navier-Stokes for viscous flow: the continuity, momentum, and energy equations.

The following analyses were performed with CFD modeling:

- Identification of significant factors affecting scour potential in catchbasin sumps.
- Shear stress evaluation in catchbasin sumps at different depths.
- Hydrodynamic behavior in a catchbasin sumps: calibration and validation
- Sediment scour in catchbasin sumps for sediment material with homogeneous particle sizes.

3.3.3 *Identification of Significant Factors Affecting Scour Potential in Catchbasin Sumps*

A 2D-CFD model was implemented in the CFD software packages *Fluent v.6.2*. This evaluation was conducted to identify the significant factors involved in the sediment scour phenomenon in catchbasin sumps. Potential factors included flow rate, sediment particle size, overlaying water depth above the sediment (or depth below the outlet), and specific gravity of the sediment material.

A 2^4-full factorial experimental design (without replicates) (Box 1978) was used to determine the significance of four factors (flow rate, sediment particle size, water depth, and specific gravity), and their interactions, on the scour of previously captured sediment from a catchbasin sump. The model was established with the continuous flow of a submersible water jet (impact geometry determined after detailed evaluations of the cascading water from the inlet flows) during a 3,600 sec (1 hr) period of time. Table 5 shows the factors with the corresponding low and high values used during the different experiments.

Table 5. Factors and Settings for the 2^4-Full Factorial Experimental Design

	Factor	**Low Values**	**High Values**
A	Flow rate (L/s)	1.6	20.8
B	Particle size (μm)	50	500
C	Water Depth (m)	0.2	1.0
D	Specific gravity	1.5	2.5

3.3.2 *Shear Stress Evaluation at Different Depths in a Catchbasin Sump*

Shear stress was calculated from a 2D-CFD model implemented with *Fluent v.6.2*. Sediment material was assumed to be in a catchbasin sump by specifying a wall-boundary layer at different depths. Two different inlet geometries were evaluated: a 0.8 m-wide rectangular inlet (representing typical gutter flows entering the catchbasin) and a 300-mm-pipe inlet (12 inches) (representing in-line conditions). The water surface in the manholes was set at 1.2 m above the manhole bottom, which corresponds to the lowest level of the outlet, and the inlet velocity was set at zero. Simulations were performed for up to 45 sec to achieve steady state in the catchbasin flow and constant acting shear stresses on the sediment surface. The acting shear stress was compared to the critical shear stress for suspension.

3.3.3 *Hydrodynamic Behavior in a Catchbasin Sump: Calibration and Validation*

Prior to the sediment scour tests with CFD modeling, calibration and validation of the hydrodynamics were performed with a 3D- and 2D-CFD model implemented in *Flow-3D v.9.2.* The calibration scenario corresponded to a catchbasin with a 50-cm rectangular inlet and a 10 L/s flow rate. The validation scenario was performed with a flow rate of 5 L/s. Simulated results were compared to experimental data.

3.3.4 *Scour of Sediment with Homogeneous Particle Sizes in Catchbasin Sumps*

Sediment scour evaluation was conducted for homogeneous sediment materials by using a 2D-CFD model implemented in *Flow-3D v.9.2.* The simulations were performed assuming a 50-cm wide rectangular inlet. A new scour model code was written and implemented that considered the limitations of the CFD software package. A total of 40 scenarios, including the calibration and validation cases, were simulated. The scenarios included combinations of three flow rates, five overlaying water depths, and four sediment particle sizes. The list of case scenarios is presented in Table 5.

Table 5. List of Case Scenarios Simulated with the 2D-CFD Model

Overlaying water depth (cm)	Diameter (μm)	Flow rate (L/s) 5	10	20
15	50	■	■	■
	180	■	■	■
	500	■	■	■
	1000	■	■	■
24	50	■	■	■
	180	■	■	■
	500	■	■	■
	1000		■	■
35	50	■	■	■
	180	■	■	■
	500		■	■
	1000			■
40	50		■	■
	180		■	■
	500			■
	1000			
45	50			■
	180			■
	500			■
	1000			

■ Simulated

The sediment scour simulations were performed assuming clear water as the influent. The use of clear water is conservative when determining the scour rate. Clear water has a larger sediment-carrying capacity and therefore a larger scour potential compared to heavily silt-laden water. However, this assumption does not greatly differ from typical conditions of stormwater runoff in urban areas. The scour tests with the full-scale physical model were performed with lake water having a maximum SSC of 6 mg/L. The National Stormwater Quality Database reported median suspended solid concentrations of 50 to 100 mg/L for different land uses for data collected throughout the U.S. (Pitt and Maestre 2008); however, concentrations as high as several thousand mg/L were also reported. Stormwater runoff with high suspended sediment concentration has lower carrying capacity and therefore less scour potential than clear water.

Using the allowable shear stresses recommended by the U.S. Bureau of Reclamation for granular materials in open channels (USDA 1977, 2007), the allowable shear for 500-µm sediment particles increases from 1.4 Pa (0.03 lb_f/ft^2) for clear water to 2.63 Pa (0.055 lb_f/ft^2) for heavily silt-laden water, which represents an approximate reduction of about 50% in the scour potential if the carrying capacity is met for this particle size. Larger particles have less of an effect, while smaller particles have a greater effect. However, these allowable shear stress values are estimated for open channels and may not be applicable to catchbasin sumps. It is also possible that small reductions of the scour potential in the catchbasin sumps may also occur with increasing consolidation of the sediment material with age, especially for any fines, and if any cohesive material, such as biofilms, oils, and possibly decomposing organic debris, are mixed with the sediment. The scour model used for the CFD simulations in this research accounts for the reduction of the carrying capacity of heavily silt-laden water associated with the sediment scoured from the sump through the effect of the drag coefficient.

3.3.5 *Advantages and Disadvantages of the CFD Software Packages*

Initially, CFD modeling was performed with *Fluent v.6.2.* The main advantage of this software package is its flexibility in generating complex computational mesh with a complementary software package called *Gambit v.2.2* (ANSYS © 2008). The model is based on the finite elements method, which allows the user to increase the resolution in specific areas, combining meshes with different geometries. However, the computational effort required by this software was substantially high, considering that the runs were made with a multi-user server from remote access. For example, in order to obtain a 10-sec simulation of the hydrodynamics of a 3D catchbasin sump, an elapsed time of about 5 hours was required. This means that running the 1,200 sec (20 min) simulation required for the scour evaluation would require about 25 days. Additionally, *Fluent v.6.2* does not combine an inviscid water-air model with sediment, so it was not possible for sediment scour to be analyzed with this software package due to the excessive required elapse time.

Flow-3D v.9.2 is a model based on the finite differences method. This model is friendlier in the generation of computational mesh. However, the geometry of the cells is limited by the finite differences method. The main advantage of this software is the speed of simulation and the real time debugging process when instability occurs during a simulation. The same scenario run with *Fluent v.6.2*, a 10-sec simulation of the hydrodynamics of a 3D catchbasin sump, only requires an elapsed time of 1 hour, which means running a 1,200 sec simulation would require about 5 days. The software package was run from the Personal Computer described above. Additionally, this model includes a module to simulate sediment scour, which is appropriate for the purpose of this research. However, this model was incompatible with the inviscid water-air model. In order to solve this issue, a new scour model code was written and implemented with some modules included by *Flow-3D*. However, only a few modules were open-coded to allow the licensed users to make modifications or create new models; ence, some alternative approaches were used and simplifications were made.

3.3.6 *Calibration and Validation Processes*

Calibration and validation were the most time-consuming processes of this research. Both processes are mandatory when computational modeling is used in order to ensure accuracy and reduce the uncertainty of the results.

The calibration and validation of the CFD model were performed manually. The selection of parameters and range of values, the adjustment of the mesh, the simulation, and the analysis of the results for each trial took several days. Issues that were addressed included determining the causes of computational instability, evaluating the sensibility of the parameters, and making appropriate decisions to increase the accuracy of the results.

CHAPTER 4

FACTORS AFFECTING SCOUR POTENTIAL

In order to determine the significant factors involved in the sediment scour phenomenon in catchbasin sumps, a series of tests with the CFD model *Fluent v.6.2* were performed. The parameters included in this analysis were flow rate, sediment particle size, overlaying water depth above the sediment (or depth below the outlet), and specific gravity of the sediment material.

4.1 Experimental Design for Four Factors

A 2^4-full factorial experimental design (without replicates) was used to determine the significance of four factors (flow rate, sediment particle size, water depth, and specific gravity), and their interactions, on the scour of previously captured sediment from a catchbasin sump. The model was established with the continuous flow of a submersible-water jet (impact geometry determined after detailed evaluations of the cascading water from the inlet flows) during a 3,600 sec (1 hr) period of time. There were obvious changes in the flow field and resulting shear stress values with time, so model results from several time periods were examined. Table 7 below shows the factors with the corresponding low and high values used during the different experiments.

A multiphase Eulerian model was implemented for the 2^4-full factorial experimental design, with which it is possible to consider two phases: water and a dense sediment bed. Because the multiphase Eulerian model is a mixture model and does not allow an immiscible water-air interphase, the flow was assumed to be a vertical-submersible water jet. The conditions of the inflow jet were separately determined by CFD modeling of the cascading water from a circular and from a rectangular inlet. Additionally, the sediment particle size was assumed to be uniform. Figure 19 shows the location of the inlet, outlet, the water depth, and the sediment depth.

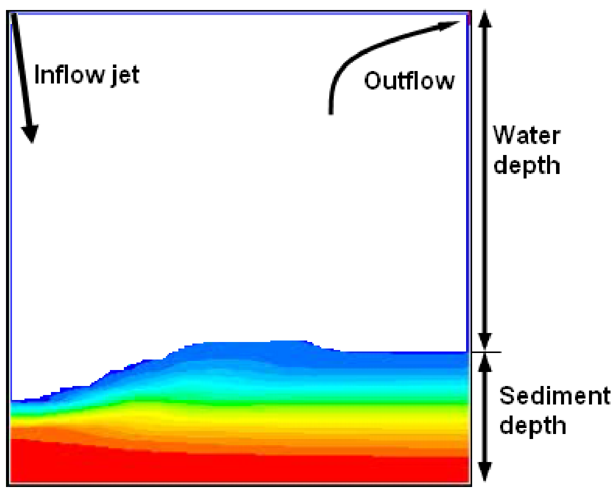

Figure 19. Inflow and outflow directions and water and sediment depth of the 2D model implemented for the 2^4-full factorial experimental design.

4.2 Results of the 2^4-Full Factorial Experimental Design

After simulating all 16 combinations of treatments for the 3,600 sec durations, the reduction of sediment depth (sediment loss) was plotted as a function of time. The sediment depth is the complement of the water protection depth (considering a total sump depth of 1.2 m); if the water depth is 0.2 m, the sediment depth is 1.0 m. Figure 20 shows the results obtained from the 2D-CFD model.

Figure 20 also shows the changes in the sediment depth with time, making it possible to see the effects of the factors and their interactions. As was expected, high flows with shallow water depths (AC) result in the fastest washout of the sediment, followed by high flows alone (A). Particle size alone (B) and particle size and specific gravity combined (BD) had little effect on scour.

The significance of the factors and their interactions were examined at six different times: 60, 300, 600, 1,000, 1,800, and 3,000 sec. Each analysis included the determination of the effects of the factors, normal probability plots of the effects, the ANOVA with no replicates, and the evaluation of resulting residuals.

Table 7. Factors and Settings for the 2^4-Full Factorial Experimental Design

	Factor	**Low Values**	**High Values**
A	Flow rate (L/s)	1.6	20.8
B	Particle size (μm)	50	500
C	Water Depth (m)	0.2	1.0
D	Specific gravity	1.5	2.5

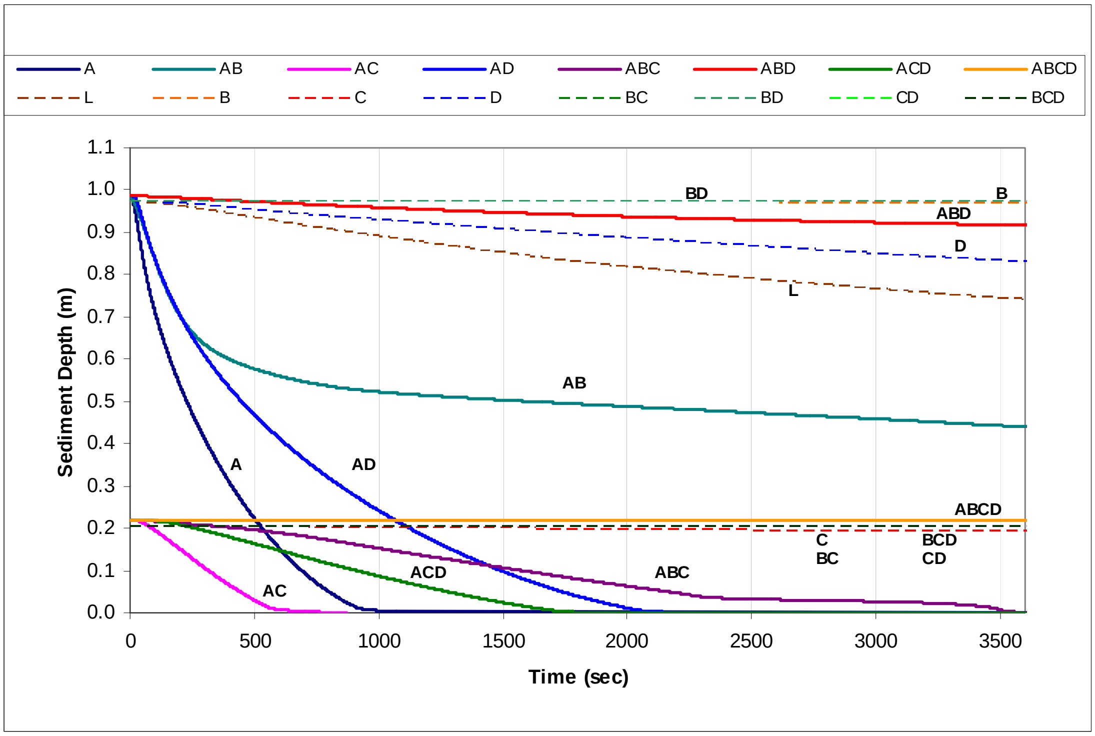

Figure 20. Reduction of sediment depth as a function of time for each treatment. Results of the 2^4-full factorial experiment (A: flow rate; B: particle size; C: water depth; and D: specific gravity).

The coefficients of the effects for all the evaluated times showed that flow rate (A), water depth (C), particle size (B), and the interaction of flow rate and water depth (AC) are the most significant factors affecting the calculated scour (Figure 21). In contrast, specific gravity (D) is located at the sixth or eighth position, which indicates that specific gravity is not as relevant as the other main factors and several of the 2-way interaction terms.

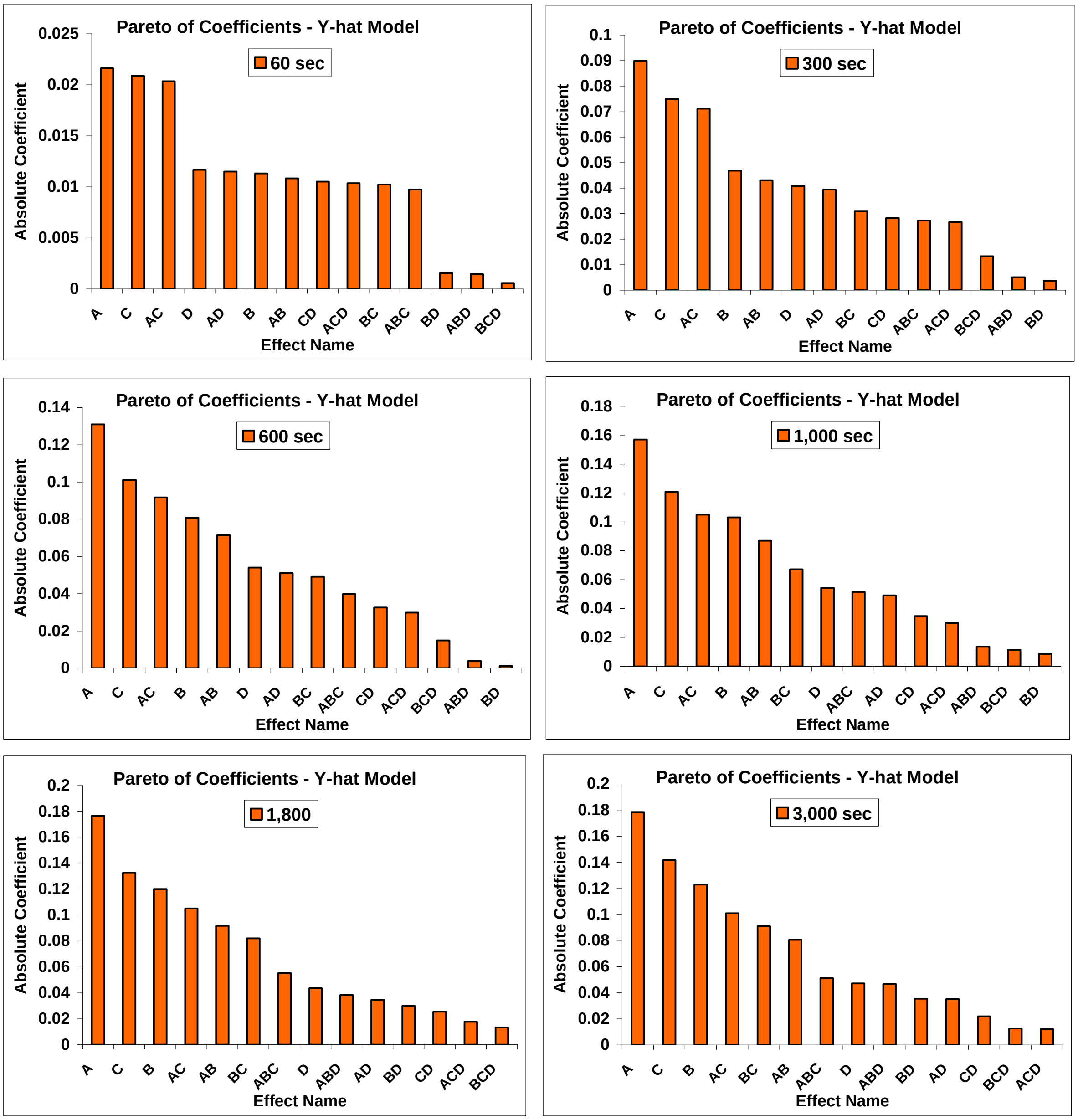

Figure 21. Coefficients of effects for each treatment at times 60, 300, 600, 1,000, 1,800, and 3,000 sec (A: flow rate; B: particle size; C: water depth; and D: specific gravity).

Similar results were obtained when the factors and interactions were examined using normal probability plots (Figure 22); flow rate (A), particle size (B), and water depth (C) were found to be significant, along with flow rate-water depth (AC) interactions for all time steps and flow rate-particle size (AB) interactions for half of the time steps. As noted above, specific gravity (D) was not identified as a significant factor, either alone or in any of the significant interaction terms. In order to further validate these results using a more quantitative criterion, an ANOVA analysis was applied to detect the significant factors and interactions at the 95%, or better, confidence level.

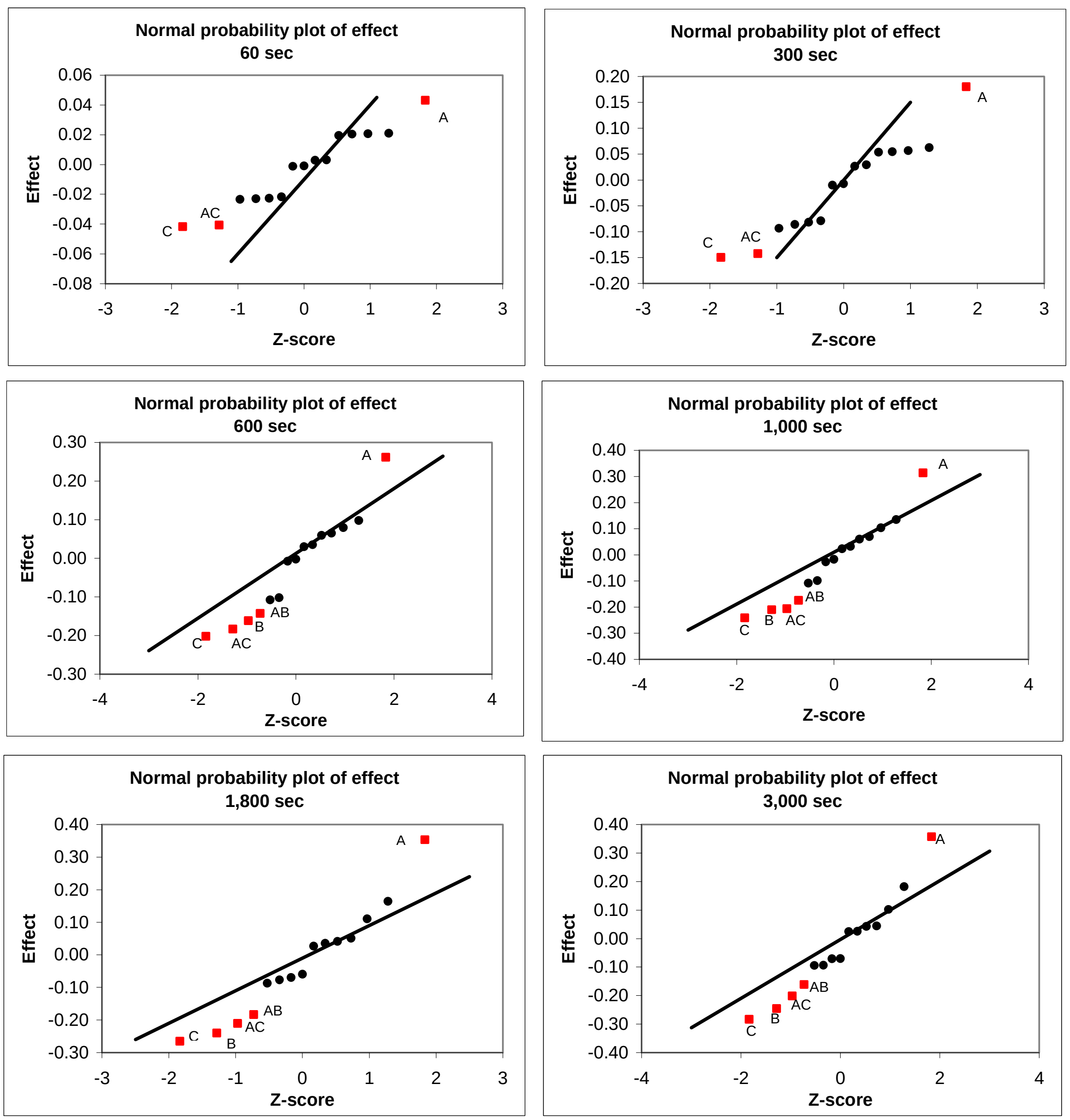

Figure 22. Normal probability plot of the effect estimated for times 60, 300, 600, 1,000, 1,800, and 3,000 sec (A: flow rate; B: particle size; C: water depth; and D: specific gravity).

An ANOVA with no replicates was used to determine the p-values for each factor and interaction (see Table 6). A confidence level of 95%, or better, would have a p-value of 0.05 or smaller, and these are indicated with values in bold typefaces. These results are the same as the previous evaluations; they show that flow rate, particle size, and water depth are significant factors for times greater that 600 sec (10 min). Additionally, the interactions of flow rate-particle size, flow rate-water depth, and particle size-water depth were also significant. However, specific gravity, or any interaction containing specific gravity, was not significant at the 95% confidence level for any of the evaluated times.

Table 6. ANOVA Results: P-Values for Each Treatment at Different Times of the Simulation with Continuous Flow (P-Values Less than 0.05 Are Bolded and Underlined)

	Time (sec)					
Treatment	60	300	600	1000	1800	3000
A	***0.02***	***0.006***	***0.003***	***0.003***	***0.003***	***0.003***
B	0.14	*0.06*	***0.02***	***0.02***	***0.01***	***0.01***
C	***0.02***	***0.01***	***0.009***	***0.009***	***0.01***	***0.008***
D	0.13	0.09	0.08	0.12	0.24	0.22
AB	0.15	*0.08*	***0.03***	***0.03***	***0.04***	*0.06*
AC	***0.02***	***0.01***	***0.01***	***0.01***	***0.02***	***0.03***
AD	0.13	0.10	0.09	0.15	0.34	0.34
BC	0.17	0.17	0.10	0.07	***0.05***	***0.04***
BD	0.82	0.86	0.97	0.77	0.41	0.34
CD	0.16	0.21	0.24	0.28	0.47	0.54

Additionally, residuals were calculated to determine normality and independency. Figure 23 shows that the residuals appear normal for times greater than 1,000 sec (17 min). However, shorter times show a lack of normality for a few extreme conditions. Considering that there are several data points, it is not possible to have a clear impression of homoscedasticity or heteroscedasticity behavior. As expected, flow rate and particle size were identified as significant factors. Moreover, the water depth was also found to be a significant factor that protects the sediment layer from being scoured. However, specific gravity was not as important as the other factors.

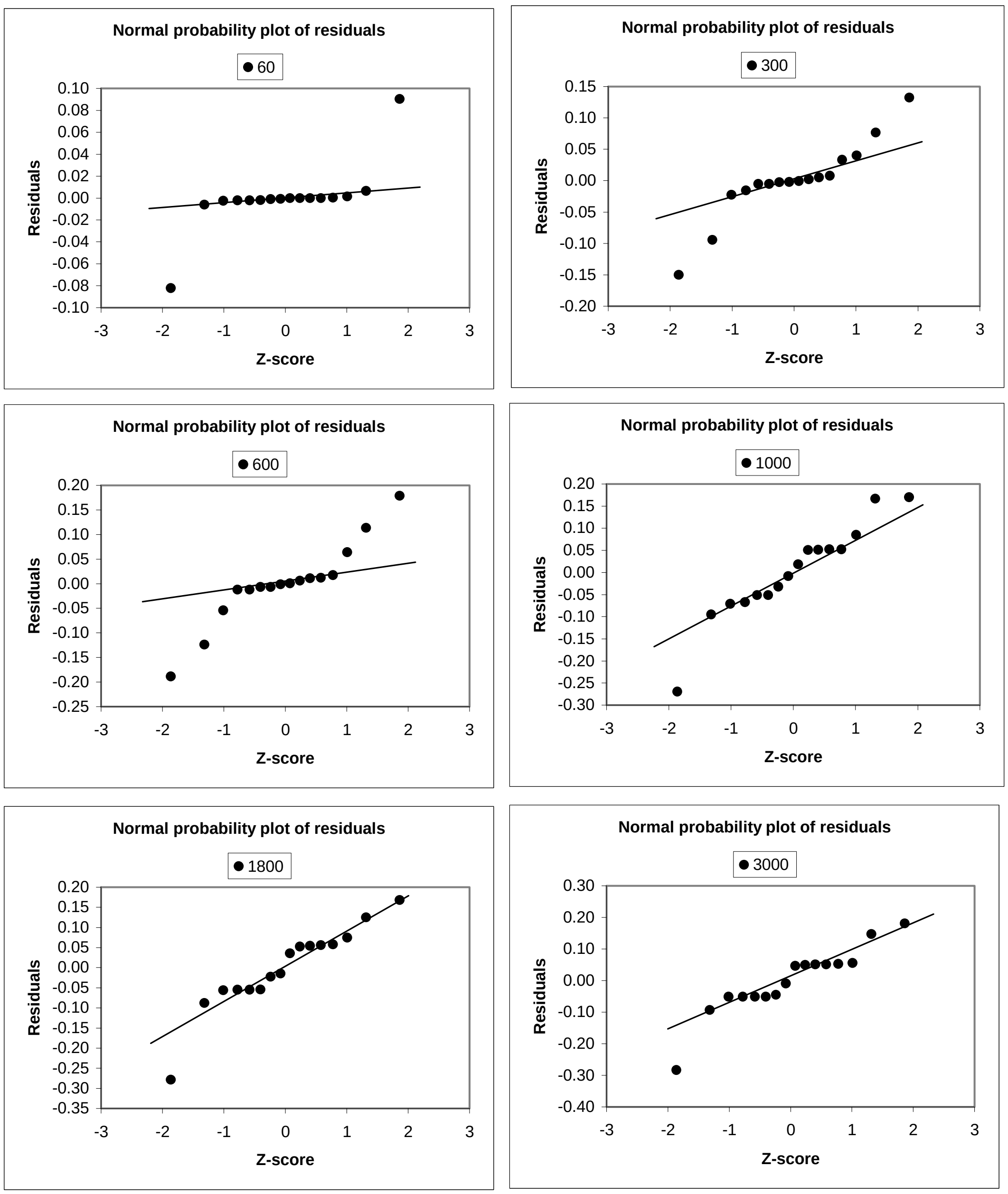

Figure 23. Normal probability plot of residuals estimated for times 60, 300, 600, 1,000, 1,800, and 3,000 sec.

These results show that flow rate, particle size, water depth, and their interactions are significant factors that affect the scour of sediment in a catchbasin sump. Specific gravity is not as important as these other factors over time under continuous flow conditions in terms of loss of sediment mass out of a catchbasin sump.

CHAPTER 5

SHEAR STRESS EVALUATION IN CATCHBASIN SUMPS

5.1 Description of the Model

A two-dimensional Computational Fluid Dynamic (2D-CFD) model, implemented in *Fluent v.6.2*, was used to evaluate the shear stress at different sediment elevations. A Volume of Fraction model (VOF) was used as a multiphase model. This multiphase model allows immiscible conditions between the water and the air, making it possible to consider the waterfall impact on the water surface in the sump. For this model, two different inlet geometries were evaluated: a 0.8 m-wide rectangular inlet (representing typical gutter flows entering the catchbasin) and a 300-mm-pipe inlet (12 inches) (representing in-line conditions). The water surface in the manholes was set at 1.2 m above the manhole bottom, which corresponds to the lowest level of the outlet, and the inlet velocity was set at zero. Figure 24 shows the three different overlaying water depths evaluated and the water surface located at 1.2 m above the bottom of the catchbasin.

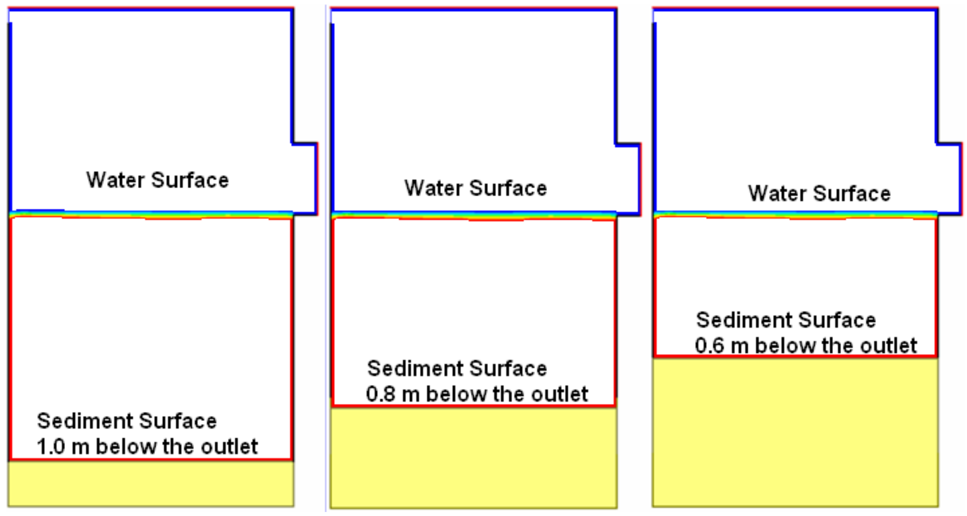

Figure 24. Water and assumed sediment surface of the 2D model implemented for the 2^4-full factorial experimental design.

5.2 Shear Stress Analysis

The critical shear stress defines the limiting condition when the sediment will move or not move from the sediment bed. Typically, the critical shear stress is determined by using the Shields' diagram (which assumes a wide flat channel) to determine the initial motion at which bed load will occur. However, in the case of scour in manholes, it is necessary to consider not only the initial motion criterion, but also the initial suspension criterion and the unique configuration of the manhole which is being studied.

Scour in manholes is defined as the migration of sediment out of the catchbasin sump chamber to the catchbasin outlet. This obviously involves the initial motion of the sediment, which will cause the sediment bed to shift (typically defined as the bed load in channels and pipes). However, because the surface of the sediment layer deposited in the manhole is located below the outlet elevation, sediment bed shifting alone will not necessarily represent migration out of the device, because the sediment does not necessarily reach the elevated outlet. Therefore, only suspended sediment will be assumed to leave the chamber.

Different shear stress criteria were reviewed for this paper in order to have a better understanding of the initial motion and initial suspension shear stress thresholds as a function of sediment characteristics. Shields, White, and Iwagaki (Garde and Ranga 1977) studied the critical shear stress for initial motion. Their results showed that dimensionless shear stress (τ_*) has the same trend for diameters between 0.1 μm to 10 μm. Their analyses are also consistent with experimental values obtained by other researchers, such as Kramer, Indri, and Chang, among others (Garde and Ranga 1977). These criteria give a better approach to the critical shear stress for initial motion, considering that they are based on theoretical and semi-theoretical analysis. They have also been widely used, especially the Shields diagram.

The Cheng-Chiew criterion (Cheng and Chiew 1999), which involves both initial motion and initial suspension, was also evaluated. This criterion relates the critical shear stress to the probability that sediment with a particular specific gravity, diameter, and settling velocity becomes bed load or gets suspended. According to Cheng and Chiew, the initial motion threshold is determined when the probability of suspension is close to zero ($1x10^{-7}$), and the initial suspension threshold is determined when the probability is about 1%. Obviously, there is not a specific line that determines when the sediment will be suspended, but usually a range is used. However, this value may be adopted for determining the initial suspension. Figure 25 shows dimensionless shear stress (τ_*) as a function of the Reynolds number of the particle (Re_*), calculated with the Cheng-Chiew criterion. Shields (initial motion), Van Rijn, and Xie criteria (initial suspension) are also included on the figure.

Figure 25 clearly shows that the dimensionless-critical shear stress calculated by using the Cheng-Chiew criterion is less than when calculated using the Shields method for Reynolds numbers less than 30. Therefore, the selection of the Cheng-Chiew criterion likely results in a conservative value for initial motion shear stress. Moreover, the Cheng-Chiew criterion involves the criteria of Xie and Van Rijn for the initial suspension threshold. Therefore, the Cheng-Chiew criterion was selected to determine the critical shear stress for initial motion and initial suspension thresholds, using a specific gravity of 2.5.

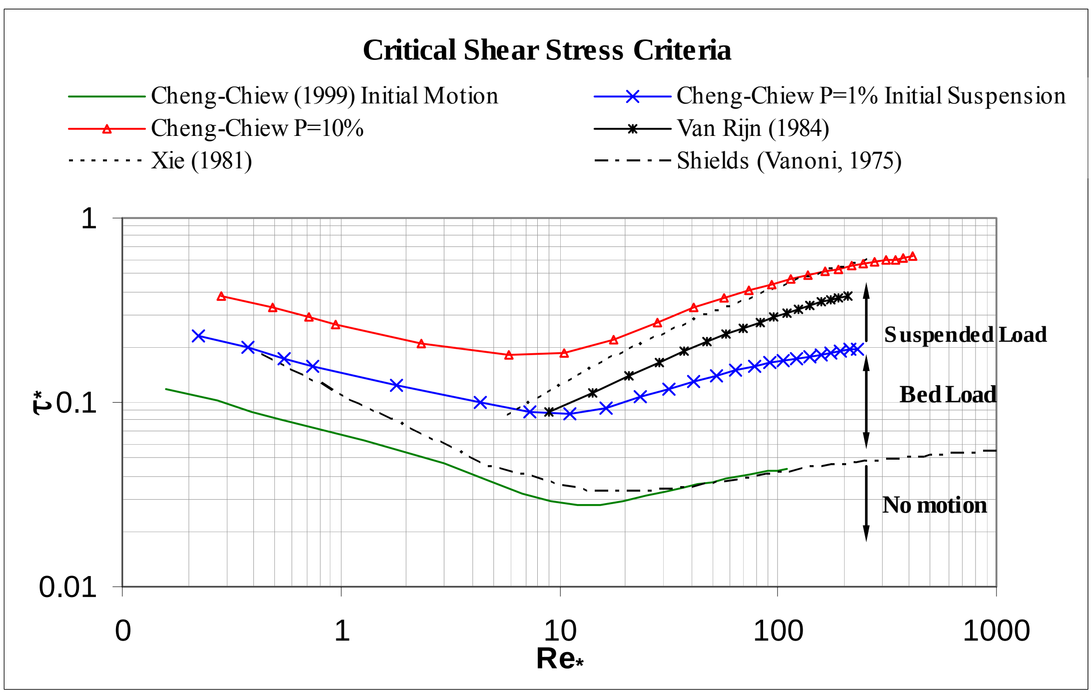

Figure 25. Critical shear stress criteria. Initial motion: Shields and Cheng-Chiew. Initial suspension: Cheng-Chiew, Xie, and Van Rijn.

Figure 26 shows the critical shear stress based on the Cheng-Chiew criterion as a function of sediment size (diameter) with a specific gravity of 2.5.

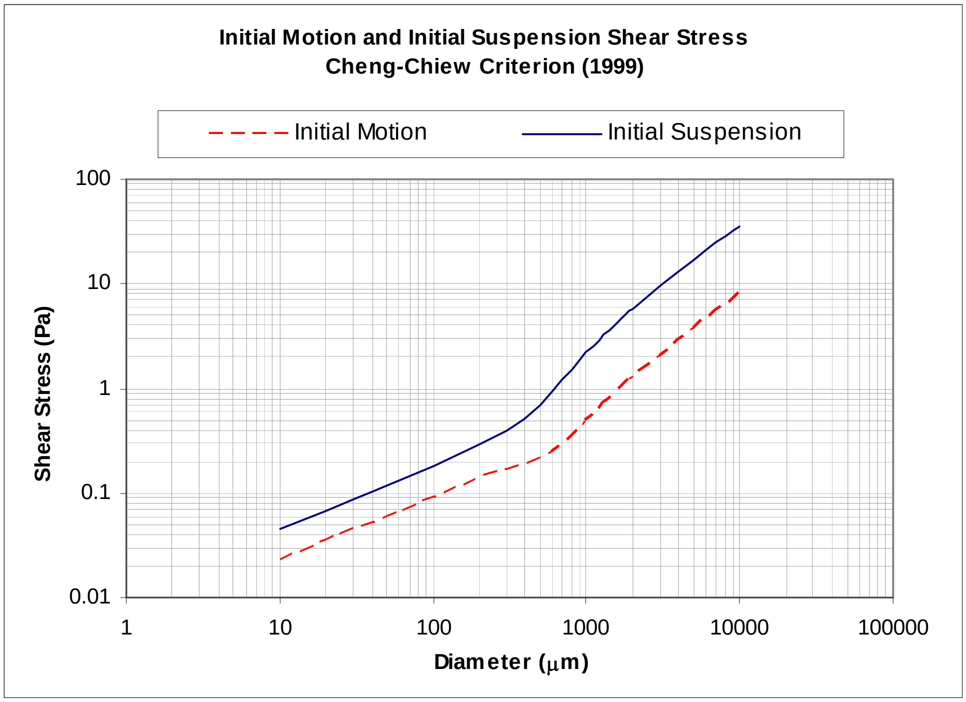

Figure 26. Initial motion and initial suspension shear stress as a function of particle size with specific gravity 2.5 – Cheng-Chiew Criterion.

Initial motion is the threshold at which the bed load is assumed to begin to move. However, bed load would not necessarily represent migration of sediment out of the catchbasin sump, because the sediment surface is located below the outlet elevation; sediment will move up and down close to the bed without reaching a suspended condition. On the other hand, initial suspension is the threshold at which the sediment will become suspended. Once the sediment becomes suspended, it is much more likely to be flushed out of the sump. When this condition occurs, the mass of sediment in the catchbasin sump will decrease with time. Therefore, scour will be defined as reduction of the height of the sediment layer.

After simulating 30 different cases, combining flow rate, sediment layer elevation, and inlet geometry, a series of graphs were developed and compared to the initial suspended threshold for a range of particle sizes up to 2,000 μm.

Rectangular inlet of 0.8-m wide. When the flow rate is 40 L/s, particle sizes smaller than about 2,000 μm are exposed to initial motion as well as to initial suspension at 0.6 m below the outlet; particle sizes smaller than 500 μm are exposed to initial suspension at 0.8 and 1.0 m.

After about 10 sec, there is no substantial difference among the shear stress magnitudes at different levels, which are between 0.5 and 1.0 Pa. This indicates that the velocity field generated by a flow rate of 40 L/s affects the whole water volume in the chamber. At 20, 10, 5, and 2 L/s flows, even though the water surface is impacted at about 0.4 sec, the shear stress begins to be important only after the velocity field starts developing. The increasing rate of the shear stress is initially manifested at 0.6 m below the outlet, then at 0.8 m, and then at 1.0 m, which is consistent with the development of the velocity field. However, once the shear stress stabilizes, there is no substantial difference of shear stress magnitudes at different elevations. Particle sizes smaller than 500 μm, 300 μm, 50 μm, and 40 μm would be exposed to initial suspension at 20, 10, 5, and 2 L/s flows, respectively, at 0.6, and 0.8 m below the outlet. At 1.0 m below the outlet, the shear stress is reduced for 10, 5, and 2 L/s flows, at which particle sizes smaller than 100 μm, 30 μm, and 20 μm, respectively, are exposed to initial suspension. Figure 27 shows these results.

Circular inlet of 300-mm diameter. When the inlet is a 300-mm diameter pipe (12 inches), the shear stress magnitudes and turbulence conditions are considerably higher than when the inlet flow is from a rectangular gutter channel. For 40 and 20 L/s flows, shear stress magnitudes of about 20 Pa exceed the critical value for 2000 μm particles for initial suspension at any elevation of the sediment surface; this shear stress is mainly caused by the impact of the water jet. However, when the flow rate is 10 L/s, the protecting water layer above the sediment surface becomes important and the shear stress is reduced to about 4.0 Pa at 0.8 m below the outlet. At 5 L/s flows, the water jet still generates shear stress values above 6.0 Pa at 0.6 m below the outlet, and particles smaller than 2000 µm are expected to become suspended. However, at 0.8 m below the outlet, the shear stress starts being more stable at about 1.0 Pa, and particles smaller than about 600 µm may become suspended for any of the three evaluated elevations. Figure 28 shows these results.

It is evident that the inlet geometry considerably affects the potential scour of sediment in a catchbasin sump. In-line catchbasin sumps with an inlet pipe without any energy-dissipating device will certainly cause more resuspension of previously deposited sediment than a typical gutter having a wide rectangular inlet.

Considering that low flow rates associated with typical rainfall events occur more often than high flow rates (Table 3, Pitt and Khambhammettu 2006), the expected sediment removal performance in the sump may be high because the hydrodynamic conditions are appropriate for particle settling. A dynamic equilibrium of scour-sedimentation of sediment may be reached in the sump, maintaining a constant sediment mass in the chamber at a specific sediment depth (as noted during prior field studies). However, if no scour protection is implemented in the catchbasin sump, a portion of the previously captured sediment may be scoured in only a few minutes if an unusually high flow rate occurs, although that has not been seen during the field activities, even with unusual flows and shallow overlaying water depths (Pitt 1979, 1985).

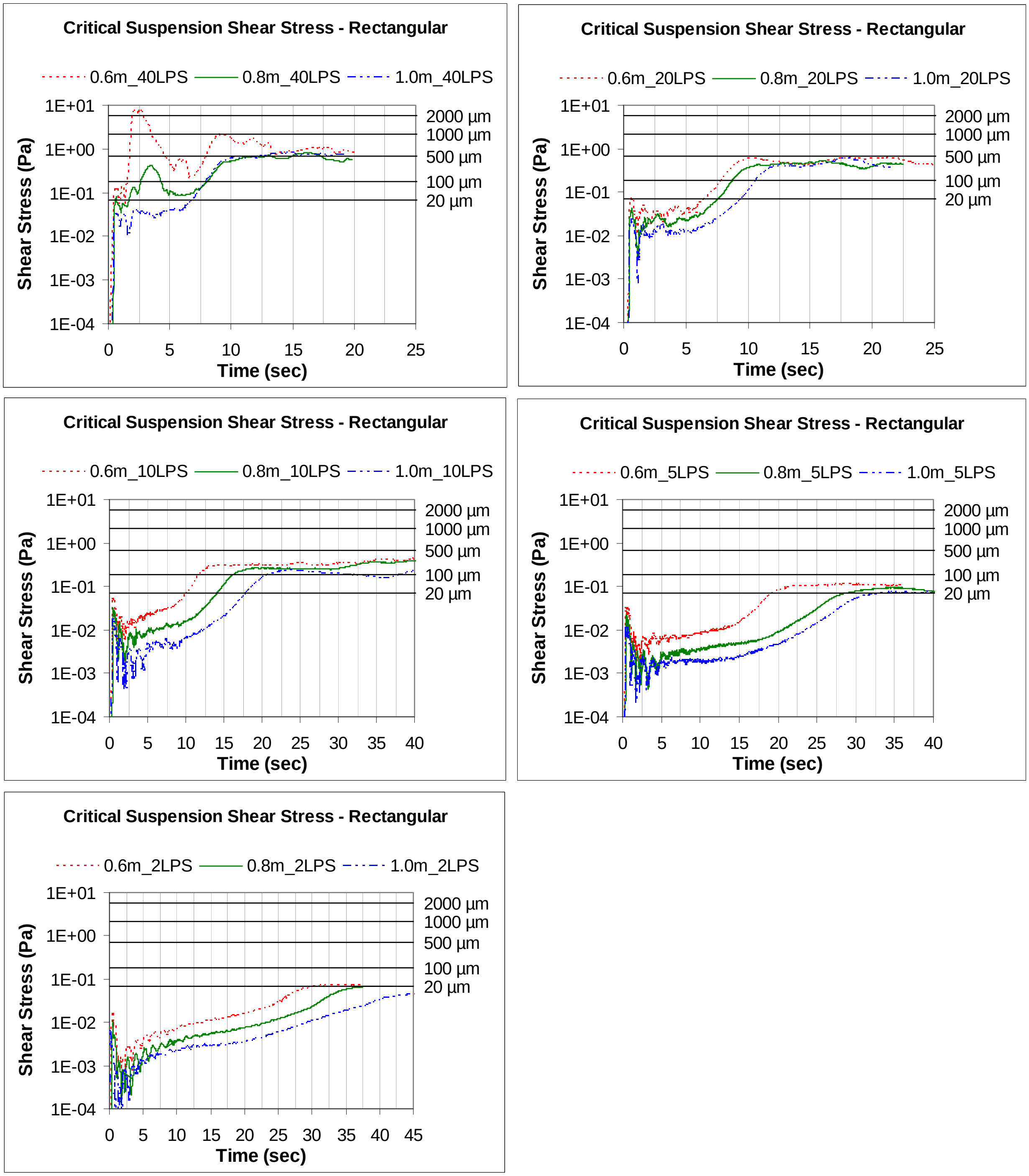

Figure 27. Shear stress on the sediment layer at different elevations in a catchbasin sump with a rectangular inlet 0.8-m wide and initial suspension threshold for different particle sizes. Series of graphs classified by flow rates: 40, 20, 10, 5, and 2 L/s.

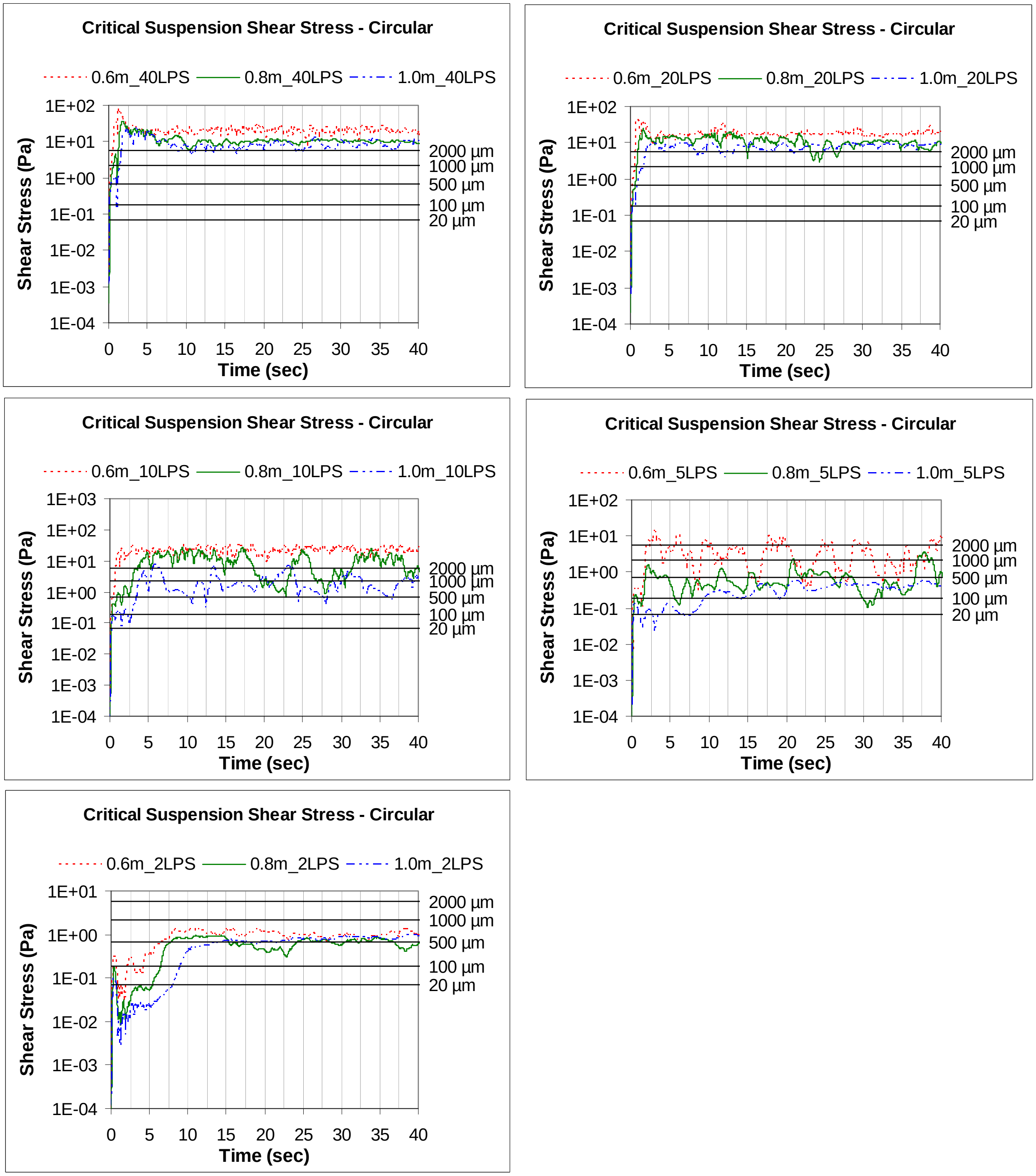

Figure 28. Shear stress on the sediment layer at different elevations in a catchbasin sump with a circular inlet 300-mm in diameter and initial suspension threshold for different particle sizes. Series of graphs classified by flow rates: 40, 20, 10, 5, and 2 L/s.

CHAPTER 6

EXPERIMENTAL RESULTS FROM A FULL-SCALE PHYSICAL MODEL OF A CATCHBASIN SUMP

6.1 Experimental Results from the Hydrodynamic Tests

Hydrodynamic tests were performed in order to determine the magnitude and direction of the velocity vectors in the control volume of a catchbasin sump under the effect of a plunging water jet. Two inlet geometries were used: a 50-cm wide rectangular channel and a 30-cm circular pipe inlet. Both were evaluated at 2.5, 5.0, and 10 L/s flow rates. Thirty instantaneous velocity measurements in x, y, and z directions were recorded at 155 locations using an Acoustic Doppler Velocity Meter (FlowTracker Handheld ADV, Sontek). The 155 points were distributed in 5 layers (16, 36, 56, 76, and 96 cm below the outlet) with 31 points each. Figure 29 shows the full-scale physical model while performing hydrodynamic tests at the facilities of the University of Alabama.

The velocity measurements were statistically analyzed to determine the significance of the type of inlet geometry, the overlaying water depth, and the flow rate.

Figure 29. Full-scale physical model while performing hydrodynamic tests.

One-way ANOVAs with Bonferroni t-tests for paired comparisons were conducted to determine the significant difference in the hydrodynamics by comparing inlet types, flow rates, and overlaying water depths. The statistical analysis was performed with aggregated samples, depending on each factor being evaluated. Using aggregated samples makes the interpretation of the results easier without reducing the collected data set. The total number of velocity magnitudes measured, including all three directions (x, y, and z), was 83,700 values.

6.1.1 *Probability Distributions of Measured Velocities*

For the analysis of the hydrodynamics, it is important to consider not only the mean velocity, but also its variation. Figure 30 shows the normal probability plot of z-velocities at 36 and 96 cm below the outlet at point 16 (located in the center of the projected top area of the control volume). This figure shows that at 36 cm below the outlet, the mean z-velocity is -1.0 cm/s, with a standard variation of 3.3 cm/s, while at 96 cm below the outlet, the z-velocity is 3.8 cm/s, with a standard variation of 3.1 cm/s. Both probability plots indicate likely normality, with p-values of 0.47 and 0.37 for the 36- and 96-cm elevations, respectively. The Anderson-Darling test compares the data to a normal distribution; a high p-value indicates that a significant difference between the data and the normal probability distributions could not be detected for the number of data points available. All the probability plots of velocity were likely normally distributed.

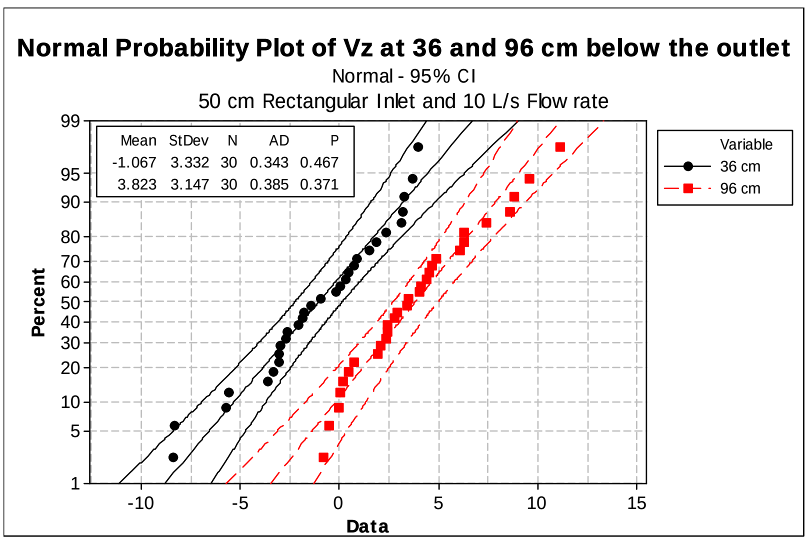

Figure 30. Normal probability plots of z-velocities at 36 and 96 cm below the outlet at point 16 (scenario with rectangular inlet and 10 L/s flow rate).

The probability plots of the experimental velocities were compared to simulated data from a 3D-CFD model implemented in *Flow-3D v.9.2* at several points located in the control volume. The mean and variations of the velocities were of greatest interest during these comparisons.

6.1.2 *Effects of Inlet Geometry on Observed Velocities in the Control Volume*

Two different inlet geometries were evaluated during the full-scale physical model tests: a 50-cm rectangular inlet representing typical gutter flows and a 30-cm diameter pipe inlet representing in-line installations (Figure 31 and 32).

Figure 31. Front view of the full-scale physical model while performing hydrodynamic tests with the 50-cm rectangular inlet (left) and with the 300-mm pipe inlet, both at 5 L/s flow rate.

Figure 32. Top view of the full-scale physical model while performing hydrodynamic tests with the 50-cm rectangular inlet (left) and with the 300-mm pipe inlet, both at 5 L/s flow rate.

Two-sample t-tests were conducted to compare the effect on the hydrodynamics generated by each inlet type. The comparison was performed by flow rate (2.5, 5, and 10 L/s) and by velocity direction (x, y, and z). Aggregated samples were created by stacking the velocity magnitudes measured in the whole water domain for each flow rate, resulting in sample sets of 4,650 velocity values for each direction (x, y, and z). Table 7 describes the sample sets used for this analysis.

Table 7. Sample Sets for Two-Sample t-Tests for Comparison of Inlet Type (Hydrodynamic Tests)

Sample	By Flow rate	By Velocity direction	Total sample sets
50-cm wide rectangular inlet	2.5, 5, and 10 L/s	Vx, Vy, and Vz	18 samples of 4,650 values each
30-cm circular inlet			

All the tests showed that the effect of the circular inlet on the whole velocity field is significantly higher than the effect generated by the rectangular inlet at 95% confidence level. The p-values obtained from the tests were highly significant (less than 0.0001). Figure 33 shows the boxplots categorized by inlet type and overlaying water depth for Vz-velocities at 2.5 L/s.

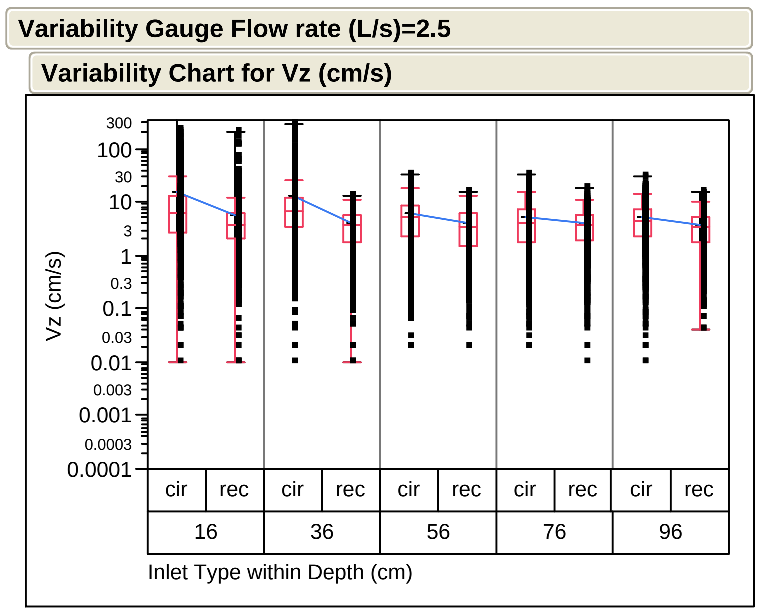

Figure 33. Boxplot of Vz-velocities measured in the whole domain at 2.5 L/s. The boxplots are categorized by inlet type (circular and rectangular) and overlaying water depth (cm).

Additionally, Figure 34 shows the maximum velocity as a function of overlaying water depth plotted by inlet type.

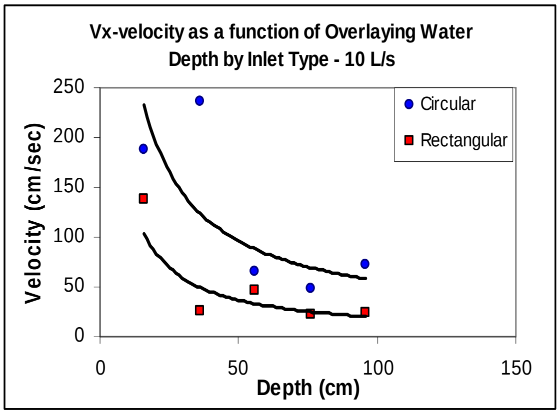

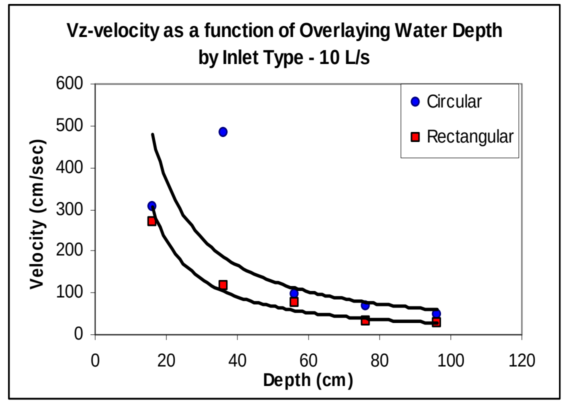

Figure 34. Maximum magnitudes of x-velocities (left) and z-velocities (right) by inlet geometry as a function of elevation below the outlet (scenario at 10 L/s flow rate).

Avila, Pitt, and Durrans (2008) evaluated the shear stresses at different elevations produced by a rectangular and circular inlet using a 2D-CFD model implemented in *Fluent v.6.2*. The results showed that the circular inlet generates significantly higher shear stress magnitudes at all overlaying water depths than generated by a rectangular inlet; therefore, the circular inlet likely causes increased scour of previously captured sediment.

These experimental hydrodynamic tests demonstrated that the inlet geometry has a major effect on the velocity field in the control volume of a catchbasin. Circular inlets cause higher velocities in the control volume than rectangular inlets. This conclusion was also found by Avila et al. (2008) and Faram et al. (2003) using CFD modeling. This phenomenon is due to the smaller area associated with the impact zone as the plunging water strikes the water surface in the catchbasin, causing more concentrated power to be transferred to a smaller area of the pooled water.

6.1.3. *Effects of Flow Rates on Velocity Distributions in the Control Volume*

Three flow rates were evaluated: 2.5, 5, and 10 L/s. One-way ANOVAs with Bonferroni t-tests for paired comparisons were conducted to compare the effects on the hydrodynamics generated by the flow rate. The comparison was performed by overlaying water depth and by inlet type. Aggregated samples were created by stacking the velocity magnitudes measured in each layer (16, 36, 56, 76, and 96 cm below the outlet). Table 8 describes the sample sets used for this analysis.

Table 8. Sample Sets for One-Way ANOVA to Evaluate Flow Rate (Hydrodynamic Tests)

<table>
<tr><th>Sample</th><th>By Depth</th><th>By Inlet Type</th><th>By Velocity direction</th><th>Total sample sets</th></tr>
<tr><td>2.5 L/s</td><td rowspan="3">16, 36, 56, 76, and 96 cm below the outlet</td><td rowspan="3">50-cm wide rectangular inlet and 30-cm circular inlet</td><td rowspan="3">Vx, Vy, and Vz</td><td rowspan="3">30 samples of 930 values each</td></tr>
<tr><td>5 L/s</td></tr>
<tr><td>10 L/s</td></tr>
</table>

The results showed that flow rate was significant at the 95% confidence level, with p-values below 0.0036. Figure 35 shows the boxplots of y-velocity (Vy) categorized by flow rate and by overlaying water depth for a rectangular inlet. The figure clearly shows how the velocity increases at each depth as the flow rate increases.

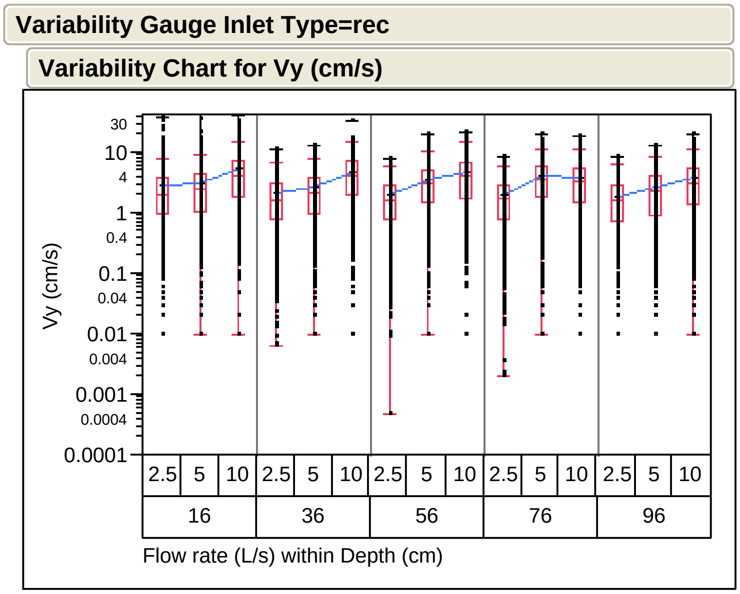

Figure 35. Boxplot of Vy-velocities using a rectangular inlet. The boxplots are categorized by flow rate (L/s) and overlaying water depth (cm).

Table 9 shows the comparison for each pair using t-tests for z-velocity at 56 cm below the outlet and with a rectangular inlet. The table shows that there is a significant difference between the mean Vz-velocities generated by each flow rate at this elevation.

Table 9. Statistical Output of Pair Comparison of Flow Rate Using a t-Test (Analysis with z-Velocities at 56 cm Below the Outlet Using a Rectangular Inlet)

Comparisons for each pair using Student's t

t	Alpha
1.96082	0.05

Level				Mean
10	A			5.4395699
5		B		4.5888280
2.5			C	3.9970000

Levels not connected by same letter are significantly different.

Level	- Level	Difference	Lower CL	Upper CL	p-Value
10	2.5	1.442570	1.069675	1.815465	<.0001*
10	5	0.850742	0.477847	1.223637	<.0001*
5	2.5	0.591828	0.218933	0.964723	0.0019*

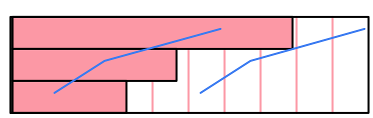

6.1.4 *Effects of the Overlaying Water Depth on Observed Velocities in the Control Volume*

Five overlaying water depths were evaluated: 16, 36, 56, 76, and 96 cm. One-way ANOVAs with Bonferroni t-tests for paired comparisons were conducted to compare the effects on the hydrodynamics generated at each depth. The comparison was performed by flow rate and by inlet type. Aggregated samples were created by stacking the velocity magnitudes measured in each layer (16, 36, 56, 76, and 96 cm below the outlet). Table 10 describes the sample sets used for this analysis.

Table 10. Sample Sets for One-Way ANOVA to Evaluate Overlaying Water Depth (Hydrodynamic Tests)

Sample	**By Flow rate**	**By Inlet Type**	**By Velocity direction**	**Total sample sets**
16 cm	2.5, 5, and 10 L/s	50-cm wide rectangular inlet and 30-cm circular inlet	Vx, Vy, and Vz	18 samples of 930 values each
36 cm				
56 cm				
76 cm				
96 cm				

The results showed that overlaying water depth was also significant at a 95% confidence level, with p-values below 0.0001. Figure 36 shows the boxplots of z-velocity (Vz), categorized by overlaying water depth and flow rate for a circular inlet. The figure clearly shows that the velocity decreases as a function of the overlaying water depth.

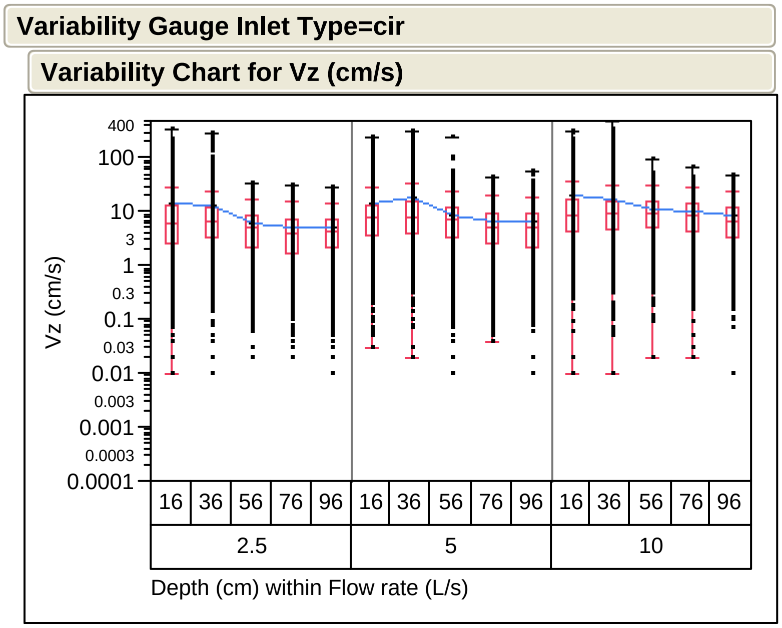

Figure 36. Boxplot of Vz-velocities using a circular inlet. The boxplots are categorized by overlaying water depth (cm) and flow rate (L/s).

The statistical results also showed that in deeper water there is no significant difference in the velocities at low flow rates, especially with rectangular inlets. In contrast, when the flow rate is high and the inlet is circular, deeper locations are significantly affected by the plunging water jet. Table 11, for example, shows the pair comparisons of z-velocities for different overlaying water depths at 2.5 L/s with a rectangular inlet. The results in the table show that the only depth that is significantly different than the others is 16 cm below the outlet. Below that depth, there is no significant difference between the z-velocities. In contrast, Table 12 shows the pair comparisons of z-velocities for different overlaying water depths at 10 L/s with a circular inlet. This table shows that the velocities at 16 and 36 cm below the outlet are significantly different than the other depths. However, depths from 56 to 96 cm below the outlet did not show any significant difference.

These results suggest that the overlaying water depth is an effective mechanism in reducing the scour potential as it reduces the velocity magnitudes and therefore the shear stress acting on the sediment surface. This is especially under high flow rates, in which the plunging water jet generates more turbulence during the impact with the water surface and increases the amount of air entrainment. The ascending velocity component due to the air buoyancy also decreases the depth that the plunging water can reach. The experimental results showed that the reduction of velocity as a function of the overlaying water depth was exponential.

Table 11. Statistical Output of Pair Comparison of Overlaying Water Depth Using t-Test (Analysis with z-Velocities at 2.5 L/s Using a Rectangular Inlet)

Comparisons for each pair using Student's t

t	Alpha
1.96047	0.05

Level		Mean
16	A	5.8443011
56	B	3.9970000
76	B	3.9950538
36	B	3.8961935
96	B	3.8293011

Levels not connected by same letter are significantly different.

Level	- Level	Difference	Lower CL	Upper CL	p-Value
16	96	2.015000	1.45644	2.573560	<.0001*
16	36	1.948108	1.38955	2.506667	<.0001*
16	76	1.849247	1.29069	2.407807	<.0001*
16	56	1.847301	1.28874	2.405861	<.0001*
56	96	0.167699	-0.39086	0.726259	0.5562
76	96	0.165753	-0.39281	0.724312	0.5607
56	36	0.100806	-0.45775	0.659366	0.7235
76	36	0.098860	-0.45970	0.657420	0.7286
36	96	0.066892	-0.49167	0.625452	0.8144
56	76	0.001946	-0.55661	0.560506	0.9945

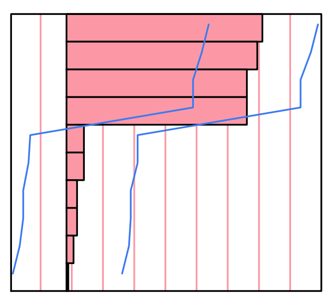

Table 12. Statistical Output of Pair Comparison of Overlaying Water Depth Using T-Test (Analysis with z-Velocities at 10 L/s Using a Circular Inlet)

Comparisons for each pair using Student's t

t	Alpha
1.96047	0.05

Level		Mean
16	A	21.314613
36	B	17.157398
56	C	10.854871
76	C	10.246602
96	C	8.644839

Levels not connected by same letter are significantly different.

Level	- Level	Difference	Lower CL	Upper CL	p-Value
16	96	12.66977	10.4446	14.89496	<.0001*
16	76	11.06801	8.8428	13.29320	<.0001*
16	56	10.45974	8.2346	12.68493	<.0001*
36	96	8.51256	6.2874	10.73775	<.0001*
36	76	6.91080	4.6856	9.13598	<.0001*
36	56	6.30253	4.0773	8.52771	<.0001*
16	36	4.15722	1.9320	6.38240	0.0003*
56	96	2.21003	-0.0152	4.43522	0.0516
76	96	1.60176	-0.6234	3.82695	0.1582
56	76	0.60827	-1.6169	2.83346	0.5920

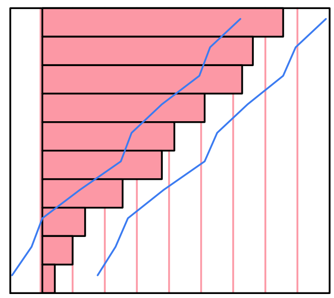

6.2 Experimental Results from the Scour Tests with Sediment Mixture

Scour tests with a sediment mixture (as pre-deposited sediment material in the sump) were performed at Lake Lurleen State Park, Northport, AL. These were once-through tests using the lake water. The tests were performed with a 50-cm wide rectangular inlet. Four overlaying water depths were evaluated: 10, 25, 46, and 106 cm. Each overlaying water depth was tested with five consecutive flow rates, each lasting 25 min; the flow rates were: 0.3, 1.3, 3.0, 6.3, and 10 L/s. Composite samples (1.0 L) were collected for the first 5 min and for the last 20 min of test. Also, a turbidity time series was recorded using a water quality sensor (HORIBA probe) adjacent to the effluent. Suspended Sediment Concentration (SSC) and Particle Size Distributions (PSD) of the composite samples were measured in the laboratory. Figure 37 shows the full-scale physical model while performing a scour test with a sediment mixture. Figure 12 shows the PSD of the sediment mixture used for these tests.

Figure 37. Full-scale physical model while performing scour tests with a sediment mixture as pre-deposited sediment material.

6.2.1 *Scour Behavior Reflected by Turbidity Measurements – Sediment Mixture*

Turbidity concentration time series were recorded at the outlet for all the tests using a time increment of 30 sec. Even though turbidity could not be directly related to particle sizes or particulate mass, it did reveal the scour pattern for different flow rates and overlaying water depths above the sediment.

The turbidity time series showed that with this specific PSD, the scour had an exponential decay pattern under steady flow conditions, having a maximum turbidity value at the beginning of the flow when the plunging impact of the incoming water had its greatest effect and decreasing exponentially over time. This pattern was more evident when the sediment was located relatively close to the outlet (with shallow water layers over the sediment), where it is more exposed to scour. With sediment at 10 cm below the outlet, for example (Figure 38), the negative exponential pattern is clear even at flows as low as 0.3 L/s. When the flow rate increased, peak turbidity values also increased, indicating a direct relationship between the peak turbidity values and the flow rate. The turbidity values decreased exponentially over time as the small particles on the surface sediment layer were washed out and bed armoring was formed. This pattern was consistent for all the evaluated flow rates. The maximum turbidity value obtained was over 1,000 NTU during the 10 L/s flow rate tests.

When the sediment was located at 25 cm below the outlet, the peak turbidity values were not as high, nor was the exponential decaying pattern as evident for low flow rates (0.3 and 1.3 L/s). For the low flows, the velocity field was not sufficient to cause significant scour. However, once the flow rate increased to 3.0 L/s, the turbidity exponential decay pattern was again evident. The maximum turbidity value at 10 L/s flow rate was 100 NTU when the overlaying water was 25 cm deep, which is approximately 10 times less than when the overlaying water depth was only 10 cm deep. With sediment at 46 cm below the outlet, the pattern was barely evident at 6.3 L/s flow rate, and a maximum turbidity value of 20 NTU was obtained at 10 L/s. At 106 cm below the outlet, the pattern was not evident for any flow condition, and the effluent turbidity values were never greater than 5 NTU. These results illustrate the significant benefit associated with the overlaying water layer in protecting the previously captured sediment in the catchbasin sump, even under the severe conditions associated with the velocity field generated by an aerated plunging water jet.

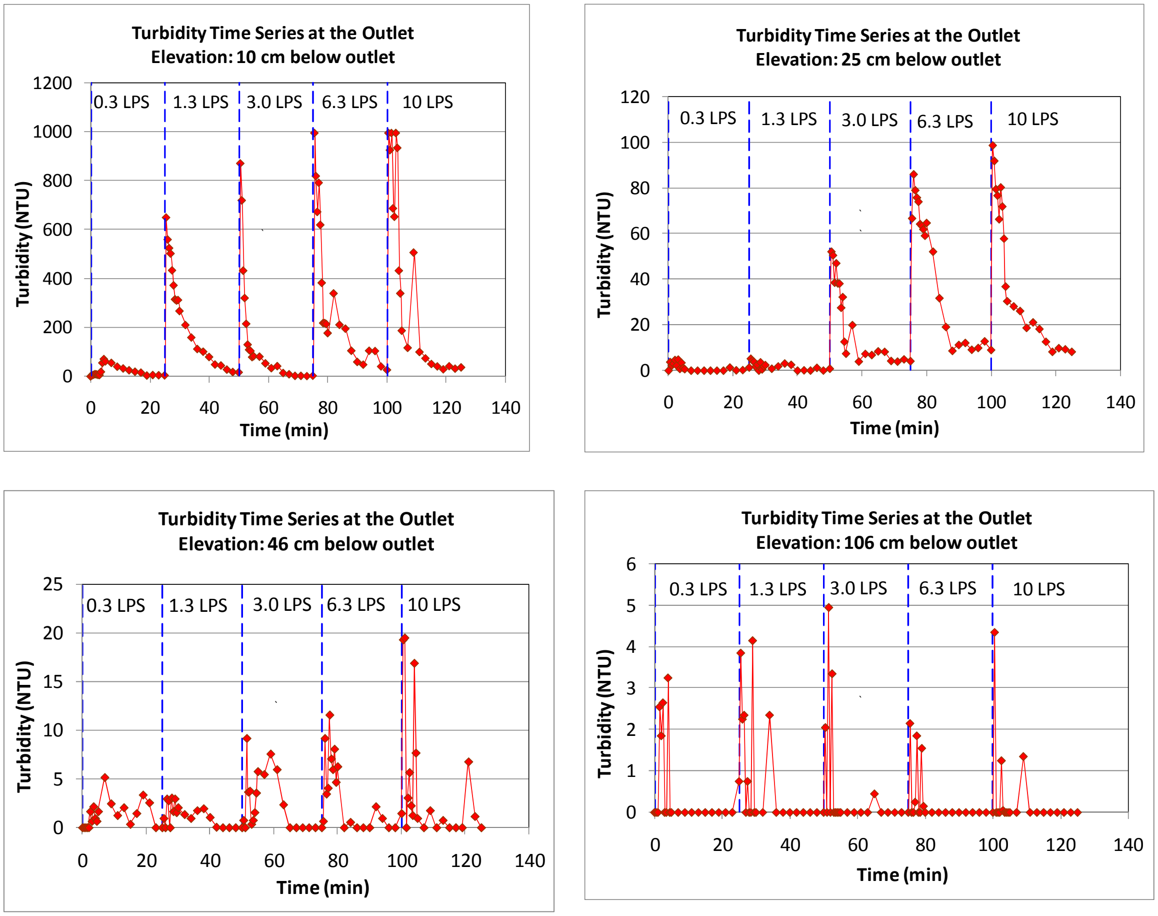

Figure 38. Turbidity time series at the outlet for scour tests: 10 cm (top left), 25 cm (top right), 46 cm (bottom left), and 106 cm (bottom right) overlaying water depths above the sediment and below the outlet (note differences in turbidity scale values).

6.2.2 *Armoring Effect on Reducing Sediment Scour*

The turbidity time series tests showed that an armoring layer of large sediment particles is formed on the sediment surface during steady flow conditions. This finding reveals that if relatively large particles (D_{75}=1500 µm, D_{90}=3350 µm, and D_{max}=4750 µm for this experiment) are present in the pre-deposited sediment in a catchbasin sump, the scour potential of underlying smaller particles is rapidly decreased as an armoring of the larger particles rapidly form on the sediment surface. Therefore, only a few centimeters of the surface sediment will be exposed to scour. However, the effectiveness of the armoring is relative to the fraction or proportion of large particles in the pre-deposited sediment and their proximity to the sediment surface. Figure 39 shows the armoring layer formed after two hours of continuous flow. Notice the presence of fine sediment next to the armoring layer, back in the sump away from the outlet structure and plunge point. This suggests that secondary currents were not strong enough to significantly erode the solids in the area of the sump.

Figure 39 Armoring layer formation on sediment mixture surface. Left: Plunging water jet impacting the water surface in catchbasin sump. Right: Armoring layer.

Two processes may be occurring, either separately or simultaneously: (1) Preferential washing of small particles from the voids around the larger particles. The shear stress defines the particle size that will remain behind, with exposed particles smaller than the size removed, until a complete armoring layer of the large particles remains behind, protecting any underlying smaller particles. (2) A "washing machine" effect occurs where the surface layer is tumbled about; the largest particles that can be suspended are also dependent on the shear stress. As this mixture moves about, smaller particles can be transported out of the system before they can resettle to the sediment layer, leaving behind the larger ones that then settle back down as the flow decreases, forming a protecting layer over the underlying sediment. The depth of the sediment that can be disturbed like this is likely dependent on the shear stress and carrying capacity of the water.

The turbidity time series presented in Figure 38 only showed the scour pattern under steady flow rates, in increasing increments, but not under rapidly fluctuating conditions at the same flow. Therefore, a fluctuating flow test was performed, applying four successive flows of 10 L/s, each lasting 3 min. Each flow was stopped at 3 min and re-started after about a minute to create the next flow burst. Thus, a total of four flow bursts were applied, and the total effective flow time was 12 min. Figure 40 shows the resulting turbidity time series for all the tests conducted with different overlaying water depths during the series of impacting flow tests.

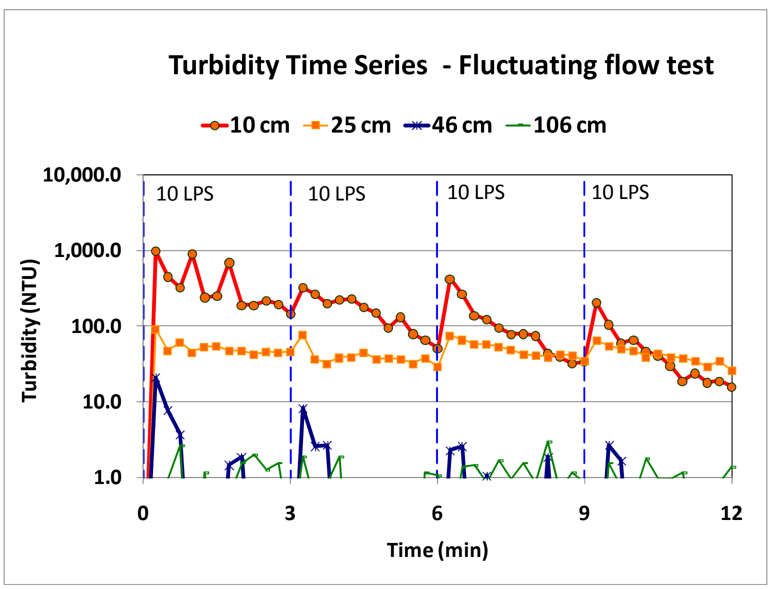

Figure 40. Turbidity time series at the outlet for the series of impacting tests using short durations of 10 L/s flows.

The turbidity values reached a peak every time the plunging jet impacted the water with the shallow 10 cm overlaying water depth and successive short duration flows of 10 L/s. However, the values of the peak decreased with each successive flow, from 1,000 NTU at the first impact to 200 NTU at the forth impact, showing that armoring is gradually protecting the sediment bed, even from the fluctuating flows that are likely during an actual runoff event. Also, with the shallow water depth, the turbidity time series still exhibited an overall negative exponential pattern, with decreasing turbidity values during the short flow durations. A similar but less dramatic scour pattern was obtained when the overlaying water depth above the sediment was increased to 25 cm; the maximum turbidity values were much less, about 90 NTU for the first impact and 64 NTU for the forth impact. However, when the water depth was increased to 46 cm above the sediment, the initial turbidity peak was only 20 NTU and decreased to maximum initial turbidity peaks of only about 5 NTU for the last two impacts. With a water layer depth of 106 cm above the sediment, no evident pattern was detected and the turbidity values were always below 5 NTU.

These findings show that sediment is more sensitive to scour under fluctuating than under steady long-term flow conditions. Additionally, the results also show that armoring is formed relatively rapidly during fluctuating flow conditions, effectively protecting the underlying sediment from scour even under the impact of plunging water jets. During these tests, armoring formed within a few minutes. The turbidity decreases as the number of impacts of flow at the same rate increases. Sediment scour is therefore highest during the initial stage of a runoff event, even if the flows keep increasing. After a few minutes at the peak runoff rate for the event, sediment scour substantially decreases as the armoring is formed at the sediment surface. Subsequent runoff events may have greatly reduced scour, unless new flows are large enough to disturb the armoring layer material. Besides large particles, other materials may help form armoring of the sediment surface, including leaves, clay soil, and other debris, if they accumulate on the sediment surface in the sump. However, if the water depth over the sediment is large (such as the 46 cm depth during these tests), the benefits of armoring are significantly decreased, as very little scour is likely to occur (at least at the 10 L/s, or less, flow rates tested).

6.2.3 *Particle Sizes Exposed to Scour*

Particle size distributions in the effluent water were determined for each flow rate and overlaying water depth test. An initial effluent water sample was collected as a composite during the first 5 minutes of flow, and a second composite sample was collected over the next 20 minutes of flow, covering the entire 25 minutes of each test. This resulted in 125 min of successively increasing flows, from 0.3 L/s to 10 L/s, for each sediment depth setup. The particle size distributions were determined by wet sieving through successive sieves: 2000, 1200, 425, 250, 150, 106, 45, 32, and 20 µm. The wet sieve analysis was performed with 10 subsamples of 100 mL, each obtained by splitting a 1.0 L composite effluent sample with a USGS/Decaport cone water sample splitter. The particle size information of the lake water was subtracted from the effluent sample observations to remove the background effects.

Table 13 summarizes the particle size distributions for both the 5-min and 20-min composite samples for each flow rate and overlaying depth over the sediment. The table shows the particle sizes for the fiftieth and ninetieth percentiles, plus the maximum scoured particle size observed in the effluent water.

Table 13. Summary of Particle Size Distribution (PSD) for the 5-Min and 20-Min Composite Samples

		Percentile					
		5-min Composite Sample			**20-min Composite Sample**		
Water Layer Depth over Sediment (cm)	**Flow rate (L/s)**	**50th (μm)**	**90th (μm)**	**Max (μm)**	**50th (μm)**	**90th (μm)**	**Max (μm)**
10	0.3	< 20	150	1200	45	150	1200
	1.3	20	150	1200	45	200	1200
	3.0	45	200	1200	106	200	1200
	6.3	106	425	4750	150	1200	4750
	10.0	1500	3200	4750	1000	3000	4750
25	0.3	< 20	150	425	< 20	350	425
	1.3	< 20	250	425	250	300	425
	3.0	20	106	425	100	425	1200
	6.3	25	150	425	45	300	1200
	10.0	32	125	1200	106	425	1200
46	0.3	45	80	106	32	125	150
	1.3	45	250	425	45	400	425
	3.0	45	200	250	45	100	106
	6.3	45	106	150	32	106	425
	10.0	106	150	1200	32	150	1200
106	0.3	< 20	< 20	< 20	< 20	106	150
	1.3	32	40	45	32	40	45
	3.0	< 20	< 20	< 20	32	106	150
	6.3	32	45	106	< 20	< 20	< 20
	10	< 20	32	45	< 20	30	45

Figure 41 and 42 show the PSD plots for different overlaying water depths (depth below the outlet) for the 6.3 L/s flow rate for the 5-min and 20-min composite samples, respectively. The original PSD of the pre-deposited sediment is also included in the figures. The figures show that as the overlaying water depth increases, the proportion of large particles scoured decreases.

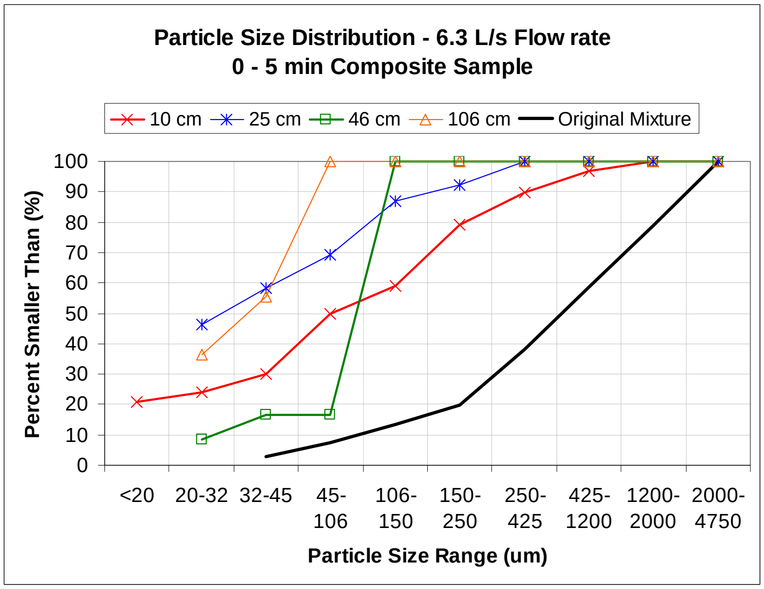

Figure 41. Particle size distribution by depth of overlaying water over the sediment for the 5-min composite sample at 6.3 L/s flow rate.

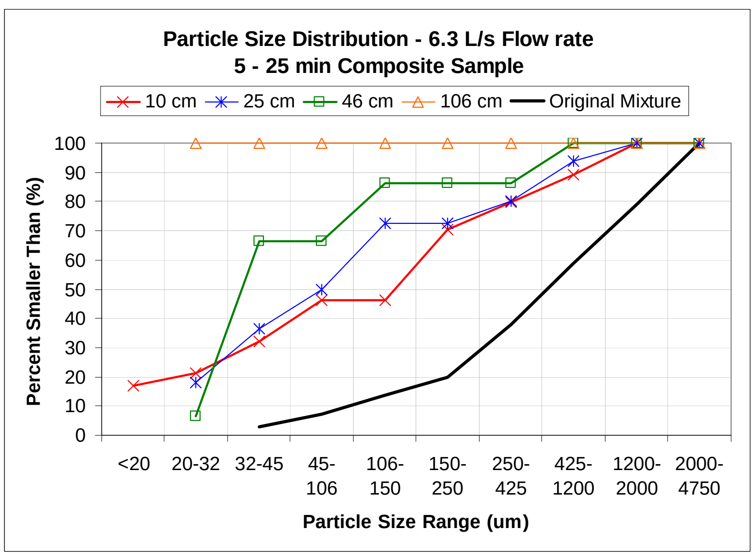

Figure 42. Particle size distribution by depth of overlaying water over the sediment for the 20-min composite samples at 6.3 L/s flow rate.

The observed maximum scoured particle size gives an indication of the significance of flow rate and overlaying water depth on the scour potential. Figure 43 and

44 show the maximum scoured particle sizes for the 5-min and 20-min composite samples. The figures show that the scour potential is directly proportional to the magnitude of flow rate and inversely proportional to the depth of water. During the first 5 min of flow for the 6.3 L/s flow rate test, for example, the maximum scoured particle size was 4,750 µm when the water layer was 10 cm thick over the sediment, 425 µm when the water layer was 25 cm thick, 150 µm when the water layer was 46 cm thick, and 106 µm when the water layer was 106 cm thick.

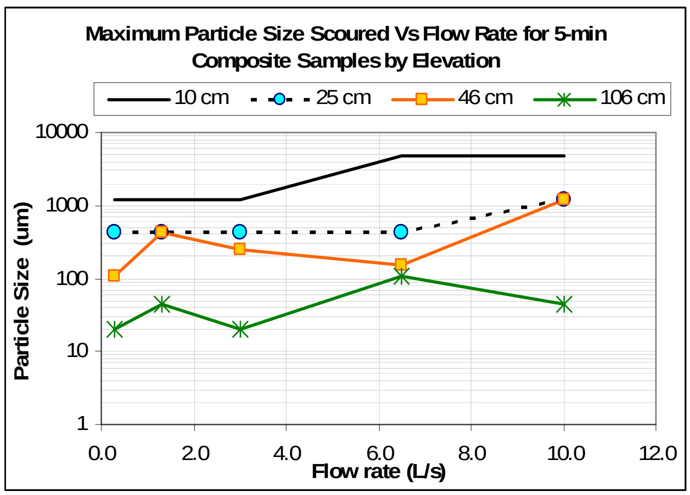

Figure 43. Maximum scoured particle size as a function of flow rate for the 5-min composite sample. Values plotted by overlaying water depth above the sediment.

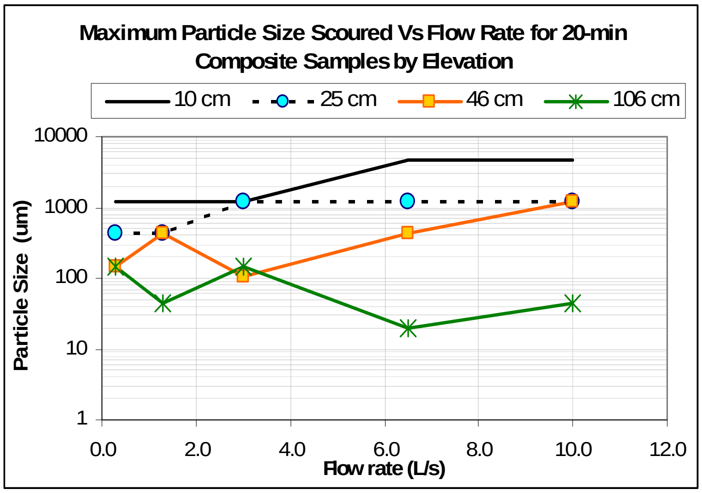

Figure 44. Maximum scoured particle size as a function of flow rate for the 20-min composite sample. Values plotted by overlaying water depth above the sediment.

6.2.4 *Effect of Flow Rate on Increasing SSC and Mass Load*

The SSC for different flow rates and overlaying water depths for the 0-5 min composite samples is shown in Table 14. SSC increases as a fractional power function of the flow rate. However, at 10 L/s, the concentration decreased for overlaying water depths of 25, 46, and 106 cm. This could be mainly attributed to dilution of the sediment mass in a higher volume of water. The incremental proportional increase in the scour mass generated from 6.3 to 10 L/s was less than the incremental proportional increase in the flow rate. However, another possible explanation is due to the scour test procedure for sediment mixture.

Table 14. Total SSC (mg/L) of Scoured Sediment for the 0 - 5-min Composite Samples

Depth below the outlet (cm)	Flow rate (L/s)				
	0.3	1.3	3.0	6.3	10.0
	SSC (mg/L)				
10	55.6	391.7	426.5	1044.6	1138.5
25	7.0	8.0	41.9	108.4	46.4
46	4.9	4.1	6.5	12.0	10.6
106	1.7	2.6	3.3	2.9	1.7

As described in the methodology, the tests were performed by applying consecutive increments of flow rates for a given sediment depth below the outlet (or overlaying water depth). Then, as the flow rate increased, a sediment armoring layer was formed, requiring a substantial increment of flow rate to break the armoring previously formed in order to expose more sediment to be scoured or a change in the location of impact of the plunging water jet to erode a different location where armoring was not formed. From 0.3 to 6.3 L/s, the flow rates were doubled at a minimum between tests, but from 6.3 to 10 L/s, the increment was only 1.6 times. This increment may not be sufficient to break the armoring formed during the test at 6.3 L/s flow rate. Moreover, the location of the plunging water jet at 10 L/s was relatively close to the location at 6.3 L/s. As a consequence, less unprotected sediment material was exposed to scour at 10 L/s than it would be if this flow rate was applied without any previous flow.

Mass load, in contrast to SSC, always shows an increasing pattern, which is consistent with the proportional relationship between mass and flow rates (except for the case at 24 cm below the outlet, where the mass load decreased from 6.3 to 10 L/s, which may be attributed to the experimental procedure). Figure 45 shows SSC and mass load for the 5-min composite sample.

A maximum SSC of 1139 mg/L was measured when the overlaying water depth was 10 cm during the 10 L/s flow rate. The difference between the flux rate at 6.5 L/s (1045 mg/L) and at 10 L/s (1139 mg/L) is not large, considering that an armoring layer had already been formed after 100 min of continuous flow at the lower rate before the 10 L/s flow rate was applied. Therefore, it is possible that the mass load for 10 L/s would actually be greater than shown here and would then decrease following the previously described exponential pattern.

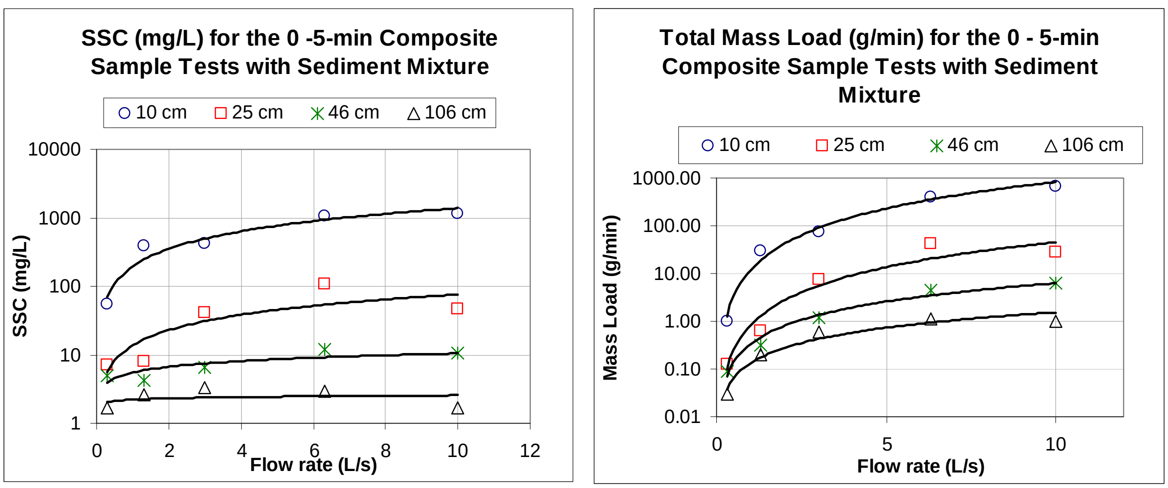

Figure 45. SSC and mass load for the 5-min composite sample obtained form the tests with sediment mixture.

The pattern for SSC and mass load for the 5-25-min composite samples are similar to the pattern seen for the 0-5-min composite samples (Table 15); SSC and mass load increase as a fractional power function of flow rate for a given water depth. Figure 46 shows SSC and mass load for the 20-min composite samples.

Table 15. Total SSC (mg/L) of Scoured Sediment for the 5-25-min Composite Samples

Depth below the outlet (cm)	Flow rate (L/s)				
	0.3	1.3	3.0	6.3	10.0
	SSC (mg/L)				
10	12.6	54.9	101.8	244.1	683.5
25	1.6	5.5	19.8	22.1	44.0
46	2.0	1.5	4.8	10.8	11.2
106	0.6	1.1	2.0	2.1	4.0

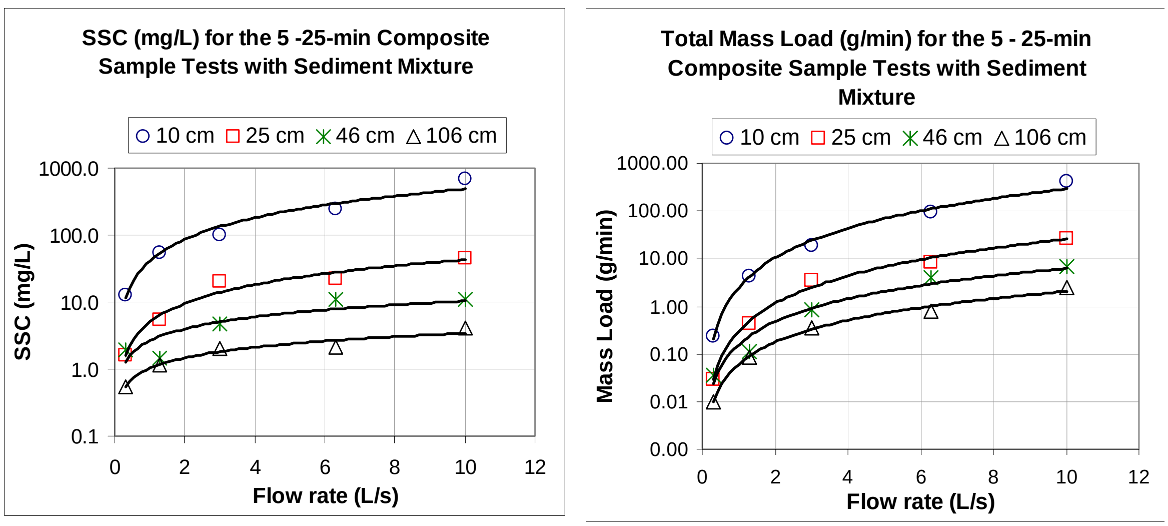

Figure 46. SSC (left) and Mass Load (right) for the 20-min composite sample obtained from the tests with sediment mixture.

Simple linear regression models, including ANOVA, were performed to determine the significance of flow rate in increasing SSC. In all 0-5 min composite samples, flow rate was significant at a 95% confidence level; except for the cases with overlaying water depth at 25 and 106 cm, with p-values of 0.27 and 0.81, respectively. However, SSC needs to be specified together with flow rate to obtain an estimation of scour mass rate.

A direct measurement of scour rate is given by mass load, which is the product of SSC and flow rate. If mass load is plotted as a function of flow rate, the confidence interval of the linear regression is reduced and the flow rate becomes significant at a 5% significance level at 106 cm and at a 10% significance level at 24 cm. However, notice that plotting mass load versus flow rate is a spurious relationship, because mass load depends on flow rate. However, mass load represents a direct measurement of scour rate, and flow rate is still an independent variable. The use of mass load artificially reduces the variability of the scour rate estimation but demonstrates this commonly used relationship.

Figure 47 shows the regression fits of SSC and mass load of the 0-5 min composite samples for the scenario with an overlaying water depth of 46 cm.

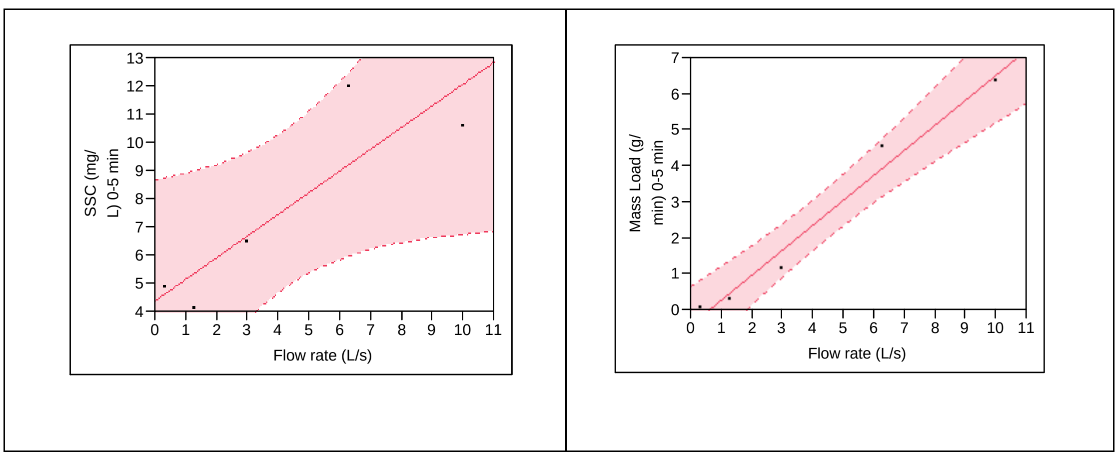

Figure 47. Simple linear regression fits of SSC and mass load of the 0-5 min composite samples for the scenario of an overlaying water depth of 46 cm.

Similarly, flow rate is highly significant in increasing SSC for the 5-25 min composite sample at 95% confidence level. All the cases showed p-values less than 0.05.

Figure 48 shows the regression fits of SSC and mass load of the 5-25 min composite samples for the scenario of an overlaying water depth of 46 cm.

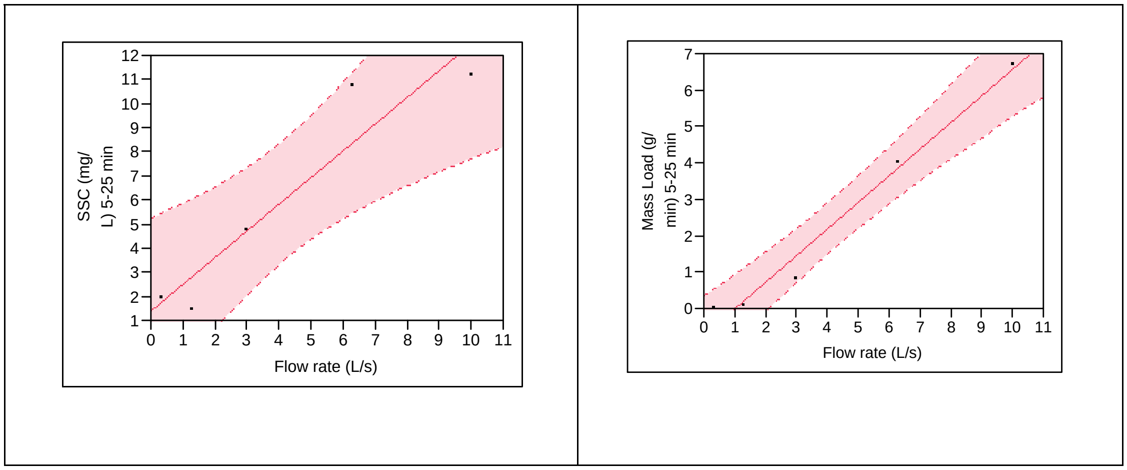

Figure 48. Simple linear regression fits of SSC and mass load of the 5-25 min composite samples for the scenario of an overlaying water depth of 46 cm.

6.2.5 *Effect of Overlaying Water Depth on the Reduction of Sediment Scour – Statistical Analysis*

The overlaying water depth was shown to be highly significant to the reduction of sediment scour. Figure 49 and 50 show SSC as a function of overlaying water depth for 0-5-min and 5-25-min composite samples, respectively; the SSC is plotted by flow rate using a logarithmic scale.

SSC decreases exponentially as a function of the overlaying water depth. However, the SSC reduction rate is so high from 10 to 24 cm below the outlet that a simple exponential regression would under-predict the scour rate at shallower depths.

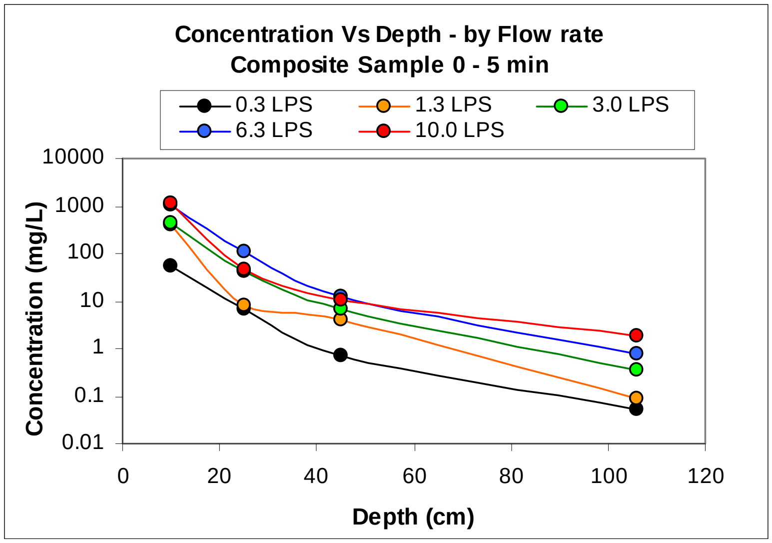

Figure 49. Suspended sediment concentration versus overlaying water depth, plotted by flow rate. Results for the 0-5-min composite samples.

At the 6.3 L/s flow rate (Figure 49), for example, an SSC of about 1045 mg/L was measured when an overlaying water depth was only 10 cm but decreased to about 3.0 mg/L when the overlaying water depth was 106 cm. This represents a reduction of almost 350 times when the water depth increased by about 100 cm.

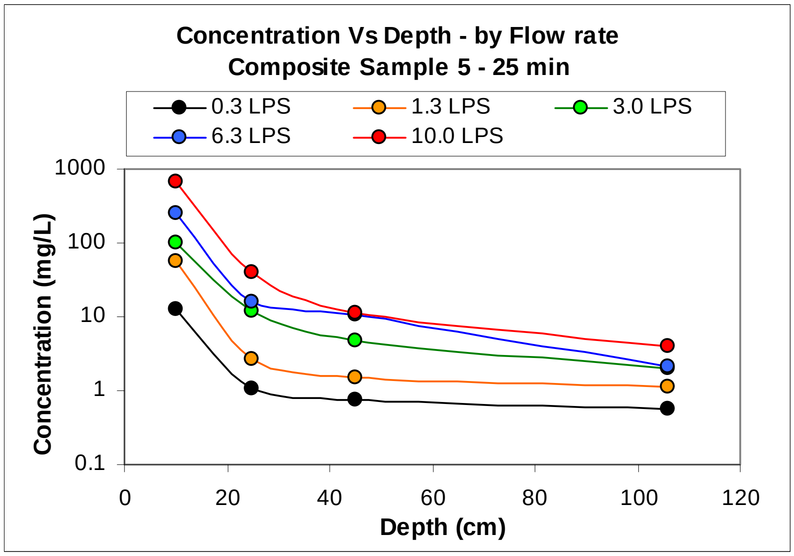

Figure 50. Suspended sediment concentration versus overlaying water depth, plotted by flow rate. Results for the 5-25-min composite samples.

A regression model with transformed variables was used to determine the significance of the overlaying water depth on the reductions of SSC. The transformation was required to normalize the data and to be able to fit both high and low SSCs simultaneously. The regression equation with transformed variables is given as:

$$\ln(SSC) = b_o + b_1\left(\frac{1}{H}\right), \qquad \text{Equation 30}$$

where *SSC* is the Suspended Sediment Concentration (mg/L), *H* is the overlaying water depth (cm), and b_o and b_1 are constants.

Figure 51 shows the experimental data and fitted regression line with a 95% confidence interval and the ANOVA table results for the 0-5-min composite sample at 3.0 L/s flow rate.

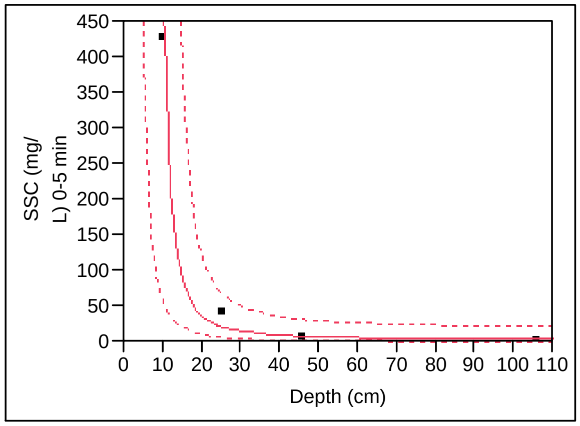

Term	Estimate	Std Error	t Ratio	Prob>|t|
Intercept	0.9462213	0.432386	2.19	0.1601
Recip(Depth (cm))	53.031859	7.841624	6.76	0.0212*

Figure 51. Experimental data and fitted regression line with a 95% confidence interval and the ANOVA table results for the 0-5 min composite sample at 3.0 L/s flow rate.

In all the cases, the overlaying water depth was shown to be highly significant in the reduction of SSC at the 95% confidence level.

Another analysis was performed with a one-way ANOVA and Bonferroni t-test for paired comparisons on the *Log(SSC)* values by overlaying water depth for both 0-5 min and 5-25 min composite samples. The transformation of the SSC was necessary to normalize the samples. Considering that only one sample was taken for each combination flow rate-overlaying water depth, sub-samples were created by combining all the SSC data by depth, including the entire flow rate range in each sub-sample. Figure 52 and 53 show the boxplots of *Log(SSC)* and *Log(Mass Load)*, respectively, with connected means and the paired comparison plots. SSC is significantly reduced as the overlaying water increases.

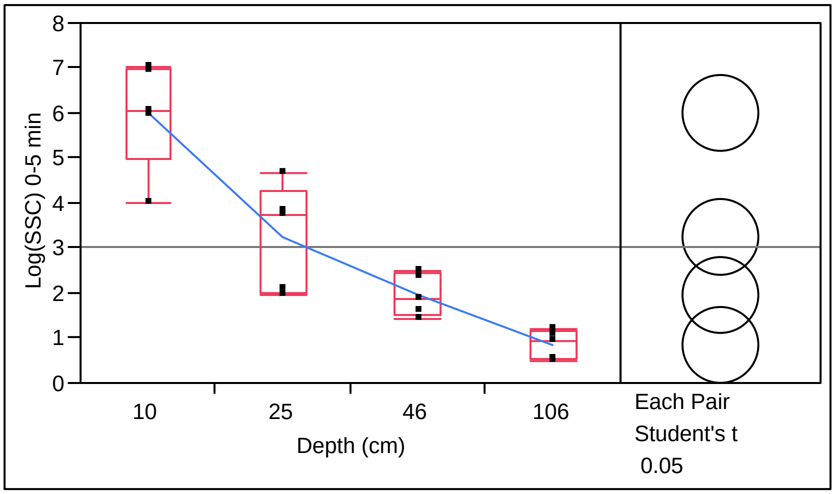

Figure 52. One-way ANOVA with Bonferroni t-test for paired comparisons analysis of overlaying water depth affecting Log(SSC) for the 0-5 min composite samples.

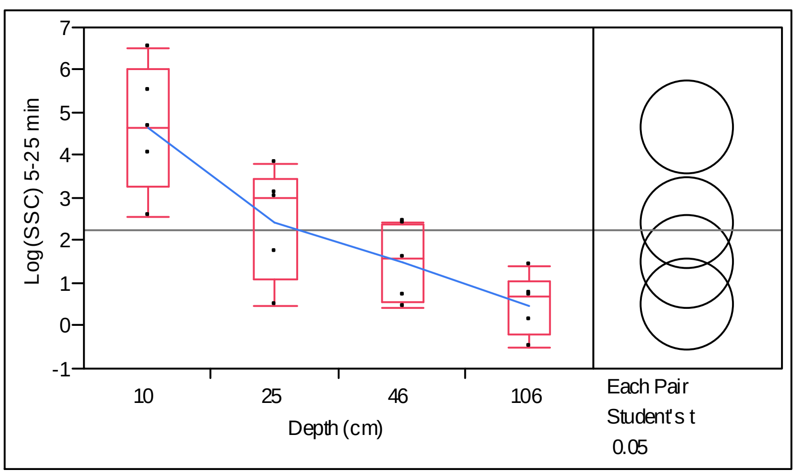

Figure 53. One-way ANOVA with Bonferroni t-test for paired comparisons analysis of overlaying water depth affecting Log(SSC) for the 5-25 min composite samples.

6.2.6 *Total Scoured Sediment Mass*

The total scoured sediment mass time series was based on the mass-flux rate. This sediment-mass time series was calculated for several particle size ranges and for the total scoured mass. The particle size ranges were: < 45, 45-150, 150-250, 250-425, 425-1200, and 1200-2000 μm. Each scour-mass time series lasted a total of 125 min, with five flow rate increments every 25 min. The flow rates examined were 0.3, 1.3, 3.0, 6.3, and 10 L/s.

Figure 54 to 57 show the scoured sediment mass time series categorized by particle size range for all tests. The flow rate is specified by a vertical dashed line plotted every 25 min. Figure 54 shows that particles as large as 1200 μm were detected in the effluent at flow rates as low as 0.3 L/s. However, the sediment mass of particles in the range of 250 to 1200 μm is less than 0.4 g over 75 min of flow. This mass may be associated with the initial impact in the first 5 min of flow. Notice that for particles as large as 4750 μm, the scoured sediment mass increased considerably when the flow rate increased to 6.3 L/s.

For any flow rate tested (up to 10 L/s), particles greater than 1200 μm were not scoured when the overlaying water depth was 25 cm. However, particles within a size range of 425 to 1200 μm were scoured at 3.0 L/s (Figure 55).

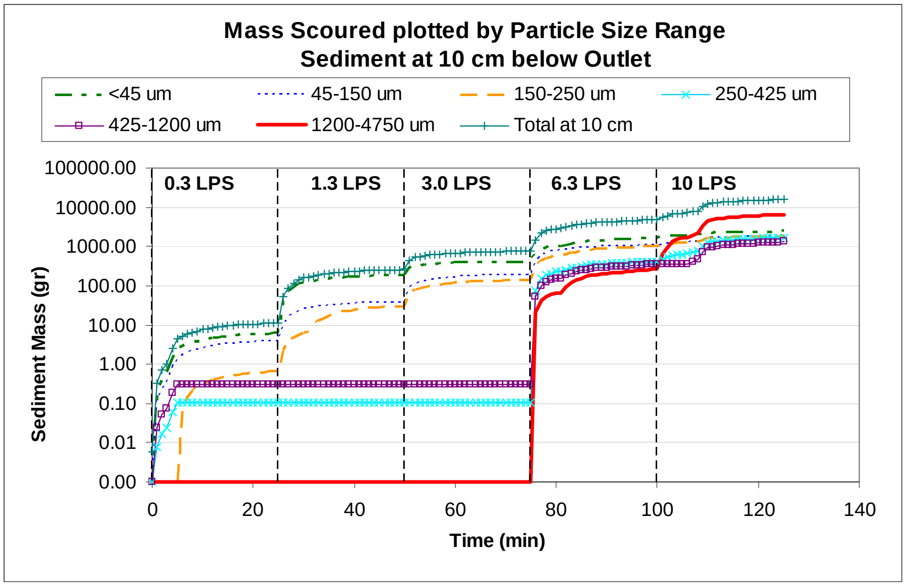

Figure 54. Sediment mass scoured by particle size range for all the scour tests performed. Overlaying water depth of 10 cm.

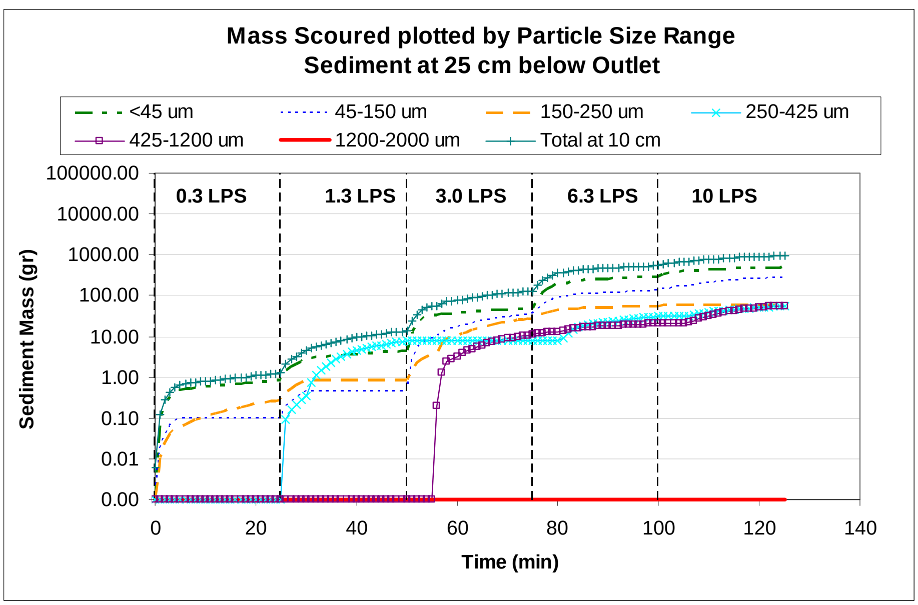

Figure 55. Sediment mass scoured by particle size range for all the scour tests performed. Overlaying water depth of 25 cm.

At 46 cm below the outlet (Figure 56), no particles larger than 1200 µm were scoured at flow rates up to 10 L/s. Particles in the size range of 425-1200 µm were scoured at 10 L/s. Particles smaller than 425 µm were also scoured at 1.3 L/s flow rate.

At 106 cm below the outlet (Figure 57), only particles up to 45 µm were scoured, with a mass of 135 g over the 125 min duration of the test. However, even including particles up to 150 µm, their scour mass was very small (less than 0.001 g).

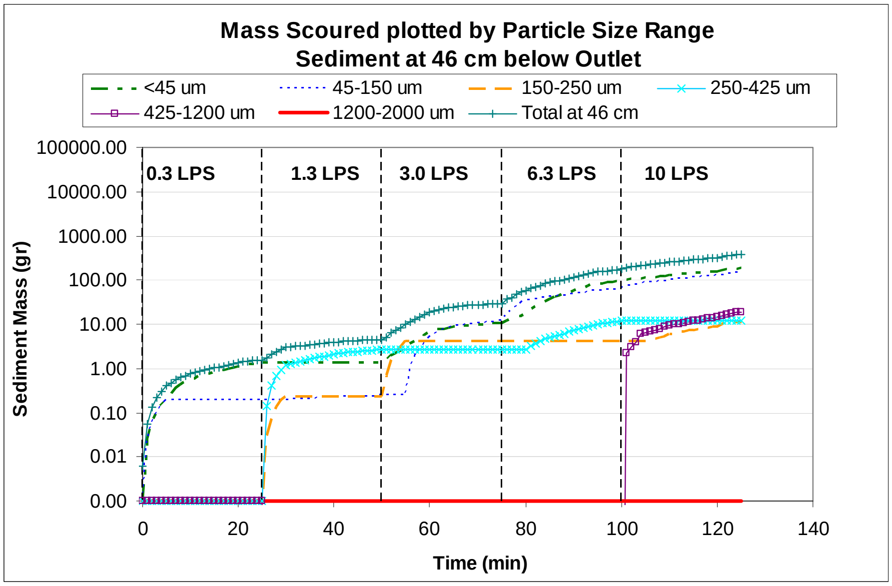

Figure 56. Sediment mass scoured by particle size range for all the scour tests performed. Overlaying water depth of 46 cm

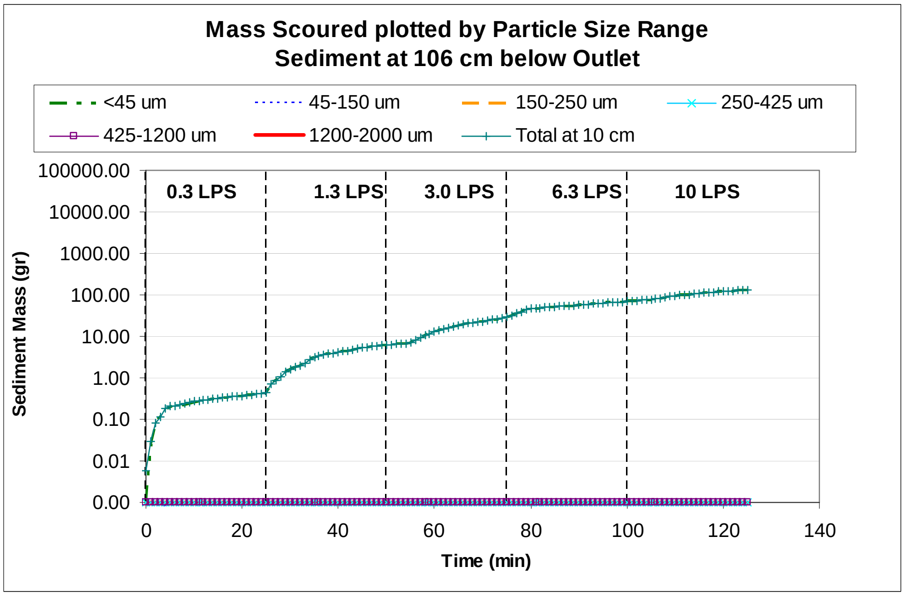

Figure 57. Sediment mass scoured by particle size range for all the scour tests performed. Overlaying water depth of 106 cm

The total scour-mass time series presented in Figure 58 shows that an increase in the overlaying water depth results in a significant reduction of the scoured mass of sediment. With an overlaying water depth of 10 cm, the maximum scoured mass, after 125 min, was about 16 Kg. The scoured particles were all smaller than 4750 µm. This scoured mass is equivalent to a scour depth of about 0.9 cm in the catchbasin. In contrast, with an overlying water depth of 25 cm, the total scoured mass, after 125 min, was reduced to less than 1 kg (930 g), which is about 17 times less than that observed with the 10 cm water depth. With an overlaying water depth of 46 cm, the total scoured mass was further reduced to only 360 g in the 120 min period of flow. With a 106 cm water depth, the total scoured mass was reduced even further to only 90 g during the 125 min test. At 106 cm below the outlet, only particles smaller than 45 µm were detected in the effluent water.

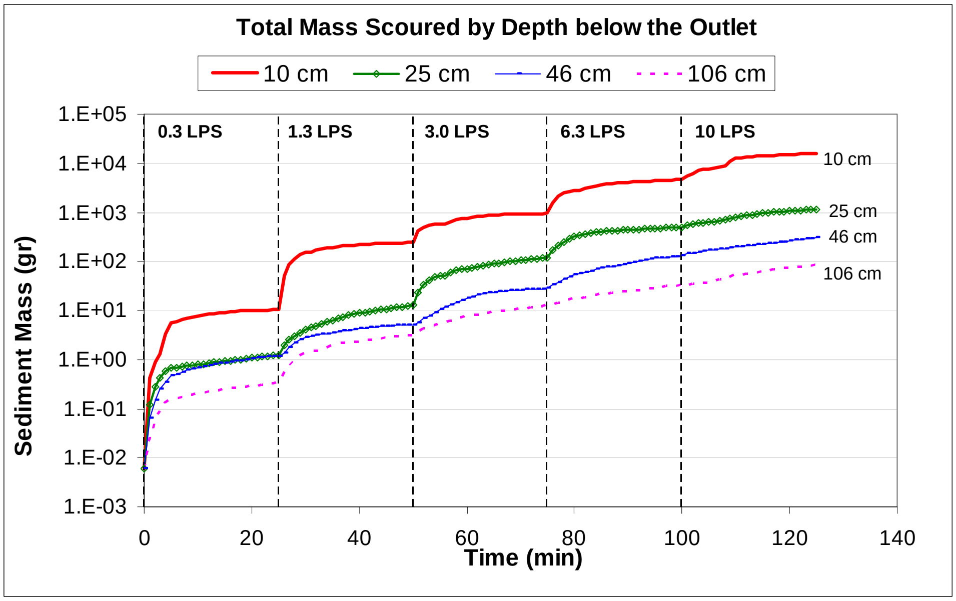

Figure 58. Total sediment mass scoured by water depth over the sediment for all the scour tests.

Regression analyses were conducted to examine the effects of overlaying water depth and the scoured sediment mass. The depth of the water was found to be a significant factor, with a highly significant p-value of 0.006. A similar conclusion was also found by Avila et al. (2007) with CFD modeling. These results show that the overlaying water depth over the sediment significantly contributes to a reduction in scour potential. Moreover, even though armoring also contributes to a reduction in scour, its benefits depend on the overlaying water depth. As the overlaying water depth increases, the armoring formation decreases, because the sediment is less exposed to scour. However, at shallow overlaying water depths, the armoring layer plays an important role in reducing the scour potential. If no armoring mechanism is present at shallow overlaying water depths, the sediment scour will be considerably higher.

6.3 Experimental Scour Tests with Homogeneous Sediment Material for CFD Model Calibration and Validation

Even though a sediment mixture includes different sediment particle sizes, it was not possible to identify the scour effect on each particle size independently, as only SSC measurements were made for these calibration and validation tests. Due to the limitations of the CFD model, only a single particle size (D_{50}) could be modeled. It was therefore necessary to run tests with the full-scale physical model using a homogenous sediment material (with D_{50} = 180 μm). Data were collected from two tests, each one at a constant flow rate of 10 L/s for 30 min. In the first tests, the sediment surface was located at 24 cm below the outlet, and in the second test, at 35 cm below the outlet.

Composite samples were collected at the influent and effluent at 3-min time intervals, which is a total of 40 3-min composite samples. Suspended Sediment Concentration (SSC) was measured for each composite sample; however, no sieve analyses were performed as the Particle Size Distribution (PSD) was fairly homogeneous. Only a 0.45 μm micro-pore filter was used to capture particulates. The data collected from these experiments were used to calibrate and validate the scour-sedimentation model implemented in the CFD model using the software package Flow-3D.

Figure 59 shows sediment placed at 24 cm below the outlet, as well as a top view of the sediment bed before performing the test.

Figure 59. Placement of sediment and measurement of initial depth below the outlet.

Figure 60 shows the full-scale physical model while a scour test is performed with the homogeneous sediment material.

Figure 60. Full-scale physical model while performing scour tests on sediment with homogeneous particle size. See the USGS/Decaport cone water sample splitter and the 1.0 L sampling bottles.

The initial and final stages of the sediment scour test, with sediment initially at 24 cm below the outlet, can be seen in Figure 61. In the left figure (initial stage of the test), the sediment level in the sump is completely horizontal. In the right figure (final stage of the test after 30 min of continuous flow), it is possible to see the scoured sediment surface.

Figure 61. Initial (left) and final (right) stages of scour test with homogeneous sediment material. Test performed with sediment at 24 cm below the outlet or overlaying water depth of 24 cm.

In order to evaluate the scour pattern at both 24 and 35 cm below the outlet, a rope was placed on the sediment surface to create an elevation contour to differentiate the location of erosion and sedimentation. Figure 62 and 63 show the elevation contour of the test at 24 and 35 cm below the outlet, respectively.

In these figures, it can be seen that the sediment scour is concentrated at the center of the sump at both elevations. When the sediment surface started at 24 cm below the outlet, a hole of 8 cm deep was measured after 30 min of continuous flow. In contrast, when the sediment surface started at 35 cm below the outlet, a hole of 3 cm deep was measured. During the hydrodynamic tests, it was observed that both the thickness and width of the rectangular water jet reduced as the vertical velocity increased by the effect of gravity. This suggests that if the distance between the water surface in the sump and the inlet is sufficiently high, the impact of a rectangular jet could be almost equivalent to a circular jet.

Also notice that a large amount of scoured mass, equivalent to the scour at the center of the sump, was located at the front sides of the sump in the direction of the flow. This occurs due to the effect of secondary currents that hit the walls of the sump and go down adjacently to the wall. This scour pattern was not observed during the scour tests with sediment mixture because the armoring layer protected the underlying sediment. The scour in the tests with sediment mixture was located in the center of the sump just below the plunging water jet.

On the other hand, with homogenous sediment material, not all the sediment that was scoured at the center and front sides of the sump left the catchbasin sump. A large portion of that sediment mass settled back to the sediment surface. This can be seen in locations where accretion occurred with +4 cm for the case of 24 cm water layers (Figure 62), and from +3 to +6 cm for the case of 35 cm water layers (Figure 63).

Finally, a symmetric pattern is observed in the contour levels for both tests at 24 and 35 cm below the outlet. Moreover, sediment scour and accretion occurred at the same locations in both tests, but with different scour masses. The accretion mostly occurred in an area surrounding the center of the sump in the same direction of the flow, indicating displacement of the sediment in the direction of the flow.

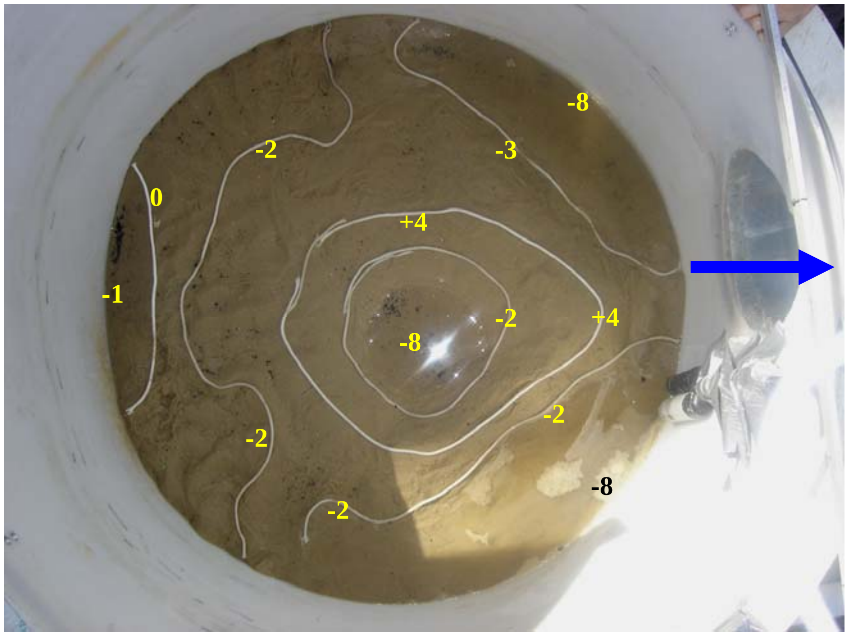

Figure 62. Final level contour lines of sediment surface after 30 min of continuous flow at 10 L/s flow rate. Test with homogenous sediment material at 24 cm below the outlet.

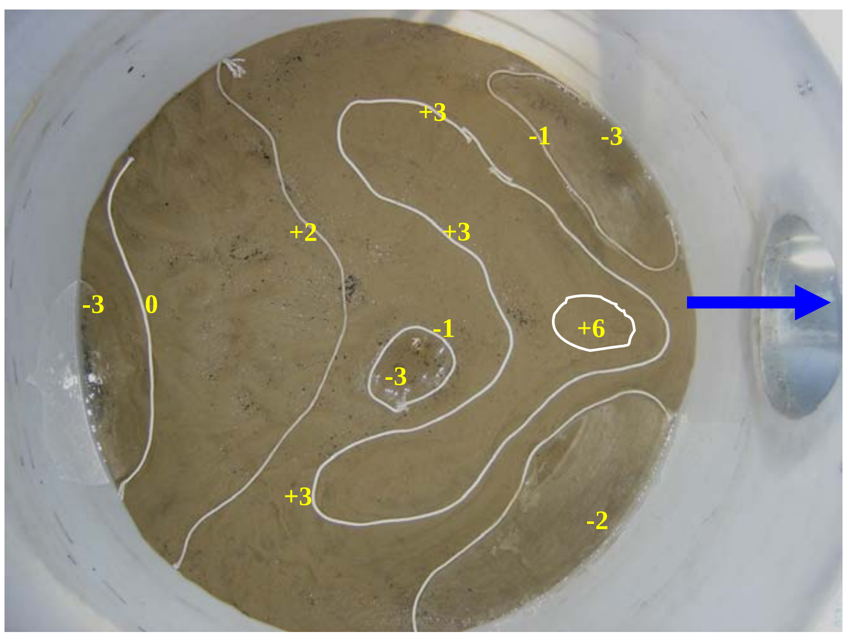

Figure 63. Final level contour lines of sediment surface after 30 min of continuous flow at 10 L/s flow rate. Test with homogenous sediment material at 35 cm below the outlet.

6.3.1 *Suspended Sediment Concentration (SSC) – Sediment with Homogeneous Particle Size*

Suspended Sediment Concentration (SSC) was measured from the composite samples taken at the influent and effluent of the catchbasin. The SSC at the influent was subtracted from the SSC at the effluent in order to obtain the net SSC discharged at the effluent. All the SSCs mentioned in this document are referred to the net SSC at the effluent, unless otherwise specified.

Table 16 shows the SSC obtained for tests with sediment at 24 and 35 cm below the outlet, 10 L/s flow rates, and with a 50-cm wide rectangular inlet.

Table 16. Experimental SSC of 3-min Composite Samples (Scour Tests with Sediment Material with Homogeneous Particle Size, Flow rate: 10 L/s, Overlaying Water Depth: 24 and 35 cm)

Composite Samples - Time Interval (min)	SSC (mg/L) at 24 cm below the outlet	SSC (mg/L) at 35 cm below the outlet
0 - 3	600	170
3 - 6	479	161
6 - 9	491	203
9 - 12	556	182
12 - 15	521	153
15 - 18	425	179
18 - 21	574	172
21 - 24	562	206
24 - 27	569	182
27 - 30	557	178

Initially, it was expected that the SSC magnitudes with homogeneous sediment material would have an exponential pattern similar to the one obtained with the sediment mixture, with high concentrations within the first minutes of flow and then substantial decreases for the remaining test time. However, the results showed that the SSC was approximately constant during the 30 min of continuous flow (Figure 64). This phenomenon is attributed to the absence of an armoring layer that protects the sediment from being scoured.

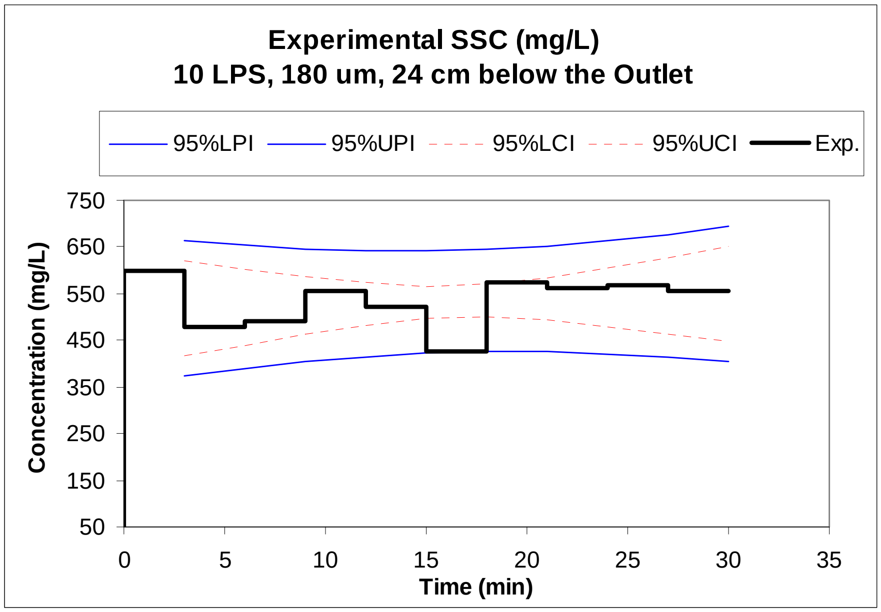

Figure 64. SSC time series of 3-min composite samples for scour tests with sediment of 180-µm particle size (homogeneous), 10 L/s flow rate, and overlaying water depth of 24 cm.

The velocity field caused by the plunging water jet continuously generates shear stresses on the sediment surface. Thus, if the critical shear stress of the sediment particles is not high enough to resist the acting shear stress, it will become suspended until a protection mechanism occurs to stop or mitigate the scour. In this case, the only protection mechanism was the overlaying water depth.

SSC will decrease only when the overlaying water depth is high enough to dissipate the eroding energy of the velocity field and reduce the acting shear stress on the sediment surface. These experimental results showed that 30 min of continuous flow at

10 L/s was not enough time to increase the overlaying water depth (creating a hole in the sediment surface) enough to significantly reduce the SSC generation.

In contrast, two protection mechanisms occurred when performing the tests with the sediment mixture: the overlaying water depth and an armoring layer. In this case, the overlaying water depth protects the sediment surface from the first impact of the plunging water jet. However, the plunging jet still has enough energy to scour the sediment material right below it. Then, due to high shear stresses generated by the first water impact, all particle sizes (large and small) are suspended. Consequently, a *"washing machine effect"* occurs with the suspended sediment as the plunging jet retreats up because of the air buoyancy. The washing machine effect consists of the preferential suspension of fine material, leaving a layer of large particles on the sediment surface, forming the armoring. Moreover, a portion of those large particles is transported with the flow as bed load, being located in the front of the catchbasin, thus protecting the underlying sediment material in those locations.

In order to determine if the SSC is statistically constant, the experimental SSC were evaluated with regression analyses, including ANOVA. Table 17 shows the statistical output which shows that the coefficient of the predictor "time" is not significant with a p-value of 0.601 and that the constant term is highly significant. This proves that the experimental SSC can be treated as a sample with a mean and standard deviation. The mean SSC was 533 mg/L, and the standard deviation was 53 mg/L.

Table 17. Statistical Output to Reject a Pattern on the Experimental SSC (mg/L) for the Calibration: Homogeneous Sediment Material with D_{50} = 180 µm, Overlaying Water Depth of 24 cm, and 10 L/s Flow Rate

Regression Analysis: SSC (mg/L) Calib. versus Time

```
The regression equation is
SSC (mg/L) Calib. = 515 + 1.12 Time

Predictor    Coef  SE Coef      T      P
Constant   514.97    38.16  13.49  0.000
Time        1.117    2.050   0.54  0.601

S = 55.8622   R-Sq = 3.6%   R-Sq(adj) = 0.0%

Analysis of Variance
Source          DF     SS    MS     F      P
Regression       1    926   926  0.30  0.601
Residual Error   8  24965  3121
Total            9  25891
```

The evaluation of residuals showed the assumption of normality, zero mean, and random pattern were satisfied (Figure 65).

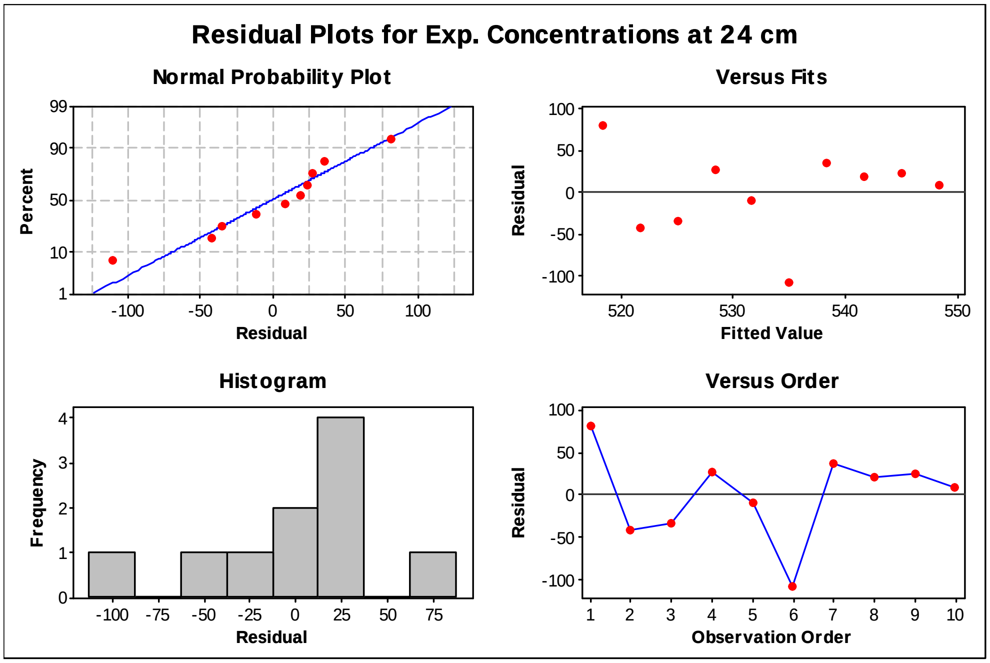

Figure 65. Probability plot of residuals, residuals versus fits, histogram of residuals, and residuals versus order. Calibration: homogeneous sediment material with D_{50} = 180 µm, overlaying water depth of 24 cm, and 10 L/s flow rate.

The same analysis was performed using the experimental SSC values obtained from the tests at 35 cm below the outlet (Figure 66). Table 18 presents the statistical output which shows that the coefficient of the prediction variable (time) is not significant with a p-value of 0.47. The constant term is highly significant.

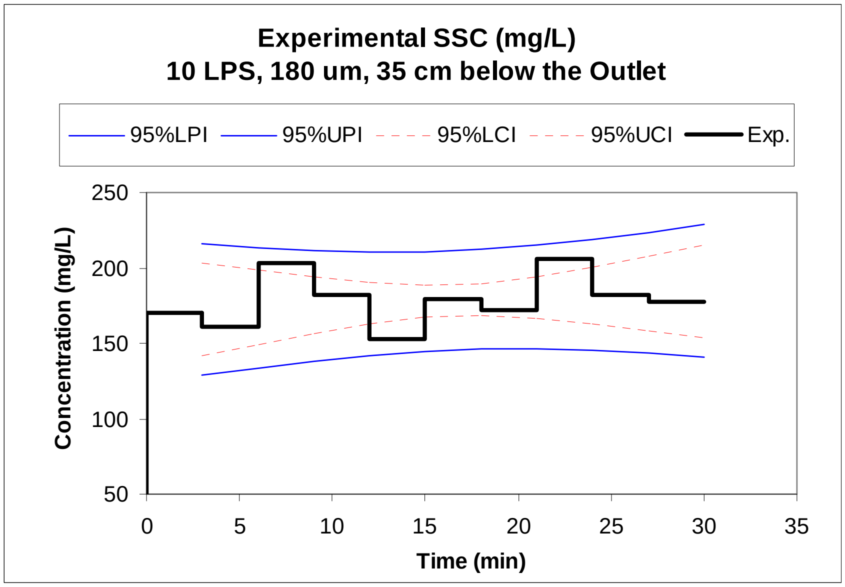

Figure 66. SSC time series of 3-min composite samples for scour tests with sediment of 180-µm particle size (homogeneous), 10 L/s flow rate, and overlaying water depth of 35 cm.

Table 18. Minitab Output to Reject a Pattern on the Experimental SSC (mg/L) for the Validation: Homogeneous Sediment Material with D_{50} = 180 µm, Overlaying Water Depth of 35 cm, and 10 L/s Flow Rate

Regression Analysis: SSC (mg/L) Valid. versus Time

```
The regression equation is
SSC (mg/L) Valid. = 171 + 0.461 Time

Predictor     Coef  SE Coef      T      P
Constant    170.89    11.51  14.85  0.000
Time        0.4613   0.6183   0.75  0.477

S = 16.8489   R-Sq = 6.5%   R-Sq(adj) = 0.0%

Analysis of Variance
Source          DF      SS     MS     F      P
Regression       1   158.0  158.0  0.56  0.477
Residual Error   8  2271.1  283.9
Total            9  2429.1
```

The residual plots are shown in Figure 67, which shows that the equation satisfies the residual assumptions.

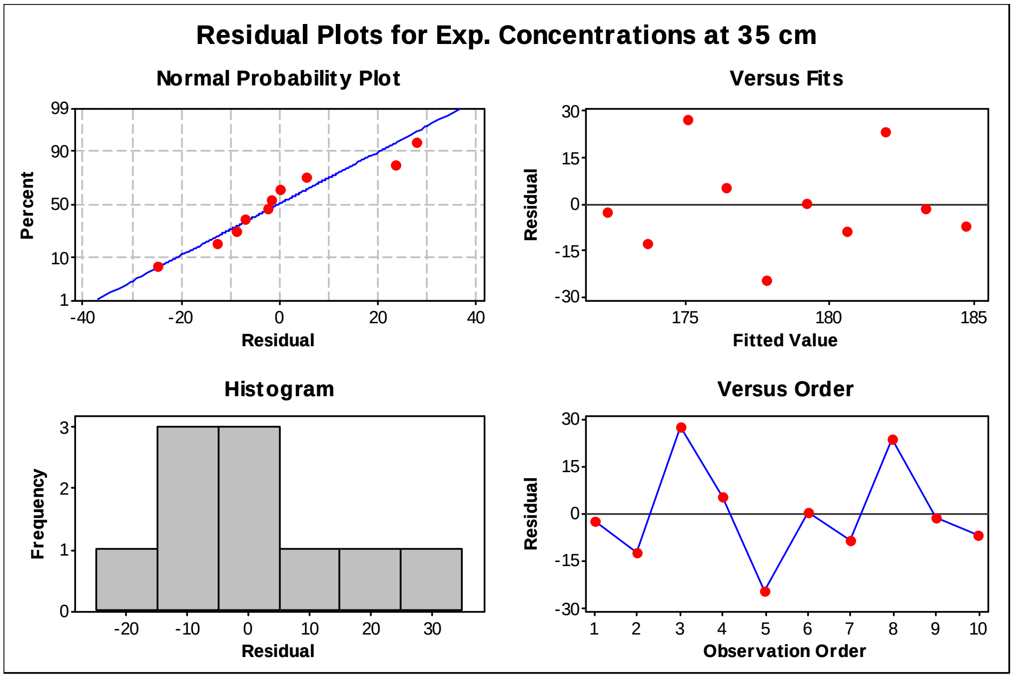

Figure 67. Probability plot of residuals, residuals versus fits, histogram of residuals, and residuals versus order. Validation: homogeneous sediment material with D_{50} = 180 µm, overlaying water depth of 35 cm, and 10 L/s flow rate.

6.3.2 *Total Scoured Sediment Mass – Homogeneous Sediment Material*

Total scoured sediment mass was determined based on the SSC obtained from the experimental data. Figure 68 shows the cumulative scoured sediment mass loss for both tests at 24 and 35 cm below the outlet. The figure shows that, consistent with the SSC magnitudes, the cumulative mass loss has a linear pattern. The maximum mass loss after 30 min of continuous flow with sediment 24 cm below the outlet was 9.6 Kg. In contrast, with sediment 35 cm below the outlet, the total mass loss was 3.2 Kg, which represents almost a 70% reduction of the total mass loss.

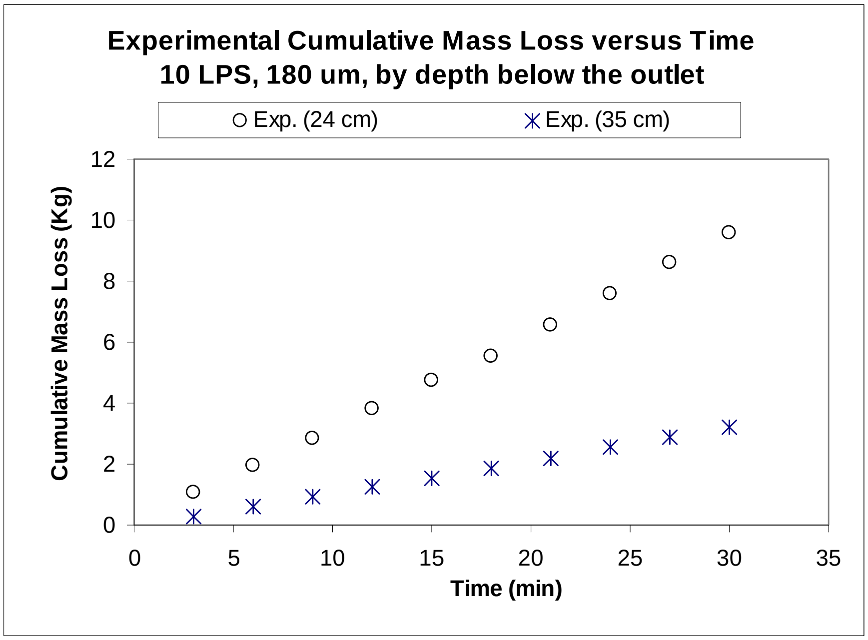

Figure 68. Experimental cumulative mass loss (Kg) based on the 3-min composite samples of scour tests with sediment with homogeneous particle size of 180 µm. Flow rate: 10 L/s.

CHAPTER 7

COMPUTATIONAL FLUID DYNAMIC (CFD) MODELING – HYDRODYNAMICS AND SEDIMENT SCOUR MODELS

CFD numerical analysis is a useful tool to evaluate the hydrodynamics in stormwater treatment devices. However, it also must be stated that the results obtained from numerical analysis contain some level of uncertainty associated with simplifications of the problem, assumption of models and parameters, and limitations of the models, among other reasons. This limitation becomes more critical when no experimental data is available or no similar simulations have been performed for comparison or validation. This is especially critical when several physical phenomena are involved in the analysis, or new sophisticated geometries and designs are proposed.

A catchbasin sump, the object of this research, had a surprisingly high level of complexity for modeling. An extensive optimization of the mesh resolution in the plunging water jet zone, a variation of turbulent mixing length for the entire control volume, high turbulent flow near the surface and low turbulent flow near the bottom of the sump, air entrainment, buoyancy, and sediment scour all simultaneously added to the complexity of the model, the computational requirements, and the uncertainty of the numerical results.

Therefore, before proceeding with simulations of the sediment scour scenarios and validation of the results with the experimental data, it is fundamentally necessary to ensure the correct hydrodynamic behavior in the control volume, considering all the relevant phenomena and parameters. Obtaining valid numerical results of sediment concentration at the outlet is not enough evidence to believe that the hydrodynamics in the control volume are correct.

7.1 Error Tolerance and Statistical Approach

It is expected that some level of error is associated with the comparison of experimental and simulated results. Errors in physical experimentation are mostly associated with the random nature of the scour phenomenon being evaluated and any human error that may occur during the measurements. However, human errors should be minimal during these tests, because controlled experiments were conducted at all times. Errors obtained with Computational Fluid Dynamic (CFD) modeling are mostly associated with approximation and simplifications of equations, numerical methods for solution, resolution of the mesh, and estimation of parameters, among other causes.

The error tolerance and statistical approach for comparison of experimental and simulated results were focused on two types of tests: hydrodynamic and scour tests.

7.1.1 *Hydrodynamic Tests*

The similarity of the experimental and simulated velocity data sets was gauged by a visual comparison of the experimental and simulated normal probability plots (two-in-one plot), especially inspecting the means and the standard deviations of both data sets.

This single procedure was applied due to the difficulty of the calibration and validation of the CFD model.

Physical experimentation of the hydrodynamics in the catchbasin sump consisted of the measurements of velocity vectors at 155 locations distributed in the entire water domain contained in the sump. Thirty instantaneous velocity measurements were taken at each location. Therefore, it was not expected to fit the mean velocities in all 155 locations but to achieve a fairly good level of similarity in a large portion of them.

7.1.2 *Scour Tests*

The error tolerance for the scour tests results was stricter than for the hydrodynamic tests, considering that the response variable, Suspended Sediment Concentration (SSC), was compared only at the effluent. Based on experimental data collected from the scour tests with a homogeneous sediment material, a percentage of error tolerance was determined by calculating the difference between the observed SSC and the prediction interval associated with the 95% confidence level. This calculation was possible because the SSC did not show any statistical evidence of having any pattern within the 30-min time period of the tests. The maximum and average errors were determined as 38% and 18%, respectively. Therefore, it was expected that the simulated results and the regression models would not exceed the maximum percentage of error. Figure 69 shows the normal probability plots of the expected percentage of error.

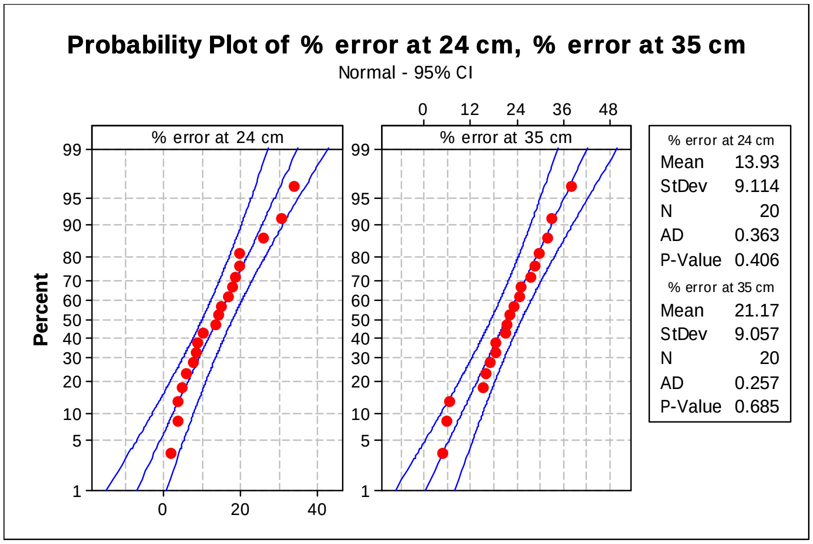

Figure 69. Normal probability plot of the percentage of SSC error obtained from experimental data with a homogeneous sediment material of D_{50} = 180 µm. Overlaying water depth of 24 cm (left) and 35 cm (right).

Additionally, standard deviations of 16 and 54 mg/L were found from the experimental samples collected at 35 and 24 cm below the outlet, respectively. This suggests that greater error percentages may be expected for concentrations lower than about 10 mg/L because at this range, the SSC magnitudes are comparable to the random variation associated with the scour phenomenon. However, considering that the range of the measured and calculated SSCs was between 0 and 1500 mg/L for the range of conditions described in previous chapters, the error at the low concentrations should not constitute major problems in the estimation of SSC.

7.2 Calibration of Hydrodynamics of the 3-Dimensional (3D) CFD Model

The calibration consisted of the estimation of relevant parameters of the model to obtain similar simulated and experimental results under a scenario of 10 L/s flow rate.

The parameters involved in the calibration were the turbulent mixing length, the air entrainment coefficient, and the air bubble diameter. The calibration was conducted under steady state conditions by analytically comparing the simulated and experimental velocities at all 155 locations distributed in the control volume.

7.2.1 *Description of the Calibration Process*

One issue of concern in the calibration process is the desired acceptable level of similarity between the simulated and experimental data. Typically, when the data is a function of time, the calibration is based on the comparison between a time series of single experimental values and the simulated time series results. However, under steady state conditions, several velocity measurements were taken at a single point, so the comparison of a single value (mean value) is not representative; the probability distribution of the data should be analyzed in order to consider the range of the velocity magnitudes. The experimental data showed that the velocities under turbulent flow and steady state are normally distributed. Therefore, the complete experimental sample at each point was considered for calibration.

One of the most time-consuming stages of the 3D-model calibration was the creation of the calculation mesh. It was necessary to find a balance between a high mesh resolution for accuracy and a low mesh resolution to reduce the computational time. The resolution of the mesh at the end of the free-falling jet, for example, had to be very high to capture the thickness of the water jet; however, a coarse mesh was applied near the bottom of the sump. This process was conducted manually until a reasonable elapsed time was reached without significantly sacrificing accuracy. The reduction of elapsed time was critical for calibration, considering that several scenarios needed to be tested and each one could take about 24 hours for a 300-sec simulation in addition to the time for analysis and modifications.

It was expected that the amount of air entrainment due to the plunging water jet was not high enough to produce a significant buoyancy effect in the flow, and the attenuation of the plunging water jet was mainly due to the impact and turbulent dissipation. However, the physical experimentation showed that the amount of air entrainment was high enough to produce significant density variations and buoyancy in the control volume. Bohrer et al. (1998) evaluated the air entrainment coefficients for developed and undeveloped free-falling water jets, finding an average estimate of 0.5 for undeveloped free-falling jets, which was the case for this research. The final calibration was achieved using an air entrainment coefficient of 0.5. The air bubble size under turbulent conditions is an inverse function of the turbulent energy dissipation, which is also a function of the turbulent kinetic energy. Hence, the greater the turbulent kinetic energy, the smaller the air bubble size. However, the model has the limitation of considering only an average bubble size. This calibrated bubble diameter size was 0.1 cm.

An initial calibration was achieved by modifying the turbulent mixing length, which is the characteristic length-scale of the energy-containing eddies (Flow Science 2007). This parameter controls the turbulence energy dissipation. The model defaults to 7% of the smallest domain dimension. However, this value varies in space and time, depending on the characteristics of the flow and geometry of the domain. Therefore, it was necessary to calibrate a value that represented the most significant flow conditions.

In this case, the turbulent mixing length was controlled mainly by the impacting zone, where the plunging jet affects the control volume in the catchbasin. A turbulent mixing length of 0.5 cm was the optimum calibrated value. This parameter was the most sensitive during the calibration. However, with the use of the turbulent mixing length, the model required customization of the air entrainment model to include changes in density and air escape from the water surface. The time demanded for this customization was long and did not result in satisfactory results.

A new attempt to calibrate the 3D model was conducted using the full transport equation to compute the dissipation. This does not depend on a constant turbulent mixing length. This alternative required more computational effort, especially in a 3D simulation. However, it does automatically consider the change in density and air escape from the water surface. The disadvantage of using this alternative was that the full transport equation subroutine was incompatible with the default scour model included in the software package. This was because the air concentration was already considered as the secondary phase, and no additional phases, such as the sediment, could be added to the model.

Nevertheless, the creation of a customized scour model coupled to the full transport equation model for the hydrodynamics was much more feasible than creating a customized air entrainment model. The software package Flow-3D could treat the packed and suspended sediment as scalars on each cell with density and drag coefficient properties which are internally considered by the full transport equation. Moreover, Flow-3D includes an advection-dispersion model to calculate the transport of suspended sediment in the control volume.

Figure 70 shows the 3D simulation of the calibrated model presenting velocity magnitudes (left) and density magnitudes (right). The velocity of the free-falling jet impacts the water surface at about 3.0 m/s, and the velocity magnitude is reduced down to about 1.0 m/s at only a few centimeters below the surface. The turbulent dissipation and the buoyancy effect caused by the air entrainment contribute to this reduction.

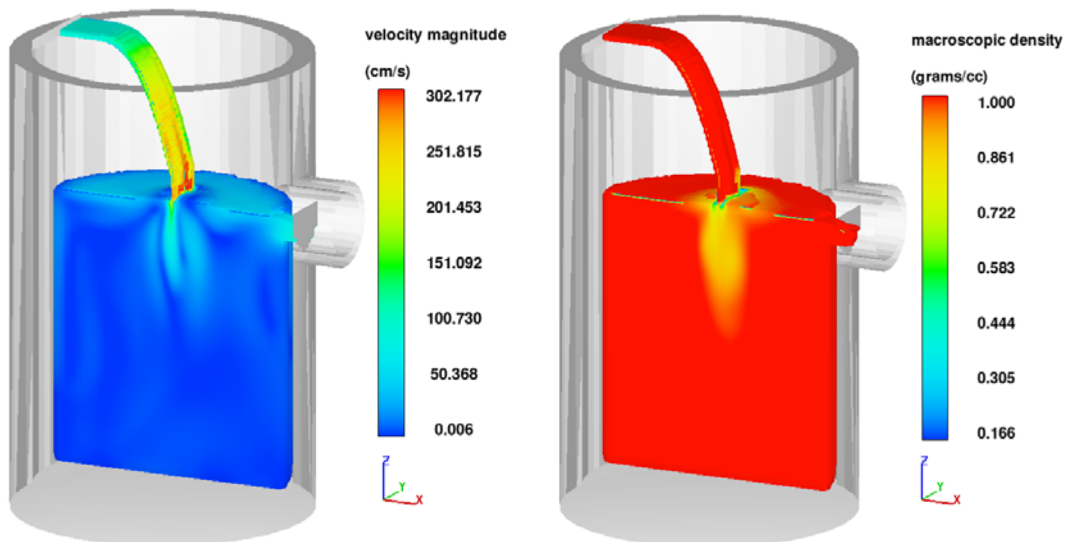

Figure 70. Scenario of rectangular inlet with a 10 L/s flow rate. Velocity magnitude in cm/s (left), and macroscopic density in gr/cm3 (right).

The calibration process was based on comparison of the normal probability plots of simulated and experimental data. Figure 71 through 73 show the comparison between simulated and experimental velocities Vx, Vy, and Vz for all the 31 points located on the layer at 76 cm below the outlet. These figures show that the simulated mean velocities are close to the experimental values in all cases. Moreover, the simulated values are also normally distributed. However, in some cases, the computational model is not capable of reproducing the velocity variation found in the experimental data. The slopes of the simulated probability plots are typically equal to or greater than the experimental data slopes, which shows that the simulated velocities fall within the range of the experimental values.

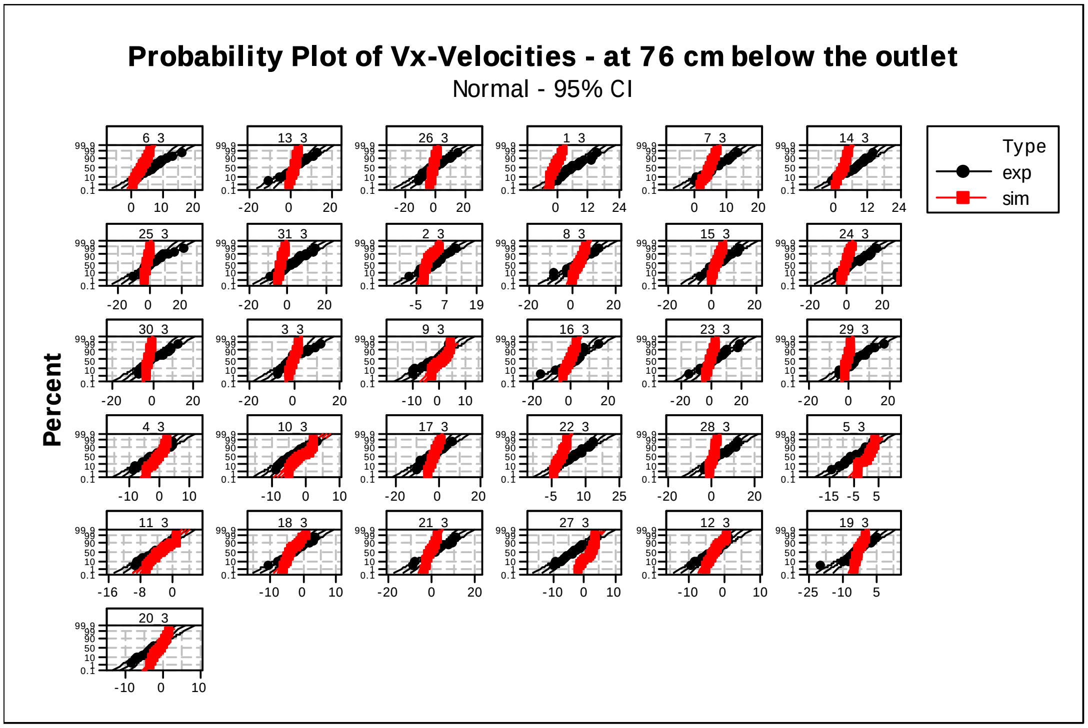

Figure 71. Probability plots of experimental and simulated v_x-velocities on 31 points located at 76 cm below the outlet (scenario of 50-cm rectangular inlet at 10 L/s flow rate).

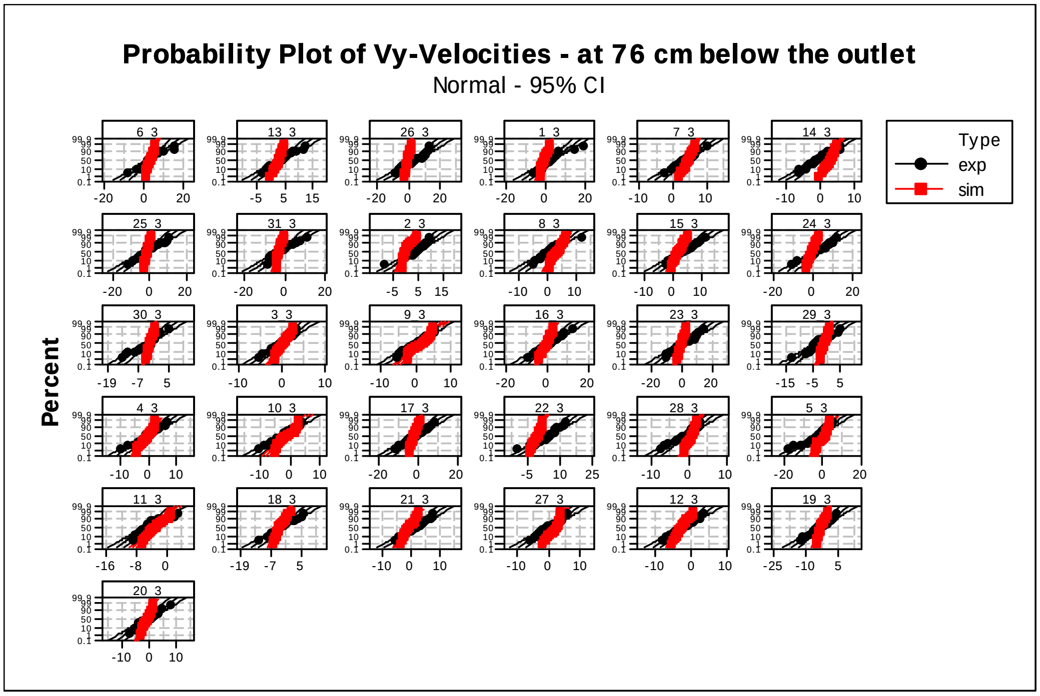

Figure 72. Probability plots of experimental and simulated v_y-velocities on 31 points located at 76 cm below the outlet (scenario of 50-cm rectangular inlet at 10 L/s flow rate).

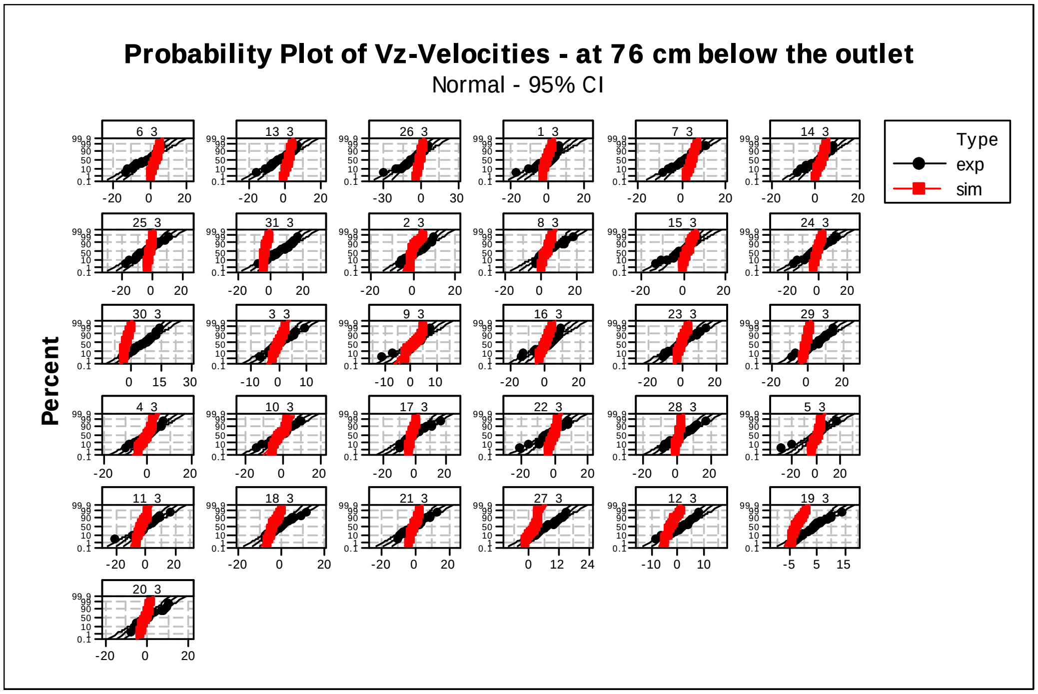

Figure 73. Probability plots of experimental and simulated v_z-velocities on 31 points located at 76 cm below the outlet (scenario of 50-cm rectangular inlet at 10 L/s flow rate).

7.2.2 *Two-Dimensional (2D) Simplification for Sediment Scour Model*

A 2D simplification was required to evaluate sediment scour in order to reduce the elapsed time for each simulation. The calibration of the hydrodynamics with the 3D model required a simulation time of 300 sec for each scenario to ensure steady state in the control volume. This steady state is achieved when the flow rate at the effluent and the water volume in the domain stay approximately constant in time. The elapsed computational time for each simulation run was about 24 hours. Additionally, the time for analysis and parameter adjustment would add 12 hours to the process. When adding sediment scour to the hydrodynamics, in order to reach steady state in terms of sediment scour, each scenario would require about 30 min of simulation, depending on the flow rate, particle size, and depth of the sediment layer. For a 30-min simulation, the run time becomes 144 hours (or 6 days) for each scenario. Therefore, the number of test cases required for a complete scour analysis (40 cases) would be excessive.

A 2D simplification was needed to reduce the elapsed computational time. This simplification was based on the symmetry of the sediment surface obtained during the scour tests. Field tests showed that the sediment surface was symmetric with respect to the center line of the flow direction (Figure 74).

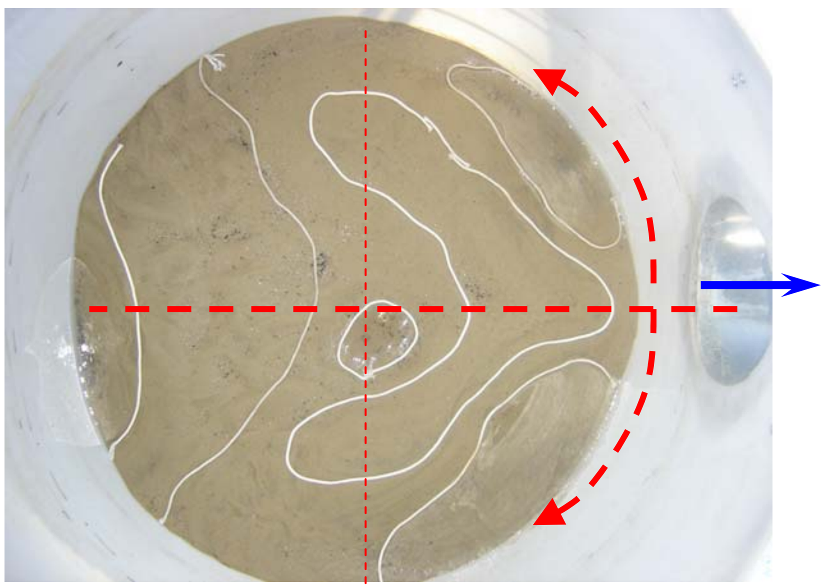

Figure 74. Symmetry of scored sediment surface.

The concentrations at the effluent were calculated as a function of the sediment mass loss. The CFD model calculates the total sediment mass in the control volume per unit width at each time interval. The depth associated with the sediment mass, using a bulk density of 1.7 g/cm^3 (measured in the laboratory), is multiplied by the area of the tank (116 cm in diameter) to calculate the sediment volume in the tank. This volume is transformed back to mass by using the bulk density to determine the remaining sediment mass in the control volume. The difference in mass at each time interval represents the sediment mass loss. Finally, the concentration at the effluent is calculated based on the flow rate.

7.2.3 *Calibration of Hydrodynamics of the 2-Dimensional (2D) CFD Model*

The 3D CFD model was adapted to a 2D CFD model. All the parameters calibrated in the 3D model were also used for the 2D model. The full transport equation model was also applied to take advantage of the air entrainment and density variation subroutines coupled to this model. However, the 2D model showed instability reflected in the drag coefficient in areas where air was trapped. Therefore, a customized drag coefficient (Equation 31) was implemented and adjusted during the calibration process. This drag coefficient is activated only in cells that contain air. Figure 75 shows the drag coefficient as a function of volume fraction of air.

$$DRG = \frac{1}{(1 - f_{air})}, \qquad \text{Equation 31}$$

where f_{air} is the volume fraction of air in cell.

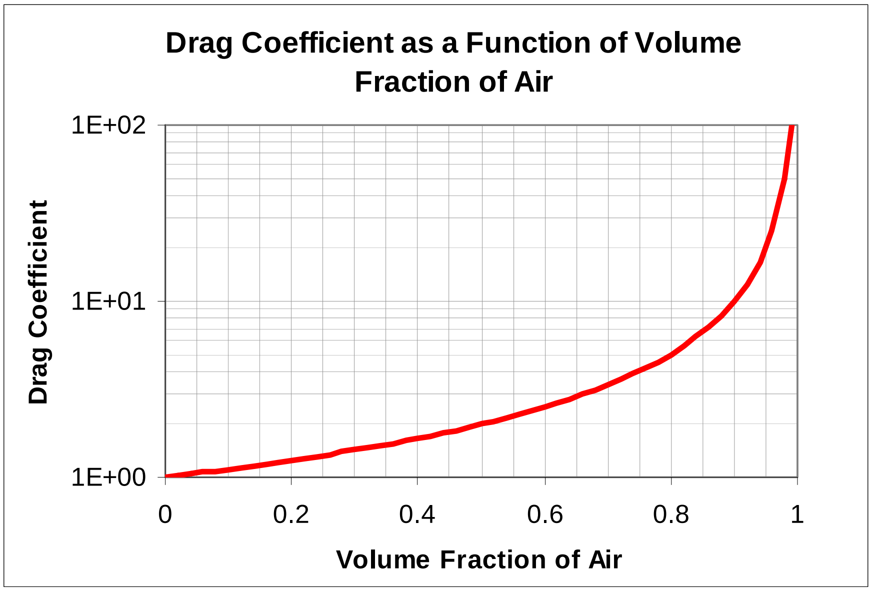

Figure 75. Drag coefficient as a function of volume fraction of air.

7.2.4 *Calibration at 10 L/s*

The calibration performed with the 10 L/s flow rate scenario consisted of determining the drag coefficient presented in Equation 31. Simulated velocities were compared to experimental velocities measured at the center line of the sump. The velocities were compared at 36 cm below the outlet, because the 3D calibration showed that the velocities at this depth were very sensitive to adjustments to the model. Figure 76 shows the velocity contours at a 10 L/s flow rate. The figure shows how the velocity of the plunging jet is rapidly reduced by turbulent dissipation and also by the ascending velocity caused by the presence of air in the control volume. These results were consistent with those obtained with the 3D model.

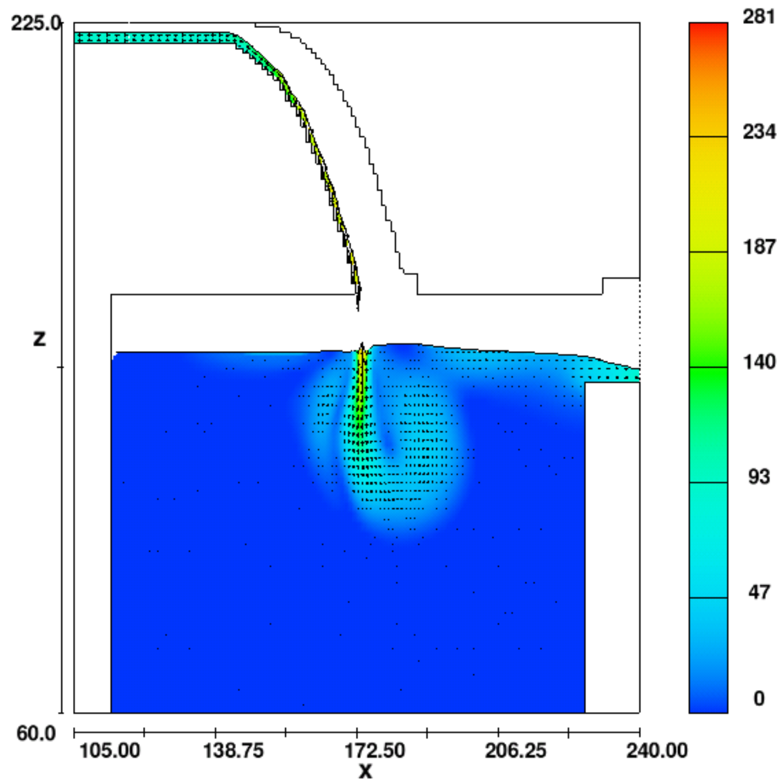

Figure 76. 2D velocity magnitude contours (cm/s) at 10 L/s inflow (calibration scenario).

Figure 77 shows the velocity vectors for the same calibration scenario.

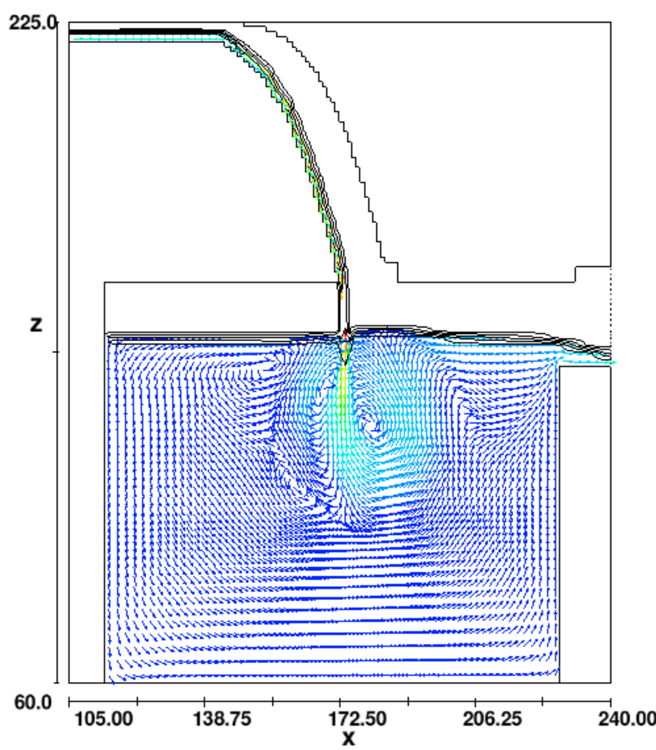

Figure 77. 2D velocity vectors (cm/s) at 10 L/s inflow (calibration scenario).

Experimental and simulated velocities were compared using normal probability plots to visually detect any difference in the mean and standard deviation of the velocities. Figure 78 shows a series of normal probability plots of the velocities. In all cases, the mean velocities of both experimental and simulated velocities are approximate. The standard deviations are also similar for three of the four cases. One of the normal probability plots had a greater standard deviation with velocities 10 cm/s higher than the experimental values. However, considering the simplification required in representing the hydrodynamics in a catchbasin sump with a 2D model, the level of approximation and uncertainty of these plots is appropriate for this case.

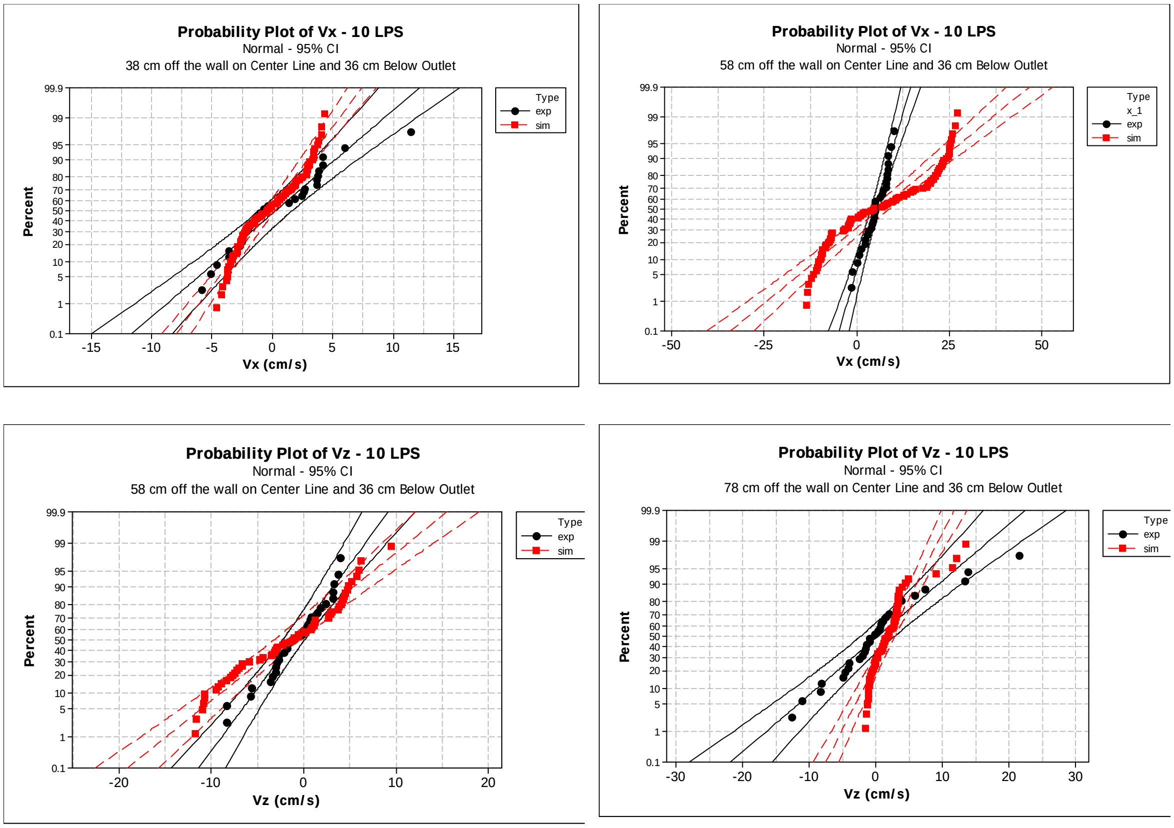

Figure 78. Normal probability plots of experimental and simulated velocities for points located on the center line at 36 cm below the outlet. (calibration scenario at 10 L/s inflow).

7.2.5 *Validation at 5 L/s*

Validation was performed by using the same equations and parameters calibrated for the 10-L/s flow rate scenario. Figure 77 shows the velocity contours at a 5 L/s flow rate. This figure shows, as expected, that the plunging water jet penetrates less than when a 10 L/s inflow is applied. The velocity vectors in Figure 79 illustrate how the velocity of the plunging jet rapidly dissipates and the ascending velocity is produced by the presence of air.

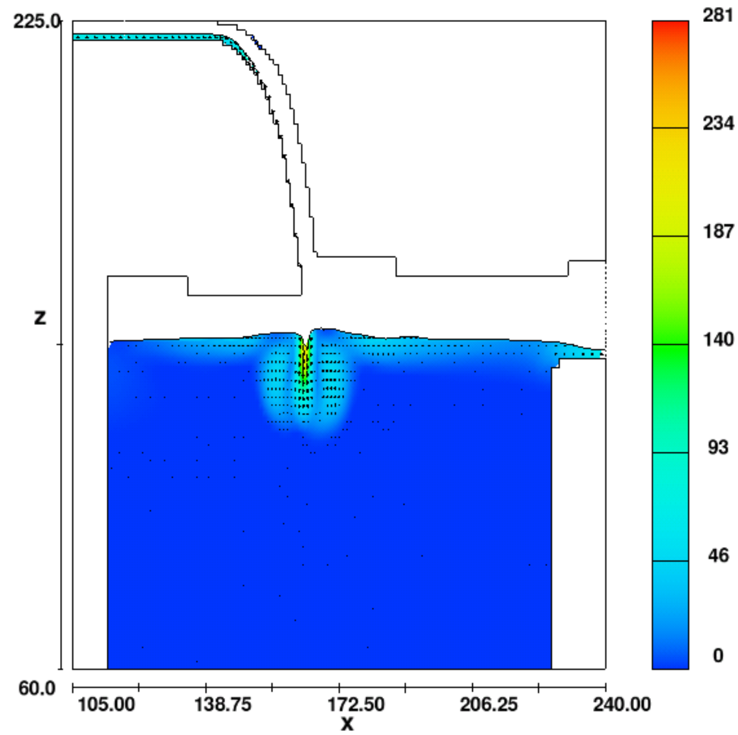

Figure 79. 2D velocity magnitude contours (cm/s) at 5 L/s inflow (calibration scenario).

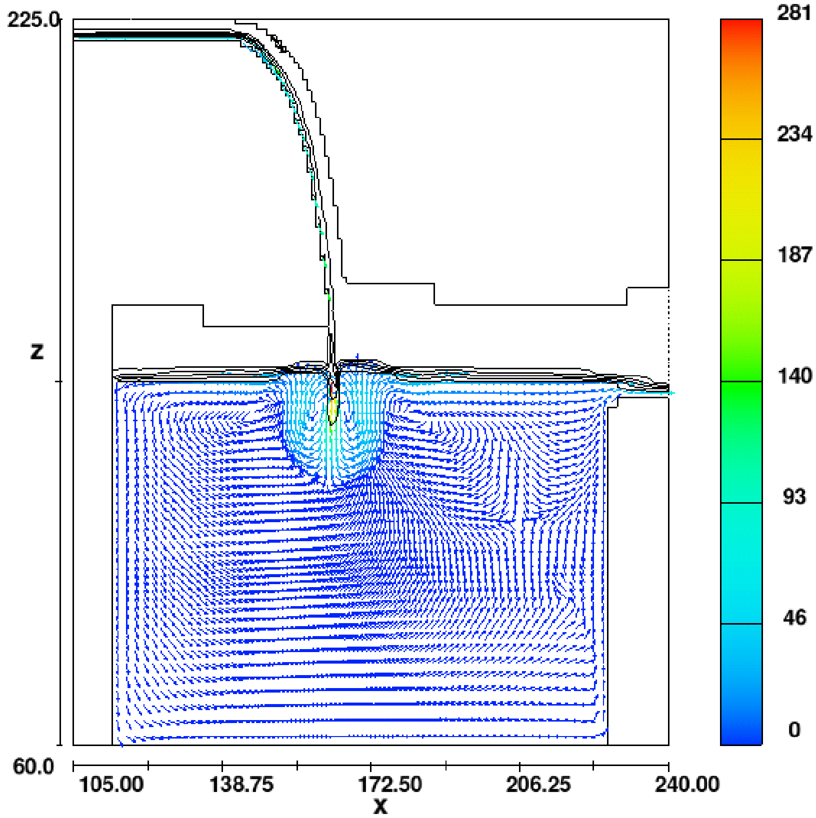

Figure 80. 2D velocity vectors (cm/s) at 5 L/s inflow (validation scenario).

The normal probability plots of the experimental and simulated velocities at 5 L/s flow rate were very similar in terms of mean and standard deviation in two of the four cases (Figure 81). However, the other two cases show a difference in the mean of about 2 cm/s for one of the plots and about 10 cm/s difference for another. Additionally, the standard deviation of those two cases is different. However, the level of similarity is still acceptable.

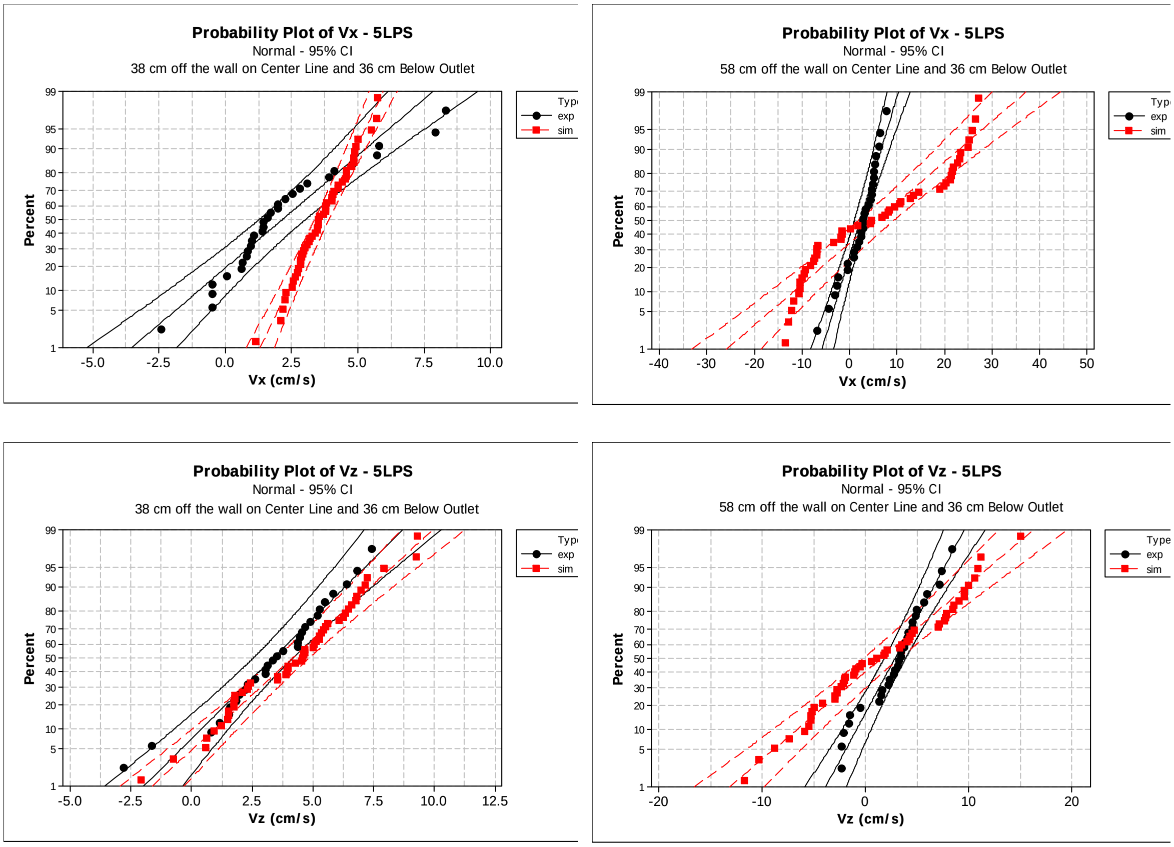

Figure 81. Normal probability plots of experimental and simulated velocities for points located on the center line at 36 cm below the outlet (calibration scenario at 10 L/s inflow).

CHAPTER 8

CREATION OF A CUSTOMIZED SCOUR MODEL

The Computational Fluid Dynamic software package Flow-3D is limited by the incompatibility of the sediment scour model with the air entrainment model. Both phenomena needed to be included in the model to evaluate sediment scour caused by the effect of a plunging water jet. Therefore, a scour model was created in FORTRAN that would evaluate the sediment scour given the hydrodynamics imposed by the flow with air entrainment. Flow-3D V.9.2 provides a series of subroutines available for licensed users to create new models or modify existing codes.

Two User's Defined Functions (UDF) were created: 1) the scour-sedimentation subroutine and 2) the drag coefficient subroutine. Other components of the model, such as the advection-dispersion model, density variation model, drift flux model, and air escape model, are implicit in Flow-3D. The UDF were compiled with the Flow-3D's solution algorithms using Fortran Compiler supported in Visual Studio v.2005.

Each UDF is composed by blocks which are shown in Table 19 and 22:

Table 19. Description of the Blocks of the Scour-Sedimentation User's Defined Function

UDF	Blocks
Scour-Sedimentation	Calculation of nominal critical shear stress for initial suspension and initial motion. Calculation of the acting shear stress Calculation of the angle or the sediment bed and the critical shear stress reduction coefficient Ka. Calculation of the effective critical shear stress Suspension from packed sediment Sedimentation of suspended sediment Calculation of new concentrations

Table 20. Description of Blocks of the Drag Coefficient User's Defined Function.

UDF	Blocks
Drag Coefficient	Drag coefficient of packed sediment Drag coefficient of suspended sediment Drag coefficient of clear water Drag coefficient for air entrainment

The assumptions and limitations of the UDF are the following:

Scour UDF:

- Only a single particle size can be simulated.
- Sediment suspension occurs directly from the packed sediment and not from bed load. A probability of sediment suspension factor (Cheng and Chiew 1999) needs to be calibrated. Cheng and Chiew defined the probability of initial motion as $1x10^{-7}$ and the probability of initial suspension as 0.01.

- There is no fraction of sediment specially assigned for bed load. Suspended sediment will behave as bed load due to an increment in the drag coefficient near the packed sediment interface.
- The particle settling velocity is smaller under turbulent flow (ASCE 1975). For this model, the settling velocity is reduced by a factor calculated as the ratio between the maximum settling velocity and the velocity associated with the turbulent kinetic energy (*tke*). The maximum particle settling velocity is reached when the *tke* is minimal.

*Drag coefficient UDF***:**

- The drag coefficient on packed sediment is infinite. No flow occurs where the sediment is packed.
- The drag coefficient imposed by the presence of suspended sediment is a function of the volume fraction of solids and the particle size.
- The drag coefficient imposed by the presence of air in water is a function of the volume fraction of air in water.

8.1 Theoretical Development

8.1.1 *Scour Model UDF*

The calculation of the critical shear stresses for initial motion and initial suspension was based on the criterion proposed by Cheng and Chiew (1999) (Figure 82). Cheng and Chiew proposed a theoretical analysis of the initiation of sediment suspension based on the probability of suspension from the bed load. The probability of suspension is associated with the vertical velocity fluctuations related to the settling velocity of the particles. Cheng and Chiew presented the probability of suspension P function that follows a Gaussian distribution as:

$$P = 0.5 - 0.5\sqrt{1 - \exp\left(-\frac{2}{\pi}\frac{w^2}{u_*^2}\right)},$$ Equation 32

where w is the particle settling velocity, $u_* = \sqrt{\frac{\tau}{\bar{\rho}}}$ is the shear velocity, τ equals acting shear stress, and $\bar{\rho}$ is the density of the fluid.

Cheng and Chiew (1999) indicated that a probability of 0.01 can be considered as the threshold for the initiation of sediment suspension from the top of the bed-load layer, and a probability of 1×10^{-7} can be considered the threshold for the initial sediment motion. The critical shear stress coefficient is then given by:

$$\Phi = \frac{\left(\sqrt{25 + 1.2D_*^2} - 5\right)^3}{\left(w/u_*\right)^2 D_*^3},$$ Equation 33

where D_* is the dimensionless diameter of particles, given by $D_* = \left[\left(\frac{\rho_s - \rho}{\rho}\right)\frac{g}{\nu^2}\right]^{1/3} D$, ρ_s is the density of the particles, ρ is the density of the water, g equals gravitational acceleration, ν equals the kinematic viscosity of the water, and D is the diameter of particles.

Using the equations above, Figure 82 shows the critical shear stress for initial motion and initial suspension thresholds using the Cheng and Chiew criteria.

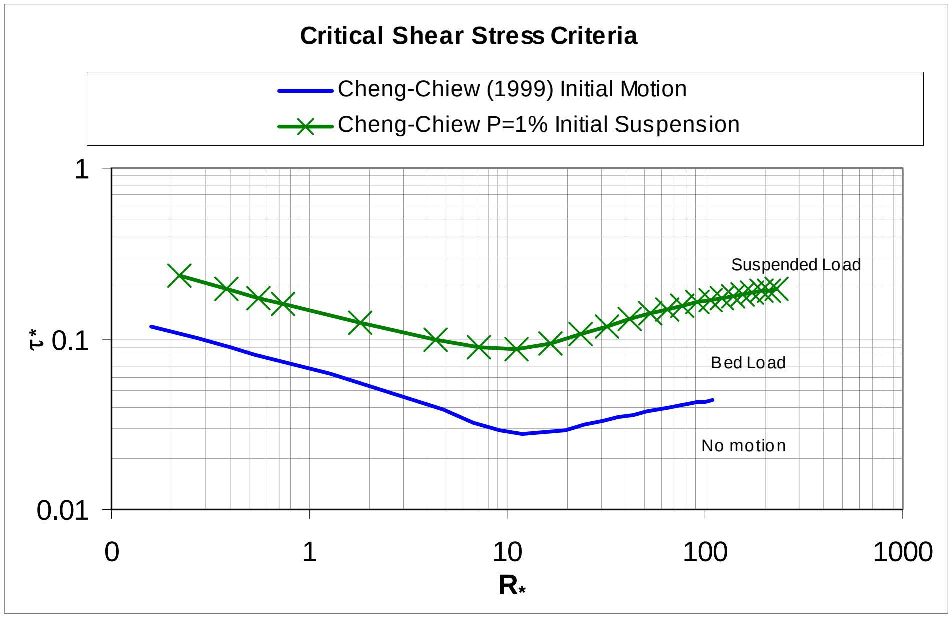

Figure 82. Incipient motion and initial suspension thresholds based on Cheng and Chiew (1999).

The sediment scour mass is associated with the lift velocity (u_{lift}), which is a function of the acting shear stress and the resistant shear stress. Brethour (2000) presented a formula for scour lift from the packed bed interface, defined as the excess shear velocity.

$$u_{lift} = \alpha \sqrt{\frac{\tau - \tau_{crit}}{\bar{\rho}}}, \qquad \text{Equation 34}$$

where α is the probability of sediment suspension, τ is the acting shear stress, τ_{crit} is the critical shear stress for either initial motion or initial suspension, and $\bar{\rho}$ is the density of the fluid.

However, considering that there is not a sediment fraction assigned to bed load for the customized scour model, and this is not coupled to the advection-dispersion model at the water-sediment interface, a net lift velocity ($\hat{u}_{lift}$) is applied instead to consider the effect of the settling velocity of the particle and to have a well balanced scour rate in the absence of the advection-dispersion model acting at the interface. The net lift velocity is defined as the difference between the nominal lift velocity given in Equation 35 and the nominal settling velocity of the particle. The net lift velocity is given as:

$$\hat{u}_{lift} = \alpha\left(\sqrt{\frac{\tau - \tau_{crit}}{\bar{\rho}}} - w_o\right), \qquad \text{Equation 35}$$

where w_o is the nominal settling velocity of the particle.

Notice that the formula for scour lift applies to suspension from the packed sediment bed and not from the bed-load layer. Also notice that the probability of initial suspension from Cheng and Chiew (1999) (1%) applies to sediment suspension from the bed load. Therefore, the approach of the proposed scour model requires the calibration of the probability of sediment suspension factor from the packed sediment, which should be a number between $1\text{x}10^{-7}$ and 0.01 for initiation of sediment suspension.

The nominal critical shear stress is given by:

$$\tau^o_{crit} = \Phi \cdot g(\rho_s - \rho)D . \qquad \text{Equation 36}$$

This nominal critical shear stress is affected by a reduction factor, *K*, which depends on the angle of repose, φ, of the sediment bed as:

$$\tau_{crit} = K \cdot \tau^o_{crit} , \qquad \text{Equation 37}$$

where

$$K = \sqrt{1 - \frac{\sin^2\varphi}{\sin^2\theta}} \qquad \text{Equation 38}$$

is the critical shear stress reduction factor and θ is the critical angle of repose. The critical angle of repose, θ, was measured during the experiment. This angle had a range between 22 and 30^{o}. θ = 30^{o} was used for the simulations.

The acting shear stress is calculated based on shear velocity u_*, derived from the turbulent kinetic energy *tke*, in Equation 39 (Flow Science 2007).

$$tke = \frac{u^2{}_*}{\sqrt{CNU}}, \qquad \text{Equation 39}$$

where *tke* is the turbulent kinetic energy (cm^2/sec^2) and *CNU* equals 0.085 for Renormalization-Group model (RNG), which is based on the k-ε model but with parameters explicitly derived. The k-ε model has a two transport equations, for the turbulent kinetic energy k and its dissipation; its parameters are empirically derived (Flow-3D 2007).

The shear velocity is given as:

$$u_* = \sqrt{\frac{\tau}{\overline{\rho}}}. \qquad \text{Equation 40}$$

Combining Equation 39 and 40, the acting shear stress, τ, is given as:

$$\tau = \sqrt{CNU} \cdot \overline{\rho} \cdot tke. \qquad \text{Equation 41}$$

The acting shear stress calculated with Equation 41 was compared to the acting shear stress calculated with Equation 42, also implemented in the customized model, which describes the theoretically definition of shear stress. However, only Equation 41 was ultimately implemented because it is not necessary to deal with the geometry of the mesh. Flow-3D automatically considers the geometry when determining the turbulent kinetic energy *tke*.

$$\tau = (\mu + \rho\varepsilon)\frac{\partial u}{\partial z}, \qquad \text{Equation 42}$$

where μ is the dynamic viscosity, ε is the eddy viscosity due to turbulence, and $\frac{\partial u}{\partial z}$ equals the strain rate.

On the other hand, the sedimentation process was based on criterion in which the sediment particles remain suspended if the upward velocity of the turbulent eddies exceeds the settling velocity of the particles. The threshold ratio between the nominal settling velocity of the particle w_o and the shear velocity u_* is presented as:

$$\frac{w_o}{u_*} = 1.25\,. \qquad \text{Equation 43}$$

Thus, if the ratio $\frac{w_o}{u_*} > 1.25$, settling will occur.

However, the effective settling velocity of the particles w, with which the settling rate is calculated, is lower than the nominal settling velocity w_o. The nominal settling velocity of the particles is normally calculated with a column of still water. However, when turbulence is imposed by the flow, the settling velocity decreases due to the fluctuating ascending velocity (ASCE 1977). The reduction of the settling velocity is related nonlinearly to the drag on the particles and the particle's velocity relative to the fluid.

A simplified model was assumed to account for reduction of the fall velocity as a function of the turbulent kinetic energy, *tke*, which is a measurement of the velocity fluctuation. The approximation assumes that the settling velocity starts decreasing when the velocity fluctuations are slightly greater than the terminal velocity. That is,

$$w = K_W \cdot w_o \,, \qquad \text{Equation 44}$$

where

$$K_W = \begin{cases} 1 & if \;\; v'_{tke} \leq w_o \\ \dfrac{w_o}{v'_{tke}} & if \;\; v'_{tke} > w_o \end{cases} \qquad \text{Equation 45}$$

is the reduction factor of settling velocity, and $v'_{tke} = \sqrt{2 \cdot tke}$ is the velocity fluctuation associated to the turbulent kinetic energy.

The motion of suspended sediment in the control volume is described by the advection-dispersion equation, which includes the lift and the settling velocity of the particles. The equation is given as:

$$\left(\frac{\partial c_s}{\partial t}\right)_x + u \cdot \nabla c_s = \hat{D} \nabla^2 c_s - u_{lift} \cdot \nabla c_s - w \cdot \nabla c_s \,, \qquad \text{Equation 46}$$

where c_s is the concentration of suspended sediment, u is the local fluid velocity, and $\hat{D}$ is the dispersion coefficient, taken as the inverse of the Schmidt number 1.0/0.7. This is a default value given by Flow-3D (Flow Science 2007).

8.1.2 *Drag Coefficient UDF*

The drag coefficient establishes the resistance of flow due to the presence of either air or sediment in the control volume. Considering that the flow contains water, air, and sediment, the drag coefficient was calculated as a function of the volume fraction of either air or sediment in the water. The drag coefficient equations were calculated based on Equation 47, given in the Flow-3D User's Manual (Flow Science 2007), with some modifications applied for this particular problem.

In the presence of suspended sediment, the drag coefficient is calculated as:

$$DRG = TSDRG \frac{f_{SED}^2}{(1 - f_{SED})^3}, \qquad \text{Equation 47}$$

where *TSDRG* is a multiplier factor for drag coefficient, and f_{SED} is the volume fraction of sediment.

If a cell is completely full of sediment, the drag coefficient *DRG* becomes effectively infinite, which means that there is no flow through the cell. Equation 47 considers the drag coefficient only as a function of the sediment concentration of sediment. However, several researchers have found a correlation between P_s/P_f and the Von Karman universal constant, *k*, where P_s is the power to support sediment suspension and P_f is the power of the fluid. The power ration is given by:

$$\frac{P_s}{P_f} = \left(1 - \frac{\gamma}{\gamma_s}\right) wg\overline{C}d, \qquad \text{Equation 48}$$

where γ is the specific weight of water, γ_s is the specific weight of the sediment particles, $\overline{C}$ is the mean concentration over the depth, d is the depth of the water in a channel.

Einstein and Chien (1952, 1955) found that as the ratio P_s/P_f increases, the Von Karman constant *k* decreases. The power ratio increases when either the concentration or the particle size increases (Figure 83).

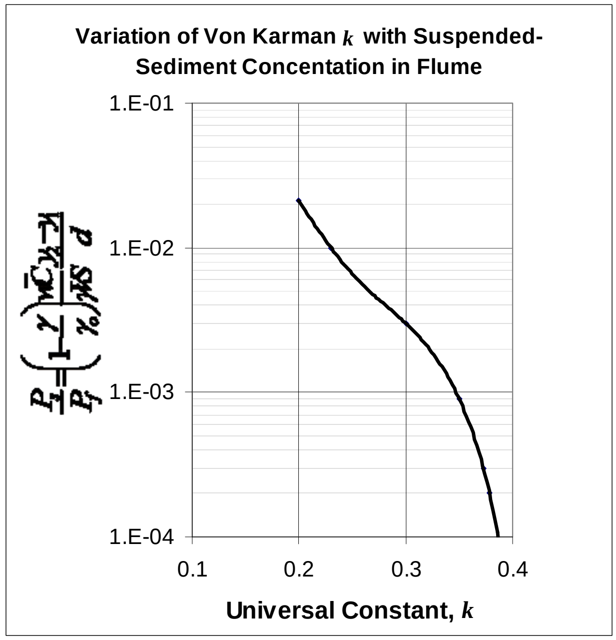

Figure 83. Reduction of the Universal Constant, *k*, with increments of either concentration or particle size of the suspended sediment.

As a consequence, if the Von Karman constant *k* decreases, the flow velocity also decreases, considering that the velocity profile in a channel flow is given as:

$$U = \frac{2.3}{k} \log\left(\frac{y}{d}\right)\sqrt{\frac{\tau_o}{\rho}} + U_{\max} . \qquad \text{Equation 49}$$

Therefore, the flow resistance is a function of both the concentration and the particle size. Moreover, from the previous analysis, it can be seen that, for a constant sediment concentration, the flow expends more energy trying to keep larger particles suspended than smaller particles (Figure 84).

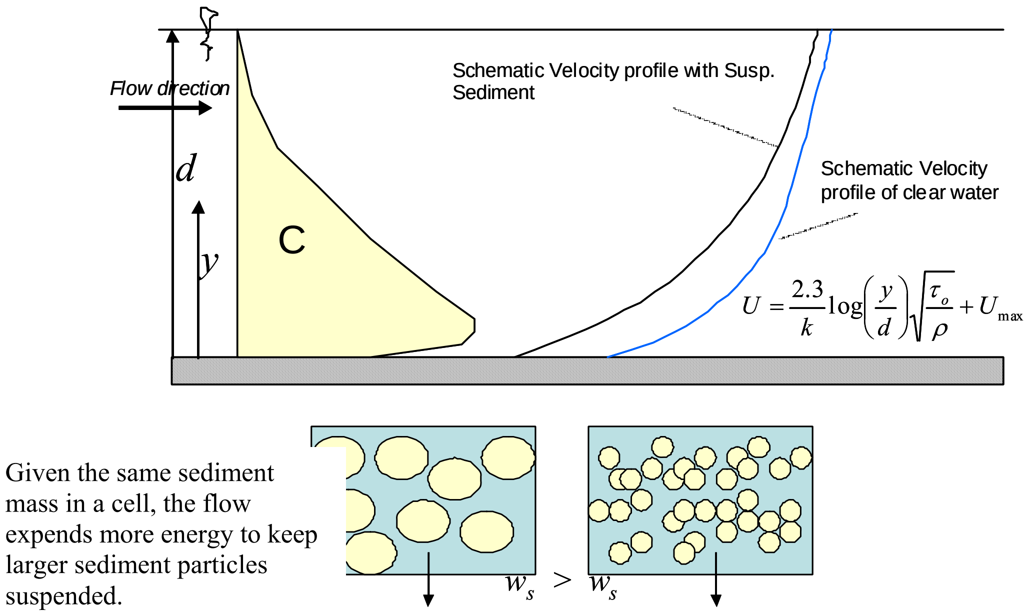

Figure 84. Schematic explanation of increment of drag coefficient by diameter reflected by the universal constant, *k*.

The analysis described above was based on results obtained by Laursen (1953) from flume experiments. Therefore, the power ratio was evaluated by particle size to determine the effect on the percentage of reduction of the Von Karman constant *k*. The Drag coefficient multiplier (TRDRG) (Figure 86) was calculated based on the ratio between the power ratio and the particle settling velocity (Figure 85). A linear regression was applied to the coefficients shown in the equations calculated in Figure 85. This linear regression represents the coefficient TRDRG (Figure 86).

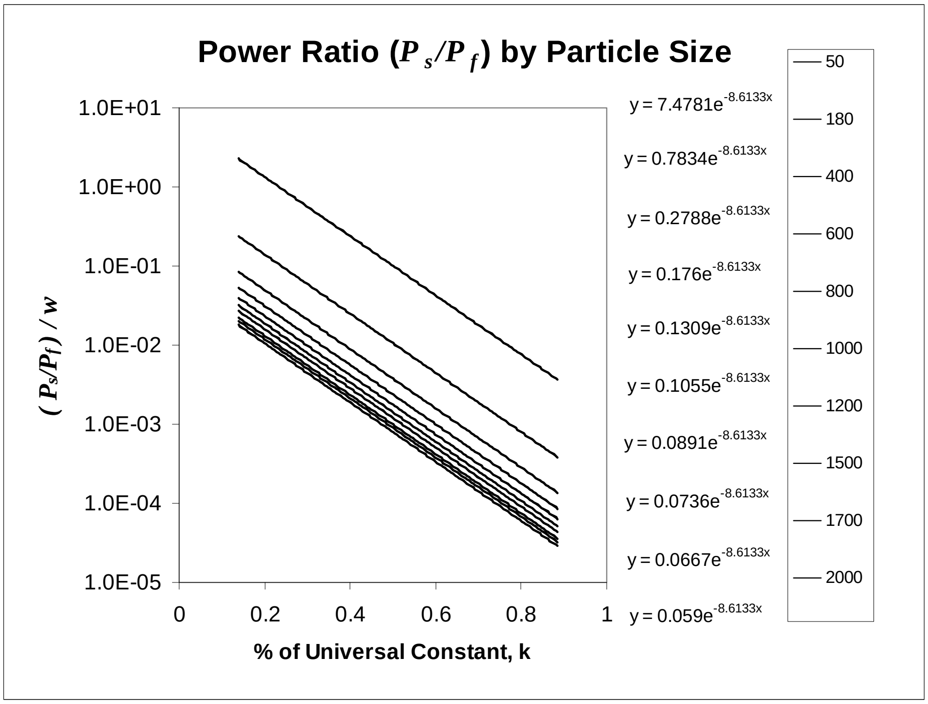

Figure 85. Reduction of the universal constant, *k*, related to the power ratio and particle settling velocity.

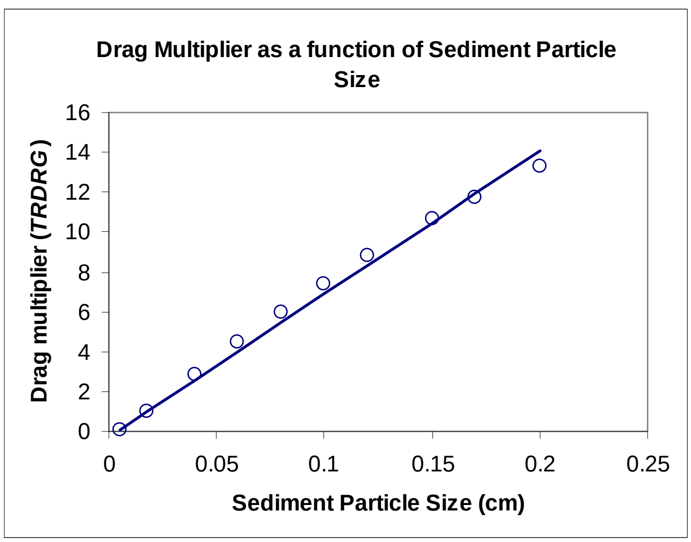

Figure 86. Drag multiplier (*TSDRG*) as a function of sediment particle size.

The final drag coefficient function is given as:

$$DRG = (71.8D - 0.3)\frac{f_{SED}^2}{(1 - f_{SED})^3}.$$ Equation 50

Figure 87 shows the drag coefficient as a function of the volume fraction of sediment plotted by particle size.

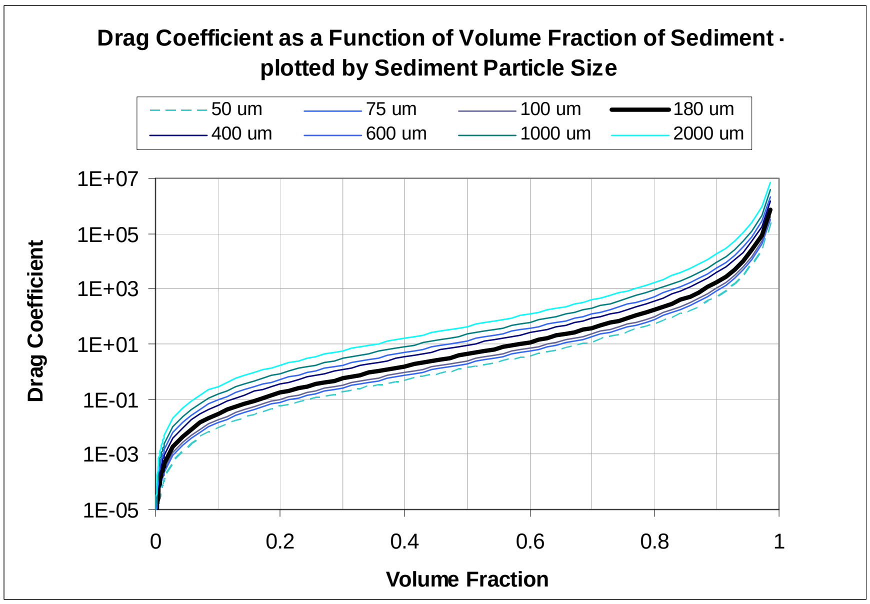

Figure 87. Drag coefficient as a function of volume fraction of sediment and sediment particle size.

8.2 Numerical Specification of the Scour Model

The scour model approach is shown in

Figure 88. The modeling approach is as follows:

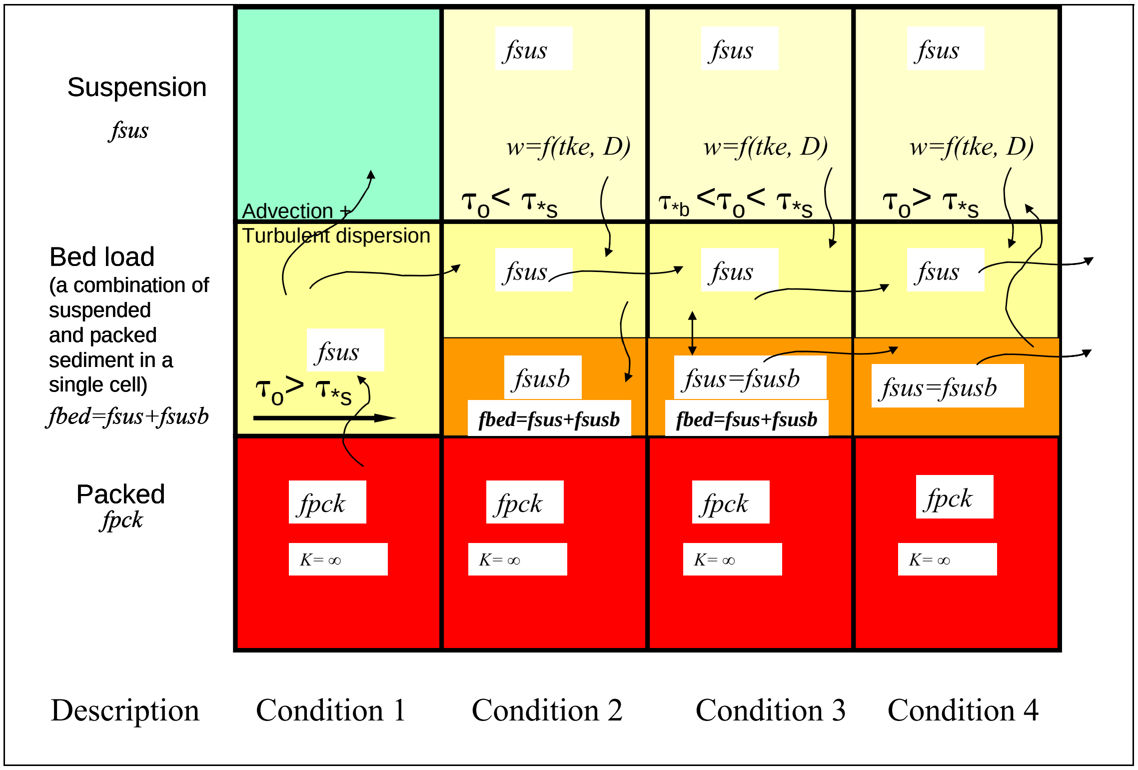

Figure 88. Schematic graphic-numerical specification of the scour-sedimentation model.

Condition 1. Initially, the total sediment mass is packed, *fpck*, from the bottom of the catchbasin sump up to the corresponding depth below the outlet. The drag coefficient of the packed sediment is assigned to be infinite, so no flow will occur in cells containing packed sediment. Suspended sediment concentration, *fsus*, is initially zero in the whole domain. Once the plunging water jet impacts the water surface, a velocity field is developed in the fluid domain. If the acting shear stress on the sediment surface is greater than the critical shear stress for initial suspension, the sediment gets suspended at a rate based on the net lift velocity. The suspended sediment mass passes to the upper cell and is transported through the fluid domain with the advection-dispersion equations included in Flow-3D.

Condition 2. Settling sediment mass is calculated and transported at a rate determined by the net settling velocity of the particles. Sedimentation occurs in cells located right above cells with packed sediment. In those cells, if the acting shear stress is less than the critical shear stress for suspension, a portion of the suspended sediment, *fsus*, is deposited in the cell as a deposited-suspended concentration, *fsusb*. This *fsusb* has the property of allowing flow through the cell but increasing the drag coefficient. The combination of *fsus* and *fsusb* is denominated as bed load.

Condition 3. In cells with *fbed*, if the acting shear stress is between the critical shear stress for incipient motion and the critical shear stress for initial suspension, a portion of the deposited-suspended sediment, *fsusb*, is resuspended back to *fsus* and added to the suspended sediment on the same cell. This process allows the *fbed* to be transported on the sediment surface as bed load. However, no sediment fraction is assigned specifically as bed load, and the bed load transport is not completely considered in this customized model, only approximated.

Condition 4. Scour does not occur in packed cells, *fpck*, with upper cells containing deposited-suspended sediment, *fsusb*. In order for scour to occur in packed cells, it is necessary that *fsusb*=0 in the upper cells. If the acting shear stress is greater than the critical shear stress for initial suspension, scour occurs on cells with $fsusb > 0$.

Finally, advection-dispersion of suspended sediment occurs in the entire fluid domain. The total mass in the control volume is calculated on each time step (approximately $1x10^{-3}$ sec). The total mass is recorded every 10 sec, so the difference in mass at every 10 sec interval represents the mass loss rate.

8.3 Calibration and Validation of the Scour Model – Sediment with Homogeneous 180-μm Particle Size

8.3.1 *Calibration of the Customized Scour Model*

The calibration scenario was performed with a homogeneous sediment material with D_{50} = 180 μm, located at 24 cm below the outlet, and a flow rate of 10 L/s. The inlet was considered to be a 50-cm wide rectangular inlet. The width of the inlet defines the depth of water at the influent. The calibration consisted of the estimation of the probability of suspension, α, used to determine the net lift velocity (Equation 51) which represents the suspension mass rate.

$$\hat{u}_{lift} = \alpha\left(\sqrt{\frac{\tau - \tau_{crit}}{\bar{\rho}}} - w_o\right). \qquad \text{Equation 51}$$

The probability of initial suspension found by Cheng and Chiew (1999) is α = 0.01, and it applies to sediment suspension from the bed load. However, the scour in the proposed model occurs directly from the packed sediment, so no bed load is produced from the packed sediment but rather from the sediment already suspended. Additionally, according to Cheng and Chiew, the probability associated with initial motion is $1x10^{-7}$. Therefore, the probability of initial suspension needs to be between $1x10^{-7}$ and 0.01. This probability is treated as a fraction of the packed sediment that is suspended.

Figure 89 shows the initial condition of the calibration scenario. The CFD model does not define the water-sediment interface as a sharp line but as a bandwidth between 0 and 1.7 g/cm^3 (sediment concentration). This approach made by the CFD model implies an approximate graphical representation of scour in the sediment surface. However, this does not affect the correct calculation of SSC and mass load.

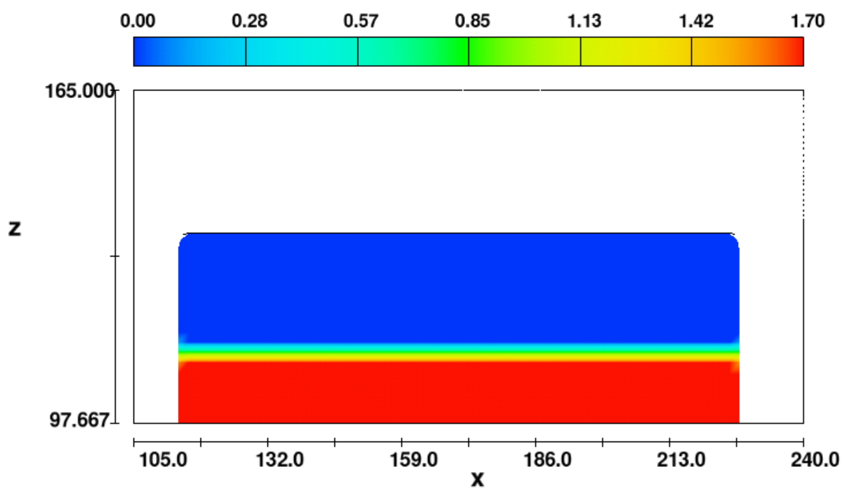

Figure 89. Initial condition of the calibration scenario. Colors represent sediment concentration with 1.7 g/cm^3 as the maximum magnitude (bulk density).

The calibrated probability of suspension α was found to be 1x10^{-4}, which is within the expected range between 1x10^{-7} and 0.01.

Figure 90 shows the experimental and simulated SSC time series. The experimental SSC is plotted at 3-min intervals to correspond with sample collection intervals of 3 min. The 95% confidence and prediction intervals of the experimental SSC are included on the graph. The simulated SSC is plotted at 10 sec intervals. The figure shows that the simulated SSC is approximately constant within the 30-min simulation, and its mean value is close to the experimental SSC. Notice that the SSC values can be treated independently of time, as was proved in previous chapters. This allows one to statistically compare the two samples. The 2D-SSC contour of the calibration scenario is shown in Figure 91.

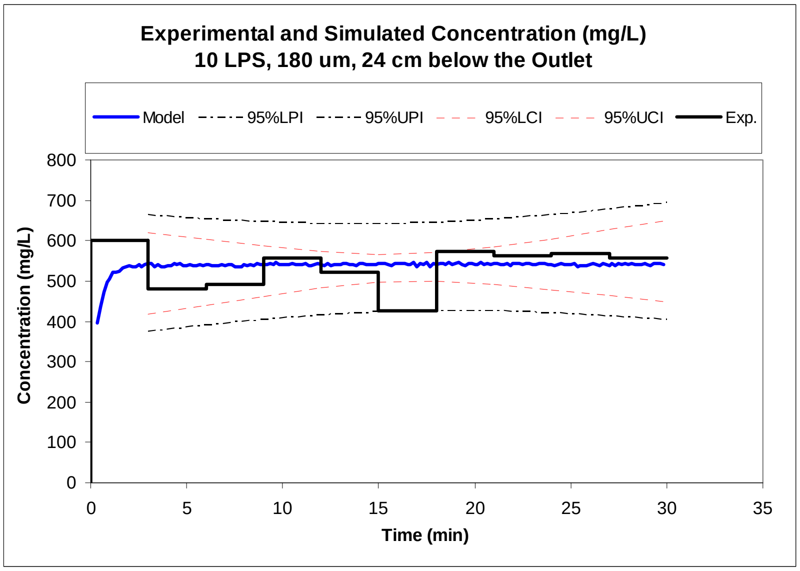

Figure 90. Experimental and simulated SSC (mg/L) for the calibration scenario. Homogeneous sediment material of D_{50} = 180 µm, flow rate: 10 L/s, overlaying water depth: 24 cm.

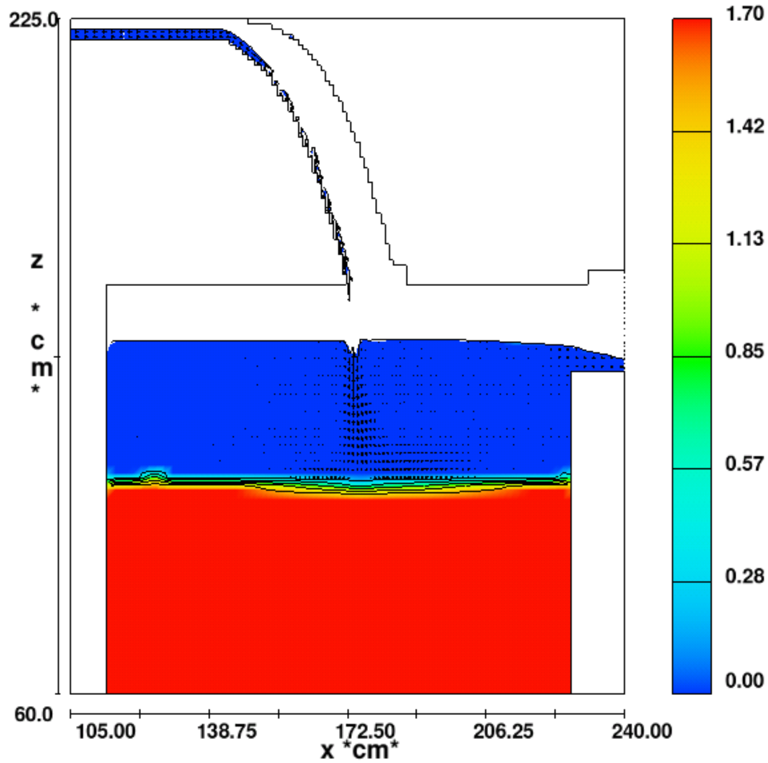

Figure 91. Total sediment concentration (g/cm3) at 20 min of continuous flow. Flow rate: 10 L/s, overlaying water depth: 24 cm, sediment particle size: 180 μm. 2D-CFD contour. Color scale represents sediment concentration (g/cm^3).

Another method to compare experimental and simulated results is the cumulative mass loss shown in Figure 92. The figure shows that both the experimental and simulated cumulative mass losses are very similar, which was expected since both mean SSC values are also similar.

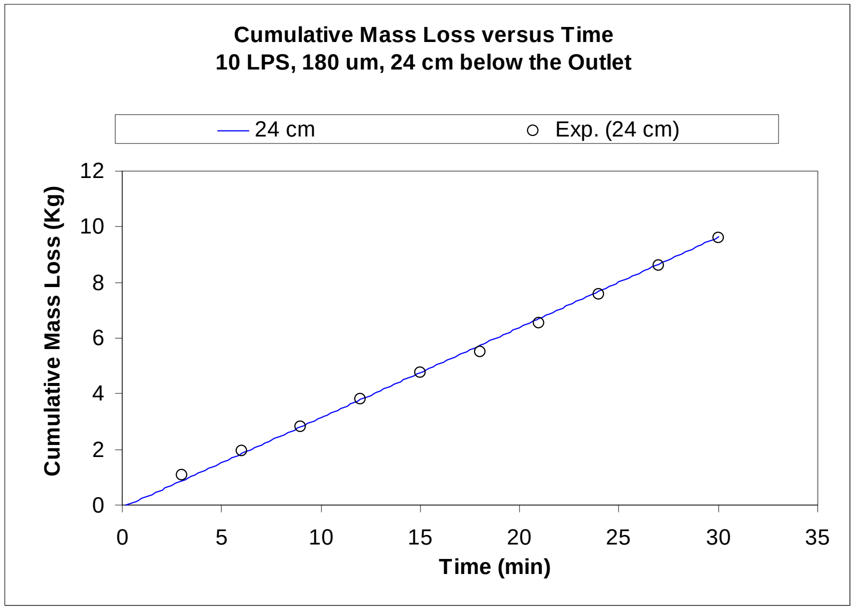

Figure 92. Experimental and simulated cumulative mass loss (Kg) for the calibration scenario. Homogeneous sediment of D_{50} = 180 µm, flow rate: 10 L/s, overlaying water depth: 24 cm.

Normal probability plots of the 3-min composites of the experimental and simulated SSC values are presented in Figure 93. The graph shows that both mean SSC values are approximately the same. However, the standard deviations are statistically different with a p-value equal to zero. Therefore, a two-sample t-test with unequal variance was performed to statistically compare the experimental and simulated SSC. The boxplots are shown in Figure 94.

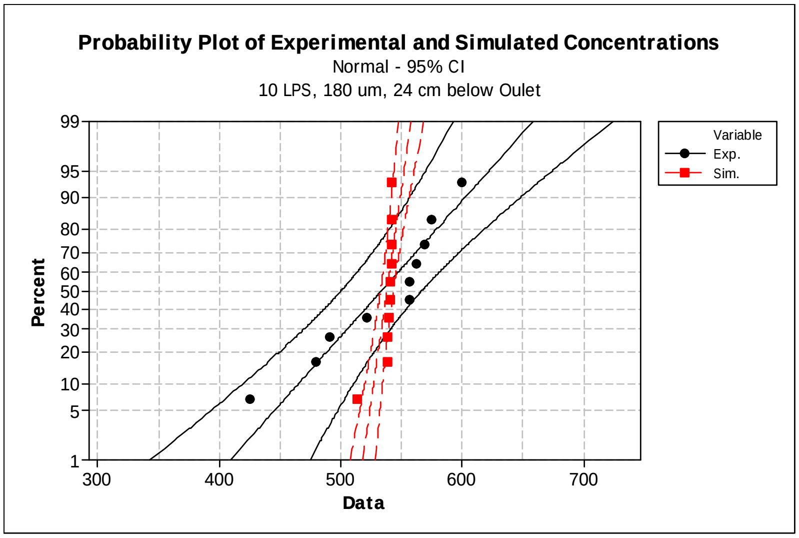

Figure 93. Comparison of normal probability plots between experimental and simulated SSC 3-min composite samples. Calibration: Homogeneous sediment material with D_{50} = 180 µm, overlaying water depth of 24 cm, and 10 L/s flow rate.

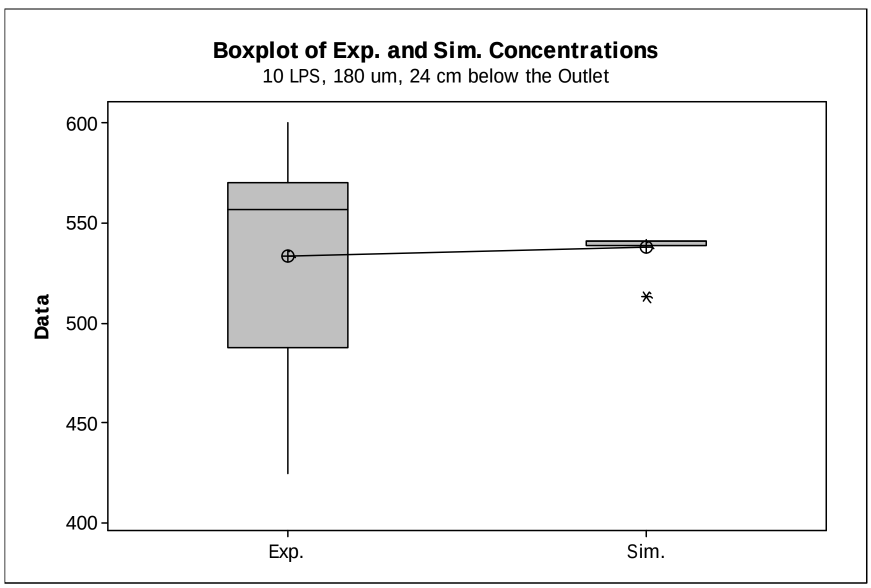

Figure 94. Comparison of boxplots between experimental and simulated SSC 3-min composite samples. Calibration: Homogeneous sediment material with D_{50} = 180 µm, overlaying water depth of 24 cm, and 10 L/s flow rate.

Table 21 shows the statistical output of a two-sample t-test to compare the 3-min composite SSC of experimental and simulated scenarios. The result shows a p-value equal to 0.8, which indicates that there is not enough evidence to reject both SSC means as equal. Hence, it can be said in the language of this evaluation that both experimental and simulated SSC means are statistically equal. The simulated SSC mean was 538 mg/L.

Table 21. 2-Sample t-Test with Unequal Variance of Experimental and Simulated 3-min Composite SSC (Calibration: Homogeneous Sediment Material with D_{50} = 180 μm, Overlaying Water Depth of 24 cm, and 10 L/s Flow Rate)

Two-Sample T-Test and CI: Exp. 24 cm, Sim. 24 cm

```
Two-sample T for Exp. 24 cm vs Sim. 24 cm

              N    Mean  StDev  SE Mean
Exp. 24 cm  10   533.4   53.6       17
Sim. 24 cm  10  537.80   8.57      2.7

Difference = mu (Exp. 24 cm) - mu (Sim. 24 cm)
Estimate for difference:  -4.4
95% CI for difference:  (-43.3, 34.4)
T-Test of difference = 0 (vs not =): T-Value = -0.26 P-Value =
0.803  DF = 9
```

8.3.2 *Validation of Customized Scour Model*

Validation of the scour model was performed using sediment with a homogeneous particle size of 180 μm, an overlaying water depth of 35 cm, and a flow rate of 10 L/s. No modification of the equations and the calibrated parameter, α, were made.

Figure 95 shows the 2D-SSC contour where it can be seen that less sediment mass was scoured. Figure 96 shows the experimental and simulated SSC time series, including the experimental confidence and prediction intervals.

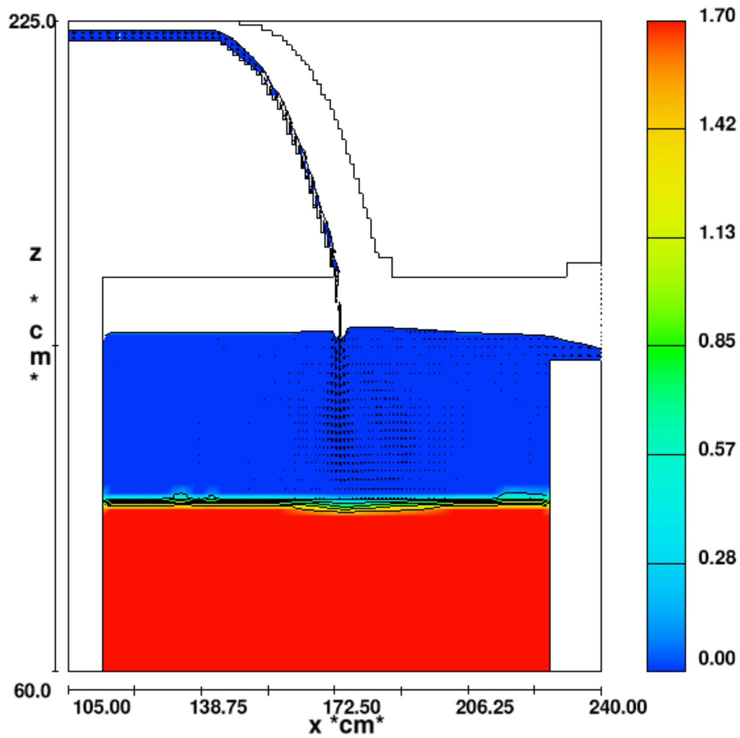

Figure 95. Total sediment concentration (g/cm^3) at 20 min of continuous flow. Flow rate: 10 L/s, overlaying water depth: 35 cm, sediment particle size: 180 µm. 2D-CFD contour. Color scale represents sediment concentration (g/cm^3).

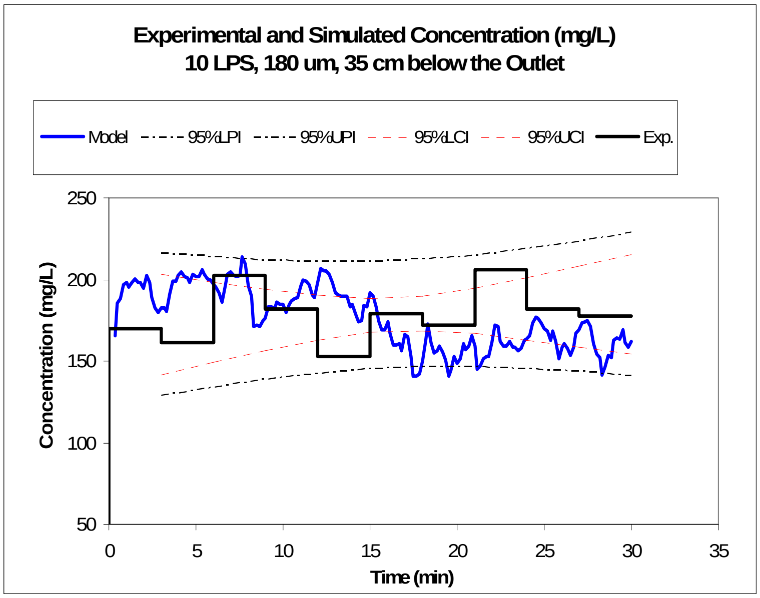

Figure 96. Experimental and simulated SSC (mg/L) for the validation scenario. Homogeneous sediment material of D_{50} = 180 μm, flow rate: 10 L/s, overlaying water depth: 24 cm.

Figure 96 shows that, in contrast to the calibration scenario with an overlaying water depth of 24 cm, the SSC fluctuates in time. This could be attributed to random oscillation of the velocity field close to the sediment surface due to the combined effect of the energy dissipation of the plunging water jet and the presence of air in the fluid domain.

Experimental and simulated cumulative mass loss are plotted in Figure 97, which shows the strong similarity between them.

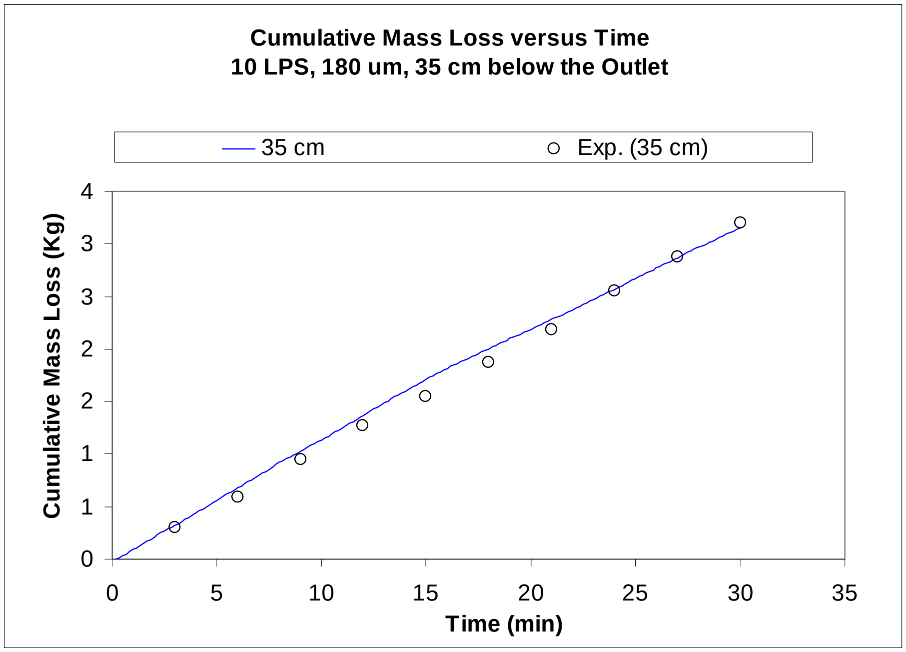

Figure 97. Experimental and simulated cumulative mass loss (Kg) for the validation scenario. Homogeneous sediment of D_{50} = 180 μm, flow rate: 10 L/s, overlaying water depth: 35 cm.

Normal probability plots of the 3-min composite of the experimental and simulated SSC are shown in Figure 98. The figure shows that both mean SSC values are very similar. Moreover, the variances of both SSC samples were not significantly different, with a p-value of 0.91. Therefore, a two-sample t-test with equal variance was performed to statistically compare the experimental and simulated SSC. Also, boxplots are shown in Figure 99.

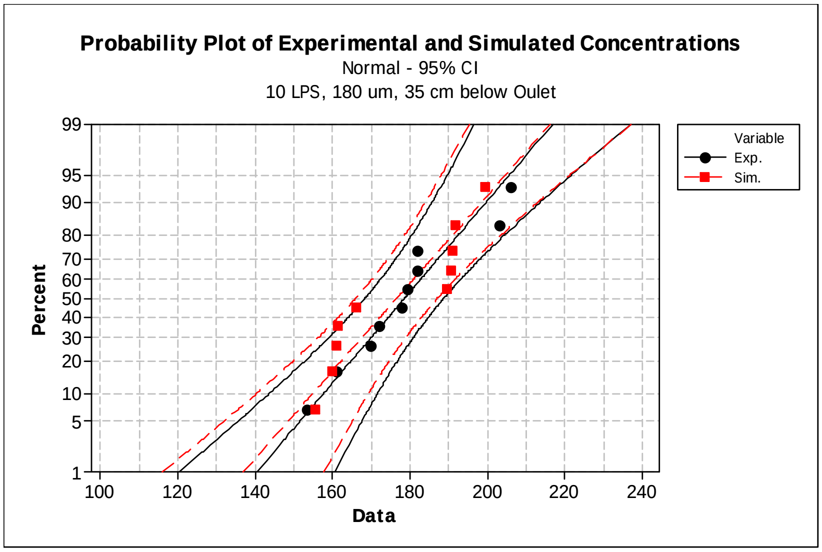

Figure 98. Comparison of normal probability plots between experimental and simulated SSC 3-min composite samples. Validation: homogeneous sediment material with D_{50} = 180 µm, overlaying water depth of 35 cm, and 10 L/s flow rate.

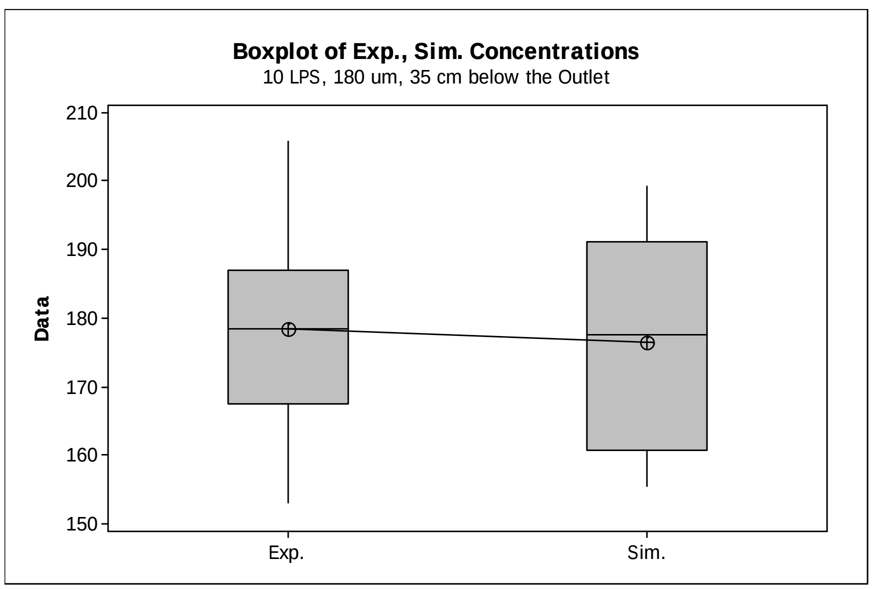

Figure 99. Comparison of boxplots between experimental and simulated SSC 3-min composite samples. Validation: homogeneous sediment material with D_{50} = 180 µm, overlaying water depth of 24 cm, and 10 L/s flow rate.

Table 22 shows the statistical output of a two-sample t-test to compare the 3-min composite SSCs from the experimental and simulated validation scenarios. The result shows a p-value equal to 0.8, which indicates that there is not enough evidence to reject the SSC means as equal. Hence, both experimental and simulated SSC means can be considered statistically equal. The simulated SSC mean was 177 mg/L.

Table 22. 2-Sample t-Test with Unequal Variance of Experimental and Simulated 3-min Composite SSC (Validation: Homogeneous Sediment Material with D_{50} = 180 µm, Overlaying Water Depth of 35 cm, and 10 L/s Flow Rate)

Two-Sample T-Test and CI: Exp. 35 cm, Sim. 35 cm

```
Two-sample T for Exp. 35 cm vs Sim. 35 cm

             N   Mean  StDev  SE Mean
Exp. 35 cm  10  178.5   16.4      5.2
Sim. 35 cm  10  176.5   17.1      5.4

Difference = mu (Exp. 35 cm) - mu (Sim. 35 cm)
Estimate for difference:  2.00
95% CI for difference:  (-13.73, 17.73)
T-Test of difference = 0 (vs not =): T-Value = 0.27  P-Value =
0.792  DF = 18
Both use Pooled StDev = 16.7425
```

CHAPTER 9

RESULTS OF SEDIMENT SCOUR WITH CFD MODELING

A total of 40 scenarios, including the calibration and validation, were simulated with the customized 2D-CFD scour model in Flow-3D. The list of scenarios is presented in Table 23.

Table 23. List of Case Scenarios Simulated with the 2D-CFD Model.

		Flow rate (L/s)		
Overlaying water depth (cm)	**Diameter (μm)**	**5**	**10**	**20**
15	50	■	■	■
	180	■	■	■
	500	■	■	■
	1000	■	■	■
24	50	■	■	■
	180	■	■	■
	500	■	■	■
	1000		■	■
35	50	■	■	■
	180	■	■	■
	500		■	■
	1000			■
40	50		■	■
	180		■	■
	500			■
	1000			
45	50			■
	180			■
	500			■
	1000			

■ Simulated

9.1 Analysis of the 2-Dimensional (2D) SSC Contours for Scour of Sediment with a Homogeneous Particle Size

Flow rate has an important effect on the scour potential, especially due to the impacting energy of the plunging water jet. At low flow rates, for example, 5 L/s (Figure 100), the mass of the plunging water jet impacting the water surface in the sump is considerably smaller than the mass at 20 L/s (Figure 101); therefore, the power at which the plunging water jet penetrates the water in the sump is relatively low. The impacting energy is rapidly dissipated by turbulence and the ascending component of the velocity caused by the buoyancy due to the air buoyancy. Therefore, the plunging jet does not reach as deeply as at higher velocities. Figure 100 shows how the plunging water jet at 5 L/s reaches the sediment located 24 cm below the outlet with relatively low velocities and is rapidly dissipated by the ascending component of the velocity. Figure 101, in contrast, shows that the plunging water jet penetrates with more energy at 20 L/s and reaches the sediment located 24 cm below the outlet. Moreover, at 20 L/s, the plunging water jet penetrates deeper and with enough energy to generate high acting shear stresses, as is shown in Figure 102 with sediment 40 cm below the outlet.

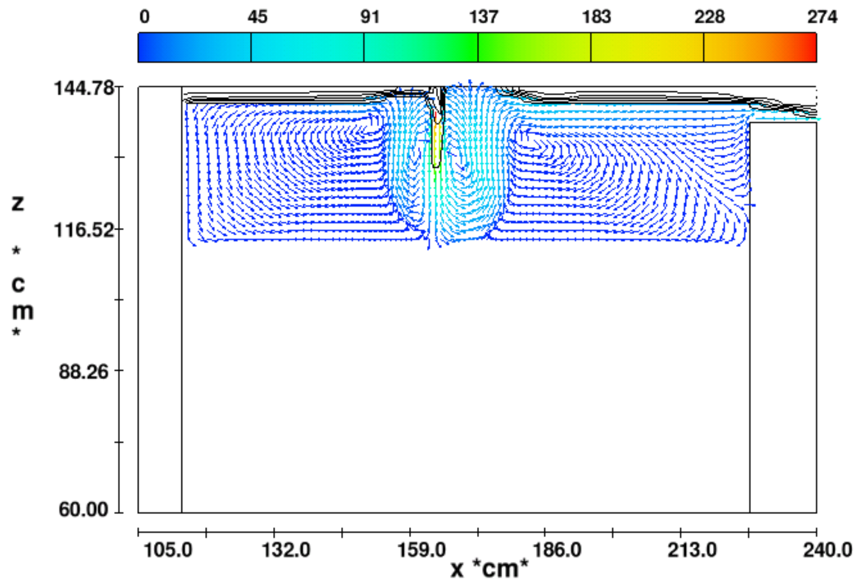

Figure 100. Velocity vectors at 5 L/s flow rate with sediment 24 cm below the outlet.

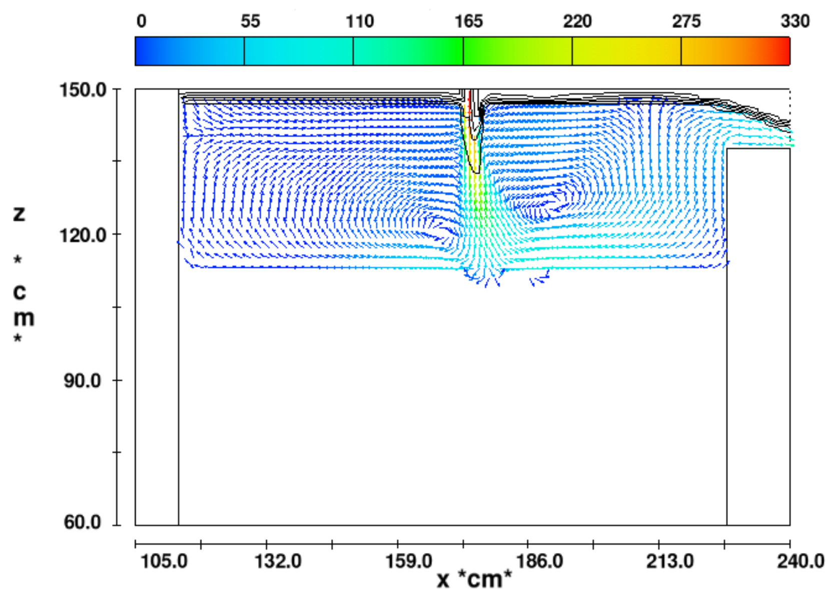

Figure 101. Velocity vectors at 20 L/s flow rate with sediment 24 cm below the outlet.

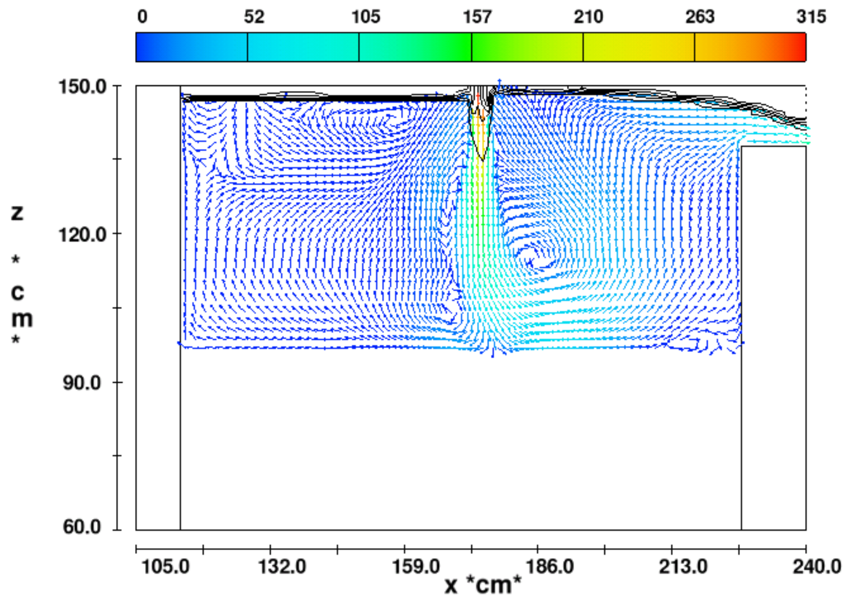

Figure 102. Velocity vectors at 20 L/s flow rate with sediment 40 cm below the outlet.

Figure 103 through 108 show representative 2D contours of the center line of a catchbasin sump. The colors in those figures represent sediment concentration in g/cm^3 and show a maximum value of 1.7 g/cm^3, which represents the bulk density of the packed sediment layer; this bulk density was measured in the laboratory. These figures will be referenced throughout this chapter to describe the differences in sediment scour under differing conditions of flow rate, overlaying water depth, and sediment particle size.

To compare the sediment scour resulting from different flow rates, Figure 103 and 104 show the total sediment concentration after 20 min of simulation for an initial overlaying water depth of 24 cm and a homogeneous sediment material of 180 μm in size. Figure 103 shows that a small sediment mass was scoured at 5 L/s right under the plunging water jet, in contrast to the same scenario at 20 L/s, where the sediment scour is considerably higher (shown in Figure 104).

It is possible to see in Figure 104 (20 L/s) that even though the plunging water jet is primarily affecting the sediment mass directly beneath it, the sediment scour is evident on the whole sediment surface. This is due to two major reasons. The first reason is that at a 20 L/s flow rate, the velocities in the whole control volume and the shear stress on a large portion of the sediment surface are high, causing more sediment suspension. The second reason is due to the angle of repose of the sediment material.

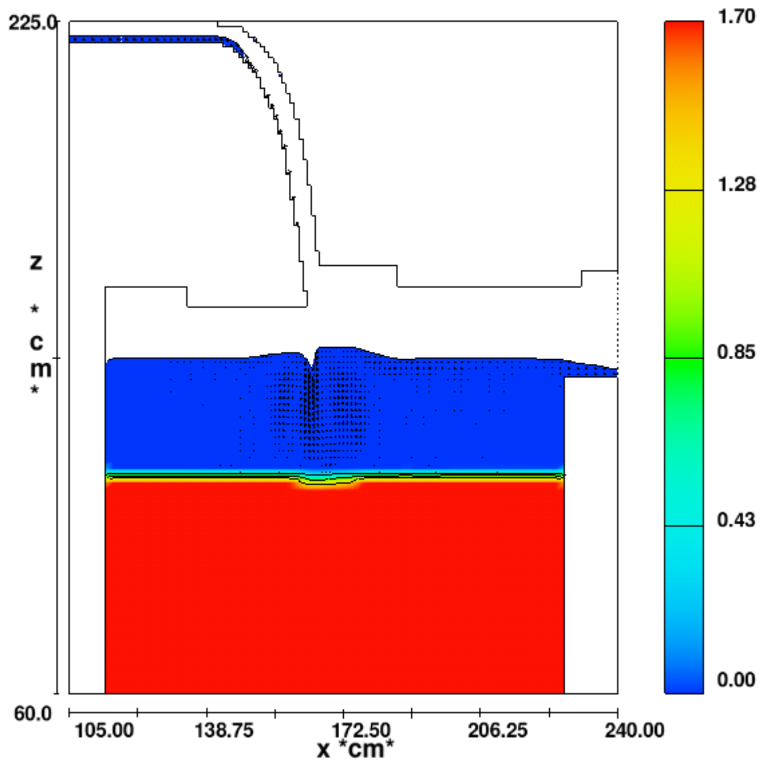

Figure 103. Total sediment concentration (g/cm^3) at 20 min of continuous flow. Flow rate: 5 L/s, overlaying water depth: 24 cm, sediment particle size: 180 μm. 2D-CFD contour. Color scale represents sediment concentration (g/cm3).

A hole is created on the sediment surface as the sediment mass beneath the plunging water jet is scoured. This increases the actual angle of repose of the sediment bed, which reduces resistant shear stress. As a consequence, the sediment material surrounding the hole is more exposed to scour, causing it to become suspended or to fall inside the hole. It will be resuspended if the plunging water jet is generating high shear stress magnitudes. In this case, the sediment scour will decrease once the overlaying water depth is large enough for the sediment material to not be so exposed to high shear stresses.

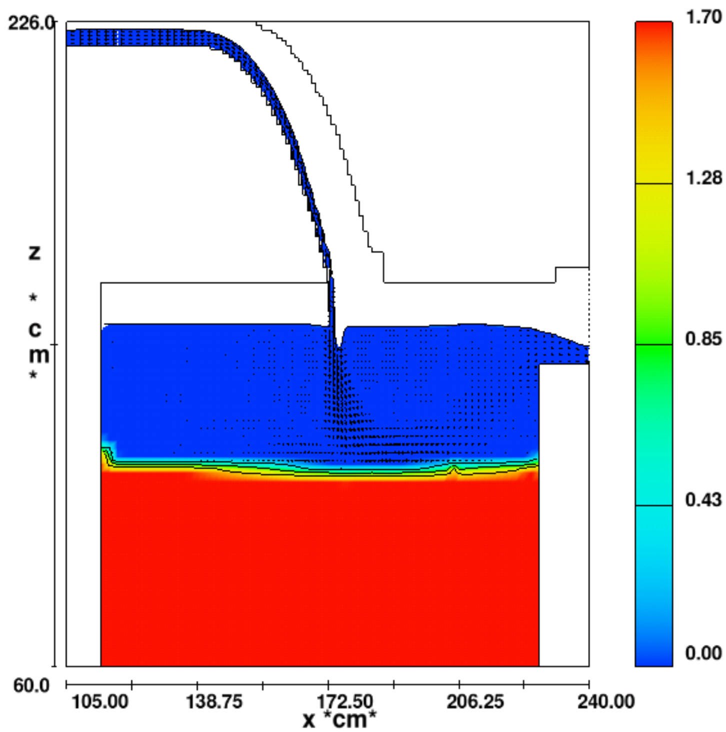

Figure 104. Total sediment concentration (g/cm^3) at 20 min of continuous flow. Flow rate: 20 L/s, overlaying water depth: 24 cm, sediment particle size: 180 µm. 2D-CFD contour. Color scale represents sediment concentration (g/cm3).

Overlaying water depth also has been shown, through the experimental and simulated data in this research, to be one of the main factors that protects sediment from being scoured in catchbasin sumps. It balances the effect of the plunging water jet. Figure 105 shows the scenario with a 20 L/s flow rate, 180-µm particle size, and overlaying water depth of 40 cm. In this scenario, the sediment scour is considerably less than when the sediment is 24 cm below the outlet. The velocities and shear stress acting on the sediment surface 40 cm below the outlet are smaller, as the energy of the plunging jet was dissipated and the velocity vectors spread in the control volume.

For sediment material with a homogeneous particle size, the overlaying water depth at which sediment scour is minimal strongly depends on the particle size, especially at high flow rates. Obviously, if the overlaying water depth is large enough to avoid direct contact with the velocity field generated by the plunging water jet, particle size becomes less important. That is the case for low flow rates in which the energy of the plunging jet is dissipated at low sediment depths.

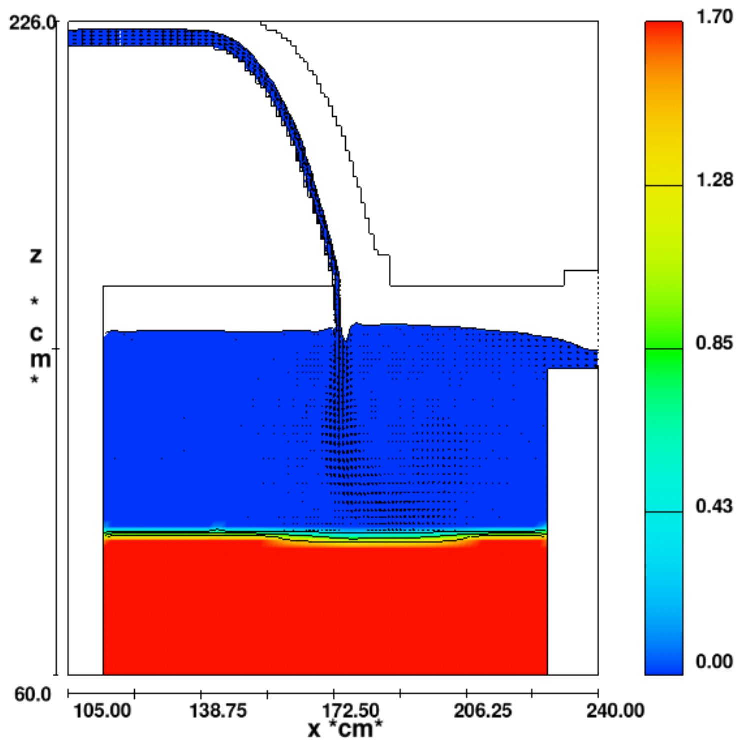

Figure 105. Total sediment concentration (g/cm^3) at 20 min of continuous flow. Flow rate: 20 L/s, overlaying water depth: 40 cm, sediment particle size: 180 µm. 2D-CFD contour. Color scale represents sediment concentration (g/cm3).

SSC values was shown to have an exponential decay pattern as a function of sediment particle size when using sediment with a homogeneous particle size

Figure 106 shows the scour after 20 min of continuous flow at 20 L/s with a sediment material with homogeneous particle size of 1000 µm located 24 cm below the outlet. The sediment scour is visually lower than the one presented in Figure 104, which has the same conditions but with a particle size of 180 µm. The critical shear stress of particles 1000 µm in size is high enough to resist the acting shear stress, so the scour mass concentrates beneath the plunging water jet and does not extend across the entire sediment surface, unlike what occurs in the scenario shown for particles 180 µm in size.

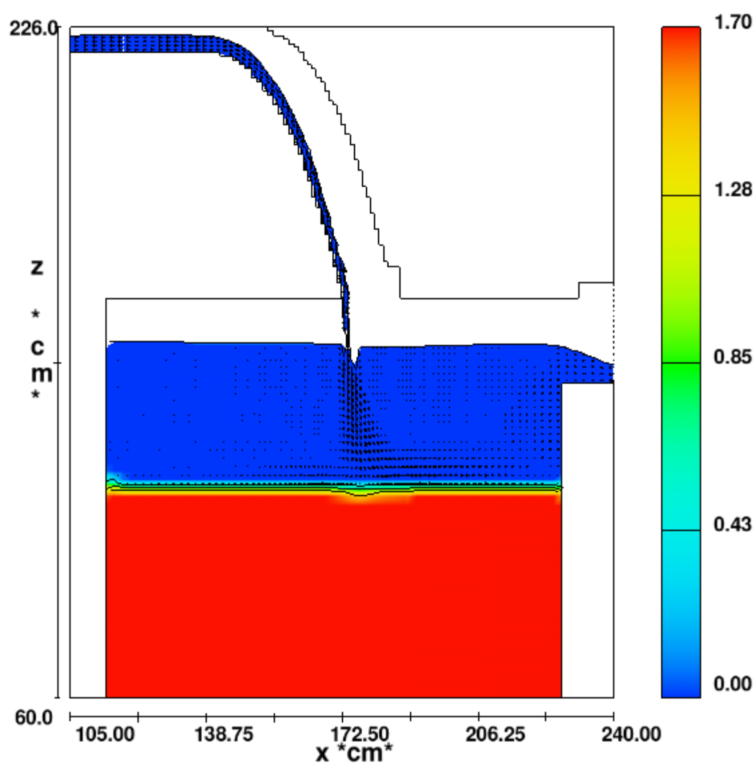

Figure 106. Total sediment concentration (g/cm^3) at 20 min of continuous flow. Flow rate: 20 L/s, overlaying water depth: 24 cm, sediment particle size: 1,000 µm. 2D-CFD contour. Color scale represents sediment concentration (g/cm3).

9.2 Analysis of SSC and Scour Mass Rate of Sediment with a Homogeneous Particle Size

Suspended Sediment Concentration (SSC) and sediment mass load for each of the 40 simulated scenarios were determined with the 2D-CFD model. Additionally, the cumulative mass loss was determined across a 20 min time period. Figure 107 and 108 present the cumulative total mass loss for several of the simulated scenarios. Figure 109 and 110 show SSC plots for the relevant scenarios described in this chapter.

As mentioned in previous chapters, one of the expected SSC results when using sediment material with a homogenous particle size was an exponential reduction in the concentration over time, similar to the pattern obtained with the sediment mixture in the full-scale physical model. However, a relatively constant SSC was obtained with both CFD modeling and full-scale physical experimentation with sediment material with a homogenous particle size. This finding is attributed to the absence of an armoring layer formed by large particles which protect smaller particles from scour within minutes after the water jet impact. In the case of sediment with a homogeneous particle size, all particles on the sediment surface were exposed continuously to scour during 20 min of continuous flow. However, the scoured mass was not large enough to increase the overlaying water depth to the point where sediment scour would decrease. Nevertheless, it is expected that after longer periods of time with continuous flow, the scour rate would decrease as the overlaying water depth increased, especially below the plunging water jet, where a hole is created in the sediment surface.

The sediment mass remaining in the control volume was recorded every 10 sec of the CFD simulation period. However, the actual time step of the simulations was about $1x10^{-3}$ sec. The difference in sediment mass between the time intervals is the mass loss in grams, which, when divided by the time interval 0.167 min (10 sec), represents the mass load in g/min.

Consequently, using the appropriate conversion factor, the SSC is calculated by dividing the mass load by the flow rate. The concentration (in mg/L) then is obtained for every 10 sec time interval.

Figure 107 shows the cumulative mass loss plotted by particle size for the scenario with a 5 L/s flow rate and sediment 24 cm below the outlet. The figure shows that for all the evaluated particle sizes, the cumulative mass loss increases linearly with time, suggesting a constant SSC within the 20 min time of simulation. The slope of each cumulative mass loss rate represents the mass load, which substantially decreases as the particle size increases.

In the scenario presented in Figure 107, the maximum total mass loss obtained after 20 min of continuous flow was 2.0 Kg, based on a sediment particle size of 50 µm. With the 180-µm sediment particle sizes, the total mass loss at 20 min decreased to 1.3 Kg, representing a reduction of 35%. Finally, with sediment particles 500 µm in size, the total mass loss was reduced to 0.1 Kg, which is a reduction of 92% in mass compared to the case with the 180-µm particle size. These reduction percentages suggest a rapidly reducing scour rate as the particle sizes increase.

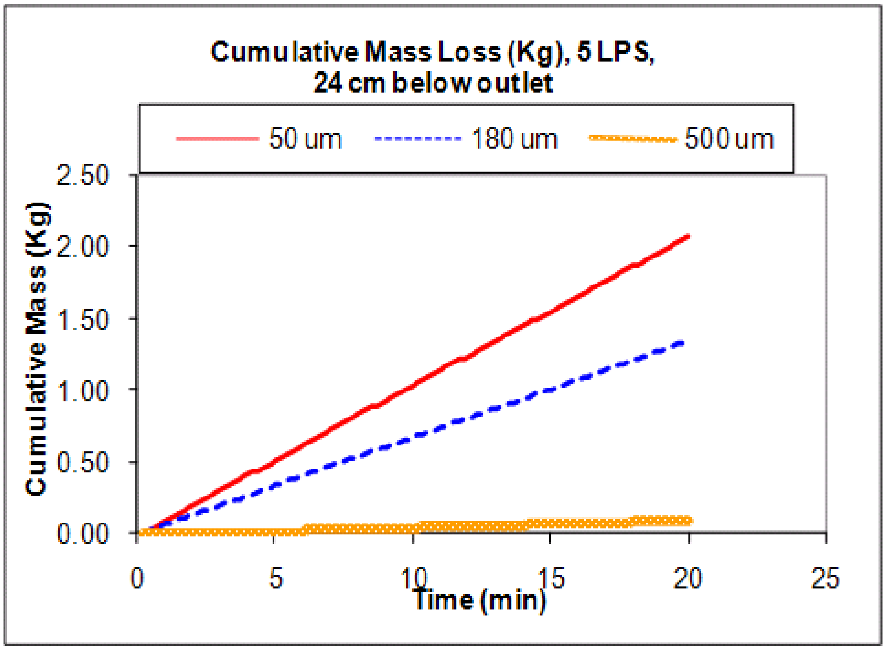

Figure 107. Cumulative mass loss (Kg) at 5 L/s and sediment at 24 cm below the outlet.

Figure 108 shows the cumulative mass load for the scenario with sediment 24 cm below the outlet and a 10 L/s flow rate. The scale of the cumulative mass loss was modified using a logarithmic scale due to the large difference in mass load between particle sizes. The total mass loss after 20 min of simulation time, with particles of 50 µm in size, was about 10 Kg, while with particles of 180 µm in size, the total mass loss was 6.4 Kg, which represents a 36% reduction. With the 500-µm particle size, the total mass loss was reduced to 2.0 Kg. Finally, the mass loss was reduced to 0.17 Kg for particles of 1000 µm in size.

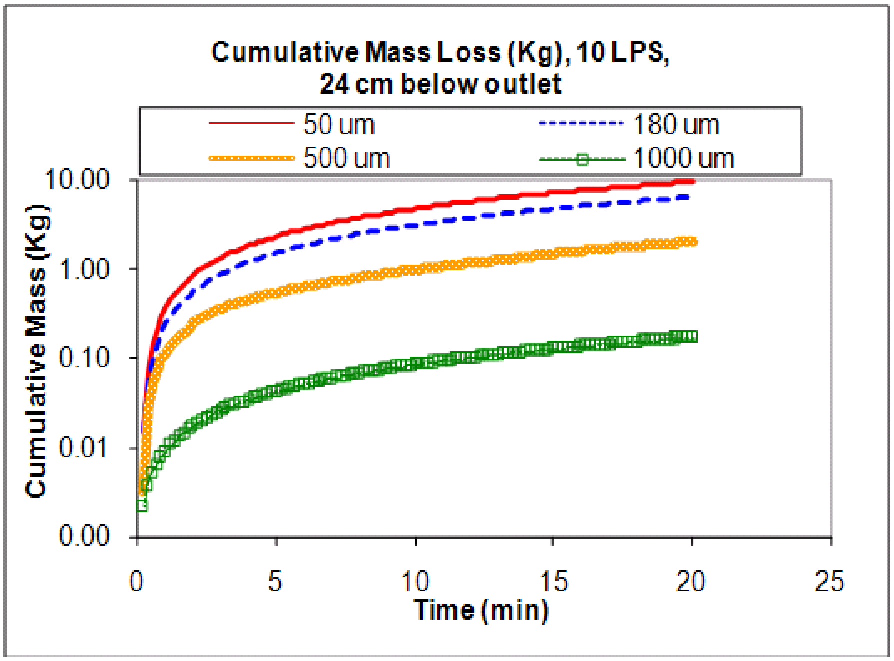

Figure 108. Cumulative mass loss (Kg) at 5 L/s and sediment 24 cm below the outlet. Cumulative mass loss in logarithmic scale.

Figure 109 shows the SSC time series over a period of 20 min with a 20 L/s flow rate, overlaying water depth of 24 cm, and particle sizes of 50, 180, 500, and 1000 µm. The SSC concentration was determined every 10 sec. The figure shows that the SSC for particles of 1000 µm in size is relatively high, 65 mg/L, when compared to the SSC at lower flow rates. In the same scenario using 5 L/s (Figure 110), the SSC of particles 1000 µm in diameter was negligible in practical terms, less than 1 mg/L.

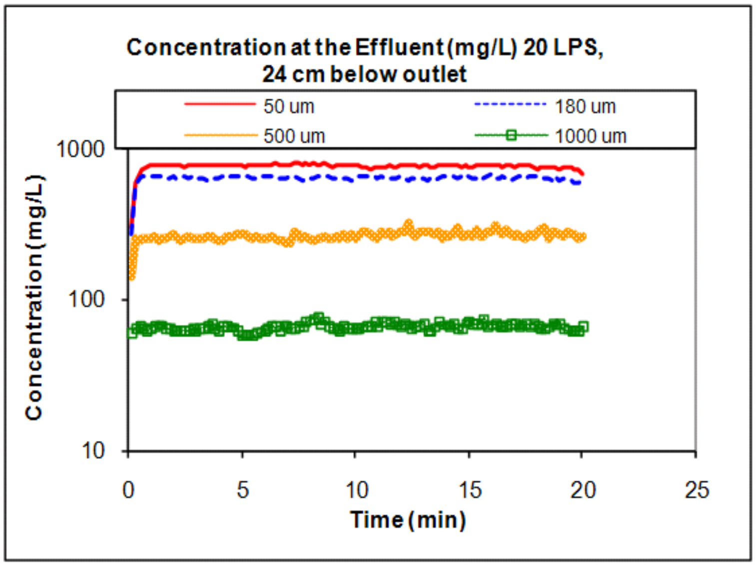

Figure 109. SSC time series plot at 20 L/s and sediment 24 cm below the outlet. Sediment material with homogeneous particle size.

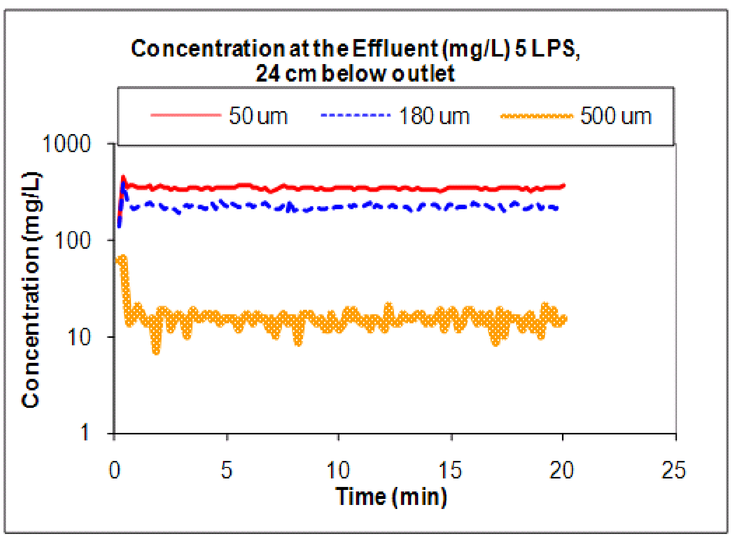

Figure 110. SSC time series plot at 5 L/s and sediment 24 cm below the outlet. Sediment material with homogeneous particle size.

When observing the SSC time series, it can be seen that the variation of SSC is higher for large overlaying water depths and lower when the depth is small. This is primarily due to the way the plunging water jet affects the sediment surface. For low overlaying water depths, the plunging water jet constantly and directly impacts the sediment surface, causing a constant scour rate. In contrast, at deeper locations, the plunging jet tends to affect the sediment surface with certain random oscillations, which are products of the turbulent conditions and the buoyancy caused by the air entrainment.

Simple linear regression was applied to all the cumulative mass loss series over the 20 min interval, using time as the predictor variable. The slope term was calculated for all the scenarios with simple linear regression, including ANOVA.

All the p-values were less than 0.001, which indicates the significance of the coefficient. The intercept terms were also significant for most of the cases, but the magnitudes were very close to zero, as is expected since at time zero the mass loss is zero. Therefore, a zero intercept was used as a constraint to determine a grand-mean mass load and a grand-mean SSC for all the scenarios.

Table 24 shows the mean SSC for all the scenarios evaluated at 10 L/s.

Table 24. SSC (mg/L) Calculated from Mass Loss as a Slope of the Cumulative Mass Loss at 10 L/s (CFD Results with Sediment Material with Homogeneous Particle Size)

Flow rate (L/s)	**Depth (cm)**	**Particle size (μm)**	**Mass Loss (g/min) (slope)**	**SSC (mg/L)**
10	15	50	777.6	1296.0
10	15	180	651.4	1085.7
10	15	500	342.8	571.3
10	15	1000	66.1	110.2
10	24	50	480.2	800.3
10	24	180	347.5	579.2
10	24	500	97.6	162.7
10	24	1000	8.4	14.0
10	35	50	316.4	527.3
10	35	180	113.2	188.7
10	35	500	22.2	37.0
10	40	50	111.2	185.3
10	40	180	24.2	40.3

Table 25 shows the percent of SSC reduction by the particle size increment for the 10 L/s flow rate scenario.

Table 25. Percentage Reduction of SSC (mg/L) by Increment of Consecutive Particle Sizes for 10 L/s Flow Rate (CFD Results)

Flow rate (L/s)	**Depth (cm)**	**SSC (mg/L)**	**Particle size (μm)**	**% Reduction of SSC by Particle Size Increment**
10	15	1296.0	50	
		1085.7	180	16
		571.3	500	47
		110.2	1000	81
	24	800.3	50	
		579.2	180	28
		162.7	500	72
		14.0	1000	91
	35	527.3	50	
		188.7	180	64
		37.0	500	80
	40	185.3	50	
		40.3	180	78

Table 26 shows the percent of SSC reduction by the increment of consecutive overlaying water depth for the 10 L/s flow rate scenario.

Table 26: Percentage Reduction of SSC (mg/L) by Increment of Consecutive Overlaying Water Depth for 10 L/s Flow Rate (CFD Results)

Flow rate (L/s)	Particle size (μm)	SSC (mg/L)	Depth (cm)	% Reduction of SSC by Depth
10	50	1296	15	
		800	24	38
		527	35	34
		185	40	65
	180	1086	15	
		579	24	47
		189	35	67
		40	40	79
	500	571	15	
		163	24	72
		37	35	77
	1000	110	15	
		14	24	87

Flow rate generally increased the SSC in most cases, as is shown in Table 27 for 180-μm particle size. However, in some cases (especially with small sediment particle sizes and small overlaying water depths), the SSC decreases as the flow rate increases. This effect is attributed to the dilution of the sediment mass at high flow rates. Mass load (Table 28) increases as a function of flow rate. However, mass load as a function of flow rate is a spurious relationship, because mass load also depends on flow rate; however, these values are shown to illustrate that the scour rate increases as a function of flow rate.

Table 27. Percentage of Change of SSC (mg/L) by Increment of Consecutive Flow Rates for 180 μm (CFD Results)

Flow rate (L/s)	**Depth (cm)**	**Particle size (μm)**	**SSC (mg/L)**	**% of Change of SSC by Flow rate**
5	15	180	1106.7	
10			1085.7	-2
20			838.1	-30
5	24		225.0	
10			579.2	61
20			635.9	9
5	35		1.0	
10			188.7	99
20			427.7	56
10	40		40.3	
20			273.8	85

Table 28. Percentage of Change of Mass Load (g/min) by Increment of Consecutive Flow Rates for 180 μm (CFD Results)

Flow rate (L/s)	**Depth (cm)**	**Particle size (μm)**	**Mass Load (g/min)**	**Total mass loss in 20 min (Kg)**	**% Increment of mass load and mass loss by Flow rate**
5	15	180	332	6.64	
10			651.4	13.028	49
20			1005.7	20.114	35
5	24		67.5	1.35	
10			347.5	6.95	81
20			763.1	15.262	54
5	35		0.3	0.006	
10			113.2	2.264	100
20			513.2	10.264	78
10	40		24.2	0.484	
20			328.5	6.57	93

CHAPTER 10

DETERMINATION OF REGRESSION MODELS TO ESTIMATE SCOURED SUSPENDED SEDIMENT CONCENTRATION IN CATCHBASIN SUMPS

10.1 SSC Results from a Full-scale Physical Experimentation – Sediment Mixture

A regression model to estimate the Suspended Sediment Concentration (SSC) in mg/L, given the flow rate (*Q*) in L/s, and the overlaying water depth above the sediment (*H*) in cm, was determined for the 0-5 min and 5-25 min experimental composite samples, respectively.

Multiple regression models available in statistical software packages (Minitab 15 and JMP 7) were evaluated with several variable transformations. However, none of the alternatives evaluated achieved satisfactory levels of fit with the response variable (SSC). Therefore, a customized regression model was created based on the trend of individual parameters with the response variables.

Initially, SSC was plotted against the overlaying water depth and the flow rate to find an approximate pattern useful to determining the most feasible mathematical form for the regression model. Figure 111 and 112 show SSC versus the overlaying water depth for both 0-5 min and 5-25 min composite samples. Figure 111 reveals a rapid reduction of the SSC as the depth of water decreases. However, experimental values could not be fitted with either an exponential or power equation, because the SSC reduction rate is much higher than with any of those equations. This would cause under-estimation of higher SSC when the overlaying water depth is small or when flow rates are high.

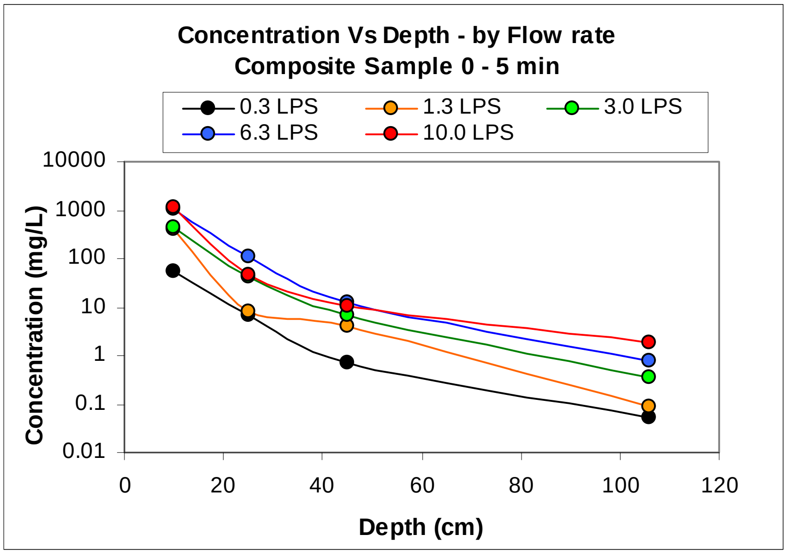

Figure 111. Suspended sediment concentration versus overlaying water depth, plotted by flow rate. Results for the 0-5 min composite samples.

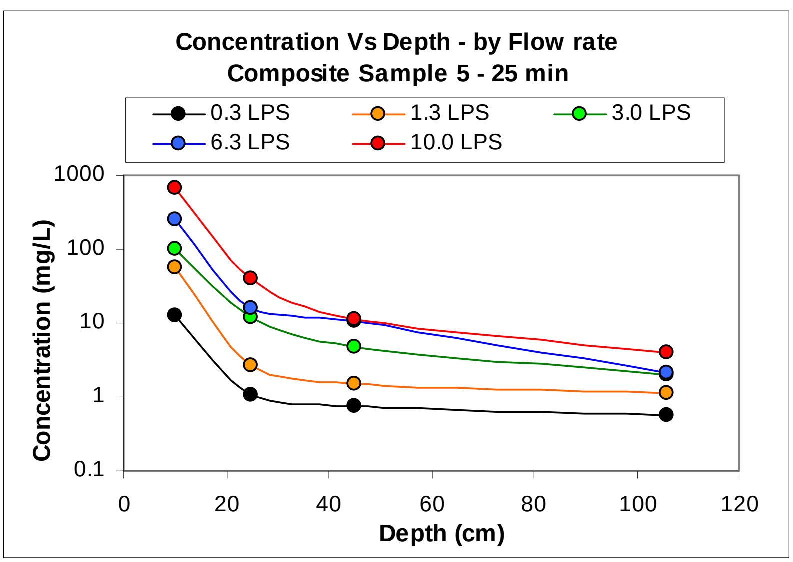

Figure 112. Suspended sediment concentration versus overlaying water depth, plotted by flow rate. Results for the 5-25 min composite samples.

Figure 113 and 114 show SSC versus flow rate, plotted by the overlaying water depth. These figures showed a fractional power trend useful to be implemented as a general regression model for SSC.

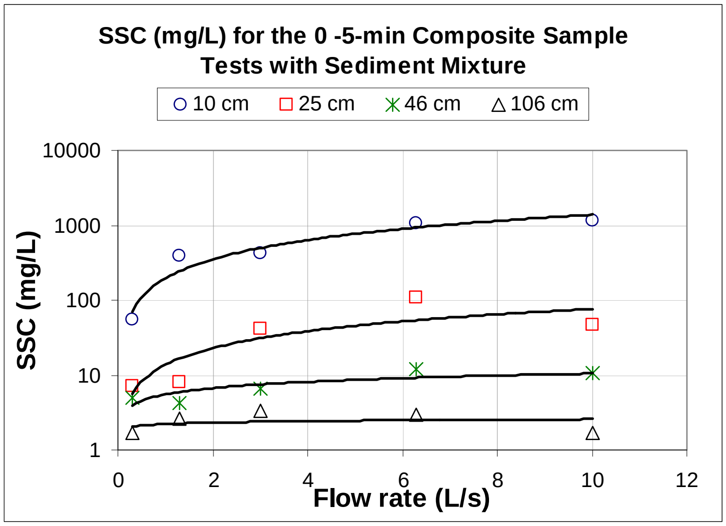

Figure 113. Suspended sediment concentration versus flow rate, plotted by overlaying water depth. Results for the 0-5 min composite samples.

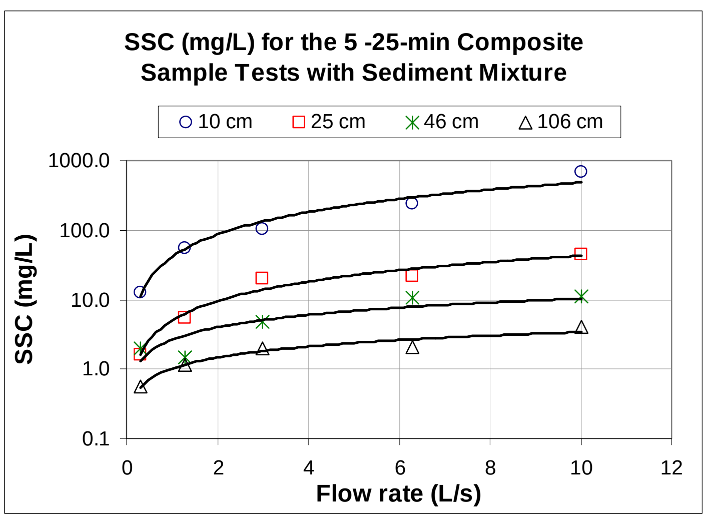

Figure 114. Suspended sediment concentration versus flow rate, plotted by overlaying water depth. Results for the 5-25 min composite samples.

The general regression model form is given by

$$SSC = f_1(H) \cdot Q^{f_2(H)}, \quad \text{Equation 52}$$

where *SSC* is the Suspended Sediment Concentration (mg/L), *H* is the overlaying water depth or depth below the outlet (cm), *Q* is the flow rate (L/s or L/s), and $f_1(H)$ and $f_2(H)$ are functions of the overlaying water depth

Table 29 shows the coefficients, $f_1(H)$, and exponents, $f_2(H)$, of each power trend line determined in Figure 115.

Table 29. $f_1(H)$ and $f_2(H)$ for 0-5 min and 5-25 min Composite Samples

0 - 5 min Composite Sample			**5 - 25 min Composite Sample**		
$f_1(H)$	$f_2(H)$	R^2	$f_1(H)$	$f_2(H)$	R^2
195.73	0.85	0.94	41.05	1.07	0.97
13.67	0.75	0.75	3.05	1.02	0.96
2.38	0.80	0.94	1.74	0.81	0.95
0.12	0.90	0.92	1.02	0.52	0.95

The preliminary *f(H)* for the 0-5 min composite samples is given by the following equations. The fitted lines of the equations are shown in Figure 115.

$$f_1(H) = (670)^2 \cdot H^{-3.36}$$ Equation 53

$$f_2(H) = 0.74 \cdot H^{0.032}$$ Equation 54

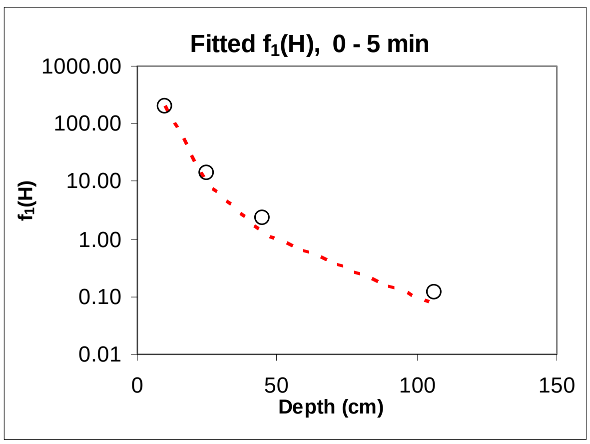

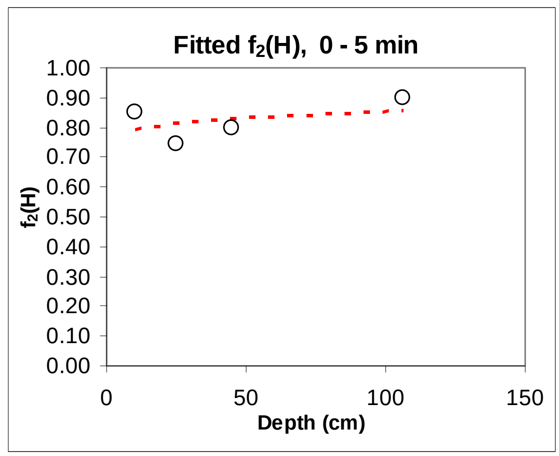

Figure 115. Fitted and observed $f_1(H)$ (left) and $f_2(H)$ (right) for the 0-5 min composite samples.

Also, the preliminary *f(H)* for the 5-25 min composite samples is given by the following equations. The fitted lines of the equations are shown in Figure 116.

$$f_1(H) = (105)^2 \cdot H^3 [\ln(H)]^{-15}$$ Equation 55

$$f_2(H) = 2.06 \cdot H^{-0.26}$$ Equation 56

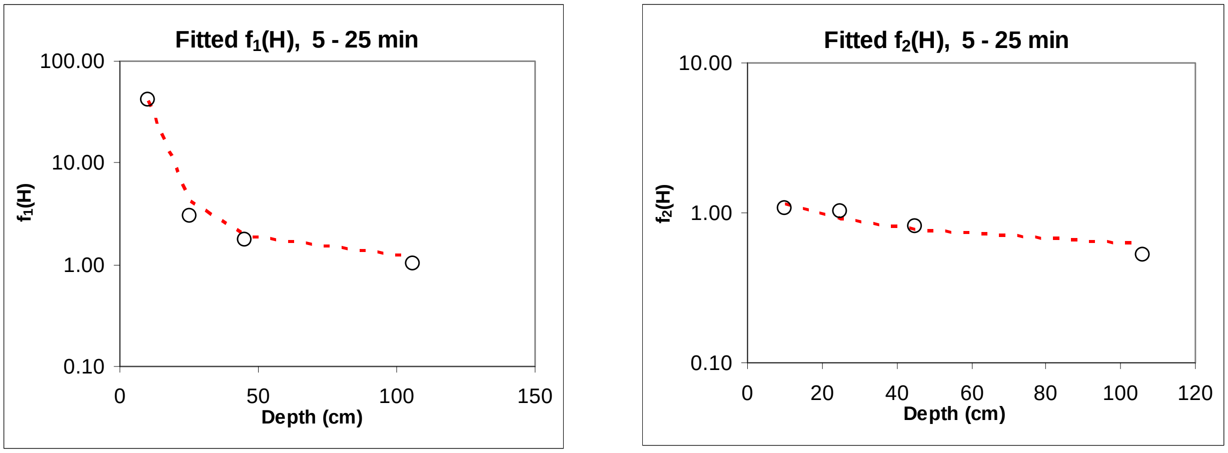

Figure 116. Fitted and observed $f_1(H)$ (left) and $f_2(H)$ (right) for the 5-25 min composite samples.

The previous equations are only a first approach to the complete form $SSC = f_1(H) \cdot Q^{f_2(H)}$, which needs to be calibrated for the whole data set, based on the functions $f_1(H)$ and $f_2(H)$ where calculated for each composite sample. The parameters for the complete form of the regression model for SSC were determined by Monte Carlo simulations. The target function of the simulations was an $R^2 = 1$. Residual analyses were performed for each equation to determine the degree of approximation.

10.1.1 *Regression Model of SSC for the 0-5 min Composite Samples*

A calibrated regression model was found for the 0-5 min composite samples with an $R^2 = 0.92$. The equation was determined as:

$$SSC = (670)^2 \cdot H^{-3.32} \cdot Q^{\left(0.92 H^{-0.15}\right)}. \qquad \text{Equation 57}$$

Figure 117 shows fitted and observed SSC magnitudes with the 95% confidence and prediction intervals. The figure shows that the equation estimates the observed concentrations fairly well. The observed versus fitted values are within the prediction interval, and the data fall close to the 45° line. It is possible to see that the confidence interval is narrower at lower concentrations and wider at higher concentrations. This is mainly due to the 80% of the 20 observed concentrations that are below 150 mg/L. Higher concentrations prove to be more difficult to estimate; however, the percentage of error at higher concentrations is relatively low in comparison to the magnitude of the concentrations, as is shown in Figure 119.

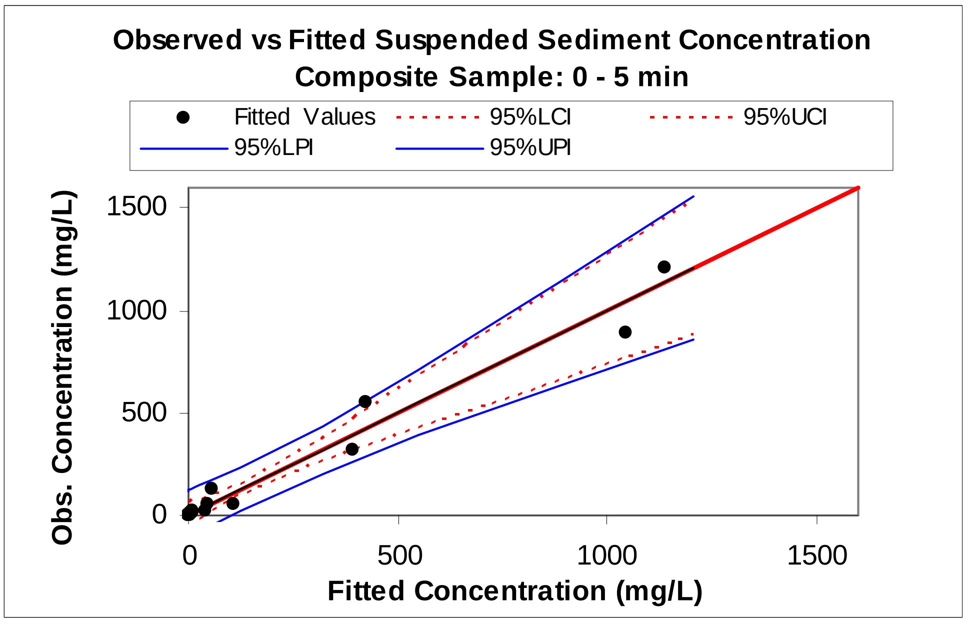

Figure 117. Observed versus fitted suspended sediment concentrations for the 0-5 min composite samples.

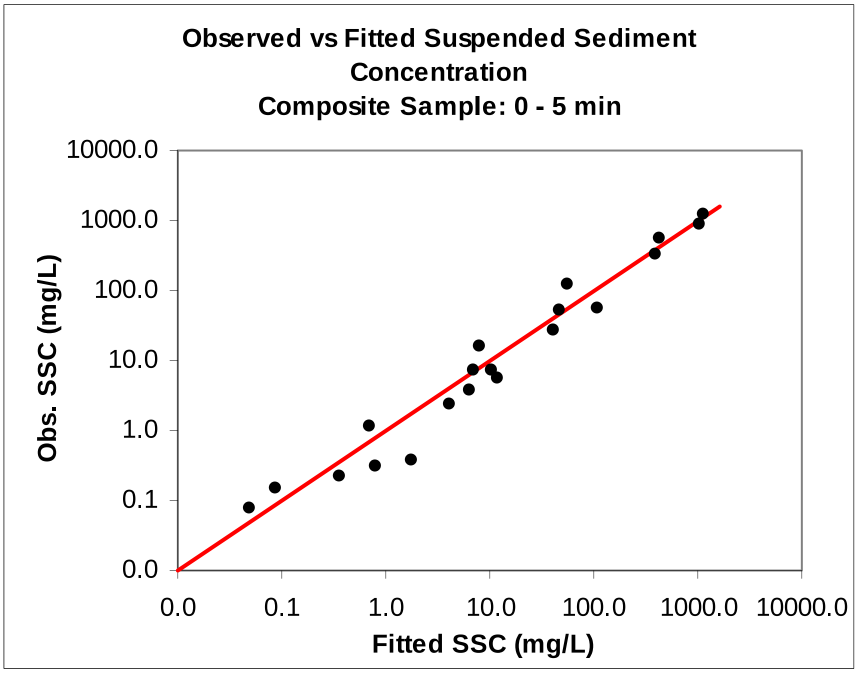

Figure 118. Observed versus fitted suspended sediment concentrations in logarithmic scale for the 0-5 min composite samples.

Residuals versus fitted values (Figure 119) do not show strong evidence of any trend. Also, the figure shows that two observations have residuals greater than 100 mg/L; however, these maximum residuals represent a percentage of error below 25%, which is acceptable given the nature of the scour phenomenon that includes an important randomized process. The maximum percentage of error found with experimental data was 38%.

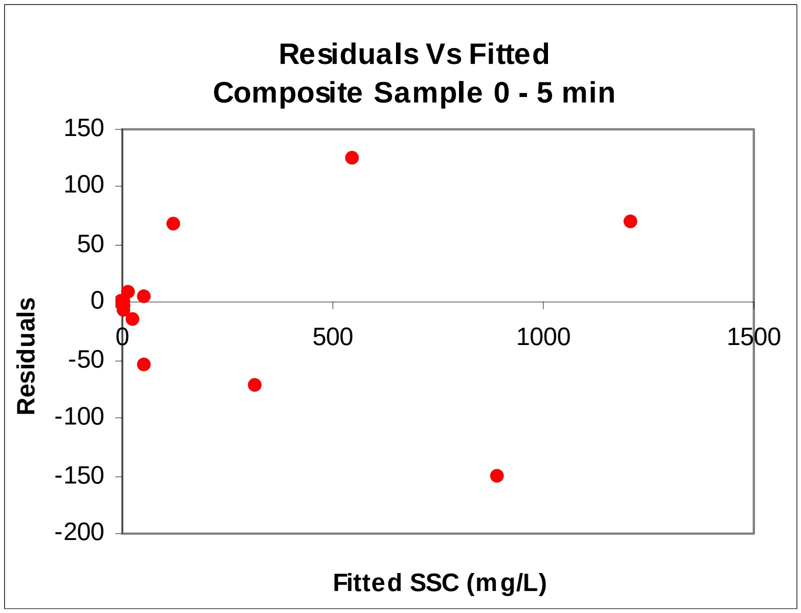

Figure 119. Residuals versus fitted values of suspended sediment concentrations for the 0-5 min composite samples.

Normality of the residuals was checked in Figure 120. The figure shows that a great portion of the residuals are close to zero, which is an indication of the good performance of the prediction equation. The unusual residuals that deviate from the normal curve appear to be small in relation to the actual values, so the error level is relatively small; 25%, which is not greater than 25% for residuals greater than 100 mg/L. It is important to clarify that the normality assumption of the residuals was achieved with other regression models; however, the percentage of error associated with the highest residuals was greater than 80%. In this case, it was decided to choose a model with the smallest residuals, even though the normality assumption of the residuals was not completely satisfied.

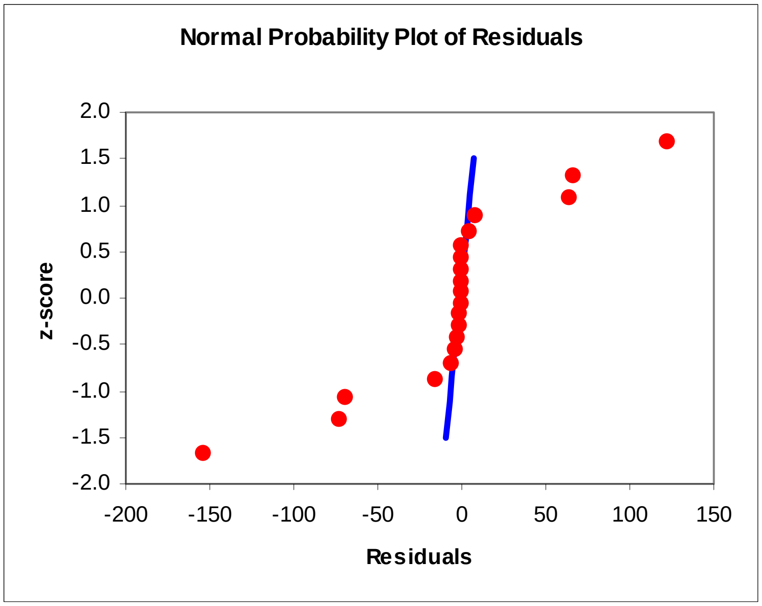

Figure 120. Normal probability plot of the residuals of suspended sediment concentrations for the 0-5 min composite samples.

In general, the regression model for Suspended Sediment Concentrations for the 0-5 min composite samples is seen to work appropriately within the range of conditions evaluated in this research.

Response surface plots of SSC for the 0-5 min composite samples were created to compare the observed and fitted concentrations. Figure 121 shows both experimental and fitted SSC response surfaces.

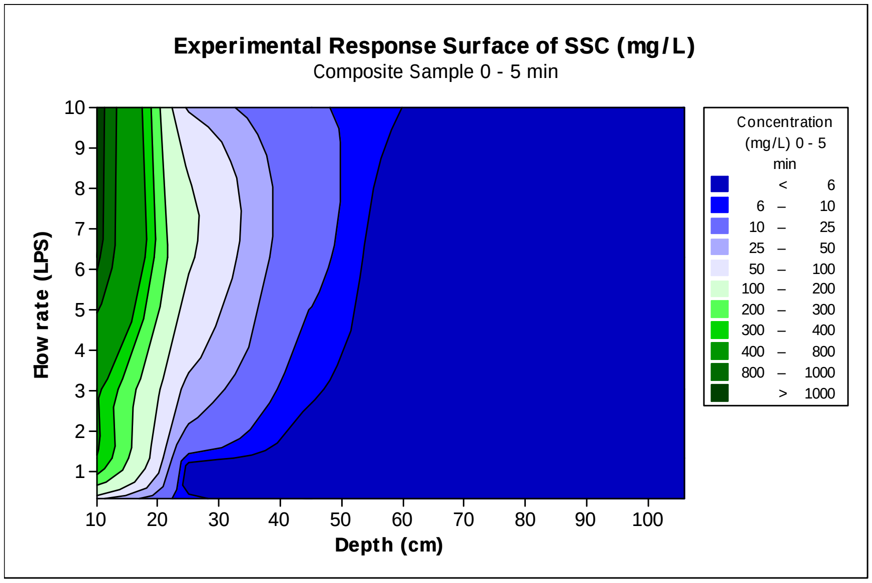

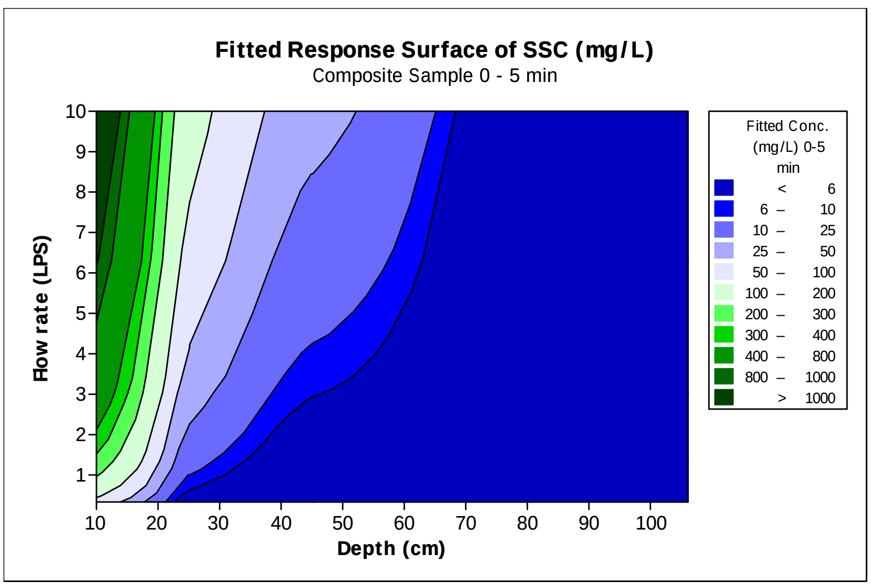

Figure 121. Response surface plots of suspended sediment concentration (SSC), mg/L as a function of flow rate (L/s) and overlaying water depth (cm). Experimental values (top) and fitted values (bottom).

The SSC response surfaces are very similar, especially for concentrations above 50 mg/L. For concentrations below 50 mg/L, the regression model tends to slightly over-estimate the concentrations for flow rates above 8.0 L/s. However, the over-estimation of the concentrations at 10 L/s by the regression model would cover the scenario at which no armoring is previously formed before this flow rate acts on the pre-deposited sediment.

10.1.2 *Regression Model of SSC for the 5-25 min Composite Sample*

The regression model of SSC for the 5-25 min composite sample was determined with an R^2= 0.93. The equation is given as:

$$SSC = (115)^2 \cdot H^3 \cdot [\ln(H)]^{-15} Q^{\left(1.6H^{-0.19}\right)}. \qquad \text{Equation 58}$$

Figure 122 shows fitted and observed SSC magnitudes with the 95% confidence and prediction intervals. The figure also shows that the regression model estimates the observed concentrations well, as the values are within the prediction interval and the linear regression line between observed and fitted values is close to the 45^{o} line. The confidence and prediction intervals are both narrower at lower concentrations and wider at higher concentrations, as 85% of the 20 observed concentrations are below 100 mg/L. Higher concentrations are shown to be difficult to estimate, but the percentage of error at higher concentrations is still relatively low in comparison to the magnitude of the concentrations.

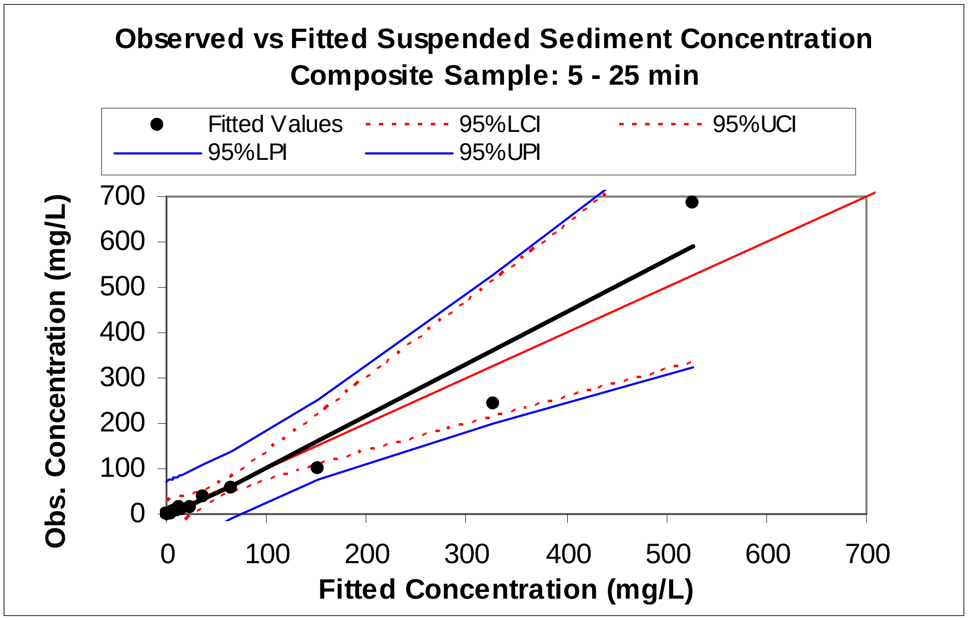

Figure 122. Observed versus fitted suspended sediment concentrations for the 5-25 min composite samples.

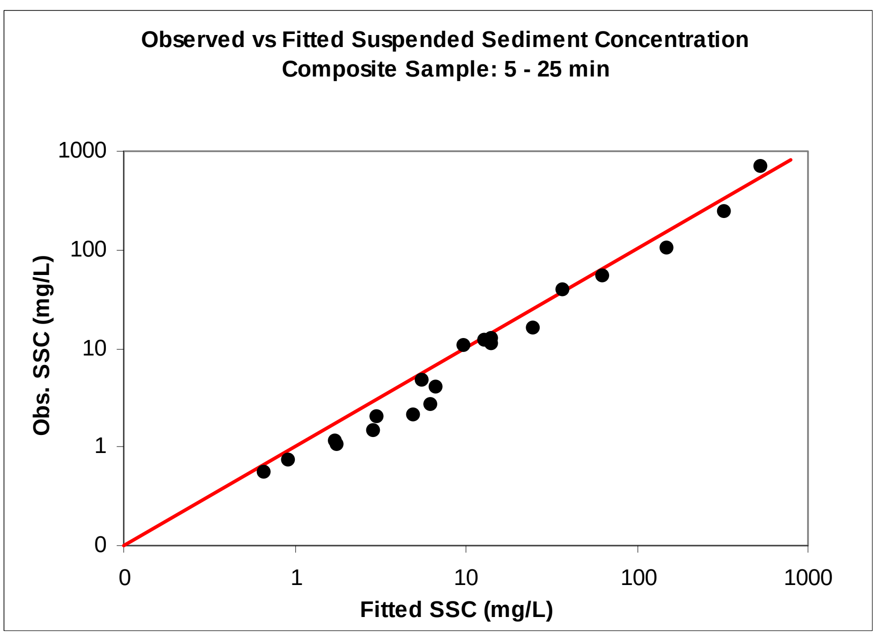

Figure 123. Observed versus fitted suspended sediment concentrations in logarithmic scale for the 5-25 min composite samples.

The residuals versus fitted values are presented in Figure 124. This figure shows that the residuals apparently have a trend. However, notice that 85% of the data is below 100 mg/L and only three values show relatively high concentrations with a maximum of 530 mg/L, so the scale of the concentration does not allow one to give a fair judgment of the random pattern of the residuals. The highest residual of 150 mg/L related to the concentration of 530 mg/L is about 28%, which is lower than the maximum percentage of error (38%) found with experimental data.

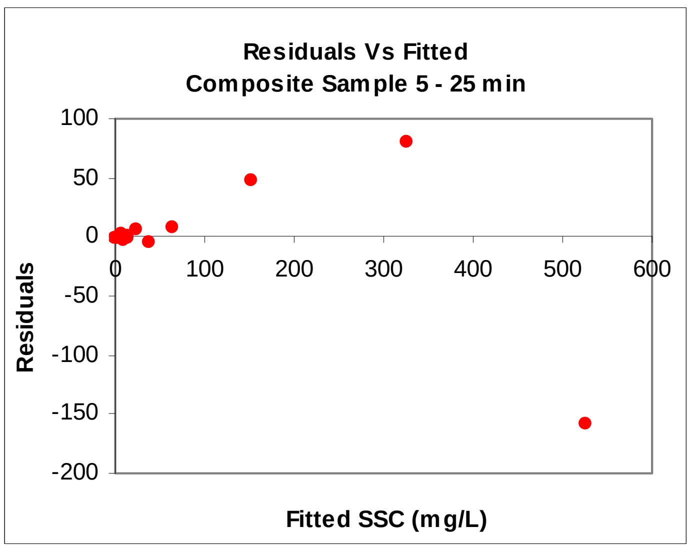

Figure 124. Residuals versus fitted values of suspended sediment concentrations for the 5-25 min composite samples.

If the residuals are plotted in a range of fitted values up to 100 mg/L, the random pattern appears to be evident and the residuals achieve the random assumption for 85% of the data.

The normal probability plot of the residuals is presented in Figure 125. With the exception of three points, the residuals look normal. Additionally, the residuals of 85% of the data are very small. The highest residuals are less than 30% in error related to their fitted concentrations.

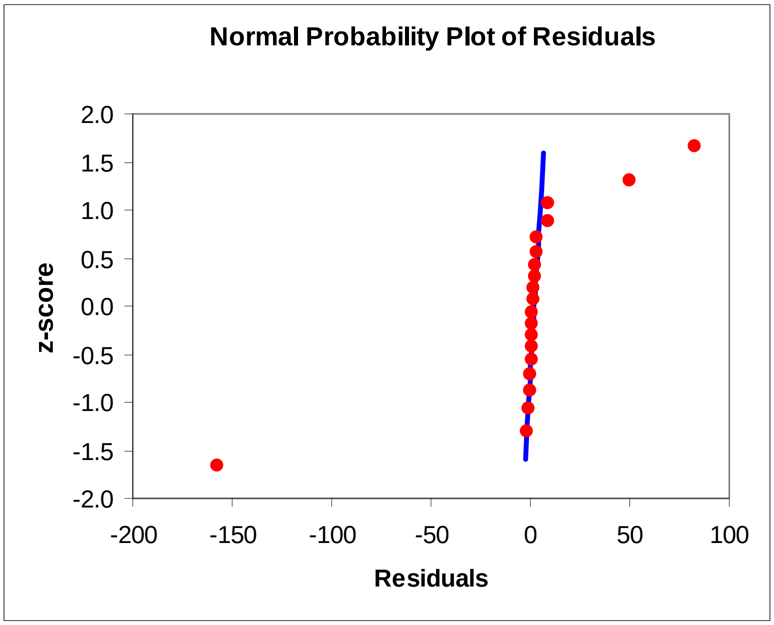

Figure 125. Normal probability plot of the residuals of suspended sediment concentrations for the 5-25 min composite samples.

The experimental and fitted SSC response surfaces for the 5-25 min composite samples are shown in Figure 126. The response surfaces show great similarity for concentrations greater than 10 mg/L. At lower concentrations, the prediction equation slightly over-predicted the SSC at a 10 L/s flow rate due to the effect of the consecutive flow rate procedure described above. This does not represent a major issue, as the concentrations on this range are small (lower than 10 mg/L), and the over-prediction of the fitted model is for scenarios where no substantial armoring was previously formed.

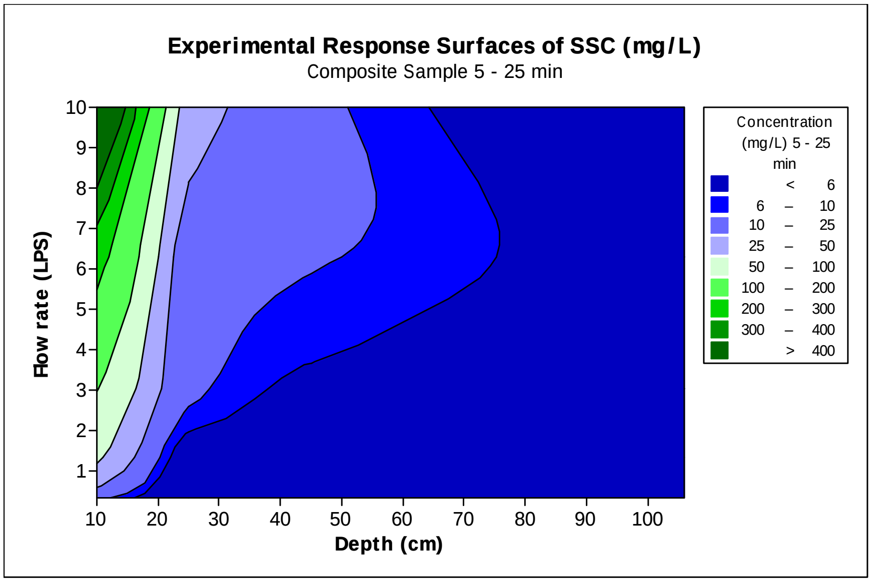

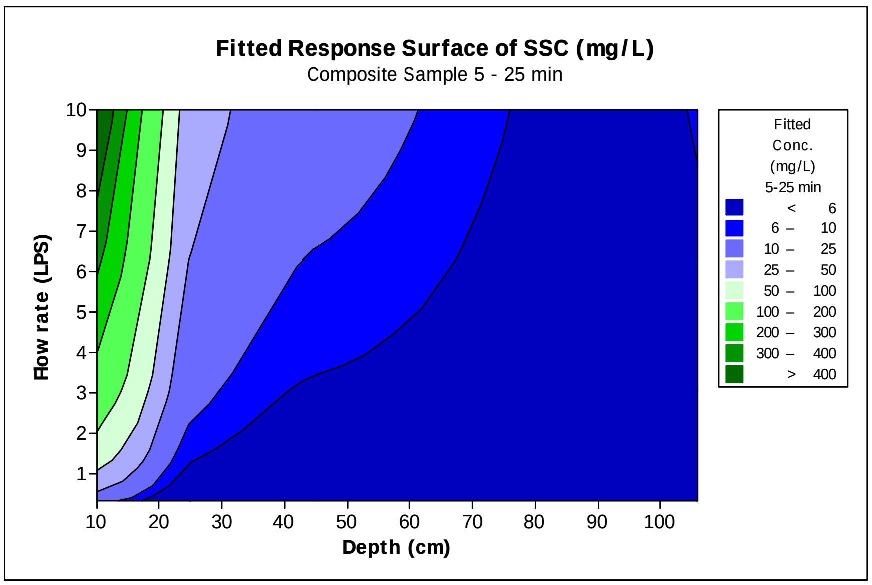

Figure 126. Response surface plots of suspended sediment concentration (SSC), mg/L as a function of flow rate (L/s) and overlaying water depth (cm). Experimental values (top) and fitted values (bottom).

Mass load is obtained by multiplying SSC by its corresponding flow rate. Figure 127 and 128 show the response surface of mass load as a function of the flow rate and overlaying water depth for the 0-5 min composite samples. Notice that the response mass load, plotted as a function of flow rate, is also correlated to flow rate (a spurious self-correlation); however, these plots present a direct measure of the scour rate in terms of mass loss per unit time for the given conditions of flow rate and overlaying water depth.

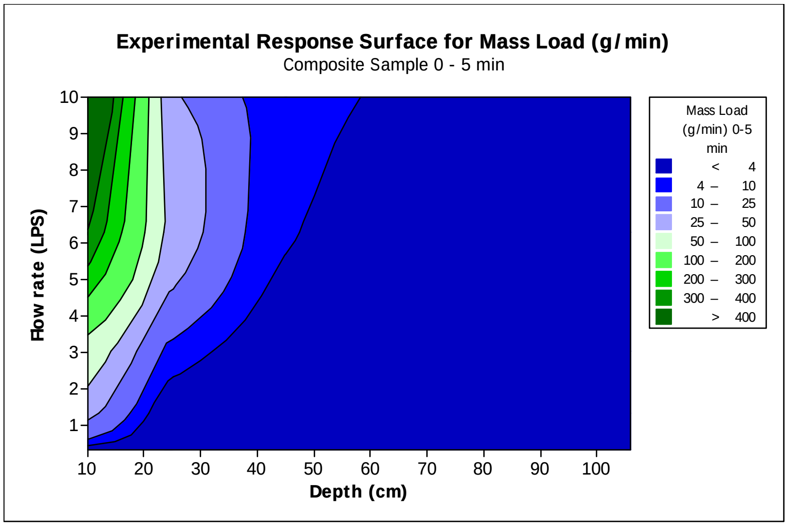

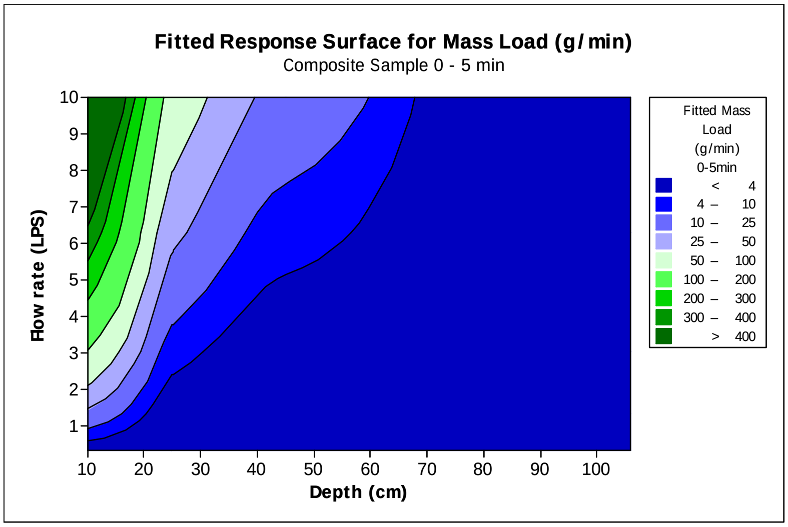

Figure 127. Response surface plots of mass load in g/min, as a function of flow rate (L/s) and overlaying water depth (cm). Experimental values (top) and fitted values (bottom) of the 0.5 min composite samples.

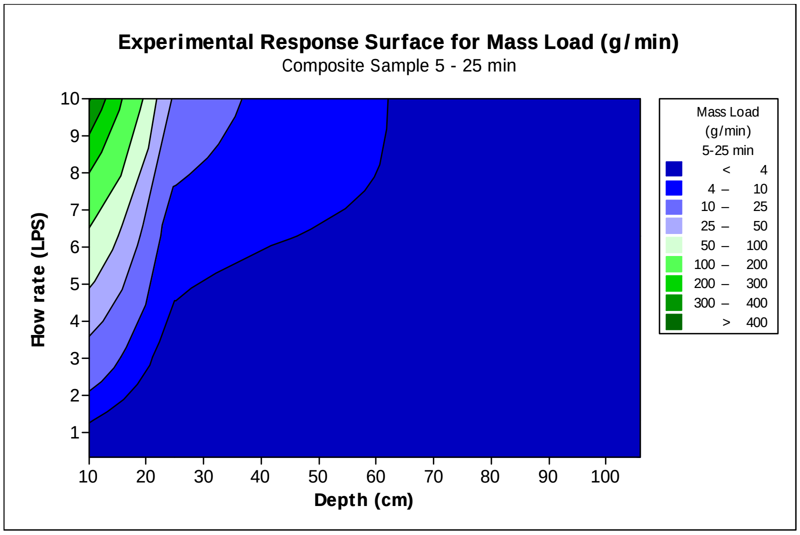

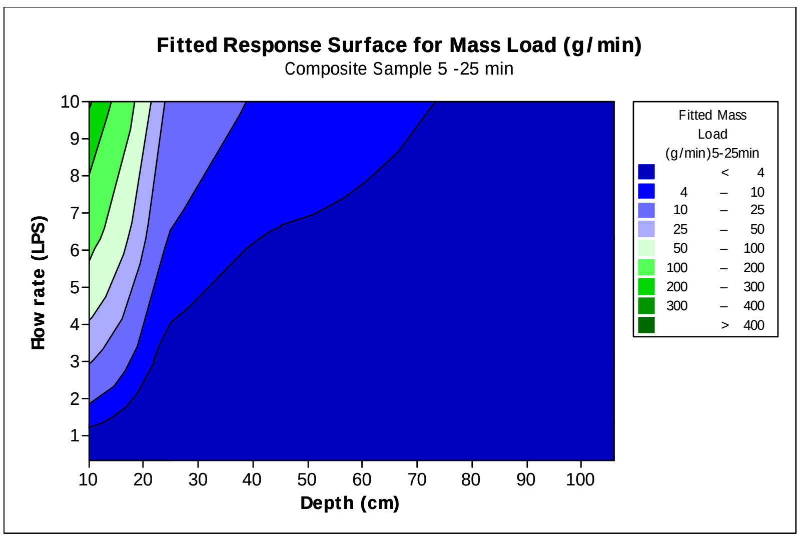

Figure 128. Response surface plots of mass load in g/min, as a function of flow rate (L/s) and overlaying water depth (cm). Experimental values (top) and fitted values (bottom) of the 5-25 min composite samples

10.2 Computational Fluid Dynamic Results – Sediment with Homogeneous Particle Sizes

Each SSC time series calculated with the 2D-CFD model showed a constant magnitude within the 20 min of simulation. These results were consistent with the experimental tests obtained with a homogeneous particle size, as described in previous chapters.

Based on the mean SSC for each simulated scenario, a series of plots were created to determine relationships between SSC and the different factors involved in the scour phenomenon, such as sediment particle size, flow rate, and overlaying water depth.

Two regression models are proposed in this chapter to determine the SSC for a range of particle sizes between 50 and 100 µm, flow rates between 5 and 20 L/s, and overlaying water depth between 15 and 45 cm. The first model is based on individual linear equations aggregated into a general mathematical form. The second one is a multiple linear regression model.

10.2.1 *Relationship between SSC and Sediment Particle Size*

Suspended Sediment Concentration was plotted as a function of sediment particle size. This relationship showed that SSC decreases exponentially as the particle size increases. Figure 129 shows the SSC versus sediment particle size scenario at 20 L/s flow rate plotted by overlaying water depth. The exponential pattern is consistent in all the scenarios.

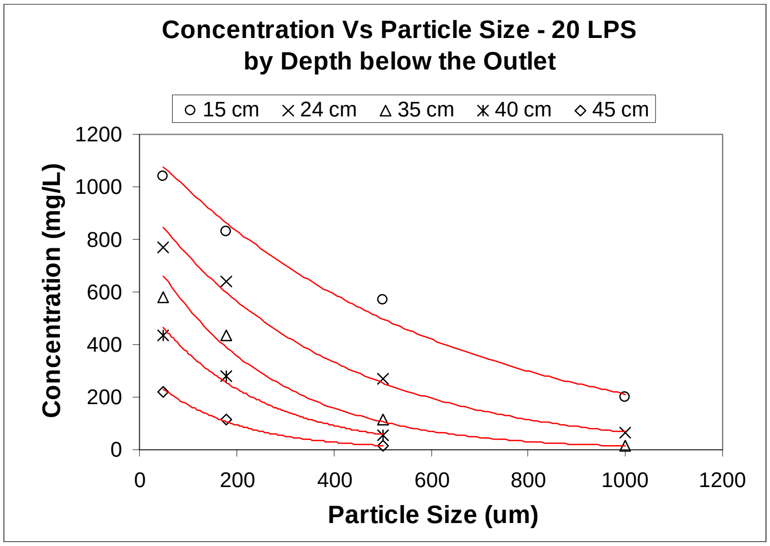

Figure 129. Suspended sediment concentration (mg/L) versus sediment particle size (µm) plotted by overlaying water depth (cm) (scenario at 20 L/s flow rate).

A direct measurement of the scour rate is given by the mass load showed in Figure 130.

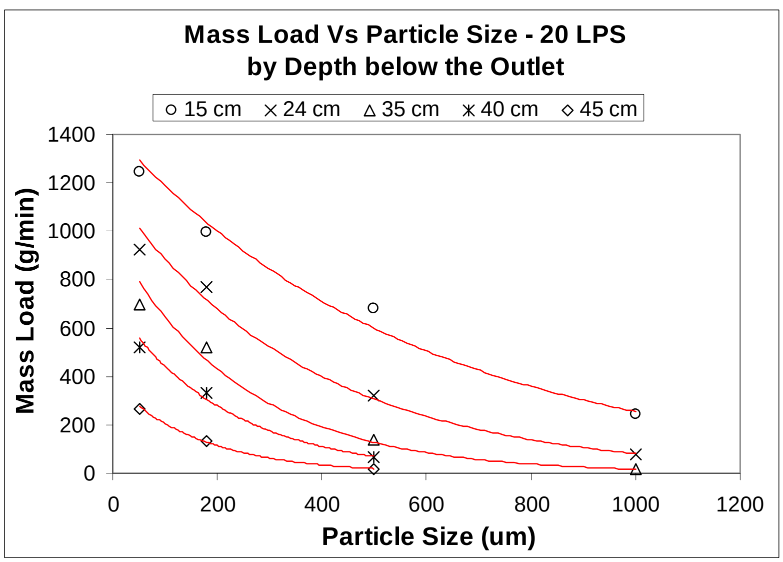

Figure 130. Mass load (g/min) versus sediment particle size (µm) plotted by overlaying water depth (cm) (scenario at 20 L/s flow rate).

10.2.2 *Relationship between SSC and Overlaying Water Depth*

When SSC is related to the overlaying water depth, the concentration decreases linearly with depth. This finding differs from the case when a sediment mixture is used as a pre-deposited material where the pattern was exponential. Figure 131 shows the linear pattern between SSC and overlaying water depth for the 20 L/s flow rate scenario. Mass load is also plotted as a function of depth in Figure 132.

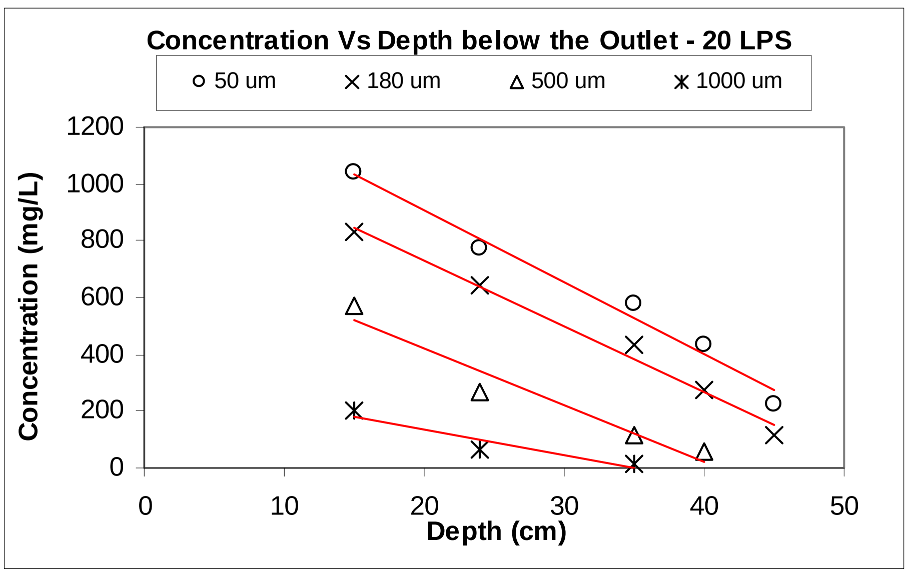

Figure 131. Suspended sediment concentration (mg/L) versus overlaying water depth (cm) plotted by sediment particle size (μm) (scenario at 20 L/s flow rate.)

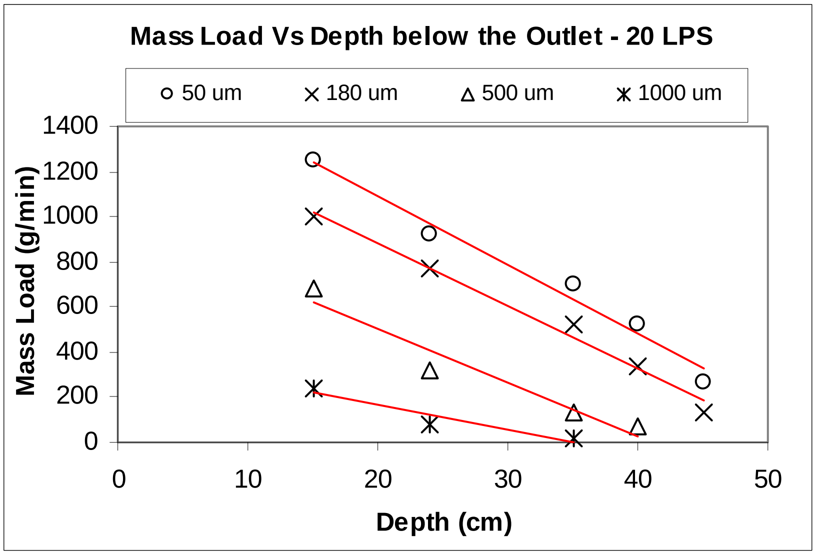

Figure 132. Mass load (g/min) versus overlaying water depth (cm) plotted by sediment particle size (µm) (scenario at 20 L/s flow rate).

The linear pattern found with a homogeneous sediment particle size is mainly due to the absence of the armoring layer which was formed when the sediment mixture was used. The sediment mixture contains large particle sizes, which rapidly protect the finer sediment a few minutes after being exposed to the plunging water jet, causing a faster reduction of the SSC.

When the pre-deposited sediment is homogeneous in size, it will always be exposed to significant scour until the sediment mass is no longer in contact with shear stresses higher than the critical shear stress corresponding to a given particle size. Field experimentation and CFD results in this research showed that the only mechanism that protects sediment with a homogeneous particle size from being scour is the overlaying water depth. The scour rate will decrease when a hole is created on the sediment surface right below the plunging water jet, reducing the magnitude of the acting shear stress on the sediment surface.

10.2.3 *Relationship between SSC and Flow Rate*

Suspended Sediment Concentrations did not show a consistent pattern with flow rate when SSC is plotted by particle size. For some particle sizes, the SSC decreases when the flow rate increases. This is attributed to the dilution of the sediment mass. When the flow rate increases, the scour mass consistently increases as well. However, the proportion of the increments in scoured-sediment mass is smaller than the proportion of the increments of flow rate, especially for small particle sizes.

Figure 133 shows that, for particles 1000 µm in size, SSC has a positive slope. As the particle size is reduced to 50 µm, the slope decreases. This observation clearly shows that sediment particle size has an important effect on the SSC that cannot be explained by these plots.

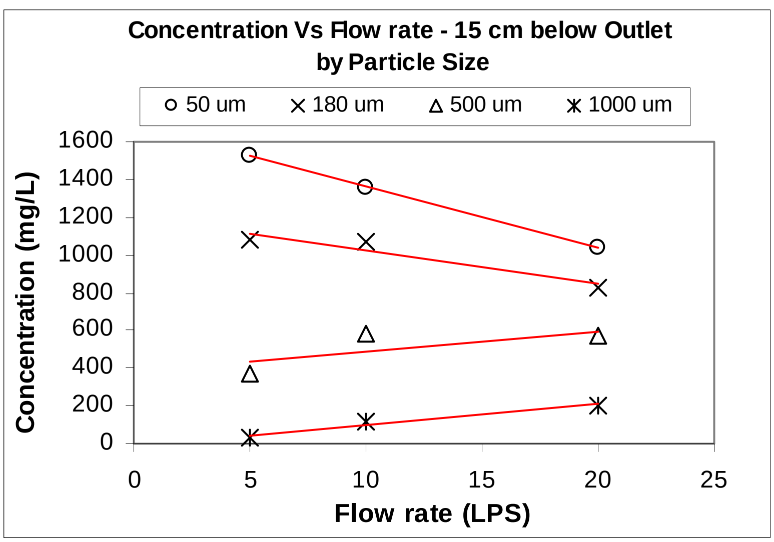

Figure 133. Suspended sediment concentration (mg/L) versus flow rate (L/s) plotted by sediment particle size (µm) (scenario of sediment 24 cm below the outlet).

However, if mass load is plotted as a function of flow rate (Figure 134) (a spurious self-correlation), it is possible to see that mass load consistently increases as flow rate increases. This indicates that the scour rate certainly increases as flow rate increases.

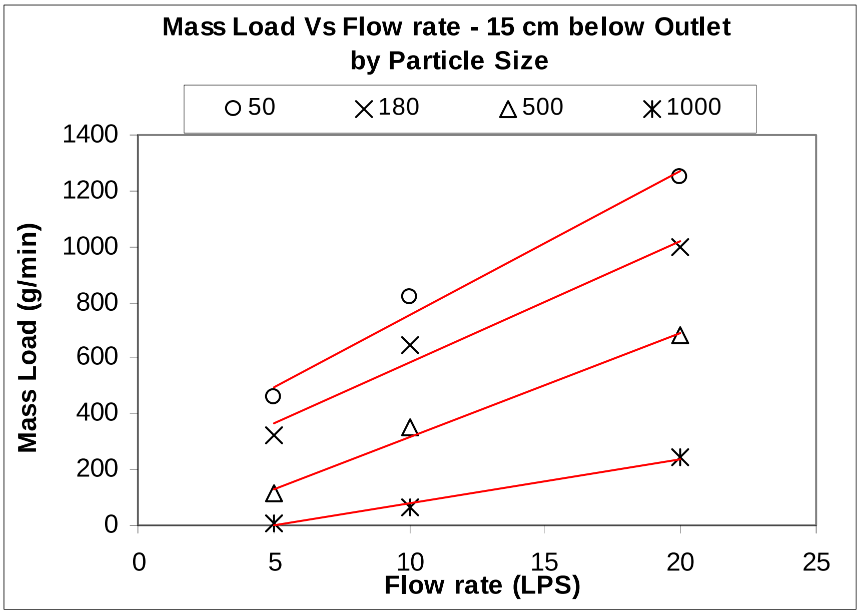

Figure 134. Suspended sediment concentration (mg/L) versus flow rate (L/s) plotted by sediment particle size (µm) (scenario of sediment 24 cm below the outlet).

10.2.4 *Regression Model for SSC Based on Individual Linear Functions*

Based on the individual patterns found between SSC, flow rate, sediment particle size, and overlaying water depths, a combined plot was created to determine a general pattern that allows one to create a response surface for SSC. ANOVA was applied for each of the individual linear regressions to determine the significant level of their factors, except in those cases with only two points. Figure 135 shows SSC as a function of overlaying water depth (or depth below the outlet), plotted by flow rate and specified by sediment particle size.

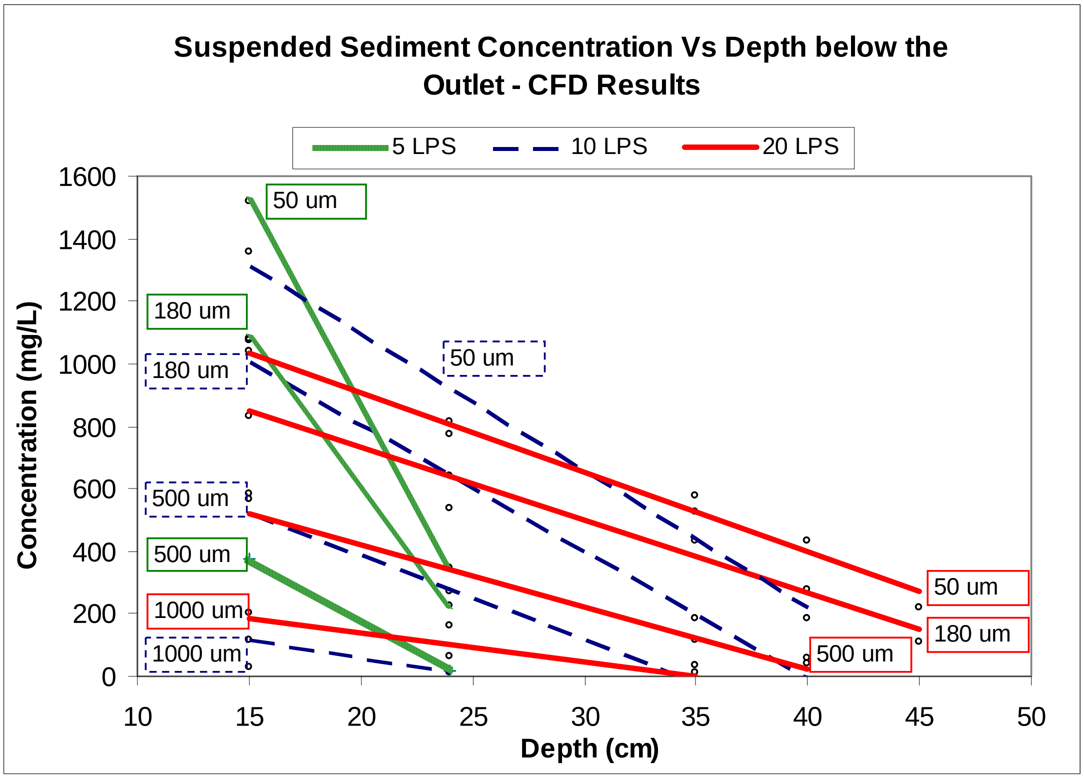

Figure 135. SSC prediction model based on individual linear functions. Suspended sediment concentration (mg/L) versus overlaying water depth (cm), plotted by flow rate (L/s) and specified by particle size (µm).

The general regression equation is given as:

$$SSC = m_{Q,D} \cdot H + b_{Q,D}\,, \qquad \text{Equation 59}$$

where *SSC* is the Suspended Sediment Concentration (mg/L), *H* is the overlaying water depth, or depth below the outlet (cm), *Q* is the flow rate (L/s), *D* is the sediment particle size (µm), and $m_{Q,D}$ and $b_{Q,D}$ are constants, given flow rate and sediment particle size. Values are given in Table 30.

Table 30. Coefficients and Intercepts for Individual SSC Regression Equations

	Diameter (μm)	***M***	***p-value***	***b***	***p-value***
5 L/s	50	-130.47	N/A*	3479	N/A
	180	-95.43	N/A	2513.7	N/A
	500	-39.9	N/A	973	N/A
10 L/s	50	-43.7	0.0152	1966	0.0069
	180	-40.45	0.0138	1612.1	0.0079
	500	-26.74	N/A	920.6	N/A
	1000	-11.05	N/A	279.4	N/A
20 L/s	50	-25.43	0.0013	1418.1	0.0003
	180	-23.2	0.0002	1196.7	0.0007
	500	-17.83	0.007	771.35	0.0034
	1000	-9.2	N/A	320.25	N/A
* Few points to estimate p-values.					

This regression model is applicable to a range of flow rates between 5 and 20 L/s, overlaying water depths greater than 15 cm, and sediment particle sizes between 50 and 1,000 µm; slope coefficients and intercept values can be interpolated for any condition within the described ranges. Extrapolations should be done with caution, since the uncertainty of the results increase.

The effect of the flow rate on the SSC is shown in Figure 135. Notice that at a 5 L/s flow rate and for a particle size of 50 µm, the SSC is higher than all the scenarios below 15 cm below the outlet. This is attributed to low mass dilution. However, the absolute value of the slope or coefficient (*m*) is very high, so the SSC rapidly decreases, because the plunging water jet does not impact with enough energy to penetrate deeper, producing relatively low shear stress magnitudes on deeper locations. Then, when the flow rate increases to 10 L/s, both the SSC and the absolute value of the slope decrease, showing the effect of water dilution and the deeper impact of the plunging water jet. Finally, the pattern continues at the 20 L/s flow rate, which has the lower absolute value of the slope indicating higher scour potential at deeper locations.

In order to see the effect of flow rate on the scour rate, mass load was plotted instead of concentration as a function of overlaying water depth. Figure 136 shows that the mass load or scour rate is proportional to the magnitude of flow rate, as is expected. However, the regression model was implemented for SSC instead of mass load, as concentration does not contain flow rate implicitly (and is therefore independent) and provides more information for water quality purposes.

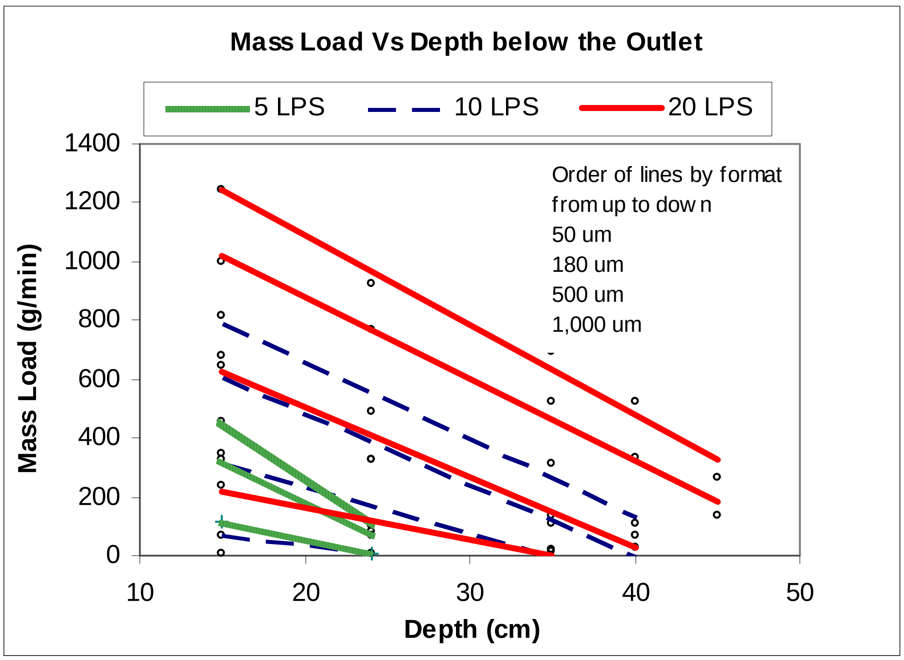

Figure 136. Mass load (g/min) versus overlaying water depth (cm), plotted by flow rate (L/s) and specified by particle size (μm).

This regression model has the advantage of estimating the SSC for a particular scenario by reducing the prediction interval imposed by each individual linear equation. In contrast, using a single multiple regression model to estimate the SSC will certainly increase the error, since the equation will try to fit all the data and the prediction interval would increase the range for the whole data set.

Figure 137 shows the observed (CFD model) versus fitted values with regression models based on individual linear function, including the 95% confidence and prediction intervals, the fitted regression line, and 45^{o} line. The figure shows a very good fit between observed and fitted values. Moreover, the confidence and prediction intervals are relatively narrow, which indicates high accuracy in the estimation of SSC.

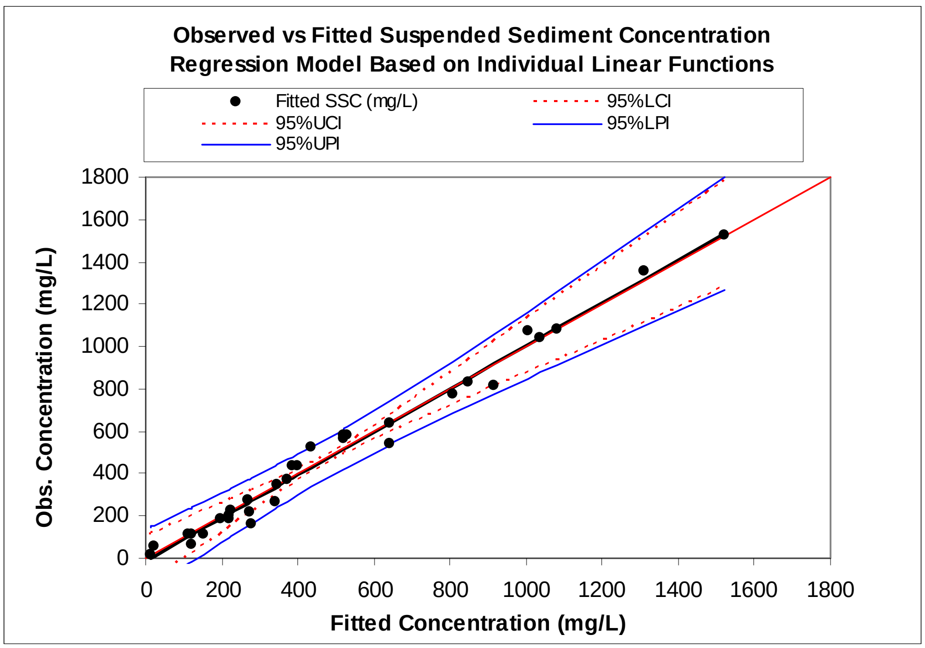

Figure 137. Observed versus fitted suspended sediment concentrations for mean SSC magnitudes of homogenous sediment material. Regression model based on linear functions. Observed data from CFD results.

Residuals versus fitted values in Figure 137 do not show evidence of having any pattern that violates the random assumption of the residuals. Also, Figure 138 shows that the residuals are approximately normally distributed.

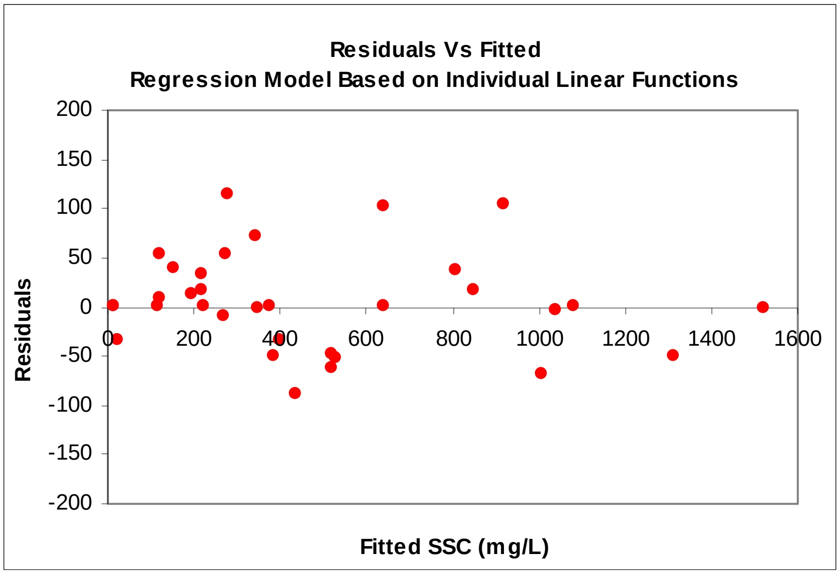

Figure 138. Residuals versus fitted suspended sediment concentrations for mean SSC magnitudes of homogenous sediment material. Regression model based on linear functions. Observed data from CFD results.

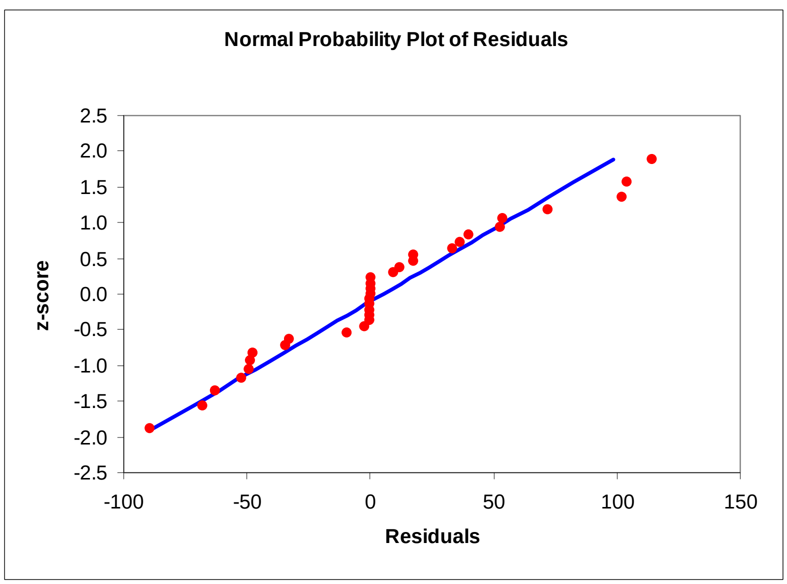

Figure 139. Normal probability plot of residuals for suspended sediment concentrations for mean SSC magnitudes of homogenous sediment material. Regression model based on linear functions. Observed data from CFD results.

Response surfaces of SSC were determined by using the regression model based on individual lineal functions. A series of SSC response surfaces by particle size are presented in Figure 140.

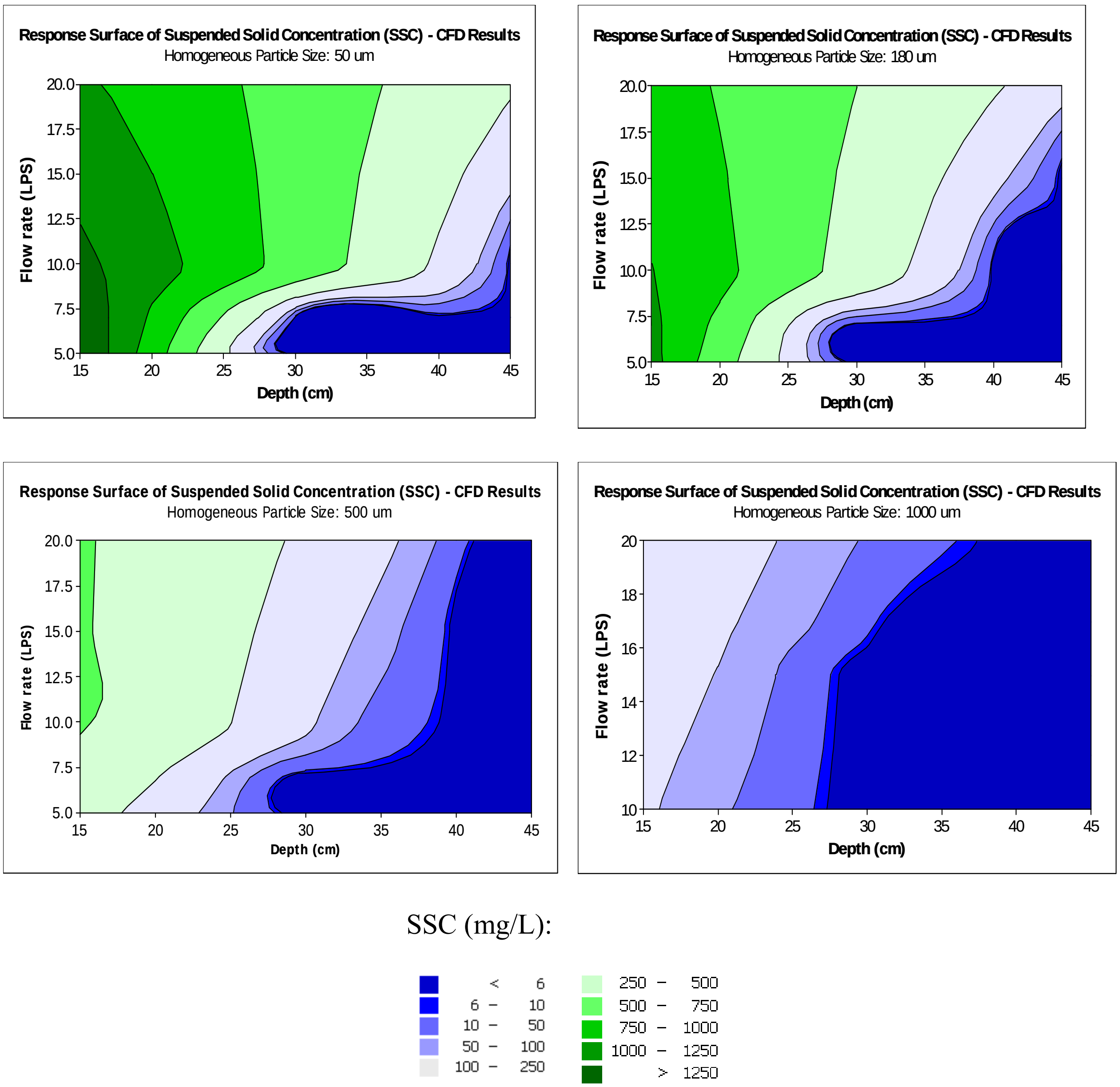

Figure 140. Suspended sediment concentration (mg/L) response surface calculated with the prediction model based on individual functions from CFD results. Model applicable to sediment material with homogeneous particle sizes of 50, 180, 500, and 1000 μm.

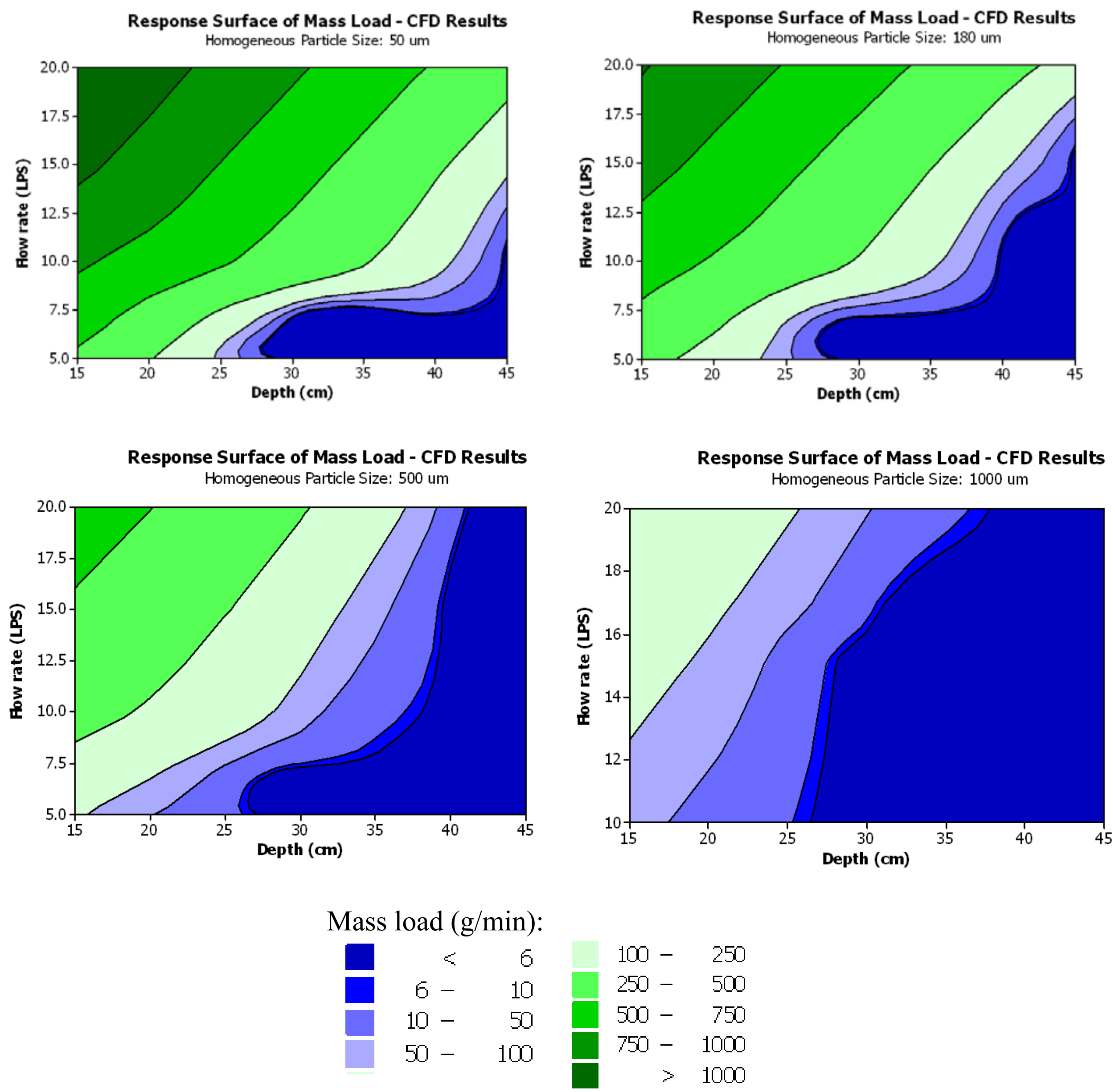

Figure 141. Mass load (g/min) response surface calculated with the prediction model based on individual functions from CFD results. Model applicable to sediment material with homogeneous particle sizes of 50, 180, 500, and 1000 µm.

Notice that SSC is higher at low flow rates; however, if mass loss is plotted instead of SSC, the scour rate is higher at high flow rates. Figure 141 shows a series of response surfaces for mass load. These response surfaces were determined from the previous response surfaces for

SSC shown in Figure 140. Mass load is only shown to illustrate the increments in sediment scour mass as a function of flow rate.

10.2.5 *Multiple Regression Model for SSC Estimation*

A multiple regression model was obtained to estimate SSC based on the CFD model results. The evaluation included ANOVA to determine significant factors and their interactions, as well as the calculation of the coefficients for each factor and interaction. The model was based on all the mean SSC within 20 min of simulation for each case scenario. The coefficient of determination of the equation was $R^2 = 0.83$.

The model is given by the following equation:

$$SSC = Max\left(0,\ b_o + b_1 \cdot Q + b_2 \cdot D + b_3 \cdot H + b_4 (Q - 13.37)(H - 27.35)\right), \qquad \text{Equation 60}$$

where *SSC* is the Suspended Sediment Concentration (mg/L), *H* is the overlaying water depth, or depth below the outlet (cm),, *Q* is the flow rate (L/s or L/s), *D* is the sediment particle size (□m), and b_o *to* b_4 are the coefficients for factors and their interactions. Values are given in Table 31.

Table 31. Coefficients and Intercepts for Individual SSC Regression Equations

Term	**Coefficient**	**Factor**	**Prob>|t|**
b_o	1341	Intercept	<.0001
b_1	18.4	Flow rate (L/s)	0.0004
b_2	-0.97	Diameter (um)	<.0001
b_3	-33.3	Depth (cm)	<.0001
b_4	1.54	(Flow rate-13.375)*(Depth-27.35)	0.0018

Figure 142 shows fitted and observed SSC magnitudes with the 95% confidence and prediction intervals. The figure shows that the regression model estimates the observed concentrations fairly well, as the values are within the prediction interval and the linear regression line between observed and fitted values is close to the 45^{o} line. However, notice that the confidence and prediction intervals are much wider than the intervals obtained with the regression model based on individual linear functions.

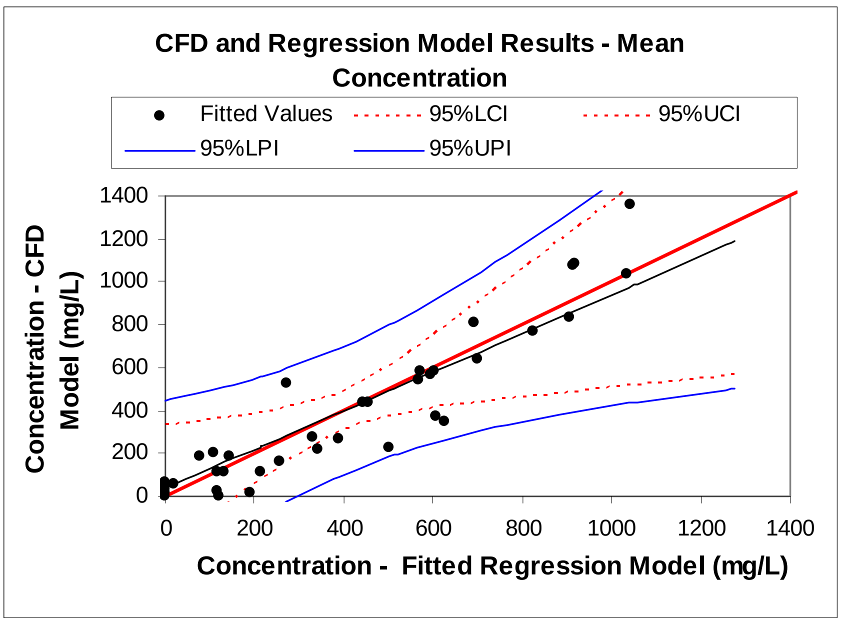

Figure 142. Observed versus fitted suspended sediment concentrations for mean SSC magnitudes of homogenous sediment material. Multiple regression model. Observed data from CFD results.

The residuals versus fitted values in Figure 143 show an apparent pattern of low values in the middle and large values in the upper and lower endings. Additionally, two residuals are greater than 300 mg/L. The largest residual is 480 mg/L, which corresponds to 46% of error related to the fitted concentration.

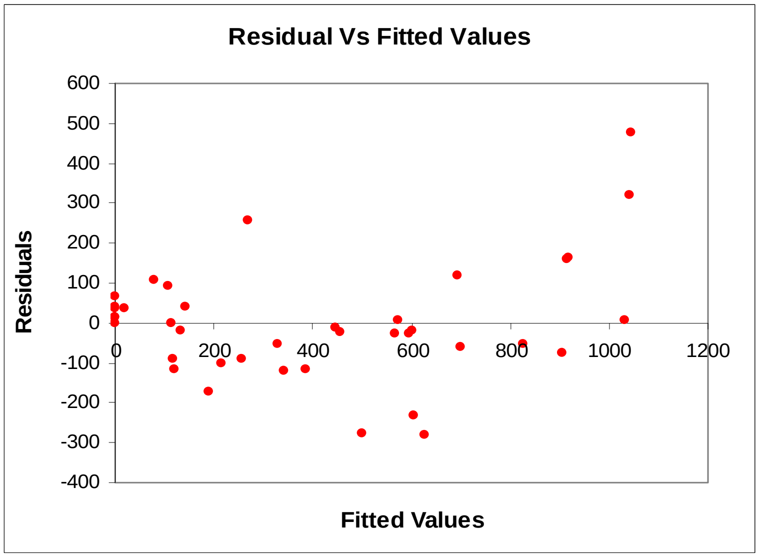

Figure 143. Residuals versus fitted suspended sediment concentrations for mean SSC magnitudes of homogenous sediment material. Regression model based on linear functions. Observed data from CFD results.

Figure 144 shows that the residuals are approximately normal distributed.

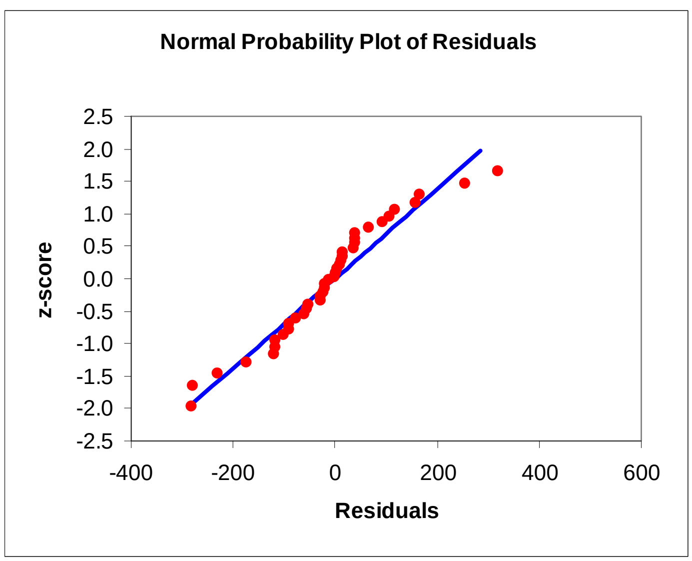

Figure 144. Normal probability plot of residuals for suspended sediment concentrations for mean SSC magnitudes of homogenous sediment material. Regression model based on linear functions. Observed data from CFD results.

Even though the multiple regression model predicts the mean concentrations fairly well, with an R^2 = 0.83; the uncertainty of the estimate is high, as the confidence and prediction intervals are very wide. The percentage of error associated with the highest residual was 45%, which is greater than the maximum percentage of error found with experimental data (38%). This could cause undesired over- or under-estimations of the SSC values and result in an inaccurate model.

CHAPTER 11

CONCLUSIONS AND FINDINGS

The conclusions and findings of this research are presented in this chapter for each hypothesis and objective proposed.

11.1 Hypothesis #1

"Scour of pre-deposited sediment from a stormwater catchbasin sump can be estimated through the knowledge of major factors involved in the process, such as flow rate, characteristics of the sediment, and overlying water depth above the sediment."

This hypothesis was proven through the determination of several regression models to estimate Suspended Sediment Concentration (SSC) for any sediment with a homogeneous particle size between 50 and 1000 μm and for a sediment mixture (shown in Figure 12) based on flow rate and overlaying water.

The error associated with the estimation of SSC was less than the maximum error tolerance calculated based on the experimental measurements of SSC.

Two regression models were shown to have good performance in estimating SSC for a sediment mixture and for sediment material with a homogeneous particle size.

11.1.1 *Sediment Mixture*

Customized regression models were determined for the 0-5 and 5-25 min composite samples. The level of adjustment was appropriate based on the residual analysis. These regression models are limited for catchbasin sumps at flow rates between 0.3 to 10 L/s and overlaying water depths between 10 and 106 cm.

The regression model for the 0-5 min composite samples is given as:

$$SSC = (670)^2 \cdot H^{-3.32} \cdot Q^{\left(0.92 H^{-0.15}\right)}. \qquad \text{Equation 61}$$

The regression model for the 5-25 min composite samples is given as:

$$SSC = (115)^2 \cdot H^3 \cdot [\ln(H)]^{-15} Q^{\left(1.6 H^{-0.19}\right)}, \qquad \text{Equation 62}$$

where *SSC* is the Suspended Sediment Concentration (mg/L), *H* is the overlaying water depth, or depth below the outlet (cm), and *Q* is the flow rate (L/s or L/s).

Response surfaces of fitted SSC were compared to experimental values for the 0-5 min composite samples (Figure 145) and the 5-25 min composite samples (Figure 146). The response surfaces showed good fit.

The maximum error associated with these regression models was less than 25% for the 0-5 min composite samples and less than 30% for the 5-25 min composite samples, both for concentrations greater than 10 mg/L. These percentages of error were less than the maximum error tolerance of 38%.

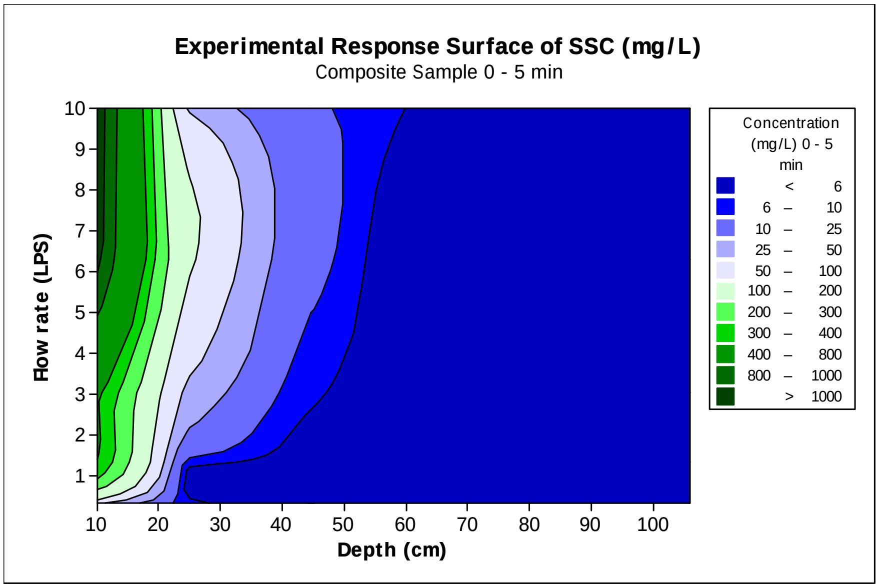

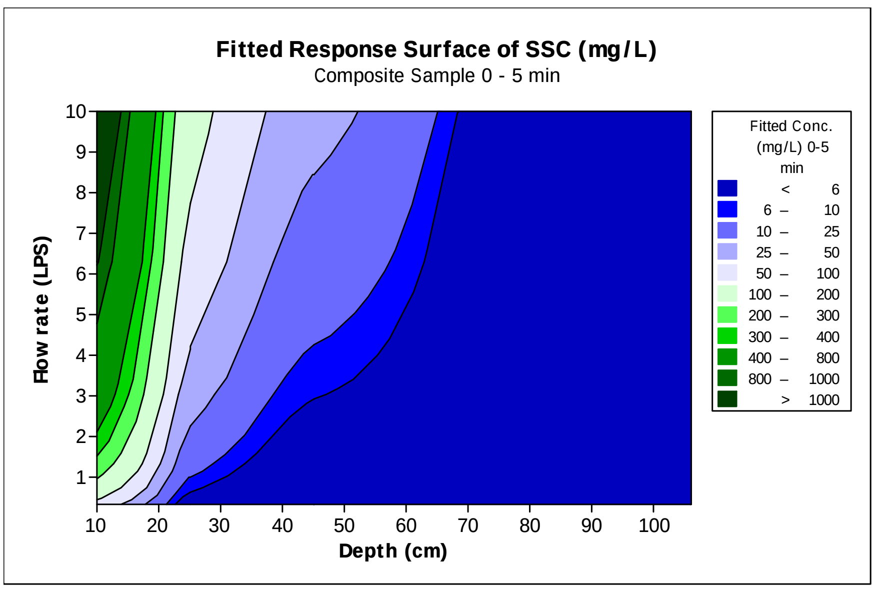

Figure 145. Response surface plots of suspended sediment concentration (SSC) mg/L as a function of flow rate (L/s) and overlaying water depth (cm) (0-5 min composite samples). Experimental values (top) and fitted values (bottom).

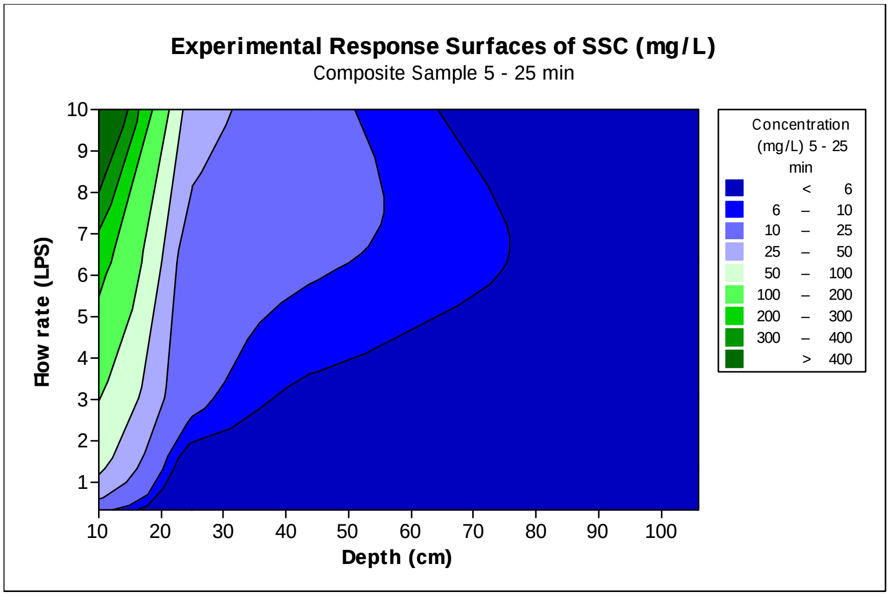

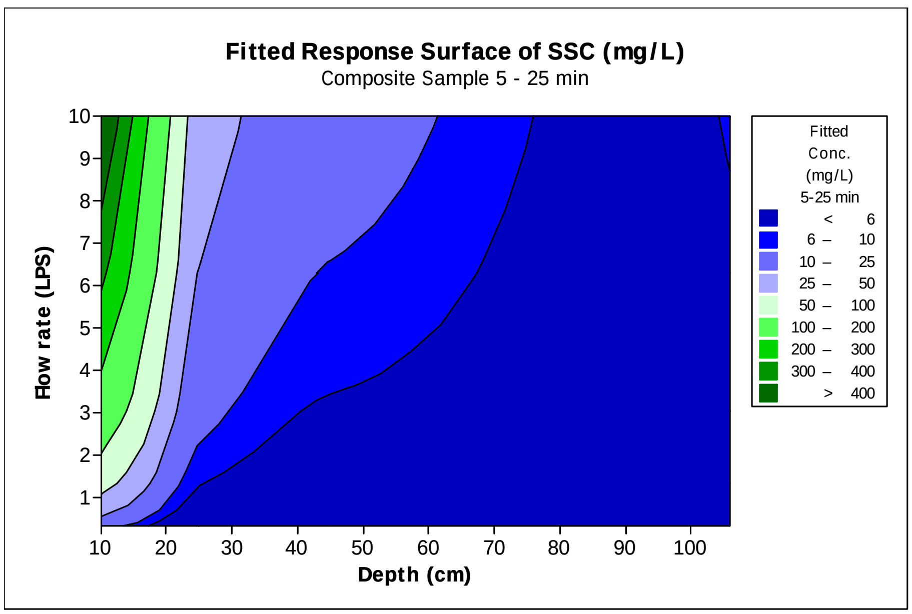

Figure 146. Response surface plots of suspended sediment concentration (SSC) mg/L as a function of flow rate (L/s) and overlaying water depth (cm) (5-25 min composite samples). Experimental values (top) and fitted values (bottom).

A multiple linear regression model was also determined; the coefficient of determination of the equation was $R^2 = 0.83$. The model is given by the following equation:

$$SSC = Max\left(0, 1341 + 18.4 \cdot Q - 0.97 \cdot D - 33.3 \cdot H + 1.54(Q - 13.37)(H - 27.35)\right) \quad \text{Equation 63}$$

where *SSC* is the Suspended Sediment Concentration (mg/L), *H* is the overlaying water depth, or depth below the outlet (cm), *Q* is the flow rate (L/s), *D* is the sediment particle size (μm), and b_o *to* b_4 are the coefficients for factors and interactions. Values are given in Table 31.

Figure 147 shows fitted and observed SSC magnitudes with the 95% confidence and prediction intervals. The figure shows that the regression model estimates the observed concentrations fairly well, as the values are within the prediction interval and the linear regression line between observed and fitted values is close to the 45^o line. However, the confidence and prediction intervals are much wider than the intervals obtained with the regression model based on individual linear functions. The multiple linear regression model showed two residuals greater than 300 mg/L, corresponding to 46% of error related to the fitted concentration, which is greater than the percentage error (38%) estimated from experimental data.

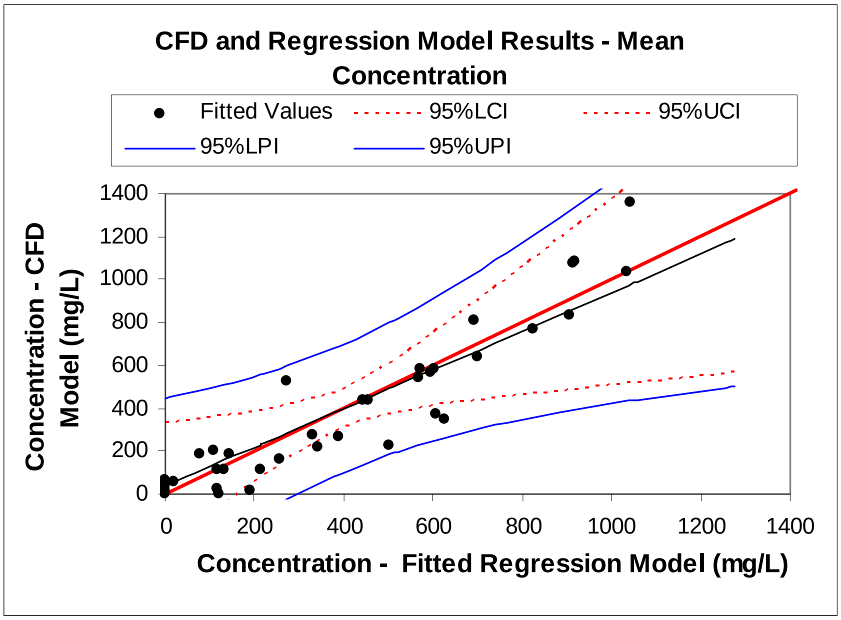

Figure 147. Observed versus fitted suspended sediment concentrations for mean SSC magnitudes of homogenous sediment material. Multiple regression model. Observed data from CFD results.

11.1.2 *Sediment Material with Homogeneous Particle Sizes*

A regression model for SSC based on individual linear functions was determined based on results obtained from CFD modeling. The general regression equation is given as:

$$SSC = m_{Q,D} \cdot H + b_{Q,D}\,, \qquad \text{Equation 64}$$

where D is the sediment particle size (µm) and $m_{Q,D}$ and $b_{Q,D}$ are constants, given flow rate and sediment particle size. See Table 32

Figure 148 shows the SSC prediction model. Response surfaces of SSC plotted by sediment particle size are shown in

Figure 149.

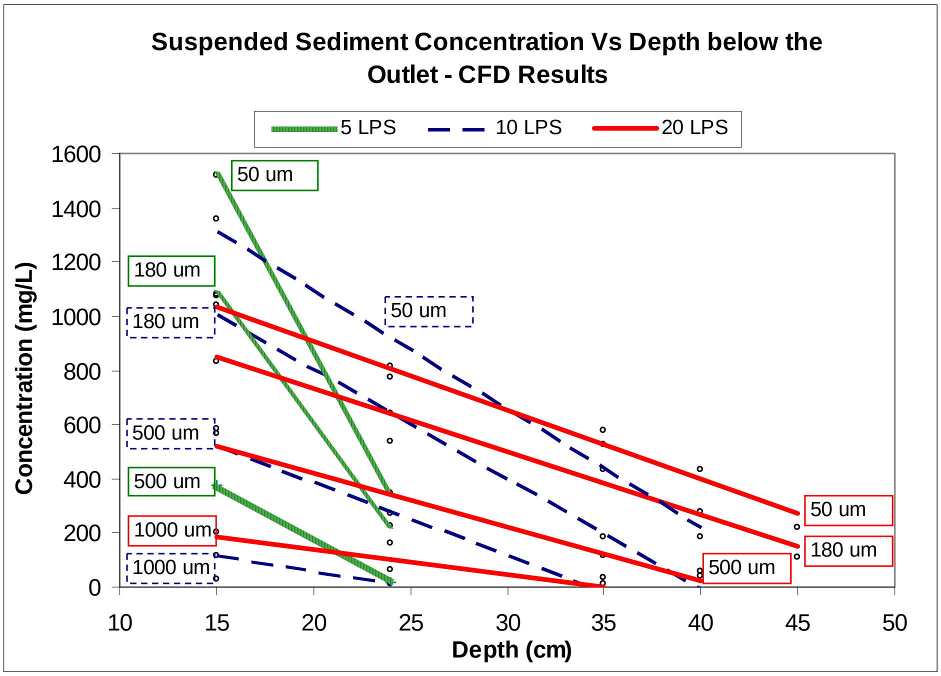

Figure 148. SSC prediction model based on individual linear functions. Suspended sediment concentration (mg/L) versus overlaying water depth (cm), plotted by flow rate (L/s) and specified by particle size (μm).

Table 32. Coefficients and Intercepts for Individual SSC Regression Equations.

	Diameter (μm)	*m*	*b*
5 L/s	50	-130.47	3479
	180	-95.43	2513.7
	500	-39.9	973
10 L/s	50	-43.7	1966
	180	-40.45	1612.1
	500	-26.74	920.6
	1000	-11.05	279.4
20 L/s	50	-25.43	1418.1
	180	-23.2	1196.7
	500	-17.83	771.35
	1000	-9.2	320.25

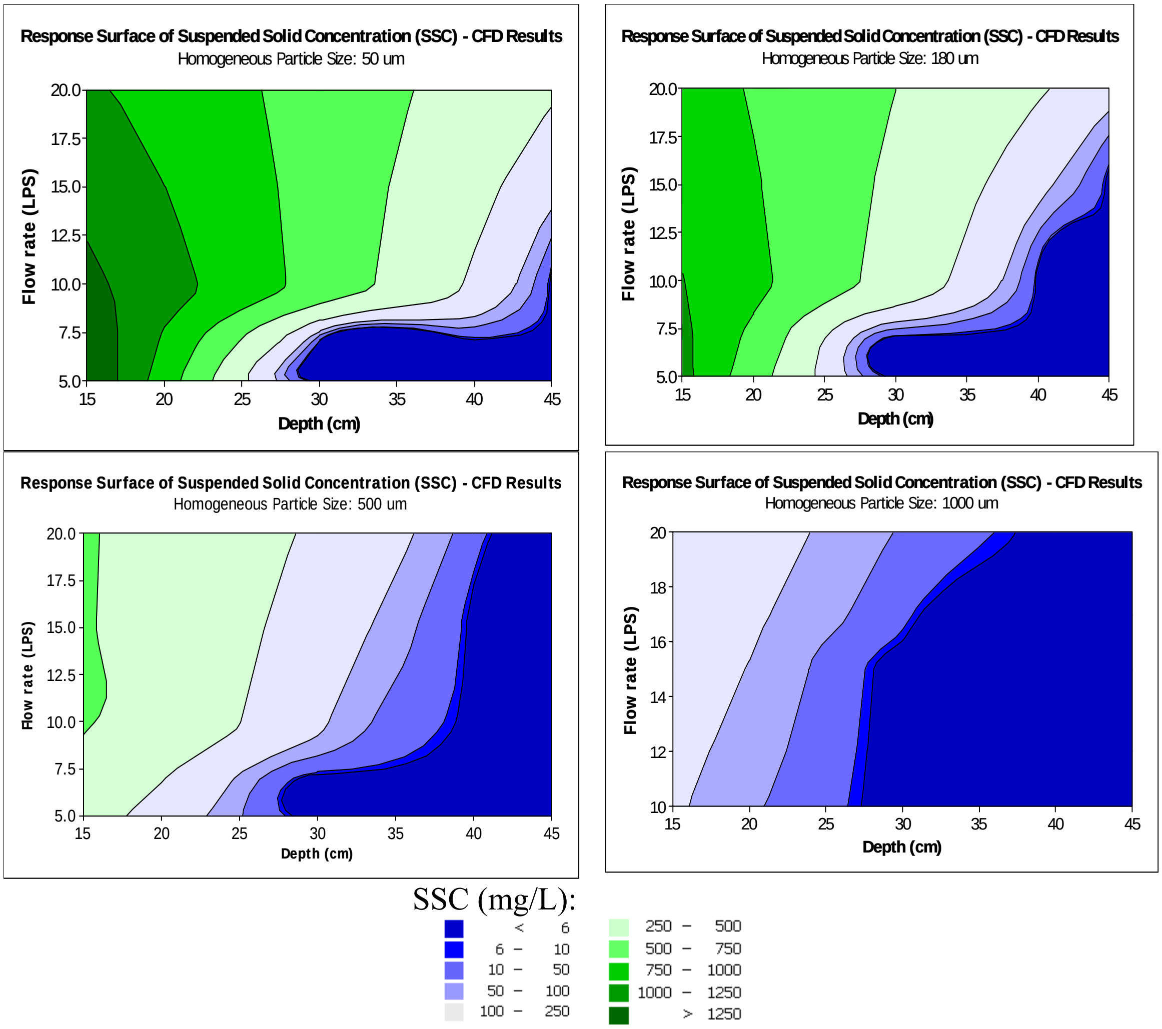

Figure 149. Suspended sediment concentration (mg/L) response surface calculated with the prediction model based on individual functions from CFD results. Model applicable to sediment material with homogeneous particle sizes of 50, 180, 500, and 1000 μm.

11.2 Hypothesis #2

"In addition to the data collected from physical experimentation to determine the relationship of scour rate with those major factors, the sediment scour rate can also be determined by using the initial motion and initial suspension threshold criteria implemented in a Computational Fluid Dynamics (CFD) model. Differences between actual field observations and the CFD model are likely caused by bed armoring, highly

variable flows, and a mixture of sediment particle sizes. The CFD modeling is highly valuable in understanding the basic processes inherent in scour from these devices."

This hypothesis was proven through the creation of a new scour model code implemented in Flow-3D v.9.2. The scour model was based on the initial motion and initial suspension threshold criteria given by Cheng and Chiew (1999). The model was calibrated and validated with experimental data. Two-sample t-tests were conducted to compare the experimental and simulated SSC and showed no evidence to reject the samples as equal. Figure 150 shows the validation scenario at a flow rate of 10 L/s with sediment material of 180-µm particle size placed 35 cm below the outlet. Figure 151 shows the 2D contour of sediment concentration for the validation scenario.

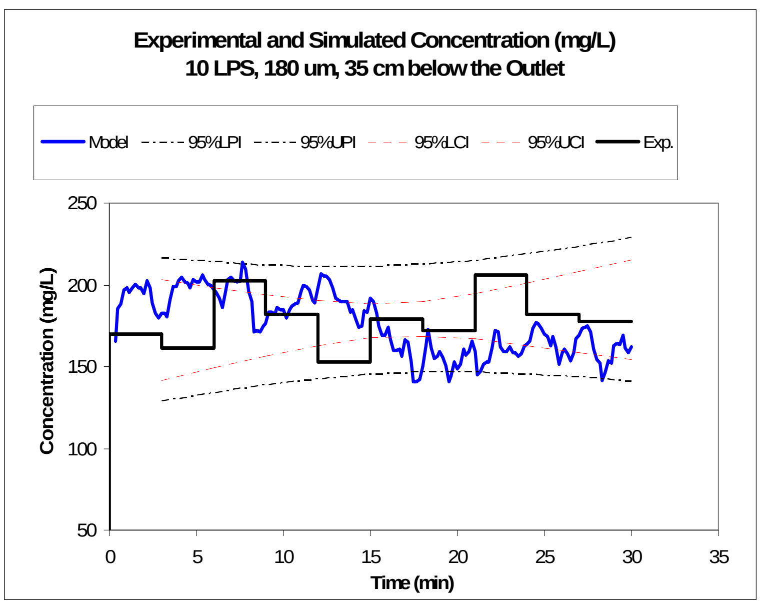

Figure 150. Experimental and simulated SSC (mg/L) for the validation scenario. Homogeneous sediment material of D_{50} = 180 µm, flow rate: 10 L/s, overlaying water depth: 24 cm.

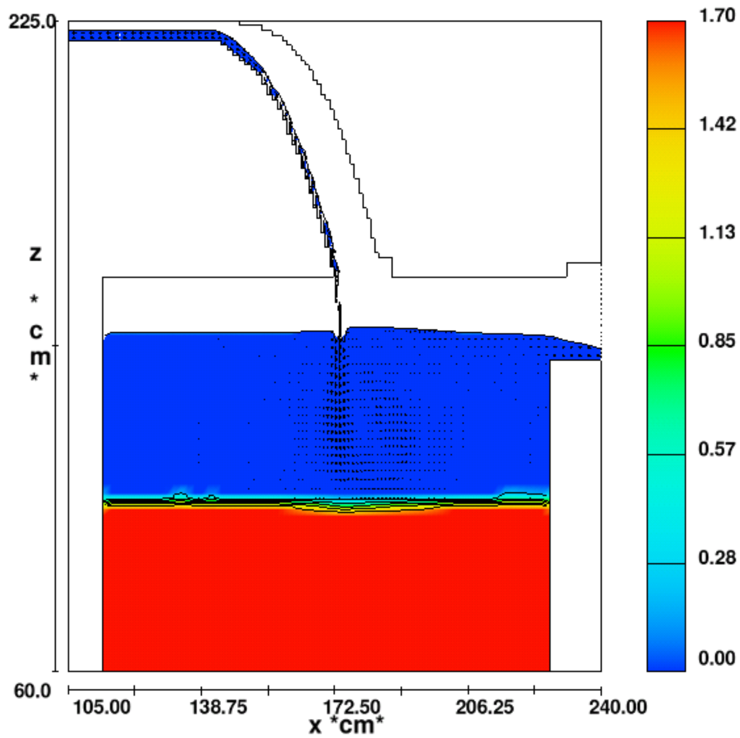

Figure 151. Total sediment concentration (g/cm^3) at 20 min of continuous flow. Flow rate: 10 L/s, overlaying water depth: 35 cm, sediment particle size: 180 µm. 2D-CFD contour. Color scale represents sediment concentration (g/cm3).

Differences in the SSC time series were found between the experimental results with a sediment mixture and the experimental results with sediment with a homogeneous particle size.

The variation of SSC over time in tests performed with a sediment mixture is reflected by the turbidity measurements in Figure 152. The results showed that the scour had a negative exponential pattern under steady flow conditions. A maximum turbidity value was measured at the beginning of every flow, when the impact of the plunging water jet has its greatest effect. After that point, the scour pattern decreased exponentially over time. This pattern was caused by the formation of an armoring layer with large particles.

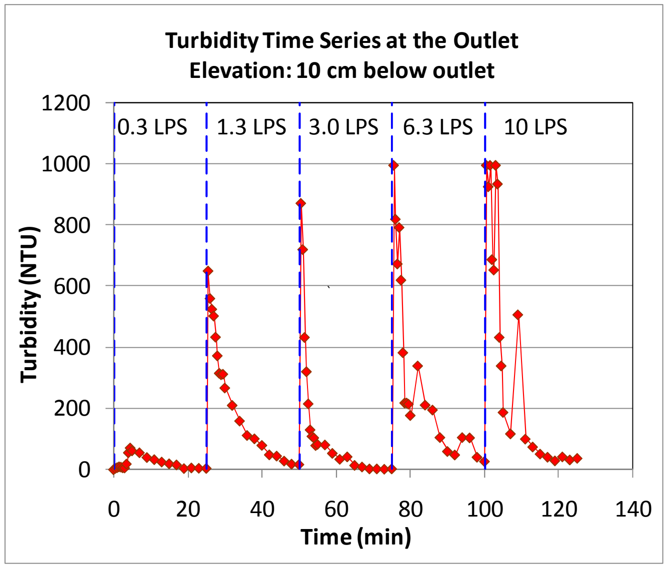

Figure 152. Turbidity time series pattern at different flow rates and with a sediment mixture at 10 cm below the outlet.

In contrast, the variation of SSC over time using sediment with homogeneous particle size showed that SSC has a magnitude that was statistically constant during the 30 min period of evaluation (Figure 153). Initially, it was expected that the SSC magnitudes with homogeneous sediment material would have an exponential decay pattern similar to the one obtained with the sediment mixture, with high concentrations within the first minutes of flow and then a substantial decrement for the remaining flow duration. However, the results showed that the SSC mantained an approximate constant magnitude. This phenomenon is attributed to the absence of an armoring layer that protects the sediment from being scoured.

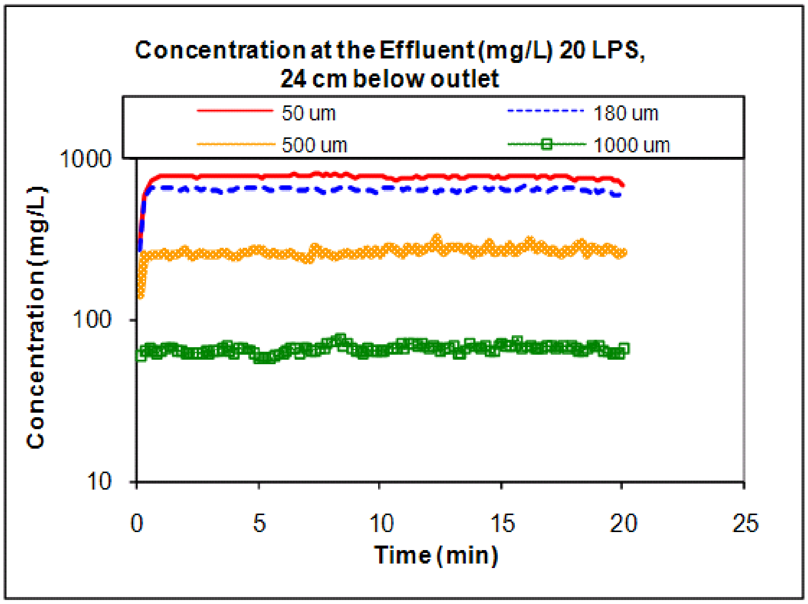

Figure 153. SSC time series plot at 20 L/s and sediment 24 cm below the outlet. Sediment material with homogeneous particle size. CFD results.

The velocity field caused by the plunging water jet continuously generates shear stresses on the sediment surface. If the critical shear stress of the sediment is not large enough to resist the acting shear stress, this sediment will get suspended permanently until a protective mechanism stops or mitigates the scour. When the pre-deposited sediment has a homogeneous particle size, the only protection mechanism is the overlaying water depth.

SSC will decrease only when the overlaying water depth is large enough to dissipate the eroding energy of the velocity field acting on the sediment surface. These experimental results showed that 30 min of continuous flow at 10 L/s was not sufficient time to increase the overlaying water depth (creating a hole in the sediment surface) to significantly reduce the SSC.

In contrast, two protection mechanisms occurred when conducting the tests with the sediment mixture: the overlaying water depth and an armoring layer. In this case, the overlaying water depth protected the sediment surface from the first impact of the plunging water jet. However, the plunging water jet still had enough energy to scour the sediment material directly below it. Then, due to the high shear stresses generated by the first water impact, all particle sizes (large and small) are suspended. Consequently, a *"washing machine effect"* occurs with the suspended sediment while the plunging water jet retreats upward because of the air buoyancy.

The washing machine effect consists of the preferential removal of fine material from the suspension of the whole mixture, leaving a layer of large particles on the sediment surface which form the armoring layer. Moreover, a portion of those large particles is transported with the flow as bed load to a location located in the front of the catchbasin, thus protecting the sediment material in those locations.

CFD modeling was shown to be a highly valuable tool in understanding the basic processes inherent in scour from stormwater hydrodynamic devices. A total of 40 scenarios with homogeneous sediment particle size were evaluated with satisfactory results. However, several limitations were found.

The first limitation was the inability to simulate scour of a sediment mixture, discriminating the sediment fraction of each particle size. Only scour of single particle sizes (D_{50}) were evaluated. The second limitation was the incompatibility of combining water, air buoyancy, and sediment scour in a single model. This issue was overcome by creating a new scour model code implemented in Flow-3D v.9.2.

A general limitation of both CFD model software packages was the excessive elapsed time required to simulate 3-dimensional (3D) scenarios, such as taking days to run a single case. Consequently, a 2-dimensional (2D) approach was preferred for this study.

11.3 Objective #1

"Determine the significant factors involved in the sediment scour phenomenon in a catchbasin sump."

Flow rate, particle size, water depth, and their interactions are significant factors that affect the scour of sediment in a catchbasin sump. Specific gravity is not significant under the evaluated conditions.

The overlaying water depth above the sediment is highly important in protecting the sediment layer from scour. High shear stresses caused by the impacting water jet will not reach the sediment surface if the water is deep. Therefore, with deeper water, the resulting shear stress conditions on the sediment surface are less than with shallower water.

Consolidation of the deposited sediment bed and the cohesive properties of clay were not included in these analyses. Table 33 shows the p-values determined with ANOVA for all main factors and interactions. The p-values are presented at 17, 33, and 50 min during a 60-min simulation with continuous flow. These results show that flow rate (A), particle size (B), and water depth (C) are significant factors. Additionally, the interactions of flow rate-particle size, flow rate-water depth, and particle size-water depth were also significant. However, specific gravity (D), or any interaction containing specific gravity, was not significant at the 95% confidence level. No 3- or 4-way interactions were found to be significant.

Table 33. ANOVA Results: p-Values for Each Treatment at Different Times of the Simulation with Continuous Flow (p-Values Less than 0.05 are Bolded and Underlined)

	Time (sec)		
Treatment	1000	1800	3000
A (Flow rate)	***0.003***	***0.003***	***0.003***
B (Particle size)	***0.02***	***0.01***	***0.01***
C (Overlaying water depth)	***0.009***	***0.01***	***0.008***
D (Specific gravity)	0.12	0.24	0.22
AB	***0.03***	***0.04***	*0.06*
AC	***0.01***	***0.02***	***0.03***
AD	0.15	0.34	0.34
BC	0.07	***0.05***	***0.04***
BD	0.77	0.41	0.34
CD	0.28	0.47	0.54

11.4 Objective #2

"Evaluate the hydrodynamic characteristics of the flow in a catchbasin sump associated with the sediment scour potential."

The inlet geometry has a significant effect on the scour potential of sediments captured in catchbasin sumps. Circular inlets, compared to the rectangular inlets, generate higher velocities in all three directions in the entire water domain of a catchbasin sump, especially close to the surface.

All the statistical tests showed that the effect of a circular inlet on the velocity field is significantly higher than that generated by a rectangular inlet (at the 95% confidence level). The p-values obtained from the tests were below 0.001.

The overlaying water depth significantly reduces the scour potential in catchbasin sumps under free-falling water jet conditions, especially under high flow rates. The ascending velocity component due to air buoyancy also reduces the impacting energy of the plunging water jet.

The experimental results showed that the reduction of velocity as a function of the overlaying water depth was exponential.

11.5 Objective #3

"Determine the Suspended Sediment Concentration (SSC) for different conditions of flow rate, sediment characteristics, and overlying water depth above the sediment."

The results showed that as the flow rate increases, SSC increases as a fractional power function of flow rate. SSC for different flow rates and overlaying water depths for the 0-5-min and 5-25 min composite samples are shown in Table 34.

Table 34. Total SSC (mg/L) of Scoured Sediment for the 5-min Composite Samples

Composite Sample	**Depth below the outlet (cm)**	**Flow rate (L/s)**				
		0.3	**1.3**	**3.0**	**6.3**	**10.0**
		SSC (mg/L)				
0 – 5 min	10	55.6	391.7	426.5	1044.6	1138.5
	25	7.0	8.0	41.9	108.4	46.4
	46	4.9	4.1	6.5	12.0	10.6
	106	1.7	2.6	3.3	2.9	1.7
5 – 25 min	10	12.6	54.9	101.8	244.1	683.5
	25	1.6	5.5	19.8	22.1	44.0
	46	2.0	1.5	4.8	10.8	11.2
	106	0.6	1.1	2.0	2.1	4.0

Figure 154 shows SSC and mass load for the 5-25 min composite samples. Notice that mass load versus flow rate is a spurious self-correlation; however, it is shown to illustrate a direct measurement of mass loss.

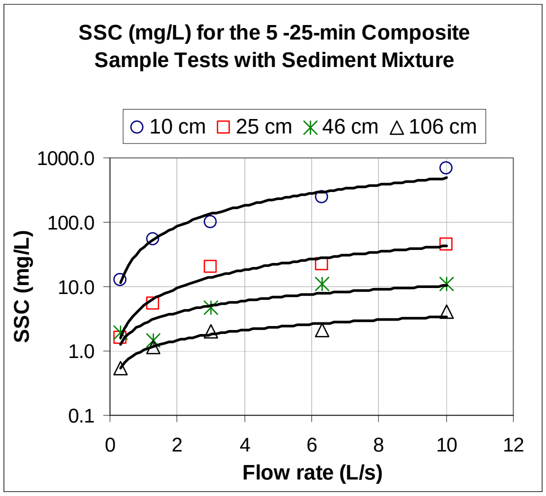

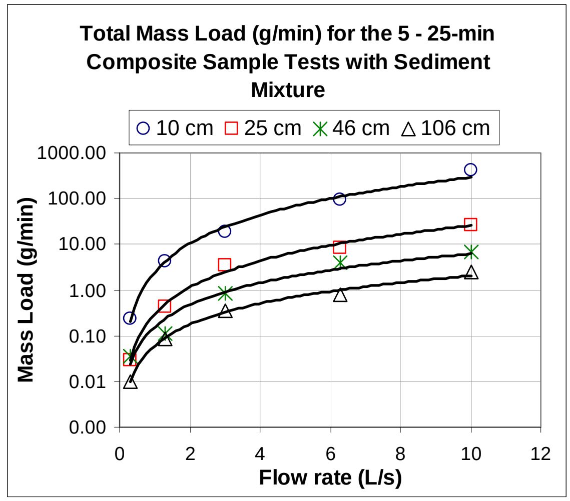

Figure 154. SSC and mass load for the 20-min composite sample obtained from the tests with sediment mixture.

Simple linear regression models, including ANOVA, were performed to determine the significance of flow rate in increasing SSC. In all 0-5 min composite samples, flow rate was significant at the 95% confidence level, except for the cases with the overlaying water depth at 25 and 106 cm, with p-values of 0.27 and 0.81, respectively. SSC needs to be specified together with flow rate to have an estimation of scour rate.

11.6 Objective #4

"Implement a Computational Fluid Dynamics model supported by physical experimentation to determine the sediment scour rate under different conditions."

A Computational Fluid Dynamic (CFD) model was implemented in the software package Flow-3D v.9.2. Hydrodynamic and sediment scour analyses were performed for a series of conditions combining flow rate, overlaying water depth, and particle size. The scour tests were performed with sediment of homogenous particle size.

A new computational code for sediment scour was created in order to overcome the limitations of Flow-3D v.9.2. The hydrodynamics and the customized scour model were calibrated and validated with experimental data. A total of 40 scenarios, including the calibration and validation, were simulated with the customized 2D-CFD model in Flow-3D.

11.7 Objective #5

"Evaluate the relationship between individual significant factors involved in the scour phenomenon and the scour rate."

Several patterns were detected between the significant factors affecting scour potential (flow rate, overlaying water depth, and sediment particle size) and the Suspended Sediment Concentration (SSC). Differences of these relationships were also found between the results obtained with a sediment mixture, which includes armoring, and a sediment material with a homogeneous particle size.

11.7.1 *Sediment Mixture*

Overlaying water depth was shown to be highly significant in the reduction of sediment scour. Figure 155 shows SSC as a function of overlaying water depth for the 0-5 min composite samples.

SSC decreases exponentially as the overlaying water depth increases. However, the SSC reduction rate is so high that a simple exponential regression would under-predict the scour rate for sediment located close to the water surface.

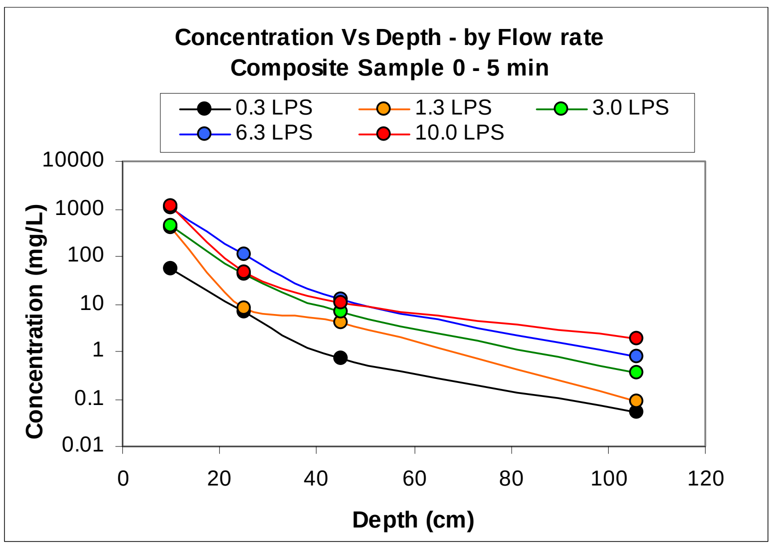

Figure 155. Suspended sediment concentration versus overlaying water depth, plotted by flow rate. Results for the 0-5 min composite samples.

A regression model with transformed variables was required to determine the significance of the overlaying water depth on the reduction of SSC. The regression equation with transformed variables is given as:

$$\ln(SSC) = b_o + b_1\left(\frac{1}{H}\right),$$ Equation 65

where *SSC* is the Suspended Sediment Concentration (mg/L) and *H* is the overlaying water depth (cm).

Figure 156 shows the experimental data and fitted regression line with a 95% confidence level and the ANOVA results for the 0-5 min composite sample at a 3.0 L/s flow rate.

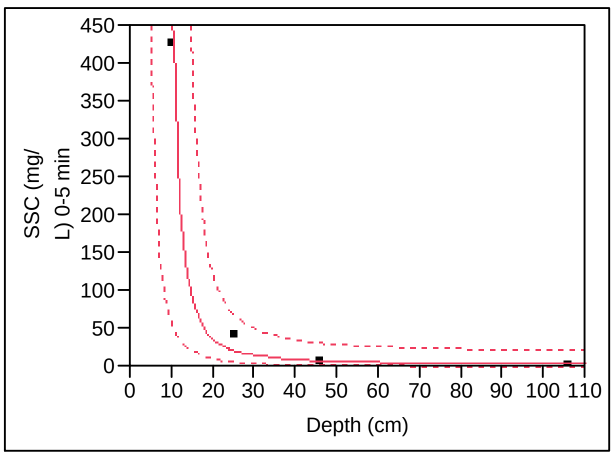

Term	**Estimate**	**Std Error**	**t Ratio**	**Prob>|t|**
Intercept	0.9462213	0.432386	2.19	0.1601
Recip(Depth (cm))	53.031859	7.841624	6.76	0.0212*

Figure 156. Experimental data and fitted regression line with a 95% confidence interval and the ANOVA results for the 0-5 min composite sample at 3.0 L/s flow rate.

In all cases, the overlaying water depth proved to be highly significant, at a 95% confidence level, in the reduction of SSC.

SSC and mass load show the fractional-power function pattern as flow rate increases for the 5-25 min composite sample (Figure 157). Statistical evaluation of the significance of flow rate is discussed in Objective #3.

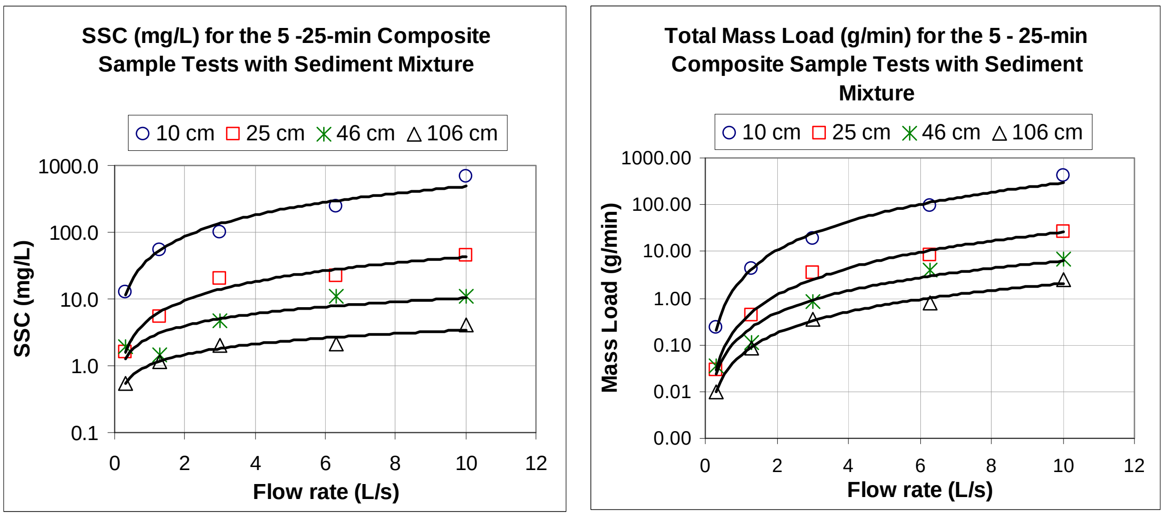

Figure 157. SSC (left) and mass load (right) for the 20-min composite sample obtained from the tests with a sediment mixture.

The relationship between SSC and sediment particle size was not evaluated for the sediment mixture.

11.7.2 *Sediment Material with Homogeneous Particle Sizes*

Overlaying water depth reduced SSC linearly as the depth increased. Figure 158 shows the linear pattern between SSC and overlaying water depth for the 20 L/s flow rate scenario. This finding differed from the case where a sediment mixture was used as a pre-deposited material in the catchbasin sump. The linear pattern found with sediment using the homogeneous particle size is mainly due to the absence of an armoring layer.

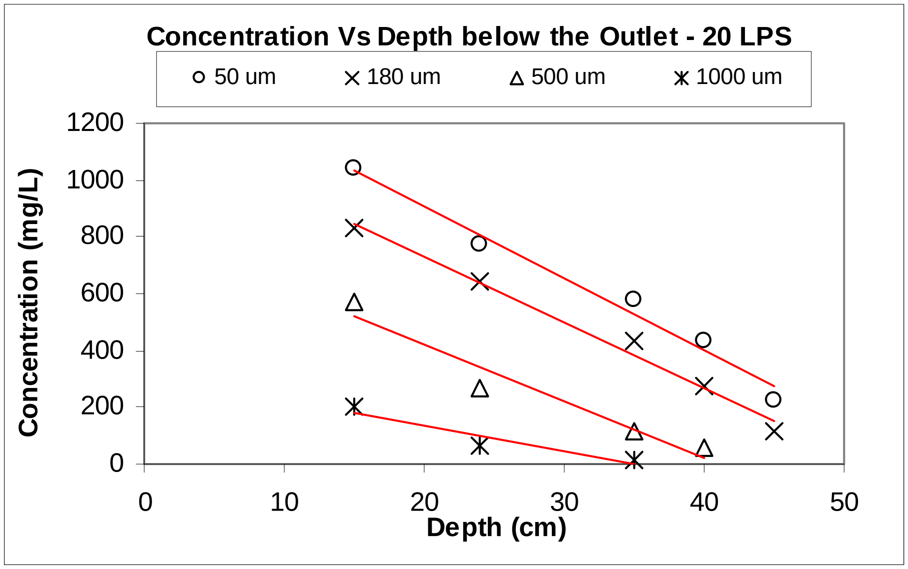

Figure 158. Suspended sediment concentration (mg/L) versus overlaying water depth (cm), plotted by sediment particle size (μm) (scenario at 20 L/s flow rate).

SSC and flow rate do not show a consistent pattern when SSC is plotted by particle size (Figure 159). The concentration and the flow rate do not increase in the same proportion; for some particle sizes, SSC decreases when the flow rate increases. This could be attributed to the dilution of the sediment mass.

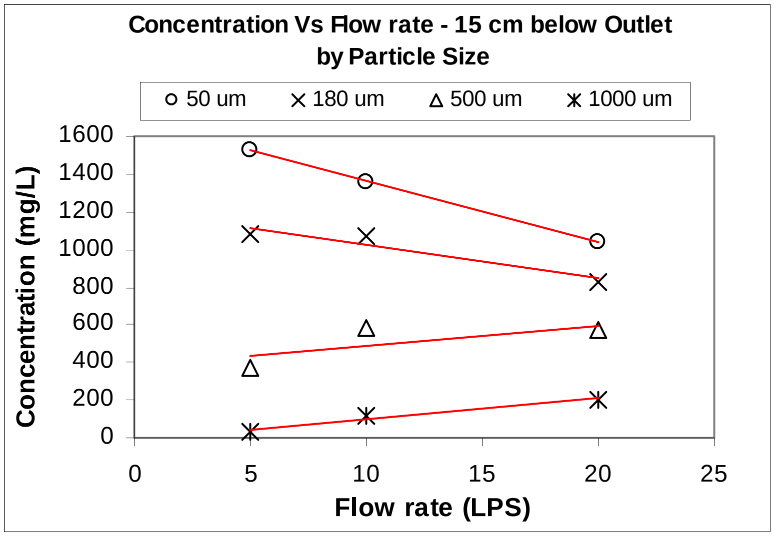

Figure 159. Suspended sediment concentration (mg/L) versus flow rate (L/s) plotted by sediment particle size (µm) (scenario of sediment 24 cm below the outlet).

When mass load is plotted as a function of flow rate (a spurious self-correlation) (Figure 160), it is possible to see that mass loss consistently increases with flow rate. This indicates that the scour rate certainly increases as flow rate increases.

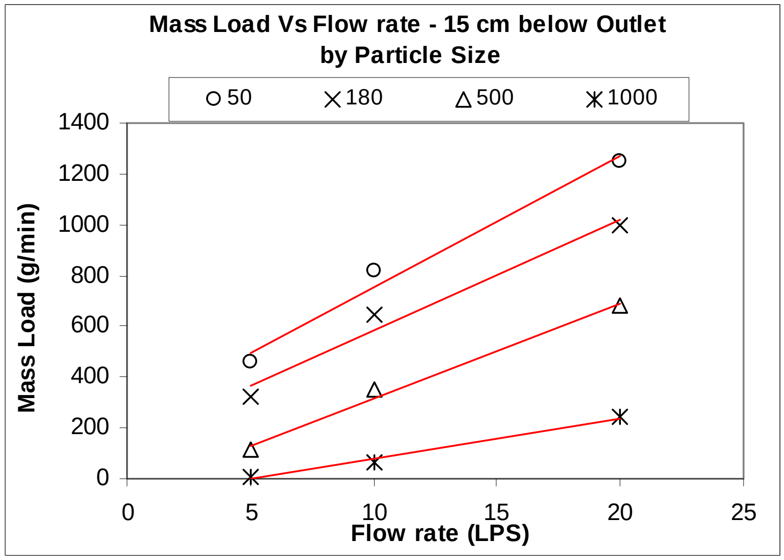

Figure 160. Mass load (g/min) versus flow rate (L/s), plotted by sediment particle size (µm) (scenario of sediment 24 cm below the outlet).

Sediment particle size reduced SSC exponentially. Figure 161 shows SSC versus sediment particle size for the 20 L/s flow rate scenario, plotted by overlaying water depth.

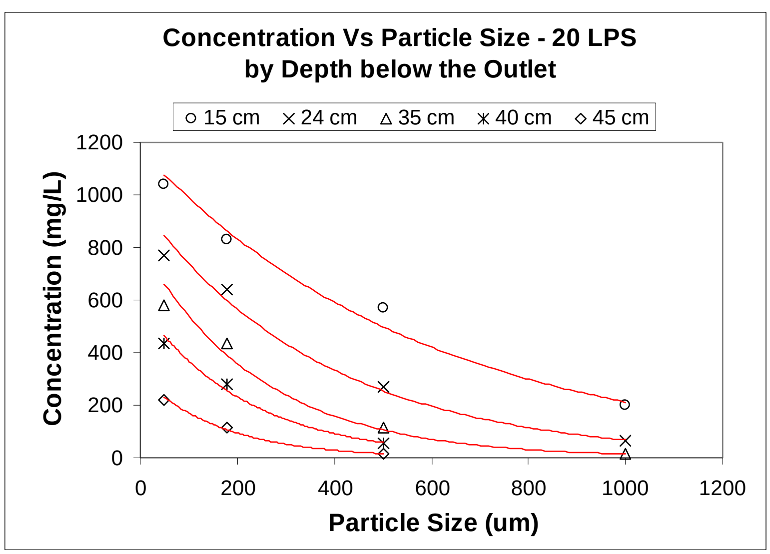

Figure 161. Suspended sediment concentration (mg/L) versus sediment particle size (µm), plotted by overlaying water depth (cm) (scenario at 20 L/s flow rate).

11.8 Objective #6

"Develop a model to predict the scour rate given the significant factors and their interactions."

This achievement is described in detail in the conclusion of Section 11.1.

11.9 Challenges

The main challenges in this research were the creation and implementation of new scour model code in Flow-3D, as well as the calibration and validation of the computational model.

Due to a limitation of the CFD model Flow-3D, not being capable of simulating scenarios with water, air buoyancy, and sediment scour simultaneously, it was necessary to create new scour model code. In principle, Flow-3D includes a scour model based on the Shields criterion of incipient motion to determine the scour rate. However, this model is only applicable with water. Separately, Flow-3D includes a drift-flux model coupled with the turbulent model equations to include air entrainment, considering changes in density and air escape from the water surface. The models are incompatible because the fraction of sediment and the fraction of air generate conflict, as only one secondary fraction could be analyzed. However, Flow-3D provides a couple of opened codes for licensed users to make customizations and/or create new models.

An initial approach was to create a customized air entrainment model to be implemented in the Flow-3D scour model; however, the hydrodynamic results were not accurate and the simulations presented high instability.

The last approach was to create a customized scour model with drag coefficient evaluation coupled with the drift-flux and turbulent models of Flow-3D. The sediment fraction was not considered as a secondary fraction but as a scalar with density and drag properties. This option was ultimately successful.

On the other hand, calibration and validation required a long time to be achieved. These processes were performed manually, by analytical trial and error, based on results obtained from each previous trial. Each trial required about four days for the 3D simulations, analysis of the results, and modifications for the next trial. The 2D scenarios took about two days. The customized scour model required not only calibration and validation, but also code debugging which required several weeks to be completed.

11.10 Research Contributions

This research made the following major contributions:

"Identifying mathematical relationships between individual significant factors involved in the scour phenomenon and the sediment scour rate in a catchbasin sump."

- Identified the significance of flow rate, overlaying water depth, and inlet type in the hydrodynamic characteristics in catchbasin sumps.
- Identified the significance of flow rate, overlaying water depth, and sediment characteristics in the scour rate of previously captured sediment in catchbasin sumps.
- Identified mathematical relationships between the sediment scour rate in catchbasin sumps and the significant factors involved in the scour phenomenon.

- Developed regression models and response surfaces to estimate the sediment scour rate through the known flow rate, overlaying water depth, and sediment characteristics. These regression models and scour rate response surfaces can be implemented in any rainfall-runoff-quality model for preventing and managing polluted stormwater runoff.

"Creating and implementing a computational model for sediment scour in catchbasin sumps."

- Created and implemented a computational model for sediment scour in catchbasin sumps based on the initial motion and initial suspension threshold criteria. This computational model, implemented in a Computational Fluid Dynamic (CFD) model, can be used to evaluate the sediment scour in any stormwater control device, including catchbasin sumps, hydrodynamic separators, and detention ponds.
- Provided a methodology for calibration and validation of a Computational Fluid Dynamic (CFD) model based on experimental data obtained from a full-scale physical model. This methodology will contribute to the performance of responsible CFD modeling.

"Contributing to the understanding and improvement of existing, and the development of new, stormwater control devices, protocols, and rules for preventing and managing polluted stormwater runoff."

- Provided a comprehensive analysis of the scour phenomenon in catchbasin sumps, on which little information was available in the existing literature.
- Identified the effect of the overlaying water depth and the armoring layer on reducing the sediment scour rate in catchbasin sumps. The understanding of these factors contributes to the improvement and development of protocols and stormwater control devices.
- Provided recommendations for sediment scour testing protocols for stormwater control devices.
- Provided a computational tool for evaluating the sediment scour in stormwater control devices with different geometries and under different flows.

11.11 Impact on Health, Welfare, and Safety of Society

It is shown in previous research studies that a great number of toxic pollutants in stormwater runoff are strongly associated with sediment particles (Pitt et al. 1982, 1984, 1999; Morquecho, Pitt, and Clark 2005). Catchbasin sumps and hydrodynamic separators have been designed and used to capture sediment particles from polluted stormwater runoff in order to prevent polluted sediment from reaching natural water bodies. However, captured sediment from these stormwater control devices is exposed to scour during rain events, allowing the polluted sediment be discharged to natural water bodies.

The benefits of understanding the scour phenomenon and quantifying the scour rate in stormwater control devices will greatly contribute to the health, welfare, and safety of society by preventing pollution of natural water bodies, which are sources of drinking water, food, recreation, and biological and ecological sustainability. This research provided a comprehensive analysis of the sediment scour phenomenon in catchbasin sumps, the identification of significant factors involved in this phenomenon, and the development of new equations and computational models for estimating the scour rate under different conditions, among other contributions. All these findings greatly contribute to preventing and managing polluted stormwater runoff.

CHAPTER 12

RECOMMENDATIONS AND FUTURE RESEARCH SUBJECTS

12.1 Recommendation for the Methodology and Protocols for Sediment Scour Tests in Stormwater Hydrodynamic Devices

The following recommendations are presented for scour test protocols:

1. The scour tests should be preferably performed with sediment having the same particle size distribution (PSD) of sediment material captured by the same stormwater control device under evaluation located in an urban area. Another option would be to perform the scour tests with sediment of a PSD similar to sediment collected from sumps from other devices previously installed in the area. A final alternative would be to perform the tests with sediment having the PSD of sump sediment found in previous studies. Using local natural soil is not recommended, as it contains greater amounts of fine particles which are not necessarily captured by these devices, resulting in excessive scour.
2. Scour tests performed using a full-scale physical setup and a representative sediment mixture showed that the scour rate within the first 5 min of flow was significantly higher than for the following 20 min of flow. Moreover, sediment was more sensitive to scour under fluctuating flow rates. The New Jersey Tier II stormwater test protocol requires the scour tests to use the manufactured treatment devices at 125% of the treatment flow rate (NJCTA 2006) at a steady

flow. However, in addition to performing the scour tests with continuous flows, it is also recommended that the tests be conducted with fluctuating flows to account for the flow variability that actually occurs during rainfall events. The tests with fluctuating flow rates should be performed with flow rates equal or greater than the maximum design flow rate of each specific stormwater control device. A one-hour fluctuating flow test should be conducted by applying flow impacts every 3 min, leaving the flow to act on the sediment surface for that period of time. The flow should then be stopped for a period of 1 min before applying the next flow, continuing in this manner for 1 hour.

3. The New Jersey Tier II stormwater test protocol also requires that scour tests be performed with a sediment load of 50 and 100% of the unit's capture capacity (NJCAT 2006). The recommendation of this research agrees with this protocol. Again, this sediment needs to have a PSD representing local sump sediment observations.

12.2 Enhancements to the Basic Geometry of a Catchbasin Sump to Reduce Scour Potential

One of the main findings in this research was the significant effect of the inlet geometry on the scour potential. The scouring effect on the hydrodynamics generated by concentrated plunging water jets (circular inlets) was significantly higher than for less concentrated water jets (rectangular inlets). This proves that reducing the flow rate per unit width at the inlet will reduce the scour potential significantly. Modifying the inlet flow is recommended to decrease the impacting energy or/and physically isolate the sediment from the impacting water.

12.3 Recommendation for Computational Modeling – Calibration and Validation Processes

A recommendation to CFD software developers is to include a calibration module in the computational model. This module should include an option to specify the number of parameters to be calibrated with their range of values, the experimental data, and a statistical sub-module to compare experimental and simulated results at certain time intervals. The variation of parameters should be performed through Monte Carlo simulations. The calibration module would set initial parameters and compare the simulated results to the observed data at certain time intervals; if the results are statistically different, the module would set new values until it gets the best scenario given a number of trials. This type of module would considerably increase the performance of responsible CFD modeling.

12.4 Future Research Subjects

The following future research subjects are proposed:

- Evaluation of the armoring properties of different sediment particle sizes. Full-scale physical experimentation can be conducted with different sediment mixtures by changing the proportion of large particles to determine the sediment scour reduction of each mixture.

- Evaluation of scour potential in swirl hydrodynamic devices. Rotational flow has been widely used in proprietary stormwater hydrodynamic devices for sediment removal, taking advantage of the rotational flow as a mechanism to separate sediment particles from the water. Scour tests could be performed with different conditions of flow rate, diameters of the sump, and sediment particle sizes, among other factors.
- Creation of CFD code to evaluate the scour of sediment mixtures. Sediment mixtures can be analyzed by assigning multiple secondary fractions or scalars, specifying the proportion and properties of each particle size in each cell of the fluid domain. Sediment armoring analysis can then be performed with this new model.

REFERENCES

Aderibigbe, O. and N. Rajaratnam. "Effect of Sediment Gradation on Erosion by Plane Turbulent Wall Jet." *Journal of Hydraulic Engineering*, vol. 124 (October 1998): 1034-1042.

Adamsson, A., V. Stovin, and L. Bergdahl. "Bed Shear Stress Boundary Conditions for Storage Tank Sedimentation." *Journal of Environmental Engineering*, vol. 129 (July 2003): 651 – 658.

APWA (American Public Work Association). "Water Pollution Aspects of Runoff." U.S. EPA Report, no. 11030DNS01/69 (NTIS PB 215 532), January 1969.

Aronson, G., D. Watson, and W. Pisano. "Evaluation of Catchbasin Performance for Urban Stormwater Pollution Control." Grant no. R-804578, EPA-600/2-83-043. Cincinnati, OH: U.S. EPA, June 1983.

ASCE (American Society of Civil Engineers). *Sedimentation Engineering*. New York, NY: Vanoni, V., 1975.

ASCE (American Society of Civil Engineers) and AWWA (American Water Works Association). *Water Treatment Plant Design*, 2nd ed. New York, NY: McGraw-Hill, 1990.

Avila, H., R. Pitt, and S. Durrans. "Factors Affecting Scour of Previously Captured Sediment from Stormwater Catchbasin Sumps." Podium Presentation, Stormwater and Urban Water Systems Modeling Conference. Toronto, Canada, February 2007.

Bohrer, J. G., S. R. Abt, and R. J. Wittler. "Predicting Plunge Pool Velocity Decay of Free Falling, Rectangular Jet." *Journal of Hydraulic Engineering*, vol. 124 (October 1998): 1043-1048.

Brethour, J. 2003. "Modeling Sediment Scour." Available from http://www.flow3d.com/pdfs/tn/FloSci-TN62.pdf. Internet; accessed October 2008.

Brethour, J.M. 2001. "Transient 3-D Model for Lifting, Transporting, and Depositing Solid Material." Available from http://www.flow3d.com/pdfs/tp/wat_env_tp/FloSci-Bib28-01.pdf. Internet; accessed October 2008.

Brzozowski, C. October 2006. “BMP Testing Protocols: Wisconsin Steps Forward.” *Stormwater Journal*. Available from: http://www.stormh2o.com/october-2006/bmp-testing-wisconsin.aspx. Internet; accessed October 2008.

Burton, A. and R. Pitt. *Stormwater Effects Handbook*. Washington D.C.: Lewis Publishers, 2002.

Butler, D. and S.H.P.G. Karunaratne. “The Suspended Solids Trap Efficiency of The Roadside Gully Pot.” *Water Research*, vol. 29, no. 2. (February 1995): 719-729.

Cheng, N. and Y. Chiew. “Analysis of Initiation of Sediment Suspension from Bed Load.” *Journal of Hydraulic Engineering*, vol. 125, no. 8 (August 1999): 855-861.

Chin, D. *Water Resources Engineering*, 2nd ed. Upper Saddle River, NJ: Prentice Hall, 2006.

Chow, V. T. *Open Channel Hydraulic*. U.S.: McGraw-Hill, 1959.

Dey, S. and S. Bose. “Bed Shear in Equilibrium Scour around a Circular Cylinder Embedded in a Loose Bed.” *Journal of Applied Mathematical Modeling*, vol. 18 (May 1994): 265-273.

Dey, S. and R. V. Raikar. “Scour Below a High Vertical Drop.” *Journal of Hydraulic Engineering*, vol. 133 (May 2007): 564-568.

Dou, X. and J. S. Jones. “A New Sediment Transport Formula for Local Scour Prediction.” *Water Resources 2000*, Joint Conference on Water Resource Engineering and Water Resources Planning and Management. Minneapolis, MN: ASCE, July-August 2000.

Einstein, H.A. and E. A. El-Samni. “Hydrodynamic Forces on a Rough Wall.” *Reviews of Modern Physics*, vol. 21, no. 3 (July 1949): 520-524.

Ervine, D. A. and H. T. Falvey. “Behavior of Turbulent Water Jets in The Atmosphere and in Plunge Pools.” Proceedings of Institution of Civil Engineers, 1987.

Fair, G. M., J. C. Geyer, and D.A. Okun. *Water and Wastewater Engineering*, vol. 2: Water Purification and Wastewater Treatment and Disposal. New York, NY: John Wiley & Sons, Inc., 1968.

Faram, M., R. Harwood, and P. Deahl. “Investigation into The Sediment Removal and Retention Capabilities of Stormwater Treatment Chambers.” StormCon Conference. Texas, USA, July 2003.

Flow Science, Inc., *Flow-3D User’s Manual, V-9*. Santa Fe, NM: Flow Science, 2007.

Fluent, Inc. 2005. *Fluent ® 6.2 Computational Fluid Dynamic (CFD) User's Manual*. Available from http://www.fluent.com/. Internet; accessed October 2008.

Garde, R. and R. K. Ranga, *Mechanics of Sediment Transportation and Alluvial Stream Problems.* New Delhi, India: John Wiley & Sons, 1977.

Goncharov, V.N. Dynamics of Channel Flow. Israel Programme for Scientific Translation. Moscow, Russia, 1964.

Hoffmans, G. and K. Pilarczyk. "Local Scour Downstream of Hydraulic Structures." *Journal of Hydraulic Engineering*, vol. 121, no. 4 (April 1995): 326-340.

Iwagaki, Y. "Hydrodynamical Study on Critical Tractive Force." Trans. *JSCE*, no. 41 (1956): 1-21.

Jia, Y., T. Kitamura, and S. Wang. "Simulation of Scour Process in Plunging Pool of Losse Bed-Material." *Journal of Hydraulic Engineering*, vol. 127, no. 3 (March 2001): 219-229.

Lager, J.A., W.G. Smith, W.G. Lynard, R.M. Finn, and E.J. Finnemore. "Urban Stormwater Management and Technology: Update and Users' Guide." U.S. EPA-600/8-77-014. Cincinnati, OH, September 1977.

Lee, C.C. and S.D. Lin. *Handbook of Environmental Engineering Calculations*. U.S.: McGraw Hill, 1999.

Li, F. and L. Cheng. "Numerical Model for Local Scour under Offshore Pipelines." *Journal of Hydraulic Engineering*, vol. 125, no. 4 (April 1999): 400-406.

McKeigh, E. J. "A Study of Air Entrainment Using Plunging Water Lets. Ph.D. Dissertation, Queen's University. Belfast, Ireland 1978.

Meilan, Q., K. Fujisak, and K. Tanaka. "Sediment Re-suspension by Turbulent Jet in an Intake Pond." *Journal Hydraulic Research*, vol. 38, no. 5 (September 1999): 323-330.

Melville, B. "Pier and Abutment Scour: Integrated Approach." *Journal of Hydraulic Engineering*, vol. 123, no. 2 (February 1997): 125-136.

Morquecho, R., R. Pitt, and S.E. Clark. "Pollutant Associations with Particulates in Stormwater." World Water & Environmental Resources Congress, ASCE/EWRI. Alaska, May 2005.

Neil, C.R. "Note on Initial Movement of Coarse Uniform Material." *Journal of Hydraulic Research*, vol. 6, no. 2, 1968.

New Jersey Corporation of Advanced Technology – NJCAT. "Technology Verification: BaySaver Technologies, Inc." December 2004.

New Jersey Corporation of Advanced Technology – NJCAT. "Technology Verification: Hydro International." February 2005.

New Jersey Corporation of Advanced Technology – NJCAT. "Technology Verification: Stormceptor." September 2004.

New Jersey Corporation of Advanced Technology – NJCAT. "Technology Verification: Stormwater Management, Inc." June 2002.

New Jersey Corporation of Advanced Technology – NJCAT. "Technology Verification: VorSentry, Stormwater Treatment System." December 2005

New Jersey Corporation of Advanced Technology – NJCAT. "Technology Verification: Vortechnics." May 2004.

New Jersey Corporation of Advanced Technology – NJCAT. "New Jersey TIER II Stormwater Test Requirements – Amendments to TARP TIER II Protocol." January, 2006.

Niño, Y., F. López, and M. García. "Threshold for Particle Entrainment into Suspension." *Journal of Sedimentology*, no. 50 (2003): 247-263.

Phipps, D., R. Alkhaddar, J. Dodd., M. Faram, and P. Deahl. "Evaluation of Deifferent Configurations of Stormwater Treatment Chamber." StormCon: 3rd North American Surface Water Quality Conference and Exposition. Palm Desert, CA, July 2004.

Pitt, R. "Characterizing and Controlling Urban Runoff through Street and Sewerage Cleaning." U.S. EPA. Contract No. R-805929012. EPA/2-85/038. PB 85-186500/AS. Cincinnati, OH, June 1985.

Pitt, R. "Demonstration of Nonpoint Pollution Abatement Through Improved Street Cleaning Practices." U.S. EPA. Grant no. S-804432. EPA-600/2-79-161. Cincinnati, OH, August 1979.

Pitt, R. 2004. "Sediment Transport in Storm Drainage Systems. Stormwater Management: Module 3." Available from http://unix.eng.ua.edu/~rpitt/Class/StormWaterManagement/MainSWM.html. Internet; accessed October 2008.

Pitt, R. and P. Bissonnette. "Bellevue Urban Runoff Program." City of Bellevue, WA, August 1984.

Pitt, R. and R. Field. "An Evaluation of Storm Drainage Inlet Devices for Stormawter Quality Treatment." Procedures WEFTEC (Water Environmental Federation Technical Exposition). Orlando, FL, 1998.

Pitt, R. and U. Khambhammettu. "Field Verification Tests of the UpFlow™ Filter. Small Business Innovative Research, Phase 2 (SBIR2)." U.S. EPA. Edison, NJ, March 2006.

Pitt, R. and A. Maestre. *The National Stormwater Quality Database - A Compilation and Analysis of NPDES Stormwater Monitoring Information*. U.S. EPA Office of Water Center for Watershed Protection Ellicott City. Washington, D.C., September 4, 2005, Updated: February 3, 2008.

Pitt, R. and J. Voorhees. *SLAMM (Source Loading and Management Model): A Water Quality Management Planning Model for Urban Stormwater Runoff*, 2000.

Pitt, R., S. Clark, and K. Parmer. "Protection of Groundwater from Intentional and Nonintentional Stormwater Infiltration." U.S. EPA. EPA/600/SR-94/051. PB94-165354AS. Storm and Combined Sewer Program. Cincinnati, Oh, May 1994.

Pitt, R., B. Robertson, and P. Barron, A. Ayyoubi, and S. Clark. "Stormwater Treatment at Critical Areas: The Multi-Chambered Treatment Train (MCTT)." U.S. EPA, Wet Weather Flow Management Program, National Risk Management Research Laboratory. EPA/600/R-99/017. Cincinnati, OH, March 1999.

Sansalone, J., S. Pathapati, J. Kim, B. Liu. "University of Florida Treatment and Maintenance of Stormwater Hydrodynamic Separators: A Case Study." 9th Biennial Conference on Stormwater Research & Watershed Management, May 2007.

Sartor, J. and G. Boyd. "Water Pollution Aspects of Street Surface Contaminants." U.S. EPA. Contract no. 14-12-921. EPA-R2-72-081. Washington D.C., November 1972.

Shields, A. "Anwendung der Aehnlichkeitsmechanik und der Turbulenzforschung auf die Geschiebebewegung." Mitteilungen der Pruessischen Versuchanstalt fur Wasserbau und Schiffbau. Berlin, 1936.

SonTek. *FlowTracker Handheld ADV® User's Manual*, 2007. Available from http://www.sontek.com/product/flowtracker/flowtracker-ov.htm. Internet; accesses October 2008.

Stormceptor®, Inc. *Study Manual, 1993 – 1995*. Available from http://www.stormceptor.com/. Internet; accessed October 2008.

U.S. Army Corps of Engineers (COE). "Sedimentation Investigations of Rivers and Reservoirs." EM 1110-24000. U.S. Army Engineer Waterways Experiment Station. Vicksburg, MS, 1995.

USDA (United States Department of Agriculture). *Design of Open Channels*. Technical Release no. 25, Soil Conservation Service. Washington, DC., 1977.

USDA (United States Department of Agriculture). *Threshold Channel Design*. National Engineering Handbook Part 654, Chapter 8 210–VI–NEH (August 2007): 21.

U.S. EPA (Environmental Protection Agency). "Storm Water Technology Fact Sheet Hydrodynamic Separators." EPA 832-F99-017. September 1999.

Valiron F. and J. P. Tabuchi. *Maitrise de la pollution urbaine par temps de pluie, étatde l_art. Lavoisier*. Paris, France, 1992.

Van Rijn, L.C. "Sediment Transport, Part II: Suspended Load Transport." *Journal of Hydraulic Engineering*, no. 110 (1984): 1613-1641.

White, C.M. "The Equilibrium of Grains on the Bed of a Stream." Proceedings RSL Series, A Mathematical and Physical Sciences, vol. 174, no. 958, February 1940.

SOFTWARE

© 2008 ANSYS, Inc. *Fluent v.6.2 CFD (Computational Fluid Dynamic)*.

© 2008 Flow Science Inc. *Flow-3D 9.2 Software*.

© 2008 Microsoft Corporation. *Microsoft Office*.

© 2008 Minitab, Inc. *Minitab 15 Statistical Software*.

© 2008 SAS. *JMP®7 Statistical Discovery Software*.

APPENDIX A

FULL-SCALE PHYSICAL MODEL

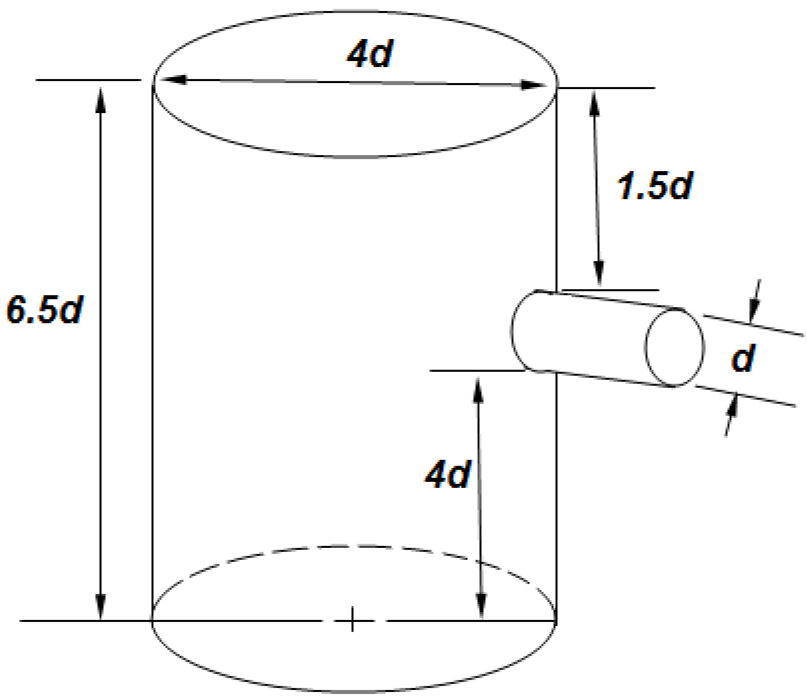

Figure A.1. Sketch of the optimal catchbasin geometry proposed by Lager et al. (1977). Diameter of the pipe, d = 30 cm (12 inches).

Figure A.2. Components of the full-scale physical model.

Table A.1. Components of the Full-Scale Physical Model

1.	A cylindrical plastic tank of 116 cm in internal diameter. The invert elevation of the outlet, which was 29 cm in diameter, was located at 116 cm above the bottom of the tank.
2.	A wooden structure placed on a trailer (6' x 10').
3.	A 50-cm wide channel placed on the wooden structure. This channel was modified to a pipe with a 30-cm diameter during the hydrodynamic tests with circular inlet.
4.	A turbulent dissipation tank located on the top of the wooden structure upstream the channel.
5.	A pump with a maximum capacity of 10 L/s and a maximum head of 6 m.
6.	Pipes of 3 inches and 1.5 inches for large and small flow rates, respectively.
7.	A set of valves to control the flow rate.
8.	Two flow meters (Midwest Instruments & Control Corp.), one for the 3-inch pipe and another for the 1.5-inch pipe. The reading ranges for the flow meters were between 2.5 and 30.0 L/s for the 3-inch pipe and between 0.65 and 8.0 L/s for the 1.5 inch pipe.
9.	A pool located downstream of the catchbasin for water recirculation during the hydrodynamic tests, also used as a sediment trap during the scour tests.

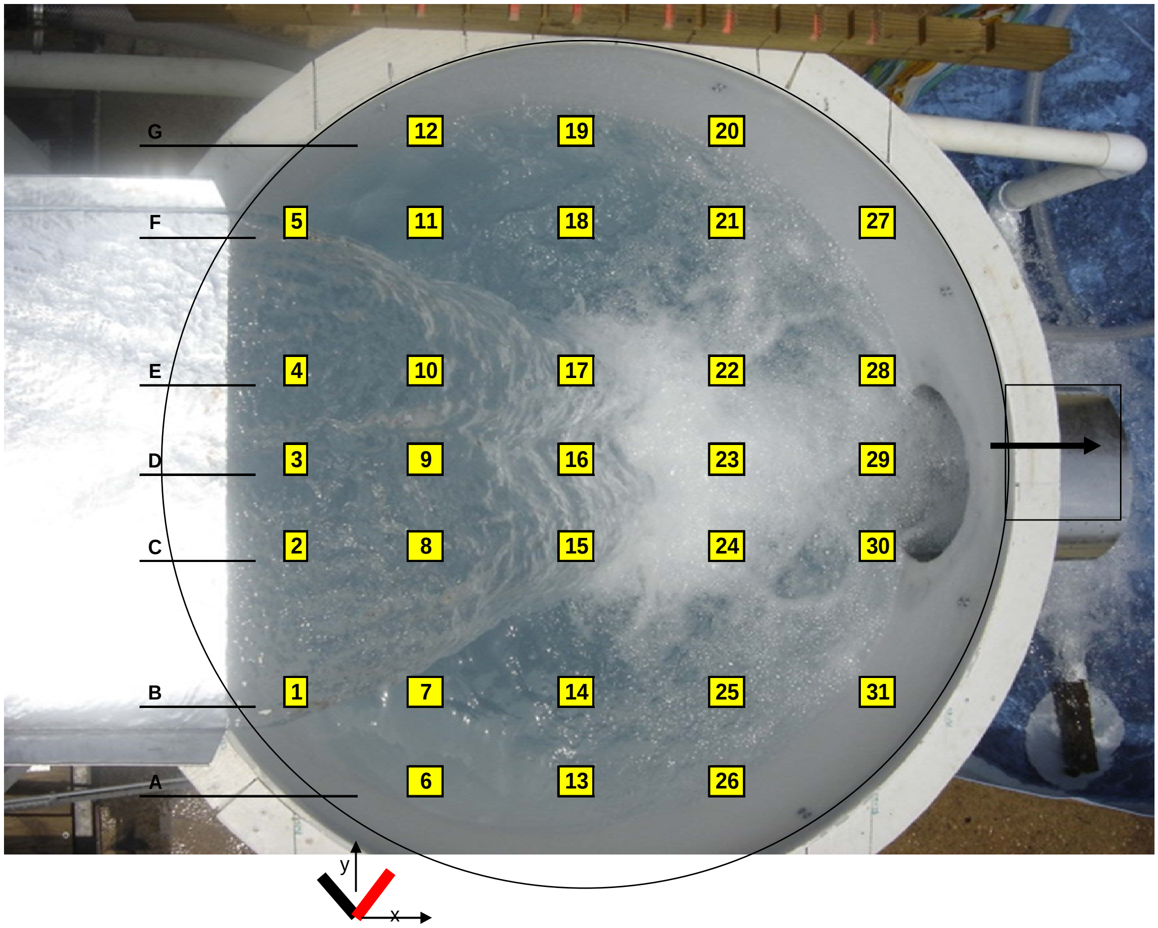

Figure A.3. Location of points for velocity measuring – Plan view of one of the five layers.

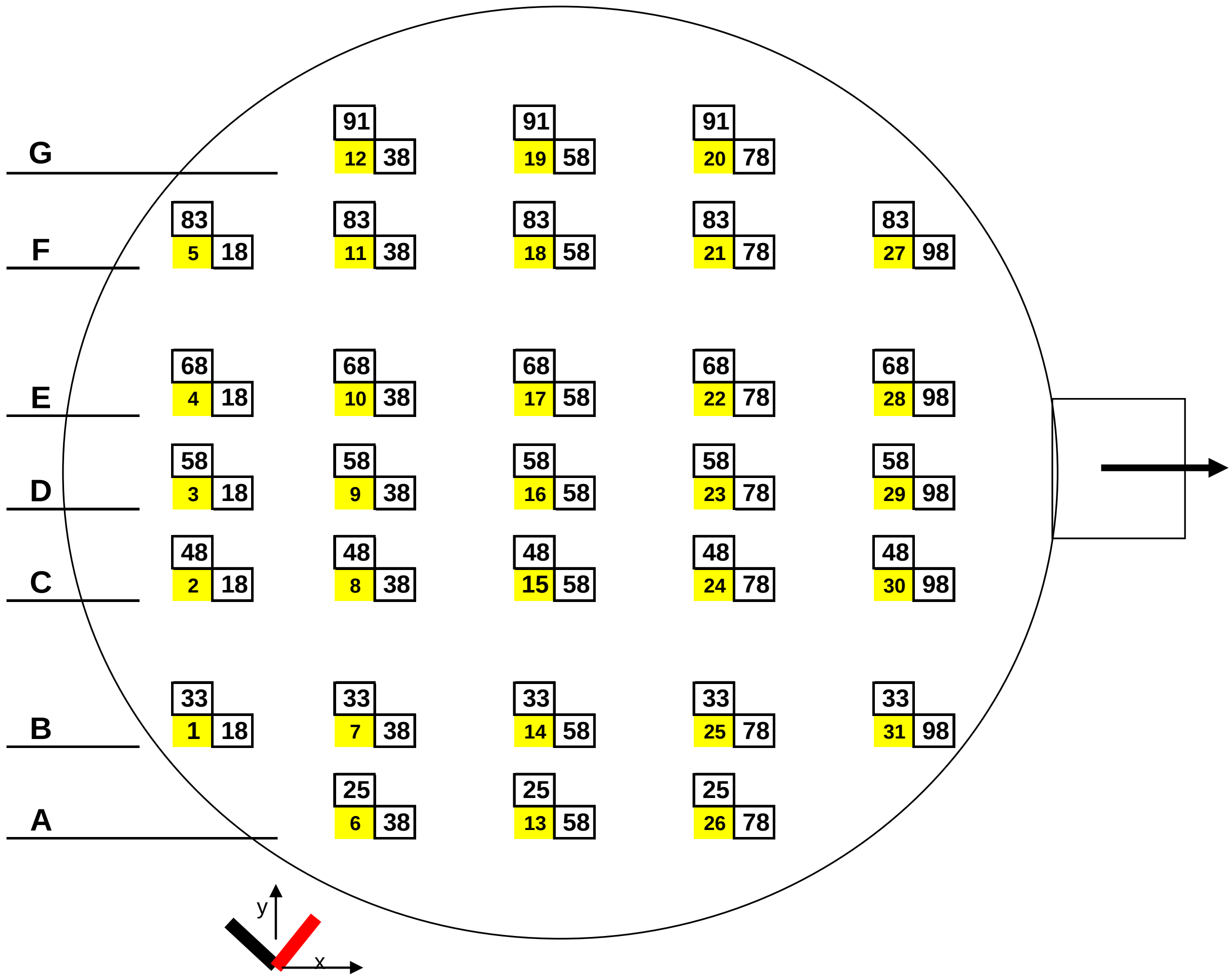

Figure A.4. Coordinates of points for velocity measuring – Plan view of one of the five layers.

Figure A.5. Location of the five layers for velocity measuring. Depth below the outlet (cm).

APPENDIX B

VELOCITIES IN A CATCHBASIN SUMP – HYDRODYNAMIC TESTS WITH RECTANGULAR AND CIRCULAR INLETS

Variability Chart for Vx (cm/s)_(y= B and F)_10 L/s

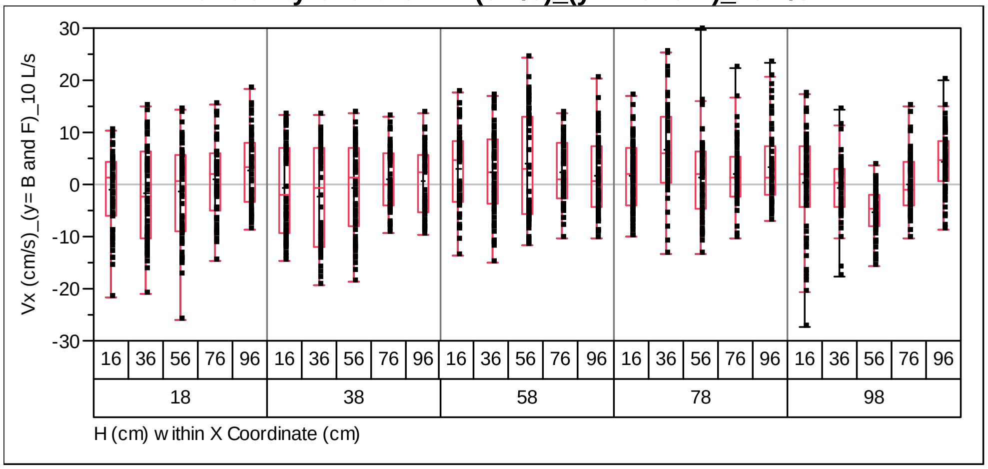

Variability Chart for Vx (cm/s)_(y= C and E)_10 L/s

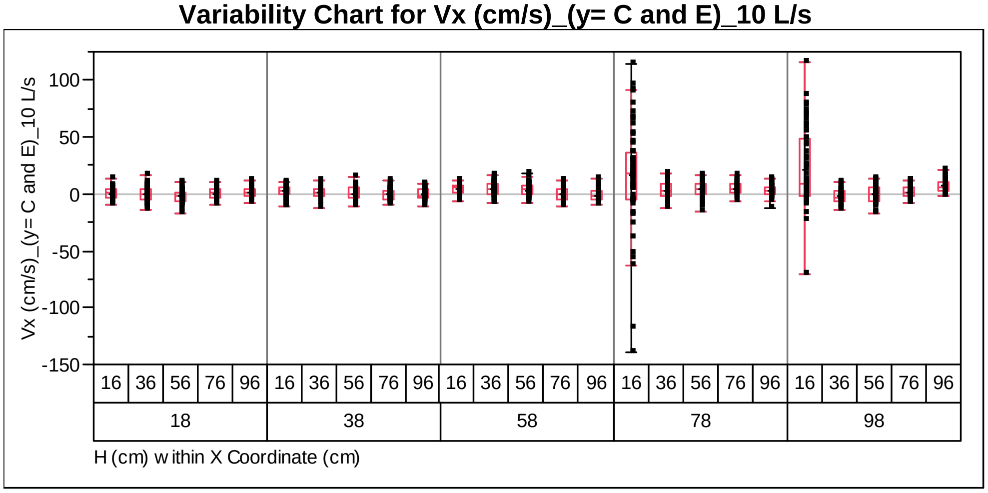

Variability Chart for Vx (cm/s)_(y= D)_10 L/s

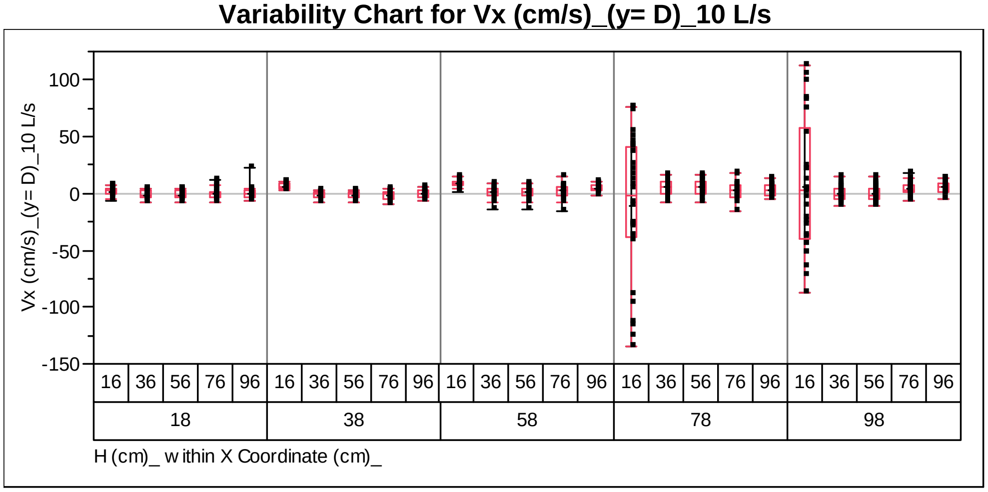

Figure B.1. Boxplots of x-velocities (Vx) at a 10 L/s flow rate with a 50-cm wide rectangular inlet.

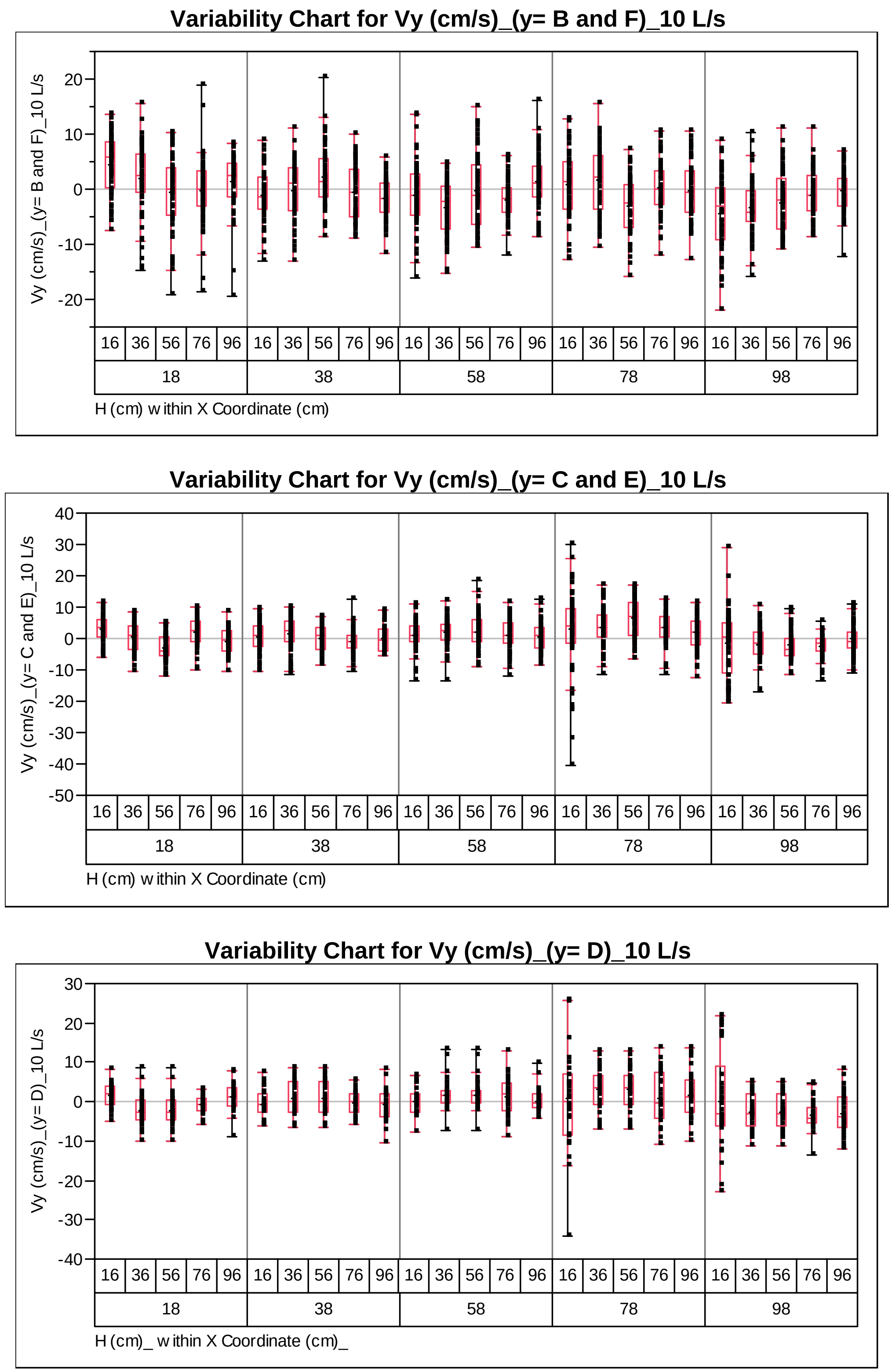

Figure B.2. Boxplots of y-velocities (Vy) at a 10 L/s flow rate with a 50-cm wide rectangular inlet.

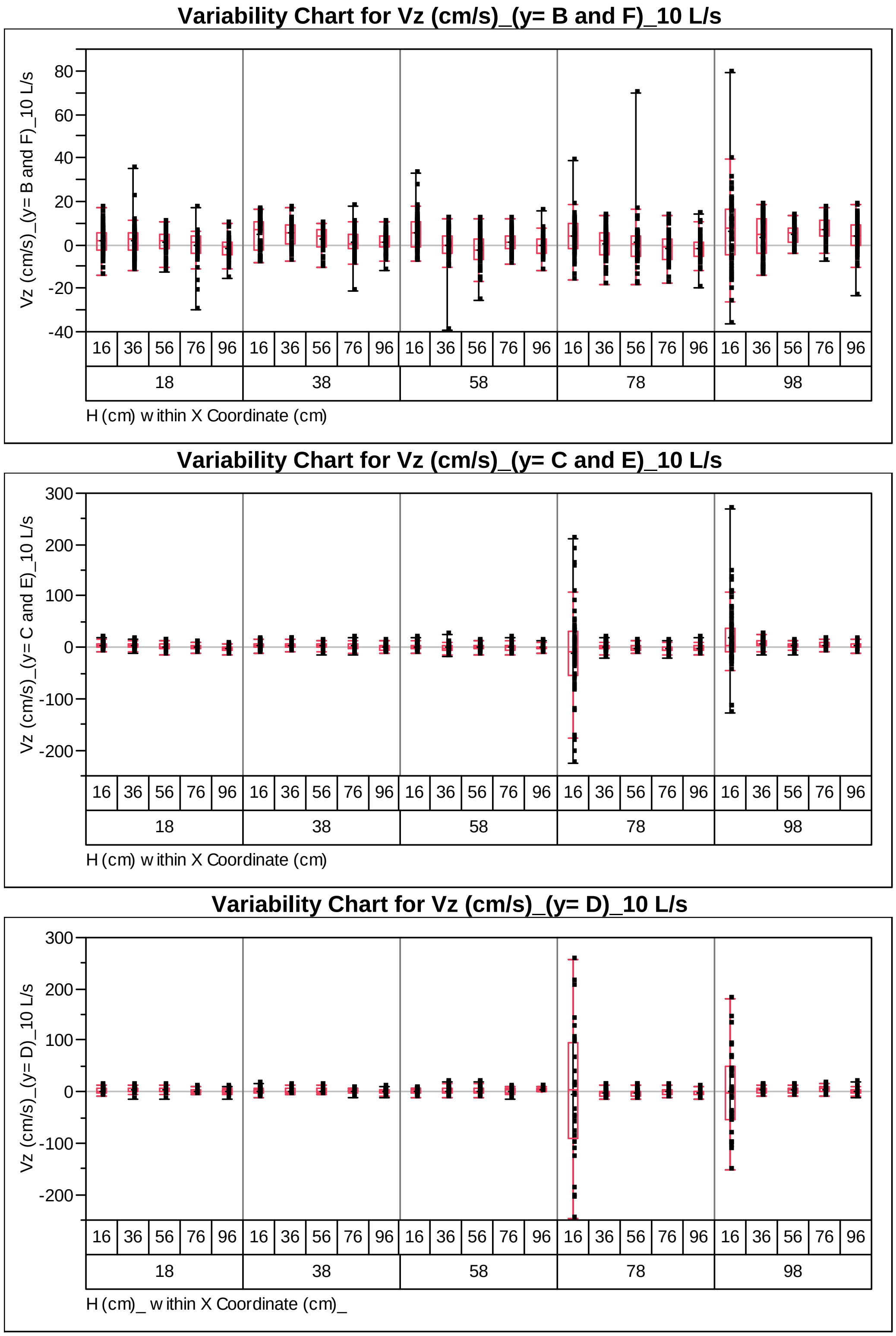

Figure B.3. Boxplots of z-velocities (Vz) at a 10 L/s flow rate with a 50-cm wide rectangular inlet.

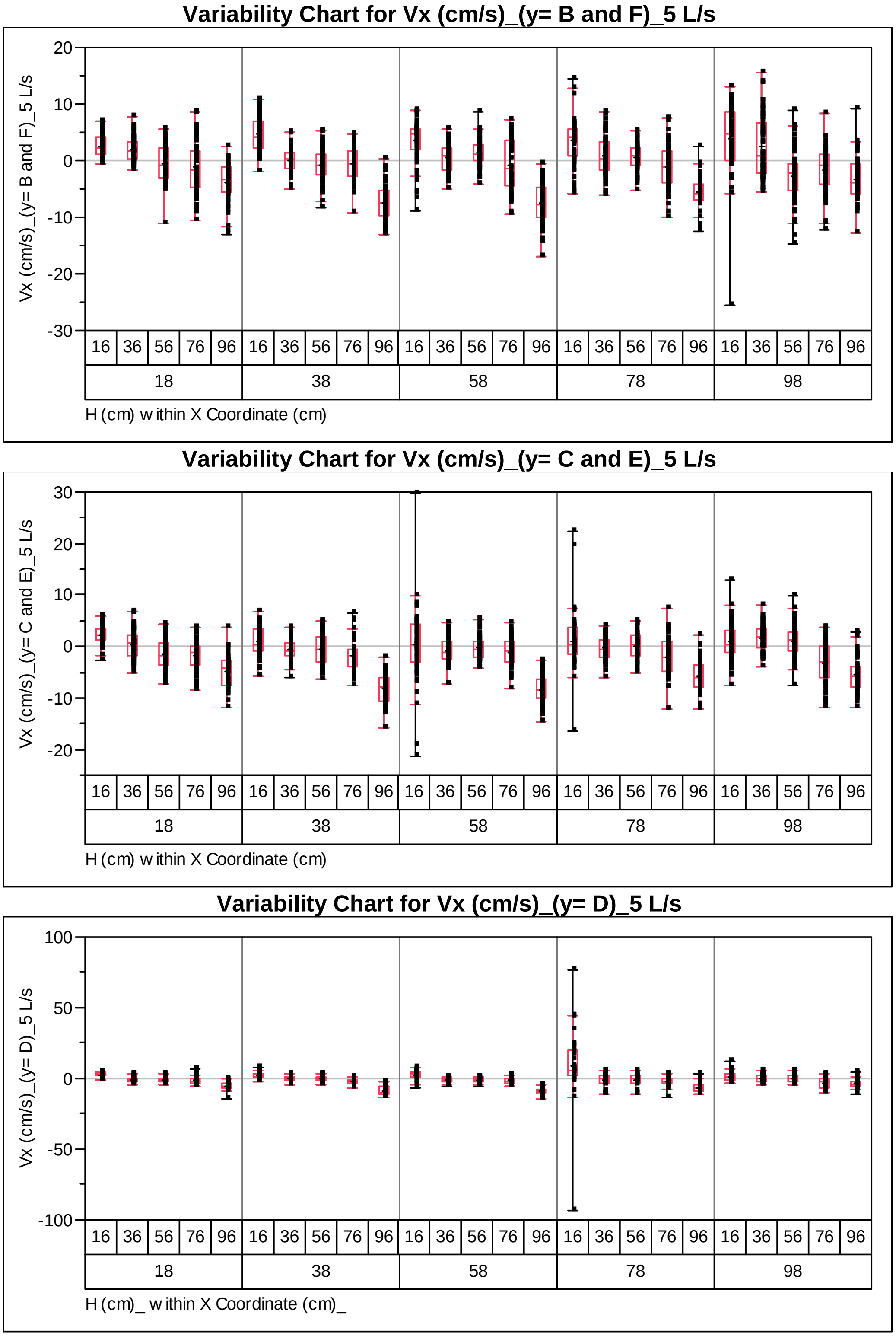

Figure B.4. Boxplots of x-velocities (Vx) at a 5 L/s flow rate with a 50-cm wide rectangular inlet.

Variability Chart for Vy (cm/s)_(y= B and F)_5 L/s

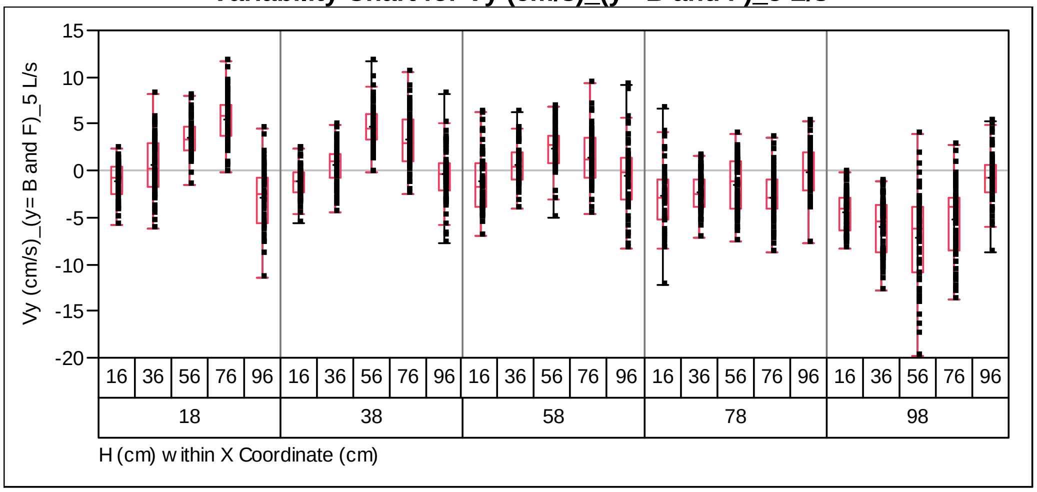

Variability Chart for Vy (cm/s)_(y= C and E)_5 L/s

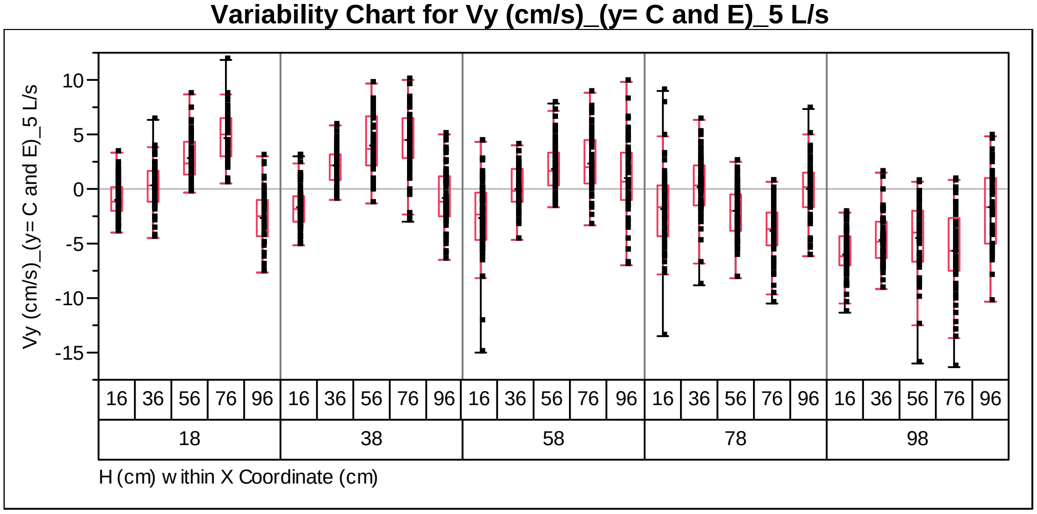

Variability Chart for Vy (cm/s)_(y= D)_5 L/s

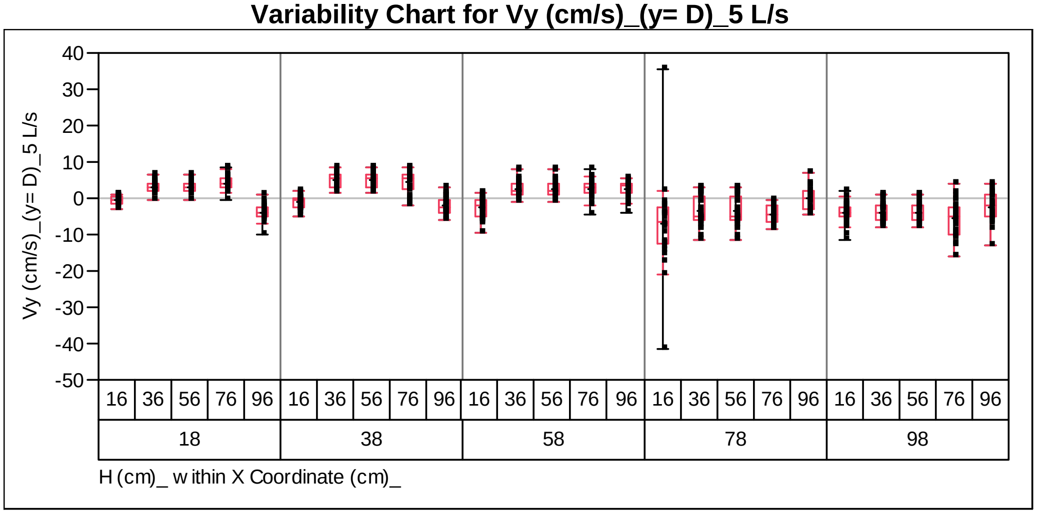

Figure B.5. Boxplots of y-velocities (Vy) at a 5 L/s flow rate with a 50-cm wide rectangular inlet.

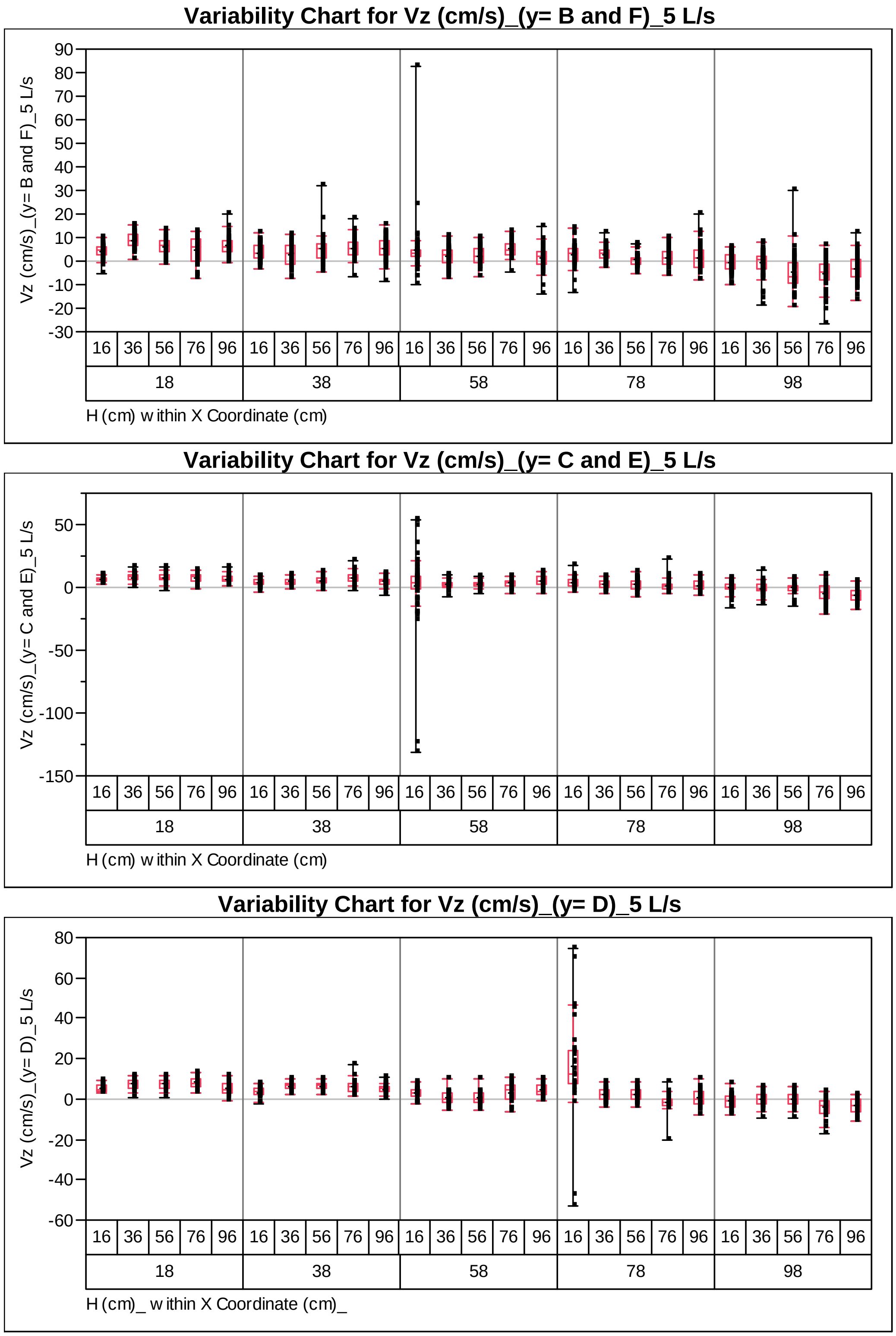

Figure B.6. Boxplots of z-velocities (Vz) at a 5 L/s flow rate with a 50-cm wide rectangular inlet.

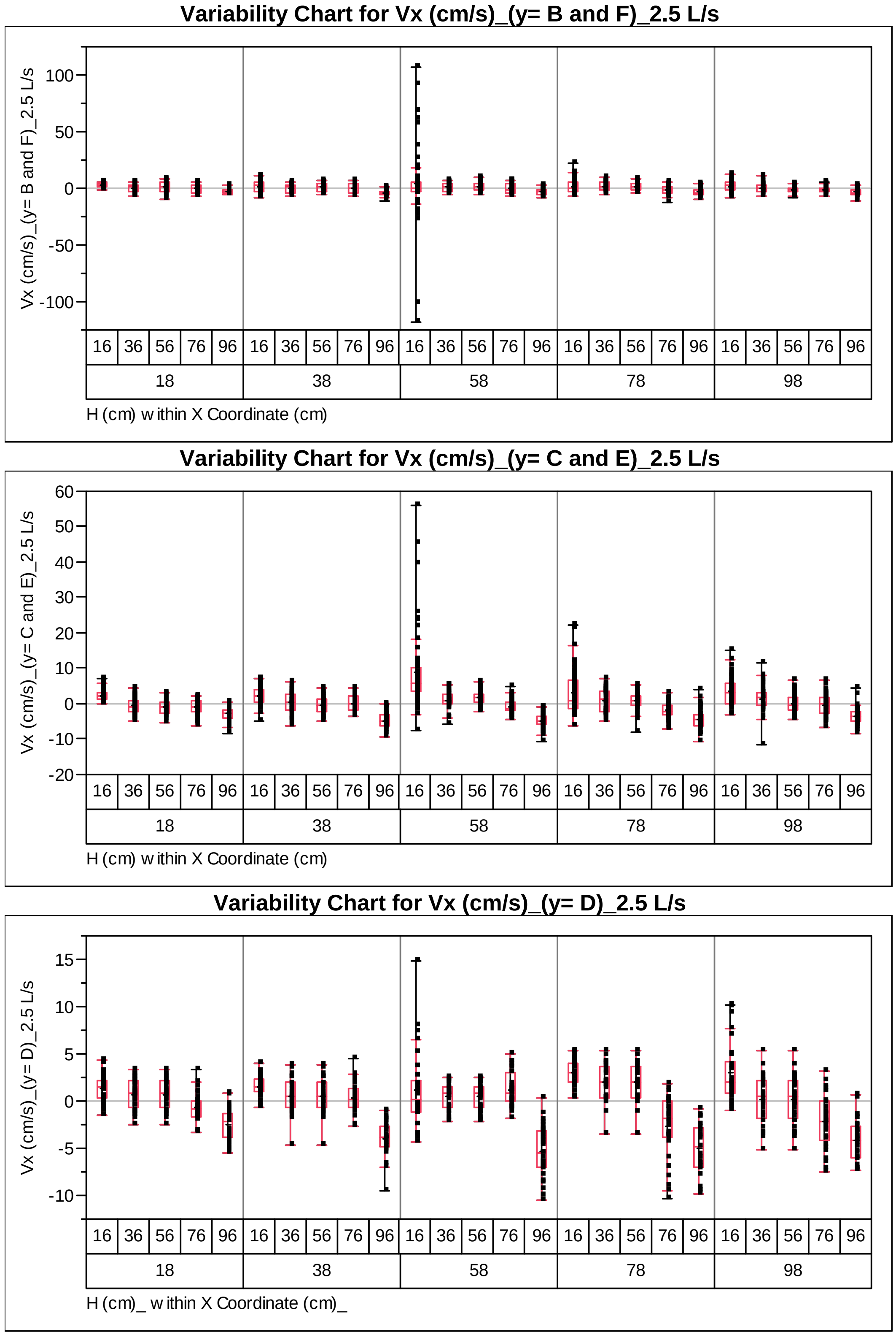

Figure B.7. Boxplots of x-velocities (Vx) at a 2.5 L/s flow rate with a 50-cm wide rectangular inlet.

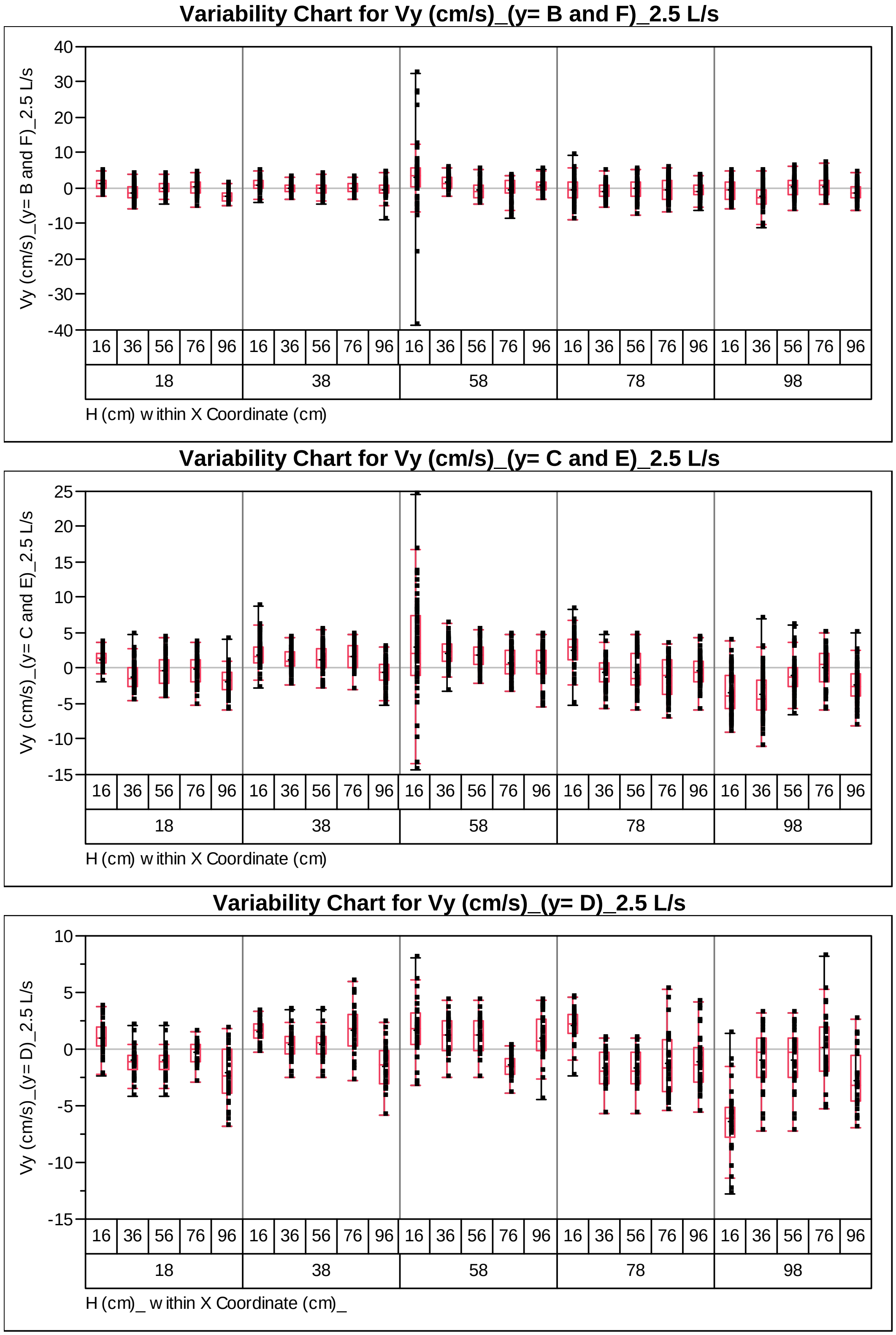

Figure B.8. Boxplots of y-velocities (Vy) at a 2.5 L/s flow rate with a 50-cm wide rectangular inlet.

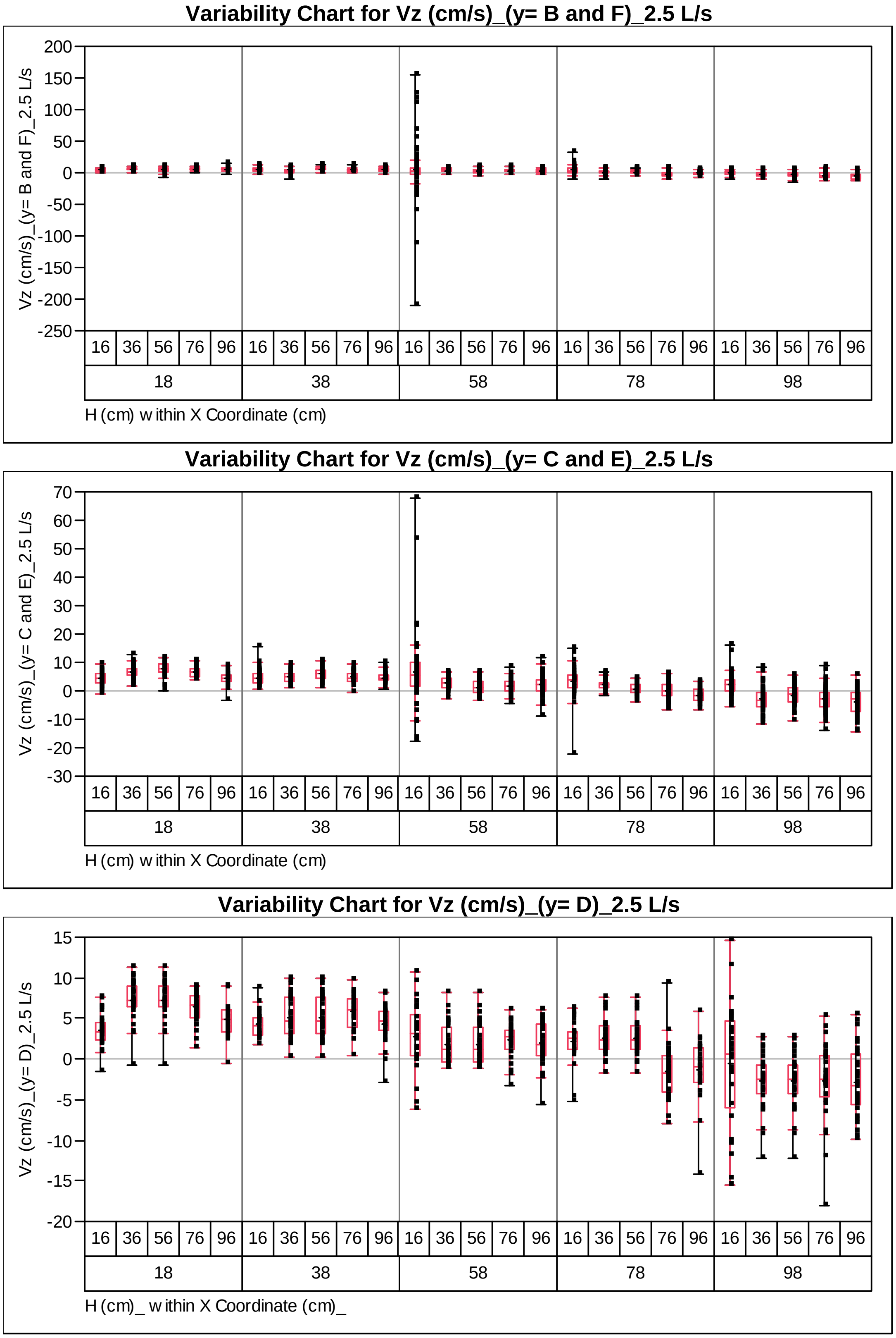

Figure B.9. Boxplots of z-velocities (Vz) at a 2.5 L/s flow rate with a 50-cm wide rectangular inlet.

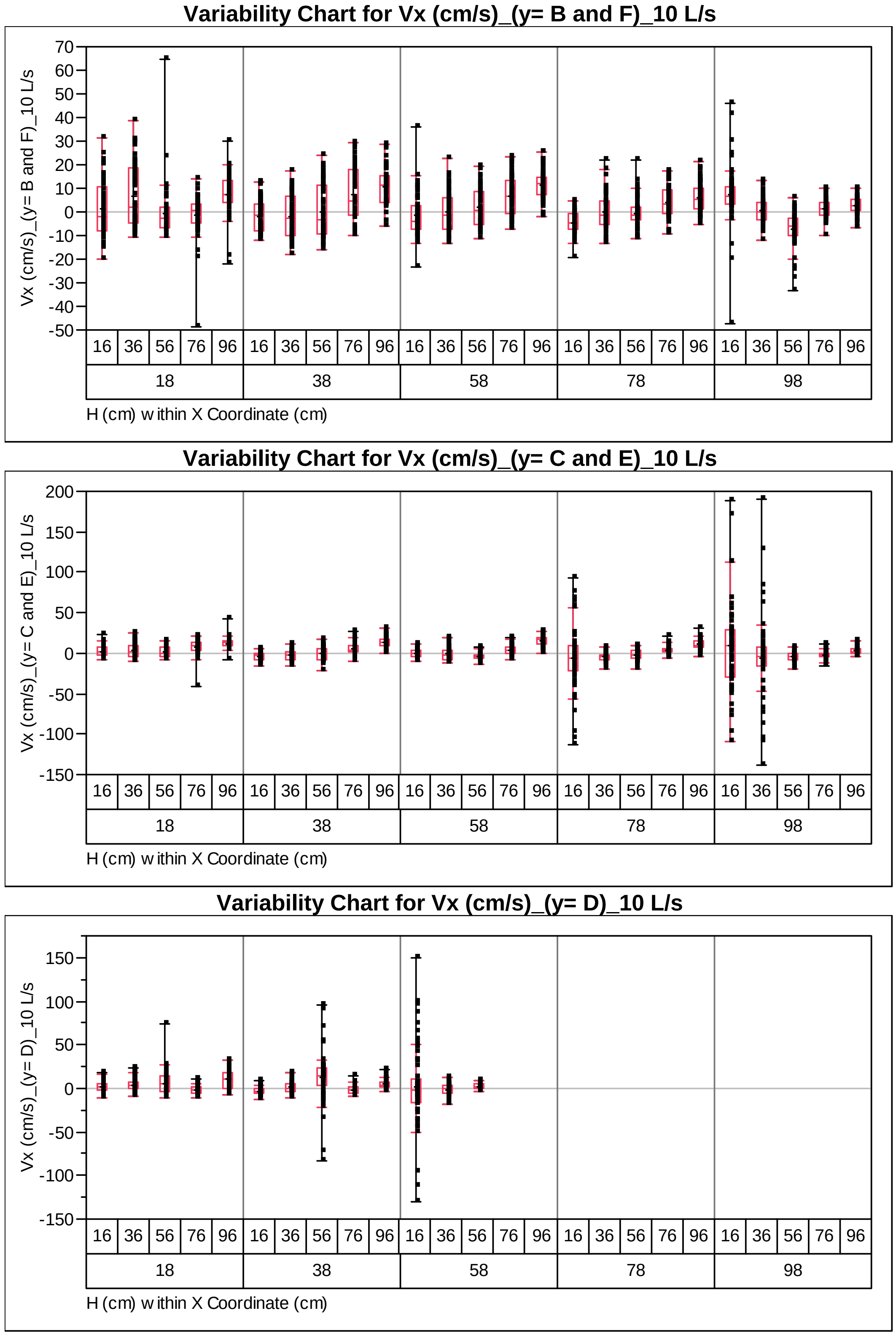

Figure B.10. Boxplots of x-velocities (Vx) at a 10 L/s flow rate with a 30-cm circular pipe inlet.

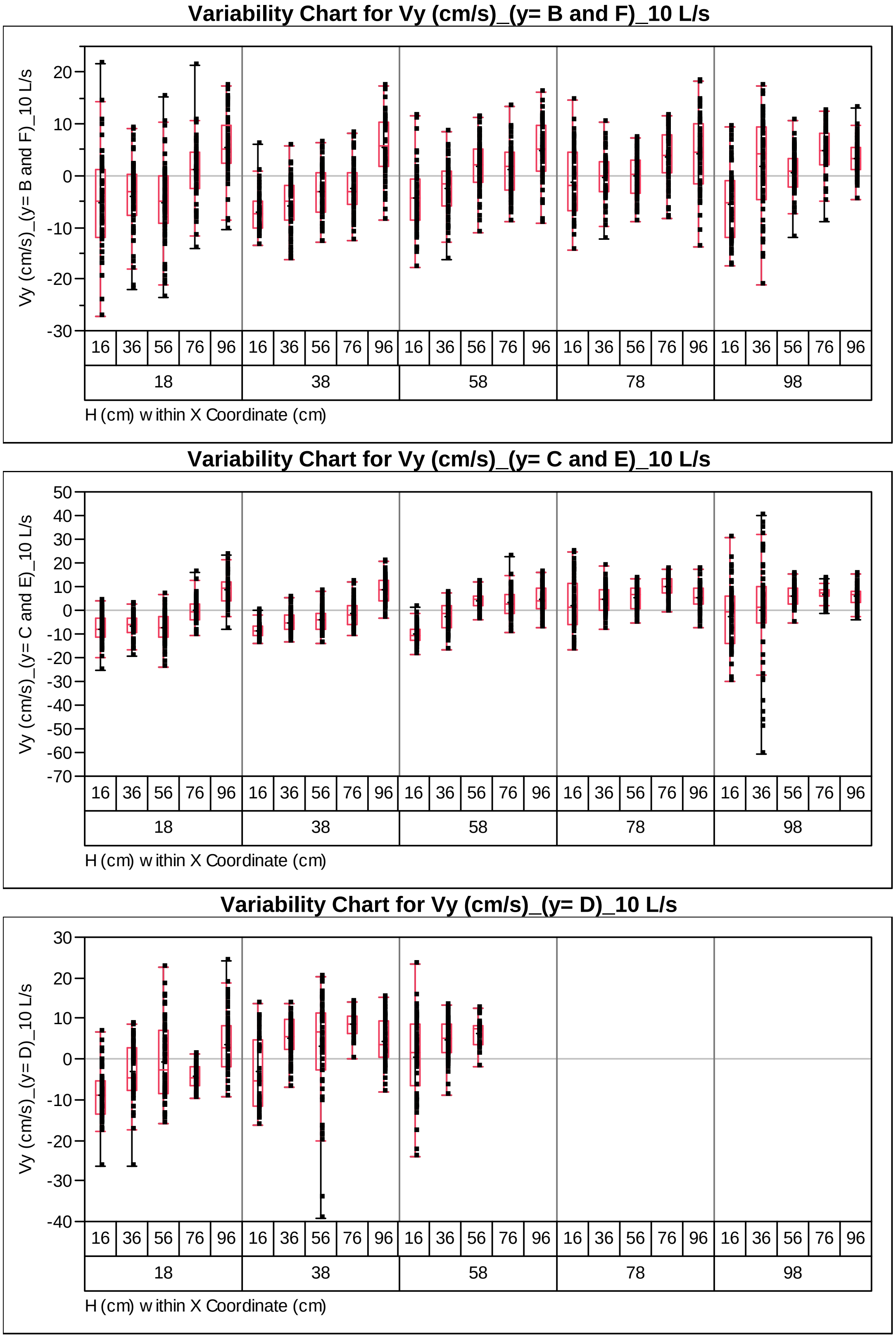

Figure B.11. Boxplots of y-velocities (Vy) at a 10 L/s flow rate with a 30-cm circular pipe inlet.

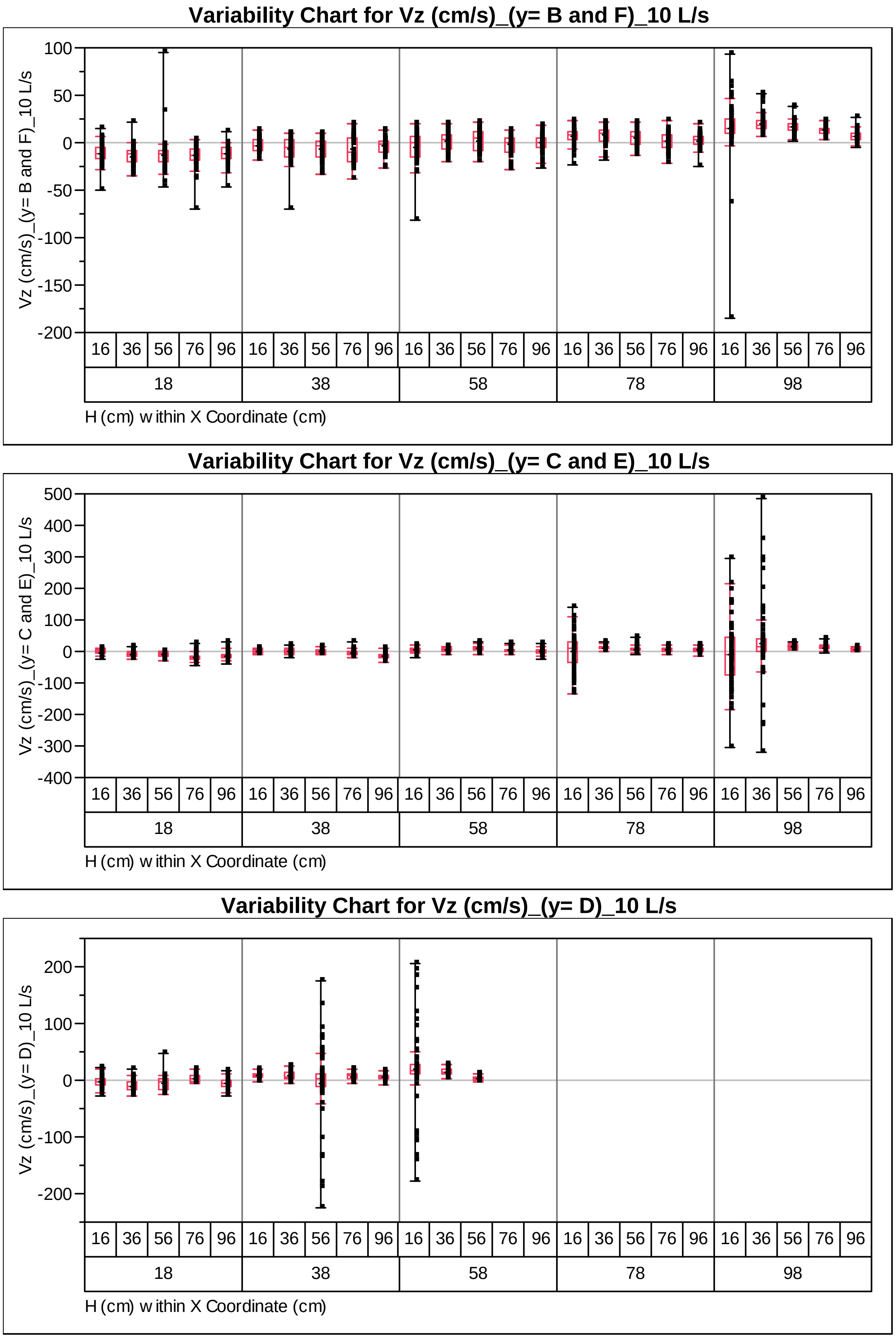

Figure B.12. Boxplots of z-velocities (Vz) at a 10 L/s flow rate with a 30-cm circular pipe inlet.

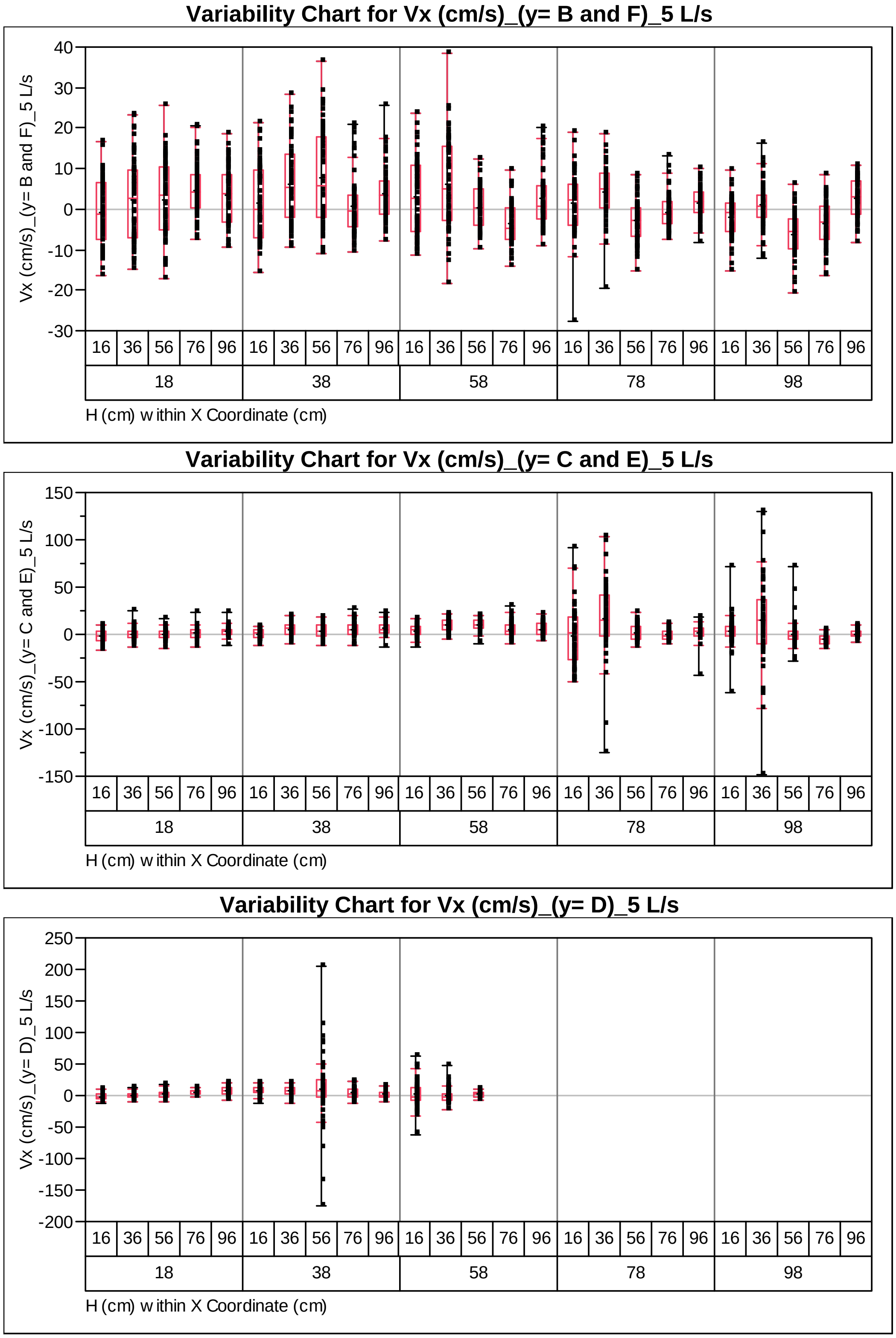

Figure B.13. Boxplots of x-velocities (Vx) at a 5 L/s flow rate with a 30-cm circular pipe inlet.

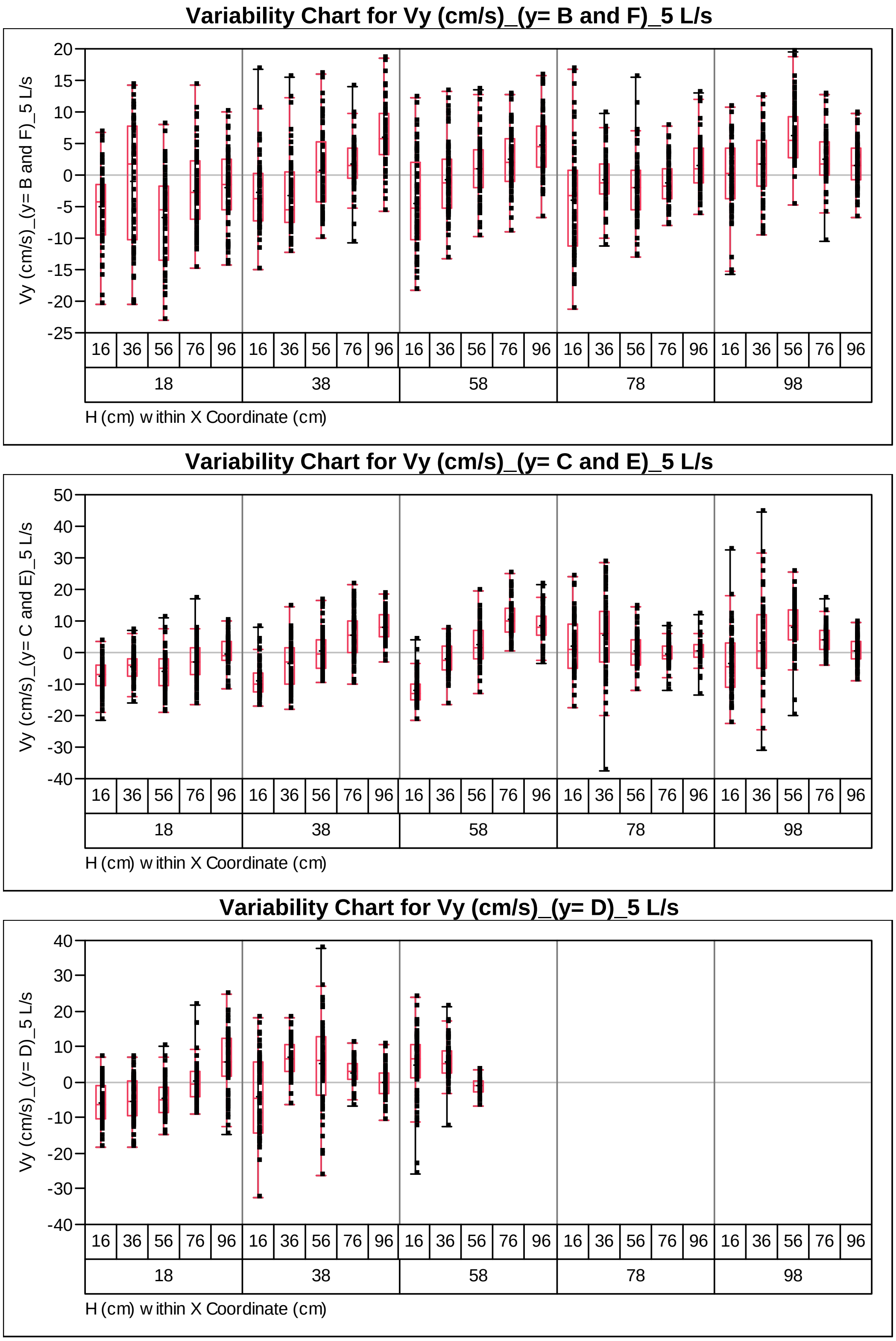

Figure B.14. Boxplots of y-velocities (Vy) at a 5 L/s flow rate with a 30-cm circular pipe inlet.

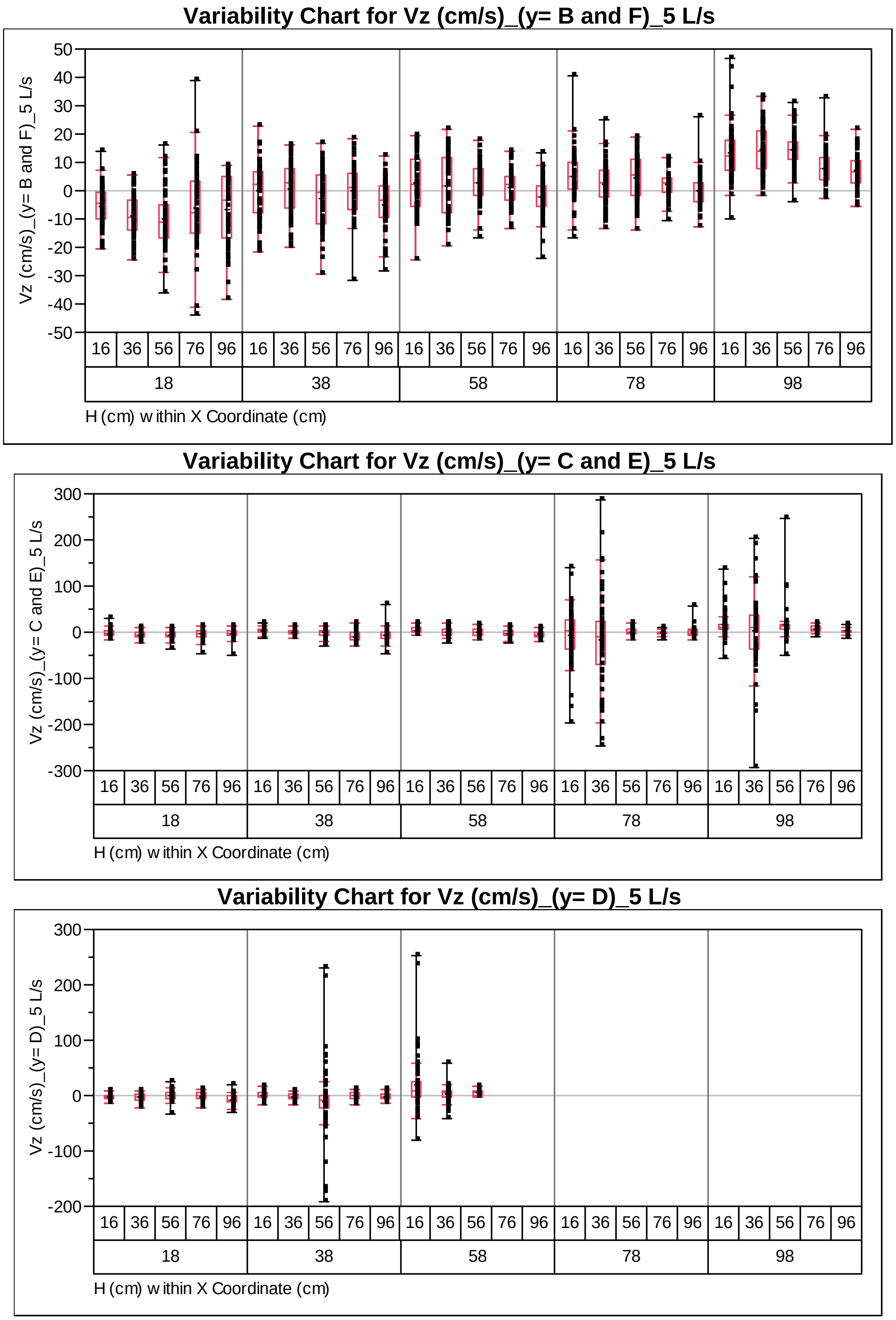

Figure B.15. Boxplots of z-velocities (Vz) at a 5 L/s flow rate with a 30-cm circular pipe inlet.

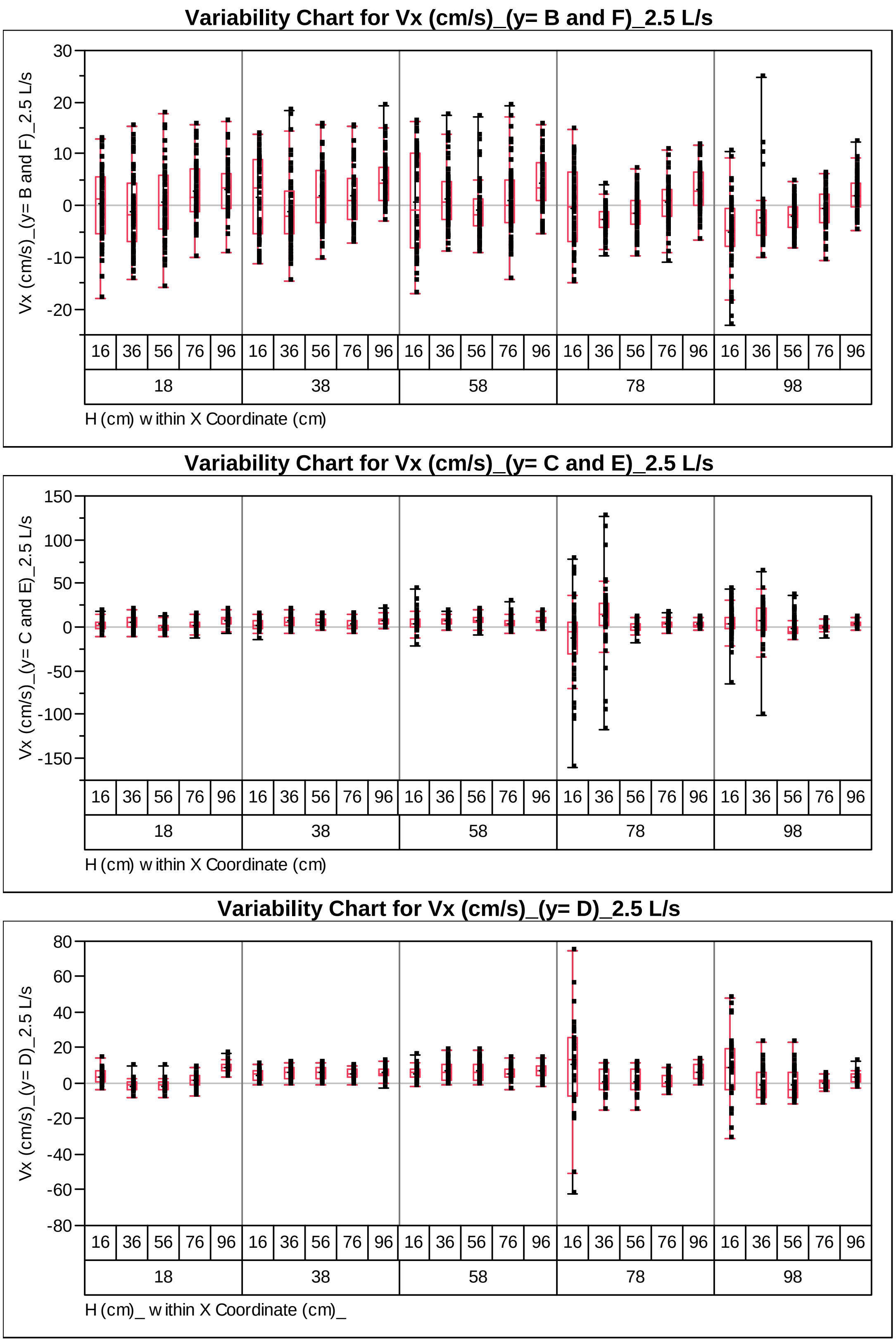

Figure B.16. Boxplots of x-velocities (Vx) at a 2.5 L/s flow rate with a 30-cm circular pipe inlet.

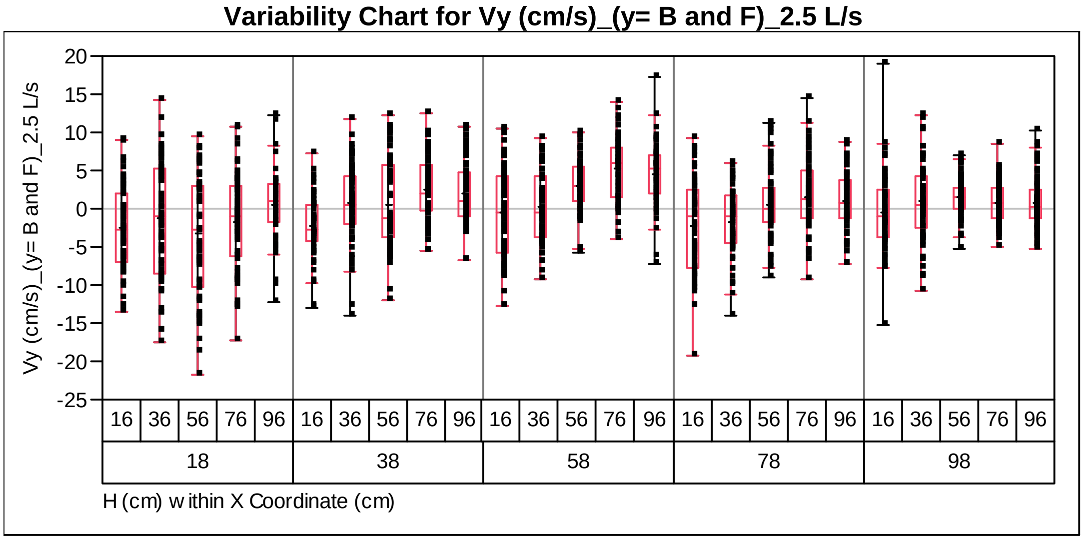

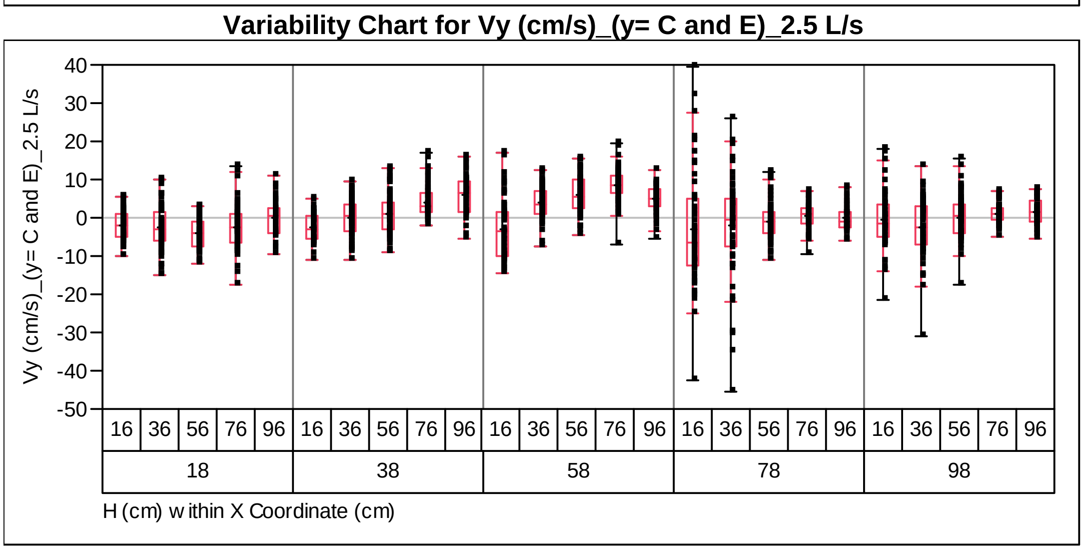

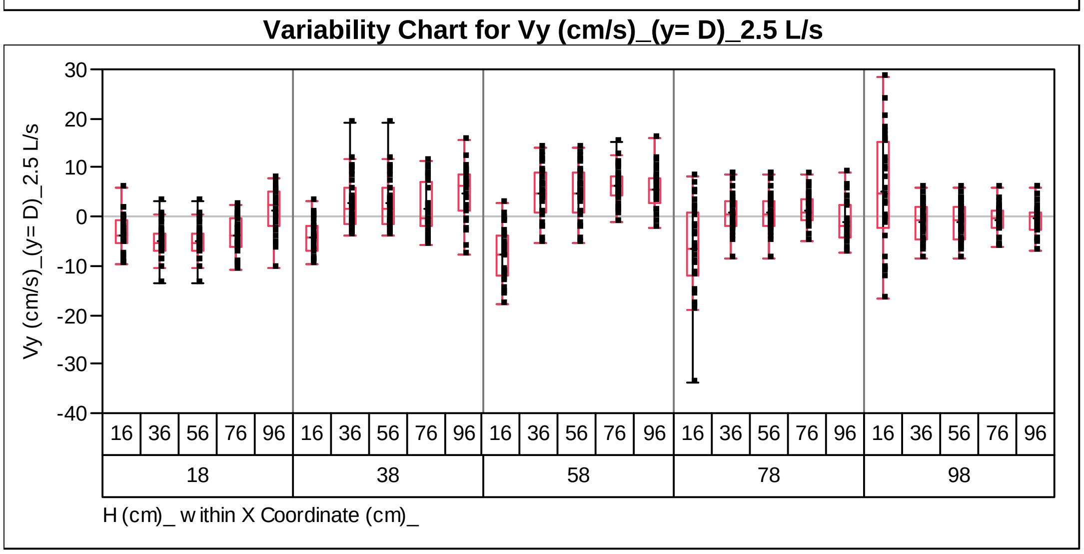

Figure B.17. Boxplots of y-velocities (Vy) at a 2.5 L/s flow rate with a 30-cm circular pipe inlet.

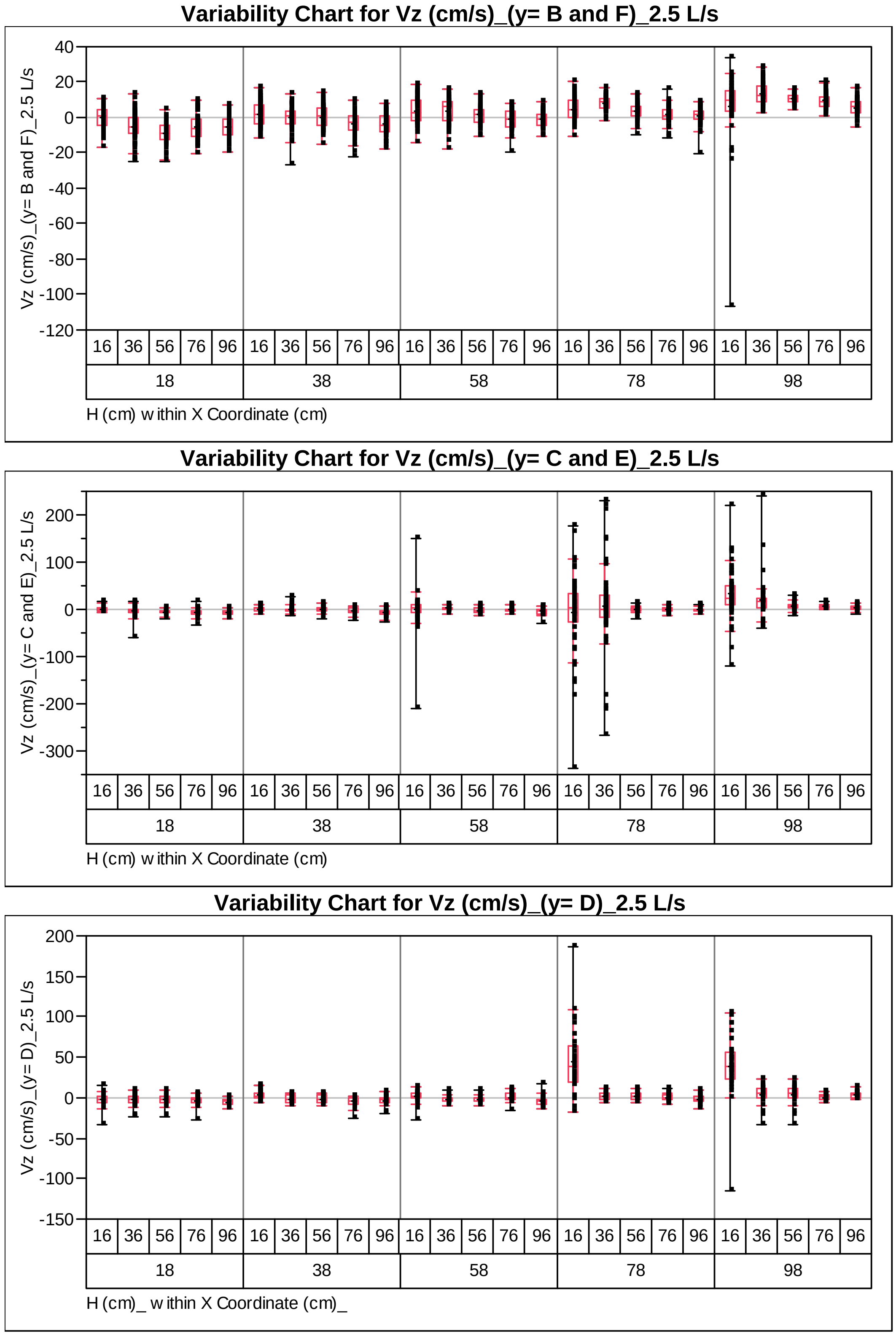

Figure B.18. Boxplots of z-velocities (Vz) at a 2.5 L/s flow rate with a 30-cm circular pipe inlet.

APPENDIX C

TWO-SAMPLE T-TEST OUTPUTS FOR COMPARISON OF CIRCULAR AND RECTANGULAR INLETS – HYDRODYNAMIC RESULTS: VELOCITIES

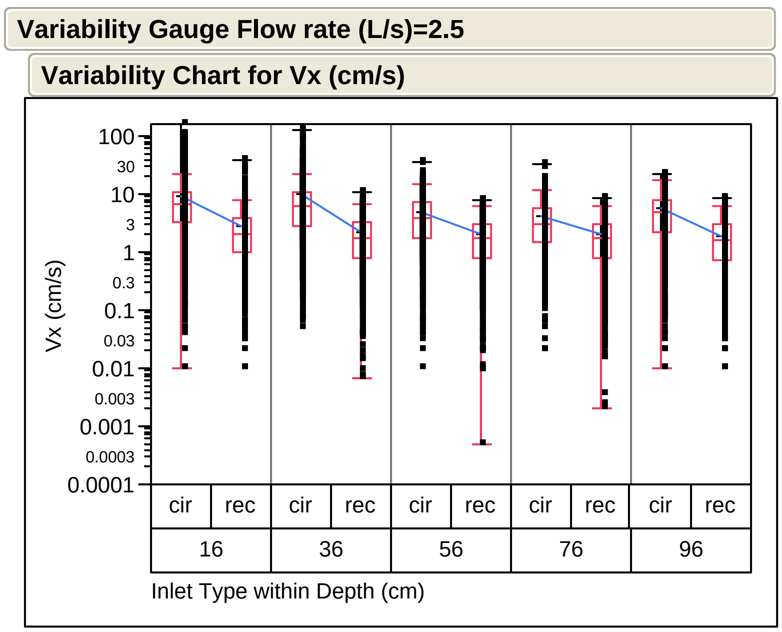

Figure C.1. Boxplots of x-velocities by inlet type and overlaying water depth at a 2.5 L/s flow rate.

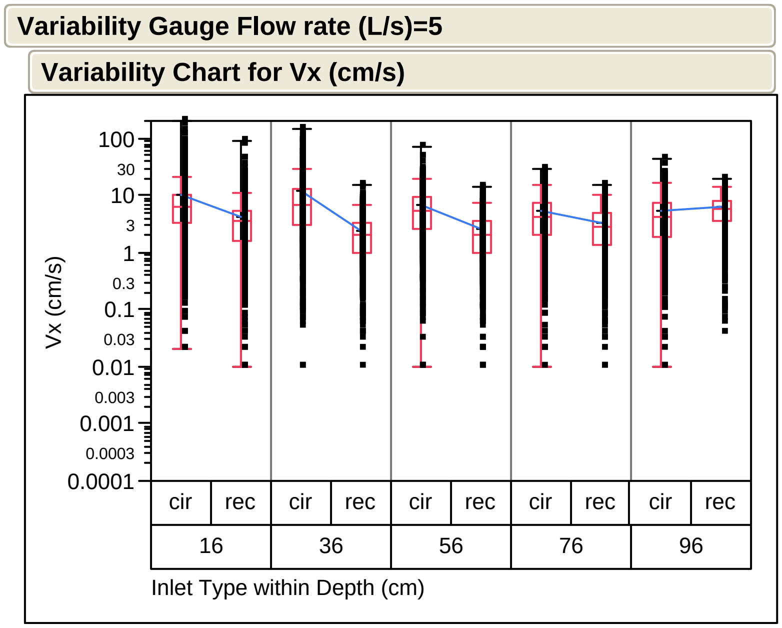

Figure C.2. Boxplots of x-velocities by inlet type and overlaying water depth at a 5 L/s flow rate.

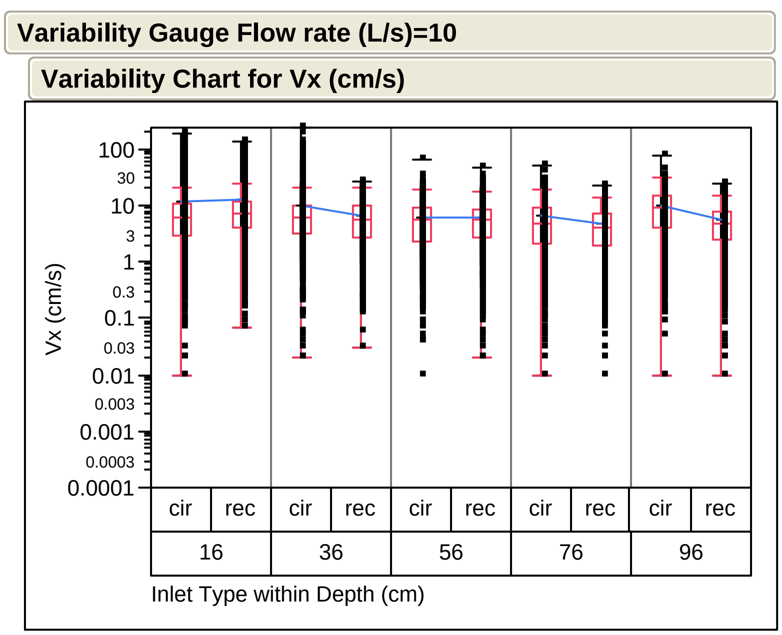

Figure C.3. Boxplots of x-velocities by inlet type and overlaying water depth at a 10 L/s flow rate.

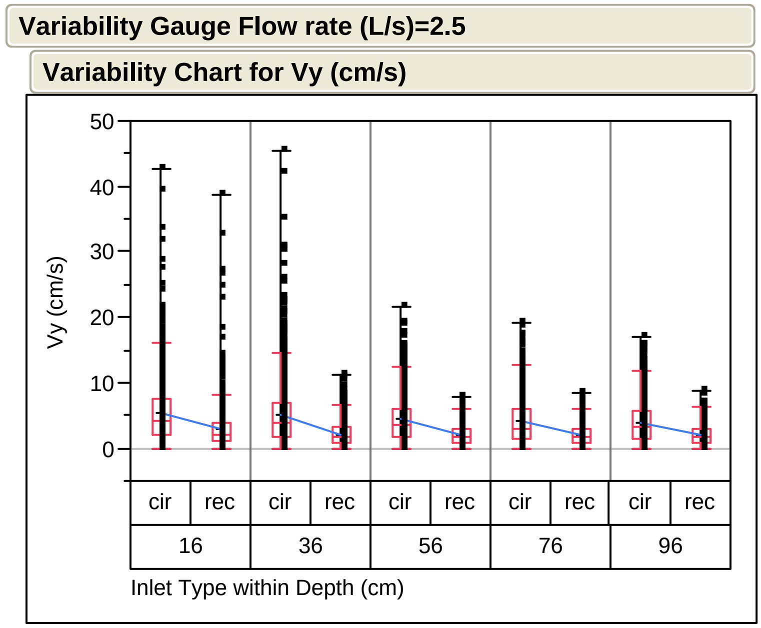

Figure C.4. Boxplots of y-velocities by inlet type and overlaying water depth at a 2.5 L/s flow rate.

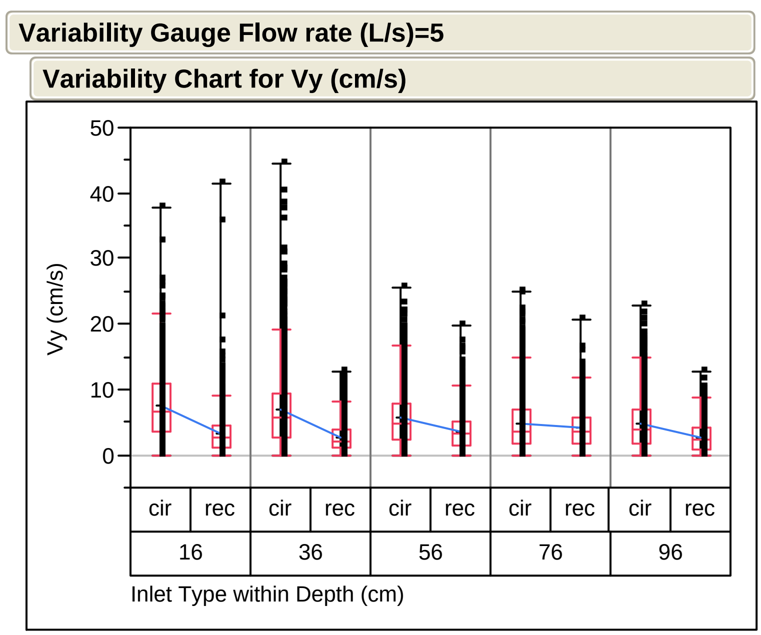

Figure C.5. Boxplots of y-velocities by inlet type and overlaying water depth at a 5 L/s flow rate.

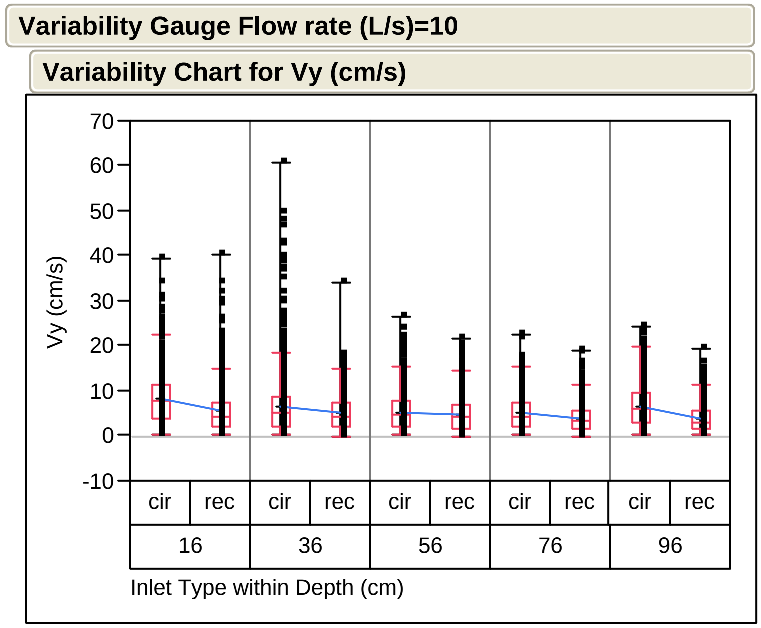

Figure C.6. Boxplots of y-velocities by inlet type and overlaying water depth at a 10 L/s flow rate.

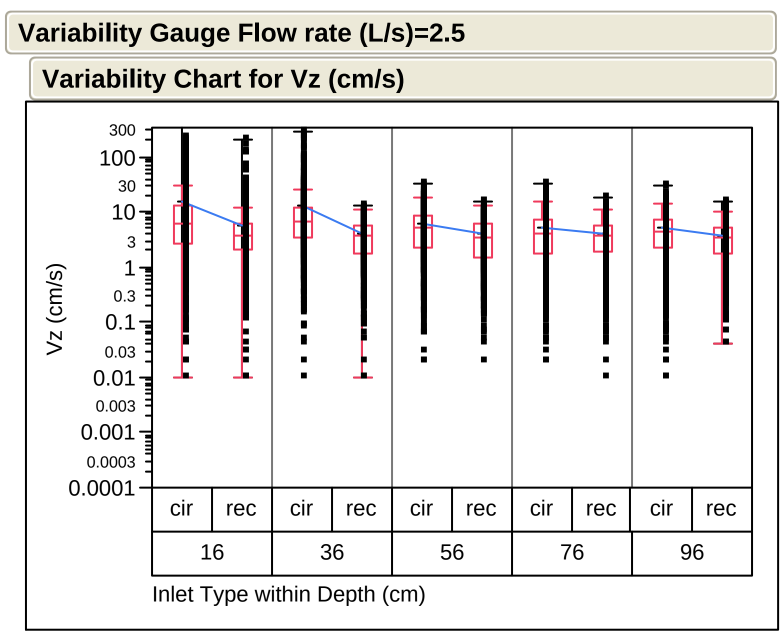

Figure C.7. Boxplots of z-velocities by inlet type and overlaying water depth at A 2.5 L/s flow rate.

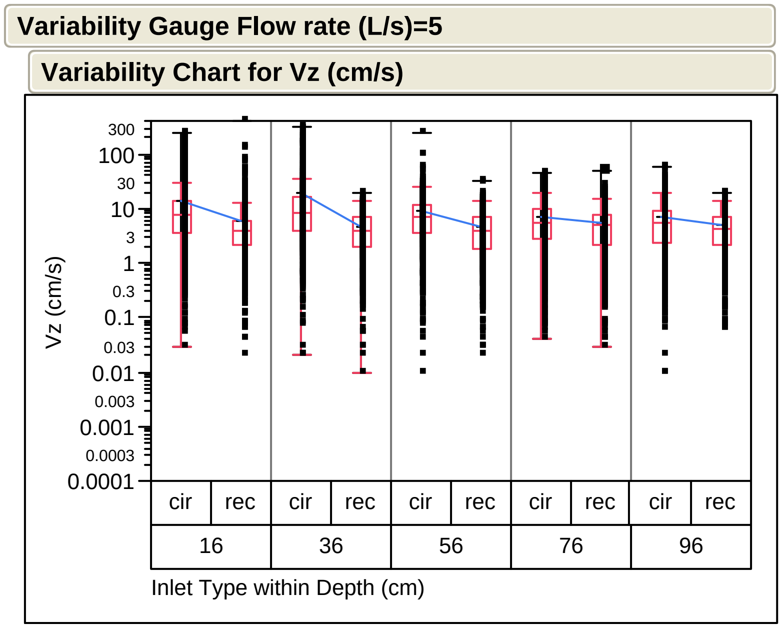

Figure C.8. Boxplots of z-velocities by inlet type and overlaying water depth at a 5 L/s flow rate.

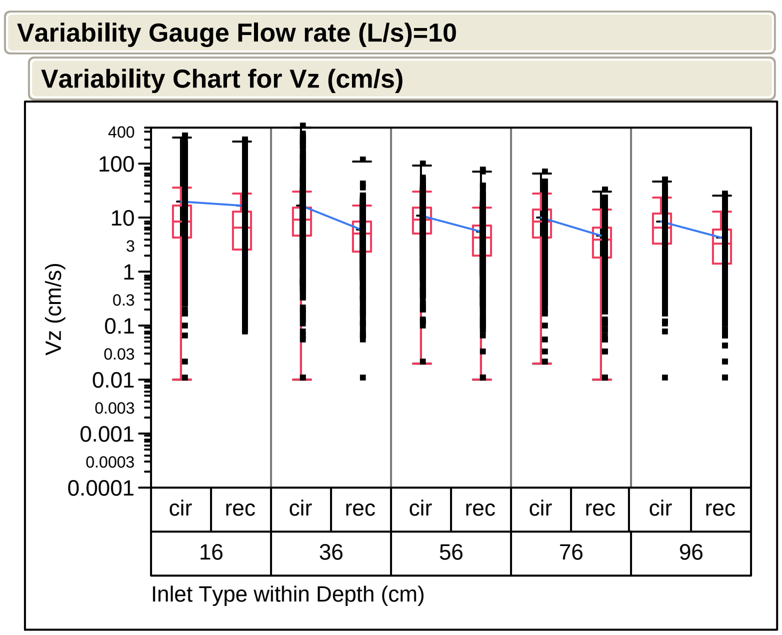

Figure C.9. Boxplots of z-velocities by inlet type and overlaying water depth at a 10 L/s flow rate.

Table C.1. Two-Sample t-Test for Inlet Type, a 30-cm Circular Pipe and a 50-cm Wide Rectangular Inlet: Evaluating x-Velocity (Vx) at 2.5 L/s

Oneway Analysis of Vx (cm/s) By Inlet Type Flow rate (L/s)=2.5

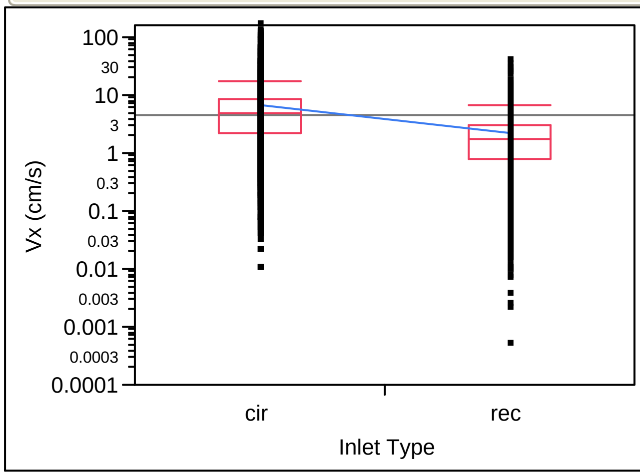

Oneway Anova

Summary of Fit

Rsquare	0.105985
Adj Rsquare	0.105889
Root Mean Square Error	6.580961
Mean of Response	4.464085
Observations (or Sum Wgts)	9300

t Test

rec-cir

Assuming equal variances

Difference	-4.5313	t Ratio	-33.2004
Std Err Dif	0.1365	DF	9298
Upper CL Dif	-4.2638	Prob > |t|	0.0000*
Lower CL Dif	-4.7988	Prob > t	1.0000
Confidence	0.95	Prob < t	0.0000*

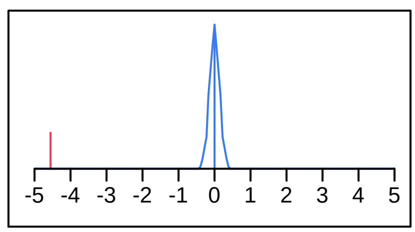

Table C.2. Two-Sample t-Test for Inlet Type, a 30-cm Circular Pipe and a 50-cm Wide Rectangular Inlet: Evaluating x-Velocity (Vx) at 5 L/s

Oneway Analysis of Vx (cm/s) By Inlet Type Flow rate (L/s)=5

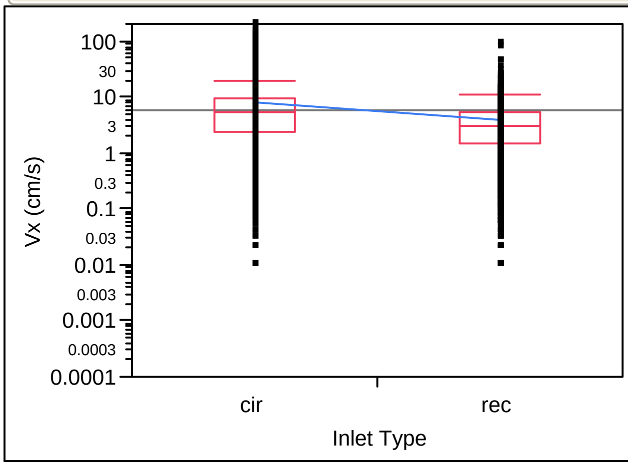

Excluded Rows 1

Oneway Anova

Summary of Fit

Rsquare	0.056069
Adj Rsquare	0.055967
Root Mean Square Error	8.59975
Mean of Response	5.890509
Observations (or Sum Wgts)	9299

t Test

rec-cir

Assuming equal variances

Difference	-4.1914	t Ratio	-23.4997
Std Err Dif	0.1784	DF	9297
Upper CL Dif	-3.8418	Prob > |t|	0.0000*
Lower CL Dif	-4.5410	Prob > t	1.0000
Confidence	0.95	Prob < t	0.0000*

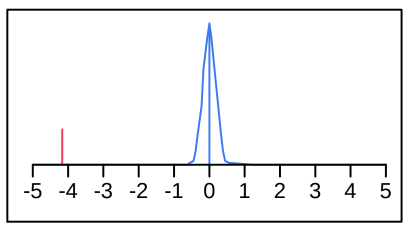

Table C.3. Two-Sample t-Test for Inlet Type, a 30-cm Circular Pipe and a 50-cm Wide Rectangular Inlet: Evaluating x-Velocity (Vx) at 10 L/s

Oneway Analysis of Vx (cm/s) By Inlet Type Flow rate (L/s)=10

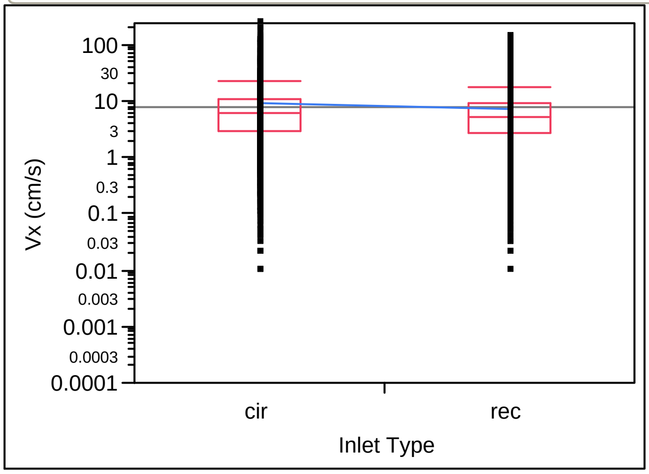

Oneway Anova

Summary of Fit

Rsquare	0.004967
Adj Rsquare	0.00486
Root Mean Square Error	11.34823
Mean of Response	8.012788
Observations (or Sum Wgts)	9300

t Test

rec-cir

Assuming equal variances

Difference	-1.6034	t Ratio	-6.81259
Std Err Dif	0.2354	DF	9298
Upper CL Dif	-1.1420	Prob > |t|	<.0001*
Lower CL Dif	-2.0647	Prob > t	1.0000
Confidence	0.95	Prob < t	<.0001*

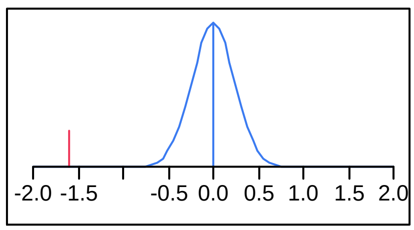

Table C.4. Two-Sample t-Test for Inlet Type, a 30-cm Circular Pipe and a 50-cm Wide Rectangular Inlet: Evaluating y-Velocity (Vy) at 2.5 L/s

Oneway Analysis of Vy (cm/s) By Inlet Type Flow rate (L/s)=2.5

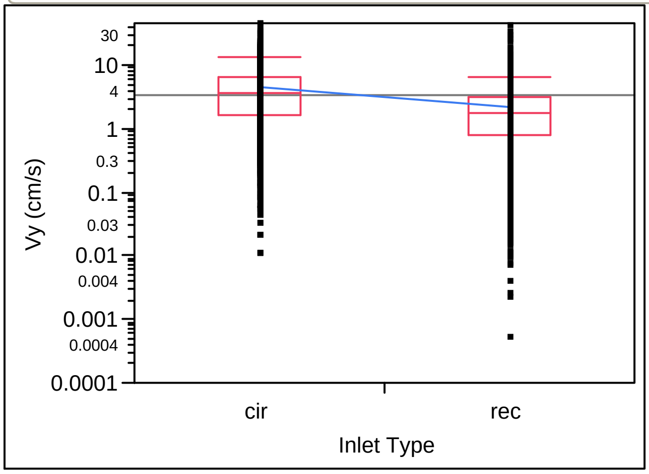

Oneway Anova

Summary of Fit

Rsquare	0.11896
Adj Rsquare	0.118865
Root Mean Square Error	3.250812
Mean of Response	3.392835
Observations (or Sum Wgts)	9300

t Test

rec-cir

Assuming equal variances

Difference	-2.3888	t Ratio	-35.4321
Std Err Dif	0.0674	DF	9298
Upper CL Dif	-2.2566	Prob > |t|	0.0000*
Lower CL Dif	-2.5209	Prob > t	1.0000
Confidence	0.95	Prob < t	0.0000*

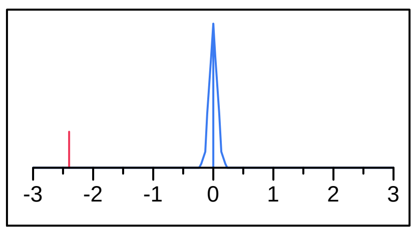

Table C.5. Two-Sample t-Test for Inlet Type, a 30-cm Circular Pipe and a 50-cm Wide Rectangular Inlet: Evaluating y-Velocity (Vy) at 5 L/s

Oneway Analysis of Vy (cm/s) By Inlet Type Flow rate (L/s)=5

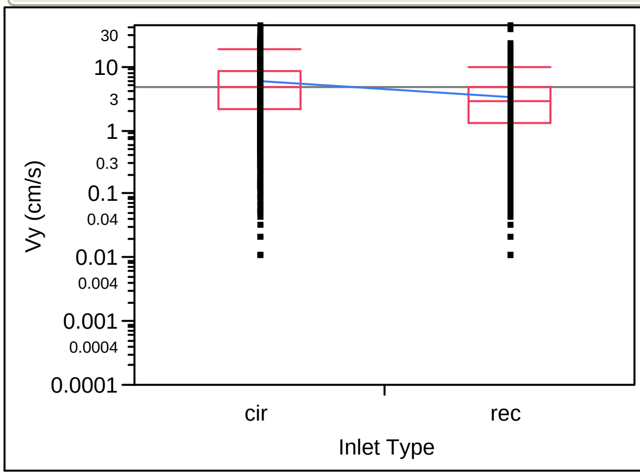

Oneway Anova

Summary of Fit

Rsquare	0.103567
Adj Rsquare	0.103471
Root Mean Square Error	4.023425
Mean of Response	4.650159
Observations (or Sum Wgts)	9300

t Test

rec-cir

Assuming equal variances

Difference	-2.7348	t Ratio	-32.7753
Std Err Dif	0.0834	DF	9298
Upper CL Dif	-2.5713	Prob > |t|	0.0000*
Lower CL Dif	-2.8984	Prob > t	1.0000
Confidence	0.95	Prob < t	0.0000*

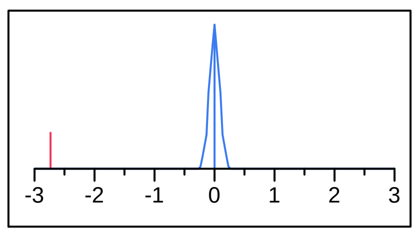

Table C.6. Two-Sample t-Test for Inlet Type, a 30-cm Circular Pipe and a 50-cm Wide Rectangular Inlet: Evaluating y-Velocity (Vy) at 10 L/s.

Oneway Analysis of Vy (cm/s) By Inlet Type Flow rate (L/s)=10

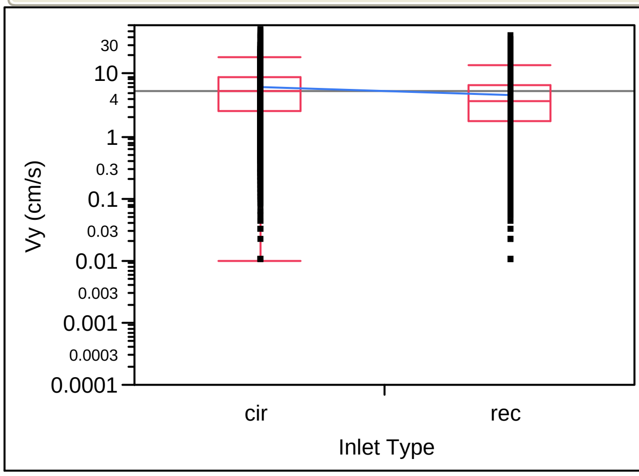

Oneway Anova

Summary of Fit

Rsquare	0.035526
Adj Rsquare	0.035422
Root Mean Square Error	4.541169
Mean of Response	5.468799
Observations (or Sum Wgts)	9300

t Test

rec-cir

Assuming equal variances

Difference	-1.7429	t Ratio	-18.5064
Std Err Dif	0.0942	DF	9298
Upper CL Dif	-1.5583	Prob > |t|	0.0000*
Lower CL Dif	-1.9275	Prob > t	1.0000
Confidence	0.95	Prob < t	0.0000*

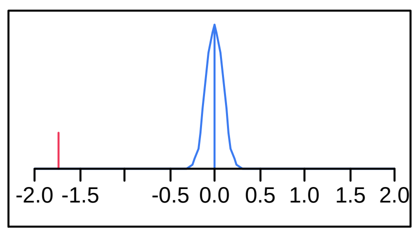

Table C.7. Two-Sample t-Test for Inlet Type, a 30-cm Circular Pipe and a 50-cm Wide Rectangular Inlets: Evaluating z-Velocity (Vz) at 2.5 L/s

Oneway Analysis of Vz (cm/s) By Inlet Type Flow rate (L/s)=2.5

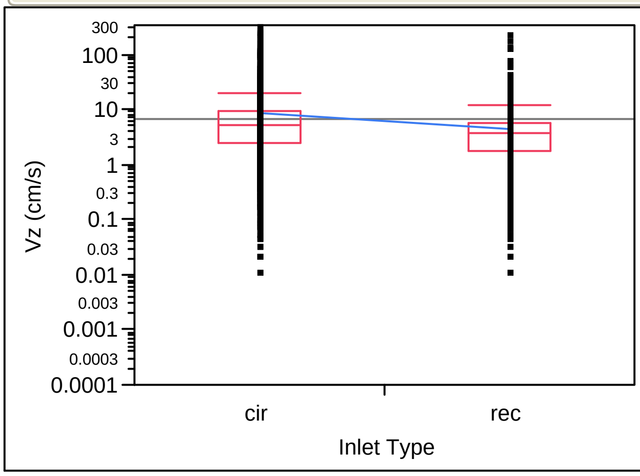

Oneway Anova

Summary of Fit

Rsquare	0.027308
Adj Rsquare	0.027203
Root Mean Square Error	13.78893
Mean of Response	6.62251
Observations (or Sum Wgts)	9300

t Test

rec-cir

Assuming equal variances

Difference	-4.6203	t Ratio	-16.1566
Std Err Dif	0.2860	DF	9298
Upper CL Dif	-4.0597	Prob > |t|	0.0000*
Lower CL Dif	-5.1808	Prob > t	1.0000
Confidence	0.95	Prob < t	0.0000*

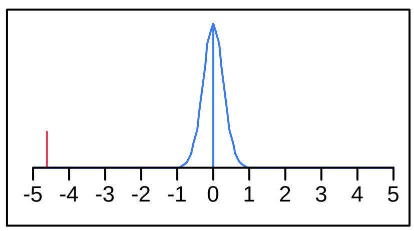

Table C.8. Two-sample t-Test for Inlet Type, a 30-cm Circular Pipe and a 50-cm Wide Rectangular Inlet: Evaluating z-Velocity (Vz) at 5 L/s

Oneway Analysis of Vz (cm/s) By Inlet Type Flow rate (L/s)=5

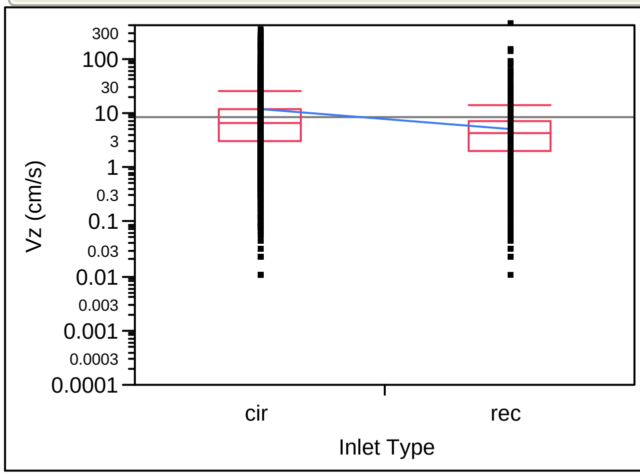

Oneway Anova

Summary of Fit

Rsquare	0.033001
Adj Rsquare	0.032897
Root Mean Square Error	16.61284
Mean of Response	8.157439
Observations (or Sum Wgts)	9300

t Test

rec-cir

Assuming equal variances

Difference	-6.1373	t Ratio	-17.8133
Std Err Dif	0.3445	DF	9298
Upper CL Dif	-5.4619	Prob > |t|	0.0000*
Lower CL Dif	-6.8126	Prob > t	1.0000
Confidence	0.95	Prob < t	0.0000*

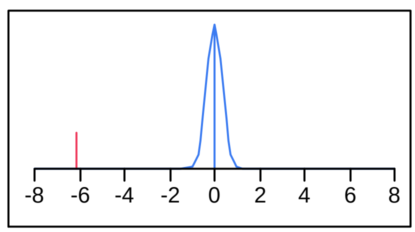

Table C.9. Two-Sample t-Test for Inlet Type, a 30-cm Circular Pipe and a 50-cm Wide Rectangular Inlet: Evaluating z-Velocity (Vz) at 10 L/s

Oneway Analysis of Vz (cm/s) By Inlet Type Flow rate (L/s)=10

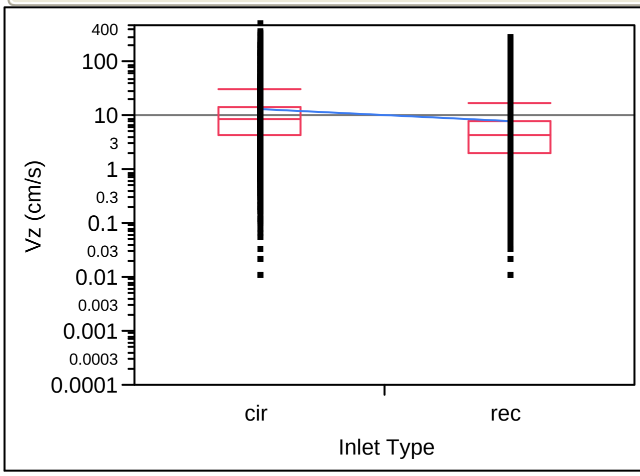

Oneway Anova

Summary of Fit

Rsquare	0.01929
Adj Rsquare	0.019184
Root Mean Square Error	21.3386
Mean of Response	10.65133
Observations (or Sum Wgts)	9300

t Test

rec-cir

Assuming equal variances

Difference	-5.9847	t Ratio	-13.5234
Std Err Dif	0.4425	DF	9298
Upper CL Dif	-5.1172	Prob > |t|	0.0000*
Lower CL Dif	-6.8521	Prob > t	1.0000
Confidence	0.95	Prob < t	0.0000*

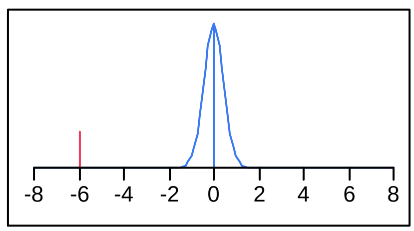

APPENDIX D

ONE-WAY ANOVA OUTPUTS FOR FLOW RATE, HYDRODYNAMIC RESULTS: VELOCITIES BY DEPTH AND BY INLET TYPE

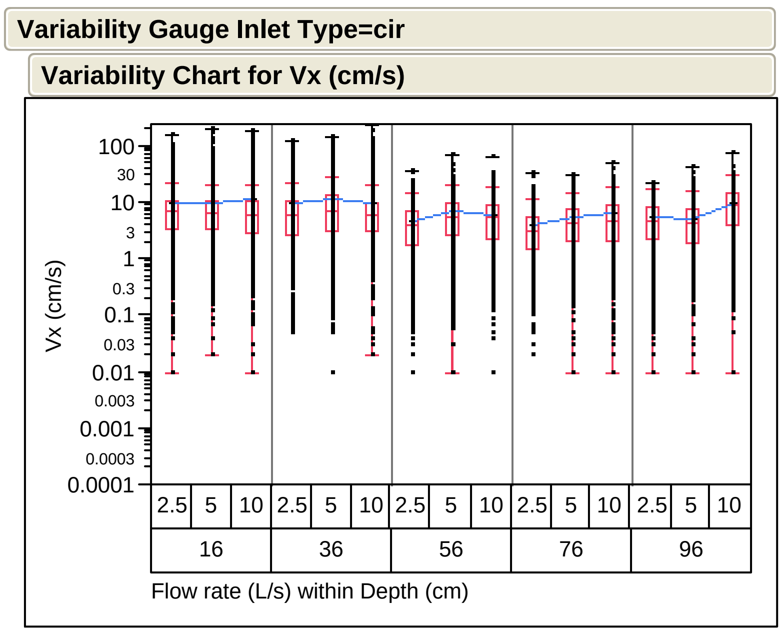

Figure D.1. Boxplots of x-velocity (Vx) by flow rate and overlaying water depth. Circular inlet.

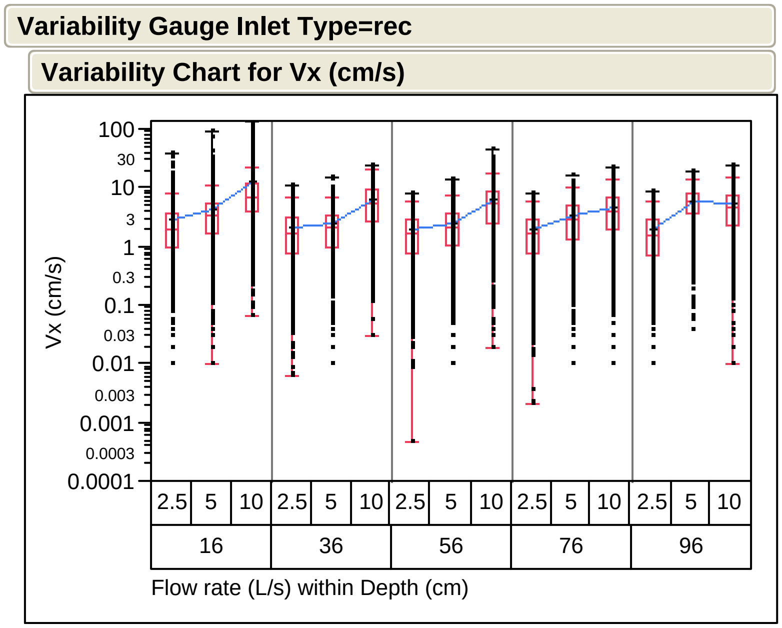

Figure D.2. Boxplots of x-velocity (Vx) by flow rate and overlaying water depth. Rectangular inlet.

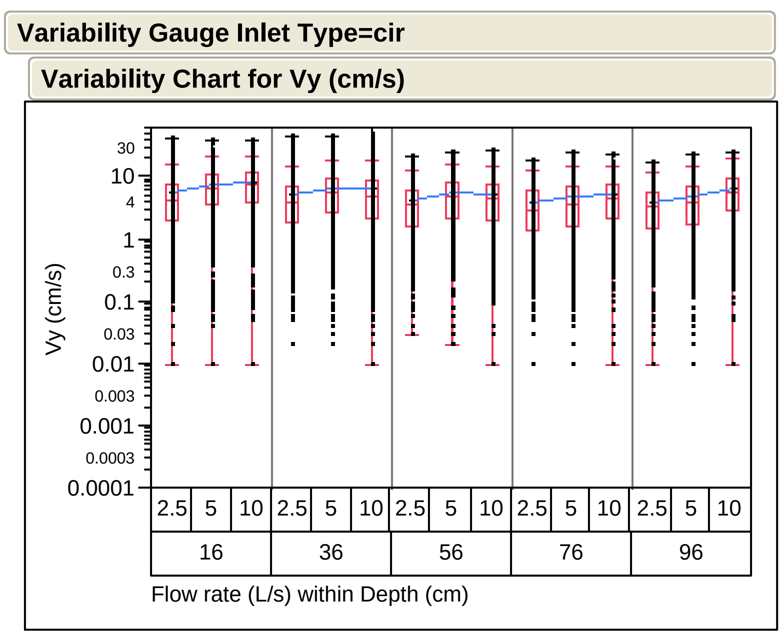

Figure D.3. Boxplots of y-velocity (Vy) by flow rate and overlaying water depth. Circular inlet.

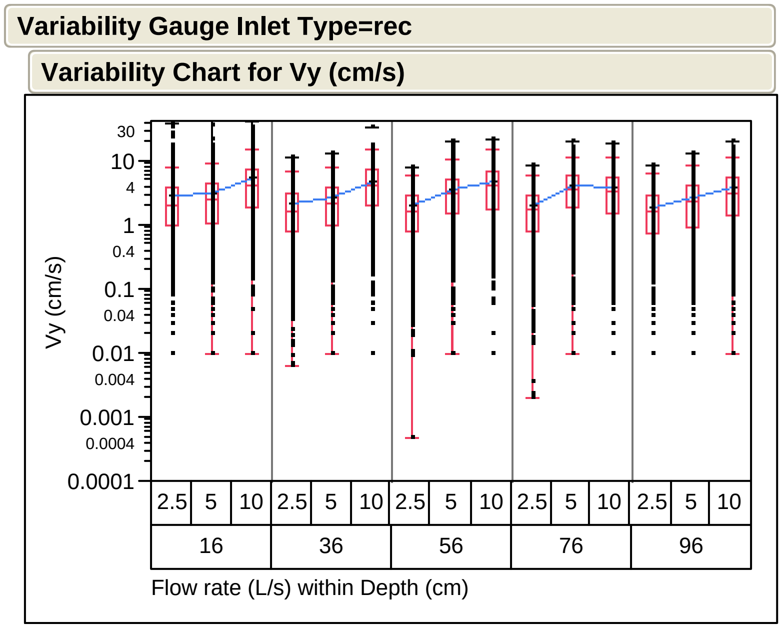

Figure D.4. Boxplots of y-velocity (Vy) by flow rate and overlaying water depth. Rectangular inlet.

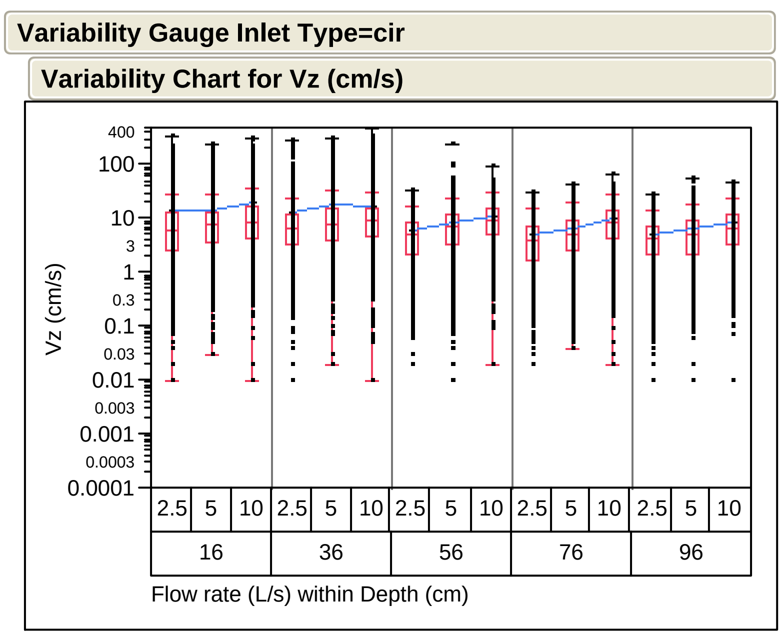

Figure D.5. Boxplots of z-velocity (Vz) by flow rate and overlaying water depth. Circular inlet.

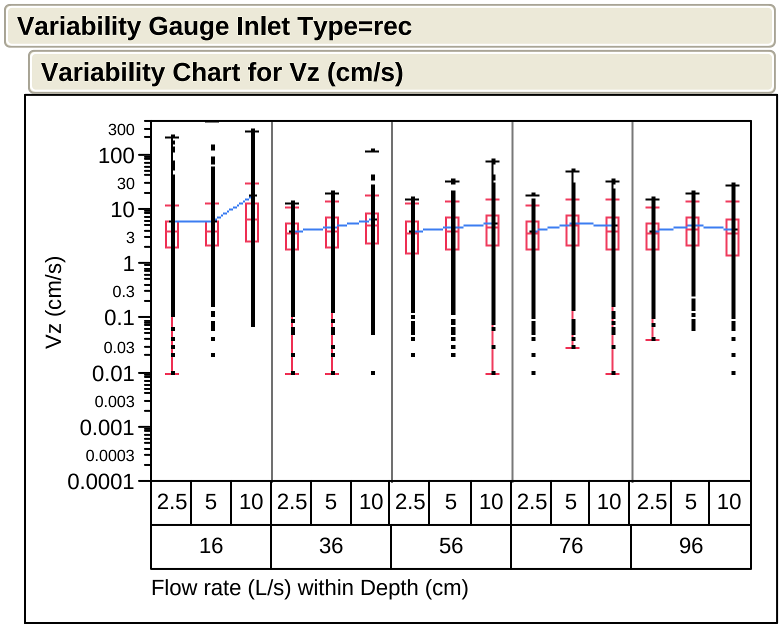

Figure D.6. Boxplots of z-velocity (Vz) by flow rate and overlaying water depth. Rectangular inlet.

Table D.1. One-Way ANOVA Output for x-Velocity by Flow Rate and Inlet Type: Overlaying Water Depth of 16 cm and Circular Inlet

Oneway Analysis of Vx (cm/s) By Flow rate (L/s) Inlet Type=cir, Depth (cm)=16

Oneway Anova

Summary of Fit

Rsquare	0.004021
Adj Rsquare	0.003306
Root Mean Square Error	16.31373
Mean of Response	10.51618
Observations (or Sum Wgts)	2790

Analysis of Variance

Source	DF	Sum of Squares	Mean Square	F Ratio	Prob > F
Flow rate (L/s)	2	2994.43	1497.22	5.6257	0.0036*
Error	2787	741725.72	266.14		
C. Total	2789	744720.15			

Means Comparisons

Comparisons for each pair using Student's t

t	Alpha
1.96082	0.05

Level	- Level	Difference	Lower CL	Upper CL	p-Value
10	2.5	2.447398	0.963980	3.930816	0.0012*
10	5	1.804570	0.321152	3.287988	0.0171*
5	2.5	0.642828	-0.840590	2.126246	0.3956

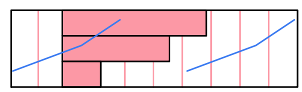

Table D.2. One-Way ANOVA Output for x-Velocity by Flow Rate and Inlet Type: Overlaying Water Depth of 36 cm and Circular Inlet

Oneway Analysis of Vx (cm/s) By Flow rate (L/s) Inlet Type=cir, Depth (cm)=36

Oneway Anova

Summary of Fit

Rsquare	0.004948
Adj Rsquare	0.004234
Root Mean Square Error	16.05232
Mean of Response	10.34688
Observations (or Sum Wgts)	2790

Analysis of Variance

Source	DF	Sum of Squares	Mean Square	F Ratio	Prob > F
Flow rate (L/s)	2	3571.03	1785.52	6.9293	0.0010*
Error	2787	718145.80	257.68		
C. Total	2789	721716.83			

Means Comparisons

Comparisons for each pair using Student's t

t	Alpha
1.96082	0.05

Level	- Level	Difference	Lower CL	Upper CL	p-Value
5	10	2.444387	0.98474	3.904035	0.0010*
5	2.5	2.352882	0.89323	3.812530	0.0016*
2.5	10	0.091505	-1.36814	1.551153	0.9022

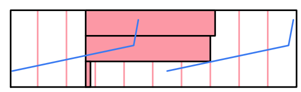

Table D.3. One-Way ANOVA Output for x-Velocity by Flow Rate and Inlet Type: Overlaying Water Depth of 56 cm and Circular Inlet

Oneway Analysis of Vx (cm/s) By Flow rate (L/s) Inlet Type=cir, Depth (cm)=56

Oneway Anova

Summary of Fit

Rsquare	0.028055
Adj Rsquare	0.027357
Root Mean Square Error	5.172035
Mean of Response	6.026885
Observations (or Sum Wgts)	2790

Analysis of Variance

Source	DF	Sum of Squares	Mean Square	F Ratio	Prob > F
Flow rate (L/s)	2	2151.922	1075.96	40.2229	<.0001*
Error	2787	74552.105	26.75		
C. Total	2789	76704.027			

Means Comparisons

Comparisons for each pair using Student's t

t	Alpha
1.96082	0.05

Level	- Level	Difference	Lower CL	Upper CL	p-Value
5	2.5	2.147495	1.677198	2.617791	<.0001*
10	2.5	1.183484	0.713187	1.653780	<.0001*
5	10	0.964011	0.493714	1.434307	<.0001*

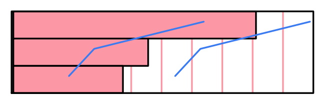

Table D.4. One-Way ANOVA Output for x-Velocity by Flow Rate and Inlet Type: Overlaying Water Depth of 76 cm and Circular Inlet

Oneway Analysis of Vx (cm/s) By Flow rate (L/s) Inlet Type=cir, Depth (cm)=76

Oneway Anova

Summary of Fit

Rsquare	0.039935
Adj Rsquare	0.039246
Root Mean Square Error	4.680811
Mean of Response	5.343978
Observations (or Sum Wgts)	2790

Analysis of Variance

Source	DF	Sum of Squares	Mean Square	F Ratio	Prob > F
Flow rate (L/s)	2	2539.995	1270.00	57.9643	<.0001*
Error	2787	61063.134	21.91		
C. Total	2789	63603.129			

Means Comparisons

Comparisons for each pair using Student's t

t	Alpha
1.96082	0.05

Level	- Level	Difference	Lower CL	Upper CL	p-Value
10	2.5	2.328226	1.902597	2.753855	<.0001*
5	2.5	1.341000	0.915371	1.766629	<.0001*
10	5	0.987226	0.561597	1.412855	<.0001*

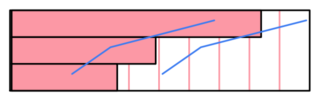

Table D.5. One-Way ANOVA Output for x-Velocity by Flow Rate and Inlet Type: Overlaying Water Depth of 96 cm and Circular Inlet

Oneway Analysis of Vx (cm/s) By Flow rate (L/s) Inlet Type=cir, Depth (cm)=96

Oneway Anova

Summary of Fit

Rsquare	0.13811
Adj Rsquare	0.137491
Root Mean Square Error	5.491689
Mean of Response	6.983043
Observations (or Sum Wgts)	2790

Analysis of Variance

Source	DF	Sum of Squares	Mean Square	F Ratio	Prob > F
Flow rate (L/s)	2	13468.562	6734.28	223.2952	<.0001*
Error	2787	84052.167	30.16		
C. Total	2789	97520.729			

Means Comparisons

Comparisons for each pair using Student's t

t	Alpha
1.96082	0.05

Level	- Level	Difference	Lower CL	Upper CL	p-Value
10	5	4.758989	4.25963	5.258352	<.0001*
10	2.5	4.556075	4.05671	5.055438	<.0001*
2.5	5	0.202914	-0.29645	0.702277	0.4257

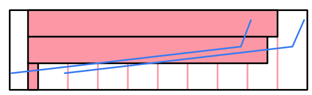

Table D.6. One-Way ANOVA Output for x-Velocity by Flow Rate and Inlet Type: Overlaying Water Depth of 16 cm and Rectangular Inlet

Oneway Analysis of Vx (cm/s) By Flow rate (L/s) Inlet Type=rec, Depth (cm)=16

Oneway Anova

Summary of Fit

Rsquare	0.127276
Adj Rsquare	0.12665
Root Mean Square Error	11.60924
Mean of Response	6.696294
Observations (or Sum Wgts)	2790

Analysis of Variance

Source	DF	Sum of Squares	Mean Square	F Ratio	Prob > F
Flow rate (L/s)	2	54779.11	27389.6	203.2253	<.0001*
Error	2787	375616.09	134.8		
C. Total	2789	430395.21			

Means Comparisons

Comparisons for each pair using Student's t

t	Alpha
1.96082	0.05

Level	- Level	Difference	Lower CL	Upper CL	p-Value
10	2.5	10.03580	8.980160	11.09143	<.0001*
10	5	8.59777	7.542139	9.65341	<.0001*
5	2.5	1.43802	0.382386	2.49366	0.0076*

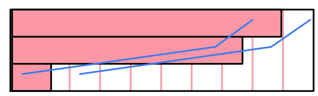

Table D.7. One-Way ANOVA Output for x-Velocity by Flow Rate and Inlet Type: Overlaying Water Depth of 36 cm and Rectangular Inlet

Oneway Analysis of Vx (cm/s) By Flow rate (L/s) Inlet Type=rec, Depth (cm)=36

Oneway Anova

Summary of Fit

Rsquare	0.294843
Adj Rsquare	0.294337
Root Mean Square Error	3.176377
Mean of Response	3.762203
Observations (or Sum Wgts)	2790

Analysis of Variance

Source	DF	Sum of Squares	Mean Square	F Ratio	Prob > F
Flow rate (L/s)	2	11757.270	5878.64	582.6562	<.0001*
Error	2787	28119.081	10.09		
C. Total	2789	39876.352			

Means Comparisons

Comparisons for each pair using Student's t

t	Alpha
1.96082	0.05

Level	- Level	Difference	Lower CL	Upper CL	p-Value
10	2.5	4.500079	4.211249	4.788909	<.0001*
10	5	4.193054	3.904224	4.481884	<.0001*
5	2.5	0.307026	0.018196	0.595856	0.0372*

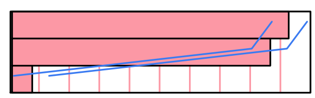

Table D.8. One-Way ANOVA Output for x-Velocity by Flow Rate and Inlet Type: Overlaying Water Depth of 36 cm and Rectangular Inlet

Oneway Analysis of Vx (cm/s) By Flow rate (L/s) Inlet Type=rec, Depth (cm)=56

Oneway Anova

Summary of Fit

Rsquare	0.263488
Adj Rsquare	0.26296
Root Mean Square Error	3.157857
Mean of Response	3.615505
Observations (or Sum Wgts)	2790

Analysis of Variance

Source	DF	Sum of Squares	Mean Square	F Ratio	Prob > F
Flow rate (L/s)	2	9942.685	4971.34	498.5271	<.0001*
Error	2787	27792.133	9.97		
C. Total	2789	37734.818			

Means Comparisons

Comparisons for each pair using Student's t

t	Alpha
1.96082	0.05

Level	- Level	Difference	Lower CL	Upper CL	p-Value
10	2.5	4.272763	3.985617	4.559909	<.0001*
10	5	3.667462	3.380316	3.954608	<.0001*
5	2.5	0.605301	0.318155	0.892447	<.0001*

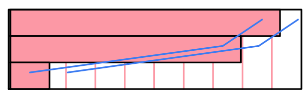

Table D.9. One-Way ANOVA Output for x-Velocity by Flow Rate and Inlet Type: Overlaying Water Depth of 76 cm and Rectangular Inlet

Oneway Analysis of Vx (cm/s) By Flow rate (L/s) Inlet Type=rec, Depth (cm)=76

Excluded Rows 1

Oneway Anova

Summary of Fit

Rsquare	0.148876
Adj Rsquare	0.148265
Root Mean Square Error	2.669878
Mean of Response	3.411324
Observations (or Sum Wgts)	2789

Analysis of Variance

Source	DF	Sum of Squares	Mean Square	F Ratio	Prob > F
Flow rate (L/s)	2	3473.734	1736.87	243.6598	<.0001*
Error	2786	19859.295	7.13		
C. Total	2788	23333.029			

Means Comparisons

Comparisons for each pair using Student's t

t	Alpha
1.96082	0.05

Level	- Level	Difference	Lower CL	Upper CL	p-Value
10	2.5	2.732556	2.489783	2.975330	<.0001*
5	2.5	1.417767	1.174928	1.660606	<.0001*
10	5	1.314790	1.071951	1.557629	<.0001*

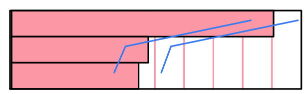

Table D.10. One-Way ANOVA Output for x-Velocity by Flow Rate and Inlet Type: Overlaying Water Depth of 96 cm and Rectangular Inlet

Oneway Analysis of Vx (cm/s) By Flow rate (L/s) Inlet Type=rec, Depth (cm)=96

Oneway Anova

Summary of Fit

Rsquare	0.257612
Adj Rsquare	0.257079
Root Mean Square Error	3.133134
Mean of Response	4.521423
Observations (or Sum Wgts)	2790

Analysis of Variance

Source	DF	Sum of Squares	Mean Square	F Ratio	Prob > F
Flow rate (L/s)	2	9493.578	4746.79	483.5507	<.0001*
Error	2787	27358.666	9.82		
C. Total	2789	36852.244			

Means Comparisons

Comparisons for each pair using Student's t

t	Alpha
1.96082	0.05

Level	- Level	Difference	Lower CL	Upper CL	p-Value
5	2.5	4.212204	3.927306	4.497102	<.0001*
10	2.5	3.522161	3.237263	3.807059	<.0001*
5	10	0.690043	0.405145	0.974941	<.0001*

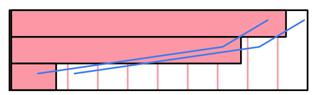

Table D.11. One-Way ANOVA Output for y-Velocity by Flow Rate and Inlet Type: Overlaying Water Depth of 16 cm and Circular Inlet

Oneway Analysis of Vy (cm/s) By Flow rate (L/s) Depth (cm)=16, Inlet Type=cir

Oneway Anova

Summary of Fit

Rsquare	0.04558
Adj Rsquare	0.044895
Root Mean Square Error	5.273737
Mean of Response	7.103935
Observations (or Sum Wgts)	2790

Analysis of Variance

Source	DF	Sum of Squares	Mean Square	F Ratio	Prob > F
Flow rate (L/s)	2	3701.729	1850.86	66.5484	<.0001*
Error	2787	77512.890	27.81		
C. Total	2789	81214.619			

Means Comparisons

Comparisons for each pair using Student's t

t	Alpha
1.96082	0.05

Level	- Level	Difference	Lower CL	Upper CL	p-Value
10	2.5	2.642925	2.16338	3.122469	<.0001*
5	2.5	2.176882	1.69734	2.656426	<.0001*
10	5	0.466043	-0.01350	0.945587	0.0568

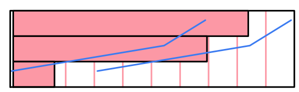

Table D.12. One-Way ANOVA Output for y-Velocity by Flow Rate and Inlet Type: Overlaying Water Depth of 16 cm and Rectangular Inlet

Oneway Analysis of Vy (cm/s) By Flow rate (L/s) Depth (cm)=16, Inlet Type=rec

Oneway Anova

Summary of Fit

Rsquare	0.082804
Adj Rsquare	0.082146
Root Mean Square Error	3.905139
Mean of Response	3.84448
Observations (or Sum Wgts)	2790

Analysis of Variance

Source	DF	Sum of Squares	Mean Square	F Ratio	Prob > F
Flow rate (L/s)	2	3837.087	1918.54	125.8052	<.0001*
Error	2787	42502.060	15.25		
C. Total	2789	46339.147			

Means Comparisons

Comparisons for each pair using Student's t

t	Alpha
1.96082	0.05

Level	- Level	Difference	Lower CL	Upper CL	p-Value
10	2.5	2.622462	2.26737	2.977559	<.0001*
10	5	2.326548	1.97145	2.681645	<.0001*
5	2.5	0.295914	-0.05918	0.651011	0.1024

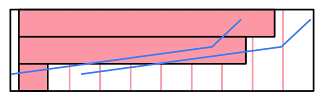

Table D.13. One-Way ANOVA Output for y-Velocity by Flow Rate and Inlet Type: Overlaying Water Depth of 36 cm and Circular Inlet

Oneway Analysis of Vy (cm/s) By Flow rate (L/s) Depth (cm)=36, Inlet Type=cir

Oneway Anova

Summary of Fit

Rsquare	0.014814
Adj Rsquare	0.014107
Root Mean Square Error	5.893276
Mean of Response	6.155473
Observations (or Sum Wgts)	2790

Analysis of Variance

Source	DF	Sum of Squares	Mean Square	F Ratio	Prob > F
Flow rate (L/s)	2	1455.516	727.758	20.9543	<.0001*
Error	2787	96794.476	34.731		
C. Total	2789	98249.992			

Means Comparisons

Comparisons for each pair using Student's t

t	Alpha
1.96082	0.05

Level	- Level	Difference	Lower CL	Upper CL	p-Value
5	2.5	1.676860	1.14098	2.212740	<.0001*
10	2.5	1.327011	0.79113	1.862890	<.0001*
5	10	0.349849	-0.18603	0.885729	0.2006

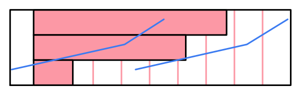

Table D.14. One-Way ANOVA Output for y-Velocity by Flow Rate and Inlet Type: Overlaying Water Depth of 36 cm and Rectangular Inlet

Oneway Analysis of Vy (cm/s) By Flow rate (L/s) Depth (cm)=36, Inlet Type=rec

Oneway Anova

Summary of Fit

Rsquare	0.158251
Adj Rsquare	0.157647
Root Mean Square Error	2.787791
Mean of Response	3.304285
Observations (or Sum Wgts)	2790

Analysis of Variance

Source	DF	Sum of Squares	Mean Square	F Ratio	Prob > F
Flow rate (L/s)	2	4072.119	2036.06	261.9811	<.0001*
Error	2787	21659.949	7.77		
C. Total	2789	25732.069			

Means Comparisons

Comparisons for each pair using Student's t

t	Alpha
1.96082	0.05

Level	- Level	Difference	Lower CL	Upper CL	p-Value
10	2.5	2.815305	2.561810	3.068801	<.0001*
10	5	2.197258	1.943762	2.450754	<.0001*
5	2.5	0.618047	0.364551	0.871543	<.0001*

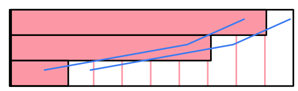

Table D.15. One-Way ANOVA Output for y-Velocity by Flow Rate and Inlet Type: Overlaying Water Depth of 56 cm and Circular Inlet

Oneway Analysis of Vy (cm/s) By Flow rate (L/s) Depth (cm)=56, Inlet Type=cir

Oneway Anova

Summary of Fit

Rsquare	0.021682
Adj Rsquare	0.02098
Root Mean Square Error	4.034564
Mean of Response	5.151487
Observations (or Sum Wgts)	2790

Analysis of Variance

Source	DF	Sum of Squares	Mean Square	F Ratio	Prob > F
Flow rate (L/s)	2	1005.414	502.707	30.8832	<.0001*
Error	2787	45365.968	16.278		
C. Total	2789	46371.381			

Means Comparisons

Comparisons for each pair using Student's t

t	Alpha
1.96082	0.05

Level	- Level	Difference	Lower CL	Upper CL	p-Value
5	2.5	1.450398	1.083532	1.817263	<.0001*
10	2.5	0.934710	0.567844	1.301575	<.0001*
5	10	0.515688	0.148823	0.882554	0.0059*

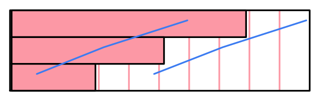

Table D.16. One-Way ANOVA Output for y-Velocity by Flow Rate and Inlet Type: Overlaying Water Depth of 56 cm and Rectangular Inlet

Oneway Analysis of Vy (cm/s) By Flow rate (L/s) Depth (cm)=56, Inlet Type=rec

Oneway Anova

Summary of Fit

Rsquare	0.146431
Adj Rsquare	0.145819
Root Mean Square Error	2.820295
Mean of Response	3.490925
Observations (or Sum Wgts)	2790

Analysis of Variance

Source	DF	Sum of Squares	Mean Square	F Ratio	Prob > F
Flow rate (L/s)	2	3802.960	1901.48	239.0577	<.0001*
Error	2787	22167.977	7.95		
C. Total	2789	25970.937			

Means Comparisons

Comparisons for each pair using Student's t

t	Alpha
1.96082	0.05

Level	- Level	Difference	Lower CL	Upper CL	p-Value
10	2.5	2.847022	2.590570	3.103473	<.0001*
5	2.5	1.657301	1.400850	1.913752	<.0001*
10	5	1.189720	0.933269	1.446172	<.0001*

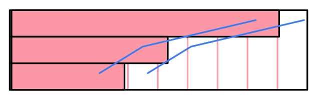

Table D.17. One-Way ANOVA Output for y-Velocity by Flow Rate and Inlet Type: Overlaying Water Depth of 76 cm and Circular Inlet

Oneway Analysis of Vy (cm/s) By Flow rate (L/s) Depth (cm)=76, Inlet Type=cir

Oneway Anova

Summary of Fit

Rsquare	0.015521
Adj Rsquare	0.014815
Root Mean Square Error	3.846495
Mean of Response	4.681341
Observations (or Sum Wgts)	2790

Analysis of Variance

Source	DF	Sum of Squares	Mean Square	F Ratio	Prob > F
Flow rate (L/s)	2	650.108	325.054	21.9697	<.0001*
Error	2787	41235.124	14.796		
C. Total	2789	41885.232			

Means Comparisons

Comparisons for each pair using Student's t

t	Alpha
1.96082	0.05

Level	- Level	Difference	Lower CL	Upper CL	p-Value
10	2.5	1.129430	0.779666	1.479194	<.0001*
5	2.5	0.867785	0.518021	1.217549	<.0001*
10	5	0.261645	-0.088119	0.611409	0.1425

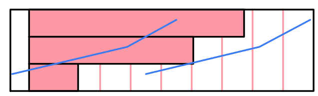

Table D.18. One-Way ANOVA Output for y-Velocity by Flow Rate and Inlet Type: Overlaying Water Depth of 76 cm and Rectangular Inlet

Oneway Analysis of Vy (cm/s) By Flow rate (L/s) Depth (cm)=76, Inlet Type=rec

Oneway Anova

Summary of Fit

Rsquare	0.114591
Adj Rsquare	0.113956
Root Mean Square Error	2.576025
Mean of Response	3.335141
Observations (or Sum Wgts)	2790

Analysis of Variance

Source	DF	Sum of Squares	Mean Square	F Ratio	Prob > F
Flow rate (L/s)	2	2393.556	1196.78	180.3489	<.0001*
Error	2787	18494.268	6.64		
C. Total	2789	20887.825			

Means Comparisons

Comparisons for each pair using Student's t

t	Alpha
1.96082	0.05

Level	- Level	Difference	Lower CL	Upper CL	p-Value
5	2.5	2.032911	1.79867	2.267151	<.0001*
10	2.5	1.888825	1.65459	2.123065	<.0001*
5	10	0.144086	-0.09015	0.378326	0.2279

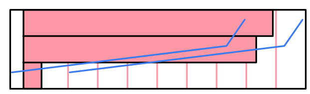

Table D.19. One-Way ANOVA Output for y-Velocity by Flow Rate and Inlet Type: Overlaying Water Depth of 96 cm and Circular Inlet

Oneway Analysis of Vy (cm/s) By Flow rate (L/s) Depth (cm)=96, Inlet Type=cir

Oneway Anova

Summary of Fit

Rsquare	0.075744
Adj Rsquare	0.075081
Root Mean Square Error	3.948343
Mean of Response	5.149548
Observations (or Sum Wgts)	2790

Analysis of Variance

Source	DF	Sum of Squares	Mean Square	F Ratio	Prob > F
Flow rate (L/s)	2	3560.603	1780.30	114.1994	<.0001*
Error	2787	43447.699	15.59		
C. Total	2789	47008.301			

Means Comparisons

Comparisons for each pair using Student's t

t	Alpha
1.96082	0.05

Level	- Level	Difference	Lower CL	Upper CL	p-Value
10	2.5	2.731086	2.372061	3.090111	<.0001*
10	5	1.751269	1.392243	2.110294	<.0001*
5	2.5	0.979817	0.620792	1.338843	<.0001*

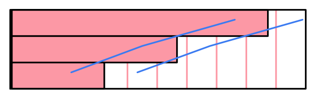

Table D.20. One-Way ANOVA Output for z-Velocity by Flow Rate and Inlet Type: Overlaying Water Depth of 16 cm and Circular Inlet

Oneway Analysis of Vz (cm/s) By Flow rate (L/s) Inlet Type=cir, Depth (cm)=16

Oneway Anova

Summary of Fit

Rsquare	0.010309
Adj Rsquare	0.009598
Root Mean Square Error	31.09924
Mean of Response	16.84723
Observations (or Sum Wgts)	2790

Analysis of Variance

Source	DF	Sum of Squares	Mean Square	F Ratio	Prob > F
Flow rate (L/s)	2	28076.0	14038.0	14.5146	<.0001*
Error	2787	2695482.5	967.2		
C. Total	2789	2723558.5			

Means Comparisons

Comparisons for each pair using Student's t

t	Alpha
1.96082	0.05

Level	- Level	Difference	Lower CL	Upper CL	p-Value
10	5	7.056720	4.22885	9.884594	<.0001*
10	2.5	6.345419	3.51755	9.173293	<.0001*
2.5	5	0.711301	-2.11657	3.539175	0.6219

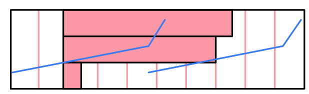

Table D.21. One-Way ANOVA Output for z-Velocity by Flow Rate and Inlet Type: Overlaying Water Depth of 36 cm and Circular Inlet

Oneway Analysis of Vz (cm/s) By Flow rate (L/s) Inlet Type=cir, Depth (cm)=36

Oneway Anova

Summary of Fit

Rsquare	0.005042
Adj Rsquare	0.004328
Root Mean Square Error	34.71919
Mean of Response	16.70448
Observations (or Sum Wgts)	2790

Analysis of Variance

Source	DF	Sum of Squares	Mean Square	F Ratio	Prob > F
Flow rate (L/s)	2	17024.8	8512.42	7.0618	0.0009*
Error	2787	3359511.6	1205.42		
C. Total	2789	3376536.4			

Means Comparisons

Comparisons for each pair using Student's t

t	Alpha
1.96082	0.05

Level	- Level	Difference	Lower CL	Upper CL	p-Value
5	2.5	5.999763	2.84273	9.156802	0.0002*
10	2.5	3.679258	0.52222	6.836296	0.0224*
5	10	2.320505	-0.83653	5.477544	0.1496

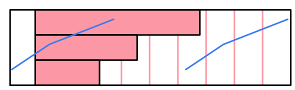

Table D.22. One-Way ANOVA Output for z-Velocity by Flow Rate and Inlet Type: Overlaying Water Depth of 56 cm and Circular Inlet

Oneway Analysis of Vz (cm/s) By Flow rate (L/s) Inlet Type=cir, Depth (cm)=56

Oneway Anova

Summary of Fit

Rsquare	0.055272
Adj Rsquare	0.054594
Root Mean Square Error	8.277129
Mean of Response	8.539796
Observations (or Sum Wgts)	2790

Analysis of Variance

Source	DF	Sum of Squares	Mean Square	F Ratio	Prob > F
Flow rate (L/s)	2	11171.03	5585.52	81.5274	<.0001*
Error	2787	190939.80	68.51		
C. Total	2789	202110.83			

Means Comparisons

Comparisons for each pair using Student's t

t	Alpha
1.96082	0.05

Level	- Level	Difference	Lower CL	Upper CL	p-Value
10	2.5	4.881957	4.129312	5.634602	<.0001*
5	2.5	2.818688	2.066043	3.571333	<.0001*
10	5	2.063269	1.310624	2.815914	<.0001*

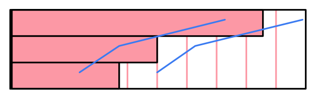

Table D.23. One-Way ANOVA Output for z-Velocity by Flow Rate and Inlet Type: Overlaying Water Depth of 76 cm and Circular Inlet

Oneway Analysis of Vz (cm/s) By Flow rate (L/s) Inlet Type=cir, Depth (cm)=76

Oneway Anova

Summary of Fit

Rsquare	0.111771
Adj Rsquare	0.111134
Root Mean Square Error	6.07167
Mean of Response	7.383032
Observations (or Sum Wgts)	2790

Analysis of Variance

Source	DF	Sum of Squares	Mean Square	F Ratio	Prob > F
Flow rate (L/s)	2	12928.81	6464.40	175.3526	<.0001*
Error	2787	102743.26	36.87		
C. Total	2789	115672.07			

Means Comparisons

Comparisons for each pair using Student's t

t	Alpha
1.96082	0.05

Level	- Level	Difference	Lower CL	Upper CL	p-Value
10	2.5	5.190312	4.638211	5.742413	<.0001*
10	5	3.400398	2.848297	3.952499	<.0001*
5	2.5	1.789914	1.237813	2.342015	<.0001*

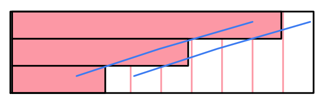

Table D.24. One-Way ANOVA Output for z-Velocity by Flow Rate and Inlet Type: Overlaying Water Depth of 96 cm and Circular Inlet

Oneway Analysis of Vz (cm/s) By Flow rate (L/s) Inlet Type=cir, Depth (cm)=96

Oneway Anova

Summary of Fit

Rsquare	0.051598
Adj Rsquare	0.050917
Root Mean Square Error	6.06445
Mean of Response	6.862778
Observations (or Sum Wgts)	2790

Analysis of Variance

Source	DF	Sum of Squares	Mean Square	F Ratio	Prob > F
Flow rate (L/s)	2	5576.45	2788.22	75.8132	<.0001*
Error	2787	102499.05	36.78		
C. Total	2789	108075.49			

Means Comparisons

Comparisons for each pair using Student's t

t	Alpha
1.96082	0.05

Level	- Level	Difference	Lower CL	Upper CL	p-Value
10	2.5	3.458129	2.906685	4.009573	<.0001*
10	5	1.888054	1.336609	2.439498	<.0001*
5	2.5	1.570075	1.018631	2.121520	<.0001*

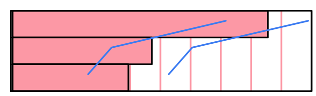

Table D.25. One-Way ANOVA Output for z-Velocity by Flow Rate and Inlet Type: Overlaying Water Depth of 16 cm and Rectangular Inlet

Oneway Analysis of Vz (cm/s) By Flow rate (L/s) Inlet Type=rec, Depth (cm)=16

Oneway Anova

Summary of Fit

Rsquare	0.050873
Adj Rsquare	0.050192
Root Mean Square Error	23.40752
Mean of Response	9.703538
Observations (or Sum Wgts)	2790

Analysis of Variance

Source	DF	Sum of Squares	Mean Square	F Ratio	Prob > F
Flow rate (L/s)	2	81847.9	40923.9	74.6907	<.0001*
Error	2787	1527030.2	547.9		
C. Total	2789	1608878.1			

Means Comparisons

Comparisons for each pair using Student's t

t	Alpha
1.96082	0.05

Level	- Level	Difference	Lower CL	Upper CL	p-Value
10	2.5	11.51895	9.39049	13.64741	<.0001*
10	5	11.46018	9.33172	13.58864	<.0001*
5	2.5	0.05876	-2.06970	2.18722	0.9568

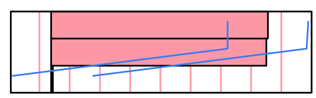

Table D.26. One-Way ANOVA Output for z-Velocity by Flow Rate and Inlet Type: Overlaying Water Depth of 36 cm and Rectangular Inlet

Oneway Analysis of Vz (cm/s) By Flow rate (L/s) Inlet Type=rec, Depth (cm)=36

Oneway Anova

Summary of Fit

Rsquare	0.049985
Adj Rsquare	0.049303
Root Mean Square Error	4.224739
Mean of Response	4.919394
Observations (or Sum Wgts)	2790

Analysis of Variance

Source	DF	Sum of Squares	Mean Square	F Ratio	Prob > F
Flow rate (L/s)	2	2617.250	1308.62	73.3188	<.0001*
Error	2787	49743.551	17.85		
C. Total	2789	52360.801			

Means Comparisons

Comparisons for each pair using Student's t

t	Alpha
1.96082	0.05

Level	- Level	Difference	Lower CL	Upper CL	p-Value
10	2.5	2.323419	1.939261	2.707578	<.0001*
10	5	1.577237	1.193078	1.961395	<.0001*
5	2.5	0.746183	0.362025	1.130341	0.0001*

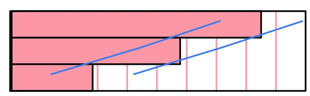

Table D.27. One-Way ANOVA Output for z-Velocity by Flow Rate and Inlet Type: Overlaying Water Depth of 56 cm and Rectangular Inlet

Oneway Analysis of Vz (cm/s) By Flow rate (L/s) Inlet Type=rec, Depth (cm)=56

Oneway Anova

Summary of Fit

Rsquare	0.020441
Adj Rsquare	0.019738
Root Mean Square Error	4.10087
Mean of Response	4.675133
Observations (or Sum Wgts)	2790

Analysis of Variance

Source	DF	Sum of Squares	Mean Square	F Ratio	Prob > F
Flow rate (L/s)	2	978.059	489.030	29.0793	<.0001*
Error	2787	46869.349	16.817		
C. Total	2789	47847.409			

Means Comparisons

Comparisons for each pair using Student's t

t	Alpha
1.96082	0.05

Level	- Level	Difference	Lower CL	Upper CL	p-Value
10	2.5	1.442570	1.069675	1.815465	<.0001*
10	5	0.850742	0.477847	1.223637	<.0001*
5	2.5	0.591828	0.218933	0.964723	0.0019*

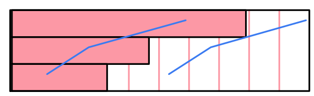

Table D.28. One-Way ANOVA Output for z-Velocity by Flow Rate and Inlet Type: Overlaying Water Depth of 76 cm and Rectangular Inlet

Oneway Analysis of Vz (cm/s) By Flow rate (L/s) Inlet Type=rec, Depth (cm)=76

Oneway Anova

Summary of Fit

Rsquare	0.024143
Adj Rsquare	0.023443
Root Mean Square Error	3.679454
Mean of Response	4.769634
Observations (or Sum Wgts)	2790

Analysis of Variance

Source	DF	Sum of Squares	Mean Square	F Ratio	Prob > F
Flow rate (L/s)	2	933.501	466.750	34.4761	<.0001*
Error	2787	37731.472	13.538		
C. Total	2789	38664.972			

Means Comparisons

Comparisons for each pair using Student's t

t	Alpha
1.96082	0.05

Level	- Level	Difference	Lower CL	Upper CL	p-Value
5	2.5	1.389688	1.055113	1.724263	<.0001*
10	2.5	0.934054	0.599479	1.268629	<.0001*
5	10	0.455634	0.121059	0.790210	0.0076*

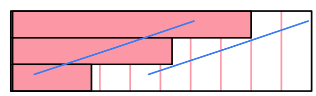

Table D.29. One-Way ANOVA Output for z-Velocity by Flow Rate and Inlet Type: Overlaying Water Depth of 96 cm and Rectangular Inlet

Oneway Analysis of Vz (cm/s) By Flow rate (L/s) Inlet Type=rec, Depth (cm)=96

Oneway Anova

Summary of Fit

Rsquare	0.017975
Adj Rsquare	0.017271
Root Mean Square Error	3.310095
Mean of Response	4.365921
Observations (or Sum Wgts)	2790

Analysis of Variance

Source	DF	Sum of Squares	Mean Square	F Ratio	Prob > F
Flow rate (L/s)	2	558.951	279.475	25.5072	<.0001*
Error	2787	30536.410	10.957		
C. Total	2789	31095.361			

Means Comparisons

Comparisons for each pair using Student's t

t	Alpha
1.96082	0.05

Level	- Level	Difference	Lower CL	Upper CL	p-Value
5	2.5	1.095688	0.7946991	1.396677	<.0001*
5	10	0.581516	0.2805270	0.882505	0.0002*
10	2.5	0.514172	0.2131829	0.815161	0.0008*

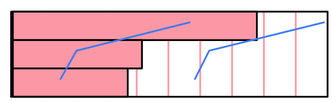

APPENDIX E

ONE-WAY ANOVA OUTPUTS FOR OVERLAYING WATER DEPTH: HYDRODYNAMIC RESULTS: VELOCITIES: BY FLOW RATE AND BY INLET TYPE

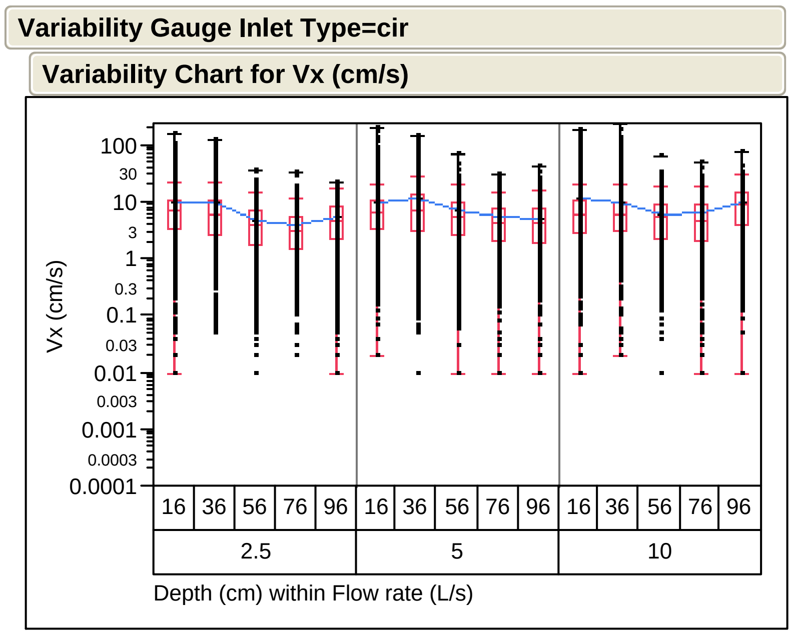

Figure E.1. Boxplots of x-velocities by overlaying water depth and by flow rate. Circular inlet.

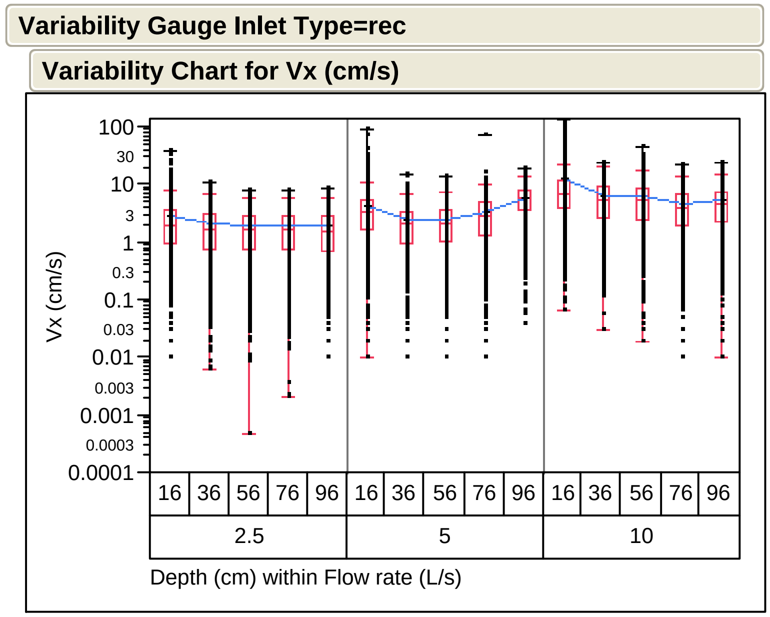

Figure E.2. Boxplots of x-velocities by overlaying water depth and by flow rate. Rectangular inlet.

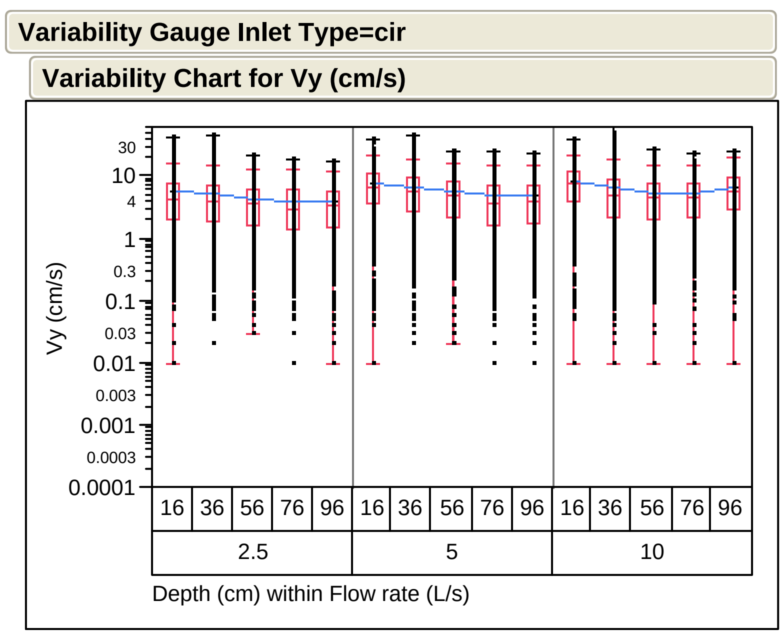

Figure E.3. Boxplots of y-velocities by overlaying water depth and by flow rate. Circular inlet.

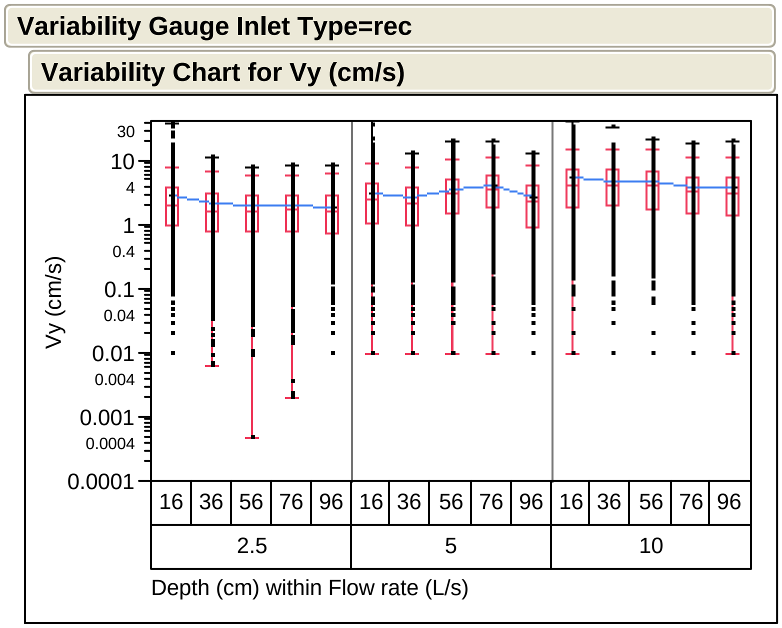

Figure E.4. Boxplots of y-velocities by overlaying water depth and by flow rate. Rectangular inlet.

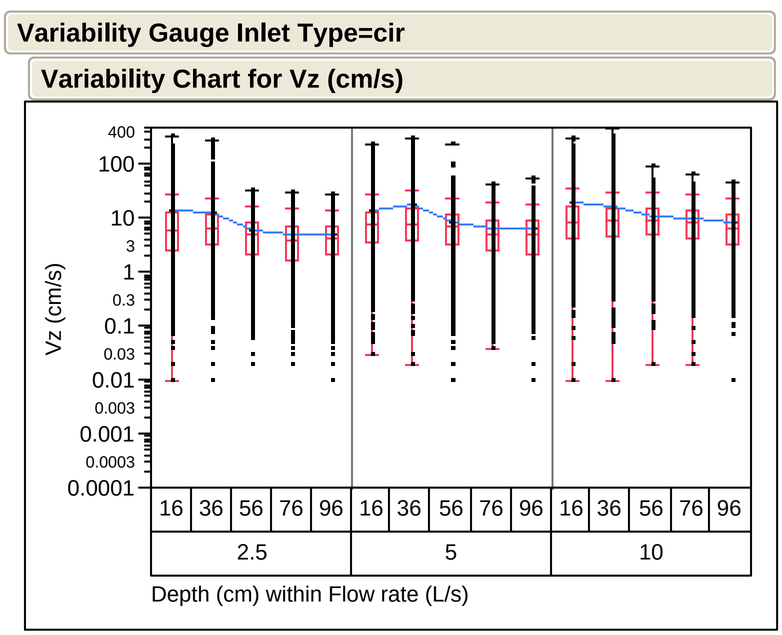

Figure E.5. Boxplots of z-velocities by overlaying water depth and by flow rate. Circular inlet.

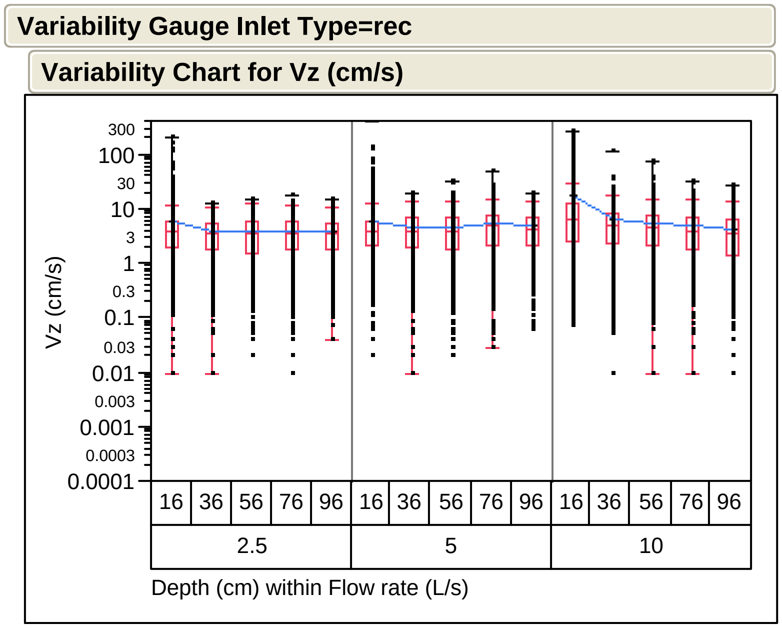

Figure E.6. Boxplots of z-velocities by overlaying water depth and by flow rate. Rectangular inlet.

Table E.1. One-Way ANOVA for Overlaying Water Depth: Evaluating x-Velocity (Vx) at 2.5 L/s Flow Rate and Circular Inlet

Oneway Analysis of Vx (cm/s) By Depth (cm) Flow rate (L/s)=2.5, Inlet Type=cir

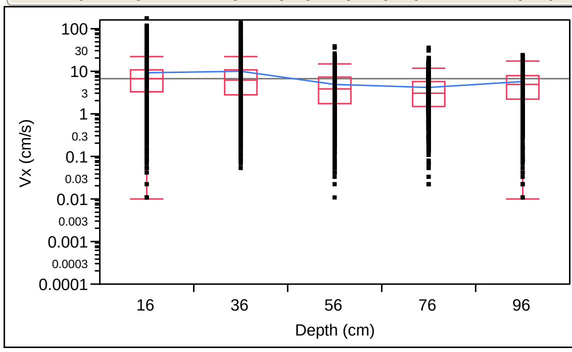

Oneway Anova

Summary of Fit

Rsquare	0.066373
Adj Rsquare	0.065569
Root Mean Square Error	8.772377
Mean of Response	6.729729
Observations (or Sum Wgts)	4650

Analysis of Variance

Source	DF	Sum of Squares	Mean Square	F Ratio	Prob > F
Depth (cm)	4	25411.85	6352.96	82.5547	<.0001*
Error	4645	357454.07	76.95		
C. Total	4649	382865.93			

Means Comparisons

Comparisons for each pair using Student's t

t	Alpha
1.96047	0.05

Level				Mean
36	A			9.5930860
16	A			9.4861075
96		B		5.5319892
56		B	C	4.9165591
76			C	4.1209032

Levels not connected by same letter are significantly different.

Level	- Level	Difference	Lower CL	Upper CL	p-Value
36	76	5.472183	4.67464	6.269722	<.0001*
16	76	5.365204	4.56767	6.162744	<.0001*
36	56	4.676527	3.87899	5.474066	<.0001*
16	56	4.569548	3.77201	5.367088	<.0001*
36	96	4.061097	3.26356	4.858636	<.0001*
16	96	3.954118	3.15658	4.751658	<.0001*
96	76	1.411086	0.61355	2.208625	0.0005*
56	76	0.795656	-0.00188	1.593195	0.0505
96	56	0.615430	-0.18211	1.412969	0.1304
36	16	0.106978	-0.69056	0.904518	0.7926

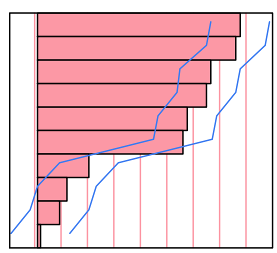

Table E.2. One-Way ANOVA for Overlaying Water Depth: Evaluating x-Velocity (Vx) at 2.5 L/s Flow Rate and Rectangular Inlet

Oneway Analysis of Vx (cm/s) By Depth (cm) Flow rate (L/s)=2.5, Inlet Type=rec

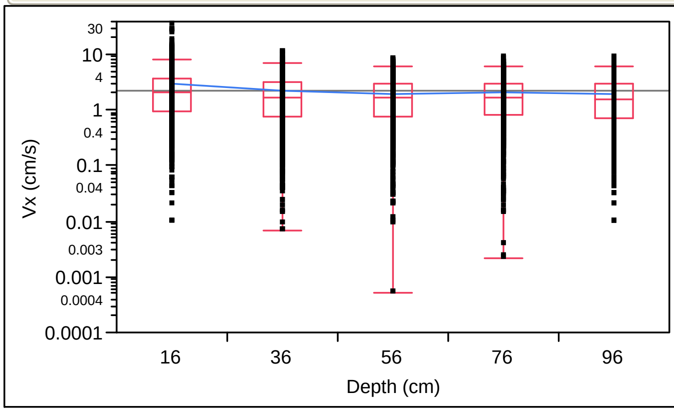

Oneway Anova

Summary of Fit

Rsquare	0.027804
Adj Rsquare	0.026967
Root Mean Square Error	2.036823
Mean of Response	2.198441
Observations (or Sum Wgts)	4650

Analysis of Variance

Source	DF	Sum of Squares	Mean Square	F Ratio	Prob > F
Depth (cm)	4	551.116	137.779	33.2106	<.0001*
Error	4645	19270.471	4.149		
C. Total	4649	19821.586			

Means Comparisons

Comparisons for each pair using Student's t

t	Alpha
1.96047	0.05

Level		Mean
16	A	2.8716882
36	B	2.1598346
76	B C	2.0278953
56	B C	1.9894839
96	C	1.9433011

Levels not connected by same letter are significantly different.

Level	- Level	Difference	Lower CL	Upper CL	p-Value
16	96	0.9283871	0.743210	1.113565	<.0001*
16	56	0.8822043	0.697027	1.067382	<.0001*
16	76	0.8437929	0.658615	1.028970	<.0001*
16	36	0.7118535	0.526676	0.897031	<.0001*
36	96	0.2165335	0.031356	0.401711	0.0219*
36	56	0.1703508	-0.014827	0.355528	0.0714
36	76	0.1319394	-0.053238	0.317117	0.1625
76	96	0.0845942	-0.100583	0.269772	0.3705
56	96	0.0461828	-0.138995	0.231360	0.6249
76	56	0.0384114	-0.146766	0.223589	0.6843

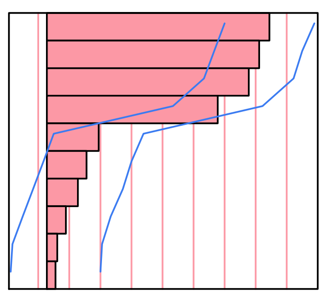

Table E.3. One-Way ANOVA for Overlaying Water Depth: Evaluating x-Velocity (Vx) at 5 L/s Flow Rate and Circular Inlet

Oneway Analysis of Vx (cm/s) By Depth (cm) Flow rate (L/s)=5, Inlet Type=cir

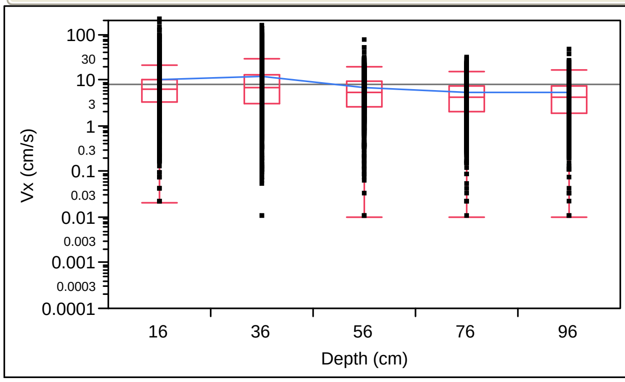

Oneway Anova

Summary of Fit

Rsquare	0.051232
Adj Rsquare	0.050415
Root Mean Square Error	11.31896
Mean of Response	7.985987
Observations (or Sum Wgts)	4650

Analysis of Variance

Source	DF	Sum of Squares	Mean Square	F Ratio	Prob > F
Depth (cm)	4	32135.05	8033.76	62.7055	<.0001*
Error	4645	595112.19	128.12		
C. Total	4649	627247.24			

Means Comparisons

Comparisons for each pair using Student's t

t	Alpha
1.96047	0.05

Level					Mean
36	A				11.945968
16		B			10.128935
56			C		7.064054
76				D	5.461903
96				D	5.329075

Levels not connected by same letter are significantly different.

Level	- Level	Difference	Lower CL	Upper CL	p-Value
36	96	6.616892	5.58783	7.645954	<.0001*
36	76	6.484065	5.45500	7.513126	<.0001*
36	56	4.881914	3.85285	5.910976	<.0001*
16	96	4.799860	3.77080	5.828922	<.0001*
16	76	4.667032	3.63797	5.696094	<.0001*
16	56	3.064882	2.03582	4.093943	<.0001*
36	16	1.817032	0.78797	2.846094	0.0005*
56	96	1.734978	0.70592	2.764040	0.0010*
56	76	1.602151	0.57309	2.631212	0.0023*
76	96	0.132828	-0.89623	1.161890	0.8002

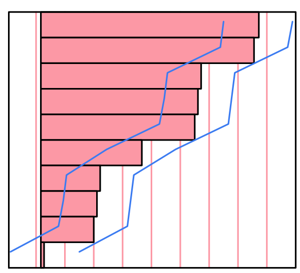

Table E.4. One-Way ANOVA for Overlaying Water Depth: Evaluating x-Velocity (Vx) at 5 L/s Flow Rate and Rectangular Inlet

Oneway Analysis of Vx (cm/s) By Depth (cm) Flow rate (L/s)=5, Inlet Type=rec

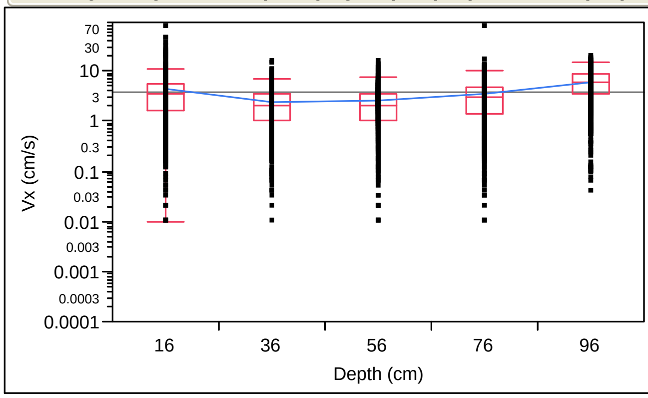

Oneway Anova

Summary of Fit

Rsquare	0.13046
Adj Rsquare	0.129711
Root Mean Square Error	3.487889
Mean of Response	3.809273
Observations (or Sum Wgts)	4650

Analysis of Variance

Source	DF	Sum of Squares	Mean Square	F Ratio	Prob > F
Depth (cm)	4	8478.123	2119.53	174.2266	<.0001*
Error	4645	56508.145	12.17		
C. Total	4649	64986.268			

Means Comparisons

Comparisons for each pair using Student's t

t	Alpha
1.96047	0.05

Level					Mean
96	A				6.1555054
16		B			4.3097097
76			C		3.5195054
56				D	2.5947849
36				D	2.4668602

Levels not connected by same letter are significantly different.

Level	- Level	Difference	Lower CL	Upper CL	p-Value
96	36	3.688645	3.37154	4.005746	<.0001*
96	56	3.560720	3.24362	3.877821	<.0001*
96	76	2.636000	2.31890	2.953101	<.0001*
96	16	1.845796	1.52869	2.162897	<.0001*
16	36	1.842849	1.52575	2.159950	<.0001*
16	56	1.714925	1.39782	2.032026	<.0001*
76	36	1.052645	0.73554	1.369746	<.0001*
76	56	0.924720	0.60762	1.241821	<.0001*
16	76	0.790204	0.47310	1.107305	<.0001*
56	36	0.127925	-0.18918	0.445026	0.4290

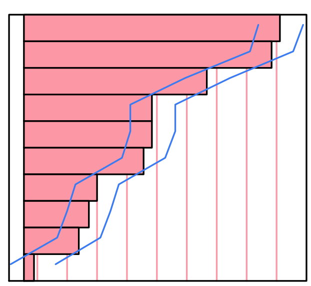

Table E.5. One-Way ANOVA for Overlaying Water Depth: Evaluating x-Velocity (Vx) at 10 L/s Flow Rate and Circular Inlet

Oneway Analysis of Vx (cm/s) By Depth (cm) Flow rate (L/s)=10, Inlet Type=cir

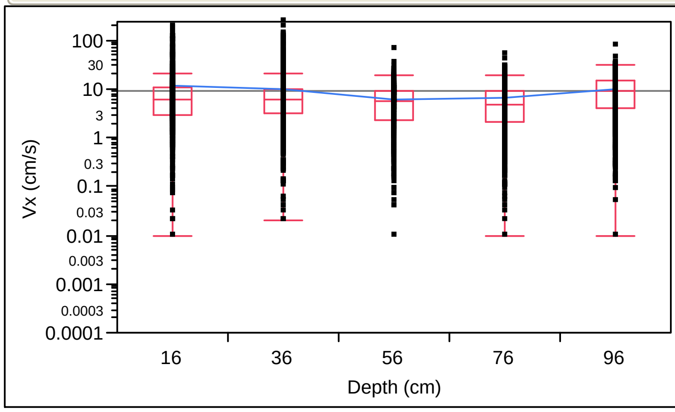

Oneway Anova

Summary of Fit

Rsquare	0.030733
Adj Rsquare	0.029898
Root Mean Square Error	12.51026
Mean of Response	8.814465
Observations (or Sum Wgts)	4650

Analysis of Variance

Source	DF	Sum of Squares	Mean Square	F Ratio	Prob > F
Depth (cm)	4	23050.51	5762.63	36.8204	<.0001*
Error	4645	726972.66	156.51		
C. Total	4649	750023.17			

Means Comparisons

Comparisons for each pair using Student's t

t	Alpha
1.96047	0.05

Level				Mean
16	A			11.933505
96		B		10.088065
36		B		9.501581
76			C	6.449129
56			C	6.100043

Levels not connected by same letter are significantly different.

Level	- Level	Difference	Lower CL	Upper CL	p-Value
16	56	5.833462	4.69609	6.970830	<.0001*
16	76	5.484376	4.34701	6.621744	<.0001*
96	56	3.988022	2.85065	5.125389	<.0001*
96	76	3.638935	2.50157	4.776303	<.0001*
36	56	3.401538	2.26417	4.538906	<.0001*
36	76	3.052452	1.91508	4.189820	<.0001*
16	36	2.431925	1.29456	3.569293	<.0001*
16	96	1.845441	0.70807	2.982809	0.0015*
96	36	0.586484	-0.55088	1.723852	0.3121
76	56	0.349086	-0.78828	1.486454	0.5474

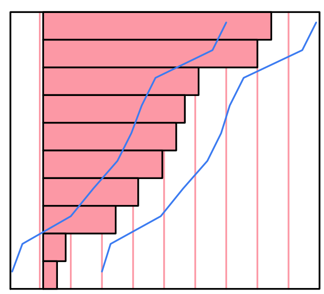

Table E.6. One-Way ANOVA for Overlaying Water Depth: Evaluating x-Velocity (Vx) at 10 L/s Flow Rate and Rectangular Inlet

Oneway Analysis of Vx (cm/s) By Depth (cm) Flow rate (L/s)=10, Inlet Type=rec

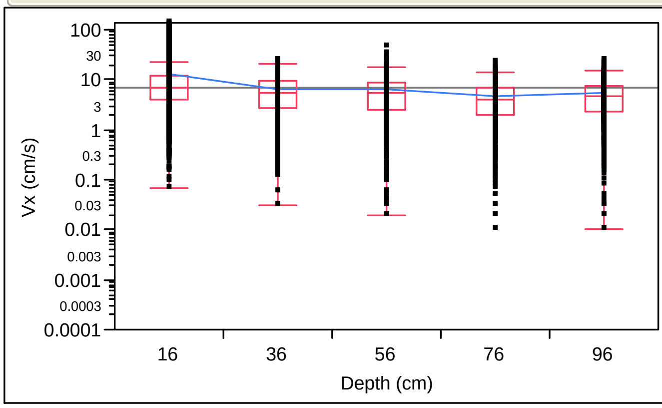

Oneway Anova

Summary of Fit

Rsquare	0.088773
Adj Rsquare	0.087988
Root Mean Square Error	9.368405
Mean of Response	7.211112
Observations (or Sum Wgts)	4650

Analysis of Variance

Source	DF	Sum of Squares	Mean Square	F Ratio	Prob > F
Depth (cm)	4	39716.44	9929.11	113.1303	<.0001*
Error	4645	407677.75	87.77		
C. Total	4649	447394.18			

Means Comparisons

Comparisons for each pair using Student's t

t	Alpha
1.96047	0.05

Level		Mean
16	A	12.907484
36	B	6.659914
56	B C	6.262247
96	C D	5.465462
76	D	4.760452

Levels not connected by same letter are significantly different.

Level	- Level	Difference	Lower CL	Upper CL	p-Value
16	76	8.147032	7.29531	8.998759	<.0001*
16	96	7.442022	6.59029	8.293749	<.0001*
16	56	6.645237	5.79351	7.496964	<.0001*
16	36	6.247570	5.39584	7.099297	<.0001*
36	76	1.899462	1.04774	2.751189	<.0001*
56	76	1.501796	0.65007	2.353523	0.0006*
36	96	1.194452	0.34272	2.046179	0.0060*
56	96	0.796785	-0.05494	1.648512	0.0667
96	76	0.705011	-0.14672	1.556738	0.1047
36	56	0.397667	-0.45406	1.249394	0.3601

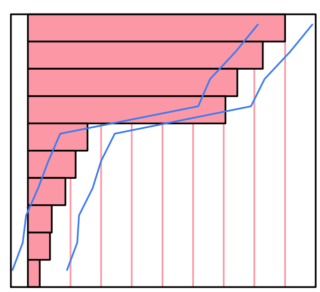

Table E.7. One-Way ANOVA for Overlaying Water Depth: Evaluating y-Velocity (Vy) at 2.5 L/s Flow Rate and Circular Inlet

Oneway Analysis of Vy (cm/s) By Depth (cm) Flow rate (L/s)=2.5, Inlet Type=cir

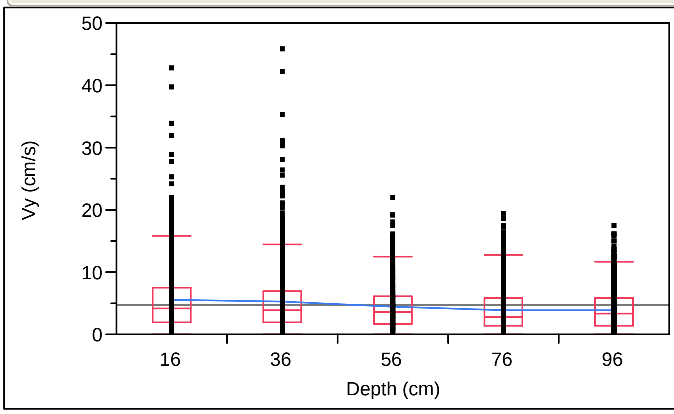

Oneway Anova

Summary of Fit

Rsquare	0.023534
Adj Rsquare	0.022693
Root Mean Square Error	4.060672
Mean of Response	4.58723
Observations (or Sum Wgts)	4650

Analysis of Variance

Source	DF	Sum of Squares	Mean Square	F Ratio	Prob > F
Depth (cm)	4	1845.950	461.487	27.9875	<.0001*
Error	4645	76591.687	16.489		
C. Total	4649	78437.637			

Means Comparisons

Comparisons for each pair using Student's t

t	Alpha
1.96047	0.05

Level				Mean
16	A			5.4973333
36	A			5.1541828
56		B		4.3564516
76		B	C	4.0156022
96			C	3.9125806

Levels not connected by same letter are significantly different.

Level	- Level	Difference	Lower CL	Upper CL	p-Value
16	96	1.584753	1.21558	1.953928	<.0001*
16	76	1.481731	1.11256	1.850907	<.0001*
36	96	1.241602	0.87243	1.610778	<.0001*
16	56	1.140882	0.77171	1.510057	<.0001*
36	76	1.138581	0.76941	1.507756	<.0001*
36	56	0.797731	0.42856	1.166907	<.0001*
56	96	0.443871	0.07470	0.813046	0.0185*
16	36	0.343151	-0.02602	0.712326	0.0685
56	76	0.340849	-0.02833	0.710025	0.0704
76	96	0.103022	-0.26615	0.472197	0.5843

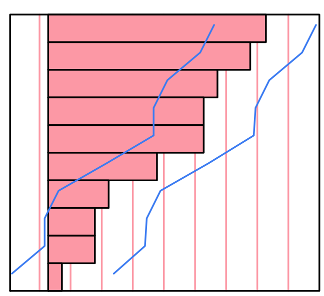

Table E.8. One-Way ANOVA for Overlaying Water Depth: Evaluating y-Velocity (Vy) at 2.5 L/s Flow Rate and Rectangular Inlet

Oneway Analysis of Vy (cm/s) By Depth (cm) Flow rate (L/s)=2.5, Inlet Type=rec

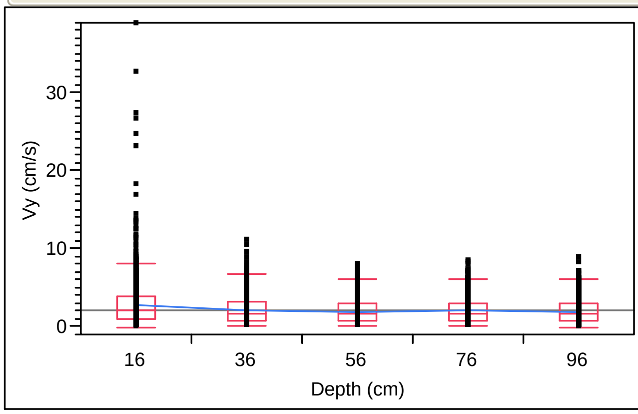

Oneway Anova

Summary of Fit

Rsquare	0.027804
Adj Rsquare	0.026967
Root Mean Square Error	2.036823
Mean of Response	2.198441
Observations (or Sum Wgts)	4650

Analysis of Variance

Source	DF	Sum of Squares	Mean Square	F Ratio	Prob > F
Depth (cm)	4	551.116	137.779	33.2106	<.0001*
Error	4645	19270.471	4.149		
C. Total	4649	19821.586			

Means Comparisons

Comparisons for each pair using Student's t

t	Alpha
1.96047	0.05

Level				Mean
16	A			2.8716882
36		B		2.1598346
76		B	C	2.0278953
56		B	C	1.9894839
96			C	1.9433011

Levels not connected by same letter are significantly different.

Level	- Level	Difference	Lower CL	Upper CL	p-Value
16	96	0.9283871	0.743210	1.113565	<.0001*
16	56	0.8822043	0.697027	1.067382	<.0001*
16	76	0.8437929	0.658615	1.028970	<.0001*
16	36	0.7118535	0.526676	0.897031	<.0001*
36	96	0.2165335	0.031356	0.401711	0.0219*
36	56	0.1703508	-0.014827	0.355528	0.0714
36	76	0.1319394	-0.053238	0.317117	0.1625
76	96	0.0845942	-0.100583	0.269772	0.3705
56	96	0.0461828	-0.138995	0.231360	0.6249
76	56	0.0384114	-0.146766	0.223589	0.6843

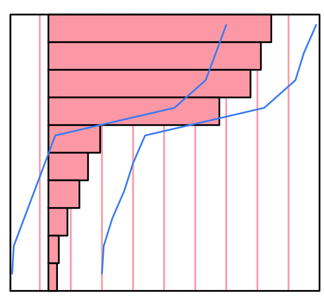

Table E.9. One-Way ANOVA for Overlaying Water Depth: Evaluating y-Velocity (Vy) at 5 L/s Flow Rate and Circular Inlet

Oneway Analysis of Vy (cm/s) By Depth (cm) Flow rate (L/s)=5, Inlet Type=cir

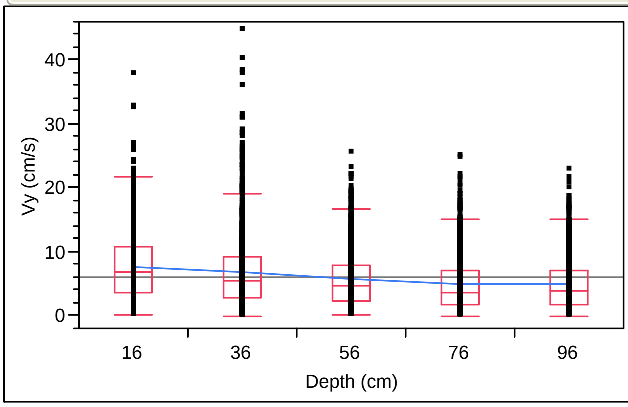

Oneway Anova

Summary of Fit

Rsquare	0.047862
Adj Rsquare	0.047042
Root Mean Square Error	4.889755
Mean of Response	6.017578
Observations (or Sum Wgts)	4650

Analysis of Variance

Source	DF	Sum of Squares	Mean Square	F Ratio	Prob > F
Depth (cm)	4	5582.79	1395.70	58.3737	<.0001*
Error	4645	111060.58	23.91		
C. Total	4649	116643.37			

Means Comparisons

Comparisons for each pair using Student's t

t	Alpha
1.96047	0.05

Level					Mean
16	A				7.6742151
36		B			6.8310430
56			C		5.8068495
96				D	4.8923978
76				D	4.8833871

Levels not connected by same letter are significantly different.

Level	- Level	Difference	Lower CL	Upper CL	p-Value
16	76	2.790828	2.34628	3.235379	<.0001*
16	96	2.781817	2.33727	3.226369	<.0001*
36	76	1.947656	1.50310	2.392207	<.0001*
36	96	1.938645	1.49409	2.383196	<.0001*
16	56	1.867366	1.42281	2.311917	<.0001*
36	56	1.024194	0.57964	1.468745	<.0001*
56	76	0.923462	0.47891	1.368014	<.0001*
56	96	0.914452	0.46990	1.359003	<.0001*
16	36	0.843172	0.39862	1.287723	0.0002*
96	76	0.009011	-0.43554	0.453562	0.9683

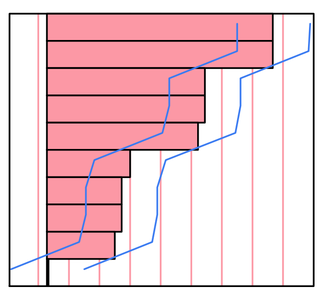

Table E.10. One-Way ANOVA for Overlaying Water Depth: Evaluating y-Velocity (Vy) at 5 L/s Flow Rate and Rectangular Inlet

Oneway Analysis of Vy (cm/s) By Depth (cm) Flow rate (L/s)=5, Inlet Type=rec

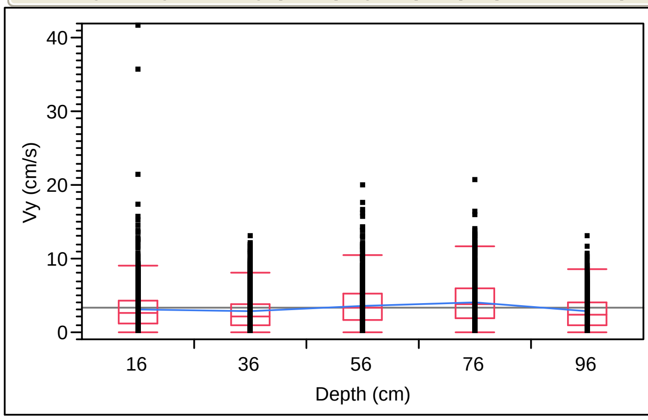

Oneway Anova

Summary of Fit

Rsquare	0.035107
Adj Rsquare	0.034276
Root Mean Square Error	2.652577
Mean of Response	3.28274
Observations (or Sum Wgts)	4650

Analysis of Variance

Source	DF	Sum of Squares	Mean Square	F Ratio	Prob > F
Depth (cm)	4	1189.154	297.288	42.2515	<.0001*
Error	4645	32682.992	7.036		
C. Total	4649	33872.146			

Means Comparisons

Comparisons for each pair using Student's t

t	Alpha
1.96047	0.05

Level					Mean
76	A				4.0608065
56		B			3.6467849
16			C		3.1676022
36				D	2.7778817
96				D	2.7606237

Levels not connected by same letter are significantly different.

Level	- Level	Difference	Lower CL	Upper CL	p-Value
76	96	1.300183	1.05902	1.541341	<.0001*
76	36	1.282925	1.04177	1.524083	<.0001*
76	16	0.893204	0.65205	1.134363	<.0001*
56	96	0.886161	0.64500	1.127320	<.0001*
56	36	0.868903	0.62774	1.110062	<.0001*
56	16	0.479183	0.23802	0.720341	<.0001*
76	56	0.414022	0.17286	0.655180	0.0008*
16	96	0.406978	0.16582	0.648137	0.0009*
16	36	0.389720	0.14856	0.630879	0.0015*
36	96	0.017258	-0.22390	0.258417	0.8884

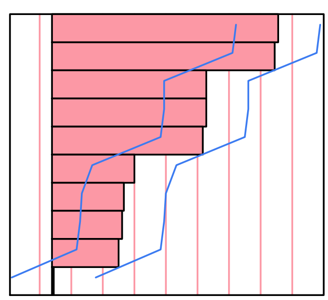

Table E.11. One-Way ANOVA for Overlaying Water Depth: Evaluating y-Velocity (Vy) at 10 L/s Flow Rate and Circular Inlet

Oneway Analysis of Vy (cm/s) By Depth (cm) Flow rate (L/s)=10, Inlet Type=cir

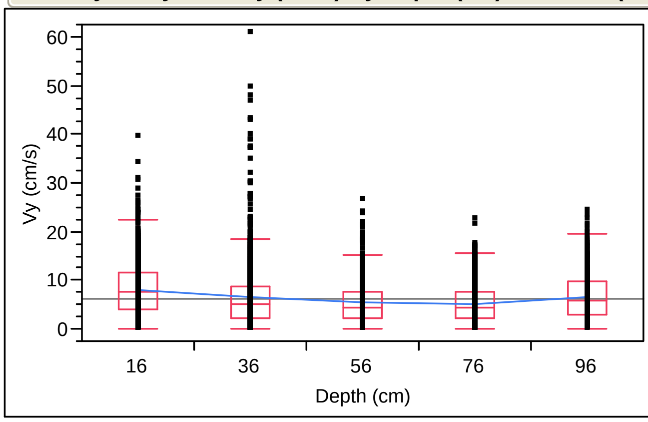

Oneway Anova

Summary of Fit

Rsquare	0.044768
Adj Rsquare	0.043945
Root Mean Square Error	5.012447
Mean of Response	6.340262
Observations (or Sum Wgts)	4650

Analysis of Variance

Source	DF	Sum of Squares	Mean Square	F Ratio	Prob > F
Depth (cm)	4	5469.41	1367.35	54.4228	<.0001*
Error	4645	116703.89	25.12		
C. Total	4649	122173.30			

Means Comparisons

Comparisons for each pair using Student's t

t	Alpha
1.96047	0.05

Level				Mean
16	A			8.1402581
96		B		6.6436667
36		B		6.4811935
56			C	5.2911613
76			C	5.1450323

Levels not connected by same letter are significantly different.

Level	- Level	Difference	Lower CL	Upper CL	p-Value
16	76	2.995226	2.53952	3.450932	<.0001*
16	56	2.849097	2.39339	3.304803	<.0001*
16	36	1.659065	1.20336	2.114770	<.0001*
96	76	1.498634	1.04293	1.954340	<.0001*
16	96	1.496591	1.04089	1.952297	<.0001*
96	56	1.352505	0.89680	1.808211	<.0001*
36	76	1.336161	0.88046	1.791867	<.0001*
36	56	1.190032	0.73433	1.645738	<.0001*
96	36	0.162473	-0.29323	0.618179	0.4846
56	76	0.146129	-0.30958	0.601835	0.5296

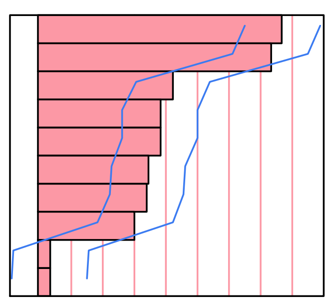

Table E.12. One-Way ANOVA for Overlaying Water Depth: Evaluating y-Velocity (Vy) at 10 L/s Flow Rate and Rectangular Inlet

Oneway Analysis of Vy (cm/s) By Depth (cm) Flow rate (L/s)=10, Inlet Type=rec

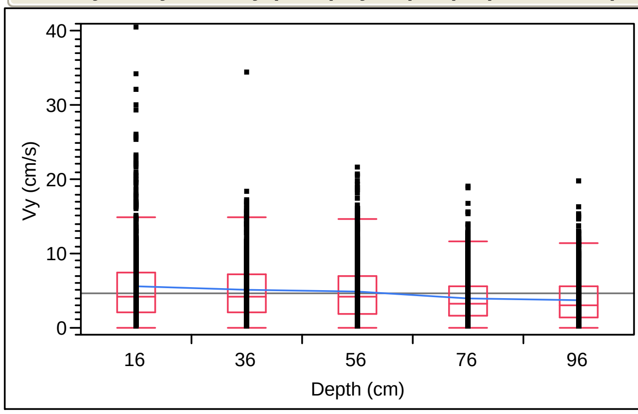

Oneway Anova

Summary of Fit

Rsquare	0.028895
Adj Rsquare	0.028059
Root Mean Square Error	3.813796
Mean of Response	4.597335
Observations (or Sum Wgts)	4650

Analysis of Variance

Source	DF	Sum of Squares	Mean Square	F Ratio	Prob > F
Depth (cm)	4	2010.317	502.579	34.5533	<.0001*
Error	4645	67561.715	14.545		
C. Total	4649	69572.032			

Means Comparisons

Comparisons for each pair using Student's t

t	Alpha
1.96047	0.05

Level				Mean
16	A			5.4941505
36		B		4.9751398
56		B		4.8365054
76			C	3.9167204
96			C	3.7641613

Levels not connected by same letter are significantly different.

Level	- Level	Difference	Lower CL	Upper CL	p-Value
16	96	1.729989	1.38326	2.076720	<.0001*
16	76	1.577430	1.23070	1.924161	<.0001*
36	96	1.210978	0.86425	1.557709	<.0001*
56	96	1.072344	0.72561	1.419075	<.0001*
36	76	1.058419	0.71169	1.405150	<.0001*
56	76	0.919785	0.57305	1.266516	<.0001*
16	56	0.657645	0.31091	1.004376	0.0002*
16	36	0.519011	0.17228	0.865741	0.0034*
76	96	0.152559	-0.19417	0.499290	0.3884
36	56	0.138634	-0.20810	0.485365	0.4332

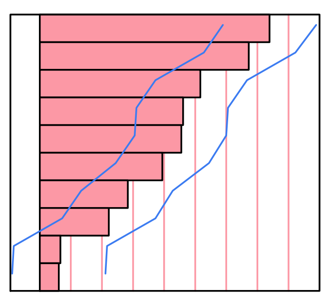

Table E.13. One-Way ANOVA for Overlaying Water Depth: Evaluating z-Velocity (Vz) at 2.5 L/s Flow Rate and Circular Inlet

Oneway Analysis of Vz (cm/s) By Depth (cm) Flow rate (L/s)=2.5, Inlet Type=cir

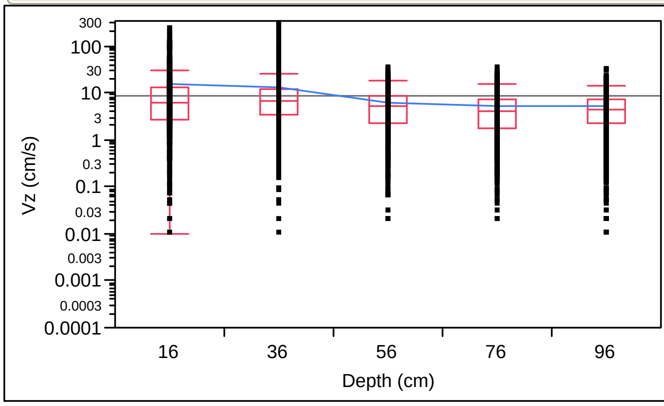

Oneway Anova

Summary of Fit

Rsquare	0.055526
Adj Rsquare	0.054713
Root Mean Square Error	17.97929
Mean of Response	8.932649
Observations (or Sum Wgts)	4650

Analysis of Variance

Source	DF	Sum of Squares	Mean Square	F Ratio	Prob > F
Depth (cm)	4	88275.2	22068.8	68.2706	<.0001*
Error	4645	1501519.6	323.3		
C. Total	4649	1589794.8			

Means Comparisons

Comparisons for each pair using Student's t

t	Alpha
1.96047	0.05

Level			Mean
16	A		14.969194
36	A		13.478140
56		B	5.972914
96		B	5.186710
76		B	5.056290

Levels not connected by same letter are significantly different.

Level	- Level	Difference	Lower CL	Upper CL	p-Value
16	76	9.912903	8.27832	11.54749	<.0001*
16	96	9.782484	8.14790	11.41707	<.0001*
16	56	8.996280	7.36169	10.63086	<.0001*
36	76	8.421849	6.78726	10.05643	<.0001*
36	96	8.291430	6.65685	9.92601	<.0001*
36	56	7.505226	5.87064	9.13981	<.0001*
16	36	1.491054	-0.14353	3.12564	0.0738
56	76	0.916624	-0.71796	2.55121	0.2717
56	96	0.786204	-0.84838	2.42079	0.3458
96	76	0.130419	-1.50417	1.76500	0.8757

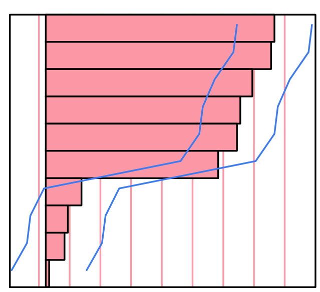

Table E.14. One-Way ANOVA for Overlaying Water Depth: Evaluating z-Velocity (Vz) at 2.5 L/s Flow Rate and Rectangular Inlet

Oneway Analysis of Vz (cm/s) By Depth (cm) Flow rate (L/s)=2.5, Inlet Type=rec

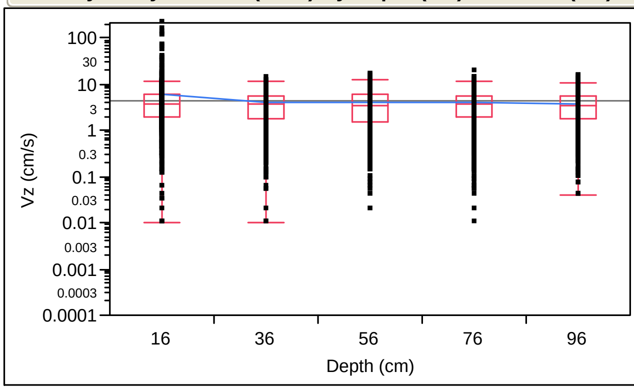

Oneway Anova

Summary of Fit

Rsquare	0.015425
Adj Rsquare	0.014577
Root Mean Square Error	6.143769
Mean of Response	4.31237
Observations (or Sum Wgts)	4650

Analysis of Variance

Source	DF	Sum of Squares	Mean Square	F Ratio	Prob > F
Depth (cm)	4	2746.77	686.693	18.1925	<.0001*
Error	4645	175329.67	37.746		
C. Total	4649	178076.44			

Means Comparisons

Comparisons for each pair using Student's t

t	Alpha
1.96047	0.05

Level			Mean
16	A		5.8443011
56		B	3.9970000
76		B	3.9950538
36		B	3.8961935
96		B	3.8293011

Levels not connected by same letter are significantly different.

Level	- Level	Difference	Lower CL	Upper CL	p-Value
16	96	2.015000	1.45644	2.573560	<.0001*
16	36	1.948108	1.38955	2.506667	<.0001*
16	76	1.849247	1.29069	2.407807	<.0001*
16	56	1.847301	1.28874	2.405861	<.0001*
56	96	0.167699	-0.39086	0.726259	0.5562
76	96	0.165753	-0.39281	0.724312	0.5607
56	36	0.100806	-0.45775	0.659366	0.7235
76	36	0.098860	-0.45970	0.657420	0.7286
36	96	0.066892	-0.49167	0.625452	0.8144
56	76	0.001946	-0.55661	0.560506	0.9945

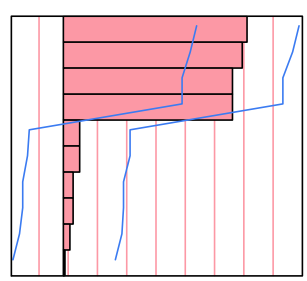

Table E.15. One-Way ANOVA for Overlaying Water Depth: Evaluating z-Velocity (Vz) at 5 L/s Flow Rate and Circular Inlet

Oneway Analysis of Vz (cm/s) By Depth (cm) Flow rate (L/s)=5, Inlet Type=cir

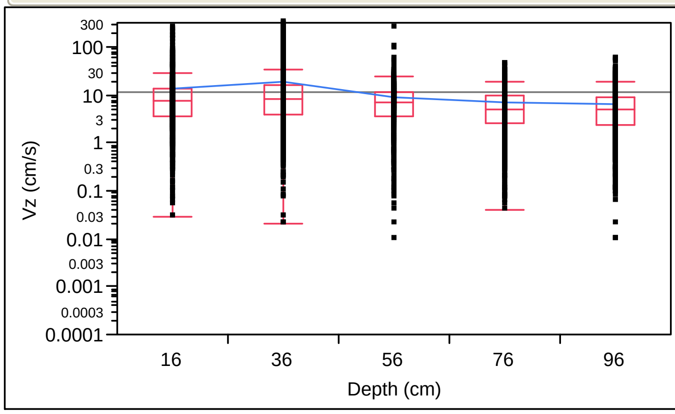

Oneway Anova

Summary of Fit

Rsquare	0.049895
Adj Rsquare	0.049077
Root Mean Square Error	21.59947
Mean of Response	11.22608
Observations (or Sum Wgts)	4650

Analysis of Variance

Source	DF	Sum of Squares	Mean Square	F Ratio	Prob > F
Depth (cm)	4	113803.2	28450.8	60.9829	<.0001*
Error	4645	2167065.2	466.5		
C. Total	4649	2280868.4			

Means Comparisons

Comparisons for each pair using Student's t

t	Alpha
1.96047	0.05

Level		Mean
36	A	19.477903
16	B	14.257892
56	C	8.791602
76	C D	6.846204
96	D	6.756785

Levels not connected by same letter are significantly different.

Level	- Level	Difference	Lower CL	Upper CL	p-Value
36	96	12.72112	10.7574	14.68483	<.0001*
36	76	12.63170	10.6680	14.59541	<.0001*
36	56	10.68630	8.7226	12.65001	<.0001*
16	96	7.50111	5.5374	9.46482	<.0001*
16	76	7.41169	5.4480	9.37540	<.0001*
16	56	5.46629	3.5026	7.43000	<.0001*
36	16	5.22001	3.2563	7.18372	<.0001*
56	96	2.03482	0.0711	3.99853	0.0423*
56	76	1.94540	-0.0183	3.90911	0.0522
76	96	0.08942	-1.8743	2.05313	0.9289

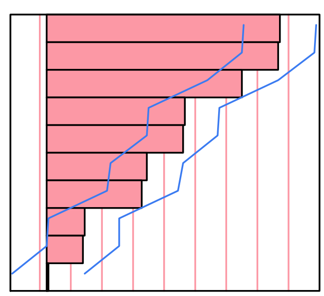

Table E.16. One-Way ANOVA for Overlaying Water Depth: Evaluating z-Velocity (Vz) at 5 L/s Flow Rate and Rectangular Inlet

Oneway Analysis of Vz (cm/s) By Depth (cm) Flow rate (L/s)=5, Inlet Type=rec

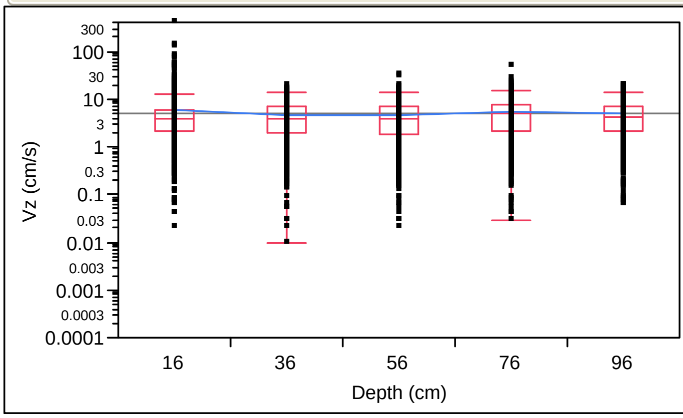

Oneway Anova

Summary of Fit

Rsquare	0.003999
Adj Rsquare	0.003142
Root Mean Square Error	7.820822
Mean of Response	5.0888
Observations (or Sum Wgts)	4650

Analysis of Variance

Source	DF	Sum of Squares	Mean Square	F Ratio	Prob > F
Depth (cm)	4	1140.84	285.210	4.6629	0.0009*
Error	4645	284112.64	61.165		
C. Total	4649	285253.48			

Means Comparisons

Comparisons for each pair using Student's t

t	Alpha
1.96047	0.05

Level		Mean
16	A	5.9030645
76	A B	5.3847419
96	B C	4.9249892
36	C	4.6423763
56	C	4.5888280

Levels not connected by same letter are significantly different.

Level	- Level	Difference	Lower CL	Upper CL	p-Value
16	56	1.314237	0.603208	2.025265	0.0003*
16	36	1.260688	0.549659	1.971717	0.0005*
16	96	0.978075	0.267046	1.689104	0.0070*
76	56	0.795914	0.084885	1.506943	0.0282*
76	36	0.742366	0.031337	1.453394	0.0407*
16	76	0.518323	-0.192706	1.229351	0.1530
76	96	0.459753	-0.251276	1.170782	0.2050
96	56	0.336161	-0.374868	1.047190	0.3540
96	36	0.282613	-0.428416	0.993642	0.4359
36	56	0.053548	-0.657480	0.764577	0.8826

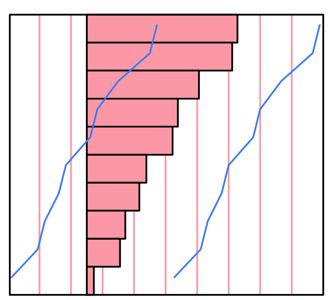

Table E.17. One-Way ANOVA for Overlaying Water Depth: Evaluating z-Velocity (Vz) at 10 L/s Flow Rate and Circular Inlet

Oneway Analysis of Vz (cm/s) By Depth (cm) Flow rate (L/s)=10, Inlet Type=cir

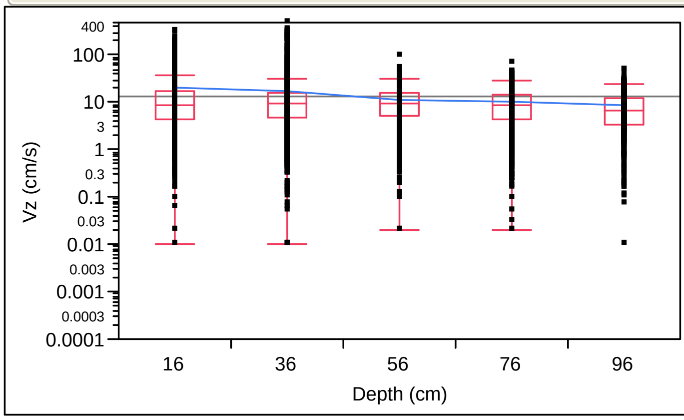

Oneway Anova

Summary of Fit

Rsquare	0.037166
Adj Rsquare	0.036337
Root Mean Square Error	24.47552
Mean of Response	13.64366
Observations (or Sum Wgts)	4650

Analysis of Variance

Source	DF	Sum of Squares	Mean Square	F Ratio	Prob > F
Depth (cm)	4	107410.8	26852.7	44.8254	<.0001*
Error	4645	2782591.4	599.1		
C. Total	4649	2890002.2			

Means Comparisons

Comparisons for each pair using Student's t

t	Alpha
1.96047	0.05

Level				Mean
16	A			21.314613
36		B		17.157398
56			C	10.854871
76			C	10.246602
96			C	8.644839

Levels not connected by same letter are significantly different.

Level	- Level	Difference	Lower CL	Upper CL	p-Value
16	96	12.66977	10.4446	14.89496	<.0001*
16	76	11.06801	8.8428	13.29320	<.0001*
16	56	10.45974	8.2346	12.68493	<.0001*
36	96	8.51256	6.2874	10.73775	<.0001*
36	76	6.91080	4.6856	9.13598	<.0001*
36	56	6.30253	4.0773	8.52771	<.0001*
16	36	4.15722	1.9320	6.38240	0.0003*
56	96	2.21003	-0.0152	4.43522	0.0516
76	96	1.60176	-0.6234	3.82695	0.1582
56	76	0.60827	-1.6169	2.83346	0.5920

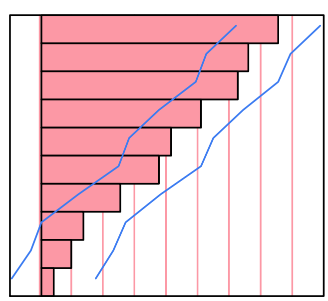

Table E.18. One-Way ANOVA for Overlaying Water Depth: Evaluating z-Velocity (Vz) at 10 L/s Flow Rate and Rectangular Inlet

Oneway Analysis of Vz (cm/s) By Depth (cm) Flow rate (L/s)=10, Inlet Type=rec

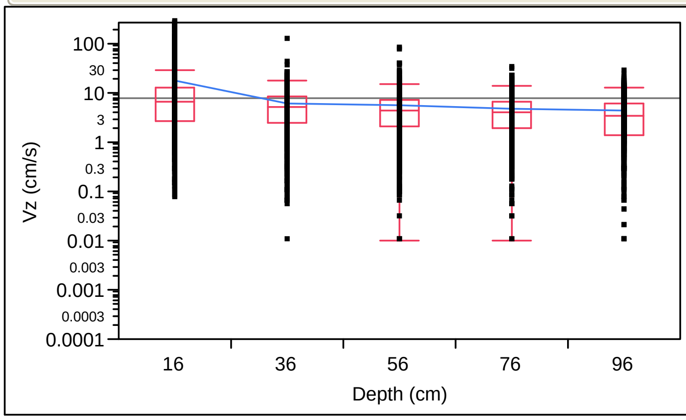

Oneway Anova

Summary of Fit

Rsquare	0.082787
Adj Rsquare	0.081997
Root Mean Square Error	16.28902
Mean of Response	7.659002
Observations (or Sum Wgts)	4650

Analysis of Variance

Source	DF	Sum of Squares	Mean Square	F Ratio	Prob > F
Depth (cm)	4	111242.1	27810.5	104.8139	<.0001*
Error	4645	1232468.7	265.3		
C. Total	4649	1343710.8			

Means Comparisons

Comparisons for each pair using Student's t

t	Alpha
1.96047	0.05

Level		Mean
16	A	17.363247
36	B	6.219613
56	B C	5.439570
76	B C	4.929108
96	C	4.343473

Levels not connected by same letter are significantly different.

Level	- Level	Difference	Lower CL	Upper CL	p-Value
16	96	13.01977	11.5389	14.50069	<.0001*
16	76	12.43414	10.9532	13.91505	<.0001*
16	56	11.92368	10.4428	13.40459	<.0001*
16	36	11.14363	9.6627	12.62455	<.0001*
36	96	1.87614	0.3952	3.35705	0.0130*
36	76	1.29051	-0.1904	2.77142	0.0876
56	96	1.09610	-0.3848	2.57701	0.1468
36	56	0.78004	-0.7009	2.26096	0.3018
76	96	0.58563	-0.8953	2.06655	0.4382
56	76	0.51046	-0.9705	1.99138	0.4992

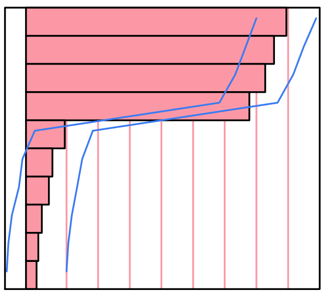

APPENDIX F

PRE-DEPOSITED SEDIMENT AND LAKE WATER CHARACTERISTICS

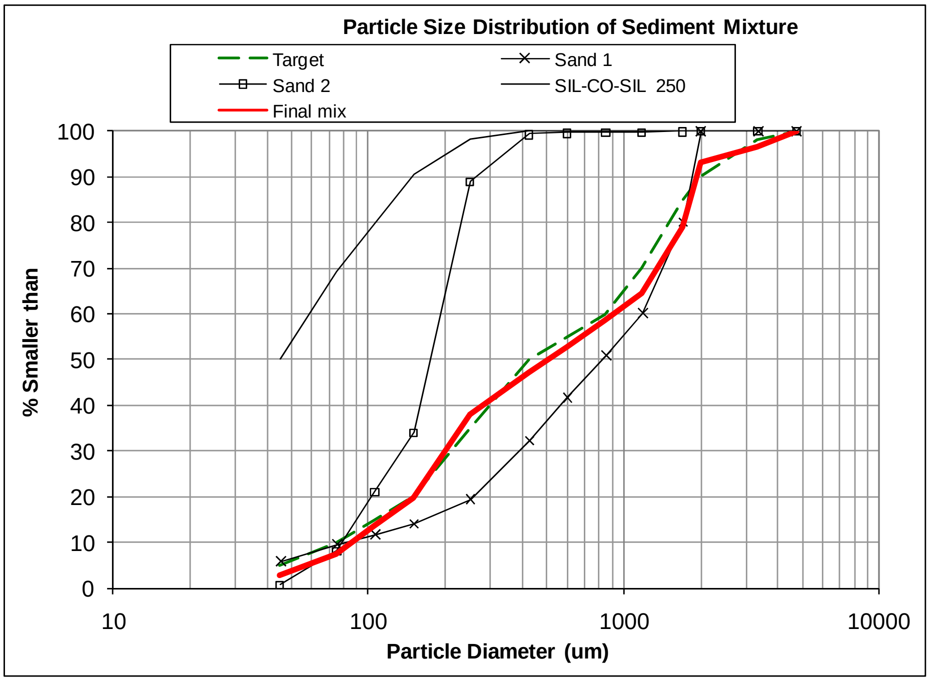

Figure F.1. Particle size distribution of sediment mixture.

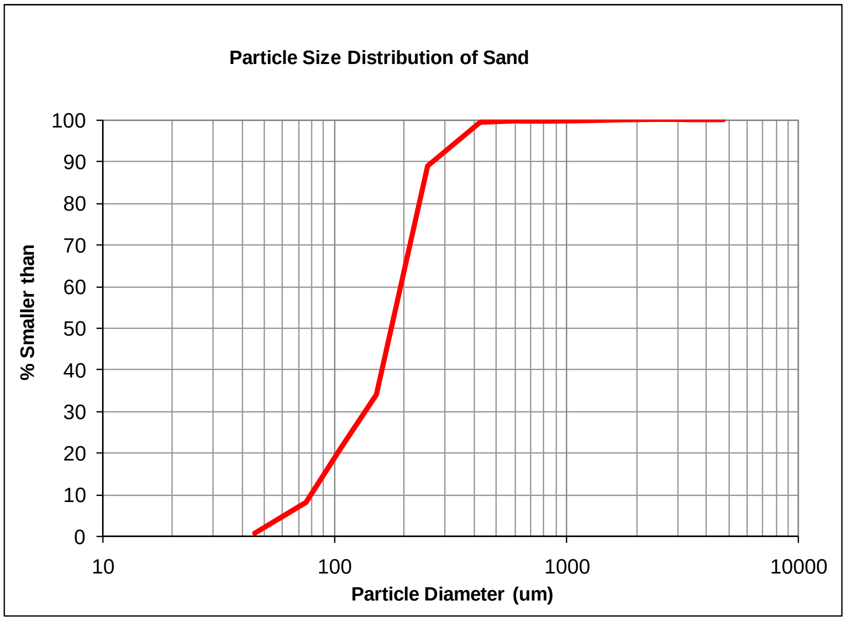

Figure F.2. Particle size distribution of sand (sediment with homogeneous particle size D_{50} = 180 μm).

Table F.1. Suspended Sediment Concentration (SSC) of Lake Water (Lake Lureen State Park, Northport, AL) – Scour of Sediment Mixture

SSC (mg/L) of Lake water (Lake (Lureen State Park, Northport, AL)		
Particle Size Range (μm)	Sample 1	Sample 2
>425	3.0	7.0
250-425	3.0	8.2
150-250	4.4	4.1
106-150	4.0	3.5
45-106	1.0	6.8
32-45	1.0	2.0
20-32	1.0	2.2
<20	1.0	1.9

\

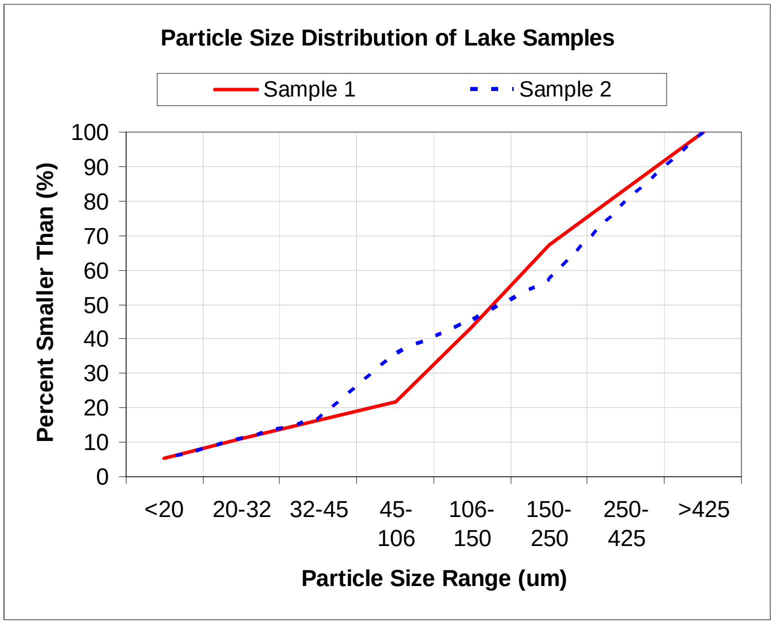

Figure F.3. Particle size distribution of lake water (Lake Lureen State Park, Northport, AL) – Scour of sediment mixture.

\

APPENDIX G

SUSPENDED SEDIMENT CONCENTRATION (SSC) OF COMPOSITE SAMPLES COLLECTED FROM SCOUR TESTS WITH SEDIMENT MIXTURE

Table G.1. Suspended Sediment Concentration (SSC) of 0–5 and 5–25 min Composite Sample: Scour of Sediment Mixture at 10 cm Below the Outlet

	SSC (mg/L) - Scour of sediment mixture at 10 cm below the outlet					
	Particle Size Range (μm)	**Flow rate (L/s)**				
		0.3	**1.3**	**3**	**6.3**	**10**
0 - 5 min composite samples	2000-4750	0.0	0.0	0.0	0.0	677.0
	1200-2000	0.0	0.0	0.0	32.3	10.0
	425-1200	0.0	0.0	0.0	73.8	0.0
	250-425	0.0	0.0	0.0	110.7	101.5
	150-250	0.0	11.3	81.6	210.3	101.0
	106-150	3.1	12.6	7.4	97.2	7.0
	45-106	15.5	44.6	118.8	207.9	93.2
	32-45	0.0	66.0	33.6	60.3	8.3
	20-32	0.0	54.4	43.1	34.2	44.5
	<20	37.1	202.9	142.0	217.8	96.0
5 - 25 min composite samples	2000-4750	0.0	0.0	0.0	0.0	274.1
	1200-2000	0.0	0.0	0.0	26.2	122.4
	425-1200	0.0	0.0	0.0	23.0	76.1
	250-425	0.0	0.0	0.0	23.0	83.6
	150-250	0.0	11.3	22.0	58.7	44.8
	106-150	2.1	0.0	20.0	0.0	0.0
	45-106	2.1	6.8	16.6	35.0	43.2
	32-45	0.0	6.8	3.3	26.0	12.5
	20-32	3.2	8.7	33.3	11.0	12.5
	<20	5.3	21.4	6.7	41.1	14.4

Table G.2. Suspended Sediment Concentration (SSC) of 0–5 and 5–25 min Composite Sample: Scour of Sediment Mixture at 25 cm Below the Outlet

	SSC (mg/L) - Scour of sediment mixture at 25 cm below the outlet					
	Particle Size Range (μm)	**Flow rate (L/s)**				
		0.3	**1.3**	**3**	**6.3**	**10**
0 - 5 min composite samples	>1200	0.0	0.0	0.0	0.0	0.0
	425-1200	0.0	0.0	0.0	0.0	0.0
	250-425	0.0	0.6	0.0	0.0	0.0
	150-250	0.8	1.9	3.0	8.3	0.0
	106-150	1.0	0.6	0.0	6.0	3.0
	45-106	0.0	0.0	8.4	19.0	7.1
	32-45	0.0	0.0	7.4	12.0	9.1
	20-32	0.0	0.0	0.0	13.0	8.1
	<20	5.3	4.9	23.1	50.1	19.2
5 - 25 min composite samples	>1200	0.0	0.0	0.0	0.0	0.0
	425-1200	0.0	0.0	4.0	1.4	2.5
	250-425	0.0	5.5	0.0	3.0	2.6
	150-250	0.6	0.0	6.3	1.7	0.0
	106-150	0.0	0.0	0.0	0.0	11.1
	45-106	0.0	0.0	6.3	5.0	8.3
	32-45	0.0	0.0	0.0	3.0	0.0
	20-32	0.0	0.0	1.1	4.0	0.0
	<20	1.1	0.0	2.1	4.0	19.5

Table G.3. Suspended Sediment Concentration (SSC) of 0–5 and 5–25 min Composite Sample: Scour of Sediment Mixture at 46 cm Below the Outlet

	SSC (mg/L) - Scour of sediment mixture at 46 cm below the outlet					
	Particle Size Range (μm)	Flow rate (L/s)				
		0.3	1.3	3	6.3	10
0 - 5 min composite samples	>1200	0.0	0.0	0.0	0.0	0.0
	425-1200	0.0	0.0	0.0	0.0	2.5
	250-425	0.0	3.6	0.0	0.0	0.0
	150-250	0.0	0.5	5.3	0.0	0.0
	106-150	0.0	0.0	0.0	0.0	4.0
	45-106	1.9	0.0	0.0	10.0	1.0
	32-45	0.0	0.0	1.1	0.0	0.0
	20-32	0.0	0.0	0.0	1.0	2.0
	<20	3.0	0.0	0.1	1.0	1.1
5 - 25 min composite samples	>1200	0.0	0.0	0.0	0.0	0.0
	425-1200	0.0	0.0	0.0	0.0	1.3
	250-425	0.0	1.5	0.0	1.5	0.0
	150-250	0.0	0.0	0.0	0.0	0.9
	106-150	0.0	0.0	0.0	0.0	0.0
	45-106	0.0	0.0	2.6	2.1	4.0
	32-45	0.3	0.0	0.0	0.0	0.0
	20-32	0.0	0.0	2.1	6.4	5.0
	<20	1.7	0.0	0.0	0.7	0.0

Table G.4. Suspended Sediment Concentration (SSC) of 0–5 and 5–25 min Composite Sample: Scour of Sediment Mixture at 106 cm Below the Outlet

	SSC (mg/L) - Scour of sediment mixture at 106 cm below the outlet					
	Particle Size Range (μm)	Flow rate (L/s)				
		0.3	1.3	3	6.3	10
0 - 5 min composite samples	>1200	0.0	0.0	0.0	0.0	0.0
	425-1200	0.0	0.0	0.0	0.0	0.0
	250-425	0.0	0.0	0.0	0.0	0.0
	150-250	0.0	0.0	0.0	0.0	0.0
	106-150	0.0	0.0	0.0	0.0	0.0
	45-106	0.0	0.0	0.0	0.0	0.0
	32-45	0.0	0.0	0.0	1.3	0.0
	20-32	0.0	0.0	2.8	0.6	0.0
	<20	1.7	2.6	0.6	1.1	1.7
5 - 25 min composite samples	>1200	0.0	0.0	0.0	0.0	0.0
	425-1200	0.0	0.0	0.0	0.0	0.0
	250-425	0.0	0.0	0.0	0.0	0.0
	150-250	0.0	0.0	0.0	0.0	0.0
	106-150	0.0	0.0	0.0	0.0	0.0
	45-106	0.0	0.0	0.0	0.0	0.0
	32-45	0.0	1.0	0.0	0.0	0.0
	20-32	0.0	0.0	0.5	0.0	0.0
	<20	0.6	0.1	1.5	2.1	4.0

APPENDIX H

PARTICLE SIZE DISTRIBUTION (PSD) OF COMPOSITE SAMPLES COLLECTED FROM SCOUR TESTS WITH A SEDIMENT MIXTURE

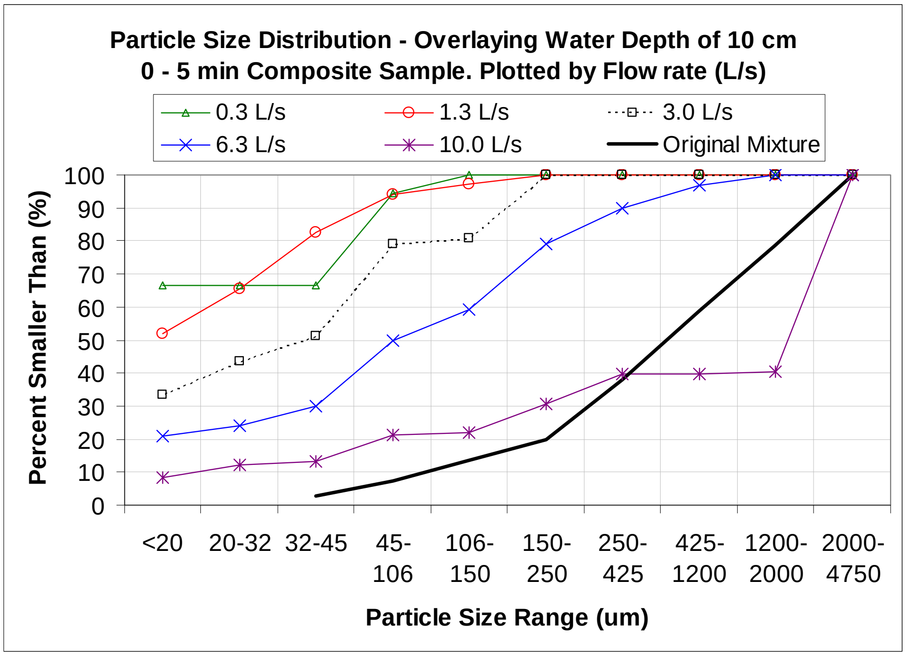

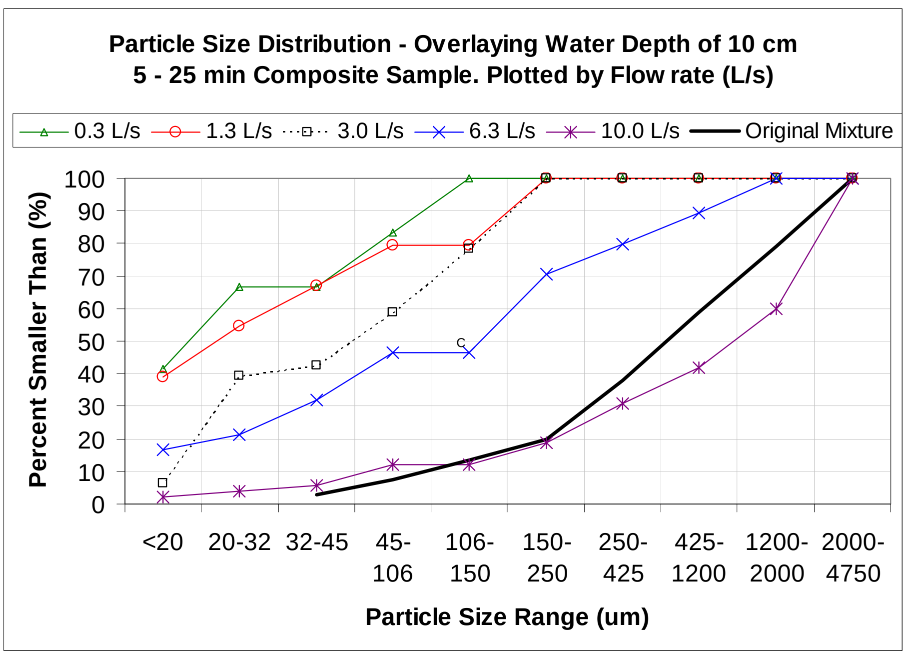

Figure H.1. PSD of scoured sediment mixture mass at 10 cm below the outlet.

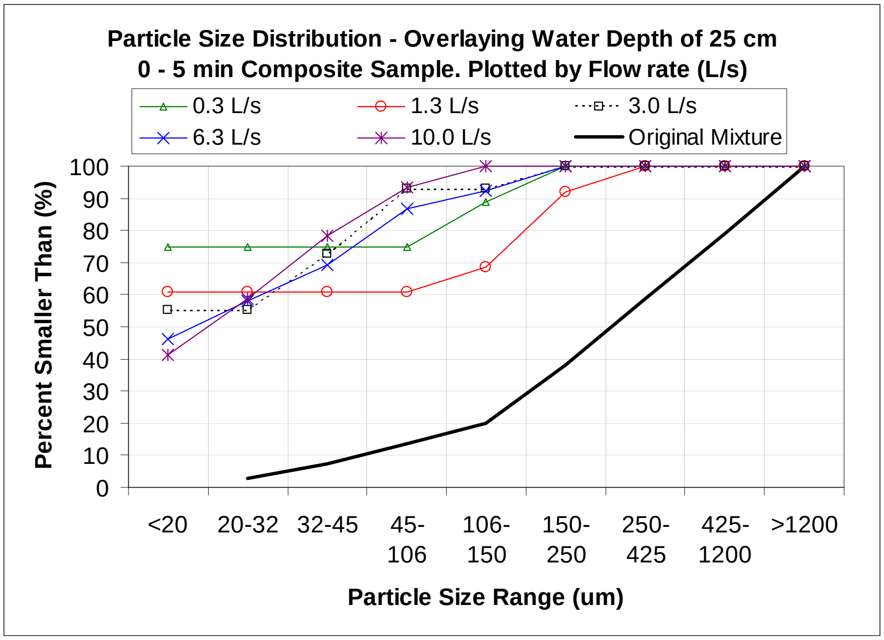

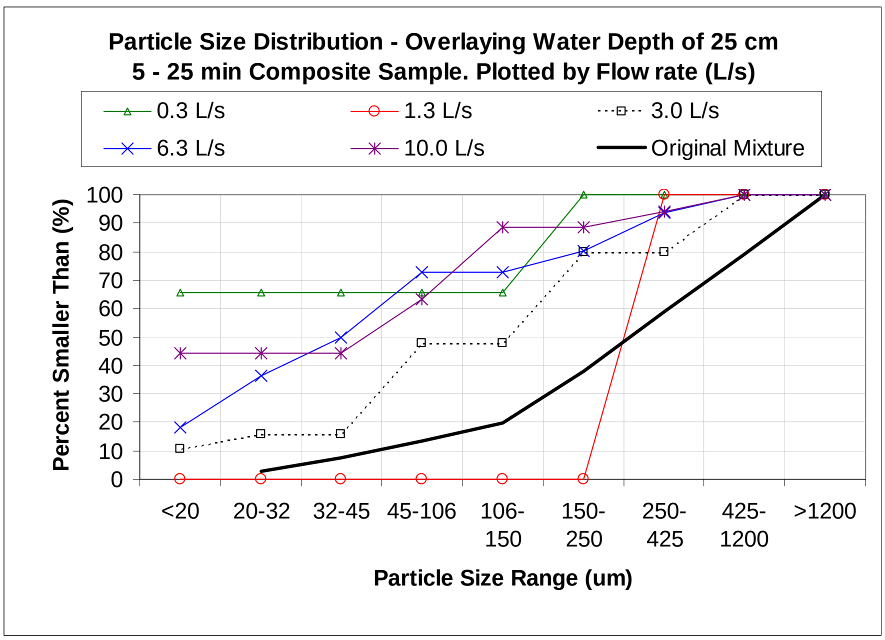

Figure H.2. PSD of scoured sediment mixture mass at 25 cm below the outlet.

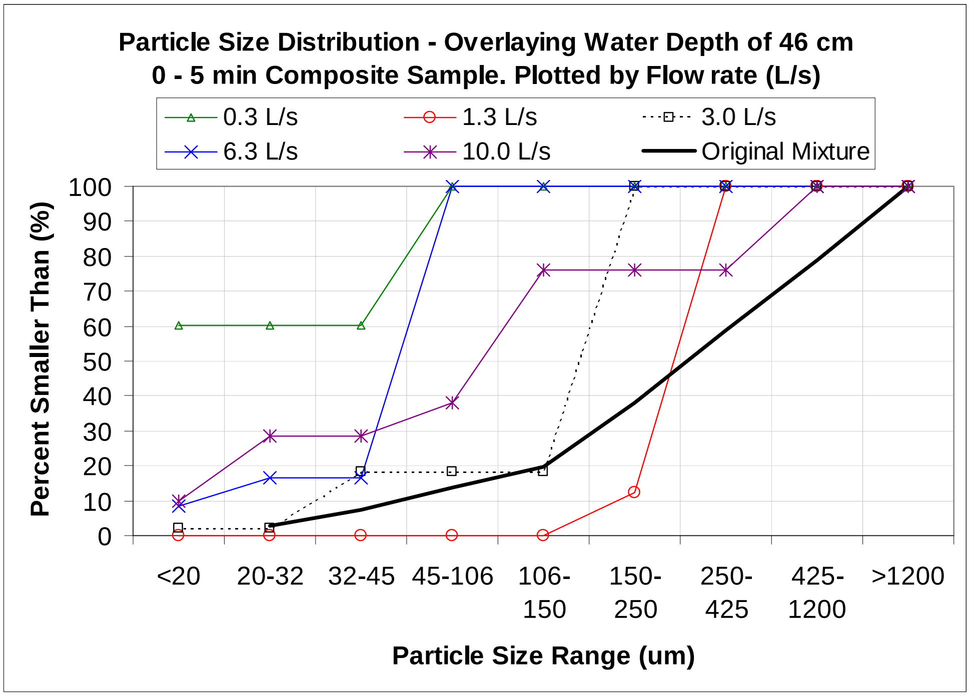

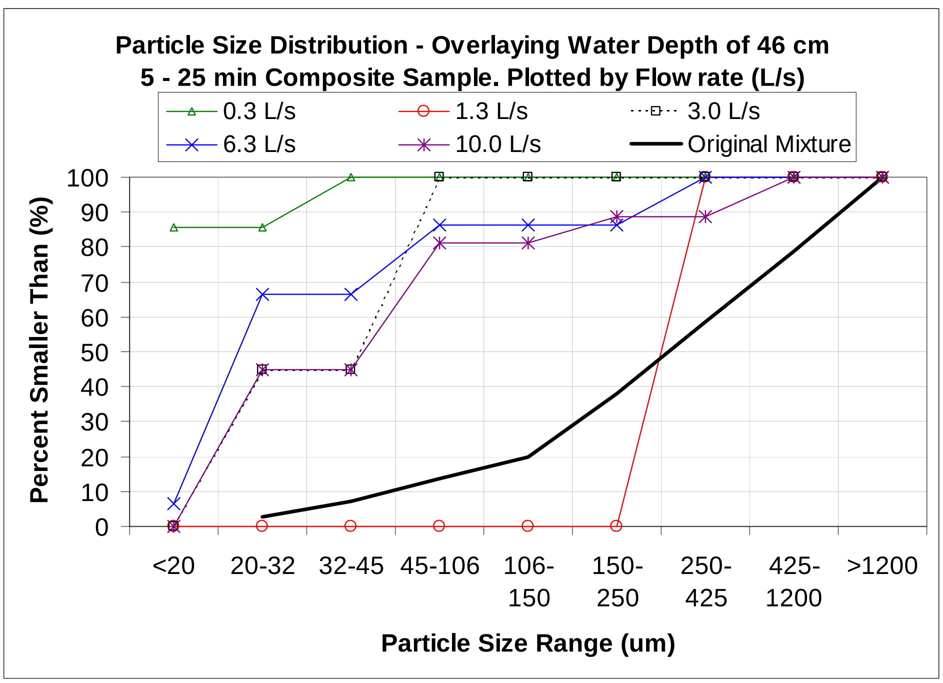

Figure H.3. PSD of scoured sediment mixture mass at 46 cm below the outlet.

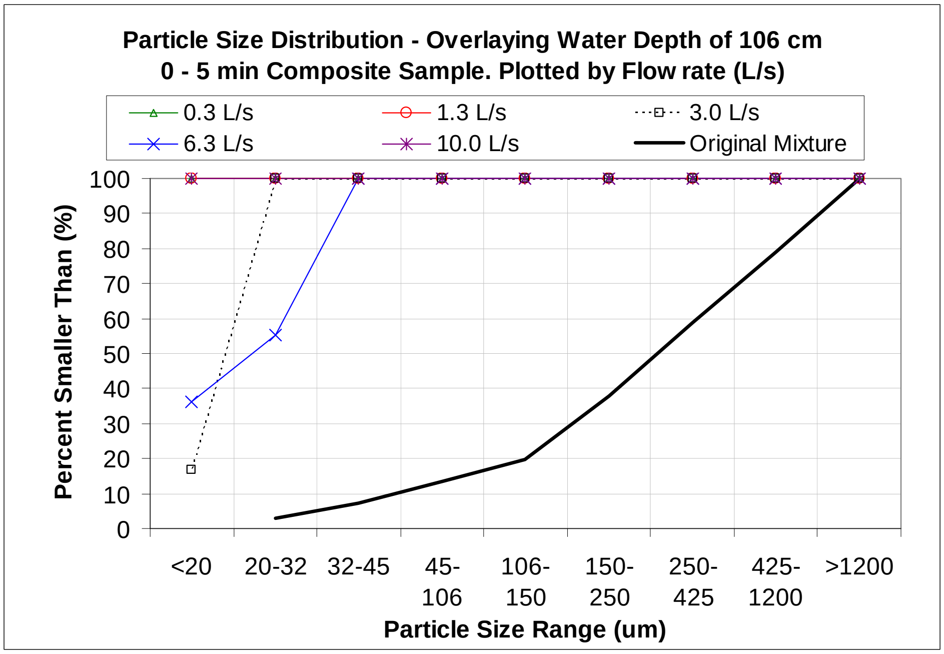

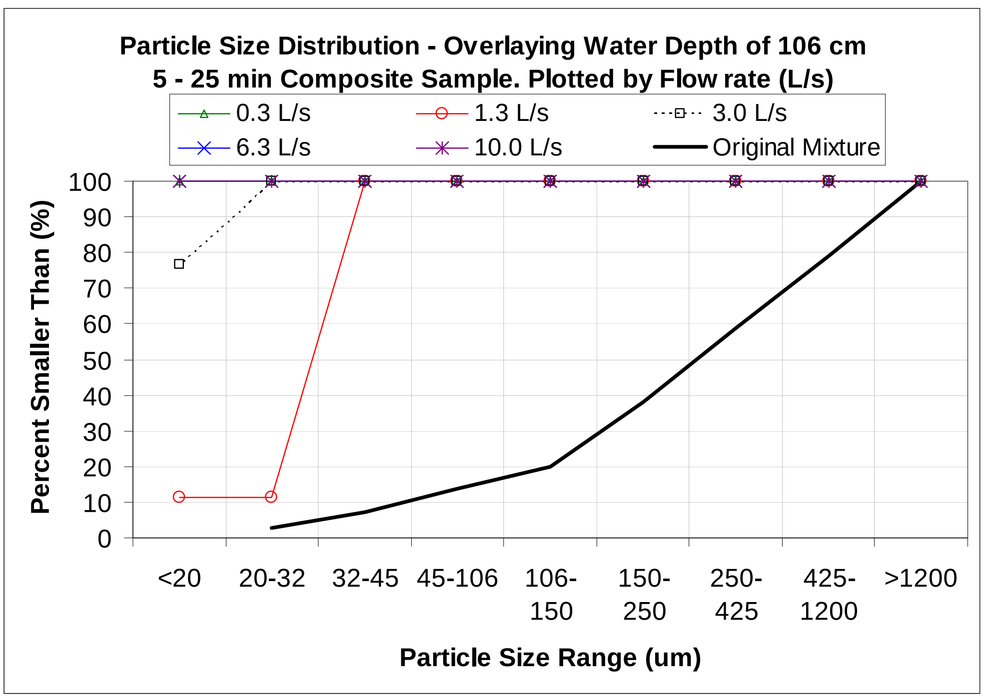

Figure H.4. PSD of scoured sediment mixture mass at 106 cm below the outlet.

APPENDIX I

STATISTICAL SUMMARY OF SUSPENDED SEDIMENT CONCENTRATION OBTAINED FROM SCOUR TESTS WITH HOMOGENOUS SEDIMENT MATERIAL

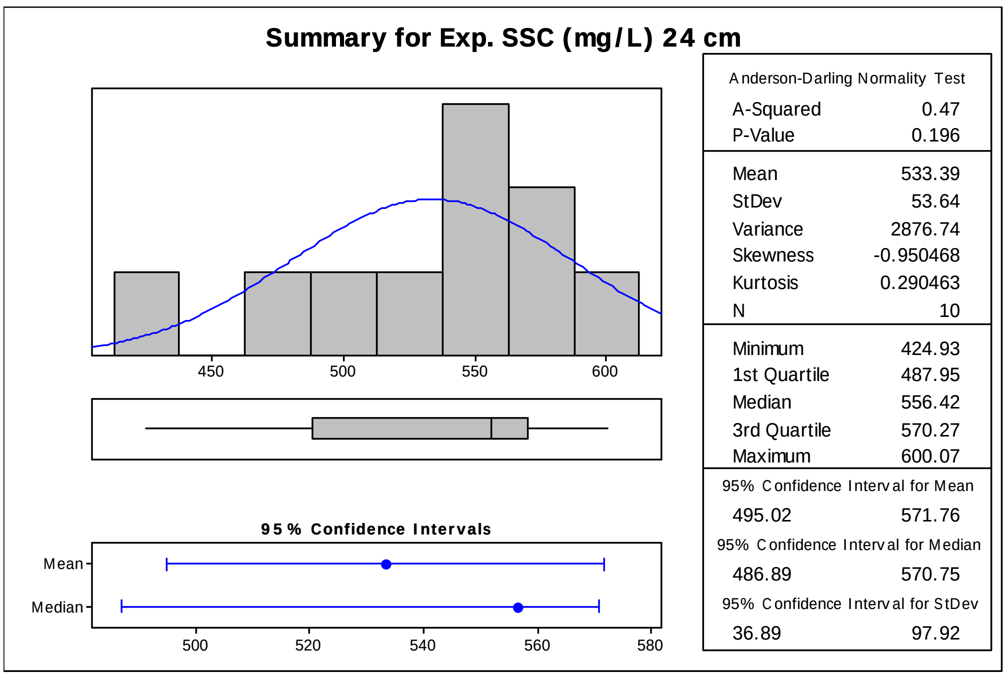

Figure I.1. SSC (mg/L) obtained from scour tests with sediment with a homogeneous particle size of 180 µm at 24 cm below the outlet, 10 L/s flow rate, and a 50-cm wide rectangular inlet.

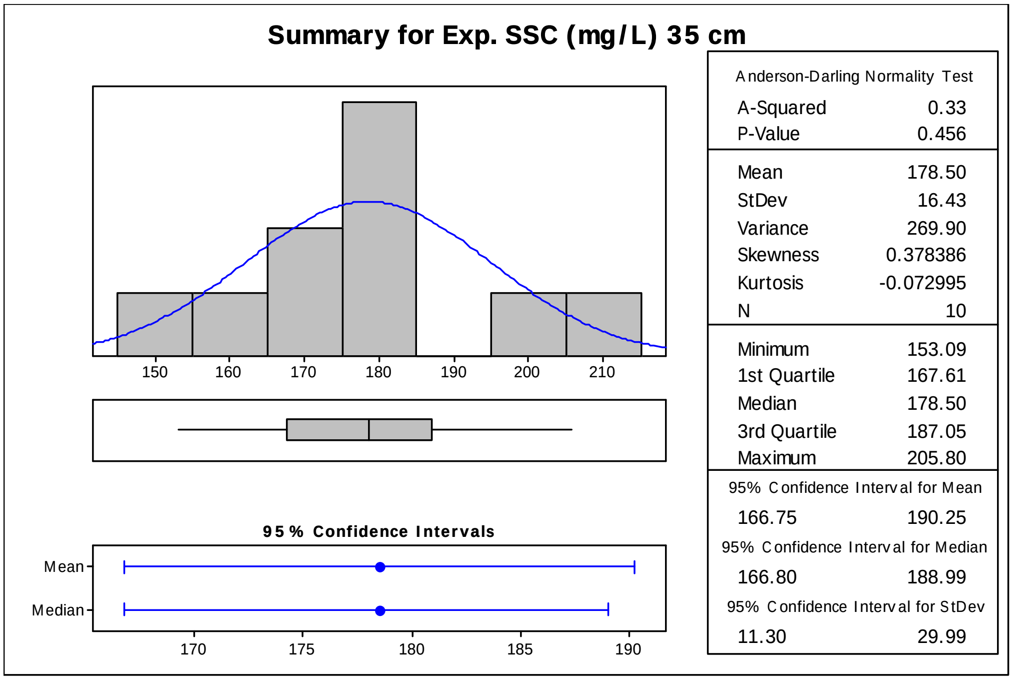

Figure I.2. SSC (mg/L) obtained from scour tests with sediment with a homogeneous particle size of 180 µm at 35 cm below the outlet, 10 L/s flow rate, and a 50-cm wide rectangular inlet.

APPENDIX J

STATISTICAL SUMMARY OF PERCENTAGE OF ERROR TOLERANCE OBTAINED FROM SCOUR TESTS WITH HOMOGENOUS SEDIMENT MATERIAL

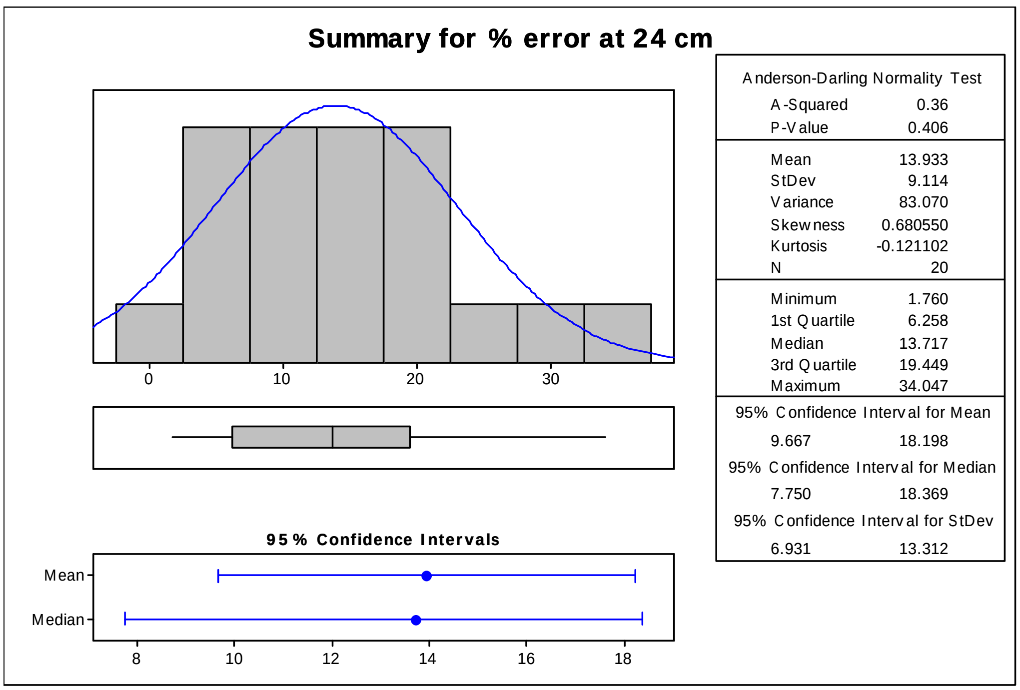

Figure J.1. Percentage of error obtained from scour tests with sediment with a homogeneous particle size of 180 μm at 24 cm below the outlet, 10 L/s flow rate.

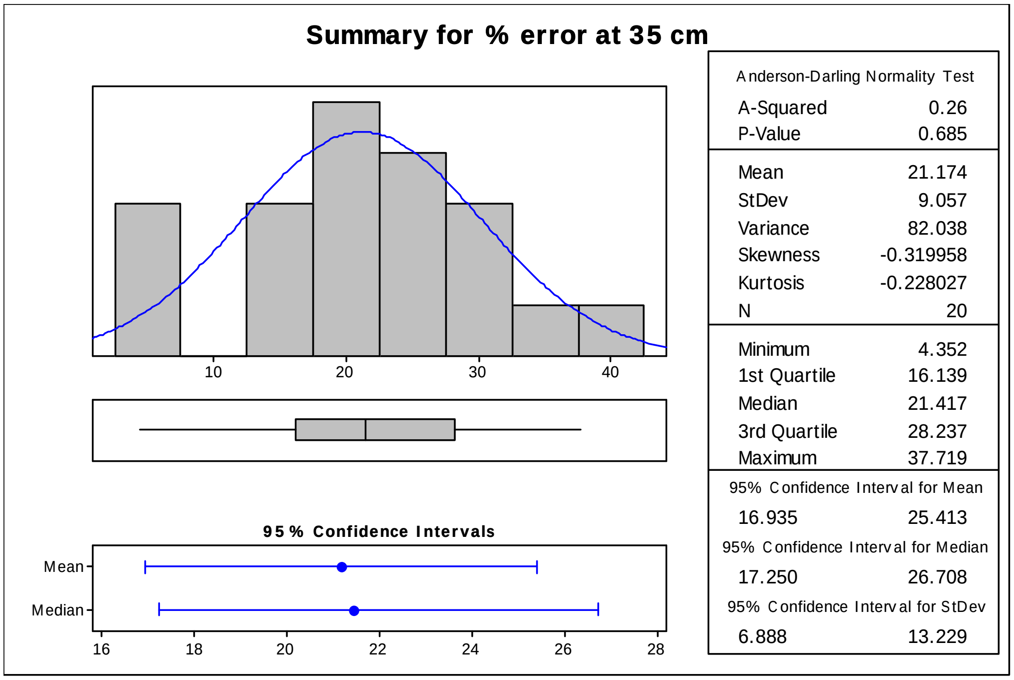

Figure J.2. Percentage of error obtained from scour tests with sediment with a homogeneous particle size of 180 µm at 35 cm below the outlet, 10 L/s flow rate.

APPENDIX K

REGRESSION FIT AND ANOVA OF SSC AS A FUNCTION OF THE OVERLAYING WATER DEPTH – SCOUR TEST WITH SEDIMENT MIXTURE

Table K.1. SSC as a Function of Overlaying Water Depth for 0-5 min Composite Samples at 0.3 L/s Flow Rate

Bivariate Fit of SSC (mg/L) 0-5 min By Depth (cm) Flow rate (L/s)=0.3

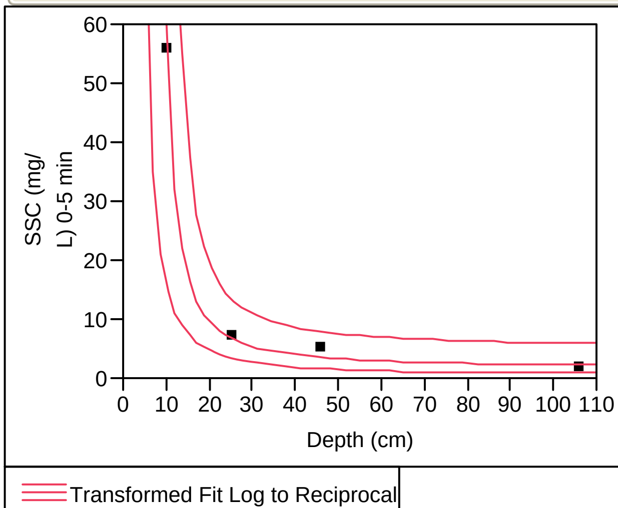

Transformed Fit Log to Reciprocal

Log(SSC (mg/L) 0-5 min) = 0.4776149 + 35.965984*Recip(Depth (cm))

Summary of Fit

RSquare	0.968043
RSquare Adj	0.952064
Root Mean Square Error	0.321352
Mean of Response	2.016717
Observations (or Sum Wgts)	4

Analysis of Variance

Source	DF	Sum of Squares	Mean Square	F Ratio
Model	1	6.2563063	6.25631	60.5837
Error	2	0.2065345	0.10327	**Prob > F**
C. Total	3	6.4628408		0.0161*

Parameter Estimates

Term	Estimate	Std Error	t Ratio	Prob>|t|
Intercept	0.4776149	0.254788	1.87	0.2017
Recip(Depth (cm))	35.965984	4.620769	7.78	0.0161*

Fit Measured on Original Scale

Sum of Squared Error	12.404289
Root Mean Square Error	2.4904105
RSquare	0.9937122
Sum of Residuals	-2.178921

Table K.2. SSC as a Function of Overlaying Water Depth for 0-5 min Composite Samples at 1.3 L/s Flow Rate

Bivariate Fit of SSC (mg/L) 0-5 min By Depth (cm) Flow rate (L/s)=1.3

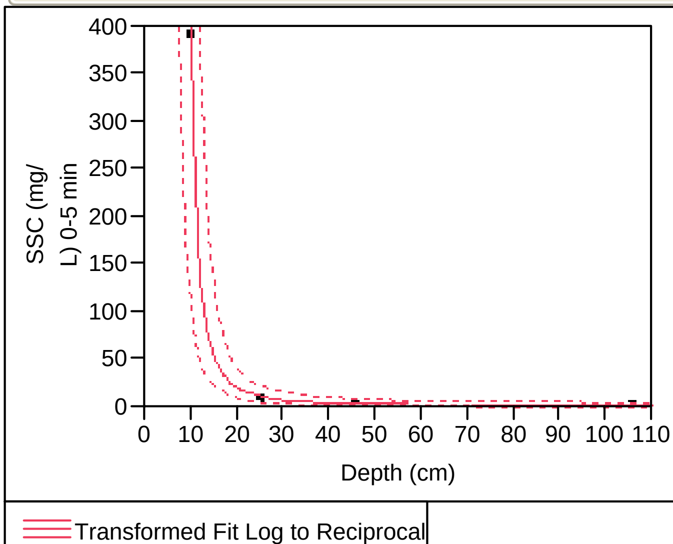

Transformed Fit Log to Reciprocal

Log(SSC (mg/L) 0-5 min) = 0.1756314 + 56.733546*Recip(Depth (cm))

Summary of Fit

RSquare	0.987191
RSquare Adj	0.980787
Root Mean Square Error	0.317795
Mean of Response	2.603446
Observations (or Sum Wgts)	4

Analysis of Variance

Source	DF	Sum of Squares	Mean Square	F Ratio
Model	1	15.567324	15.5673	154.1418
Error	2	0.201987	0.1010	**Prob > F**
C. Total	3	15.769311		0.0064*

Parameter Estimates

Term	Estimate	Std Error	t Ratio	Prob>|t|
Intercept	0.1756314	0.251968	0.70	0.5579
Recip(Depth (cm))	56.733546	4.569615	12.42	0.0064*

Fit Measured on Original Scale

Sum of Squared Error	2025.3096
Root Mean Square Error	31.822237
RSquare	0.9819572
Sum of Residuals	41.91298

Table K.3. SSC as a Function of Overlaying Water Depth for 0-5 min Composite Samples at 3 L/s Flow Rate

Bivariate Fit of SSC (mg/L) 0-5 min By Depth (cm) Flow rate (L/s)=3

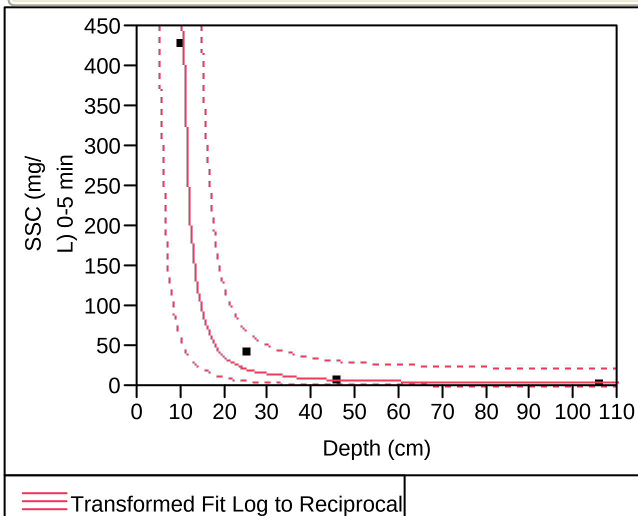

Transformed Fit Log to Reciprocal

Log(SSC (mg/L) 0-5 min) = 0.9462213 + 53.031859*Recip(Depth (cm))

Summary of Fit

RSquare	0.958103
RSquare Adj	0.937155
Root Mean Square Error	0.545347
Mean of Response	3.215628
Observations (or Sum Wgts)	4

Analysis of Variance

Source	DF	Sum of Squares	Mean Square	F Ratio
Model	1	13.602158	13.6022	45.7364
Error	2	0.594807	0.2974	**Prob > F**
C. Total	3	14.196965		0.0212*

Parameter Estimates

Term	Estimate	Std Error	t Ratio	Prob>|t|
Intercept	0.9462213	0.432386	2.19	0.1601
Recip(Depth (cm))	53.031859	7.841624	6.76	0.0212*

Fit Measured on Original Scale

Sum of Squared Error	8739.1932
Root Mean Square Error	66.102924
RSquare	0.9309367
Sum of Residuals	-73.42362

Table K.4. SSC as a Function of Overlaying Water Depth for 0-5 min Composite Samples at 6.3 L/s Flow Rate

Bivariate Fit of SSC (mg/L) 0-5 min By Depth (cm) Flow rate (L/s)=6.3

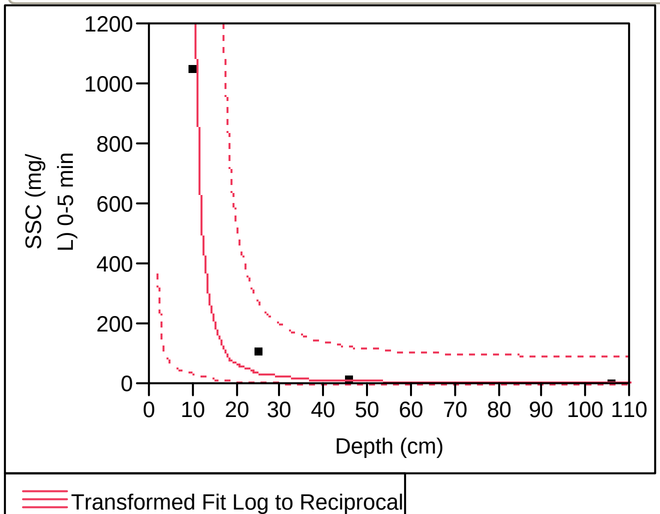

Transformed Fit Log to Reciprocal

Log(SSC (mg/L) 0-5 min) = 1.174505 + 61.313418*Recip(Depth (cm))

Summary of Fit

RSquare	0.913849
RSquare Adj	0.870774
Root Mean Square Error	0.925764
Mean of Response	3.798307
Observations (or Sum Wgts)	4

Analysis of Variance

Source	DF	Sum of Squares	Mean Square	F Ratio
Model	1	18.182147	18.1821	21.2151
Error	2	1.714077	0.8570	**Prob > F**
C. Total	3	19.896224		0.0440*

Parameter Estimates

Term	Estimate	Std Error	t Ratio	Prob>|t|
Intercept	1.174505	0.734004	1.60	0.2507
Recip(Depth (cm))	61.313418	13.31169	4.61	0.0440*

Fit Measured on Original Scale

Sum of Squared Error	202526.76
Root Mean Square Error	318.21907
RSquare	0.7342243
Sum of Residuals	-376.7257

Table K.5. SSC as a Function of Overlaying Water Depth for 0-5 min Composite Samples at 10 L/s Flow Rate

Bivariate Fit of SSC (mg/L) 0-5 min By Depth (cm) Flow rate (L/s)=10

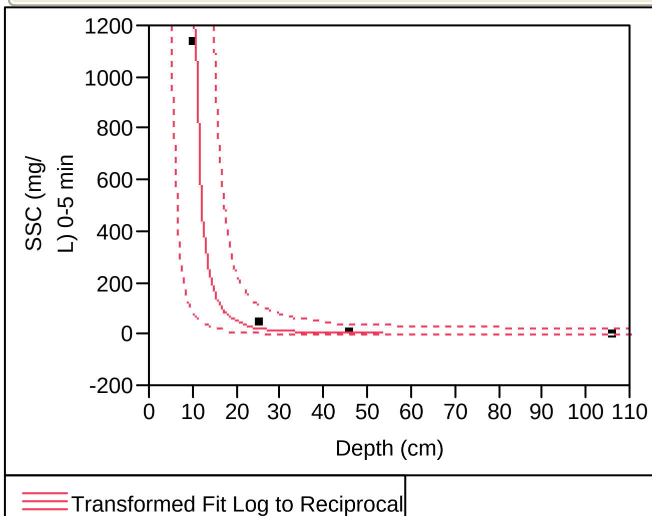

Transformed Fit Log to Reciprocal

Log(SSC (mg/L) 0-5 min) = 0.5722034 + 67.070908*Recip(Depth (cm))

Summary of Fit

RSquare	0.957672
RSquare Adj	0.936509
Root Mean Square Error	0.693409
Mean of Response	3.442387
Observations (or Sum Wgts)	4

Analysis of Variance

Source	DF	Sum of Squares	Mean Square	F Ratio
Model	1	21.757174	21.7572	45.2505
Error	2	0.961632	0.4808	**Prob > F**
C. Total	3	22.718805		0.0214*

Parameter Estimates

Term	Estimate	Std Error	t Ratio	Prob>|t|
Intercept	0.5722034	0.549778	1.04	0.4073
Recip(Depth (cm))	67.070908	9.970623	6.73	0.0214*

Fit Measured on Original Scale

Sum of Squared Error	97468.682
Root Mean Square Error	220.75856
RSquare	0.8963133
Sum of Residuals	-289.6289

Table K.6. SSC as a Function of Overlaying Water Depth for 5-25 min Composite Samples at 0.3 L/s Flow Rate

Bivariate Fit of SSC (mg/L) 5-25 min By Depth (cm) Flow rate (L/s)=0.3

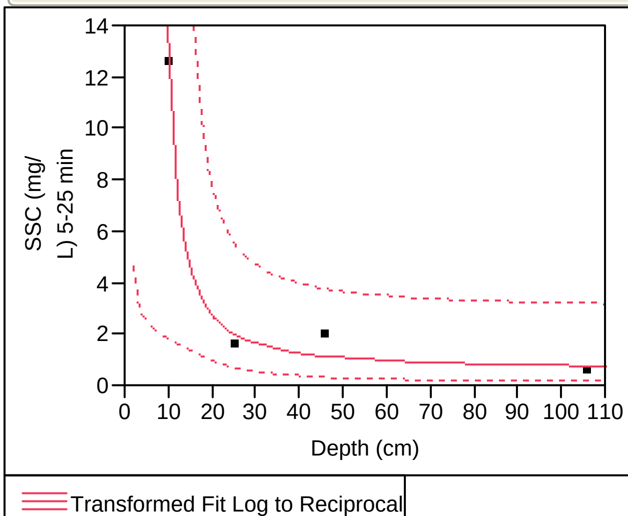

Transformed Fit Log to Reciprocal

Log(SSC (mg/L) 5-25 min) = -0.495989 + 30.203213*Recip(Depth (cm))

Summary of Fit

RSquare	0.910784
RSquare Adj	0.866176
Root Mean Square Error	0.464857
Mean of Response	0.796505
Observations (or Sum Wgts)	4

Analysis of Variance

Source	DF	Sum of Squares	Mean Square	F Ratio
Model	1	4.4120499	4.41205	20.4174
Error	2	0.4321848	0.21609	**Prob > F**
C. Total	3	4.8442347		0.0457*

Parameter Estimates

Term	Estimate	Std Error	t Ratio	Prob>|t|
Intercept	-0.495989	0.368568	-1.35	0.3107
Recip(Depth (cm))	30.203213	6.68425	4.52	0.0457*

Fit Measured on Original Scale

Sum of Squared Error	0.9318435
Root Mean Square Error	0.6825846
RSquare	0.9902035
Sum of Residuals	0.2951422

Table K.7. SSC as a Function of Overlaying Water Depth for 5-25 min Composite Samples at 1.3 L/s Flow Rate

Bivariate Fit of SSC (mg/L) 5-25 min By Depth (cm) Flow rate (L/s)=1.3

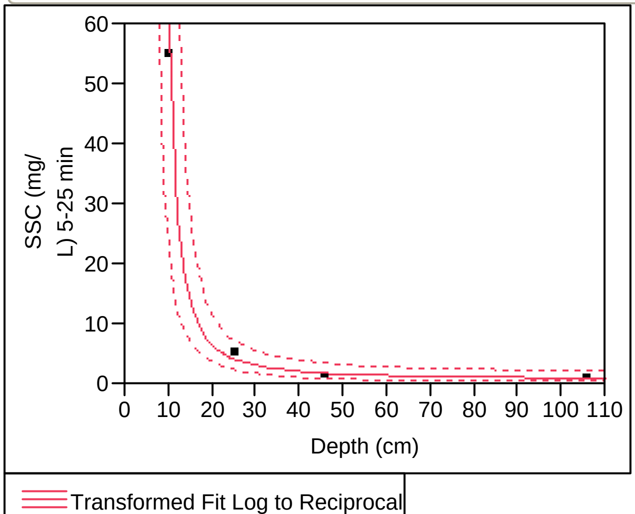

Transformed Fit Log to Reciprocal

Log(SSC (mg/L) 5-25 min) = -0.328878 + 43.970402*Recip(Depth (cm))

Summary of Fit

RSquare	0.986433
RSquare Adj	0.979649
Root Mean Square Error	0.253585
Mean of Response	1.552759
Observations (or Sum Wgts)	4

Analysis of Variance

Source	DF	Sum of Squares	Mean Square	F Ratio
Model	1	9.3509338	9.35093	145.4141
Error	2	0.1286111	0.06431	**Prob > F**
C. Total	3	9.4795449		0.0068*

Parameter Estimates

Term	Estimate	Std Error	t Ratio	Prob>|t|
Intercept	-0.328878	0.201058	-1.64	0.2435
Recip(Depth (cm))	43.970402	3.64634	12.06	0.0068*

Fit Measured on Original Scale

Sum of Squared Error	14.483461
Root Mean Square Error	2.6910464
RSquare	0.9929537
Sum of Residuals	-2.589594

Table K.8. SSC as a Function of Overlaying Water Depth for 5-25 min Composite Samples at 3.0 L/s Flow Rate

Bivariate Fit of SSC (mg/L) 5-25 min By Depth (cm) Flow rate (L/s)=3

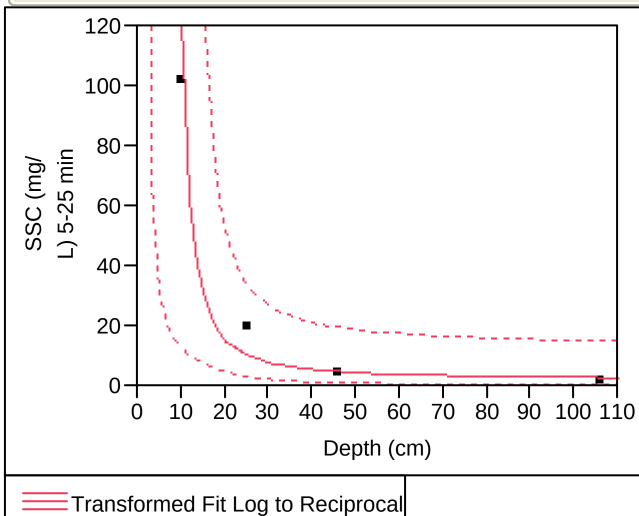

Transformed Fit Log to Reciprocal

Log(SSC (mg/L) 5-25 min) = 0.6982176 + 41.34753*Recip(Depth (cm))

Summary of Fit

RSquare	0.93209
RSquare Adj	0.898135
Root Mean Square Error	0.548832
Mean of Response	2.467614
Observations (or Sum Wgts)	4

Analysis of Variance

Source	DF	Sum of Squares	Mean Square	F Ratio
Model	1	8.2686243	8.26862	27.4508
Error	2	0.6024325	0.30122	**Prob > F**
C. Total	3	8.8710568		0.0346*

Parameter Estimates

Term	Estimate	Std Error	t Ratio	Prob>|t|
Intercept	0.6982176	0.435148	1.60	0.2498
Recip(Depth (cm))	41.34753	7.891728	5.24	0.0346*

Fit Measured on Original Scale

Sum of Squared Error	652.95689
Root Mean Square Error	18.068714
RSquare	0.9019684
Sum of Residuals	-15.59905

Table K.9. SSC as a Function of Overlaying Water Depth for 5-25 min Composite Samples at 6.3 L/s Flow Rate

Bivariate Fit of SSC (mg/L) 5-25 min By Depth (cm) Flow rate (L/s)=6.3

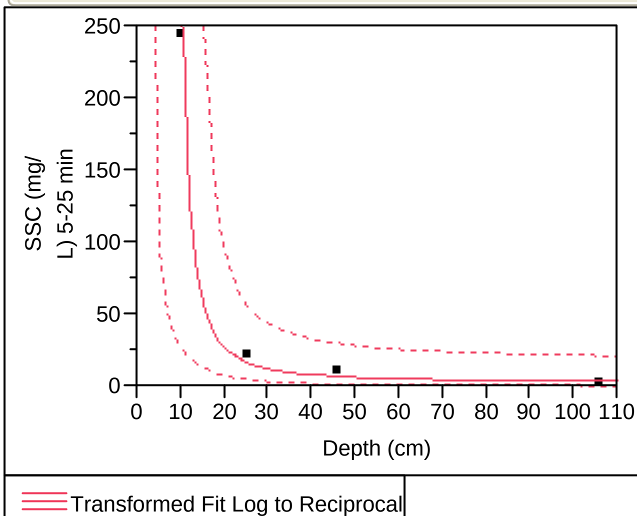

Transformed Fit Log to Reciprocal

Log(SSC (mg/L) 5-25 min) = 0.8847731 + 47.761867*Recip(Depth (cm))

Summary of Fit

RSquare	0.942154
RSquare Adj	0.913231
Root Mean Square Error	0.581981
Mean of Response	2.92866
Observations (or Sum Wgts)	4

Analysis of Variance

Source	DF	Sum of Squares	Mean Square	F Ratio
Model	1	11.033079	11.0331	32.5746
Error	2	0.677405	0.3387	**Prob > F**
C. Total	3	11.710483		0.0294*

Parameter Estimates

Term	Estimate	Std Error	t Ratio	Prob>|t|
Intercept	0.8847731	0.461431	1.92	0.1952
Recip(Depth (cm))	47.761867	8.368392	5.71	0.0294*

Fit Measured on Original Scale

Sum of Squared Error	1928.4352
Root Mean Square Error	31.051854
RSquare	0.9526416
Sum of Residuals	-35.3344

Table K.10. SSC as a Function of Overlaying Water Depth for 5-25 min Composite Samples at 10 L/s Flow Rate

Bivariate Fit of SSC (mg/L) 5-25 min By Depth (cm) Flow rate (L/s)=10

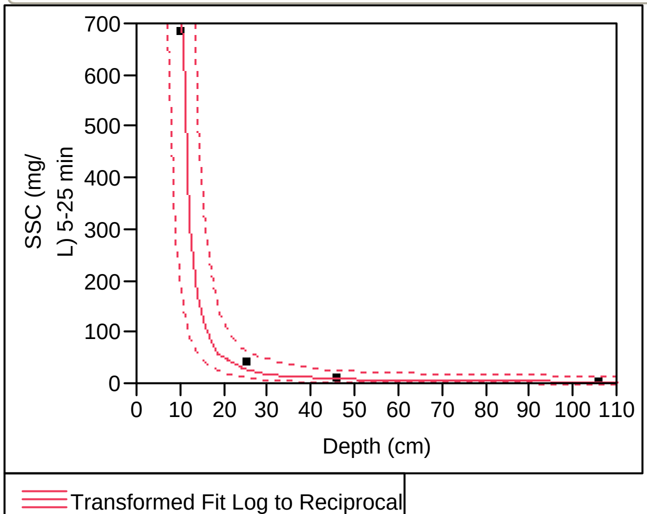

Transformed Fit Log to Reciprocal

Log(SSC (mg/L) 5-25 min) = 1.1773341 + 54.940224*Recip(Depth (cm))

Summary of Fit

RSquare	0.980792
RSquare Adj	0.971188
Root Mean Square Error	0.378091
Mean of Response	3.528406
Observations (or Sum Wgts)	4

Analysis of Variance

Source	**DF**	**Sum of Squares**	**Mean Square**	**F Ratio**
Model	1	14.598726	14.5987	102.1226
Error	2	0.285906	0.1430	**Prob > F**
C. Total	3	14.884632		0.0097*

Parameter Estimates

Term	**Estimate**	**Std Error**	**t Ratio**	**Prob>|t|**
Intercept	1.1773341	0.299774	3.93	0.0591
Recip(Depth (cm))	54.940224	5.436625	10.11	0.0097*

Fit Measured on Original Scale

Sum of Squared Error	11449.453
Root Mean Square Error	75.661923
RSquare	0.9654459
Sum of Residuals	-92.15397

APPENDIX L

ONE-WAY ANOVA WITH PAIRED COMPARISON OF OVERLAYING WATER DEPTH – SCOUR TESTS WITH A SEDIMENT MIXURE

Table L.1. One-Way ANOVA for Overlaying Water Depth: Evaluating Log(SSC) for 0-5 min Composite Samples

Oneway Analysis of Log(SSC) 0-5 min By Depth (cm)

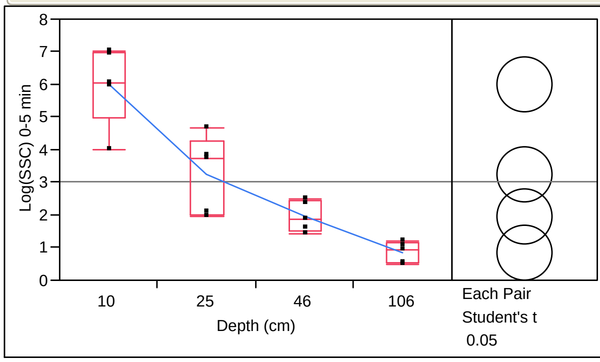

Oneway Anova

Summary of Fit

Rsquare	0.851937
Adj Rsquare	0.824176
Root Mean Square Error	0.897546
Mean of Response	3.015297
Observations (or Sum Wgts)	20

Analysis of Variance

Source	DF	Sum of Squares	Mean Square	F Ratio	Prob > F
Depth (cm)	3	74.164423	24.7215	30.6874	<.0001*
Error	16	12.889428	0.8056		
C. Total	19	87.053852			

Means for Oneway Anova

Level	Number	Mean	Std Error	Lower 95%	Upper 95%
10	5	6.00673	0.40139	5.1558	6.8576
25	5	3.25720	0.40139	2.4063	4.1081
46	5	1.94568	0.40139	1.0948	2.7966
106	5	0.85159	0.40139	0.00067	1.7025

Std Error uses a pooled estimate of error variance

Means Comparisons

Comparisons for each pair using Student's t

t	Alpha
2.11991	0.05

Abs(Dif)-LSD

	10	25	46	106
10	-1.2034	1.5461	2.8577	3.9518
25	1.5461	-1.2034	0.1081	1.2022
46	2.8577	0.1081	-1.2034	-0.1093
106	3.9518	1.2022	-0.1093	-1.2034

Positive values show pairs of means that are significantly different.

Level				Mean
10	A			6.0067254
25		B		3.2571967
46			C	1.9456791
106			C	0.8515865

Levels not connected by same letter are significantly different.

Level	- Level	Difference	Lower CL	Upper CL	p-Value
10	106	5.155139	3.95176	6.358520	<.0001*
10	46	4.061046	2.85766	5.264428	<.0001*
10	25	2.749529	1.54615	3.952910	0.0002*
25	106	2.405610	1.20223	3.608992	0.0006*
25	46	1.311518	0.10814	2.514899	0.0345*
46	106	1.094093	-0.10929	2.297474	0.0719

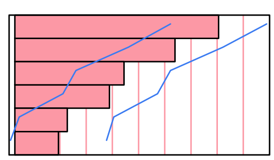

Table L.2. One-Way ANOVA for Overlaying Water Depth: Evaluating Log(Mass Load) for 0-5 min Composite Samples

Oneway Analysis of Log(Mass Load) 0-5 min By Depth (cm)

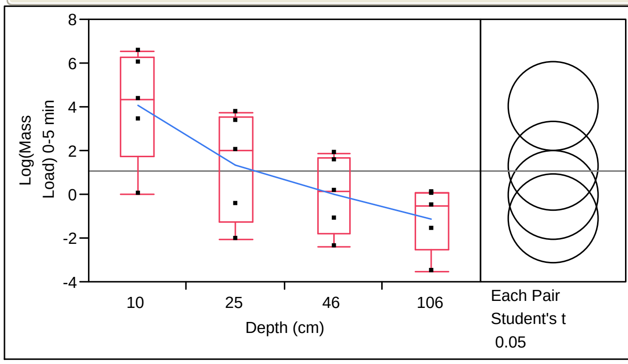

Oneway Anova

Summary of Fit

Rsquare	0.501683
Adj Rsquare	0.408248
Root Mean Square Error	2.145735
Mean of Response	1.061914
Observations (or Sum Wgts)	20

Analysis of Variance

Source	DF	Sum of Squares	Mean Square	F Ratio	Prob > F
Depth (cm)	3	74.16442	24.7215	5.3694	0.0095*
Error	16	73.66689	4.6042		
C. Total	19	147.83132			

Means for Oneway Anova

Level	Number	Mean	Std Error	Lower 95%	Upper 95%
10	5	4.0533	0.95960	2.019	6.0876
25	5	1.3038	0.95960	-0.730	3.3381
46	5	-0.0077	0.95960	-2.042	2.0266
106	5	-1.1018	0.95960	-3.136	0.9325

Std Error uses a pooled estimate of error variance

Means Comparisons

Comparisons for each pair using Student's t

t	Alpha
2.11991	0.05

Abs(Dif)-LSD

	10	25	46	106
10	-2.8769	-0.1274	1.1842	2.2783
25	-0.1274	-2.8769	-1.5654	-0.4713
46	1.1842	-1.5654	-2.8769	-1.7828
106	2.2783	-0.4713	-1.7828	-2.8769

Positive values show pairs of means that are significantly different.

Level			Mean
10	A		4.053342
25	A	B	1.303814
46		B	-0.007704
106		B	-1.101796

Levels not connected by same letter are significantly different.

Level	- Level	Difference	Lower CL	Upper CL	p-Value
10	106	5.155139	2.27825	8.032025	0.0016*
10	46	4.061046	1.18416	6.937932	0.0086*
10	25	2.749529	-0.12736	5.626415	0.0598
25	106	2.405610	-0.47128	5.282496	0.0953
25	46	1.311518	-1.56537	4.188403	0.3482
46	106	1.094093	-1.78279	3.970979	0.4319

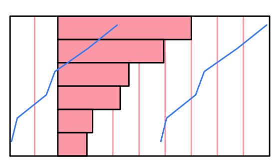

Table L.3. One-Way ANOVA for Overlaying Water Depth: Evaluating Log(SSC) for 5-25 min Composite Samples

Oneway Analysis of Log(SSC) 5-25 min By Depth (cm)

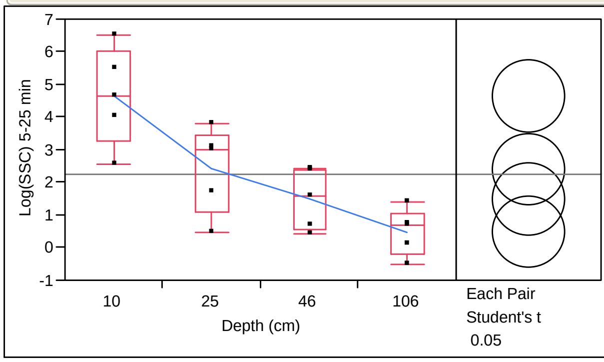

Oneway Anova

Summary of Fit

Rsquare	0.68557
Adj Rsquare	0.626614
Root Mean Square Error	1.162386
Mean of Response	2.254789
Observations (or Sum Wgts)	20

Analysis of Variance

Source	DF	Sum of Squares	Mean Square	F Ratio	Prob > F
Depth (cm)	3	47.135434	15.7118	11.6286	0.0003*
Error	16	21.618251	1.3511		
C. Total	19	68.753685			

Means for Oneway Anova

Level	Number	Mean	Std Error	Lower 95%	Upper 95%
10	5	4.63740	0.51983	3.535	5.7394
25	5	2.40804	0.51983	1.306	3.5100
46	5	1.49254	0.51983	0.391	2.5945
106	5	0.48117	0.51983	-0.621	1.5832

Std Error uses a pooled estimate of error variance

Means Comparisons

Comparisons for each pair using Student's t

t	Alpha
2.11991	0.05

Abs(Dif)-LSD

	10	25	46	106
10	-1.5585	0.6709	1.5864	2.5978
25	0.6709	-1.5585	-0.6430	0.3684
46	1.5864	-0.6430	-1.5585	-0.5471
106	2.5978	0.3684	-0.5471	-1.5585

Positive values show pairs of means that are significantly different.

Level				Mean
10	A			4.6374050
25		B		2.4080402
46		B	C	1.4925376
106			C	0.4811727

Levels not connected by same letter are significantly different.

Level	- Level	Difference	Lower CL	Upper CL	p-Value
10	106	4.156232	2.59777	5.714696	<.0001*
10	46	3.144867	1.58640	4.703331	0.0006*
10	25	2.229365	0.67090	3.787829	0.0079*
25	106	1.926867	0.36840	3.485331	0.0185*
46	106	1.011365	-0.54710	2.569829	0.1879
25	46	0.915503	-0.64296	2.473966	0.2309

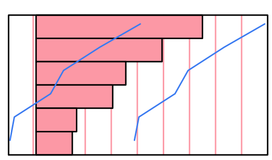

Table L.4. One-Way ANOVA for Overlaying Water Depth: Evaluating Log(Mass Load) for 5-25 min Composite Samples

Oneway Analysis of Log(Mass Load) 5-25 min By Depth (cm)

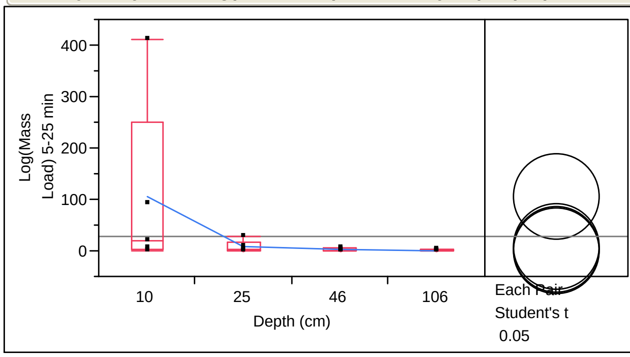

Oneway Anova

Summary of Fit

Rsquare	0.240285
Adj Rsquare	0.097838
Root Mean Square Error	87.46915
Mean of Response	28.97424
Observations (or Sum Wgts)	20

Analysis of Variance

Source	DF	Sum of Squares	Mean Square	F Ratio	Prob > F
Depth (cm)	3	38717.36	12905.8	1.6868	0.2098
Error	16	122413.64	7650.9		
C. Total	19	161131.00			

Means for Oneway Anova

Level	Number	Mean	Std Error	Lower 95%	Upper 95%
10	5	105.049	39.117	22.12	187.97
25	5	7.755	39.117	-75.17	90.68
46	5	2.360	39.117	-80.56	85.29
106	5	0.733	39.117	-82.19	83.66

Std Error uses a pooled estimate of error variance

Means Comparisons

Comparisons for each pair using Student's t

t	Alpha
2.11991	0.05

Abs(Dif)-LSD

	10	25	46	106
10	-117.27	-19.98	-14.59	-12.96
25	-19.98	-117.27	-111.88	-110.25
46	-14.59	-111.88	-117.27	-115.65
106	-12.96	-110.25	-115.65	-117.27

Positive values show pairs of means that are significantly different.

Level		Mean
10	A	105.04880
25	A	7.75495
46	A	2.36033
106	A	0.73288

Levels not connected by same letter are significantly different.

Level	- Level	Difference	Lower CL	Upper CL	p-Value
10	106	104.3159	-12.958	221.5898	0.0776
10	46	102.6885	-14.585	219.9624	0.0819
10	25	97.2939	-19.980	214.5678	0.0977
25	106	7.0221	-110.252	124.2960	0.9006
25	46	5.3946	-111.879	122.6685	0.9235
46	106	1.6274	-115.646	118.9013	0.9769

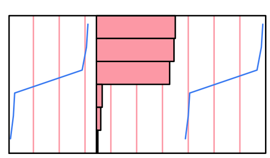

APPENDIX M

REGRESSION FIT AND ANOVA OF SSC AS A FUNCTION OF FLOW RATE – SCOUR TEST WITH A SEDIMENT MIXTURE

Table M.1. SSC as a Function of Flow Rate for 0-5 min Composite Samples with Sediment Mixture at 10 cm below the Outlet

Bivariate Fit of SSC (mg/L) 0-5 min By Flow rate (L/s) Depth (cm)=10

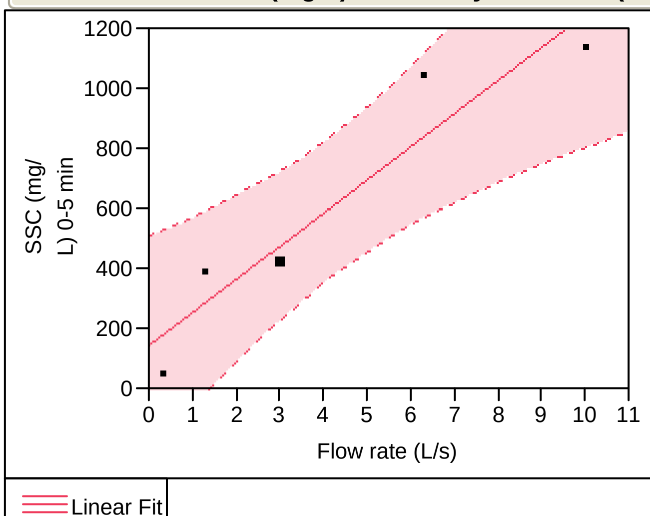

Linear Fit

SSC (mg/L) 0-5 min = 148.19136 + 110.80991*Flow rate (L/s)

Summary of Fit

RSquare	0.90446
RSquare Adj	0.872613
Root Mean Square Error	165.1805
Mean of Response	611.3768
Observations (or Sum Wgts)	5

Analysis of Variance

Source	DF	Sum of Squares	Mean Square	F Ratio
Model	1	774892.81	774893	28.4004
Error	3	81853.76	27285	**Prob > F**
C. Total	4	856746.57		0.0129*

Parameter Estimates

Term	Estimate	Std Error	t Ratio	Prob>|t|
Intercept	148.19136	114.0661	1.30	0.2847
Flow rate (L/s)	110.80991	20.79297	5.33	0.0129*

Table M.2. SSC as a Function of Flow Rate for 0-5 min Composite Samples with Sediment Mixture at 25 cm below the Outlet

Bivariate Fit of SSC (mg/L) 0-5 min By Flow rate (L/s) Depth (cm)=25

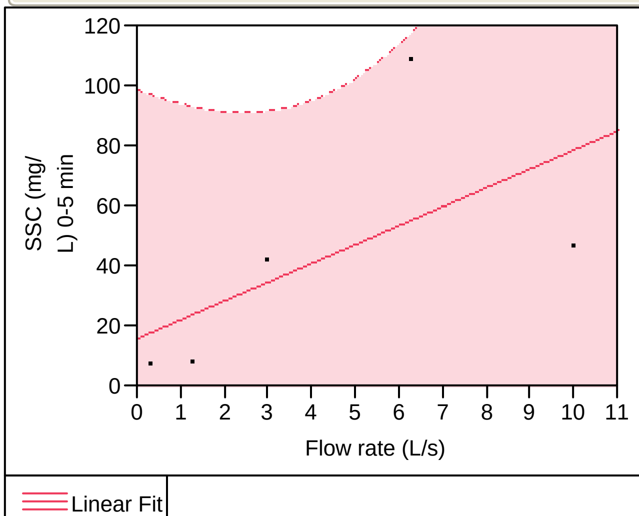

Linear Fit

SSC (mg/L) 0-5 min = 15.825007 + 6.3446151*Flow rate (L/s)

Summary of Fit

RSquare	0.373107
RSquare Adj	0.164143
Root Mean Square Error	37.71958
Mean of Response	42.3455
Observations (or Sum Wgts)	5

Analysis of Variance

Source	DF	Sum of Squares	Mean Square	F Ratio
Model	1	2540.3583	2540.36	1.7855
Error	3	4268.2995	1422.77	**Prob > F**
C. Total	4	6808.6578		0.2738

Parameter Estimates

Term	Estimate	Std Error	t Ratio	Prob>|t|
Intercept	15.825007	26.04741	0.61	0.5864
Flow rate (L/s)	6.3446151	4.748152	1.34	0.2738

Table M.3. SSC as a Function of Flow Rate for 0-5 min Composite Samples with Sediment Mixture at 46 cm below the Outlet

Bivariate Fit of SSC (mg/L) 0-5 min By Flow rate (L/s) Depth (cm)=46

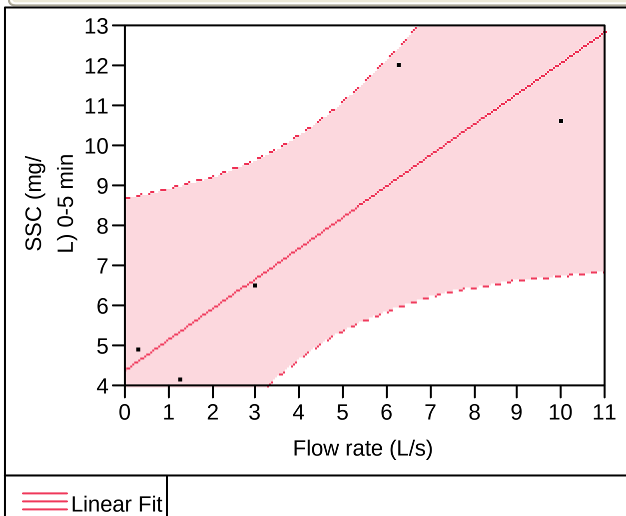

Linear Fit

SSC (mg/L) 0-5 min = 4.4083874 + 0.7709853*Flow rate (L/s)

Summary of Fit

RSquare	0.764481
RSquare Adj	0.685974
Root Mean Square Error	1.962717
Mean of Response	7.631106
Observations (or Sum Wgts)	5

Analysis of Variance

Source	DF	Sum of Squares	Mean Square	F Ratio
Model	1	37.512554	37.5126	9.7378
Error	3	11.556777	3.8523	**Prob > F**
C. Total	4	49.069331		0.0524

Parameter Estimates

Term	Estimate	Std Error	t Ratio	Prob>|t|
Intercept	4.4083874	1.355363	3.25	0.0474*
Flow rate (L/s)	0.7709853	0.247067	3.12	0.0524

Table M.4. SSC as a Function of Flow Rate for 0-5 min Composite Samples with Sediment Mixture at 106 cm below the Outlet

Bivariate Fit of SSC (mg/L) 0-5 min By Flow rate (L/s) Depth (cm)=106

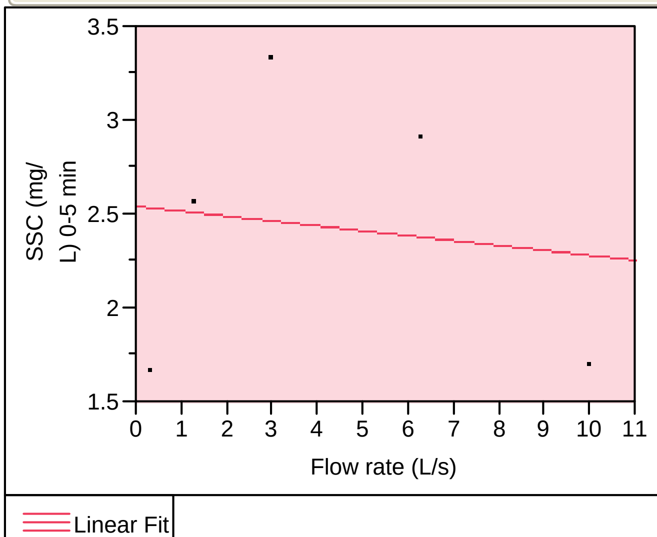

Linear Fit

SSC (mg/L) 0-5 min = 2.5487151 - 0.0269363*Flow rate (L/s)

Summary of Fit

RSquare	0.020994
RSquare Adj	-0.30534
Root Mean Square Error	0.843645
Mean of Response	2.436121
Observations (or Sum Wgts)	5

Analysis of Variance

Source	DF	Sum of Squares	Mean Square	F Ratio
Model	1	0.0457888	0.045789	0.0643
Error	3	2.1352081	0.711736	**Prob > F**
C. Total	4	2.1809970		0.8162

Parameter Estimates

Term	Estimate	Std Error	t Ratio	Prob>|t|
Intercept	2.5487151	0.582582	4.37	0.0221*
Flow rate (L/s)	-0.026936	0.106198	-0.25	0.8162

Table M.5. SSC as a Function of Flow Rate for 5-25 min Composite Samples with Sediment Mixture at 10 cm below the Outlet

Bivariate Fit of SSC (mg/L) 5-25 min By Flow rate (L/s) Depth (cm)=10

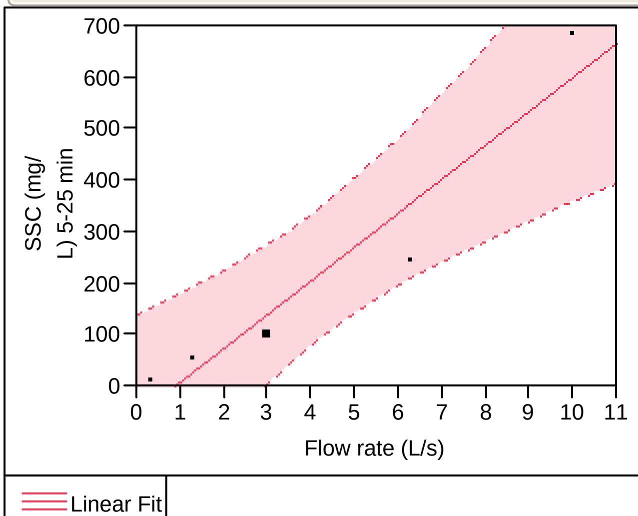

Linear Fit

SSC (mg/L) 5-25 min = -56.71262 + 66.050865*Flow rate (L/s)

Summary of Fit

RSquare	0.918797
RSquare Adj	0.89173
Root Mean Square Error	90.06075
Mean of Response	219.38
Observations (or Sum Wgts)	5

Analysis of Variance

Source	DF	Sum of Squares	Mean Square	F Ratio
Model	1	275322.33	275322	33.9446
Error	3	24332.82	8111	**Prob > F**
C. Total	4	299655.15		0.0101*

Parameter Estimates

Term	Estimate	Std Error	t Ratio	Prob>|t|
Intercept	-56.71262	62.19183	-0.91	0.4291
Flow rate (L/s)	66.050865	11.33687	5.83	0.0101*

Table M.6. SSC as a Function of Flow Rate for 5-25 min Composite Samples with Sediment Mixture at 25 cm below the Outlet

Bivariate Fit of SSC (mg/L) 5-25 min By Flow rate (L/s) Depth (cm)=25

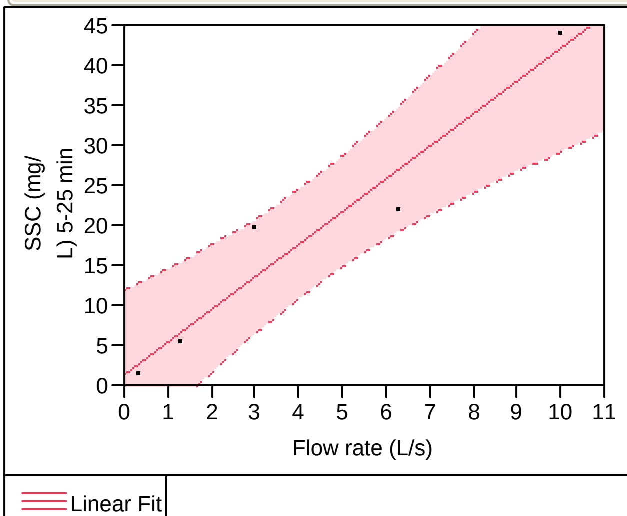

Linear Fit

SSC (mg/L) 5-25 min = 1.542993 + 4.0806237*Flow rate (L/s)

Summary of Fit

RSquare	0.938705
RSquare Adj	0.918273
Root Mean Square Error	4.78253
Mean of Response	18.6
Observations (or Sum Wgts)	5

Analysis of Variance

Source	DF	Sum of Squares	Mean Square	F Ratio
Model	1	1050.8422	1050.84	45.9433
Error	3	68.6178	22.87	**Prob > F**
C. Total	4	1119.4600		0.0066*

Parameter Estimates

Term	Estimate	Std Error	t Ratio	Prob>|t|
Intercept	1.542993	3.302596	0.47	0.6722
Flow rate (L/s)	4.0806237	0.602026	6.78	0.0066*

Table M.7. SSC as a Function of Flow Rate for 5-25 min Composite Samples with Sediment Mixture at 46 cm below the Outlet

Bivariate Fit of SSC (mg/L) 5-25 min By Flow rate (L/s) Depth (cm)=46

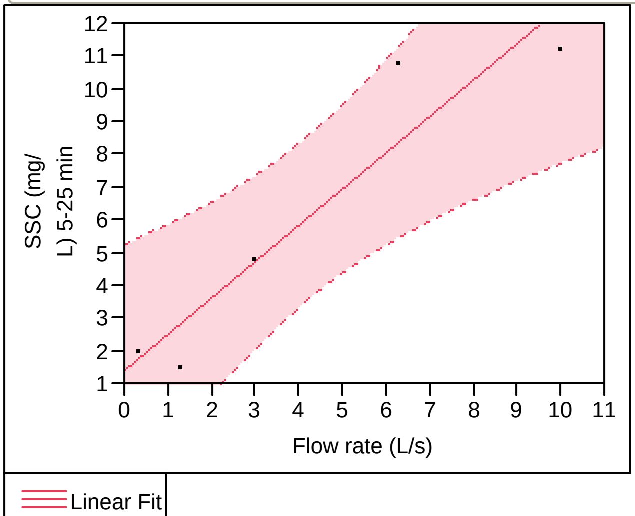

Linear Fit

SSC (mg/L) 5-25 min = 1.4012487 + 1.1145338*Flow rate (L/s)

Summary of Fit

RSquare	0.893334
RSquare Adj	0.857779
Root Mean Square Error	1.766366
Mean of Response	6.06
Observations (or Sum Wgts)	5

Analysis of Variance

Source	DF	Sum of Squares	Mean Square	F Ratio
Model	1	78.391850	78.3919	25.1252
Error	3	9.360150	3.1200	**Prob > F**
C. Total	4	87.752000		0.0153*

Parameter Estimates

Term	Estimate	Std Error	t Ratio	Prob>|t|
Intercept	1.4012487	1.219772	1.15	0.3339
Flow rate (L/s)	1.1145338	0.222351	5.01	0.0153*

Table M.8. SSC as a Function of Flow Rate for 5-25 min Composite Samples with Sediment Mixture at 106 cm below the Outlet

Bivariate Fit of SSC (mg/L) 5-25 min By Flow rate (L/s) Depth (cm)=106

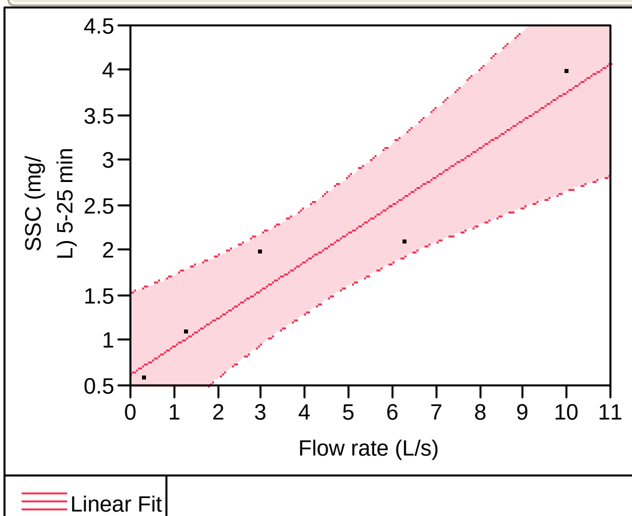

Linear Fit

SSC (mg/L) 5-25 min = 0.6435 + 0.3149521*Flow rate (L/s)

Summary of Fit

RSquare	0.924393
RSquare Adj	0.899191
Root Mean Square Error	0.413123
Mean of Response	1.96
Observations (or Sum Wgts)	5

Analysis of Variance

Source	DF	Sum of Squares	Mean Square	F Ratio
Model	1	6.2599888	6.25999	36.6788
Error	3	0.5120112	0.17067	**Prob > F**
C. Total	4	6.7720000		0.0090*

Parameter Estimates

Term	Estimate	Std Error	t Ratio	Prob>|t|
Intercept	0.6435	0.285284	2.26	0.1094
Flow rate (L/s)	0.3149521	0.052004	6.06	0.0090*

Table M.9. Mass Load as a Function of Flow Rate for 0-5 min Composite Samples with Sediment Mixture at 10 cm below the Outlet

Bivariate Fit of Mass Load (g/min) 0-5 min By Flow rate (L/s) Depth (cm)=10

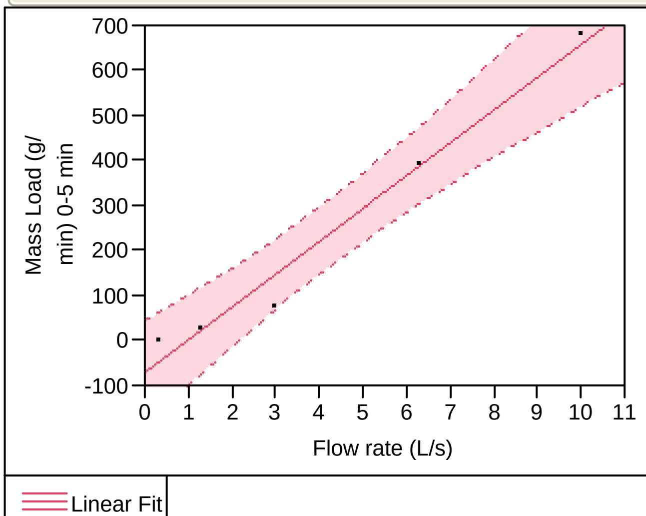

Linear Fit

Mass Load (g/min) 0-5 min = -69.42813 + 73.367783*Flow rate (L/s)

Summary of Fit

RSquare	0.976468
RSquare Adj	0.968624
Root Mean Square Error	52.23798
Mean of Response	237.2492
Observations (or Sum Wgts)	5

Analysis of Variance

Source	DF	Sum of Squares	Mean Square	F Ratio
Model	1	339699.74	339700	124.4866
Error	3	8186.42	2729	**Prob > F**
C. Total	4	347886.16		0.0015*

Parameter Estimates

Term	Estimate	Std Error	t Ratio	Prob>|t|
Intercept	-69.42813	36.07315	-1.92	0.1500
Flow rate (L/s)	73.367783	6.575733	11.16	0.0015*

Table M.10. Mass Load as a Function of Flow Rate for 0-5 min Composite Samples with Sediment Mixture at 25 cm below the Outlet

Bivariate Fit of Mass Load (g/min) 0-5 min By Flow rate (L/s) Depth (cm)=25

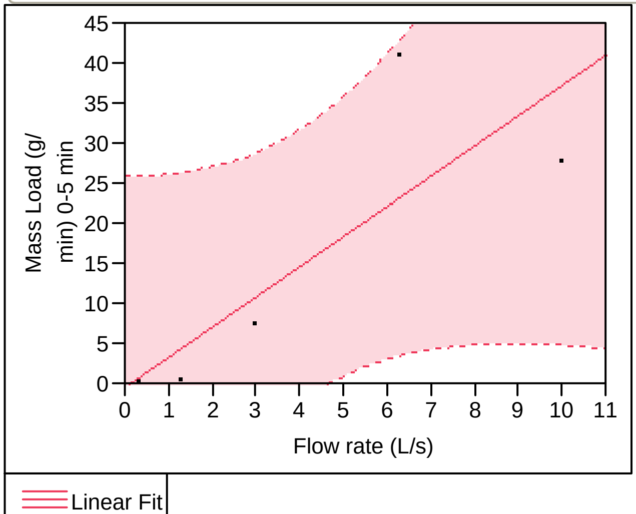

Linear Fit

Mass Load (g/min) 0-5 min = -0.328373 + 3.7687503*Flow rate (L/s)

Summary of Fit

RSquare	0.677577
RSquare Adj	0.570102
Root Mean Square Error	11.92375
Mean of Response	15.425
Observations (or Sum Wgts)	5

Analysis of Variance

Source	DF	Sum of Squares	Mean Square	F Ratio
Model	1	896.3531	896.353	6.3045
Error	3	426.5277	142.176	**Prob > F**
C. Total	4	1322.8808		0.0869

Parameter Estimates

Term	Estimate	Std Error	t Ratio	Prob>|t|
Intercept	-0.328373	8.233998	-0.04	0.9707
Flow rate (L/s)	3.7687503	1.500966	2.51	0.0869

Table M.11. Mass Load as a Function of Flow Rate for 0-5 min Composite Samples with Sediment Mixture at 46 cm below the Outlet

Bivariate Fit of Mass Load (g/min) 0-5 min By Flow rate (L/s) Depth (cm)=46

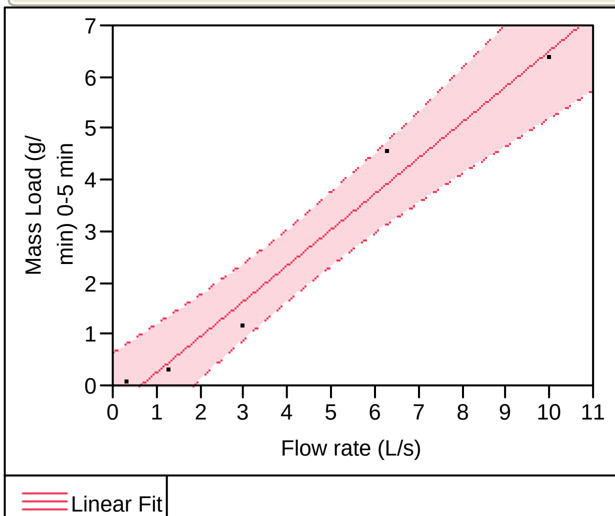

Linear Fit

Mass Load (g/min) 0-5 min = -0.41971 + 0.6979559*Flow rate (L/s)

Summary of Fit

RSquare	0.976798
RSquare Adj	0.969063
Root Mean Square Error	0.493371
Mean of Response	2.497745
Observations (or Sum Wgts)	5

Analysis of Variance

Source	DF	Sum of Squares	Mean Square	F Ratio
Model	1	30.742589	30.7426	126.2969
Error	3	0.730246	0.2434	**Prob > F**
C. Total	4	31.472835		0.0015*

Parameter Estimates

Term	Estimate	Std Error	t Ratio	Prob>|t|
Intercept	-0.41971	0.3407	-1.23	0.3057
Flow rate (L/s)	0.6979559	0.062106	11.24	0.0015*

Table M.12. Mass Load as a Function of Flow Rate for 0-5 min Composite Samples with Sediment Mixture at 106 cm below the Outlet

Bivariate Fit of Mass Load (g/min) 0-5 min By Flow rate (L/s) Depth (cm)=106

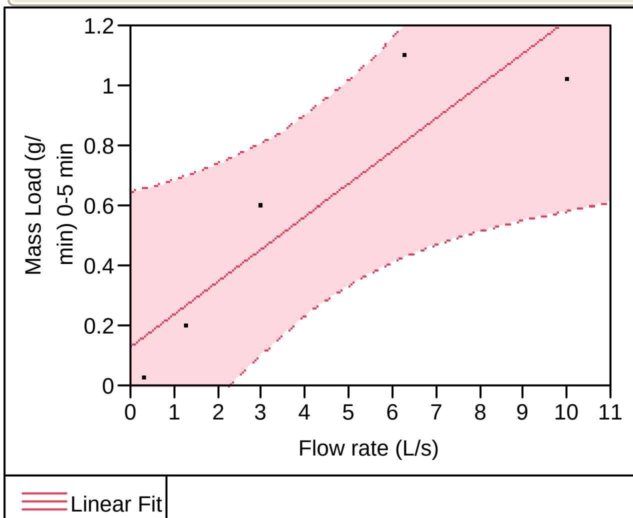

Linear Fit

Mass Load (g/min) 0-5 min = 0.1349592 + 0.1090003*Flow rate (L/s)

Summary of Fit

RSquare	0.820732
RSquare Adj	0.760977
Root Mean Square Error	0.233647
Mean of Response	0.590581
Observations (or Sum Wgts)	5

Analysis of Variance

Source	DF	Sum of Squares	Mean Square	F Ratio
Model	1	0.74979052	0.749791	13.7348
Error	3	0.16377217	0.054591	**Prob > F**
C. Total	4	0.91356269		0.0341*

Parameter Estimates

Term	Estimate	Std Error	t Ratio	Prob>|t|
Intercept	0.1349592	0.161346	0.84	0.4643
Flow rate (L/s)	0.1090003	0.029412	3.71	0.0341*

Table M.13. Mass Load as a Function of Flow Rate for 5-25 min Composite Samples with Sediment Mixture at 10 cm below the Outlet

Bivariate Fit of Mass Load (g/min) 5-25 min By Flow rate (L/s) Depth (cm)=10

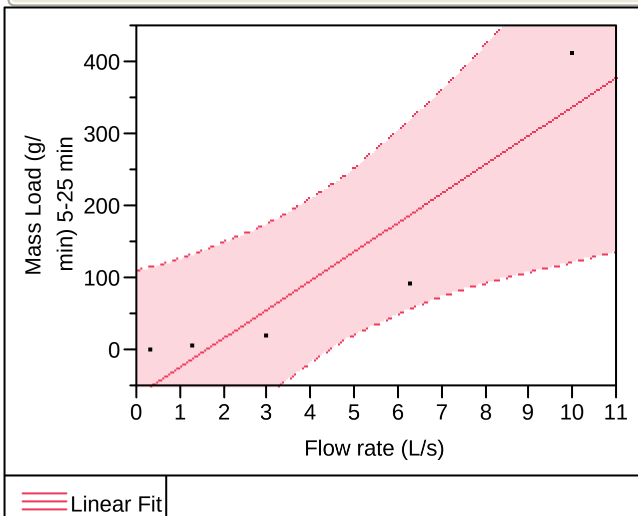

Linear Fit

Mass Load (g/min) 5-25 min = -63.7006 + 40.370672*Flow rate (L/s)

Summary of Fit

RSquare	0.843779
RSquare Adj	0.791705
Root Mean Square Error	79.67152
Mean of Response	105.0488
Observations (or Sum Wgts)	5

Analysis of Variance

Source	DF	Sum of Squares	Mean Square	F Ratio
Model	1	102852.86	102853	16.2036
Error	3	19042.65	6348	**Prob > F**
C. Total	4	121895.51		0.0275*

Parameter Estimates

Term	Estimate	Std Error	t Ratio	Prob>|t|
Intercept	-63.7006	55.0175	-1.16	0.3307
Flow rate (L/s)	40.370672	10.02907	4.03	0.0275*

Table M.14. Mass Load as a Function of Flow Rate for 5-25 min Composite Samples with Sediment Mixture at 25 cm below the Outlet

Bivariate Fit of Mass Load (g/min) 5-25 min By Flow rate (L/s) Depth (cm)=25

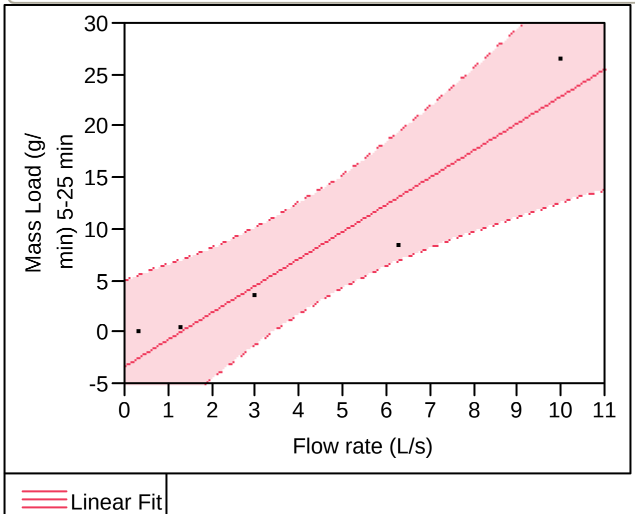

Linear Fit

Mass Load (g/min) 5-25 min = -3.231471 + 2.6283295*Flow rate (L/s)

Summary of Fit

RSquare	0.909087
RSquare Adj	0.878783
Root Mean Square Error	3.812161
Mean of Response	7.754947
Observations (or Sum Wgts)	5

Analysis of Variance

Source	DF	Sum of Squares	Mean Square	F Ratio
Model	1	435.95738	435.957	29.9986
Error	3	43.59772	14.533	**Prob > F**
C. Total	4	479.55511		0.0120*

Parameter Estimates

Term	Estimate	Std Error	t Ratio	Prob>|t|
Intercept	-3.231471	2.632504	-1.23	0.3072
Flow rate (L/s)	2.6283295	0.479876	5.48	0.0120*

Table M.15. Mass Load as a Function of Flow Rate for 5-25 min Composite Samples with Sediment Mixture at 46 cm below the Outlet

Bivariate Fit of Mass Load (g/min) 5-25 min By Flow rate (L/s) Depth (cm)=46

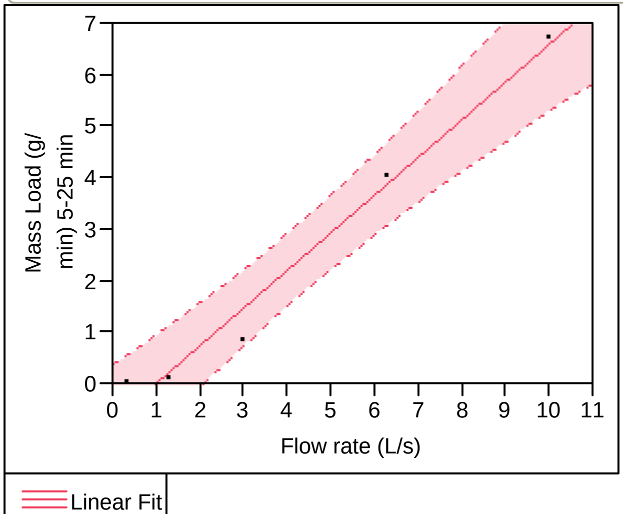

Linear Fit

Mass Load (g/min) 5-25 min = -0.705617 + 0.7334803*Flow rate (L/s)

Summary of Fit

RSquare	0.979166
RSquare Adj	0.972222
Root Mean Square Error	0.490709
Mean of Response	2.360331
Observations (or Sum Wgts)	5

Analysis of Variance

Source	DF	Sum of Squares	Mean Square	F Ratio
Model	1	33.951689	33.9517	140.9980
Error	3	0.722386	0.2408	**Prob > F**
C. Total	4	34.674075		0.0013*

Parameter Estimates

Term	Estimate	Std Error	t Ratio	Prob>|t|
Intercept	-0.705617	0.338861	-2.08	0.1287
Flow rate (L/s)	0.7334803	0.061771	11.87	0.0013*

Table M.16. Mass Load as a Function of Flow Rate for 5-25 min Composite Samples with Sediment Mixture at 106 cm below the Outlet

Bivariate Fit of Mass Load (g/min) 5-25 min By Flow rate (L/s) Depth (cm)=106

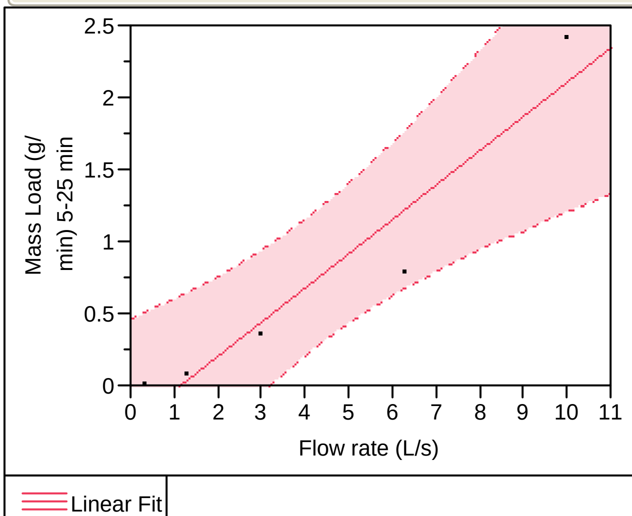

Linear Fit

Mass Load (g/min) 5-25 min = -0.261085 + 0.2377916*Flow rate (L/s)

Summary of Fit

RSquare	0.914739
RSquare Adj	0.886319
Root Mean Square Error	0.33297
Mean of Response	0.732884
Observations (or Sum Wgts)	5

Analysis of Variance

Source	DF	Sum of Squares	Mean Square	F Ratio
Model	1	3.5684327	3.56843	32.1861
Error	3	0.3326064	0.11087	**Prob > F**
C. Total	4	3.9010391		0.0108*

Parameter Estimates

Term	Estimate	Std Error	t Ratio	Prob>|t|
Intercept	-0.261085	0.229934	-1.14	0.3387
Flow rate (L/s)	0.2377916	0.041914	5.67	0.0108*

APPENDIX N

2D-PLOTS OF SEDIMENT SCOUR AT 20 MIN OF SIMULATION – RESULTS FROM A COMPUTATIONAL FLUID DYNAMICS (CFD) MODEL

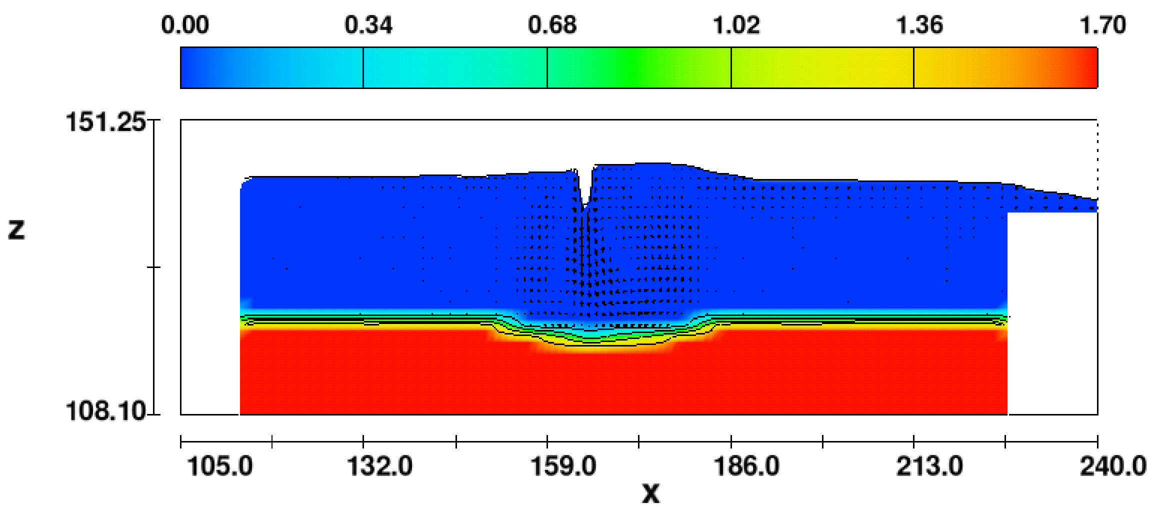

Figure N.1. Flow rate: 5 L/s, Overlaying water depth: 15 cm, Sediment particle size: 50 µm. Colors represent sediment concentration (g/cm^3).

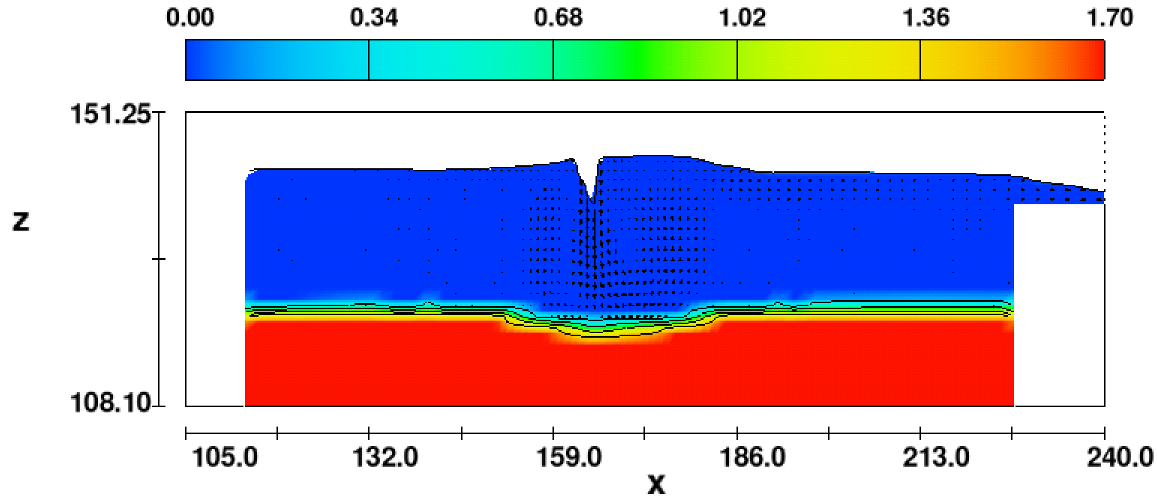

Figure N.2. Flow rate: 5 L/s, Overlaying water depth: 15 cm, Sediment particle size: 180 μm. Colors represent sediment concentration (g/cm^3).

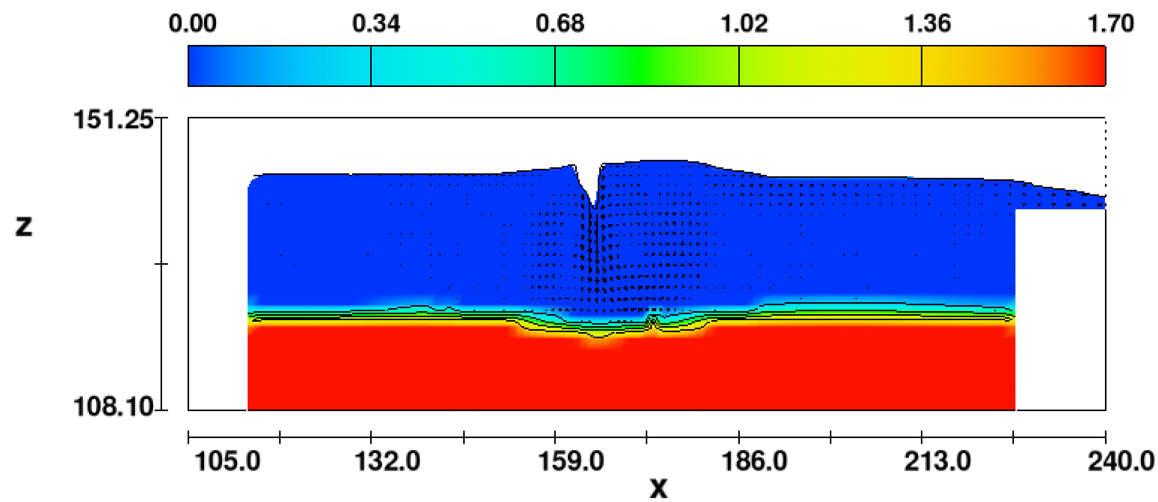

Figure N.3. Flow rate: 5 L/s, Overlaying water depth: 15 cm, Sediment particle size: 500 μm. Colors represent sediment concentration (g/cm^3).

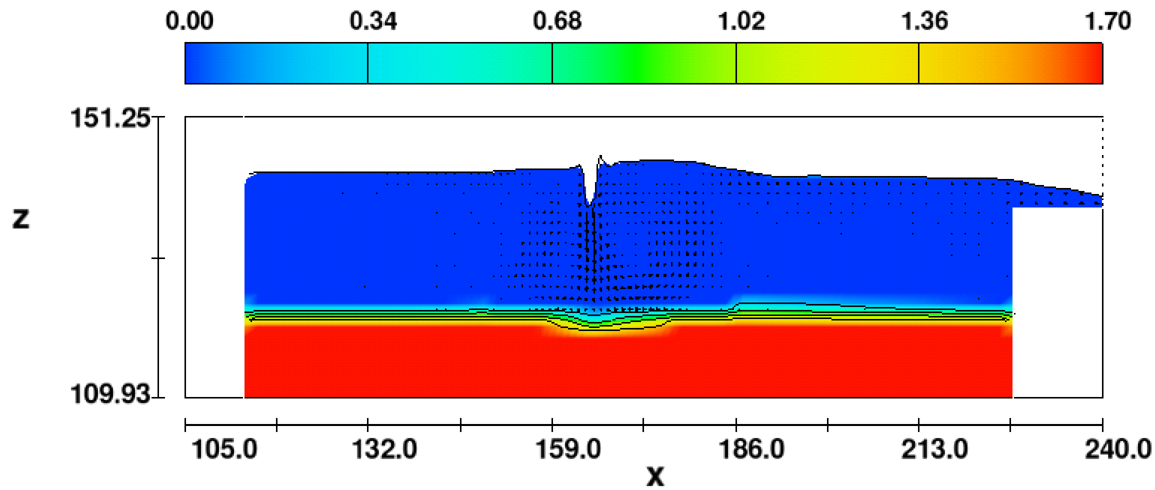

Figure N.4. Flow rate: 5 L/s, Overlaying water depth: 15 cm, Sediment particle size: 1000 µm. Colors represent sediment concentration (g/cm^3).

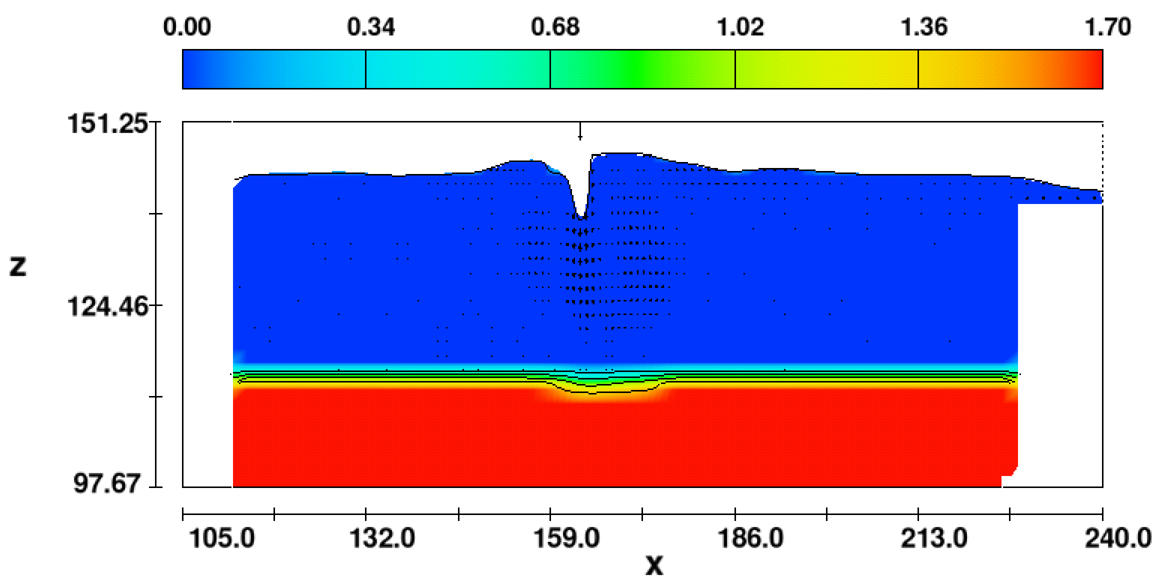

Figure N.5. Flow rate: 5 L/s, Overlaying water depth: 24 cm, Sediment particle size: 50 µm. Colors represent sediment concentration (g/cm^3).

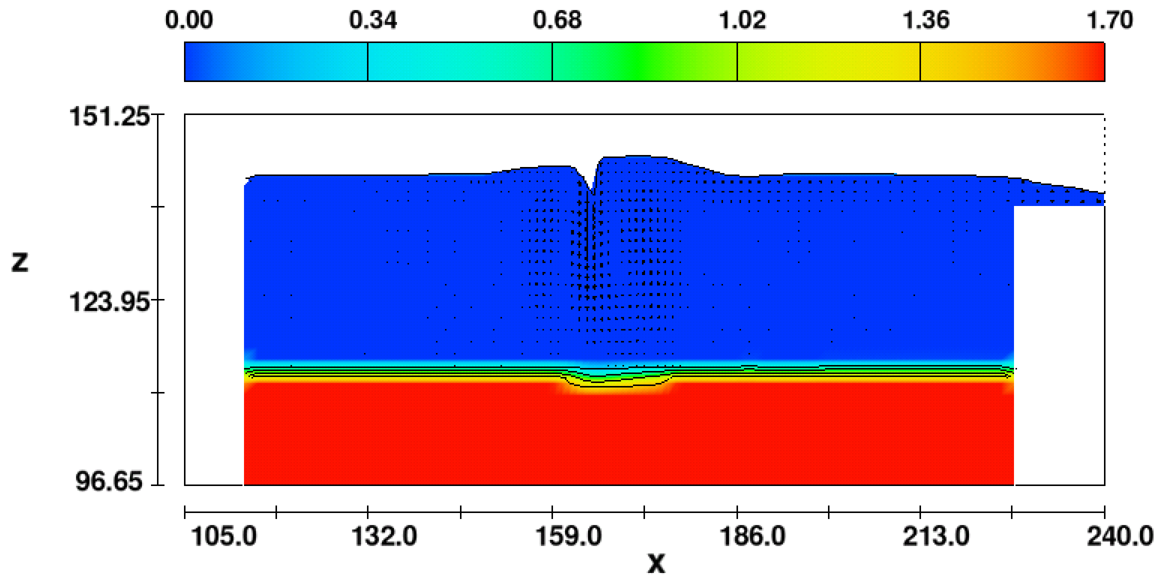

Figure N.6. Flow rate: 5 L/s, Overlaying water depth: 24 cm, Sediment particle size: 180 μm. Colors represent sediment concentration (g/cm^3).

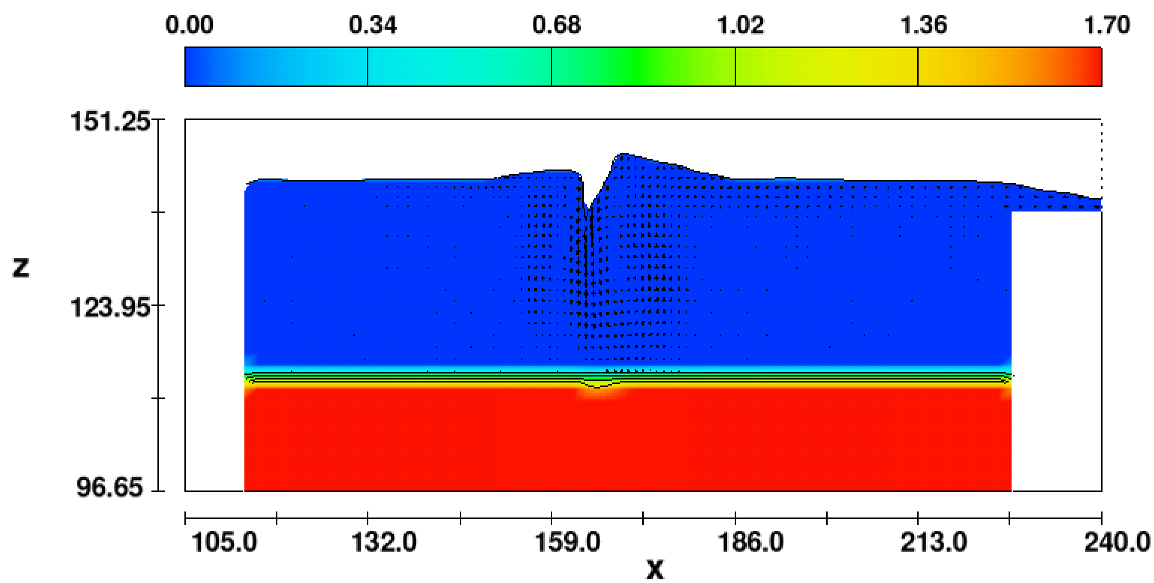

Figure N.7. Flow rate: 5 L/s, Overlaying water depth: 24 cm, Sediment particle size: 500 μm. Colors represent sediment concentration (g/cm^3).

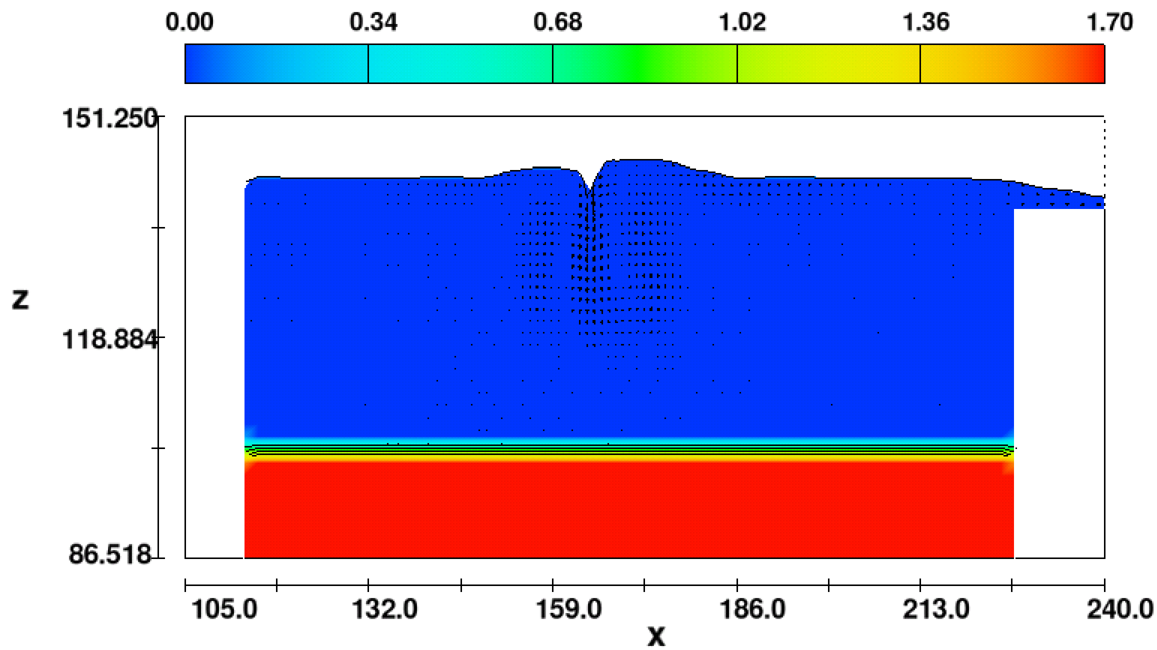

Figure N.8. Flow rate: 5 L/s, Overlaying water depth: 35 cm, Sediment particle size: 50 µm. Colors represent sediment concentration (g/cm^3).

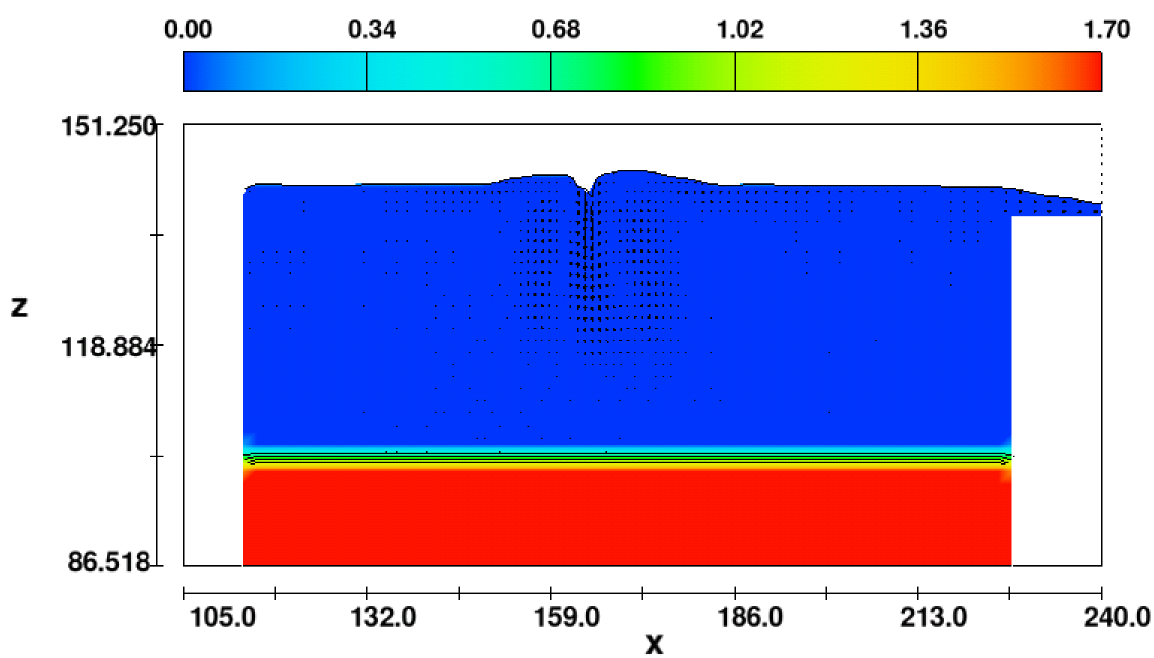

Figure N.9. Flow rate: 5 L/s, Overlaying water depth: 35 cm, Sediment particle size: 180 µm. Colors represent sediment concentration (g/cm^3).

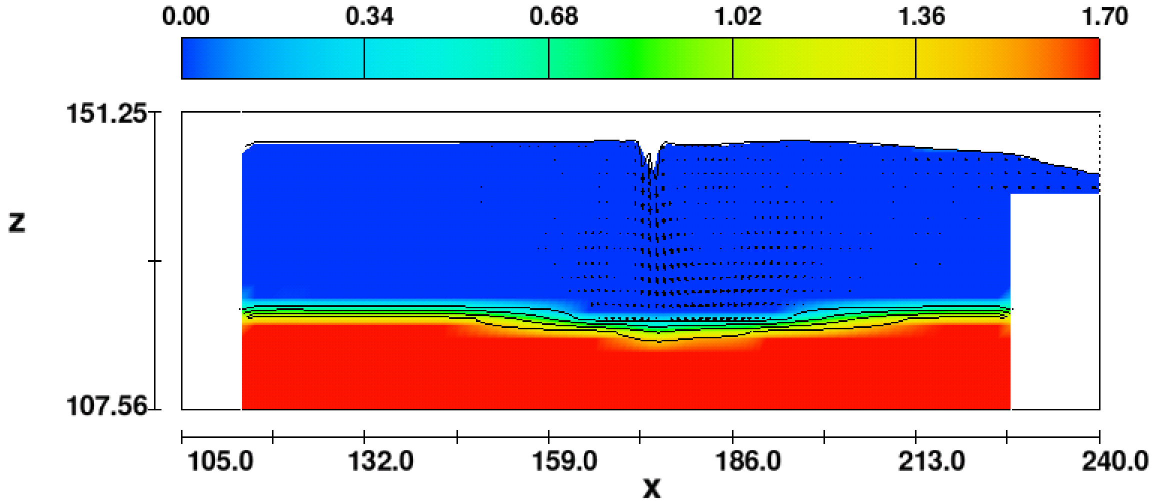

Figure N.10. Flow rate: 10 L/s, Overlaying water depth: 15 cm, Sediment particle size: 50 µm. Colors represent sediment concentration (g/cm^3).

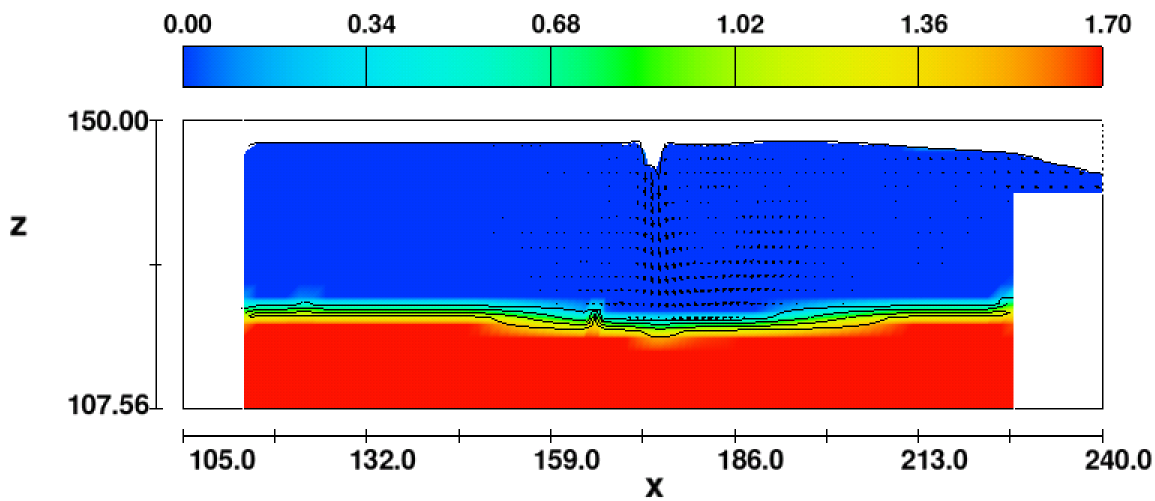

Figure N.11. Flow rate: 10 L/s, Overlaying water depth: 15 cm, Sediment particle size: 180µm. Colors represent sediment concentration (g/cm^3).

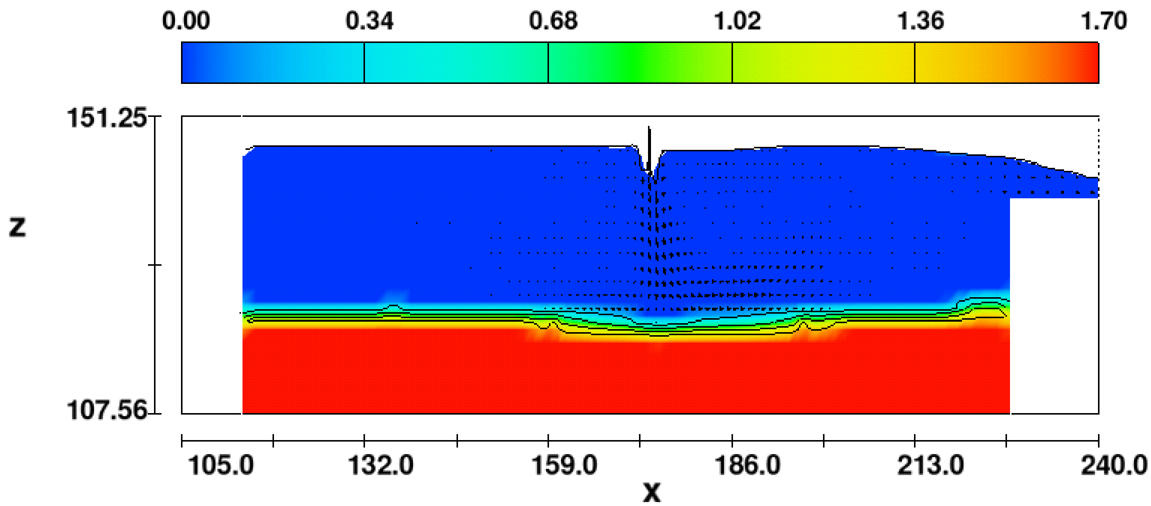

Figure N.12. Flow rate: 10 L/s, Overlaying water depth: 15 cm, Sediment particle size: 500μm. Colors represent sediment concentration (g/cm^3).

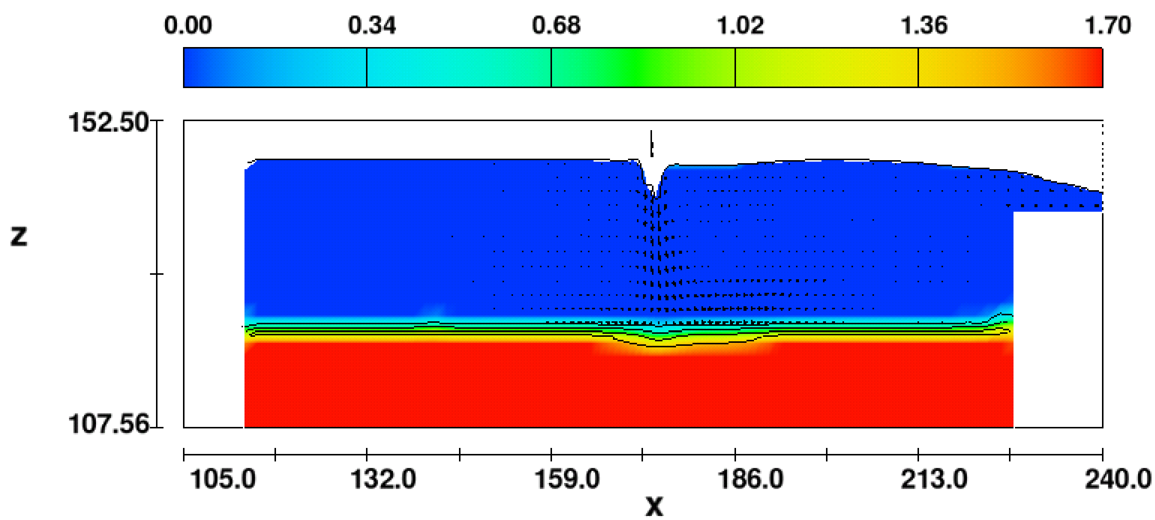

Figure N.13. Flow rate: 10 L/s, Overlaying water depth: 15 cm, Sediment particle size: 1000μm. Colors represent sediment concentration (g/cm^3).

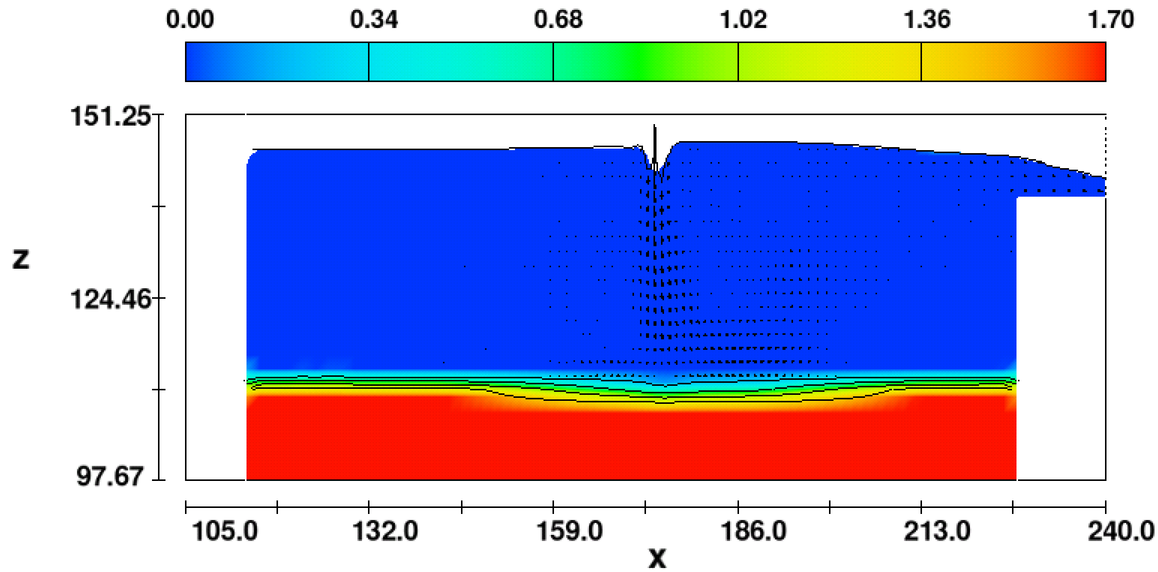

Figure N.14. Flow rate: 10 L/s, Overlaying water depth: 24 cm, Sediment particle size: 50μm. Colors represent sediment concentration (g/cm^3).

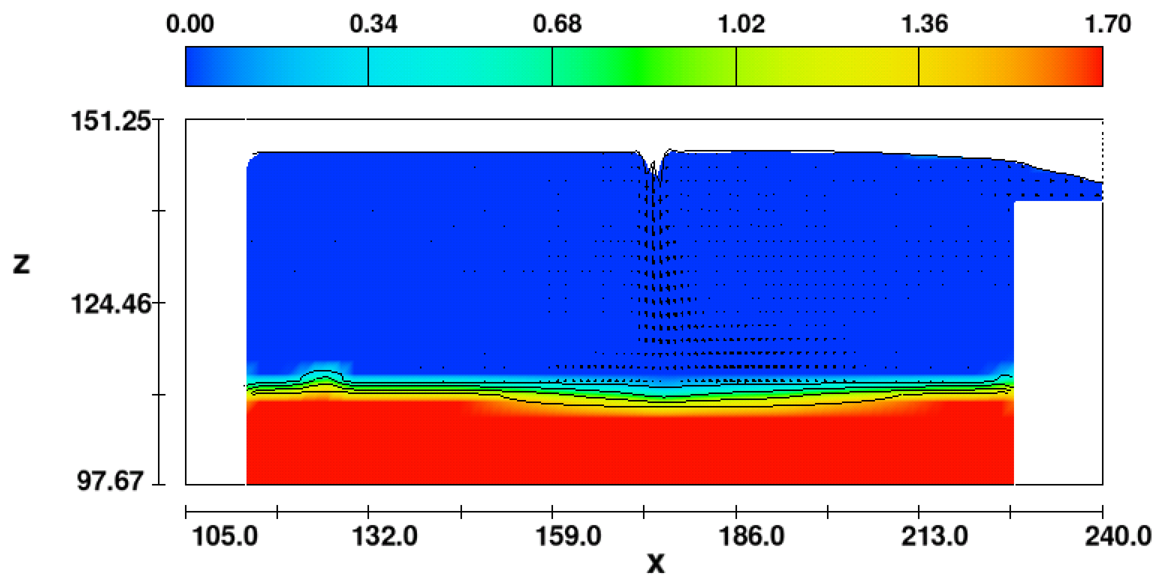

Figure N.15. Flow rate: 10 L/s, Overlaying water depth: 24 cm, Sediment particle size: 180 μm. Colors represent sediment concentration (g/cm^3).

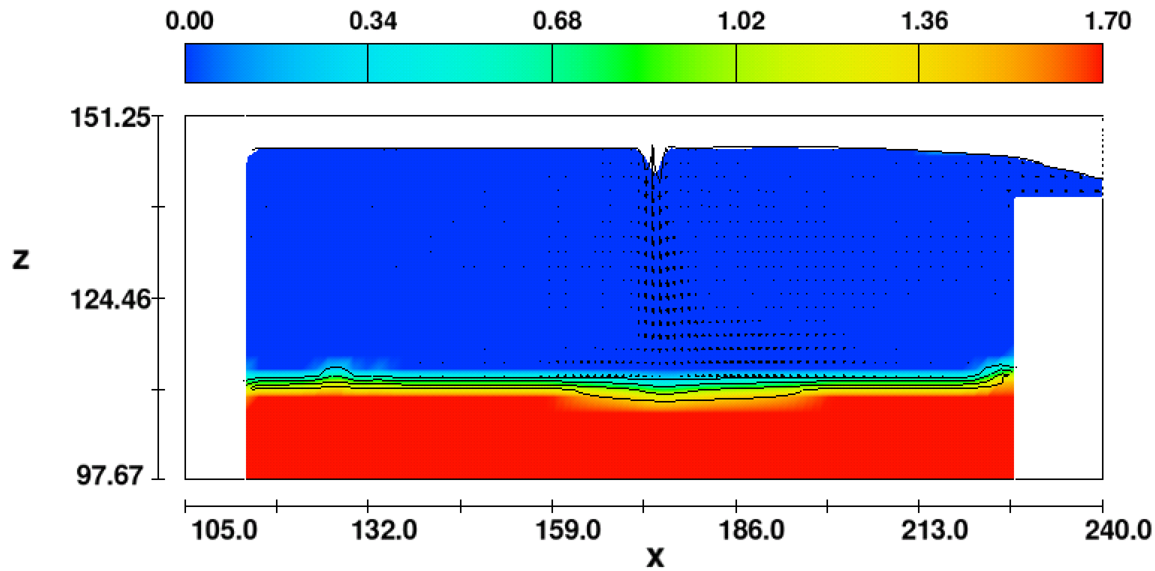

Figure N.16. Flow rate: 10 L/s, Overlaying water depth: 24 cm, Sediment particle size: 500 μm. Colors represent sediment concentration (g/cm^3).

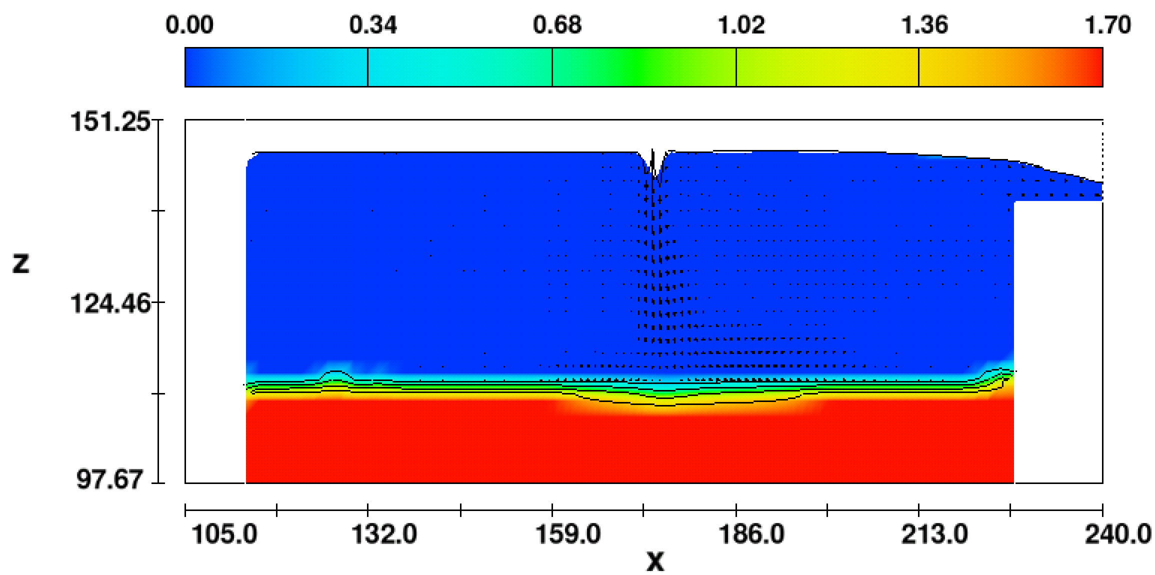

Figure N.17. Flow rate: 10 L/s, Overlaying water depth: 24 cm, Sediment particle size: 1000 μm. Colors represent sediment concentration (g/cm^3).

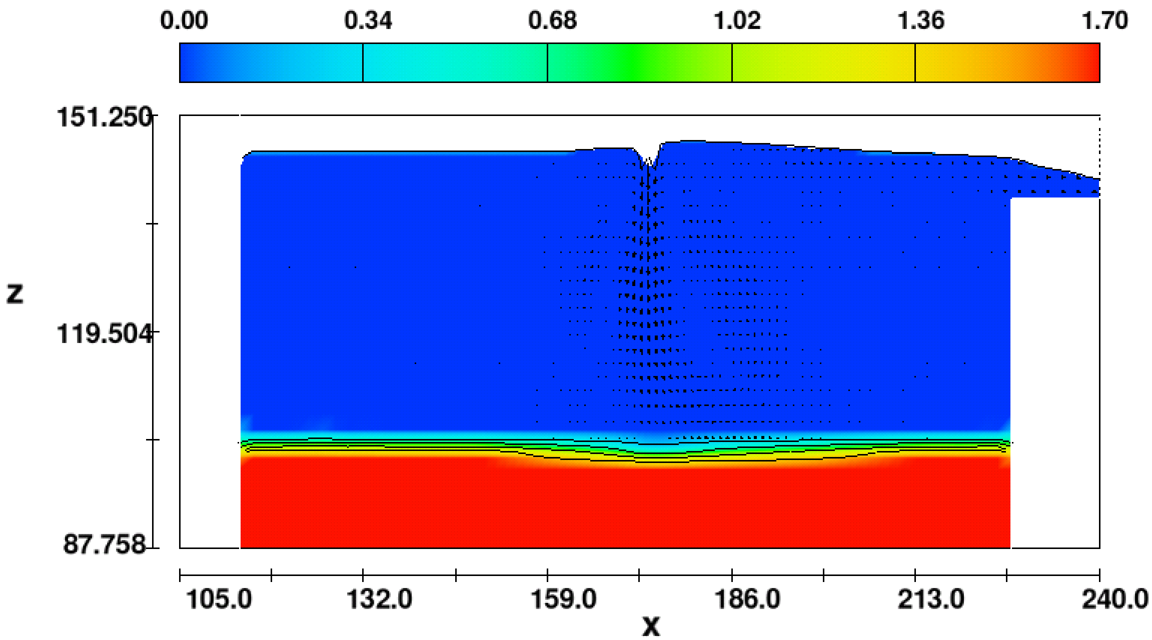

Figure N.18. Flow rate: 10 L/s, Overlaying water depth: 35 cm, Sediment particle size: 50 µm. Colors represent sediment concentration (g/cm^3).

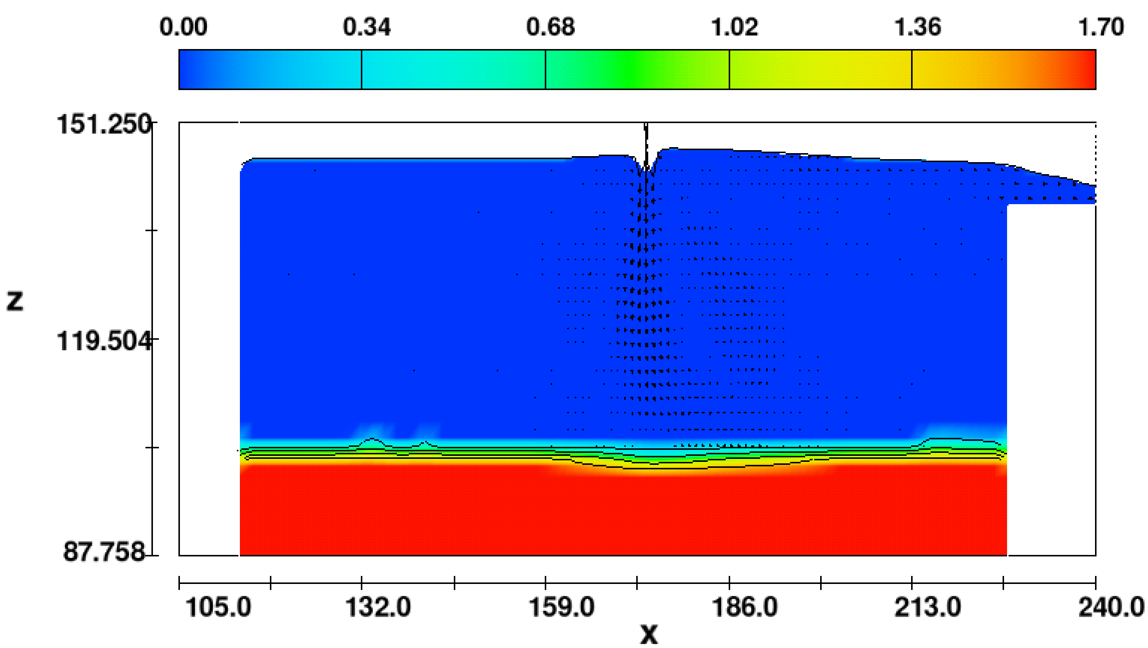

Figure N.19. Flow rate: 10 L/s, Overlaying water depth: 35 cm, Sediment particle size: 180 µm. Colors represent sediment concentration (g/cm^3).

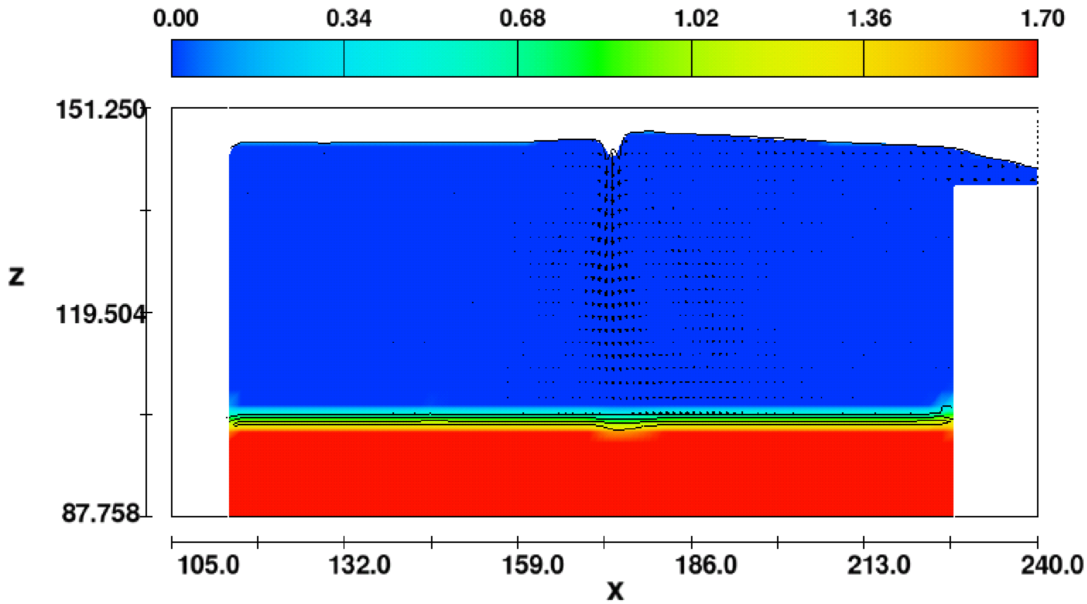

Figure N.20. Flow rate: 10 L/s, Overlaying water depth: 35 cm, Sediment particle size: 500 μm. Colors represent sediment concentration (g/cm^3).

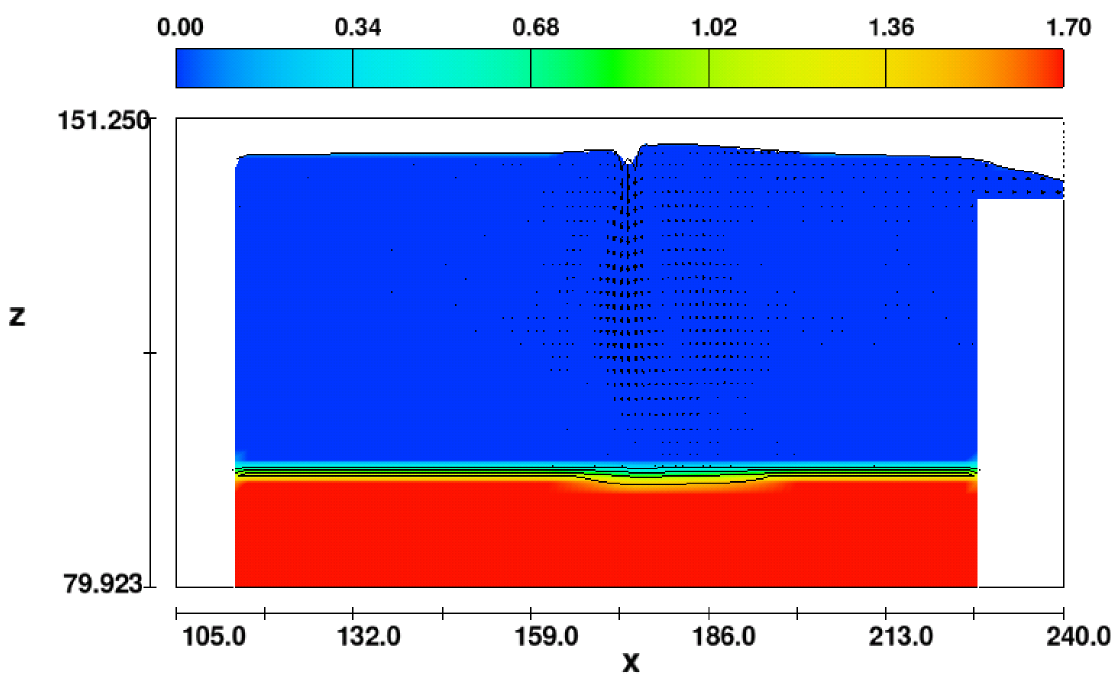

Figure N.21. Flow rate: 10 L/s, Overlaying water depth: 40 cm, Sediment particle size: 50 μm. Colors represent sediment concentration (g/cm^3).

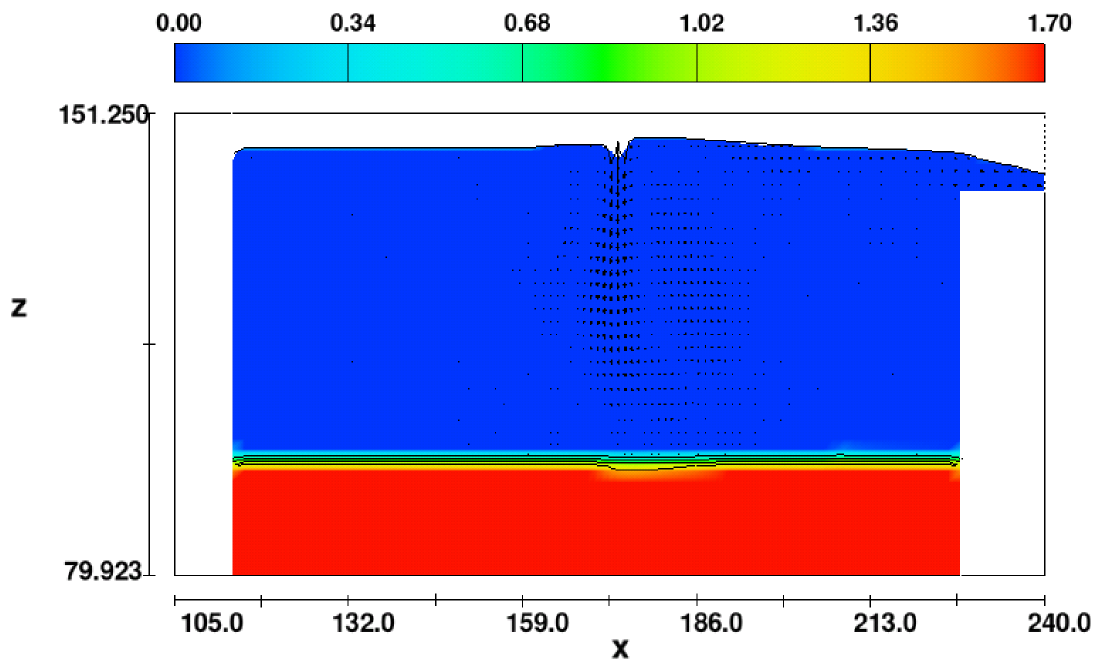

Figure N.22. Flow rate: 10 L/s, Overlaying water depth: 40 cm, Sediment particle size: 180 µm. Colors represent sediment concentration (g/cm^3).

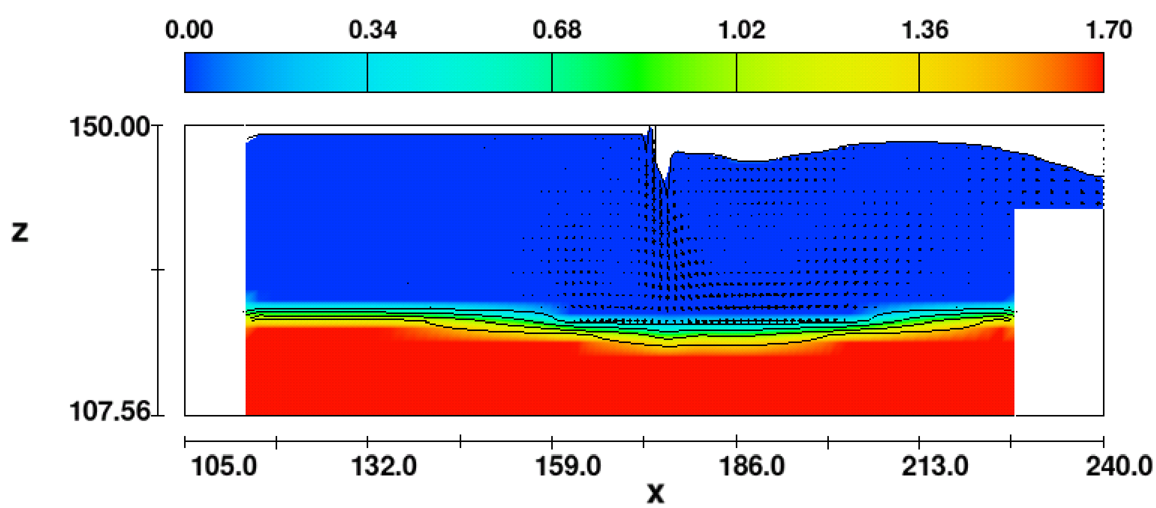

Figure N.23. Flow rate: 20 L/s, Overlaying water depth: 15 cm, Sediment particle size: 50 µm. Colors represent sediment concentration (g/cm^3).

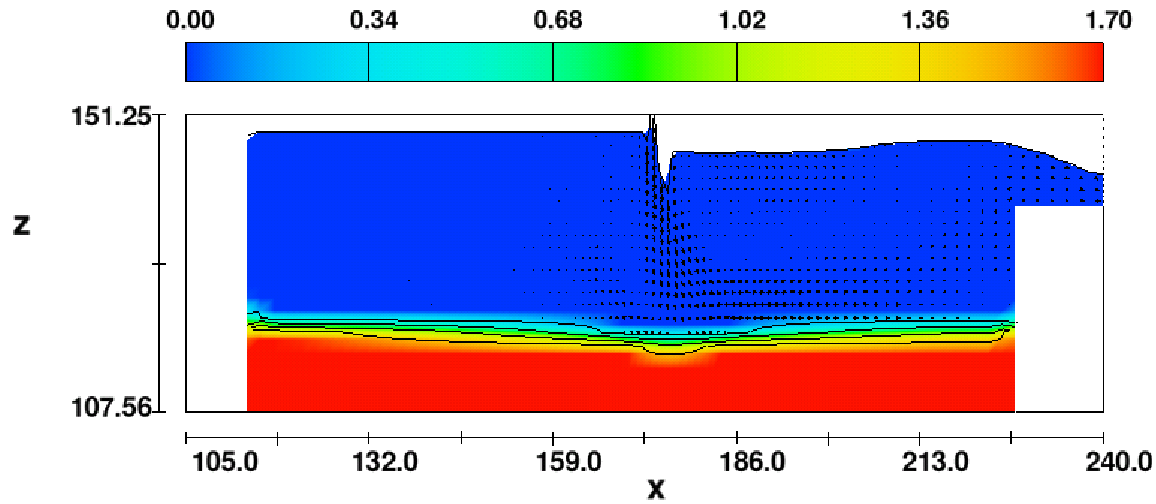

Figure N.24. Flow rate: 20 L/s, Overlaying water depth: 15 cm, Sediment particle size: 180 µm. Colors represent sediment concentration (g/cm^3).

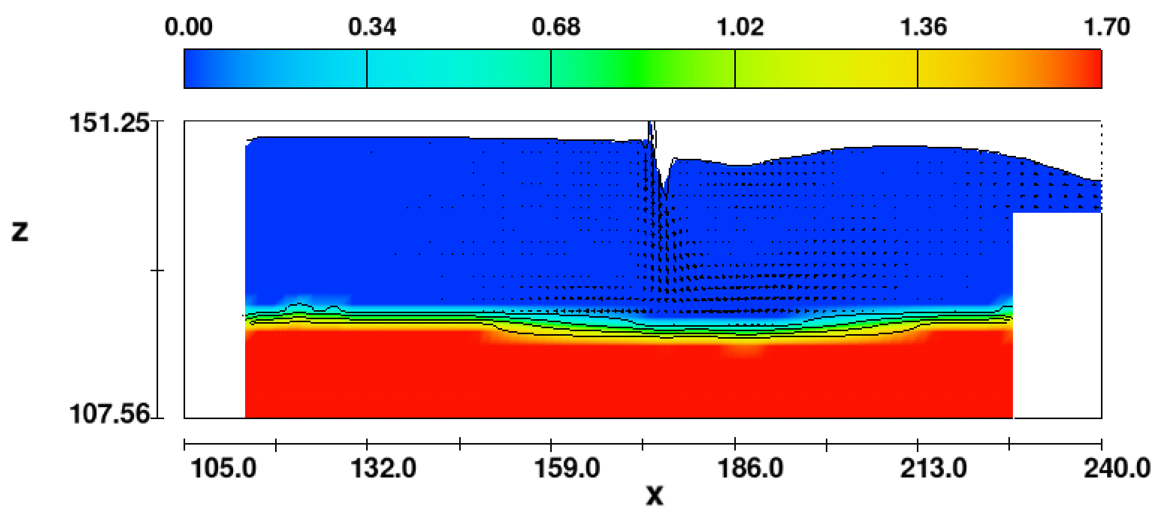

Figure N.25. Flow rate: 20 L/s, Overlaying water depth: 15 cm, Sediment particle size: 500 µm. Colors represent sediment concentration (g/cm^3).

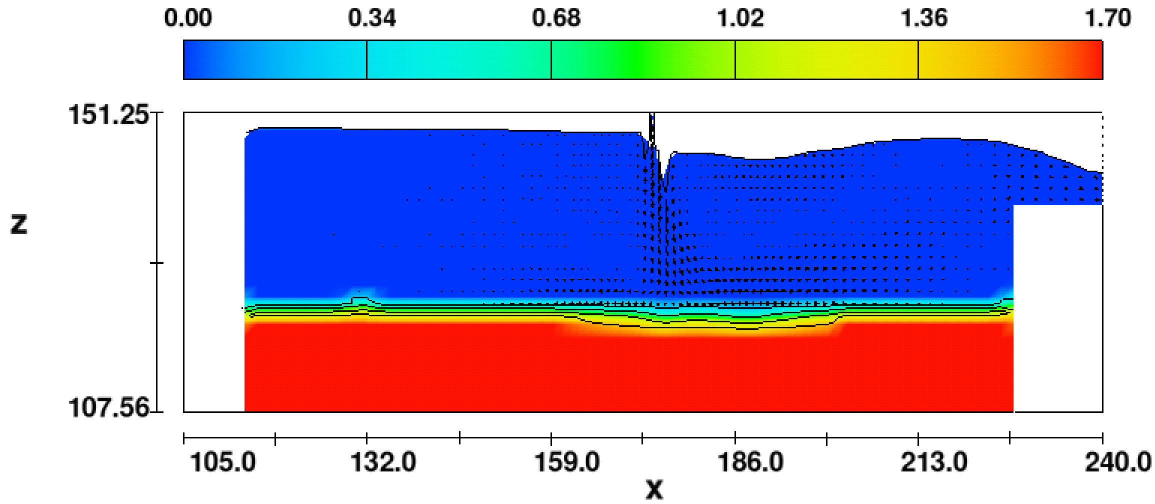

Figure N.26. Flow rate: 20 L/s, Overlaying water depth: 15 cm, Sediment particle size: 1000 μm. Colors represent sediment concentration (g/cm^3).

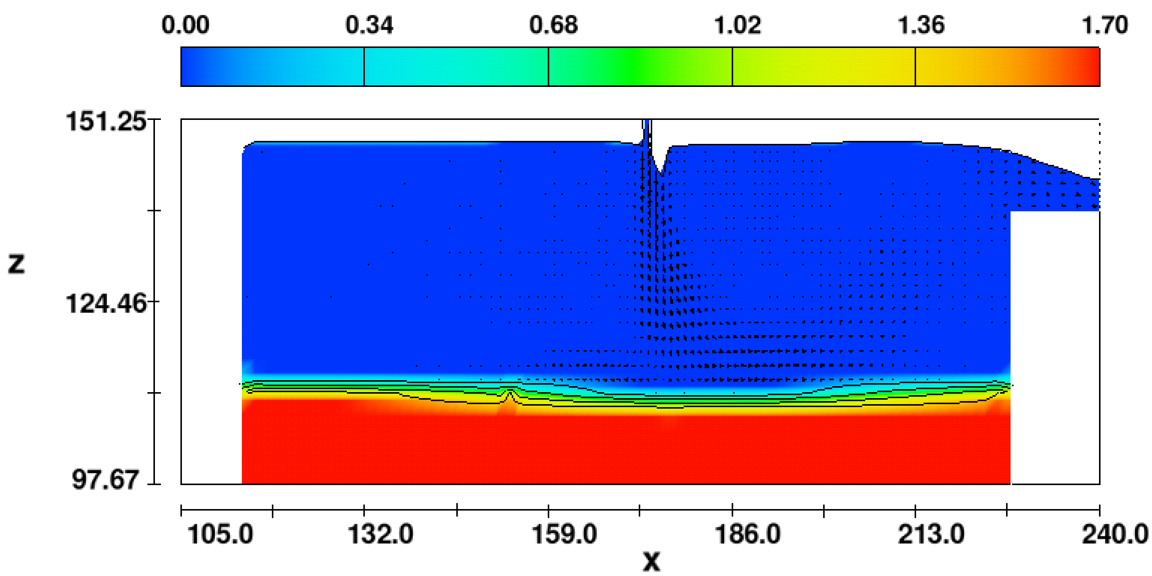

Figure N.27. Flow rate: 20 L/s, Overlaying water depth: 24 cm, Sediment particle size: 50 μm. Colors represent sediment concentration (g/cm^3).

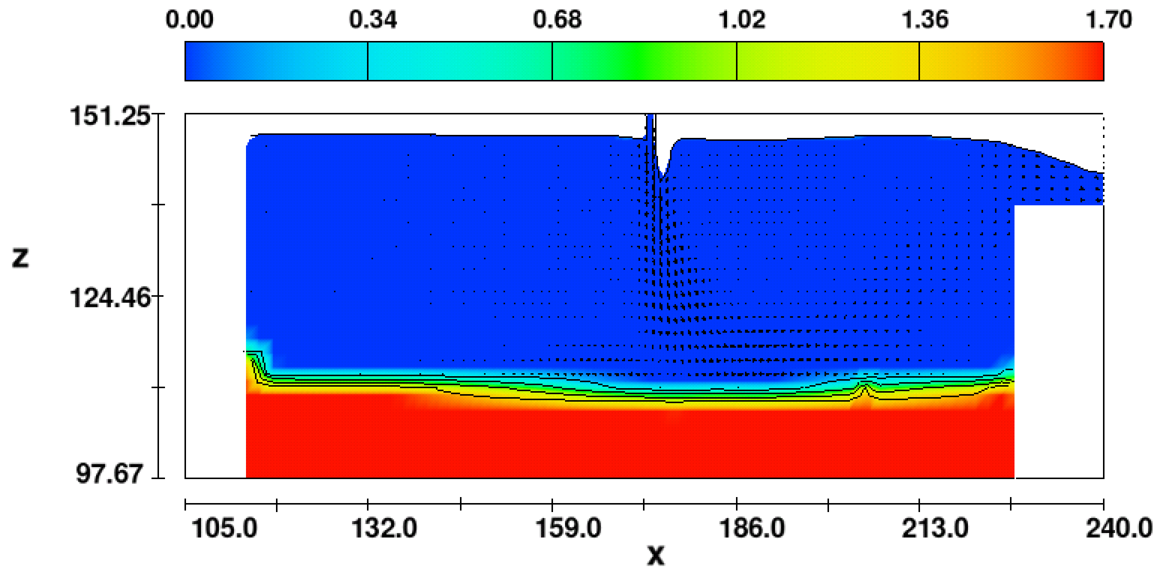

Figure N.28. Flow rate: 20 L/s, Overlaying water depth: 24 cm, Sediment particle size: 180 µm. Colors represent sediment concentration (g/cm^3).

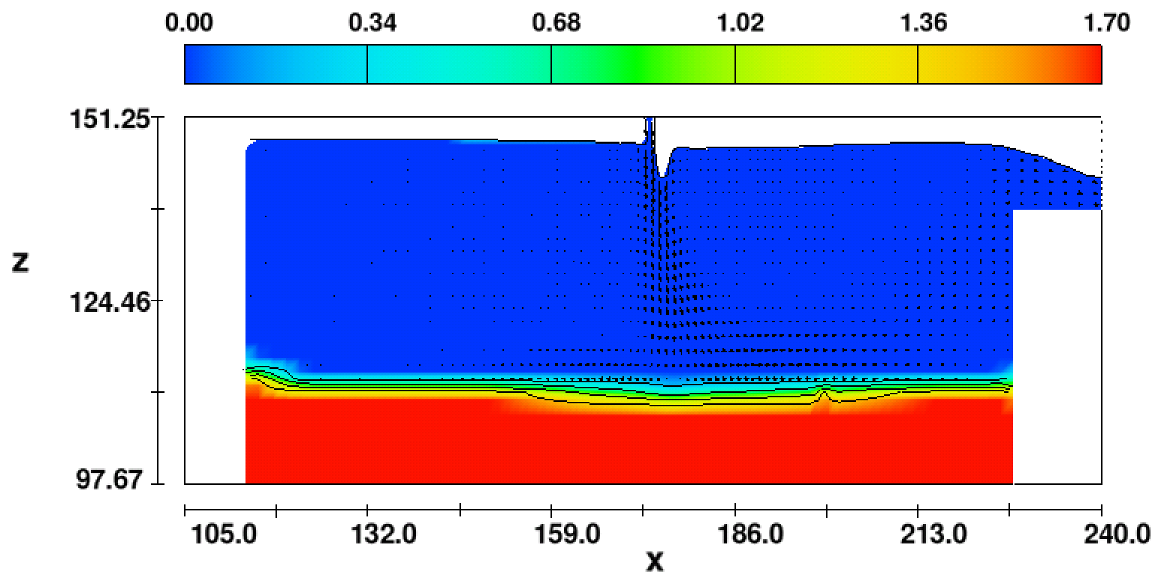

Figure N.29. Flow rate: 20 L/s, Overlaying water depth: 24 cm, Sediment particle size: 500 µm. Colors represent sediment concentration (g/cm^3).

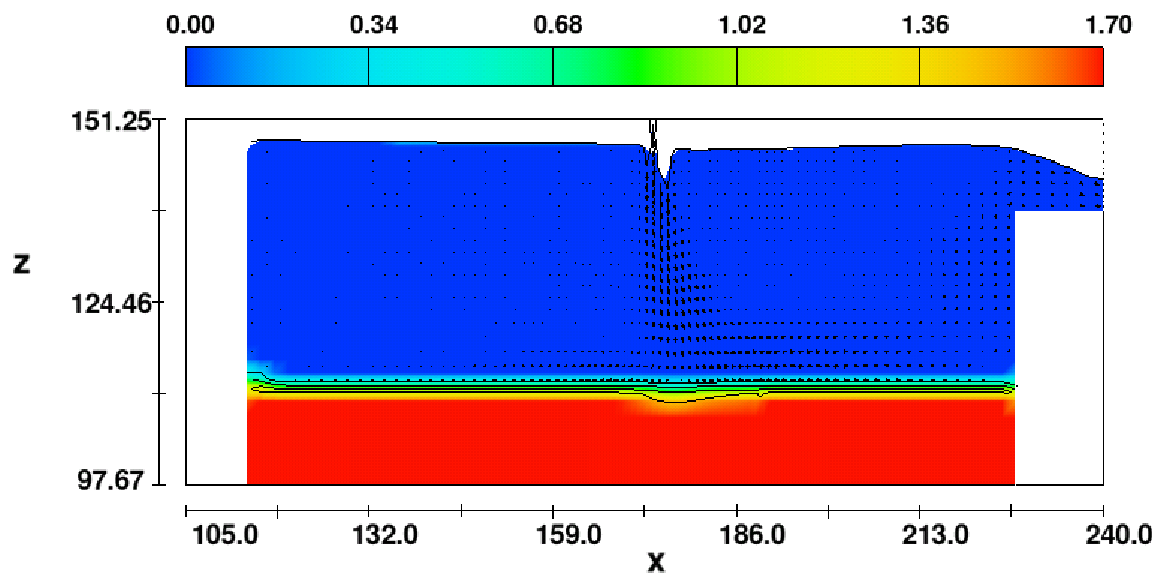

Figure N.30. Flow rate: 20 L/s, Overlaying water depth: 24 cm, Sediment particle size: 1000 μm. Colors represent sediment concentration (g/cm^3).

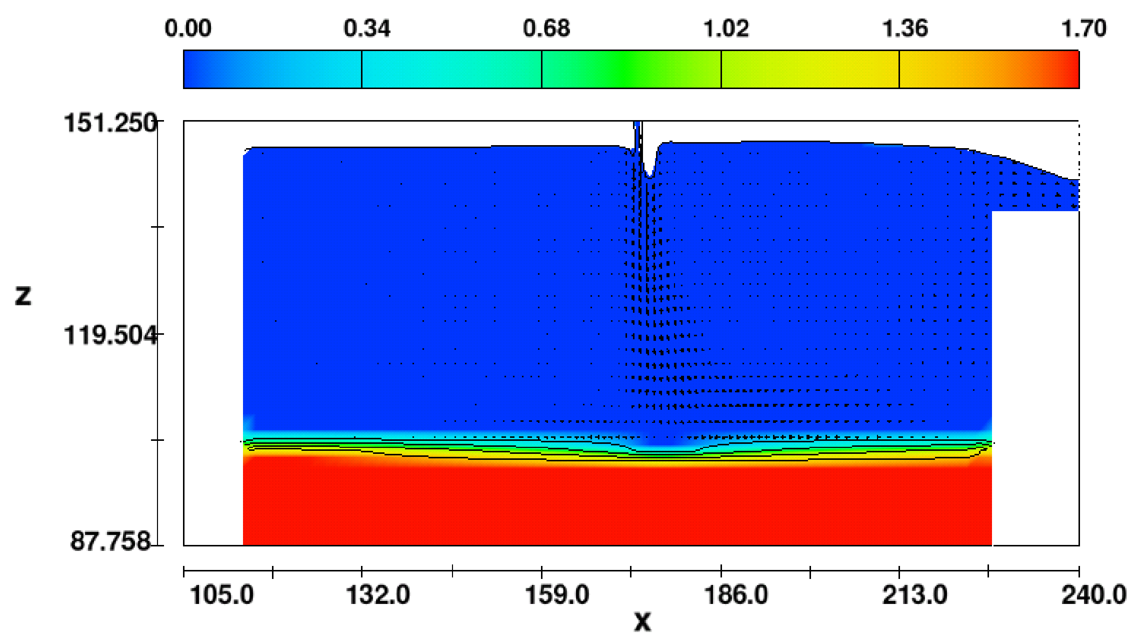

Figure N.31. Flow rate: 20 L/s, Overlaying water depth: 35 cm, Sediment particle size: 50 μm. Colors represent sediment concentration (g/cm^3).

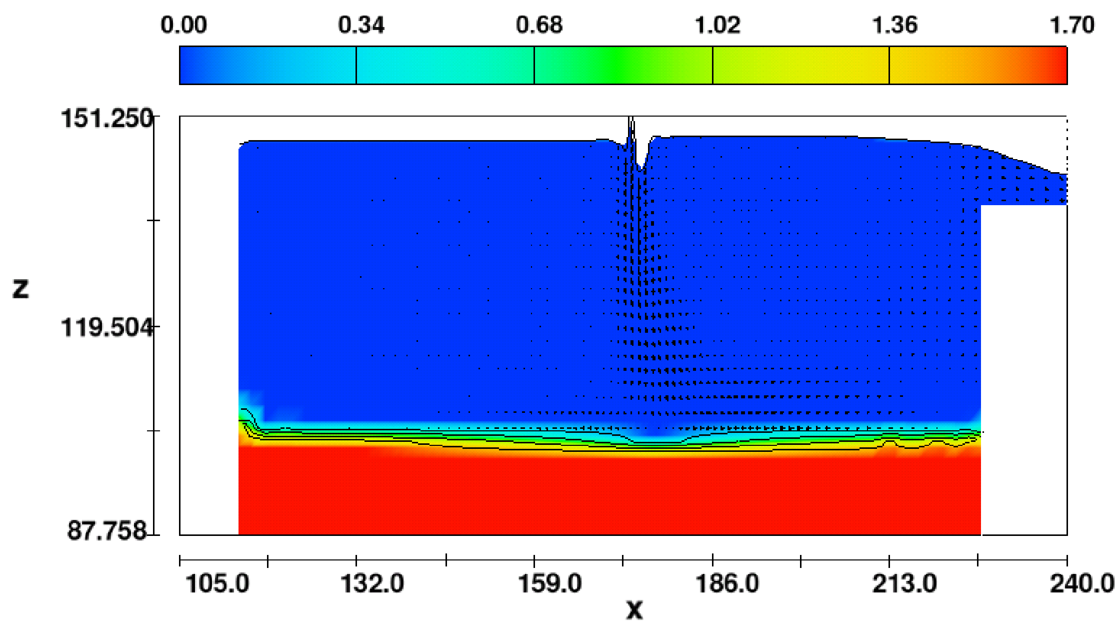

Figure N.32. Flow rate: 20 L/s, Overlaying water depth: 35 cm, Sediment particle size: 180 µm. Colors represent sediment concentration (g/cm^3).

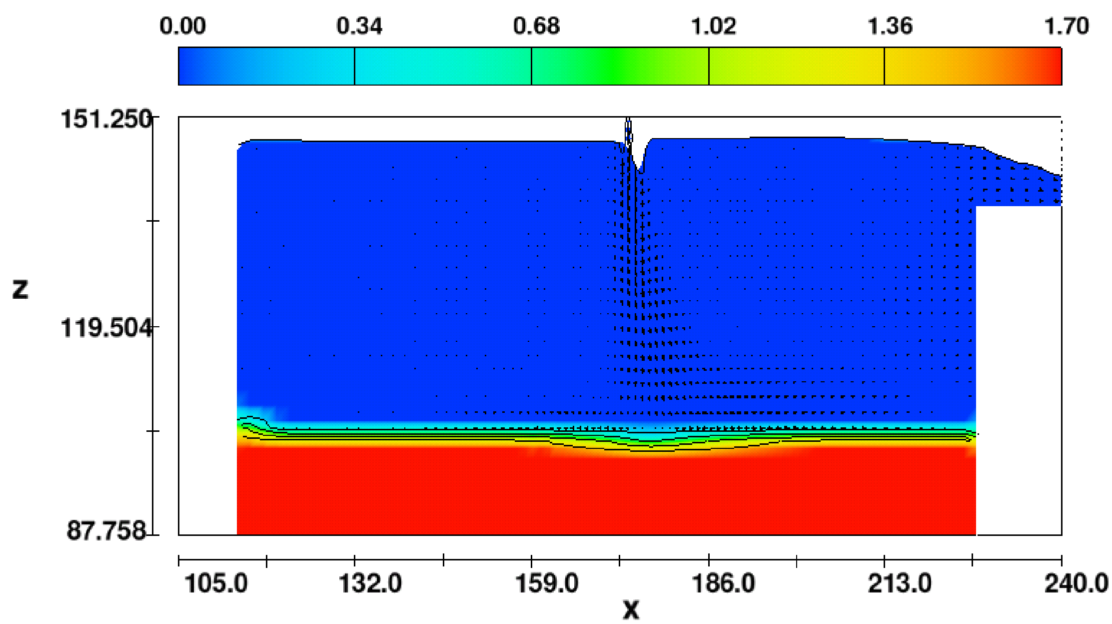

Figure N.33. Flow rate: 20 L/s, Overlaying water depth: 35 cm, Sediment particle size: 500 µm. Colors represent sediment concentration (g/cm^3).

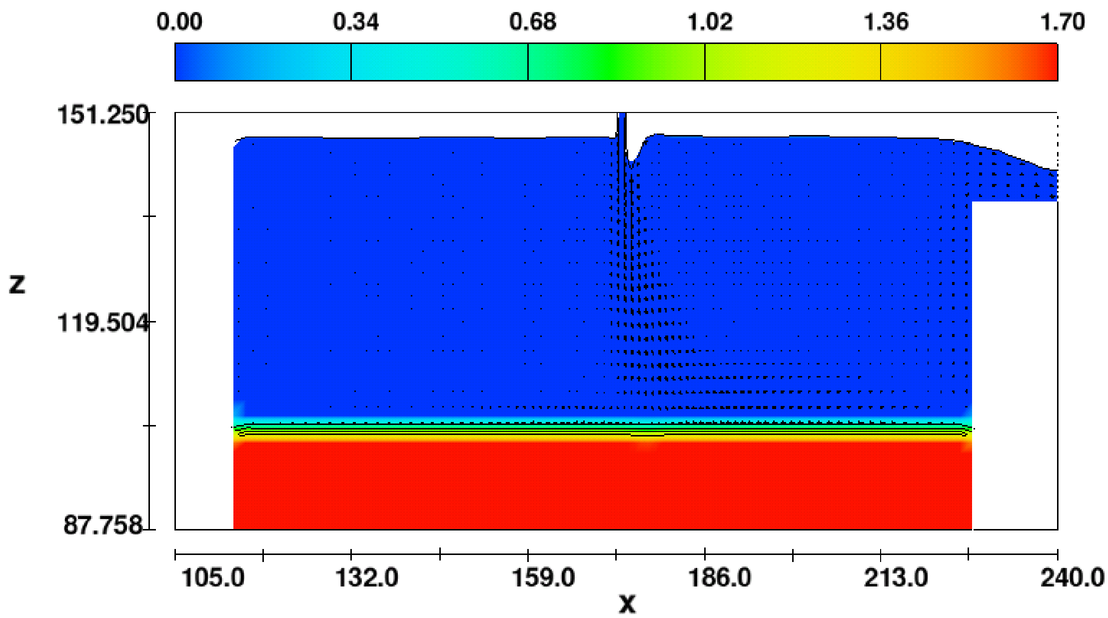

Figure N.34. Flow rate: 20 L/s, Overlaying water depth: 35 cm, Sediment particle size: 1000 µm. Colors represent sediment concentration (g/cm^3).

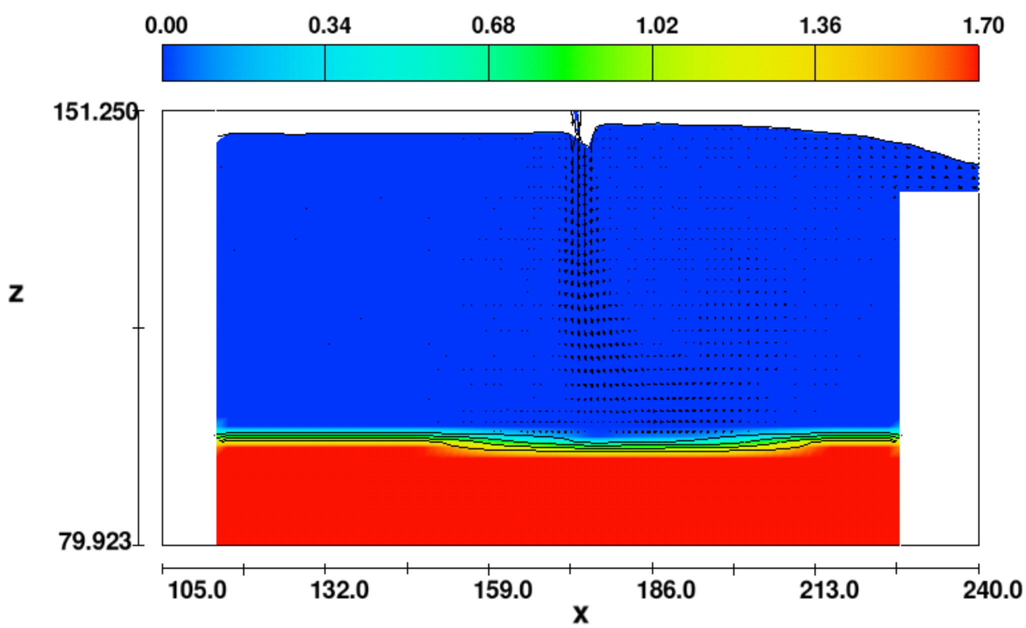

Figure N.35. Flow rate: 20 L/s, Overlaying water depth: 40 cm, Sediment particle size: 50 µm. Colors represent sediment concentration (g/cm^3).

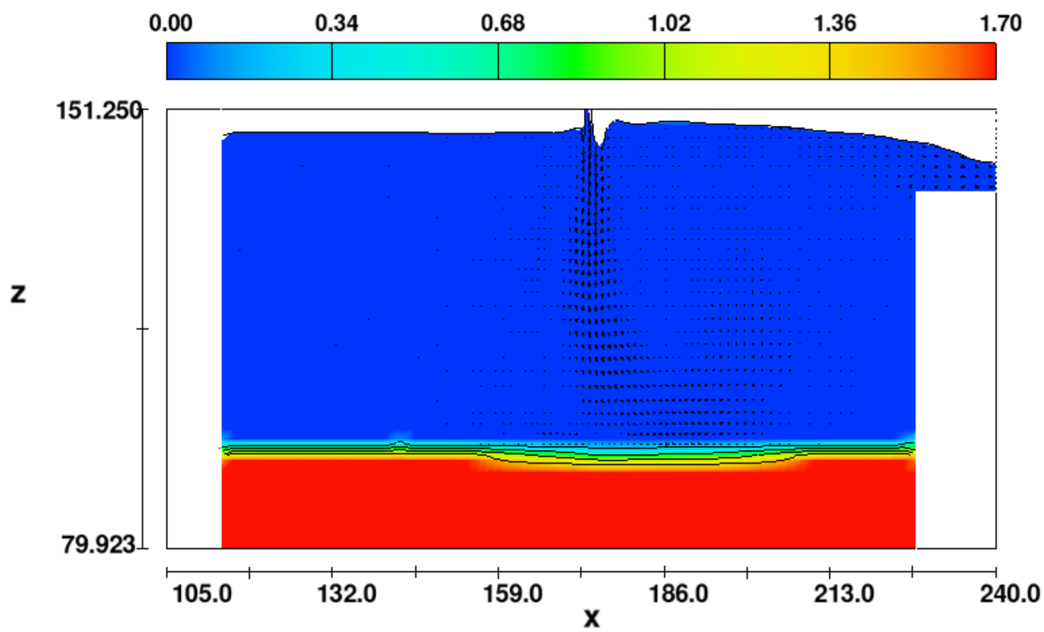

Figure N.36. Flow rate: 20 L/s, Overlaying water depth: 40 cm, Sediment particle size: 180 µm. Colors represent sediment concentration (g/cm^3).

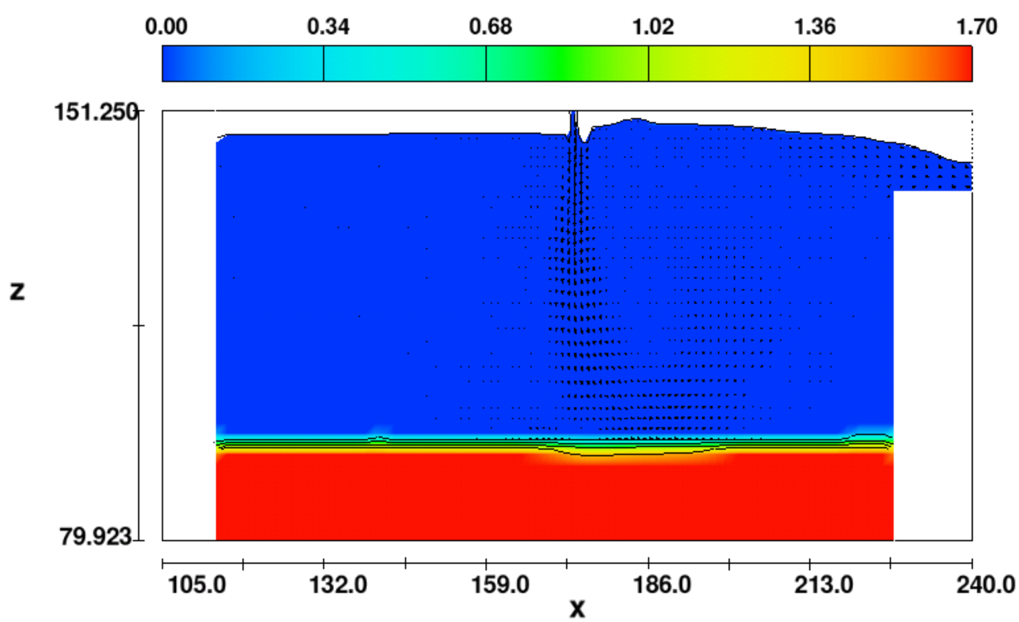

Figure N.37. Flow rate: 20 L/s, Overlaying water depth: 40 cm, Sediment particle size: 500 µm. Colors represent sediment concentration (g/cm^3).

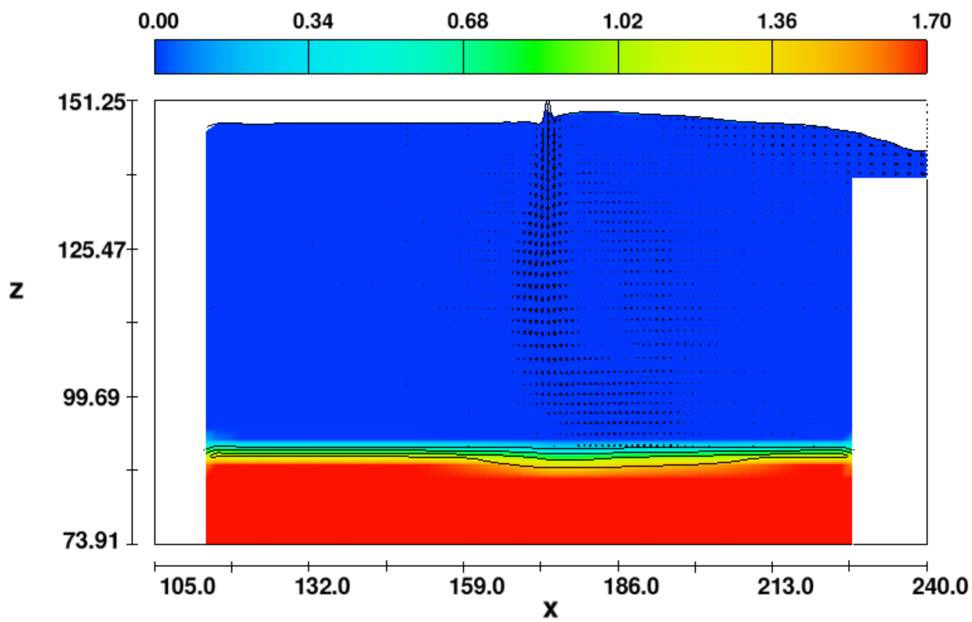

Figure N.38. Flow rate: 20 L/s, Overlaying water depth: 45 cm, Sediment particle size: 50 μm. Colors represent sediment concentration (g/cm^3).

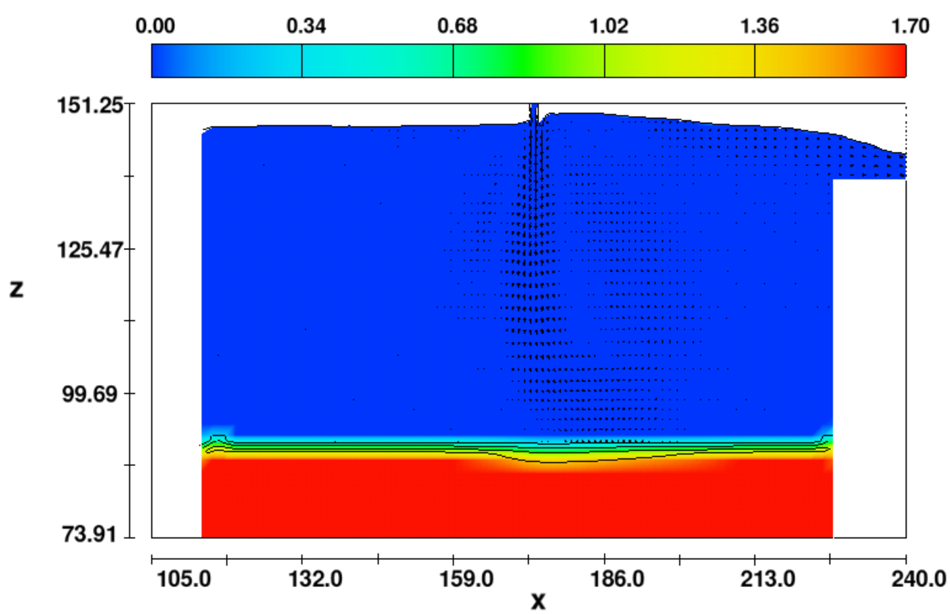

Figure N.39. Flow rate: 20 L/s, Overlaying water depth: 45 cm, Sediment particle size: 180 μm. Colors represent sediment concentration (g/cm^3).

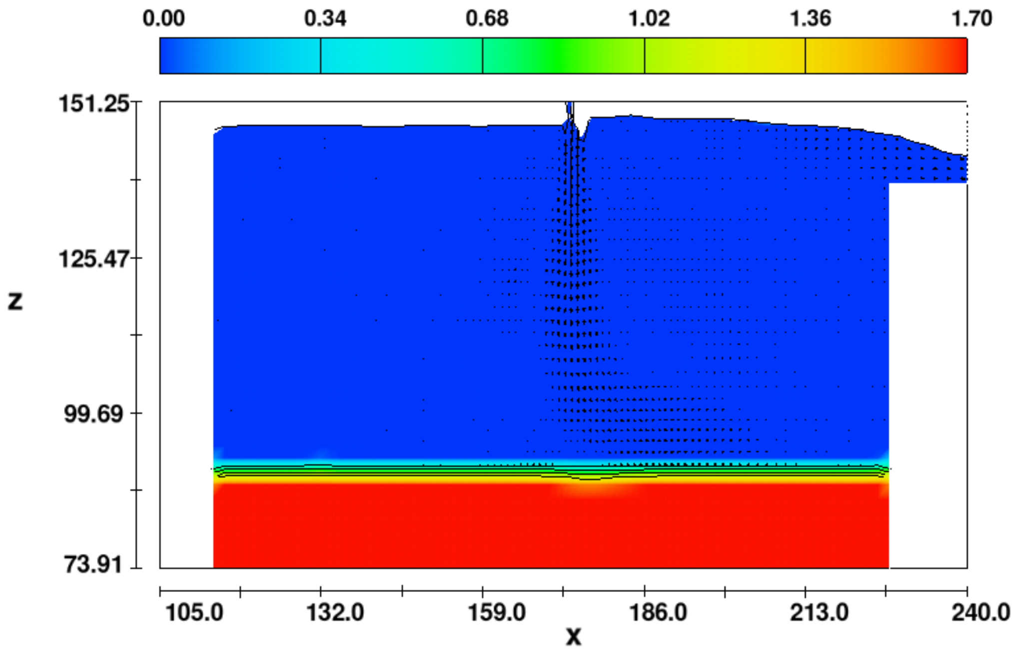

Figure N.40. Flow rate: 20 L/s, Overlaying water depth: 45 cm, Sediment particle size: 500 µm. Colors represent sediment concentration (g/cm^3).

APPENDIX O

SUSPENDED SEDIMENT CONCENTRATION (SSC) TIME SERIES – RESULTS FROM A 2D-CFD MODEL

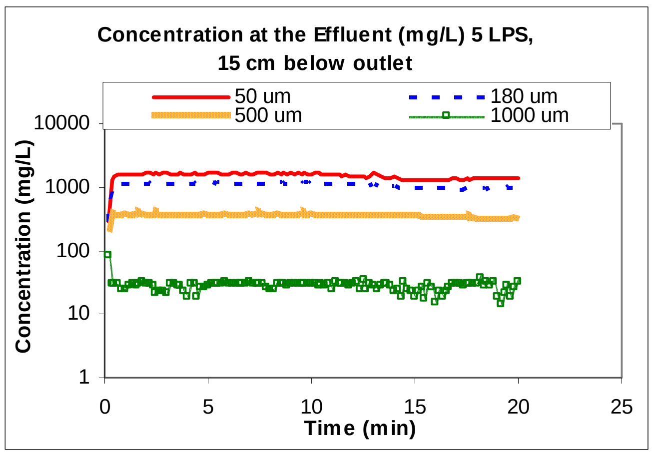

Figure O.1. SSC (mg/L) at 5 L/s flow rate and 15 cm below the outlet.

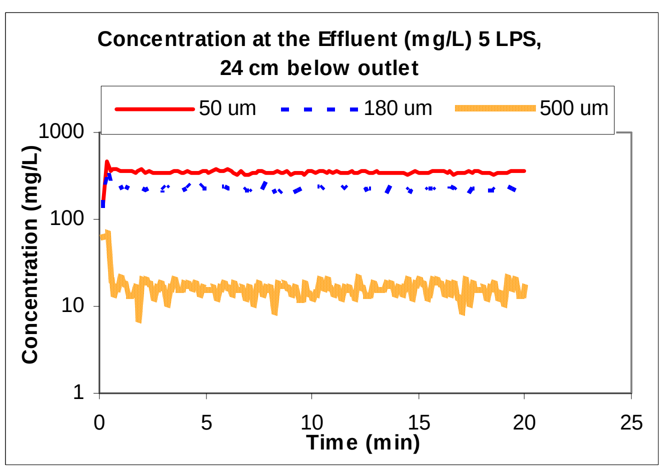

Figure O.2. SSC (mg/L) at 5 L/s flow rate and 24 cm below the outlet.

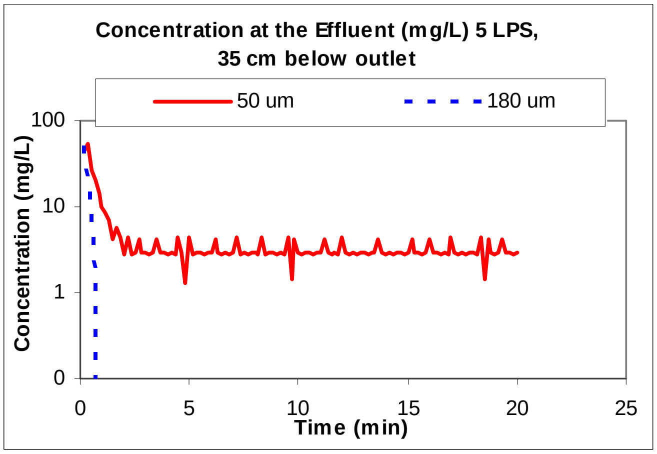

Figure O.3. SSC (mg/L) at 5 L/s flow rate and 35 cm below the outlet.

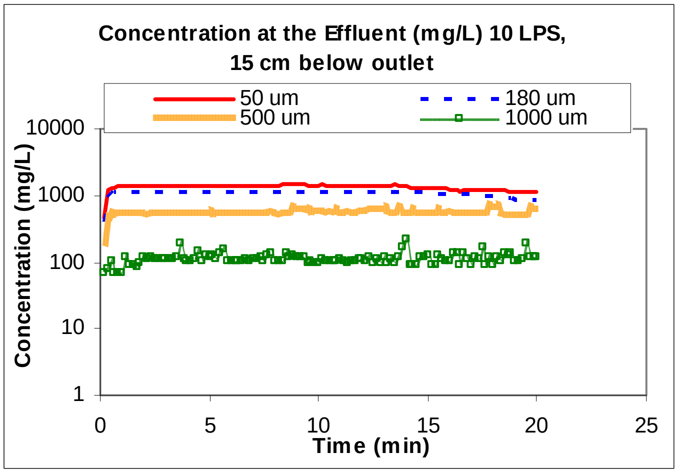

Figure O.4. SSC (mg/L) at 10 L/s flow rate and 15 cm below the outlet.

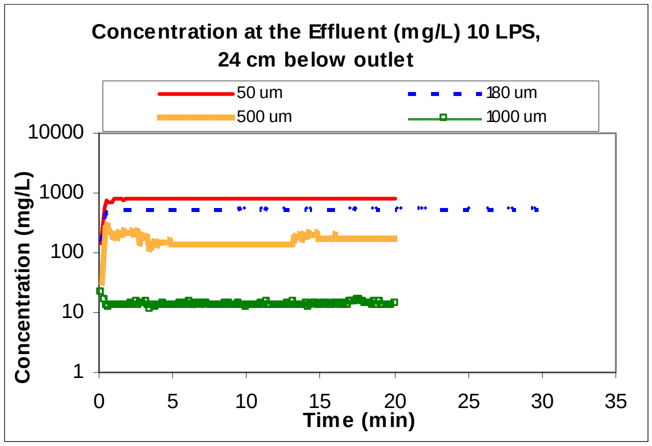

Figure O.5. SSC (mg/L) at 10 L/s flow rate and 24 cm below the outlet.

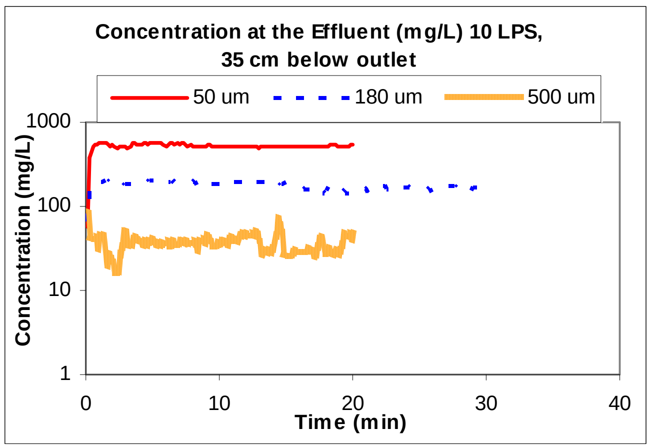

Figure O.6. SSC (mg/L) at 10 L/s flow rate and 35 cm below the outlet.

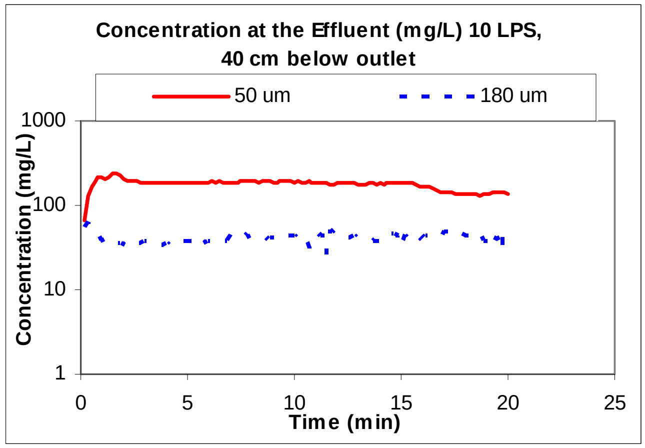

Figure O.7. SSC (mg/L) at 10 L/s flow rate and 40 cm below the outlet.

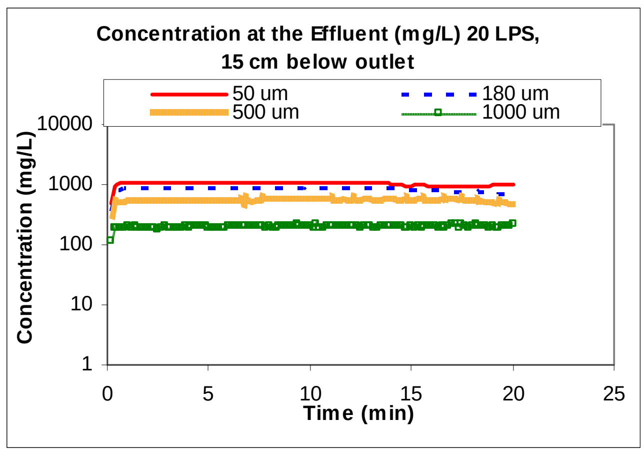

Figure O.8. SSC (mg/L) at 20 L/s flow rate and 15 cm below the outlet.

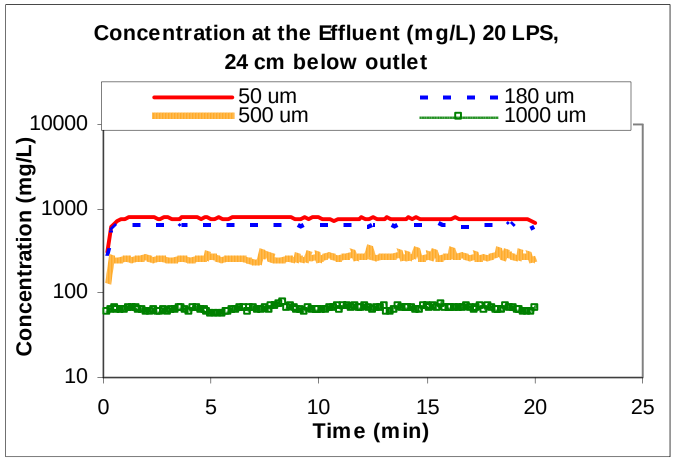

Figure O.9. SSC (mg/L) at 20 L/s flow rate and 24 cm below the outlet.

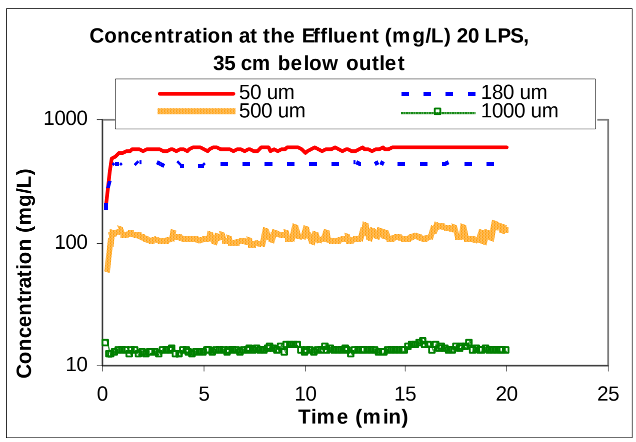

Figure O.10. SSC (mg/L) at 20 L/s flow rate and 35 cm below the outlet.

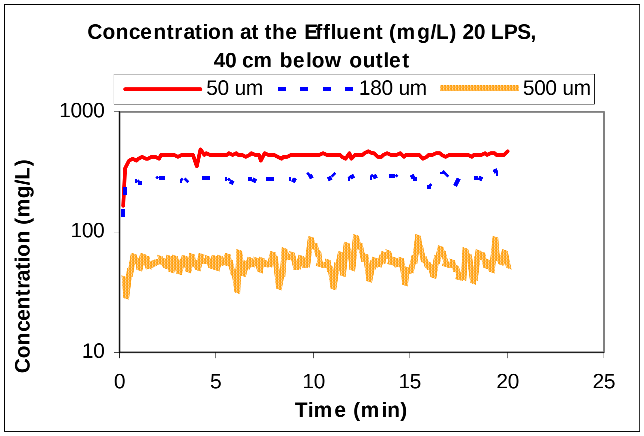

Figure O.11. SSC (mg/L) at 20 L/s flow rate and 40 cm below the outlet.

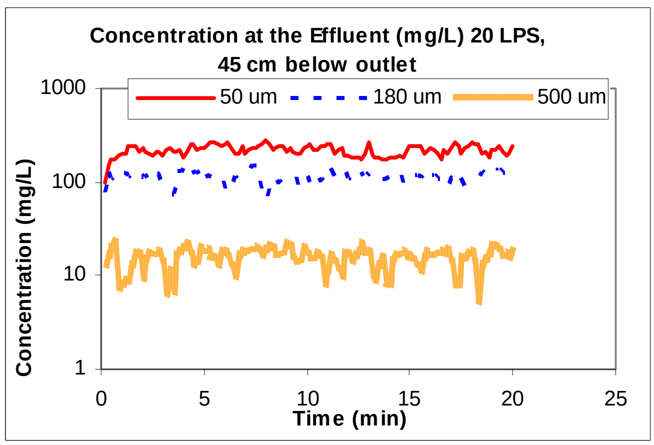

Figure O.12. SSC (mg/L) at 20 L/s flow rate and 45 cm below the outlet.

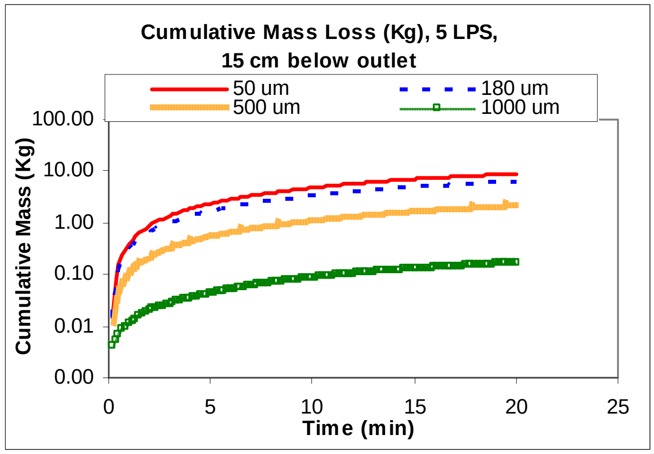

Figure O.13. Cumulative mass loss (Kg) at 5 L/s flow rate and 15 cm below the outlet.

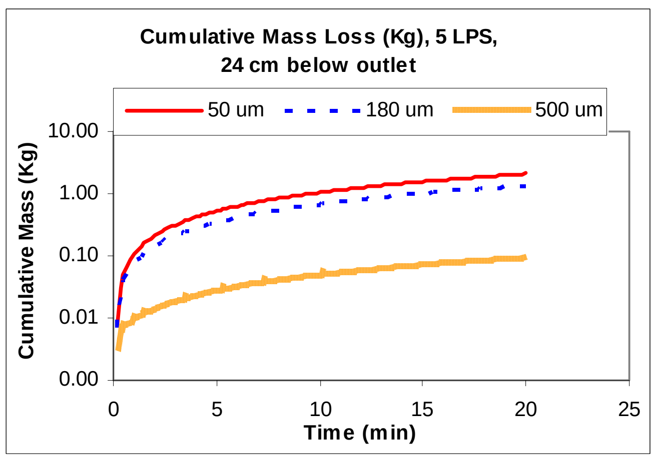

Figure O.14. Cumulative mass loss (Kg) at 5 L/s flow rate and 24 cm below the outlet.

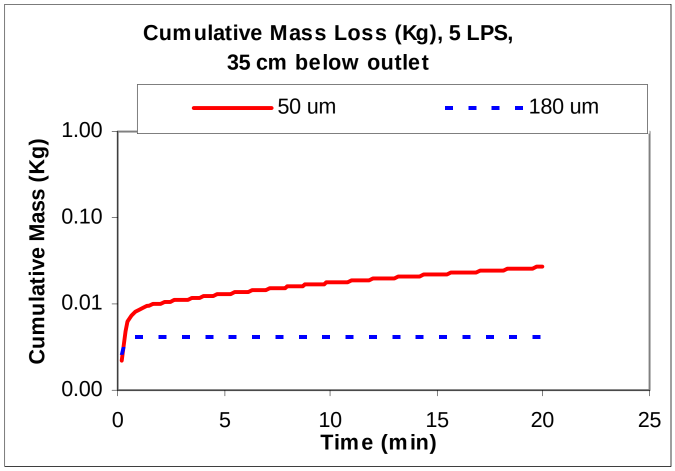

Figure O.15. Cumulative mass loss (Kg) at 5 L/s flow rate and 35 cm below the outlet.

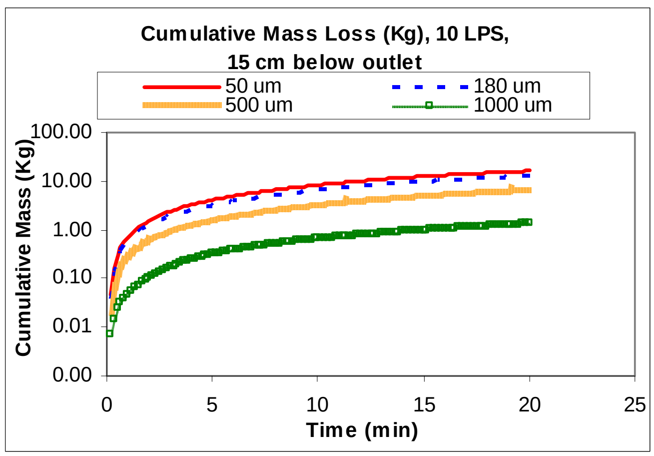

Figure O.16. Cumulative mass loss (Kg) at 10 L/s flow rate and 15 cm below the outlet.

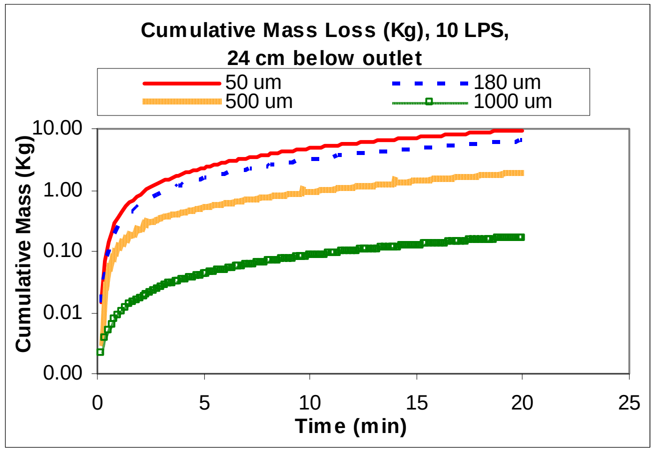

Figure O.17. Cumulative mass loss (Kg) at 10 L/s flow rate and 24 cm below the outlet.

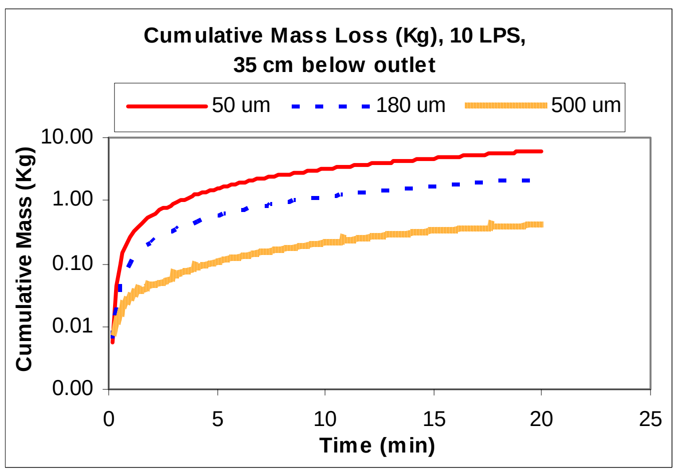

Figure O.18. Cumulative mass loss (Kg) at 10 L/s flow rate and 35 cm below the outlet.

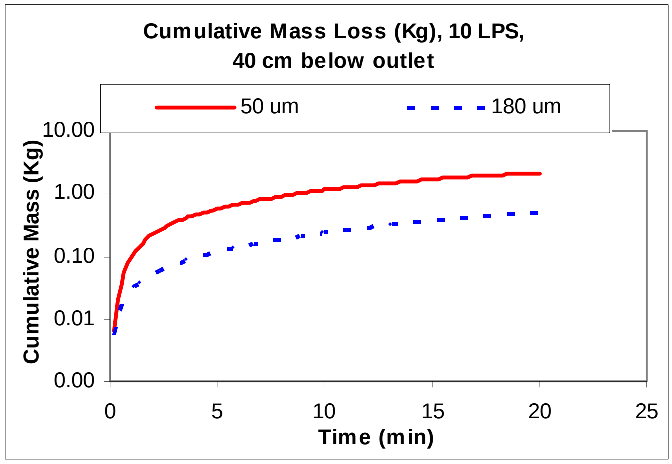

Figure O.19. Cumulative mass loss (Kg) at 10 L/s flow rate and 40 cm below the outlet.

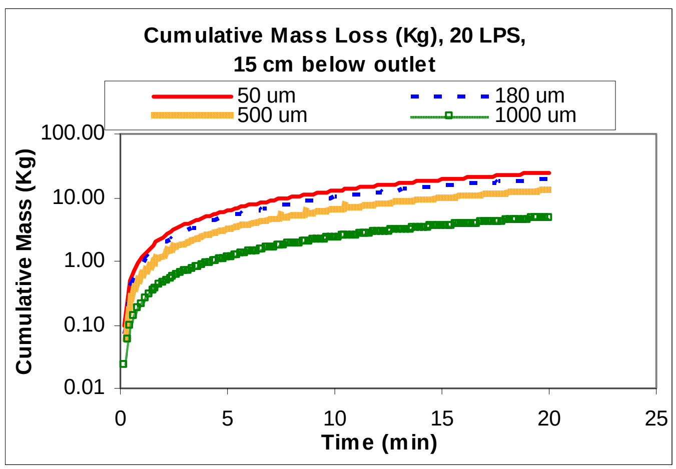

Figure O.20. Cumulative mass loss (Kg) at 20 L/s flow rate and 15 cm below the outlet.

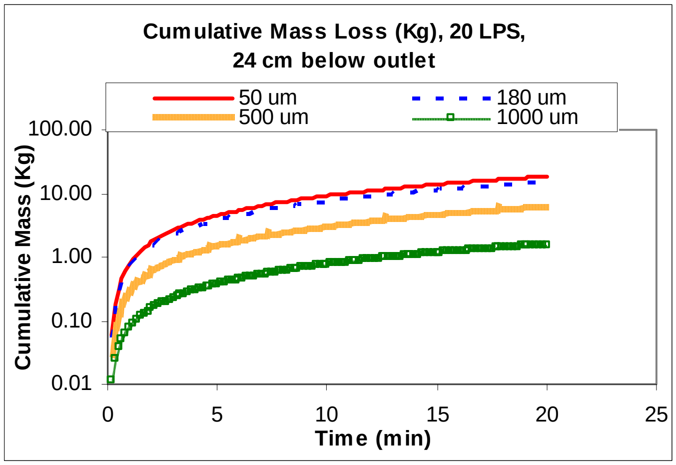

Figure O.21. Cumulative mass loss (Kg) at 20 L/s flow rate and 24 cm below the outlet.

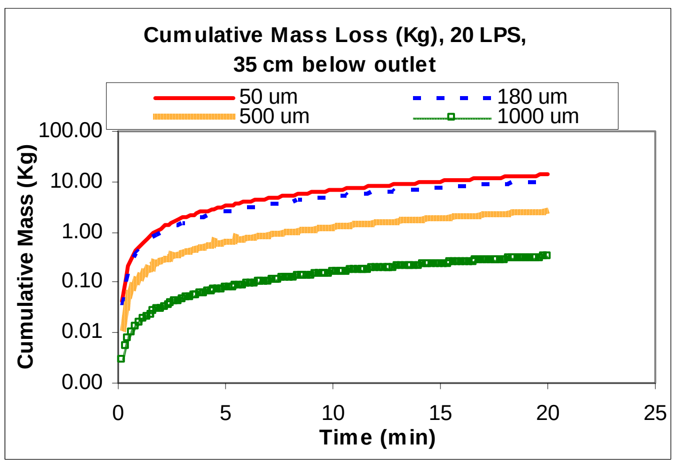

Figure O.22. Cumulative mass loss (Kg) at 20 L/s flow rate and 35 cm below the outlet.

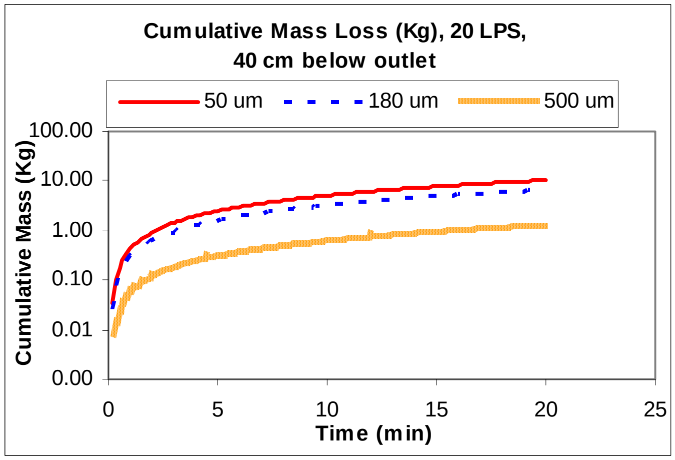

Figure O.23. Cumulative mass loss (Kg) at 20 L/s flow rate and 40 cm below the outlet.

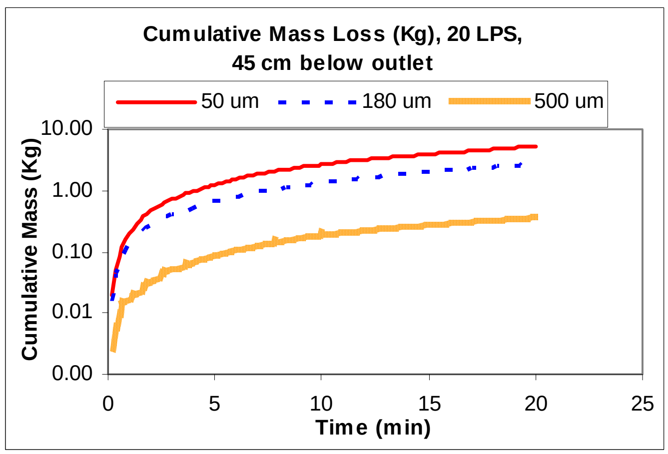

Figure O.24. Cumulative mass loss (Kg) at 20 L/s flow rate and 45 cm below the outlet.

APPENDIX P

SSC AND MASS LOAD OBTAINED FROM A 2D-CFD MODEL

Table P.1. Mean SSC and Mass Loss Based on the Cumulative Mass Loss Slope

Scenario	Flow rate (L/s)	Overlaying water depth (cm)	Sediment particle size (μm)	Mass Loss (g/min) (slope)	Concentration (mg/L)
1	5	15	50	466.3	1554.3
2	5	15	180	332.0	1106.7
3	5	15	500	114.2	380.7
4	5	15	1000	8.6	28.7
5	5	24	50	104.4	348.0
6	5	24	180	67.5	225.0
7	5	24	500	5.0	16.7
8	5	35	50	1.5	5.0
9	5	35	180	0.3	1.0
10	10	15	50	777.6	1296.0
11	10	15	180	651.4	1085.7
12	10	15	500	342.8	571.3
13	10	15	1000	66.1	110.2
14	10	24	50	480.2	800.3
15	10	24	180	347.5	579.2
16	10	24	500	97.6	162.7
17	10	24	1000	8.4	14.0
18	10	35	50	316.4	527.3
19	10	35	180	113.2	188.7
20	10	35	500	22.2	37.0
21	10	40	50	111.2	185.3
22	10	40	180	24.2	40.3
23	20	15	50	1261.2	1051.0
24	20	15	180	1005.7	838.1
25	20	15	500	677.7	564.8
26	20	15	1000	238.0	198.3
27	20	24	50	919.3	766.1
28	20	24	180	763.1	635.9
29	20	24	500	317.0	264.2
30	20	24	1000	77.8	64.8
31	20	35	50	680.0	566.7
32	20	35	180	513.2	427.7
33	20	35	500	133.1	110.9
34	20	35	1000	15.8	13.2
35	20	40	50	513.5	427.9
36	20	40	180	328.5	273.8
37	20	40	500	66.5	55.4
38	20	45	50	262.0	218.3
39	20	45	180	133.8	111.5
40	20	45	500	18.4	15.3

Table P.2. Percentage Reduction of SSC by Particle Size Increment

Flow rate (L/s)	Depth (cm)	SSC (mg/L)	Particle size (µm)	% Reduction of SSC by Particle Size Increment
5	15	1554.3	50	
		1106.7	180	29
		380.7	500	66
		28.7	1000	92
	24	348.0	50	
		225.0	180	35
		16.7	500	93
	35	5.0	50	
		1.0	180	80
10	15	1296.0	50	
		1085.7	180	16
		571.3	500	47
		110.2	1000	81
	24	800.3	50	
		579.2	180	28
		162.7	500	72
		14.0	1000	91
	35	527.3	50	
		188.7	180	64
		37.0	500	80
	40	185.3	50	
		40.3	180	78
20	15	1051.0	50	
		838.1	180	20
		564.8	500	33
		198.3	1000	65
	24	766.1	50	
		635.9	180	17
		264.2	500	58
		64.8	1000	75
	35	566.7	50	
		427.7	180	25
		110.9	500	74
		13.2	1000	88
	40	427.9	50	
		273.8	180	36
		55.4	500	80
	45	218.3	50	
		111.5	180	49
		15.3	500	86

Table P.3. Percentage Reduction of SSC by Overlaying Water Depth

Flow rate (L/s)	Particle size (μm)	SSC (mg/L)	Depth (cm)	% Reduction of SSC by Depth
5	50	1554	15	
		348	24	78
		5	35	99
	180	1107	15	
		225	24	80
		1	35	99
	500	381	15	
		17	24	96
10	50	1296	15	
		800	24	38
		527	35	34
		185	40	65
	180	1086	15	
		579	24	47
		189	35	67
		40	40	79
	500	571	15	
		163	24	72
		37	35	77
	1000	110	15	
		14	24	87
20	50	1051	15	
		766	24	27
		567	35	26
		428	40	24
		218	45	49
	180	838	15	
		636	24	24
		428	35	33
		274	40	36
		112	45	59
	500	565	15	
		264	24	53
		111	35	58
		55	40	50
		15	45	72
	1000	198	15	
		65	24	67
		13	35	80

Table P.4. Percentage of Change of SSC by Flow Rate

Flow rate (L/s)	Depth (cm)	Particle size (µm)	SSC (mg/L)	% of Change of SSC by Flow rate
5	15	50	1554.3	
10			1296.0	-20
20			1051.0	-23
5	24		348.0	
10			800.3	57
20			766.1	-4
5	35		5.0	
10			527.3	99
20			566.7	7
10	40		185.3	
20			427.9	57
5	15	180	1106.7	
10			1085.7	-2
20			838.1	-30
5	24		225.0	
10			579.2	61
20			635.9	9
5	35		1.0	
10			188.7	99
20			427.7	56
10	40		40.3	
20			273.8	85
5	15	500	380.7	
10			571.3	33
20			564.8	-1
5	24		16.7	
10			162.7	90
20			264.2	38
10	35		37.0	
20			110.9	67
5	15	1000	28.7	
10			110.2	74
20			198.3	44
10	24		14.0	
20			64.8	78

Table P.5. Percentage of Increment of Mass Load by Flow Rate

Flow rate (L/s)	Depth (cm)	Particle size (μm)	Mass Load (g/min)	Total mass loss in 20 min (Kg)	% Increment of mass loss by Flow rate
5	15	50	466.3	9.326	
10			777.6	15.552	40
20			1261.2	25.224	38
5	24		104.4	2.088	
10			480.2	9.604	78
20			919.3	18.386	48
5	35		1.5	0.03	
10			316.4	6.328	100
20			680	13.6	53
10	40		111.2	2.224	
20			513.5	10.27	78
5	15	180	332	6.64	
10			651.4	13.028	49
20			1005.7	20.114	35
5	24		67.5	1.35	
10			347.5	6.95	81
20			763.1	15.262	54
5	35		0.3	0.006	
10			113.2	2.264	100
20			513.2	10.264	78
10	40		24.2	0.484	
20			328.5	6.57	93
5	15	500	114.2	2.284	
10			342.8	6.856	67
20			677.7	13.554	49
5	24		5	0.1	
10			97.6	1.952	95
20			317	6.34	69
10	35		22.2	0.444	
20			133.1	2.662	83
5	15	1000	8.6	0.172	
10			66.1	1.322	87
20			238	4.76	72
10	24		8.4	0.168	
20			77.8	1.556	89

APPENDIX Q

REGRESSION WITH ANOVA OF CUMULATIVE MASS LOSS VERSUS TIME TO DETERMINE MASS LOAD – RESULTS FROM A 2D-CFD MODEL

Table Q.1. Cumulative Mass Loss for 5 L/s, 15 cm and 50 μm (Left), and 5 L/s, 15 cm and 180 μm (Right)

Bivariate Fit of 15 cm_50 um_5LPS By time (min)

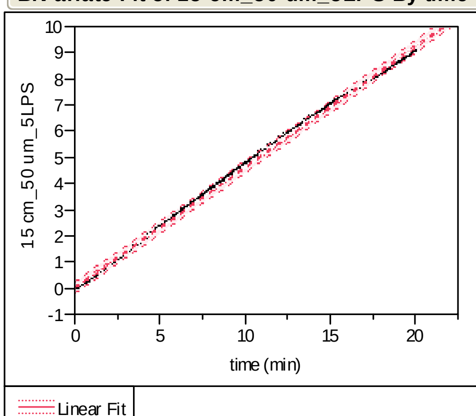

Linear Fit

15 cm_50 um_5LPS = 0.0633078 + 0.4615992*time (min)

Summary of Fit

RSquare	0.998135
RSquare Adj	0.998119
Root Mean Square Error	0.116158
Mean of Response	4.717767
Observations (or Sum Wgts)	120

Analysis of Variance

Source	DF	Sum of Squares	Mean Square	F Ratio
Model	1	852.16038	852.160	63157.19
Error	118	1.59214	0.013	Prob > F
C. Total	119	853.75252		<.0001 *

Parameter Estimates

Term	Estimate	Std Error	t Ratio	Prob>|t|
Intercept	0.0633078	0.021341	2.97	0.0036 *
time (min)	0.4615992	0.001837	251.31	<.0001 *

Bivariate Fit of 15 cm_180 um_5LPS By time (min)

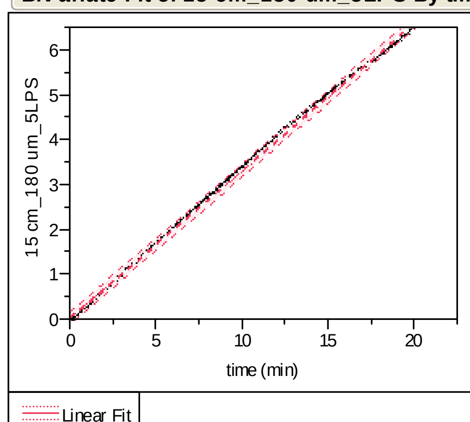

Linear Fit

15 cm_180 um_5LPS = 0.0442325 + 0.3288942*time (min)

Summary of Fit

RSquare	0.998645
RSquare Adj	0.998633
Root Mean Square Error	0.070542
Mean of Response	3.360582
Observations (or Sum Wgts)	120

Analysis of Variance

Source	DF	Sum of Squares	Mean Square	F Ratio
Model	1	432.61697	432.617	86937.10
Error	118	0.58719	0.004976	Prob > F
C. Total	119	433.20416		<.0001 *

Parameter Estimates

Term	Estimate	Std Error	t Ratio	Prob>|t|
Intercept	0.0442325	0.012961	3.41	0.0009 *
time (min)	0.3288942	0.001115	294.85	<.0001 *

Table Q.2. Cumulative Mass Loss for 5 L/s, 15 cm and 500 µm (Left), and 5 L/s, 24 cm and 50 µm (Right)

Biv ariate Fit of 15 cm_500 um_5LPS By time (min)

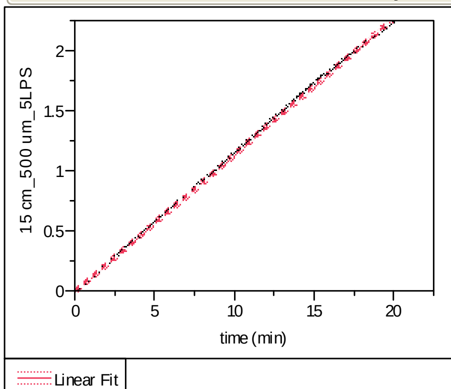

Linear Fit

15 cm_500 um_5LPS = 0.0049981 + 0.113793*time (min)

Summary of Fit

RSquare	0.999644
RSquare Adj	0.999641
Root Mean Square Error	0.0125
Mean of Response	1.152411
Observations (or Sum Wgts)	120

Analysis of Variance

Source	DF	Sum of Squares	Mean Square	F Ratio
Model	1	51.787224	51.7872	331422.0
Error	118	0.018438	0.000156	**Prob > F**
C. Total	119	51.805663		<.0001 *

Parameter Estimates

Term	Estimate	Std Error	t Ratio	Prob>|t|
Intercept	0.0049981	0.002297	2.18	0.0315 *
time (min)	0.113793	0.000198	575.69	<.0001 *

Biv ariate Fit of 24 cm_50 um_5LPS By time (min)

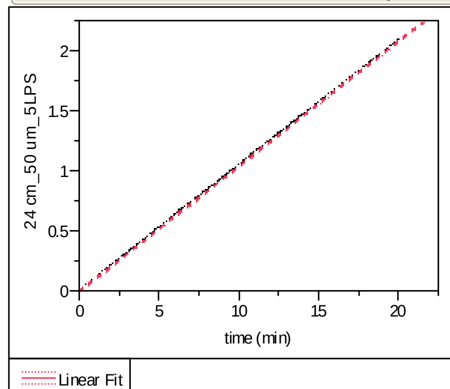

Linear Fit

24 cm_50 um_5LPS = 0.0037337 + 0.104155*time (min)

Summary of Fit

RSquare	0.999954
RSquare Adj	0.999954
Root Mean Square Error	0.004113
Mean of Response	1.053964
Observations (or Sum Wgts)	120

Analysis of Variance

Source	DF	Sum of Squares	Mean Square	F Ratio
Model	1	43.386221	43.3862	2564391
Error	118	0.001996	0.000017	**Prob > F**
C. Total	119	43.388218		<.0001 *

Parameter Estimates

Term	Estimate	Std Error	t Ratio	Prob>|t|
Intercept	0.0037337	0.000756	4.94	<.0001 *
time (min)	0.104155	0.000065	1601.4	<.0001 *

Table Q.3. Cumulative Mass Loss for 5 L/s, 24 cm and 180 μm (Left), and 10 L/s, 15 cm and 50 μm (Right)

Bivariate Fit of 24 cm_180 um_5LPS By time (min)

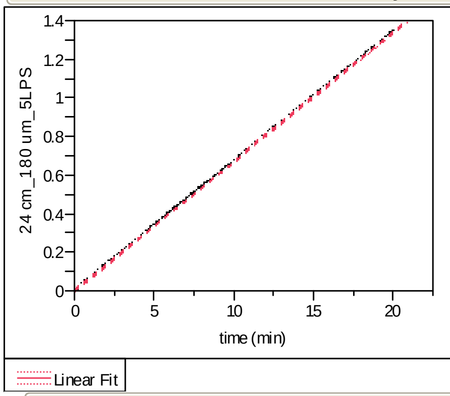

Linear Fit

24 cm_180 um_5LPS = 0.0077322 + 0.0669248*time (min)

Summary of Fit

RSquare	0.999944
RSquare Adj	0.999944
Root Mean Square Error	0.002915
Mean of Response	0.682557
Observations (or Sum Wgts)	120

Analysis of Variance

Source	DF	Sum of Squares	Mean Square	F Ratio
Model	1	17.912864	17.9129	2107787
Error	118	0.001003	8.498e-6	**Prob > F**
C. Total	119	17.913866		<.0001 *

Parameter Estimates

Term	Estimate	Std Error	t Ratio	Prob>|t|
Intercept	0.0077322	0.000536	14.44	<.0001 *
time (min)	0.0669248	0.000046	1451.8	<.0001 *

Bivariate Fit of 15 cm_50 um_10LPS By time (min)

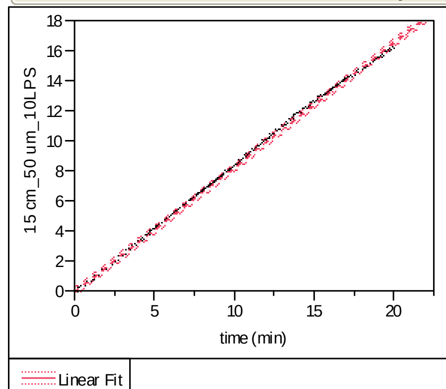

Linear Fit

15 cm_50 um_10LPS = -0.013789 + 0.8307718*time (min)

Summary of Fit

RSquare	0.999194
RSquare Adj	0.999187
Root Mean Square Error	0.137396
Mean of Response	8.36316
Observations (or Sum Wgts)	120

Analysis of Variance

Source	DF	Sum of Squares	Mean Square	F Ratio
Model	1	2760.2903	2760.29	146219.9
Error	118	2.2276	0.018878	**Prob > F**
C. Total	119	2762.5179		<.0001 *

Parameter Estimates

Term	Estimate	Std Error	t Ratio	Prob>|t|
Intercept	-0.013789	0.025243	-0.55	0.5859
time (min)	0.8307718	0.002173	382.39	<.0001 *

Table Q.4. Cumulative Mass Loss for 10 L/s, 15 cm and 180 µm (Left), and 10 L/s, 15 cm and 500 µm (Right)

Bivariate Fit of 15 cm_180 um_10LPS By time (min)

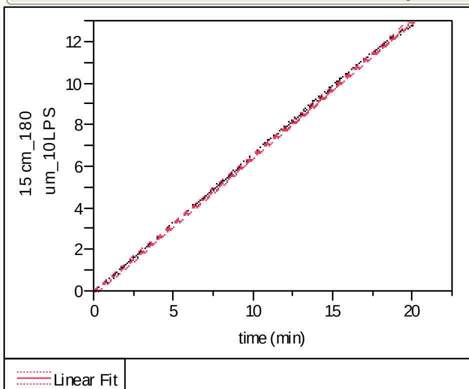

Linear Fit

15 cm_180 um_10LPS = -0.044982 + 0.6547238*time (min)

Summary of Fit

RSquare	0.999749
RSquare Adj	0.999747
Root Mean Square Error	0.0604
Mean of Response	6.556816
Observations (or Sum Wgts)	120

Analysis of Variance

Source	DF	Sum of Squares	Mean Square	F Ratio
Model	1	1714.3816	1714.38	469934.8
Error	118	0.4305	0.003648	**Prob > F**
C. Total	119	1714.8121		<.0001 *

Parameter Estimates

Term	Estimate	Std Error	t Ratio	Prob>|t|
Intercept	-0.044982	0.011097	-4.05	<.0001 *
time (min)	0.6547238	0.000955	685.52	<.0001 *

Bivariate Fit of 15 cm_500 um_10LPS By time (min)

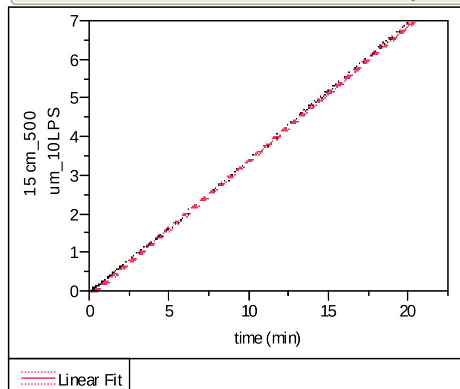

Linear Fit

15 cm_500 um_10LPS = -0.113335 + 0.3512462*time (min)

Summary of Fit

RSquare	0.999805
RSquare Adj	0.999803
Root Mean Square Error	0.028552
Mean of Response	3.428397
Observations (or Sum Wgts)	120

Analysis of Variance

Source	DF	Sum of Squares	Mean Square	F Ratio
Model	1	493.41742	493.417	605256.0
Error	118	0.09620	0.000815	**Prob > F**
C. Total	119	493.51362		<.0001 *

Parameter Estimates

Term	Estimate	Std Error	t Ratio	Prob>|t|
Intercept	-0.113335	0.005246	-21.60	<.0001 *
time (min)	0.3512462	0.000451	777.98	<.0001 *

Table Q.5. Cumulative Mass Loss for 10 L/s, 15 cm and 1000 μm (Left), and 10 L/s, 24 cm and 50 μm (Right)

Bivariate Fit of 15 cm_1000 um_10LPS By time (min)

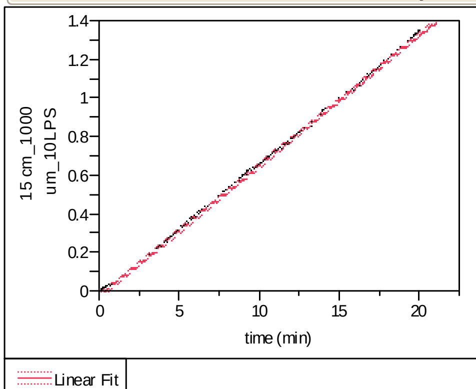

Linear Fit

15 cm_1000 um_10LPS = -0.022107 + 0.0677024*time (min)

Summary of Fit

RSquare	0.999728
RSquare Adj	0.999726
Root Mean Square Error	0.006502
Mean of Response	0.660559
Observations (or Sum Wgts)	120

Analysis of Variance

Source	DF	Sum of Squares	Mean Square	F Ratio
Model	1	18.331569	18.3316	433589.5
Error	118	0.004989	4.228e-5	**Prob > F**
C. Total	119	18.336558		<.0001 *

Parameter Estimates

Term	Estimate	Std Error	t Ratio	Prob>|t|
Intercept	-0.022107	0.001195	-18.51	<.0001 *
time (min)	0.0677024	0.000103	658.48	<.0001 *

Bivariate Fit of 24 cm_50 um_10LPS By time (min)

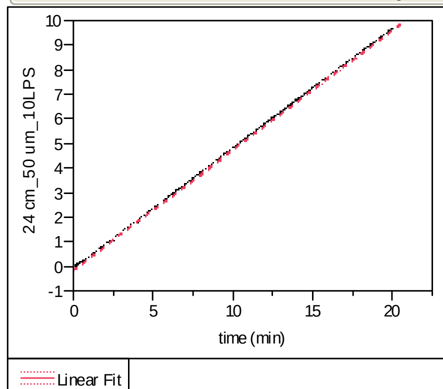

Linear Fit

24 cm_50 um_10LPS = -0.110527 + 0.4884282*time (min)

Summary of Fit

RSquare	0.999967
RSquare Adj	0.999967
Root Mean Square Error	0.01622
Mean of Response	4.814458
Observations (or Sum Wgts)	120

Analysis of Variance

Source	DF	Sum of Squares	Mean Square	F Ratio
Model	1	954.09731	954.097	3626536
Error	118	0.03104	0.000263	**Prob > F**
C. Total	119	954.12835		<.0001 *

Parameter Estimates

Term	Estimate	Std Error	t Ratio	Prob>|t|
Intercept	-0.110527	0.00298	-37.09	<.0001 *
time (min)	0.4884282	0.000256	1904.3	<.0001 *

Table Q.6. Cumulative Mass Loss for 10 L/s, 24 cm and 180 µm (Left), and 10 L/s, 24 cm and 1000 µm (Right)

Bivariate Fit of 24 cm_180 um_10LPS By time (min)

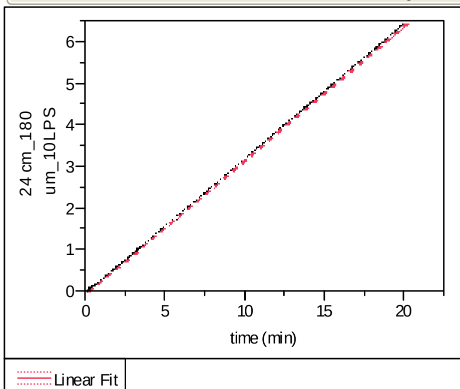

Linear Fit

24 cm_180 um_10LPS = -0.083807 + 0.3237611*time (min)

Summary of Fit

RSquare	0.999967
RSquare Adj	0.999967
Root Mean Square Error	0.010796
Mean of Response	3.180784
Observations (or Sum Wgts)	120

Analysis of Variance

Source	DF	Sum of Squares	Mean Square	F Ratio
Model	1	419.21859	419.219	3596917
Error	118	0.01375	0.000117	**Prob > F**
C. Total	119	419.23235		<.0001 *

Parameter Estimates

Term	Estimate	Std Error	t Ratio	Prob>|t|
Intercept	-0.083807	0.001983	-42.25	<.0001 *
time (min)	0.3237611	0.000171	1896.6	<.0001 *

Bivariate Fit of 24 cm_1000 um_10LPS By time (min)

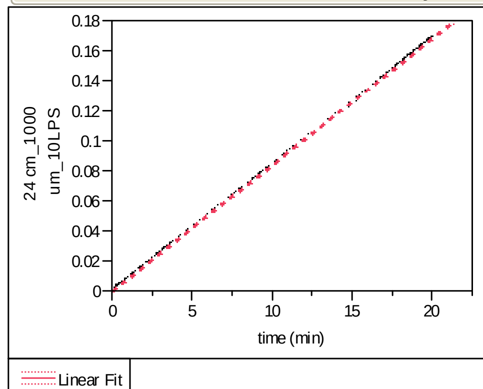

Linear Fit

24 cm_1000 um_10LPS = 0.0005423 + 0.0084002*time (min)

Summary of Fit

RSquare	0.999908
RSquare Adj	0.999907
Root Mean Square Error	0.00047
Mean of Response	0.085245
Observations (or Sum Wgts)	120

Analysis of Variance

Source	DF	Sum of Squares	Mean Square	F Ratio
Model	1	0.28221127	0.282211	1279810
Error	118	0.00002602	2.205e-7	**Prob > F**
C. Total	119	0.28223729		<.0001 *

Parameter Estimates

Term	Estimate	Std Error	t Ratio	Prob>|t|
Intercept	0.0005423	8.628e-5	6.29	<.0001 *
time (min)	0.0084002	7.425e-6	1131.3	<.0001 *

Table Q.7. Cumulative Mass Loss for 10 L/s, 35 cm and 50 µm (Left), and 10 L/s, 35 cm and 180 µm (Right)

Bivariate Fit of 35 cm_50 um_10LPS By time (min)

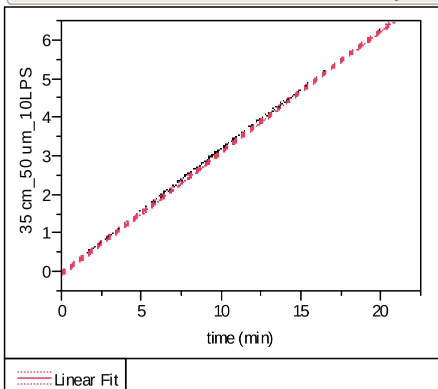

Linear Fit

35 cm_50 um_10LPS = -0.020496 + 0.3149048*time (min)

Summary of Fit

RSquare	0.999775
RSquare Adj	0.999773
Root Mean Square Error	0.027499
Mean of Response	3.154794
Observations (or Sum Wgts)	120

Analysis of Variance

Source	DF	Sum of Squares	Mean Square	F Ratio
Model	1	396.59734	396.597	524472.2
Error	118	0.08923	0.000756	**Prob > F**
C. Total	119	396.68657		<.0001 *

Parameter Estimates

Term	Estimate	Std Error	t Ratio	Prob>|t|
Intercept	-0.020496	0.005052	-4.06	<.0001 *
time (min)	0.3149048	0.000435	724.20	<.0001 *

Bivariate Fit of 35 cm_180 um_10LPS By time (min)

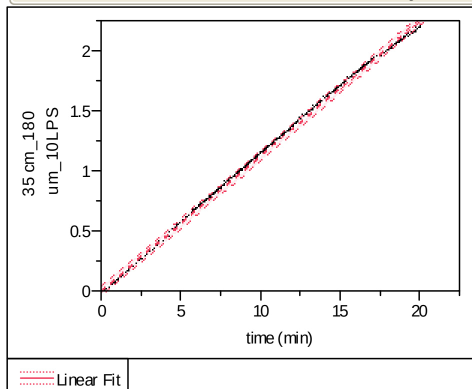

Linear Fit

35 cm_180 um_10LPS = 0.0084949 + 0.1126072*time (min)

Summary of Fit

RSquare	0.998973
RSquare Adj	0.998965
Root Mean Square Error	0.021018
Mean of Response	1.143951
Observations (or Sum Wgts)	120

Analysis of Variance

Source	DF	Sum of Squares	Mean Square	F Ratio
Model	1	50.713472	50.7135	114803.7
Error	118	0.052125	0.000442	**Prob > F**
C. Total	119	50.765597		<.0001 *

Parameter Estimates

Term	Estimate	Std Error	t Ratio	Prob>|t|
Intercept	0.0084949	0.003862	2.20	0.0298 *
time (min)	0.1126072	0.000332	338.83	<.0001 *

Table Q.8. Cumulative Mass Loss for 10 L/s, 35 cm and 500 μm (Left), and 10 L/s, 40 cm and 50 μm (Right)

Bivariate Fit of 35 cm_500 um_10LPS By time (min)

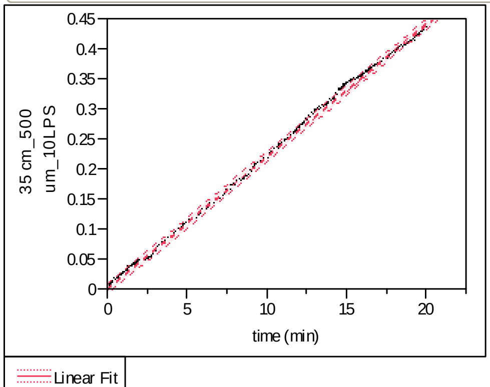

Linear Fit

35 cm_500 um_10LPS = 0.0016848 + 0.0220599*time (min)

Summary of Fit

RSquare	0.998875
RSquare Adj	0.998865
Root Mean Square Error	0.004311
Mean of Response	0.224122
Observations (or Sum Wgts)	120

Analysis of Variance

Source	DF	Sum of Squares	Mean Square	F Ratio
Model	1	1.9462425	1.94624	104734.0
Error	118	0.0021928	1.858e-5	**Prob > F**
C. Total	119	1.9484352		<.0001 *

Parameter Estimates

Term	Estimate	Std Error	t Ratio	Prob>|t|
Intercept	0.0016848	0.000792	2.13	0.0355 *
time (min)	0.0220599	6.816e-5	323.63	<.0001 *

Bivariate Fit of 40 cm_50 um_10LPS By time (min)

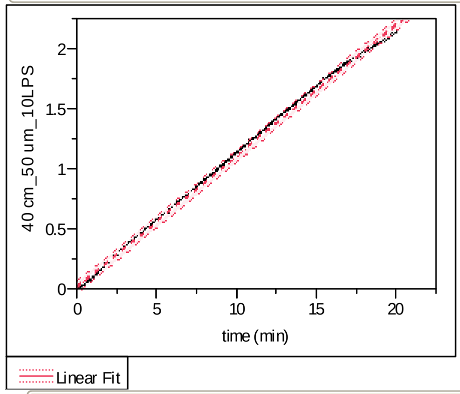

Linear Fit

40 cm_50 um_10LPS = 0.0233055 + 0.1094632*time (min)

Summary of Fit

RSquare	0.998461
RSquare Adj	0.998448
Root Mean Square Error	0.025021
Mean of Response	1.127059
Observations (or Sum Wgts)	120

Analysis of Variance

Source	DF	Sum of Squares	Mean Square	F Ratio
Model	1	47.921181	47.9212	76548.04
Error	118	0.073871	0.000626	**Prob > F**
C. Total	119	47.995053		<.0001 *

Parameter Estimates

Term	Estimate	Std Error	t Ratio	Prob>|t|
Intercept	0.0233055	0.004597	5.07	<.0001 *
time (min)	0.1094632	0.000396	276.67	<.0001 *

Table Q.9. Cumulative Mass Loss for 10 L/s, 40 cm and 180 µm (Left), and 20 L/s, 15 cm and 50 µm (Right)

Bivariate Fit of 40 cm_180 um_10LPS By time (min)

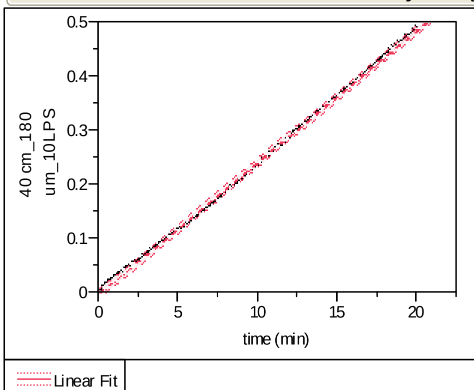

Linear Fit

40 cm_180 um_10LPS = -0.003846 + 0.0244615*time (min)

Summary of Fit

RSquare	0.999116
RSquare Adj	0.999109
Root Mean Square Error	0.004235
Mean of Response	0.242807
Observations (or Sum Wgts)	120

Analysis of Variance

Source	DF	Sum of Squares	Mean Square	F Ratio
Model	1	2.3930790	2.39308	133407.2
Error	118	0.0021167	0.000018	Prob > F
C. Total	119	2.3951957		<.0001 *

Parameter Estimates

Term	Estimate	Std Error	t Ratio	Prob>|t|
Intercept	-0.003846	0.000778	-4.94	<.0001 *
time (min)	0.0244615	0.000067	365.25	<.0001 *

Bivariate Fit of 15 cm_50 um_20LPS By time (min)

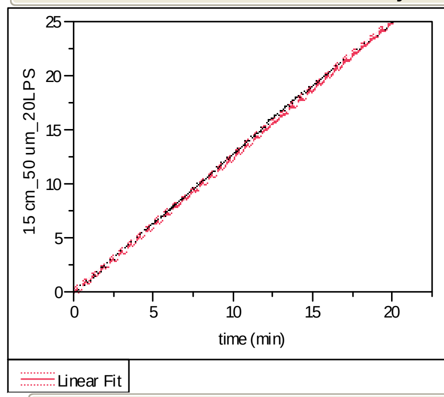

Linear Fit

15 cm_50 um_20LPS = 0.0290162 + 1.2590275*time (min)

Summary of Fit

RSquare	0.999475
RSquare Adj	0.999471
Root Mean Square Error	0.167934
Mean of Response	12.72421
Observations (or Sum Wgts)	120

Analysis of Variance

Source	DF	Sum of Squares	Mean Square	F Ratio
Model	1	6339.5966	6339.60	224792.7
Error	118	3.3278	0.028202	Prob > F
C. Total	119	6342.9245		<.0001 *

Parameter Estimates

Term	Estimate	Std Error	t Ratio	Prob>|t|
Intercept	0.0290162	0.030854	0.94	0.3489
time (min)	1.2590275	0.002655	474.12	<.0001 *

Table Q.10. Cumulative Mass Loss for 20 L/s, 15 cm and 180 µm (Left), and 20 L/s, 15 cm and 500 µm (Right)

Bivariate Fit of 15 cm_180 um_20LPS By time (min)

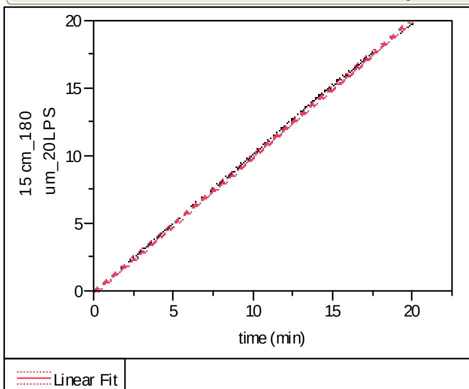

Linear Fit

15 cm_180 um_20LPS = -0.058593 + 1.010126*time (min)

Summary of Fit

RSquare	0.999734
RSquare Adj	0.999732
Root Mean Square Error	0.095962
Mean of Response	10.12684
Observations (or Sum Wgts)	120

Analysis of Variance

Source	DF	Sum of Squares	Mean Square	F Ratio
Model	1	4080.7719	4080.77	443145.5
Error	118	1.0866	0.009209	Prob > F
C. Total	119	4081.8585		<.0001 *

Parameter Estimates

Term	Estimate	Std Error	t Ratio	Prob>|t|
Intercept	-0.058593	0.017631	-3.32	0.0012 *
time (min)	1.010126	0.001517	665.69	<.0001 *

Bivariate Fit of 15 cm_500 um_20LPS By time (min)

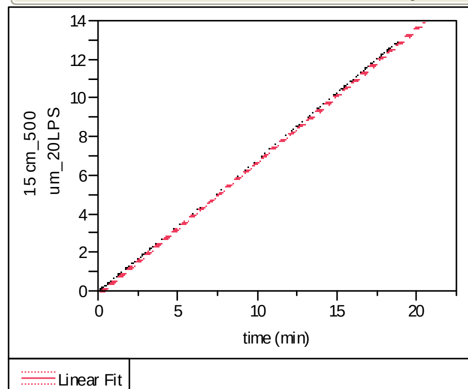

Linear Fit

15 cm_500 um_20LPS = -0.147881 + 0.6887035*time (min)

Summary of Fit

RSquare	0.99988
RSquare Adj	0.999879
Root Mean Square Error	0.043916
Mean of Response	6.796546
Observations (or Sum Wgts)	120

Analysis of Variance

Source	DF	Sum of Squares	Mean Square	F Ratio
Model	1	1896.9499	1896.95	983597.3
Error	118	0.2276	0.001929	Prob > F
C. Total	119	1897.1775		<.0001 *

Parameter Estimates

Term	Estimate	Std Error	t Ratio	Prob>|t|
Intercept	-0.147881	0.008069	-18.33	<.0001 *
time (min)	0.6887035	0.000694	991.76	<.0001 *

Table Q.11. Cumulative Mass Loss for 20 L/s, 15 cm and 1000 µm (Left), and 20 L/s, 24 cm and 50 µm (Right)

Bivariate Fit of 15 cm_1000 um_20LPS By time (min)

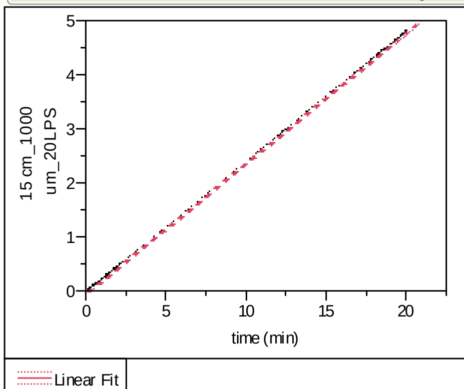

Linear Fit

15 cm_1000 um_20LPS = -0.049804 + 0.2417229*time (min)

Summary of Fit

RSquare	0.999911
RSquare Adj	0.99991
Root Mean Square Error	0.013313
Mean of Response	2.387569
Observations (or Sum Wgts)	120

Analysis of Variance

Source	DF	Sum of Squares	Mean Square	F Ratio
Model	1	233.68281	233.683	1318433
Error	118	0.02091	0.000177	Prob > F
C. Total	119	233.70372		<.0001 *

Parameter Estimates

Term	Estimate	Std Error	t Ratio	Prob>|t|
Intercept	-0.049804	0.002446	-20.36	<.0001 *
time (min)	0.2417229	0.000211	1148.2	<.0001 *

Bivariate Fit of 24 cm_50 um_20LPS By time (min)

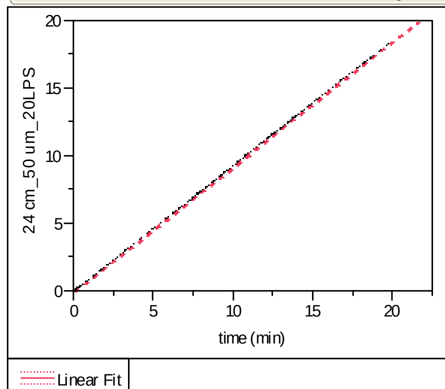

Linear Fit

24 cm_50 um_20LPS = -0.124864 + 0.928634*time (min)

Summary of Fit

RSquare	0.999951
RSquare Adj	0.999951
Root Mean Square Error	0.037775
Mean of Response	9.238862
Observations (or Sum Wgts)	120

Analysis of Variance

Source	DF	Sum of Squares	Mean Square	F Ratio
Model	1	3448.8982	3448.90	2416911
Error	118	0.1684	0.001427	Prob > F
C. Total	119	3449.0666		<.0001 *

Parameter Estimates

Term	Estimate	Std Error	t Ratio	Prob>|t|
Intercept	-0.124864	0.00694	-17.99	<.0001 *
time (min)	0.928634	0.000597	1554.6	<.0001 *

Table Q.12. Cumulative Mass Loss for 20 L/s, 24 cm and 180 μm (Left), and 20 L/s, 24 cm and 500 μm (Right)

Bivariate Fit of 24 cm_180 um_20LPS By time (min)

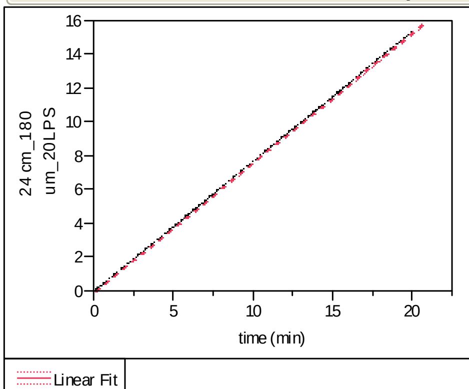

Linear Fit

24 cm_180 um_20LPS = -0.086365 + 0.7695083*time (min)

Summary of Fit

RSquare	0.999975
RSquare Adj	0.999975
Root Mean Square Error	0.022254
Mean of Response	7.672844
Observations (or Sum Wgts)	120

Analysis of Variance

Source	DF	Sum of Squares	Mean Square	F Ratio
Model	1	2368.1970	2368.20	4782092
Error	118	0.0584	0.000495	**Prob > F**
C. Total	119	2368.2554		<.0001 *

Parameter Estimates

Term	Estimate	Std Error	t Ratio	Prob>|t|
Intercept	-0.086365	0.004089	-21.12	<.0001 *
time (min)	0.7695083	0.000352	2186.8	<.0001 *

Bivariate Fit of 24 cm_500 um_20LPS By time (min)

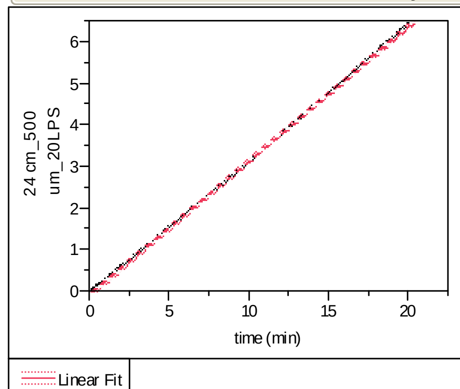

Linear Fit

24 cm_500 um_20LPS = -0.083464 + 0.323184*time (min)

Summary of Fit

RSquare	0.999699
RSquare Adj	0.999696
Root Mean Square Error	0.032674
Mean of Response	3.175309
Observations (or Sum Wgts)	120

Analysis of Variance

Source	DF	Sum of Squares	Mean Square	F Ratio
Model	1	417.72556	417.726	391283.9
Error	118	0.12597	0.001068	**Prob > F**
C. Total	119	417.85154		<.0001 *

Parameter Estimates

Term	Estimate	Std Error	t Ratio	Prob>|t|
Intercept	-0.083464	0.006003	-13.90	<.0001 *
time (min)	0.323184	0.000517	625.53	<.0001 *

Table Q.13. Cumulative Mass Loss for 20 L/s, 24 cm and 1000 µm (Left), and 20 L/s, 35 cm and 50 µm (Right)

Bivariate Fit of 24 cm_1000 um_20LPS By time (min)

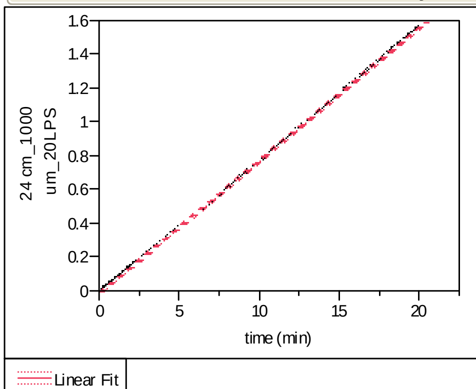

Linear Fit

24 cm_1000 um_20LPS = -0.012549 + 0.0787635*time (min)

Summary of Fit

RSquare	0.999808
RSquare Adj	0.999807
Root Mean Square Error	0.006351
Mean of Response	0.78165
Observations (or Sum Wgts)	120

Analysis of Variance

Source	DF	Sum of Squares	Mean Square	F Ratio
Model	1	24.810837	24.8108	615088.5
Error	118	0.004760	4.034e-5	Prob > F
C. Total	119	24.815597		<.0001 *

Parameter Estimates

Term	Estimate	Std Error	t Ratio	Prob>|t|
Intercept	-0.012549	0.001167	-10.75	<.0001 *
time (min)	0.0787635	0.0001	784.28	<.0001 *

Bivariate Fit of 35 cm_50 um_20LPS By time (min)

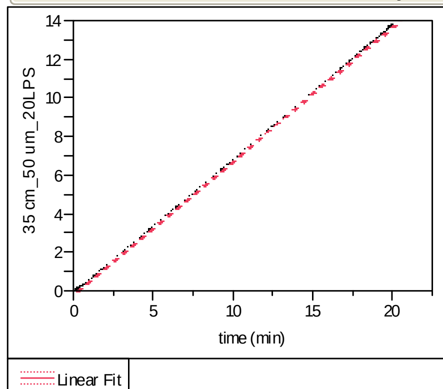

Linear Fit

35 cm_50 um_20LPS = -0.195085 + 0.6944928*time (min)

Summary of Fit

RSquare	0.999914
RSquare Adj	0.999913
Root Mean Square Error	0.037551
Mean of Response	6.807718
Observations (or Sum Wgts)	120

Analysis of Variance

Source	DF	Sum of Squares	Mean Square	F Ratio
Model	1	1928.9757	1928.98	1368028
Error	118	0.1664	0.00141	Prob > F
C. Total	119	1929.1421		<.0001 *

Parameter Estimates

Term	Estimate	Std Error	t Ratio	Prob>|t|
Intercept	-0.195085	0.006899	-28.28	<.0001 *
time (min)	0.6944928	0.000594	1169.6	<.0001 *

Table Q.14. Cumulative Mass Loss for 20 L/s, 35 cm and 180 µm (Left), and 20 L/s, 35 cm and 500 µm (Right)

Bivariate Fit of 35 cm_180 um_20LPS By time (min)

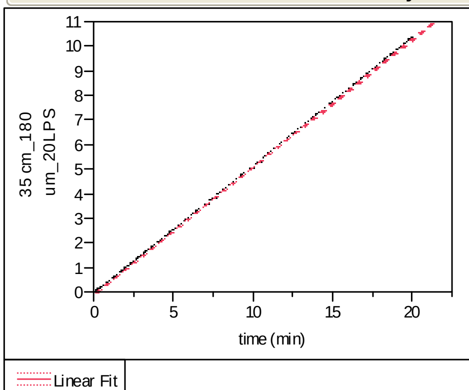

Linear Fit

35 cm_180 um_20LPS = -0.093475 + 0.520146*time (min)

Summary of Fit

RSquare	0.999952
RSquare Adj	0.999952
Root Mean Square Error	0.02099
Mean of Response	5.15133
Observations (or Sum Wgts)	120

Analysis of Variance

Source	DF	Sum of Squares	Mean Square	F Ratio
Model	1	1082.0360	1082.04	2455932
Error	118	0.0520	0.000441	**Prob > F**
C. Total	119	1082.0880		<.0001 *

Parameter Estimates

Term	Estimate	Std Error	t Ratio	Prob>|t|
Intercept	-0.093475	0.003856	-24.24	<.0001 *
time (min)	0.520146	0.000332	1567.1	<.0001 *

Bivariate Fit of 35 cm_500 um_20LPS By time (min)

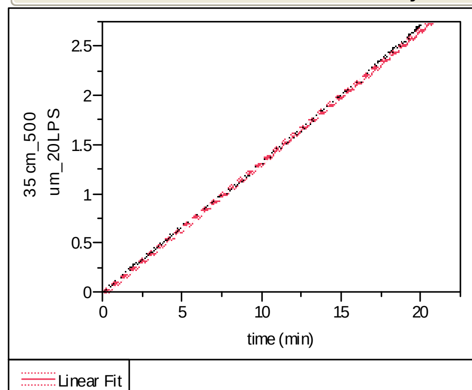

Linear Fit

35 cm_500 um_20LPS = -0.018222 + 0.1344466*time (min)

Summary of Fit

RSquare	0.999611
RSquare Adj	0.999608
Root Mean Square Error	0.015439
Mean of Response	1.337448
Observations (or Sum Wgts)	120

Analysis of Variance

Source	DF	Sum of Squares	Mean Square	F Ratio
Model	1	72.292069	72.2921	303272.7
Error	118	0.028128	0.000238	**Prob > F**
C. Total	119	72.320197		<.0001 *

Parameter Estimates

Term	Estimate	Std Error	t Ratio	Prob>|t|
Intercept	-0.018222	0.002837	-6.42	<.0001 *
time (min)	0.1344466	0.000244	550.70	<.0001 *

Table Q.15. Cumulative Mass Loss for 20 L/s, 35 cm and 1000 µm (Left), and 20 L/s, 40 cm and 50 µm (Right)

Bivariate Fit of 35 cm_1000 um_20LPS By time (min)

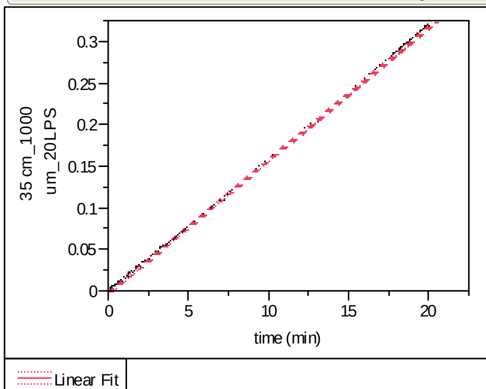

Linear Fit

35 cm_1000 um_20LPS = -0.00236 + 0.0160109*time (min)

Summary of Fit

RSquare	0.999797
RSquare Adj	0.999796
Root Mean Square Error	0.001327
Mean of Response	0.159083
Observations (or Sum Wgts)	120

Analysis of Variance

Source	DF	Sum of Squares	Mean Square	F Ratio
Model	1	1.0252299	1.02523	582528.0
Error	118	0.0002077	1.76e-6	**Prob > F**
C. Total	119	1.0254376		<.0001 *

Parameter Estimates

Term	Estimate	Std Error	t Ratio	Prob>|t|
Intercept	-0.00236	0.000244	-9.68	<.0001 *
time (min)	0.0160109	0.000021	763.24	<.0001 *

Bivariate Fit of 40 cm_50 um_20LPS By time (min)

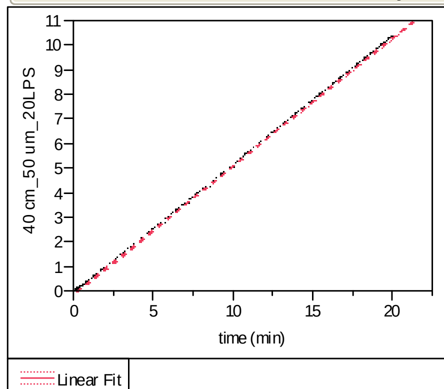

Linear Fit

40 cm_50 um_20LPS = -0.120026 + 0.5224782*time (min)

Summary of Fit

RSquare	0.999961
RSquare Adj	0.99996
Root Mean Square Error	0.019066
Mean of Response	5.148296
Observations (or Sum Wgts)	120

Analysis of Variance

Source	DF	Sum of Squares	Mean Square	F Ratio
Model	1	1091.7608	1091.76	3003388
Error	118	0.0429	0.000364	**Prob > F**
C. Total	119	1091.8037		<.0001 *

Parameter Estimates

Term	Estimate	Std Error	t Ratio	Prob>|t|
Intercept	-0.120026	0.003503	-34.26	<.0001 *
time (min)	0.5224782	0.000301	1733.0	<.0001 *

Table Q.16. Cumulative Mass Loss for 20 L/s, 40 cm and 180 µm (Left), and 20 L/s, 40 cm and 500 µm (Right)

Bivariate Fit of 40 cm_180 um_20LPS By time (min)

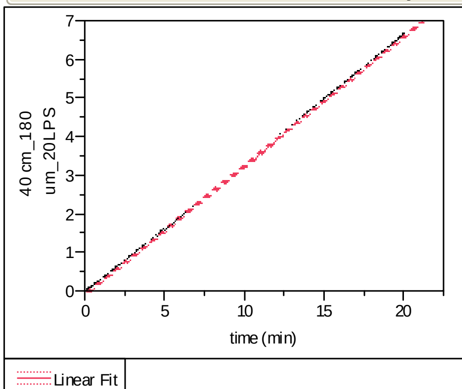

Linear Fit

40 cm_180 um_20LPS = -0.079273 + 0.3344095*time (min)

Summary of Fit

RSquare	0.999854
RSquare Adj	0.999853
Root Mean Square Error	0.023527
Mean of Response	3.29269
Observations (or Sum Wgts)	120

Analysis of Variance

Source	DF	Sum of Squares	Mean Square	F Ratio
Model	1	447.24803	447.248	808020.0
Error	118	0.06531	0.000554	**Prob > F**
C. Total	119	447.31335		<.0001 *

Parameter Estimates

Term	Estimate	Std Error	t Ratio	Prob>|t|
Intercept	-0.079273	0.004323	-18.34	<.0001 *
time (min)	0.3344095	0.000372	898.90	<.0001 *

Bivariate Fit of 40 cm_500 um_20LPS By time (min)

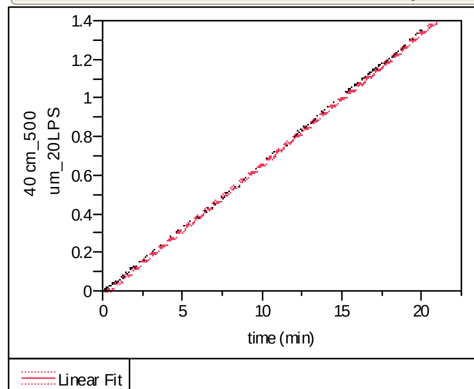

Linear Fit

40 cm_500 um_20LPS = -0.017373 + 0.0677923*time (min)

Summary of Fit

RSquare	0.999742
RSquare Adj	0.999739
Root Mean Square Error	0.006346
Mean of Response	0.666199
Observations (or Sum Wgts)	120

Analysis of Variance

Source	DF	Sum of Squares	Mean Square	F Ratio
Model	1	18.380274	18.3803	456449.5
Error	118	0.004752	4.027e-5	**Prob > F**
C. Total	119	18.385025		<.0001 *

Parameter Estimates

Term	Estimate	Std Error	t Ratio	Prob>|t|
Intercept	-0.017373	0.001166	-14.90	<.0001 *
time (min)	0.0677923	0.0001	675.61	<.0001 *

Table Q.17. Cumulative Mass Loss for 20 L/s, 45 cm and 50 µm (Left), and 20 L/s, 45 cm and 180 µm (Right)

Bivariate Fit of 45 cm_50 um_20LPS By time (min)

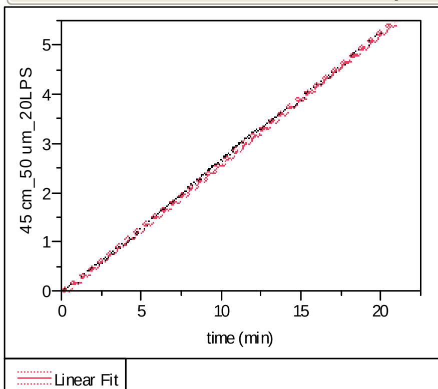

Linear Fit

45 cm_50 um_20LPS = -0.044034 + 0.2651687*time (min)

Summary of Fit

RSquare	0.999435
RSquare Adj	0.999431
Root Mean Square Error	0.036691
Mean of Response	2.62975
Observations (or Sum Wgts)	120

Analysis of Variance

Source	DF	Sum of Squares	Mean Square	F Ratio
Model	1	281.21320	281.213	208887.2
Error	118	0.15886	0.001346	**Prob > F**
C. Total	119	281.37205		<.0001 *

Parameter Estimates

Term	Estimate	Std Error	t Ratio	Prob>|t|
Intercept	-0.044034	0.006741	-6.53	<.0001 *
time (min)	0.2651687	0.00058	457.04	<.0001 *

Bivariate Fit of 45 cm_180 um_20LPS By time (min)

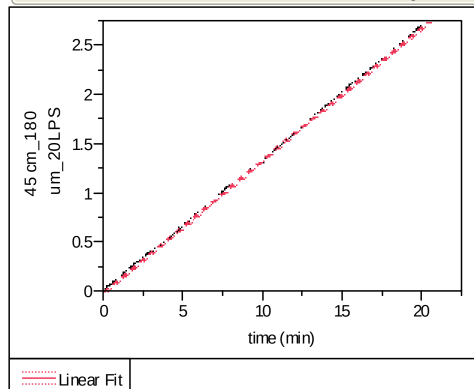

Linear Fit

45 cm_180 um_20LPS = -0.014397 + 0.134862*time (min)

Summary of Fit

RSquare	0.999847
RSquare Adj	0.999846
Root Mean Square Error	0.009713
Mean of Response	1.345461
Observations (or Sum Wgts)	120

Analysis of Variance

Source	DF	Sum of Squares	Mean Square	F Ratio
Model	1	72.739500	72.7395	771041.1
Error	118	0.011132	9.434e-5	**Prob > F**
C. Total	119	72.750632		<.0001 *

Parameter Estimates

Term	Estimate	Std Error	t Ratio	Prob>|t|
Intercept	-0.014397	0.001785	-8.07	<.0001 *
time (min)	0.134862	0.000154	878.09	<.0001 *

APPENDIX R

CUSTOMIZED SCOUR MODEL CODE

(This code was written on the subroutine *qsadd* in Flow-3D v.9.2 which Flow Science (2007) makes available for licensed users to create new computational codes)

```fortran
subroutine qsadd
c
c     this subroutine is called when nsc>0.  the call is near the
c     end of the cycle, after the pressure/velocity update and fluid
c     advection and diffusion,
c     but before new cells are initialized, nf's are set,
c     and the chemistry routine is called.
c
c    **************************************************************
c    **                          notice 1                        **
c    **        This subprogram was created by Humberto Avila     **
c    **                        SCOUR MODEL                       **
c    **                                                          **
c    **                copyright 2008 Humberto Avila             **
c    **                      ALL RIGHTS RESERVED                 **
c    **************************************************************
c    **************************************************************
c    **                          notice 2                        **
c    **  this subprogram contains flow science, inc. proprietary **
c    **       trade secret and confidential information.         **
c    **                                                          **
c    **                unauthorized use prohibited               **
c    **           copyright 1985-2006 flow science, inc.         **
c    **************************************************************
use mblock_module
c
use arrays_module
c
use arrayp_module
c
use meshcb_module
c
use voids_module
c
use obsijk_module
c
#ifdef SINGLE
include '../comdeck/precis4.f'
#else
include '../comdeck/precis.f'
#endif
include '../comdeck/params.f'
include '../comdeck/dparam.f'
include '../comdeck/cntrl.f'
include '../comdeck/const.f'
include '../comdeck/dumn.f'
include '../comdeck/phiou.f'
include '../comdeck/scala.f'
include '../comdeck/state.f'
include '../comdeck/pardat.f'
include '../comdeck/obsd.f'
c             scalar species sources and sinks
```

```
c
c     (not currently implemented)
c
c      variable        description
c      --------        --------------------------------
c       ijk            current cell index
c       ipjk             cell to right
c       imjk             cell to left
c       ijpk             cell to back
c       ijmk             cell to front
c       ijkp             cell to top
c       ijkm             cell to bottom
c       i                current x index
c       j                current y index
c       k                current z index
c
c       t                time
c       delt             time step size
c
c       nbl              current mesh block number
c
c       x(i)             mesh coordinate at right of cell ijk
c       xi(i)            cell ijk center
c       y(j)             mesh coordinate at back of cell ijk
c       yj(j)            cell ijk center
c       z(k)             mesh coordinate at top of cell ijk
c       zk(k)            cell ijk center
c       delx(i)          cell size in x direction
c       dely(j)          cell size in y direction
c       delz(k)          cell size in z direction
c       rri(i)           correction factor for cylindrical coordinates
c                        i.e., delta y at x(i) is dely(j)/rri(i)
c
c       vf(ijk)        open volume fraction in cell
c       afr(ijk)       open area fraction at right face
c       afb(ijk)       open area fraction at back face
c       aft(ijk)       open area fraction at top face
c
c       u(ijk)         x velocity at right face
c       v(ijk)         y velocity at back face
c       w(ijk)         z velocity at top face
c       fn(ijk)        fluid fraction in cell at beginning of cycle
c       p(ijk)         pressure in cell
c       tn(ijk)        temperature in cell
c       rhoe(ijk)      density*specific energy in cell
c       arint(ijk)     free surface area in cell
c       rho(ijk)       density in cell (only for variable density)
c
c       nf(ijk)        free surface indicator in cell
c          =0           interior fluid cell
c          =1           surface cell - fluid at left
c          =2           surface cell - fluid at right
c          =3           surface cell - fluid at front
c          =4           surface cell - fluid at back
c          =5           surface cell - fluid at bottom
c          =6           surface cell - fluid at top
c          =7           surface cell - cavitating cell
```

```
c          >=8          void cell -- void id number
c
c       nsc            number of scalars
c       sclr(ijk,ns)   concentration of scalar ns at cell ijk
c                      after advection and diffusion
c                      (update this variable to change scalar
c                      concentration)
c       sclrn(ijk,ns)  concentration of scalar ns at cell ijk
c                      at beginning of time step
c
c
c      skip over if no scalars exist and this subroutine is used for
c         scalar sources
c      if(nsc.eq.0) return
c
c
=======================================================================
c --- DEFINTTION OF CONSTANTS
diased=dum1
shcoef=dum2
rhosed=dum3
crpkc=dum4
coh=dum5
codrg=dum6
cobed=dum7
cosusp=dum8
coeros=dum9
vsett=dum12
angres=dum13
vslop=dum14
c --- critical solid fraction
fscrit=crpkc*rhosed
fmxpk=maxpak*rhosed
fsusp=csusp*rhosed
c --- critical shear stress
crtshr=shcoef*980.0*(rhosed-1.0)*diased
c =================================================================
c ---  CALCULATION OF ACTING SHEAR STRESS
do 100 k=kprb,kprt
do 100 j=jprf,jprbk
do 100 i=iprl,iprr
c -----  calculate current cell index
include '../comdeck/ijk.f'
c ------  skip non-active mesh cells
if(ijk.ge.ijklim_bc) cycle
c ------  skip calculation for completely blocked cells
if(vf(ijk).lt.em6) goto 100
c --------  calculate "neighbor indices"
include '../comdeck/mijk.f'
include '../comdeck/pijk.f'
c ----------  skip empty (void) cells
if(fn(ijk).lt.emf .and. nmat.eq.1) go to 100
c
c --- shear stress --------------------------
pvelshr=tke(ijk)*0.2915
sclr(ijk,6)=pvelshr*1.0
c----------------------------------------------
```

```
c --- volume of cell
sclr(ijk,10)=delx(i)*dely(j)*delz(k)
c---------------------------------------------
c --- mass calculation --------------------------
if(sclr(ijk,11).gt.ztest) then
sclr(ijk,9)=max(sclr(ijk,11),sclr(ijk,12)+sclr(ijk,3))
else
sclr(ijk,9)=sclr(ijk,12)+sclr(ijk,3)
endif
c---------------------------------------------
100   continue
c================================================================
c --- CALCULATION OF SEDIMENT DEPTH IN CELLS
do 110 k=kprb,kprt
do 110 j=jprf,jprbk
do 110 i=iprl,iprr
c -----  calculate current cell index
include '../comdeck/ijk.f'
c ------  skip non-active mesh cells
if(ijk.ge.ijklim_bc) cycle
c ------  skip calculation for completely blocked cells
if(vf(ijk).lt.em6) goto 110
c --------  calculate "neighbor indices"
include '../comdeck/mijk.f'
include '../comdeck/pijk.f'
c ----------  skip empty (void) cells
if(fn(ijk).lt.emf .and. nmat.eq.1) go to 110
c
sclr(ijk,13)=zero
if (sclr(ijk,11).gt.ztest) then
fracpack=sclr(ijk,11)/rhosed/crpkc
sclr(ijk,13)=delz(k)*fracpack
endif
c
if (sclr(ijkm,8).eq.one .and. sclr(ijk,8).eq.zero) then
fracbed=sclr(ijk,12)/rhosed/crpkc
sclr(ijk,13)=delz(k)*fracbed
endif
c
110    continue
c================================================================
c --- LOOP FOR CALCULATION ANGLE OF SEDIMENT SURFACE AND K COEFFICIENT
do 120 k=kprb,kprt
do 120 j=jprf,jprbk
do 120 i=iprl,iprr
c -----  calculate current cell index
include '../comdeck/ijk.f'
c ------  skip non-active mesh cells
if(ijk.ge.ijklim_bc) cycle
c ------  skip calculation for completely blocked cells
if(vf(ijk).lt.em6) goto 120
c --------  calculate "neighbor indices"
include '../comdeck/mijk.f'
include '../comdeck/pijk.f'
c ----------  skip empty (void) cells
if(fn(ijk).lt.emf .and. nmat.eq.1) go to 120
c – initialization of scalars
```

```
sclr(ijk,14)=zero
sclr(ijk,15)=zero
sclr(ijk,19)=zero
sclr(ijk,20)=zero
c ---------------------------------
if(sclr(ijk,8).eq.one .or. sclr(ijkm,8).eq.one)then
if (f(imjk).lt.ztest .or. vf(imjk).lt.em6)then
xangm=0.0
else
sclr(ijk,19)=abs((delx(i)+delx(im))/2.0)
sclr(ijk,15)=abs(sclr(ijk,13)- sclr(imjk,13))
xangm=sclr(ijk,15)/sclr(ijk,19)
endif
c
if (f(ipjk).lt.ztest .or. vf(ipjk).lt.em6)then
xangp=0.0
else
sclr(ijk,19)=abs((delx(i)+delx(ip))/2.0)
sclr(ijk,15)=abs(sclr(ijk,13)- sclr(ipjk,13))
xangp=sclr(ijk,15)/sclr(ijk,19)
endif
c
xang=max(xangm,xangp)
xang=max(zero,xang)
xang=min(60.0,xang)
c
angx=max(0.0,atan(xang))
angx=min(angx,angres)
c--- angle of sediment surface
sclr(ijk,14)=angx
sinsed=sin(angx)/sin(angres)
sinsed2=sinsed**2
c--- K (Coefficient of critical shear stress reduction)
sclr(ijk,20)=sqrt(1.0-sinsed2)
endif
c-------------------------------------------
120    continue
c ============================================================
c ---   SEDIMENT SCOUR
do 200 k=kprb,kprt
do 200 j=jprf,jprbk
do 200 i=iprl,iprr
c -----  calculate current cell index
include '../comdeck/ijk.f'
c ------  skip non-active mesh cells
if(ijk.ge.ijklim_bc) cycle
c ------  skip calculation for completely blocked cells
if(vf(ijk).lt.em6) goto 200
c --------  calculate "neighbor indices"
include '../comdeck/mijk.f'
include '../comdeck/pijk.f'
c ----------  skip empty (void) cells
if(fn(ijk).lt.emf .and. nmat.eq.1) go to 200
c----------
sclr(ijk,7)=zero
sedbed=cobed*sclr(ijk,20)*crtshr
sedcrit=sclr(ijk,20)*crtshr
```

```
sclr(ijk,5)=sedcrit
sclr(ijk,23)=zero

c--- RESUSPENSION OF BEDLOAD SEDIMENT
if (sclr(ijk,12).gt.ztest .and. sclr(ijkp,6).gt.sedcrit)then
susfrc=sclr(ijkp,3)/rhosed
rhomed=susfrc*rhosed+1.0*(1.0-(susfrc/crpkc))
ulift=max(zero,sqrt((sclr(ijkp,6)-sedcrit)/1.0)-vsett)
dlift=coeros*ulift*delt
areacel=delx(i)*dely(j)
avalsed=sclr(ijk,12)*sclr(ijk,10)
avaleros=max(zero,(fscrit-sclr(ijkp,3))*sclr(ijkp,10))
eros=min(avalsed,dlift*areacel*fscrit)
eros=min(eros,avaleros)
sclr(ijk,7)=eros
c --- suspension of sediment
sclr(ijkp,3)=sclr(ijkp,3)+eros/sclr(ijkp,10)
c --- remaining packing concentration
sclr(ijk,12)=max(zero,sclr(ijk,12)-eros/sclr(ijk,10))
elseif (sclr(ijk,12).gt.ztest .and. sclr(ijkp,6).gt.sedbed)then
susfrc=sclr(ijkp,3)/rhosed
rhomed=susfrc*rhosed+1.0*(1.0-(susfrc/crpkc))
ulift=cosusp*sqrt((sclr(ijkp,6)-sedbed)/1.0)
dlift=ulift*delt
areacel=delx(i)*dely(j)
eros=min(sclr(ijk,12)*sclr(ijk,10),dlift*areacel*fscrit)
sclr(ijk,7)=eros
c --- suspension of sediment
sclr(ijk,3)=sclr(ijk,3)+eros/sclr(ijk,10)
c --- remaining packing concentration
sclr(ijk,12)=max(zero,sclr(ijk,12)-eros/sclr(ijk,10))
endif
c =================================================================
c--- SCOUR ON PACKED SEDIMENT
if (sclr(ijk,11).gt.ztest .and. sclr(ijkp,6).gt.sedcrit)then
if (sclr(ijkp,11).eq.zero .and. sclr(ijkp,12).eq.zero) then
sclr(ijk,8)=one
susfrc=sclr(ijkp,3)/rhosed
rhomed=susfrc*rhosed+1.0*(1.0-(susfrc/crpkc))
ulift=max(zero,sqrt((sclr(ijkp,6)-sedcrit)/1.0)-vsett)
dlift=coeros*ulift*delt
areacel=delx(i)*dely(j)
avalsed=sclr(ijk,11)*sclr(ijk,10)
avaleros=max(zero,(fscrit-sclr(ijkp,3))*sclr(ijkp,10))
eros=min(avalsed,dlift*areacel*fscrit)
eros=min(eros,avaleros)
sclr(ijk,7)=eros
c --- suspension of sediment
sclr(ijkp,3)=sclr(ijkp,3)+eros/sclr(ijkp,10)
c --- remaining packing concentration
sclr(ijk,11)=max(zero,sclr(ijk,11)-eros/sclr(ijk,10))
packing=sclr(ijk,11)
sclr(ijk,2)=packing
if(sclr(ijk,11).lt.ztest)then
sclr(ijk,8)=zero
sclr(ijk,2)=zero
sclr(ijk,11)=zero
```

```
endif
endif
endif

c--- total sediment mass in cells ---------------
if(sclr(ijk,11).gt.ztest) then
sclr(ijk,9)=max(sclr(ijk,11),sclr(ijk,12)+sclr(ijk,3))
else
sclr(ijk,9)=sclr(ijk,12)+sclr(ijk,3)
endif
c-----------------------------------------------
200   continue
c========================================================================
======
c --- SEDIMENT SETTLING
c---------------
do 400 k=kprb,kprt
do 400 j=jprf,jprbk
do 400 i=iprl,iprr
c -----  calculate current cell index
include '../comdeck/ijk.f'
c ------  skip non-active mesh cells
if(ijk.ge.ijklim_bc) cycle
c ------  skip calculation for completely blocked cells
if(vf(ijk).lt.em6) goto 400
c --------  calculate "neighbor indices"
include '../comdeck/mijk.f'
include '../comdeck/pijk.f'
c ----------  skip empty (void) cells
if(fn(ijk).lt.emf .and. nmat.eq.1) go to 400
c
sclr(ijk,16)=zero
sclr(ijk,17)=zero
sclr(ijk,22)=zero
sclr(ijk,18)=zero
if (sclr(ijk,11).lt.fscrit .and. sclr(ijk,6).lt.crtshr)then
c
vxyz=sqrt(2.0*tke(ijk))
pervel=min(1.0,abs(vsett)/vxyz)
vset=pervel*abs(vsett)
sclr(ijk,18)=vset
c
sedavam=(sclr(ijkm,11)+sclr(ijkm,12)+sclr(ijkm,3))*sclr(ijkm,10)
sedavaf=fscrit*sclr(ijkm,10)
sclr(ijk,22)=max(zero,sedavaf-sedavam)
dsed=sclr(ijk,18)*delt
areacel=delx(i)*dely(j)
sclr(ijk,16)=dsed*areacel*sclr(ijk,3)
sclr(ijk,17)=min(sclr(ijk,16),sclr(ijk,3)*sclr(ijk,10))
sclr(ijk,17)=min(sclr(ijk,17),sclr(ijk,22))
c
endif
c-----------------------------------------------
400   continue
c ================================================================
c ================================================================
c --- CALCULATION OF SEDIMENT CONCENTRATION IN CELLS
```

```
do 500 k=kprb,kprt
do 500 j=jprf,jprbk
do 500 i=iprl,iprr
c -----  calculate current cell index
include '../comdeck/ijk.f'
c ------  skip non-active mesh cells
if(ijk.ge.ijklim_bc) cycle
c ------  skip calculation for completely blocked cells
if(vf(ijk).lt.em6) goto 500
c --------  calculate "neighbor indices"
include '../comdeck/mijk.f'
include '../comdeck/pijk.f'
c ----------  skip empty (void) cells
if(fn(ijk).lt.emf .and. nmat.eq.1) go to 500
c
if (sclr(ijk,8).eq.zero)then
sclr(ijk,4)=(sclr(ijkp,17)-sclr(ijk,17))/sclr(ijk,10)
sclr(ijk,3)=max(zero,sclr(ijk,3)+sclr(ijk,4))
endif
if (sclr(ijk,8).eq.one .and. sclr(ijk,11).lt.fscrit)then
sclr(ijk,4)=(sclr(ijkp,17)-sclr(ijk,17))/sclr(ijk,10)
sclr(ijk,11)=max(zero,sclr(ijk,11)+sclr(ijk,4))
endif
c
if(sclr(ijk,11).gt.ztest) then
sclr(ijk,9)=max(sclr(ijk,11),sclr(ijk,12)+sclr(ijk,3))
else
sclr(ijk,9)=sclr(ijk,12)+sclr(ijk,3)
endif
c
if(sclr(ijk,9).ge.fscrit)then
rescon=sclr(ijk,9)-fscrit
sclr(ijk,2)=fscrit
sclr(ijk,11)=fscrit
sclr(ijk,12)=zero
sclr(ijk,3)=zero
sclr(ijkp,12)=sclr(ijkp,12)+rescon*sclr(ijk,10)/sclr(ijkp,10)
sclr(ijk,8)=one
sclr(ijkp,8)=zero
endif
c -----------------------------------------
500   continue
c
========================================================================
c --- SEDIMENTATION
do 510 k=kprb,kprt
do 510 j=jprf,jprbk
do 510 i=iprl,iprr
c -----  calculate current cell index
include '../comdeck/ijk.f'
c ------  skip non-active mesh cells
if(ijk.ge.ijklim_bc) cycle
c ------  skip calculation for completely blocked cells
if(vf(ijk).lt.em6) goto 510
c --------  calculate "neighbor indices"
include '../comdeck/mijk.f'
include '../comdeck/pijk.f'
```

```
c ----------  skip empty (void) cells
if(fn(ijk).lt.emf .and. nmat.eq.1) go to 510
c----------
sedbed=cobed*sclr(ijk,20)*crtshr
if (sclr(ijk,3).gt.ztest .and. sclr(ijkp,6).lt.crtshr)then
if(sclr(ijk,8).eq.zero .and. sclr(ijkm,8).eq.one)then
areacel=delx(i)*dely(j)
sedsett=vsett*delt*areacel*sclr(ijk,3)/sclr(ijk,10)
sedsett=min(sedsett,sclr(ijk,3))
sclr(ijk,12)=sclr(ijk,12)+sedsett
sclr(ijk,3)=max(zero,sclr(ijk,3)-sedsett)
endif
endif
c
sclr(ijk,23)=sclr(ijk,12)+sclr(ijk,3)
if(sclr(ijk,23).ge.fscrit)then
rescon=sclr(ijk,23)-fscrit
sclr(ijk,11)=fscrit
sclr(ijk,2)=fscrit
sclr(ijk,12)=zero
sclr(ijk,3)=zero
sclr(ijkp,12)=sclr(ijkp,12)+rescon*sclr(ijk,10)/sclr(ijkp,10)
sclr(ijk,8)=one
endif
sclr(ijk,23)=sclr(ijk,12)+sclr(ijk,3)
c
if(sclr(ijk,12).gt.ztest .and. sclr(ijkm,8).eq.one)then
if(sclr(ijkm,11).lt.fscrit)then
sedavam1=sclr(ijkm,11)*sclr(ijkm,10)
sedavam2=fscrit*sclr(ijkm,10)
sedavam=sedavam2-sedavam1
sedavam=max(zero,sedavam)
sedavap=sclr(ijk,12)*sclr(ijk,10)
sedown=min(sedavam,sedavap)
sclr(ijkm,11)=sclr(ijkm,11)+sedown/sclr(ijkm,10)
repacking=sclr(ijkm,11)
sclr(ijkm,2)=repacking
sclr(ijk,12)=max(zero,sclr(ijk,12)-sedown/sclr(ijk,10))
sclr(ijk,2)=sclr(ijk,11)
endif
endif
c
if(sclr(ijk,11).gt.ztest) then
sclr(ijk,9)=max(sclr(ijk,11),sclr(ijk,12)+sclr(ijk,3))
else
sclr(ijk,9)=sclr(ijk,12)+sclr(ijk,3)
endif
c=================================================================
510   continue
c
return
end
```

APPENDIX S

CUSTOMIZED DRAG COEFFICIENT MODEL CODE

(This code was written on the subroutine *drgcst* in Flow-3D v.9.2 which Flow Science (2007) makes available for licensed users to create new computational codes)

```
subroutine drgcst(ijk,drgcof)
c
c   customied drag coefficient routine
c   called once per time step for every cell
c
c    **************************************************************
c    **                          notice 1                        **
c    **        This subprogram was created by Humberto Avila     **
c    **                        SCOUR MODEL                       **
c    **                                                          **
c    **                copyright 2008 Humberto Avila             **
c    **                      ALL RIGHTS RESERVED                 **
c    **************************************************************
c    **************************************************************
c    **                          notice 2                        **
c    **  this subprogram contains flow science, inc. proprietary **
c    **       trade secret and confidential information.         **
c    **                                                          **
c    **                unauthorized use prohibited               **
c    **            copyright 1985-2006 flow science, inc.        **
c    **************************************************************
c
use mblock_module
c
use arrays_module
c
use arrayp_module
c
use meshcb_module
c
use voids_module
c
#ifdef SINGLE
include '../comdeck/precis4.f'
#else
include '../comdeck/precis.f'
#endif
include '../comdeck/params.f'
include '../comdeck/cntrl.f'
include '../comdeck/const.f'
include '../comdeck/dumn.f'
include '../comdeck/phiou.f'
include '../comdeck/scala.f'
include '../comdeck/state.f'
include '../comdeck/pardat.f'
c
c             scalar species sources and sinks
c
c     (not currently implemented)
c
c      variable        description
c      --------        --------------------------------
c       ijk            current cell index
c       ipjk             cell to right
c       imjk             cell to left
c       ijpk             cell to back
c       ijmk             cell to front
```

```
c       ijkp             cell to top
c       ijkm             cell to bottom
c       i                current x index
c       j                current y index
c       k                current z index
c
c       t                time
c       delt             time step size
c
c       nbl              current mesh block number
c
c       x(i)             mesh coordinate at right of cell ijk
c       xi(i)            cell ijk center
c       y(j)             mesh coordinate at back of cell ijk
c       yj(j)            cell ijk center
c       z(k)             mesh coordinate at top of cell ijk
c       zk(k)            cell ijk center
c       delx(i)          cell size in x direction
c       dely(j)          cell size in y direction
c       delz(k)          cell size in z direction
c       rri(i)           correction factor for cylindrical coordinates
c                        i.e., delta y at x(i) is dely(j)/rri(i)
c
c       vf(ijk)        open volume fraction in cell
c       afr(ijk)       open area fraction at right face
c       afb(ijk)       open area fraction at back face
c       aft(ijk)       open area fraction at top face
c
c       u(ijk)         x velocity at right face
c       v(ijk)         y velocity at back face
c       w(ijk)         z velocity at top face
c       fn(ijk)        fluid fraction in cell at beginning of cycle
c       p(ijk)         pressure in cell
c       tn(ijk)        temperature in cell
c       rhoe(ijk)      density*specific energy in cell
c       arint(ijk)     free surface area in cell
c       rho(ijk)       density in cell (only for variable density)
c
c       nf(ijk)        free surface indicator in cell
c          =0           interior fluid cell
c          =1           surface cell - fluid at left
c          =2           surface cell - fluid at right
c          =3           surface cell - fluid at front
c          =4           surface cell - fluid at back
c          =5           surface cell - fluid at bottom
c          =6           surface cell - fluid at top
c          =7           surface cell - cavitating cell
c          >=8          void cell -- void id number
c
c       nsc            number of scalars
c       sclr(ijk,ns)   concentration of scalar ns at cell ijk
c                      after advection and diffusion
c                      (update this variable to change scalar
c                      concentration)
c       sclrn(ijk,ns)  concentration of scalar ns at cell ijk
c                      at beginning of time step
c
```

```
c   user's code here ...
c
c Definition: dU/dt = <forces and acelerations> - drgcof*U
c
c solidification and porous obstacle contributions are added to drgcof
c after the call to drgcst
c
c  drgcof - coefficient of linear drag term
c     U   - flow velocity
c
c ---INITIALIZATON OF DRAG COEFFICIENT
drgeval=idum1
if (drgeval.lt.1) then
drgcof=zero
goto 100
endif
c --- DEFINITION OF CONSTANTS
diased=dum1
shcoef=dum2
rhosed=dum3
crpkc=dum4
coh=dum5
codrg=dum6
cobed=dum7
cosusp=dum8
exscor=dum10
cdensed=dum11
exair1=dum14
exair2=dum15
c --- solid fractions
fscrit=crpkc*rhosed
fmxpk=maxpak*rhosed
fsusp=csusp*rhosed
fdens=cdensed*rhosed
c=====================================================================
c ---  DRAG INDICATOR IN CELLS
if (cycle.eq.0) then
do 50 k=kprb,kprt
do 50 j=jprf,jprbk
do 50 i=iprl,iprr
c -----  calculate current cell index
include '../comdeck/ijk.f'
c ------  skip non-active mesh cells
if(ijk.ge.ijklim_bc) cycle
c ------  skip calculation for completely blocked cells
if(vf(ijk).lt.em6) goto 50
c --------  calculate "neighbor indices"
include '../comdeck/mijk.f'
include '../comdeck/pijk.f'
c ----------  skip empty (void) cells
c             if(fn(ijk).lt.emf .and. nmat.eq.1) go to 50
c ----------
if(sclr(ijk,2).ge.fscrit)then
sclr(ijk,11)=fscrit
sclr(ijk,8)=one
else
sclr(ijk,11)=zero
```

```
sclr(ijk,8)=zero
endif
sclr(ijk,12)=zero
if(sclr(ijk,8).eq.one)then
sclr(ijk,20)=one
sclr(ijkp,20)=one
endif
if(sclr(ijk,8).eq.one)then
sclr(ijk,5)=crtshr
endif
c--
if(sclr(ijk,11).gt.ztest) then
sclr(ijk,9)=max(sclr(ijk,11),sclr(ijk,12)+sclr(ijk,3))
else
sclr(ijk,9)=sclr(ijk,12)+sclr(ijk,3)
endif
c
50    continue
endif
c ===================================================================
c --- DRAG COEFFICIENT CALCULATON
c --- TRDRG coefficient
diacof=71.8*diased-0.2925
c --- drag coefficient
if (sclr(ijk,11).gt.ztest)then
drgcof=1.0/ztest
elseif(sclr(ijk,12).gt.ztest) then
frsedsus=(sclr(ijk,12)+sclr(ijk,3))/rhosed
drgcof=diacof*frsedsus**codrg/(crpkc-frsedsus)**exscor
elseif (sclr(ijk,idfair).gt.ztest)then
drgcof=sclr(ijk,idfair)**exair1/(1.0-sclr(ijk,idfair))**exair2
else
drgcof=zero
endif
c =======================================
100   continue
return
end
```